Talanta

The International Journal of Pure and Applied Analytical Chemistry

Publication information: *Talanta* (ISSN 0039-9140). For 2008, volumes 74–76 are scheduled for publication. Subscription prices are available upon request from the Publisher or from the Regional Sales Office nearest you or from this journal's website (http://www.elsevier.com/locate/talanta). Further information is available on this journal and other Elsevier products through Elsevier's website: (http://www.elsevier.com). Subscriptions are accepted on a prepaid basis only and are entered on a calendar year basis. Issues are sent by standard mail (surface within Europe, air delivery outside Europe). Priority rates are available upon request. Claims for missing issues should be made within six months of the date of dispatch.

Orders, claims, and journal enquiries: please contact the Customer Service Department at the Regional Sales Office nearest you:
Orlando: Elsevier, Customer Service Department, 6277 Sea Harbor Drive, Orlando, FL 32887-480 USA; phone: (+1) (877) 8397126 [toll free number for US customers], or (+1) (407) 3454020 [customers outside US]; fax: (+1) (407) 3631354; e-mail: usjcs@elsevier.com
Amsterdam: Elsevier, Customer Service Department, PO Box 211, 1000 AE Amsterdam, The Netherlands; phone: (+31) (20) 4853757; fax: (+31) (20) 4853432; e-mail: nlinfo-f@elsevier.com
Tokyo: Elsevier, Customer Service Department, 4F Higashi-Azabu, 1-Chome Bldg, 1-9-15 Higashi-Azabu, Minato-ku, Tokyo 106-0044, Japan; phone: (+81) (3) 5561 5037; fax: (+81) (3) 5561 5047; e-mail: jp.info@elsevier.com
Singapore: Elsevier, Customer Service Department, 3 Killiney Road, #08-01 Winsland House I, Singapore 239519; phone: (+65) 63490222; fax: (+65) 67331510; e-mail: asiainfo@elsevier.com

USA mailing notice: *Talanta* (ISSN 0039-9140) is published monthly by Elsevier B.V. (P.O. Box 211, 1000 AE Amsterdam, The Netherlands). Annual subscription price in the USA US$ 4,085 (valid in North, Central and South America), including air speed delivery. Application to mail at periodical postage rate is paid at Rathway, NJ and additional mailing offices.
USA POSTMASTER: Send address changes to *Talanta*, Publications Expediting Inc., 200 Meacham Avenue, Elmont, NY 11003.
AIRFREIGHT AND MAILING in the USA by Publications Expediting Inc., 200 Meacham Avenue, Elmont, NY 11003.

Available online at www.sciencedirect.com
ScienceDirect
Talanta 76 (2008) 40–43
Talanta
www.elsevier.com/locate/talanta

Novel PVC membrane-based thoron ion selective electrode and its application: Determination of zirconium

Hassan A. Arida *

Hot Laboratories Center, Atomic Energy Authority, Inshass, 13759 Cairo, Egypt

Received 15 October 2007; received in revised form 28 January 2008; accepted 31 January 2008
Available online 9 February 2008

Abstract

The construction, electrochemical evaluation and application of new electrode selective to the thoron reagent are reported. The electrode incorporates bathophenanthroline iron: thoron ion pair as electroactive sensing material, *o*-nitrophenyl octyl ether as plasticizer and PVC as support matrix, exhibits a Nernstian response to thoron with a slope of -29.7 ± 1 mV per decade in a range of concentration from 1.0×10^{-6} to 5.0×10^{-2} mol L^{-1}, a detection limit of 6.0×10^{-7} mol L^{-1} and fast response time of less than 30 s. The proposed electrode is successfully applied to zirconium ion determination in aqueous samples using indirect potentiometry and the results obtained are compared with those provided by spectrophotometric analysis using thoron as complexing agent.

Keywords: Thoron; Ion selective electrode; Zirconium determination; Indirect potentiometry

1. Introduction

So far little work has been reported on the determination of anionic organic reagents, despite they widely used for the detection and quantitative determination of many metal cations as well as they had played an increasing important role in chemical methods and functional analysis. The preparation, characterisation and analytical application of most of these reagents have been reported [1–3]. Different methods have been also reported for the organic reagents determination [4–12], based on fluorometric [4], voltametric [5–9], chemiluminescence [10], polarographic [11] and spectrophotometric methods of analysis [12]. However, most of these techniques necessitate the use of sophisticated and relatively costly apparatus and require complicated pre-treatment procedures which not suitable for on-line or field monitoring. In contrast, suggesting of ion selective electrodes is an attractive alternative method for organic and inorganic species detection, due to its inherent advantages of being simple, rapid, reliable, low cost and non-destructive characteristics. Hence, a number of ion selective electrodes for measuring anionic reagents have been reported [13–21]. These electrodes have proven useful quantitative determination of anionic surfactants [13–15], molybdate anion [16], gibberellic acid [17], ethylenediaminetetraacetatobismuthate III anion [18], orthophosphate [19], cysteine [20] and flufenamic acid anion [21]. In our previous work, we have also developed a new ion selective electrode for the determination of 8-hydroxyquinoline and its application in the determination of some metal ions [22]. In addition, some modified calixarenes and macrocyclic receptors have been recently, developed and applied as sensing materials for selective determination of chromate, monohydrogen phosphate, carbonate and phosphate, respectively [23–26].

It has already well documented that, on the other hand, thoron (Fig. 1) reagent (thorin or thoron (1) indicator; 4((2-arsonophenyl)azo)-3-hydroxy-2,7-naphthalenedisulfonic acid), was used as a selective reagent for zirconium, thorium, beryllium and lanthanum [8,27,28]. In such studies, thoron has been extensively used in a significant selective determination of some rare earths due to its high ability to chelate specific cations. There has been, however, not any ion selective electrode being reported for the determination of thoron reagent.

The goal of this work was to develop an ion selective electrode for thoron detection and study its applicability in the potentiometric determination of some metal ions. The electrode based on bathophenanthroline iron(II): thoron ion pair shows a stable and reproducible potentiometric response towards thoron anion with a linear concentration range and fast response time. The

* Tel.: +20 2 44620774; fax: +20 2 44620806.
E-mail address: aridaha@hotmail.com.

0039-9140/$ – see front matter © 2008 Elsevier B.V. All rights reserved.
doi:10.1016/j.talanta.2008.01.061

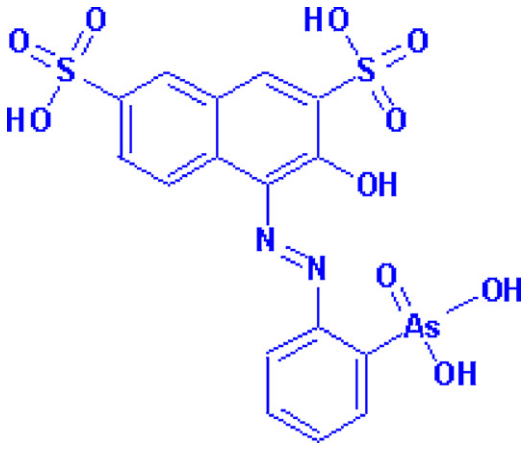

Fig. 1. Chemical structure of thoron.

electrode has been applied to the determination of zirconium (as an example) with satisfactory results.

2. Experimental

2.1. Reagents and apparatus

In the preparation of solutions, deionized bi-distilled water was used throughout. Analytical reagents chemicals were used without any additional purification. Thoron; 4((2-arsonophenyl)azo)-3-hydroxy-2,7-naphthalenedisulfonic acid disodium salt was obtained from B.D.H. Laboratory Reagents. Poly (vinyl chloride) powder, *o*-nitrophenyl octyl ether, tetrahydrofurane (THF) and ethanol were obtained from Aldrich Chemicals Co. Bathophenanthroline (4,7-diphenyl-1,10-phenanthroline), iron(II) sulphate and zirconyl chloride were obtained from Fluka AG (Buchs, Switzerland). Standard stock solutions of 0.1 and 0.05 mol L^{-1} for zirconyl chloride and thoron reagent, respectively, were prepared in deionized bi-distilled water. The working solutions were prepared by rigorous dilution and the pH was adjusted by addition of very small aliquots of nitric acid or sodium hydroxide solutions.

All potentiometric measurements were performed at 25 ± 1 °C using Hanna digital pH/mV meter (Model 8417) with PVC membrane-based thoron electrode in conjunction with a Hanna single-junction Ag/AgCl reference electrode containing 10% (w/v) potassium chloride. A combined glass pH electrode (Hanna HI 1131 B) was used for all pH measurements.

2.2. Membrane and electrode preparation

The bathophenanthroline iron: thoron ion pair was prepared by addition of 50 mg 4,7-diphenyl-1,10-phenanthroline dissolved in 10 mL 95% (v/v) ethanol: water mixture to 0.2 mL of 0.1 mol L^{-1} iron(II) sulphate. This mixture was stirred at room temperature for 5 min and thoron reagent (5 mL of 5×10^{-2} mol L^{-1}) was slowly added. The resulting orange precipitate of the ion pair complex was filtered off, washed with deionized bi-distilled water and dried at room temperature for 24 h. Infrared spectra of the final product agreed with the formation of [(Fe (bphen)$_3$)$^{2+}$ thoron^{2-}] ion pair complex.

Master PVC membrane of approximately 0.1 mm thick was optimized and prepared as described elsewhere [22] by mixing a 10 mg portion of thoron-based ion pair complex with 0.35 mL of *o*-nitrophenyl octyl ether plasticizer, 190 mg of PVC matrix, and 6 mL THF. The viscous solution thus obtained was poured in a glass Petridish (3 cm diameter) and the solvent was allowed to evaporate for bout 24 h at room temperature.

The master PVC membrane was sectioned with a cork borer (10 mm diameter) and attached to a polyethylene tubing (3 cm length and 8 mm i.d.) using THF. A home made electrode body was used which consists of a glass tube, to one end of which the polyethylene tubing was tightly inserted and filled with an equimolar mixture of 10^{-2} mol L^{-1} KCl and thoron as an internal reference solution. An Ag/AgCl internal reference wire electrode was immersed in the internal reference solution. This assembly was used as a sensitive electrode in the potentiometric measurements of thoron. The electrode was conditioned by soaking in 10^{-3} mol L^{-1} thoron solution for 2 h before use and stored in the same solution when not in use.

2.3. Analytical characterization of thoron electrode

The proposed electrode was calibrated by measuring the e.m.f. values after stabilization to ±0.5 mV in a series of thoron solutions covering the concentration range 1.0×10^{-8}–1.0×10^{-1} mol L^{-1} thoron. The e.m.f. values were plotted on a semilogarithmic paper as a function of thoron concentration. The obtained calibration curve was used for subsequent determination of the unknown thoron samples.

The selectivity coefficients for foreign ions were determined by the separate solution method [29] in which the potential readings (mV) of the two separate solutions one containing only the thoron ion at the concentration level of 10^{-3} mol L^{-1} and the other containing the interferent ions at the same concentration level were measured. The selectivity coefficients $K^{\mathrm{Pot}}_{\mathrm{thoron}^-,\mathrm{B}^-}$ were calculated using the experimentally obtained slope.

The response time ($t_{95\%}$) of the proposed electrode was also, tested by measuring the time required to achieve a 95% steady potential for the test solutions, when the thoron ion concentration was rapidly increased by one decade from 1.0×10^{-6} to 1.0×10^{-1} mol L^{-1}. The potential readings were recorded against time (min).

The lifetime of the investigated thoron electrode was measured from the response potential to the varying thoron concentration 2 days a week for more than 2 months. At least two electrodes have been used and not less than three repeated calibrations have been done for this purpose.

3. Results and discussion

3.1. Influence of pH on the potentiometric response of thoron electrode

The influence of the pH of a test solution on the proposed thoron electrode potentiometric response was studied at two thoron concentrations (1.0×10^{-3} and 1.0×10^{-4} mol L^{-1}),

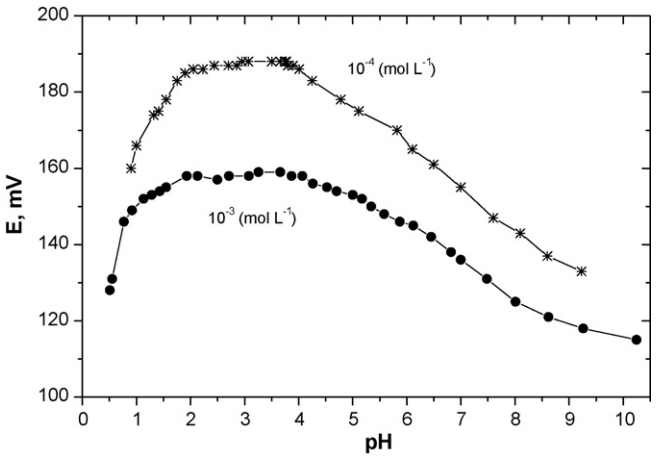

Fig. 2. Effect of pH on the potentiometric response of thoron electrode.

where the pH was adjusted from 1 to 10 with HNO_3 or NaOH solutions. The results observed are presented in Fig. 2. As it can be seen, the potential is independent on the pH changes in the range of ca. 1.8–4.2. Thus, this range may be chosen as the working pH for the electrode assembly. At pH < 1.8, the thoron anion was protonated, whereas, at relatively high pH the potential decreases more significantly probably due to membrane response to OH^-.

3.2. The response time and selectivity coefficient

The dynamic response time for the thoron electrode from lower concentration (1.0×10^{-6} mol L^{-1}) to higher concentration (5.0×10^{-2} mol L^{-1}) was recorded. The actual potential versus time tracer is presented in Fig. 3. As it can be seen, the proposed thoron electrode provides fast response time (<30 s.) to reach 95% of its final steady state potential in the tested concentration range.

The selectivity of the ion selective electrode under consideration was also, investigated with respect to some common anions using separate solutions method. The data obtained, showed that

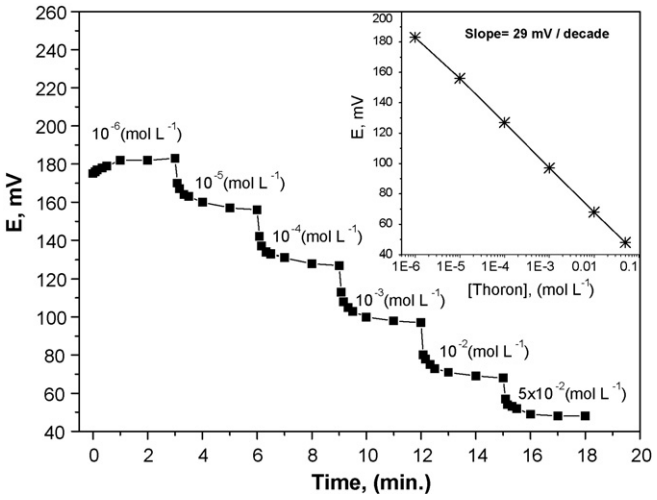

Fig. 3. Potentiometric dynamic response of thoron electrode.

Table 1
Potentiometric response characteristics of PVC based thoron electrode

Parameter	Thoron electrode
Slope (mV/decade)	-29.7 ± 1
Linear range (mol L^{-1})	1.0×10^{-6}–5.0×10^{-2}
Lower limit of linear range (mol L^{-1})	1.0×10^{-6}
Lower limit of detection (mol L^{-1})	6.0×10^{-7}
Response time (s).	<30
Working pH range	1.8–4.2
Life time (months)	>2

the selectivity coefficients ($K^{\mathrm{Pot}}_{\mathrm{Thoron}^{2-},\mathrm{B}^-}$) values ranging from 3.6×10^{-2} to 7.8×10^{-4} for the tested anions. These values clearly indicate that, the proposed electrode was fairly selective to thoron anion over different tested anions. The selectivity of the electrode towards the tested common anions increases with the lipophilic characteristics of the tested anions in accordance with the Hofmeister series. Nevertheless, for all of the diverse ions used, the selectivity coefficients were lower than 3.6×10^{-2} indicating that the studied common anions would not significantly disturb the determination of thoron.

3.3. Thoron electrode response characteristics

The proposed bathophenanthroline iron: thoron ion pair complex was prepared, identified and examined as electroactive sensing material in PVC membrane-based electrode responsive for thoron anion. The electrochemical performance characteristics of the electrode were systematically evaluated according to IUPAC recommendations [30], and the results obtained are given in Table 1. The electrode exhibits a Nernstian linear and stable response for thoron over the concentration range 1.0×10^{-6}–5.0×10^{-2} mol L^{-1} with anionic slope of -29.7 ± 1 mV/decade (Fig. 4). The limit of detection evaluated according to IUPAC recommendation from the intersection of the two extrapolated segments of the calibration graph was found to be 6.0×10^{-7} mol L^{-1}. The proposed electrode does not show appreciable decay of the slope for more than 2 months. During this period, the electrode continued to generate reproducible

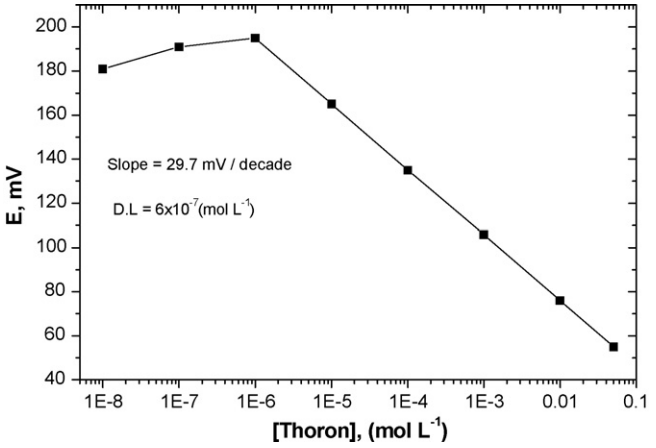

Fig. 4. Potentiometric calibration response of thoron electrode.

Table 2
Potentiometric determination of Zirconium using thoron electrode

Sample number	Suggested method ($mol\,L^{-1}$)	Spectrophotometry ($mol\,L^{-1}$)	Relative error (%)
1	1.80×10^{-4} (16.4 ppm)	1.96×10^{-4} (17.8 ppm)	−8.1
2	7.70×10^{-4} (70.2 ppm)	8.20×10^{-4} (74.8 ppm)	−6.0
3	2.62×10^{-3} (238.9 ppm)	2.44×10^{-3} (222.5 ppm)	7.3

potential. The standard deviation of the electrode potential and slope for 8 measurements are found to be 4 and 1 mV, respectively. There is no noticeable hysteresis of the potentiometric response provided that the electrode was stored in $1.0 \times 10^{-3}\,mol\,L^{-1}$ thoron solution when not in use.

3.4. Analytical application of thoron electrode

The analytical usefullness of the developed thoron electrode in the determination of some metal cations has been assessed using indirect potentiometry. Zirconium has been selected in this study as an example to investigate the reliability of the proposed electrode. Since, thoron has already been used as a selective chelating reagent for zirconium, thorium, beryllium and lanthanum [8,27,28].

In such study, to aliquots of zirconium oxychloride solution containing about 15–250 ppm a sixfold of the thoron reagent was added. After complete colour development and equilibration as described elsewhere [27], the concentration of zirconium cations has been determined by indirect potentiometry using the proposed thoron electrode. The results obtained are given in Table 2. These results were compared with those provided by the analysis of the same samples using a previously reported spectrophotometric method [27]. It can be seen that, the results obtained by the proposed electrode was in good agreement with those obtained by spectrophotometric analysis with a relative error less than 8.1%.

4. Conclusion

A New sensitive thoron-based electrode incorporating bathophenanthroline iron: thoron ion pair complex as the electroactive materials, *o*-nitrophenyl octyl ether as a solvent mediator and PVC matrix has been developed. The electrode can be used to determine thoron anions in the concentration range 1.0×10^{-6} to $5.0 \times 10^{-2}\,mol\,L^{-1}$ with a Nernstian slope of -29.7 ± 1 mV/decade of concentration. The electrode works in a relatively wide, independent pH range (1.8–4.2), and exhibits a fast response, high sensitivity and selectivity for thoron anions. The proposed electrode was successfully applied to the determination of zirconium cations concentration by indirect potentiometry. The results obtained show a satisfactory agreement with those obtained using independent spectrophotometric method.

References

[1] S.B. Savin, J. Anal. Chem. 58 (2003) 289.
[2] A.E. Friedman, L.A. Mauck, T.R. Kissel, US Patent 5,372,932 (1994).
[3] N. Souka, F. Abdel-Rahim, M.R. Mahmoud, Radioanal. Nucl. Chem. 125 (1988) 47.
[4] J.F. Garcia-Reyes, P. Ortega-Barrales, A. Molina-Diaz, Anal. Sci. 23 (2007) 423.
[5] V. Supalkova, J. Petrek, L. Havel, S. krizkova, J. Petrlova, V. Adam, D. Potesil, P. Babula, M. Beklova, A. Horna, R. Kizek, Sensors 6 (2006) 1483.
[6] J. Barek, J.C. Moreira, J. Zima, Sensors 5 (2005) 148.
[7] L. Zhao, B. Lv, H. Yuan, Z. Zhou, D. Xiao, Sensors 7 (2007) 578.
[8] A. Watson, W.F. Smyth, G. Svehla, K. Vadasdi, Z. Anal. Chem. 253 (1971) 106.
[9] V. Supalkova, D. Huska, V. Diopan, P. Hanustiak, O. Zitka, K. Stejskal, J. Baloun, J. Pikula, L. Havel, J. Zehanlek, V. Adam, L. Trnkova, M. Beklova, R. Kizek, Sensors 7 (2007) 932.
[10] I. Cukrowski, J.M. Zhang, Electroanalysis 16 (2004) 612.
[11] F.G. Banica, J.C. Moreira, A.G. Fogg, Analyst 119 (1994) 309.
[12] S. Kar, B. Sarkar, S. Ghumaan, M. Leboschka, J. Fiedler, W. Kaim, G.K. Lahiri, Dalton Trans. (2007) 1934.
[13] F.G. Binas, F.B. Sevilla, IEEE (2005) 43.
[14] J. Sánchez, M. del Valle, Crit. Rev. Anal. Chem. 35 (2005) 15.
[15] M.J. Seguí, J. Lizondo-Sabater, A. Benito, R. Martínez-Máñez, T. Pardo, F. Sancenón, J. Soto, Talanta 71 (2007) 333.
[16] Z. Fang, Z. Han, X. Zhang, G. Shen, R. Yu, Anal. Sci. 22 (2006) 949.
[17] E.M.G. Santos, C.M.C.M. Couto, M.C.B.S.M. Montenegro, M.G.P.M.S. Neves, S.L.H. Rebelo, J.A.S. Cavaleiro, B.F. Reis, Anal. Bioanal. Chem. 375 (2003) 511.
[18] S.V. Kharitonov, N.B. Minevich, I.P. Gorelov, J. Anal. Chem. 57 (2002) 632.
[19] Y. Alifragis, G. Konstantinidis, A. Georgakilas, N. Chaniotakis, Electroanalysis 17 (2005) 527.
[20] R. Volf, T.V. Shishkanova, V. Kral, J. Incl. Phenom. Macr. Chem. 35 (1999) 111.
[21] S. Kiru, Y. Oda, M. Sasaki, Chem. Pharm. Bull. (Tokyo) 31 (1983) 1089.
[22] H.A. Arida, Anal. Lett. 35 (2002) 2421.
[23] A.K. Jain, V.K. Gupta, L.P. Singh, P. Srivastava, J.R. Raisoni, Talanta 65 (2005) 716.
[24] V.K. Gupta, R. Ludwig, S. Agarwal, Anal. Chim. Acta 538 (2005) 213.
[25] A.K. Jain, V.K. Gupta, J.R. Raisoni, Electrochim. Acta 52 (2006) 951.
[26] A.K. Jain, V.K. Gupta, J.R. Raisoni, Talanta 69 (2006) 1007.
[27] G.P. Gupta, K.N. Munshi, Z. Anal. Chem. 277 (1975) 206.
[28] R. Keil, Z. Anal. Chem. 262 (1972) 273.
[29] Y. Umezaw, P. Bühlmann, K. Umezaw, K. Tohda, S. Amemiya, Pure Appl. Chem. 72 (2000) 1851.
[30] R.P. Buck, E. Lindner, Pure Appl. Chem. 66 (1994) 2527.

Talanta 76 (2008) 111–115

Contents lists available at ScienceDirect

Talanta

journal homepage: www.elsevier.com/locate/talanta

An investigation of the reaction of copper ions with dimethylindodicarbocyanine dye
An application for the determination of Cu(I), Cu(II) and Cu(III)

Ioseph S. Balogh[a], Michael Ruschak[b], Vasil Andruch[c,*], Yaroslav Bazel'[c]

[a] Department of Chemistry, College of Nyíregyháza, Sóstói u. 31/B, 4400 Nyiregyháza, Hungary
[b] Department of Analytical Chemistry, Užhorod National University, Pidhirna 46, 88000 Užhorod, Ukraine
[c] Department of Analytical Chemistry, University of P.J. Šafárik, Moyzesova 14, SK-04154 Košice, Slovak Republic

ARTICLE INFO

Article history:
Received 13 November 2007
Received in revised form 7 February 2008
Accepted 14 February 2008
Available online 10 March 2008

Keywords:
Speciation
Spectroscopy
Separation
Semiconductor materials

ABSTRACT

In this work, the reactions of various copper ions with 1,3,3-trimethyl-2-[5-(1,3,3-trimethyl-1,3-dihydroindol-2-ylidene)-penta-1,3-dienyl]-3*H*-indolium – more commonly known as dimethylindodicarbocyanine polymethyne dye (DIDC) – as well as the application of the results obtained for the development of a spectrophotometric method for the determination of Cu(I), Cu(II) and Cu(III) are described. Cu(I) and Cu(II) in the presence of chloride ions and DIDC reagent are extractable by a variety of organic solvents. It is important to emphasize that Cu(I) was extracted under considerably different experimental conditions than Cu(II). The optimum conditions for the extraction of the Cu ion associates with DIDC by amyl acetate and the determination of Cu(I) and Cu(II) were found to be: pH 3–5 and pH 3–6 and chloride concentrations of 0.5–0.8 mol L^{-1} and 3–6 mol L^{-1} for Cu(I) and Cu(II), respectively. The molar absorptivities for Cu(I) and Cu(II) are 1.8×10^5 L mol^{-1} cm^{-1} and 1.2×10^5 L mol^{-1} cm^{-1}, respectively. A reaction mechanism is suggested. Cu(III) does not extract in the presence of chloride ions. However, Cu(III) is a strong oxidative agent which can cause the decolourisation of the DIDC reagent. The optimum conditions for Cu(III) determination were found to be: 2×10^{-5} mol L^{-1} DIDC; pH 8; water:acetone 4:1 medium. The developed procedures were tested for the determination of Cu(I), Cu(II) and Cu(III) in semiconductor samples.

1. Introduction

The occurrence of copper in the earth's crust is approximately 0.01%. In nature, copper is found primarily in the form of compounds with sulphur. Copper can be combined with other metals to form alloys such as brass, bronze and various Cu–Ni alloys. Copper alloys are widely used in a variety of industries. In chemical compounds, copper is most often found in the Cu(II) form. In addition, copper may also exist in compounds in the form of copper(I) and copper(III) [1]. Interest in Cu(III) compounds increased in the middle of 20th century as a result of research on superconductors.

Copper is an important bioelement that is present in animals, plants and microorganisms. It is both vital and toxic to many biological systems, depending on the level of concentration. In biosystems copper exists in two characteristic forms, with oxidation numbers of I and II and takes part in oxidation–reduction processes. One notable function of copper is its influence on the metabolism of iron. Another function is its direct influence on the activity of some enzymes [2].

A number of techniques for copper determination have been reported, including AAS, UV–vis spectrophotometry and FIA. Numerous spectrophotometric methods using various colorimetric reagents have also been described for the determination of copper. The methods most commonly reported are those for the determination of Cu(II) and Cu(I). The most popular spectral reagents for copper determination are dithiocarbamate, 1,10-phenanthroline and dithizone [1,3]. A comparison of the selected spectrophotometric reagents is presented in Table 1.

Separation and/or preconcentration are often a prerequisite for the determination of trace elements. The most widely used techniques for the separation/preconcentration of Cu are liquid–liquid extraction, solid-phase extraction and cation exchange resins. Numerous procedures for the preconcentration of copper have been reported. These include using copper's ability to form ion-pairs with 1,10-phenanthroline and tetraphenylborate on naphthalene [16], using bathocuproine to form a complex which can then be collected on a nitrocellulose membrane filter [17], using

* Corresponding author.
E-mail address: vasil.andruch@upjs.sk (V. Andruch).

0039-9140/$ – see front matter © 2008 Elsevier B.V. All rights reserved.
doi:10.1016/j.talanta.2008.02.011

Table 1
Comparison of selected reagents for the spectrophotometric determination of copper

Reagent	λ (nm)	ε (L mol^{-1} cm^{-1})	Analytical range	Ref.
2-(5-Bromo-2-pyridylazo)-5-diethylamino phenol, polyglycol octylphenyl ether	560	1.5×10^5	0.0–18 μg	[4]
1,5-Bis(di-2-pyridylmethylene) thiocarbonohydrazide	500	4.2×10^4		[5]
Diethyldithiocarbamate, β-cyclodextrin	436	1.3×10^4	0–150 μg/25 mL	[6]
Bis(acetylacetone)ethylenediimine	370	–	up to 80 μg/mL	[7]
Poly[allylamine-*co*-*N*-4-(8-aminoquinolyl-5-azo)benzylideneallylamine]	590	4.1×10^4	0–l.0 μg/mL	[8]
3,3′-(1,3-Propanediyldiimine)bis-[3-methyl-2-butanone]dioxime	525	2.95×10^4	0.5–350 μg/L	[9]
1-[Pyridyl-(2)-azo]-naphthol-(2), TX-100, *N*,*N*′-diphenylbenzamidine	520	1.14×10^5	up to 0.6 μg/mL	[10]
S,*S*′-bis(2-aminophenyl)oxalate	504	5365	0.4–150 μg/mL	[11]
3-{2-[2-(2-Hydroxyimino-1-methyl-propylideneamino)-ethylamino]-ethyl-imino}-butan-2-one oxime	570	0.16×10^4	0.2–225 mg/L	[12]
Naphthazarin	330	1.84×10^4	up to 4.5 ppm	[13]
1-Phenyl-1,2-propanedione-2-oxime thiosemi-carbazone	465	5.56×10^3	0.38–7.63 μg/mL	[14]
Thiomichlersketone, polyethylene octyl phenyl ether	500	5.7×10^4	0–15 μg/25 mL	[15]

ammonium pyrrolidinedithiocarbamate to form a chelate which is then adsorbed on an activated carbon minicolumn [18] and using a C_{18} column loaded with sodium diethyldithiocarbamate to extract copper and cadmium from seawater [19], etc. [20–22].

Titrimetric [23–25] and voltammetric [24] methods are often used for Cu(III) determination, though spectrophotometric methods have also been reported [26,27]. Copper(III) solutions yield a pink-coloured product with *p*-anisidine in the presence of acetic acid with molar absorptivity, $\varepsilon_{533} = 415\ \text{L mol}^{-1}\ \text{cm}^{-1}$ [27].

Frequently, the methods reported have been applicable for the determination of total copper concentration, but not for the determination of the specific oxidative forms of copper, such as Cu(I), Cu(II) and Cu(III).

The aim of this work was to study the reactions of various copper ions with 1,3,3-trimethyl-2-[5-(1,3,3-trimethyl-1,3-dihydro-indol-2-ylidene)-penta-1,3-dienyl]-3*H*-indolium – more commonly known as dimethylindodicarbocyanine polymethyne dye (DIDC) – as well as the application of the results obtained for the development of a spectrophotometric method for the determination of Cu(I), Cu(II) and Cu(III).

The main characteristics of DIDC have been investigated previously: the protonation constant, the hydrolysis constant, the optimum wavelength and the molar absorptivity were found to be $pK_{pr} = -0.05 \pm 0.01$, $pK_h = 12.12 \pm 0.10$, $\lambda_{max} = 644$ nm, $\varepsilon_{644} = 18.2 \times 10^4\ \text{L mol}^{-1}\ \text{cm}^{-1}$, respectively [28]. The chemical structure of DIDC is shown in Fig. 1. The merits of the reagent include its stability and high intensity of colour. The reagent has been previously suggested for the determination of Cr(VI) [29] and Se [30].

2. Experimental

2.1. Reagents

All chemicals and solvents used were analytical-grade reagents and were used without further purification. Double-distilled water was used throughout the work. A stock solution containing 0.01 mol L^{-1} of Cu(II) was prepared by dissolving $CuSO_4 \cdot 5H_2O$ in water and standardizing by EDTA titration. The working solutions, in concentrations ranging from 1×10^{-3} mol L^{-1} to 1×10^{-5} mol L^{-1} of Cu, were prepared by dilution of the stock solution prior to use. A 2% solution of ascorbic acid was used as a reducing agent for the preparation of the Cu(I) solution. A stock solution containing 0.05 mol L^{-1} Cu(III) was prepared according to the recommendation described in Refs. [26,31].

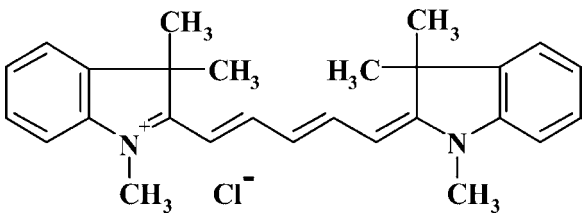

Fig. 1. The structure of DIDC.

A 1×10^{-3} mol L^{-1} aqueous solution of DIDC dye reagent was prepared by directly dissolving the precise weight of its chloride in water. The required concentration of chloride ions was reached by the addition of a 3 mol L^{-1} solution of NaCl or a 10.5 mol L^{-1} solution of LiCl. The required acidity of the aqueous phase was set by adding 1.5 mL of 1 mol L^{-1} HOAc–NH_4OH buffer solution (in the range of pH 4–9) or by the addition of 0.01 or 1 mol L^{-1} HCl solution (in the range of pH ≤ 3).

2.2. Apparatus

An SF-10 double-beam UV–vis scanning spectrophotometer and a Carl Zeiss Spekol-11 spectrophotometer were used for recording the absorption spectra and for routine measurements, respectively, with matched cells of 3 mm or 5 mm path length. The pH measurements were made using a pH-121 potentiometer with a glass electrode.

2.3. Calibration of the method for the determination of Cu(I) and Cu(II)

The extraction was carried out in graduated test tubes at room temperature. The working solution of Cu(II) was introduced to individual test tubes in amounts ranging from 0 μg to 12 μg of Cu. In the case of Cu(I), 0.5 mL of a 2% solution of ascorbic acid was added as a reducing agent. The required concentration of chloride (0.2 mol L^{-1} for Cu(I) and 4.5 or 6 mol L^{-1} for Cu(II)) was reached by the addition of a solution of NaCl and LiCl, respectively. A pH of 3 was set by the addition of 0.01 mol L^{-1} of HCl. Then 0.3 mL 1×10^{-3} mol L^{-1} of DIDC was added, and the volume was filled with water to the level of 5 mL. After the addition of each reagent, the solution was thoroughly mixed. Next, the ion associate was extracted using 5 mL of amyl acetate. After the extraction, the organic phase was separated and the absorbance was measured against that of a blank test.

2.4. Calibration of the method for the determination of Cu(III)

To the test tubes containing a constant concentration (2×10^{-5} mol L^{-1}) of DIDC, 1 mL of acetone, 1.5 mL of buffer solution with pH 8 and varying amounts of Cu(III) were added. The volume was filled with water to a level of 5 mL. After the addition of each reagent, the solution was mixed thoroughly. The decrease in the absorbance was then measured.

2.5. Procedure for real samples

A precise weight of a sample of semiconductor material was dissolved in 0.01 mol L^{-1} HCl, transferred to a volumetric flask and filled up to the calibration mark with water. An aliquot containing a maximum of 12 μg of Cu was pipetted into the test tube. All of the required reagents were then added and the analysis continued as described in the calibration procedure. Five repeated measurements were taken for each sample.

3. Results and discussion

Despite the fact that numerous articles have been devoted to copper determination in various kinds of samples, the determination of copper speciation has until now been a difficult task. As seen from an overview of the literature, the methods reported are applicable for the determination of total copper concentration, but not for the determination of the specific oxidative forms of copper, such as Cu(I), Cu(II) and Cu(III). The methods most commonly reported are those for the determination of Cu(II). Very few articles, however, have been presented that deal with the determination of Cu(I) in real samples and fewer still that deal with the determination of Cu(III) in real samples. Since a valid method for the determination of various copper species in semiconductor materials, as well as the reference materials for the investigated samples having a certified value of various copper species, is unavailable, it is difficult to assess the accuracy of the obtained results. Therefore, the accuracy and precision of the suggested method were verified by using the method of standard additions, by repeating determinations for each sample, by analysing different copper concentrations (different amounts of each sample), by the determination of total Cu by the AAS method and by comparison with theoretical data calculated from synthesis.

3.1. Preliminary investigations

The preliminary investigations carried out showed that Cu(I) and Cu(II) in the presence of chloride ions and DIDC reagent become extractable by a variety of organic solvents. It is important to emphasize that Cu(I) has extracted under considerably different experimental conditions than has Cu(II). On the other hand, Cu(III) does not extract in the presence of chloride ions. However, Cu(III) is a strong oxidative agent which can cause the decolorisation of the DIDC reagent. Therefore, a selective spectrophotometric determination of Cu(I), Cu(II) and Cu(III) should be possible.

In order to find the optimum conditions for the formation of complexes and for the extraction process, various factors influencing the reaction between the Cu ions and DIDC—factors such as pH, the concentration of chloride ions, the concentration of DIDC, the nature of the organic solvent.

3.2. Investigation of the appropriate reaction conditions

3.2.1. Medium acidity

The reaction of Cu(I) and Cu(II) with DIDC and the extraction of the ion associates formed by the organic solvents strongly depend on the pH of the aqueous phase due to the fact that the value of the pH influences some equilibria, for example, the protonation and the hydrolysis of DIDC and/or the hydrolysis of Cu. Fig. 2 shows that the appropriate pH for the extraction of the Cu ion associates with DIDC by amyl acetate is in the ranges of pH 3–5 and pH 3–6 for Cu(I) and Cu(II), respectively.

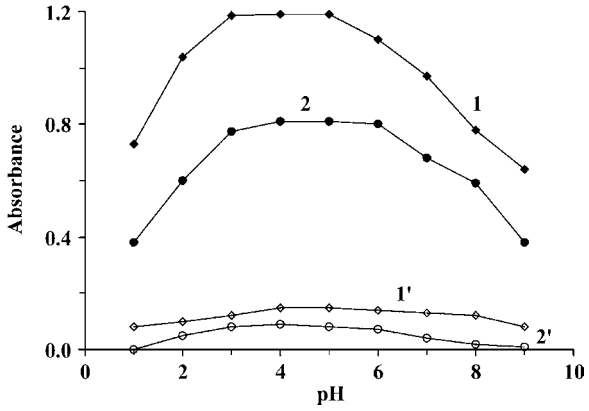

Fig. 2. The effect of the pH of the aqueous phase on the extraction of Cu(I) (1) and Cu(II) (2) ion associates with DIDC by amyl acetate. 2×10^{-5} mol L^{-1} of Cu(I) or Cu(II); LiCl, mol L^{-1}: 0.2 for Cu(I) and 4.5 for Cu(II); 6×10^{-5} mol L^{-1} DIDC; $l = 0.3$ cm; (1′) and (2′) are blank tests.

3.2.2. Concentration of ligand

The extractability of Cu ion associate with DIDC depends on the concentration of chloride ions in aqueous phase since it affects the formation of the anionic complex of the metal according to the equation:

$$M^{n+} + mL^{-} = [ML_m]^{(m-n)-}$$

The effect of chloride ion concentration on the extraction of Cu is shown in Fig. 3. With an increase in the chloride concentration, the degree of extraction increases, reaches a maximum and then remains constant for some time. With a further increase in the chloride concentration, the absorbance decreases, probably due to the formation of the complexes with higher charge, such as $CuCl_3^{2-}$, which is not extractable by organic solvent in the form of ion associate with DIDC.

The appropriate concentration of chloride ions for the extraction of the Cu(I) ion associates with DIDC by amyl acetate and toluene is thus, in the range 0.2–0.8 mol L^{-1} and 0.2–0.5 mol L^{-1}, respectively. Cu(II) does not form ion associates with DIDC that are extractable by toluene. However, extraction of Cu(II) by amyl acetate is possible, but only in the presence of a relatively higher concentration of chloride, that is, of 3–5 mol L^{-1}.

3.2.3. Reaction mechanism

Extraction equilibrium is reached within 60 s and the absorbance of the extracts remains stable for 2.5 h. The molar

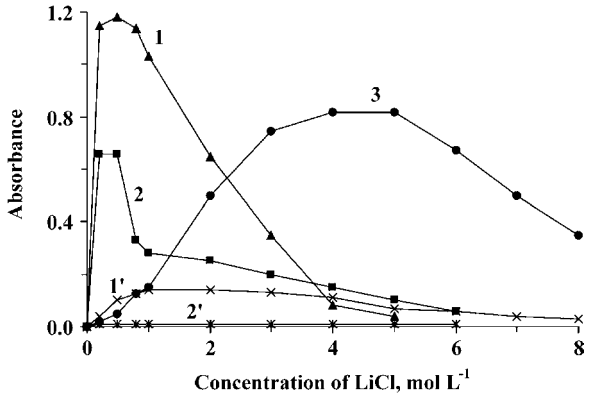

Fig. 3. The effect of the concentration of chloride on the extraction by amyl acetate (1 and 3) and toluene (2) of Cu(I) (1 and 2) and Cu(II) (3) ion associates with DIDC. 2×10^{-5} mol L^{-1} of Cu(I) or Cu(II); pH 3; 6×10^{-5} mol L^{-1} DIDC; $l = 0.3$ cm; (1′) the amyl acetate blank; (2′) the toluene blank.

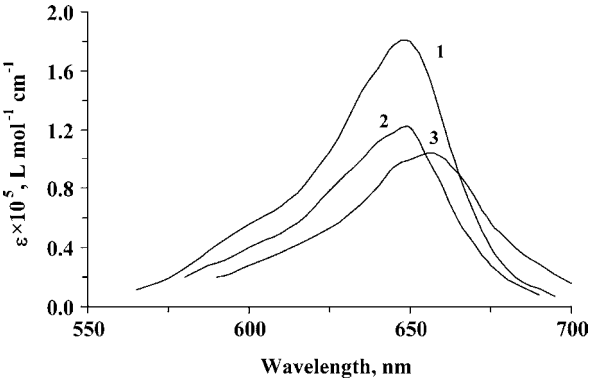

Fig. 4. The spectra of copper(I) (1 and 3) and copper(II) (2) ion associates with DIDC during extraction with amyl acetate (1 and 2) and toluene (3). 2×10^{-5} mol L^{-1} of Cu(I) or Cu(II); LiCl, mol L^{-1}: 0.2 for Cu(I) and 4.5 for Cu(II); pH 3; 6×10^{-5} mol L^{-1} DIDC; l = 0.5 cm.

ratio of Cu(I) or Cu(II), chloride ions and the DIDC in the extracted coloured complexes was determined under the appropriate conditions for complexation and extraction using various spectrophotometric methods. It was found that the Cu(I):Cl:R molar ratio is 1:2:1 and the Cu(II):Cl:R molar ratio is 1:3:1. Based on these results, it can be assumed that the copper ion associates extracts as $[CuCl_2]^-R^+$ or $[CuCl_3]^-R^+$ where R^+ is the single charged cation of DIDC.

In our opinion, the reaction mechanism may be expressed by the following chemical equations:

$$Cu_{(aq)}{}^{+} + 2Cl_{(aq)}{}^{-} + R_{(aq)}{}^{+} + nS_{(org)} = [CuCl_2]^-R^+ \times nS_{(org)}$$

$$Cu_{(aq)}{}^{2+} + 3Cl_{(aq)}{}^{-} + R_{(aq)}{}^{+} + mS_{(org)} = [CuCl_3]^-R^+ \times mS_{(org)}$$

where S is the extractant, (aq) is the aqueous phase and (org) is the organic phase.

3.2.4. The effect of an organic solvent

The absorbance of ion associate extracts depends largely on the nature of the organic solvent. Acetic esters and aromatic hydrocarbons were tested as extractants. The best extractants appeared to be amyl acetate and toluene (Fig. 4). The absorption spectra of the Cu(I) and Cu(II) ion associate during the extraction by various organic solvents under optimum conditions were recorded, and the main spectrophotometric characteristics were calculated (Table 2). The molar absorptivities are in the range of 0.7–1.8 × 10^5 L mol^{-1} cm^{-1}, depending on the extractant.

3.2.5. Analytical application

The absorbance of the coloured extracts obeys Beer's law in the range of 0.07–0.51 mg L^{-1} of Cu(I) or Cu(II). Most common elements that generally occur with copper in semiconductor samples do not interfere with its determination. The determination of Cu(I) is not interfered with by the presence of the alkaline and alkaline-earth elements, $HPO_4{}^{2-}$, CH_3COO^-, $SO_4{}^{2-}$ or $NO_3{}^-$, nor levels of Al(III), Co(II), Ni(II), Mn(II), Cd(II), Zn(II), Ag(I) and Fe(II) that are 100 times greater than the level of Cu(I). In real semiconductor samples, the determination of Cu(I) is possible even in the presence of Cu(II) which is at a level 1000 times that of Cu(I), and the determination of Cu(II) is possible in the presence of 1000 times the relative amount of Cu(I) (at 6 mol L^{-1} LiCl). The method was used for the determination of Cu(I) and Cu(II) in semiconductor materials. The results are shown in Table 3.

Table 2
Spectrophotometric characteristics of extracted ion associates of Cu(I) and Cu(II) with DIDC

System	Organic solvent	λ_{max} (nm)	$\varepsilon \times 10^5$ (L mol^{-1} cm^{-1})
$[CuCl_2]^-R^+$	Benzene	655	1.1
	Toluene	656	1.05
	Butyl acetate	648	1.4
	Amyl acetate	650	1.8
	iso-Amyl acetate	650	1.5
$[CuCl_3]^-R^+$	Butyl acetate	649	0.7
	Amyl acetate	650	1.2

Where R^+ is the cation of DIDC.

Table 3
Determination of copper in semiconductor materials

Samples	Cu(I) (%/Cu)	Cu(II) (%/Cu)
Cu_6PS_5Cl	99.9	0.09
Cu_7GeS_5Cl	99.8	0.19
Cu_6PS_5Br	99.9	0.05

The results are given in w/w percentage per total copper (%/Cu)

3.2.6. Investigation of the reaction of Cu(III) with DIDC

Preliminary experiments were performed in order to study the reaction of copper(III) with DIDC. The experiments proved that Cu(III) reacted with the DIDC reagent instantly in aqueous–organic media, forming a product that decreases the absorbance of the reagent. It involves a redox reaction which causes the reduction of Cu(III) to Cu(II) and decolourisation of DIDC as a result of oxidation of the dye reagent. Hence the concentration of Cu(III) can be determined based on the decolourisation of the DIDC solution.

Factors that can affect the reaction of Cu(III) with DIDC include, e.g., the pH, nature and concentration of organic solvent in aqueous–organic media, optimum wavelength, and the concentration range.

As follows from Fig. 5, the maximum absorbance of DIDC in the presence of Cu(III) remains constant over a wide range of pH. Further experiments were conducted at pH 8 because the stock solution of Cu(III) prepared according to recommendations described in the literature has a pH in this range.

Other non-aqueous solvents (ethanol, propanol, dioxane, dimethylsulphoxide DMSO, dimethylformamide DMFA) as well as the concentration of the non-aqueous solvent were also investigated. Fig. 6 shows that the best results were obtained with acetone as the non-aqueous solvent in the volume ratio of water:acetone 4:1. For further experiments, a 4:1 water–acetone medium was used.

The absorption spectra of DIDC in the presence of various concentrations of Cu(III) were recorded (Fig. 7). The absorbance obeys Beer's law in the range of 1.3–7.7 mg L^{-1} Cu(III).

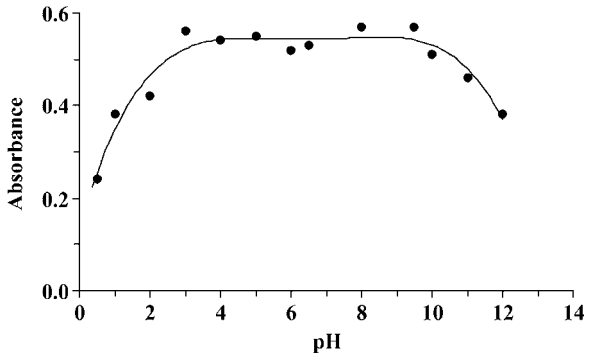

Fig. 5. The effect of the pH of the aqueous–acetone (4:1) media on the absorbance of DIDC in the presence of Cu(III). 2×10^{-5} mol L^{-1} DIDC; 8×10^{-5} mol L^{-1} of Cu(III); 1 mL of acetone; l = 0.3 cm.

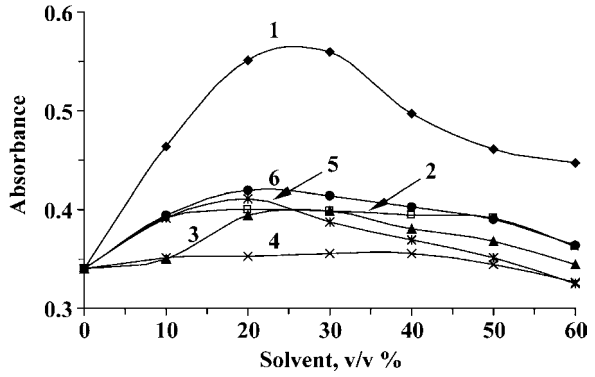

Fig. 6. The effect of the nature and concentration of a non-aqueous solvent on the absorbance of DIDC in the presence of Cu(III). 2×10^{-5} mol L^{-1} DIDC; 8×10^{-5} mol L^{-1} of Cu(III); 1.5 mL of buffer solution with pH 8; $l = 0.3$ cm: (1): acetone; (2): ethanol; (3): DMSO; (4): DMFA; (5): dioxan; (6): propanol.

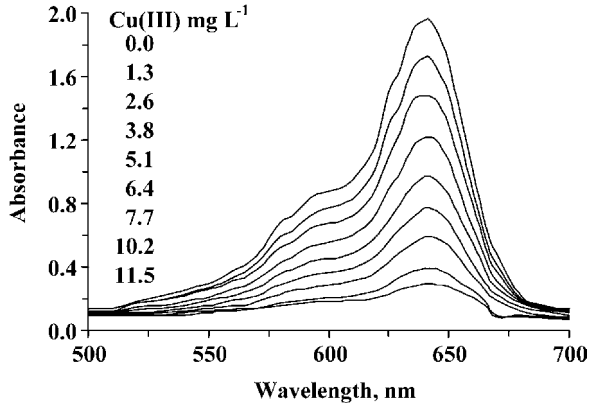

Fig. 7. The absorption spectra of DIDC in the presence of various concentrations of Cu(III). 2×10^{-5} mol L^{-1} DIDC; 1 mL of acetone; 1.5 mL of buffer solution with pH 8.0; $l = 0.5$ cm.

Table 4
Determination of copper in semiconductor materials

Samples	Cu(III) determined	
	μg	w/w (%)
Y–Sr–Cu–O	3.1	0.78
Y–Ba–Cu–O	2.5	0.63

It is important to emphasize that quantities of Cu(II) 100 times greater than the amount of Cu(III) does not interfere in Cu(III) determination. The method was used for the determination of Cu(III) in semiconductor materials. The results obtained are shown in Table 4.

4. Conclusion

The reactions of copper ions with 1,3,3-trimethyl-2-[5-(1,3,3-trimethyl-1,3-dihydro-indol-2-ylidene)-penta-1,3-dienyl]-3*H*-indolium as well as the application of the results obtained for the development of a spectrophotometric method for the determination of Cu(I), Cu(II) and Cu(III) are described. Cu(I) and Cu(II) in the presence of chloride ions and DIDC reagent are extractable by a variety of organic solvents. It is important to emphasize that Cu(I) was extracted under considerably different experimental conditions than Cu(II). Cu(III) does not extract in the presence of chloride ions. However, Cu(III) is a strong oxidative agent which can cause the decolourisation of the DIDC reagent. The optimum conditions for Cu(I), Cu(II) and Cu(III) determination were found. The developed procedures were tested for the determination of Cu(I), Cu(II) and Cu(III) in semiconductor samples.

Acknowledgements

This work has been supported by the Scientific Grant Agency of the Ministry of Education of the Slovak Republic and the Slovak Academy of Sciences (Grant No. 1/4451/07). Ya.B. says thank you for the support from MVTS Grant No. Mad'/Ukr/SR/UPJŠ07.

References

[1] V.N. Podchinova, L.N. Simonova, The Copper, Nauka, Moscow, 1990 (in Russian).
[2] W. Kaim, B. Schwederski, Bioinorganic Chemistry. Inorganic Elements in the Chemistry of Life, John Wiley & Sons, New York, 1991.
[3] Z. Marczenko, Separation and Spectrophotmeric Determination of Elements, Horwood, Chichester, 1986.
[4] S. Yi, Microchem. J. 36 (1987) 386.
[5] C. Bosch Ojeda, A. Garcia de Torres, F. Sanchez Rojas, J.M. Cano Pavón, Microchem. J. 35 (1987) 164.
[6] S.H. Li, S.Q. Li, A. Chen, Talanta 40 (1993) 1085.
[7] N. Chimpalee, D. Chimpalee, S. Lohwithee, L. Nakwatchara, D. Thorburn Burns, Anal. Chim. Acta 329 (1996) 315.
[8] H.-M. Ma, Y.-X. Huang, S.-C. Liang, Anal. Chim. Acta 334 (1996) 213.
[9] S. Karaböcek, S. Nohut, Ö. Dalman, S. Güner, Anal. Chim. Acta 408 (2000) 163.
[10] M. Thakur, M.K. Deb, Talanta 49 (1999) 561.
[11] S. Nohut, S. Karaböcek, S. Güner, Y. Gök, J. Pharm. Biomed. Anal. 20 (1999) 309.
[12] Ö. Dalman, M. Tüfekçi, S. Nohut, S. Güner, S. Karaböcek, J. Pharm. Biomed. Anal. 27 (2002) 183.
[13] R. Chaisuksant, W. Palkawong-na-ayuthaya, K. Grudpan, Talanta 53 (2000) 579.
[14] K. Hussain Reddy, N.B.L. Prasad, T. Sreenivasulu Reddy, Talanta 59 (2003) 425.
[15] D. Fu, D. Yuan, Spectrochim. Acta A 66 (2007) 434.
[16] M. Satake, G. Kano, B.K. Puri, S. Usami, Anal. Chim. Acta 199 (1987) 209.
[17] I. Kasahara, T. Ogawa, N. Hata, S. Taguchi, K. Goto, M. Ohta, K. Ohzeki, Water Res. 23 (1989) 933.
[18] R.E. Santelli, M. Gallego, M. Valcárcel, Talanta 41 (1994) 817.
[19] M.H. Wang, A.I. Yuzefovsky, R.G. Michel, Microchem. J. 48 (1993) 326.
[20] M. Endo, K. Suzuki, S. Abe, Anal. Chim. Acta 364 (1998) 13.
[21] Y. Yamini, A. Tamaddon, Talanta 49 (1999) 119.
[22] I. Isıldak, A. Asan, M. Andaç, Talanta 48 (1999) 219.
[23] Y.S. Kamentsev, V.A. Luginin, N.E. Pozdnyakova, L.T. Dubrovina, J. Anal. Chem. 47 (1992) 669.
[24] A. De Backer, J. Yperman, B. Ogorevc, G. Tavčar, D. Franco, J. Mullens, L.C. Van Poucke, Anal. Chim. Acta 334 (1996) 103.
[25] Y. Saito, T. Noji, K. Hirokawa, A. Endo, N. Matsuzaki, M. Katsumata, N. Higuchi, Jpn. J. Appl. Phys. 26 (1987) L838–L839.
[26] R.P. Pantaler, N.B. Lebed, Zh. Anal. Khim. 44 (1989) 1888.
[27] N. Krishna Murthy, B. Sreerama Murthy, Talanta 42 (1995) 101.
[28] I.S. Balog, P.P. Kish, A.A. Ishchenko, I.L. Mushkalo, V.A. Andrukh, J. Anal. Chem. 45 (1990) 344.
[29] I.S. Balogh, I.M. Maga, Á. Hargitai-Tóth, V. Andruch, Talanta 53 (2000) 543.
[30] I.S. Balog, V.A. Andrukh, I.L. Mushkalo, J. Terek, Ukr. Khim. Zh. 66 (2000) 46.
[31] D.A. Keyworth, K.G. Stone, Anal. Chem. 27 (1955) 833.

Talanta 76 (2008) 234

Contents lists available at ScienceDirect

Talanta

journal homepage: www.elsevier.com/locate/talanta

Reply to the Letter to the Editor

Dr. Christian,

This note addresses the Letter to the Editor by Pardus et al., on our manuscript, "The determination of tungsten, molybdenum, and phosphorus oxyanions by high performance liquid chromatography inductively coupled plasma mass spectrometry", by A.J. Bednar, J.E. Mirecki, L.S. Inouye, L.E. Winfield, S.L. Larson, D.B. Ringelberg, published in Talanta.

The comments in the Letter to the Editor are focused on at statement made in the Introduction of our article, "Recently, interest in tungsten geochemistry and occurrence in groundwater has increased due to specific human toxicological events, specifically the cancer cluster located in Fallon, NV, and suspected cases in Sierra Vista, AZ and Elk Grove, CA, all related to local natural deposits of tungsten ore [1,2]." In review, it seems that this statement could be interpreted to directly implement tungsten as the cause of the cancer in the human population of the area, this was not our intent. We were simply paraphrasing similar statements by Selier et al., Koutsospyros et al., and Sheppard et al. (the latter was inadvertently not cited), about the interest in tungsten and its occurrence in the Fallon area, the investigation of the CDC, etc. To date, there has not been a direct correlation established between tungsten and the cancer clusters, as the comments in the Letter to the Editor point out.

We should have more clearly stated that these multiple recent scientific studies in Fallon, NV, are evidence of the increased interest in tungsten. However, one reason tungsten interest has increased is due to the co-occurrence of tungsten in groundwater and the cancer cluster in the area. Again, we agree that to date, no direct linkage between the occurrence of tungsten in groundwater and the human cancer cases has been made, and reference to the CDC report should have been made.

Also of interest is the paper of Sheppard et al. [3], who state, "Neither tungsten nor cobalt has yet to be definitively associated with childhood leukaemia . . .", but also state, ". . . This cluster had a 'very small' likelihood of being a random event (Expert Panel, 2004), and Fallon has been declared 'one of the most convincing clusters of childhood cancer ever reported' (Steinmaus et al., 2004)".

The statement in Sheppard et al. [3] has much stronger implication of tungsten occurrence to the cancer clusters than our statement indicating the occurrence of the cancer cluster has helped increase interest in tungsten. We greatly appreciate the interest in our research and article. We regret and apologize for any misunderstanding or misinterpretation of our statement, as we did not mean to state that tungsten has been directly implicated in these cancer clusters.

References

[1] R.L. Seiler, K.G. Stollenwerk, J.R. Garbarino, Appl. Geochem. 20 (2005) 423.
[2] A. Koutsospyros, W. Braida, C. Christodoulatos, D. Dermatas, N. Strigul, J. Hazard. Mater. 136 (2006) 1.
[3] P.R. Sheppard, G. Ridenour, R.J. Speakman, M.L. Witten, Appl. Geochem. 21 (2006) 152.

Anthony J. Bednar
US Army Corps of Engineers, ERDC, EP-C, 3909 Halls Ferry Road, Vicksburg, MS 39180, United States
E-mail address: Anthony.J.Bednar@usace.army.mil

Available online 23 February 2008

0039-9140/$ – see front matter. Published by Elsevier B.V.
doi:10.1016/j.talanta.2008.02.016

Talanta 76 (2008) 146–153

Contents lists available at ScienceDirect

Talanta

journal homepage: www.elsevier.com/locate/talanta

Determination of albendazole metabolites by direct injection of bovine plasma and multidimensional achiral–chiral high performance liquid chromatography

Kátia Roberta A. Belaz, Quezia B. Cass, Regina V. Oliveira*

Departamento de Química, Universidade Federal de São Carlos, Rod. Washington Luiz, Km 235, 13565-905 São Carlos, SP, Brazil

ARTICLE INFO

Article history:
Received 7 November 2007
Received in revised form 11 February 2008
Accepted 15 February 2008
Available online 10 March 2008

Keywords:
Restricted access media (RAM)
Direct injection
Antihelmintics
Bovine plasma
Albendazole metabolites
Polysaccharide chiral phases

ABSTRACT

The development and validation of a fully automated achiral–chiral high performance liquid chromatography (HPLC) method for the simultaneous determination of albendazole metabolites: enantiomers of albendazole sulphoxide (ABZ-SO), albendazole sulphone (ABZ-SO_2) and albendazole 2-aminosulphone (ABZ-SO_2NH_2) in bovine plasma are described. This method involves an octyl restricted access media bovine serum albumin column (C_8-RAM-BSA) (50 mm × 4.6 mm I.D.) for sample clean-up, followed by enantioselective analysis on a column containing an amylose tris(3,5-dimethylphenylcarbamate) stationary phase (150 mm × 4.6 mm I.D.). The chromatographic separations of all target compounds were performed at 30 °C using a mobile phase composed of phosphate buffer (10 mmol L^{-1}; pH 7.5):acetonitrile (60:40, v/v), flow rate of 0.5 mL min^{-1} and fluorescence detection at 290 nm and 320 nm, excitation and emission, respectively. The influence of different organic modifiers and chiral selector of the stationary phase on enantioseparation of ABZ-SO was investigated. The method developed was fully validated. The calibration curves were linear in the concentration range of 40.00–1280 ng mL^{-1} for each albendazole sulphoxide enantiomer, 10.0–320 ng mL^{-1} for albendazole sulphone and 20.0–320 ng mL^{-1} for albendazole 2-aminosulphone. The inter- and intra-day precision ranged from 0.760% to 7.79% relative standard deviation (R.S.D.), and the accuracy ranged 101% from 114% of the nominal values while the transfer efficiency was in the range of 84.4–103%. The method showed good linearity, precision, accuracy, sensitivity and selectivity allowing it to be appropriate for further pharmacokinetics and metabolism studies of albendazole.

1. Introduction

Albendazole (ABZ; Fig. 1), methyl-[(5-propylthio)-1*H*-benzimidazol-2-yl] carbamate, is a broad-spectrum anthelmintic agent active against the most common helminth parasites and is widely used for treatment of veterinary and human helminthiasis [1].

ABZ is a prodrug and requires biotransformation via both cytochrome P450s (CYP) and flavin-containing monoxygenases (FMO) in order to exert its cytotoxic activity [2]. After administration, ABZ undergoes extensive metabolism to its therapeutically active metabolite, albendazole sulphoxide (ABZ-SO) [3,4]. Further ABZ-SO is oxidized to albendazole sulphone (ABZ-SO_2) [3,5], in a process catalyzed by cytochrome P450 and, finally, to albendazole 2-aminosulphone (ABZ-SO_2NH_2), the *N*-deacetylation product of albendazole sulphone [6].

Of all three metabolites, pharmacokinetics studies indicate that ABZ-SO exhibit anthelmintic activity [7] and toxic effects [8], whereas ABZ-SO_2 and ABZ-SO_2NH_2 are considered biologically inactive [8,9]. Chemical structures of albendazole and its metabolites are displayed in Fig. 1.

Albendazole sulphoxide has a stereogenic center at the sulphur atom existing as two enantiomers, (+)-ABZ-SO and (−)-ABZ-SO. Clinical studies have demonstrated that (+)-sulphoxide is the predominant form in plasma of human and animal species [10]. Thus, it is important that clinical studies include an enantioselective determination of the disposition of (+)- and (−)-ABZ-SO, as well as quantification of ABZ-SO_2 and ABZ-SO_2NH_2, which may provide additional information about the overall metabolism.

Furthermore, pharmacokinetic profiles of benzimidazoles in biological fluids have become increasingly important in order to evaluate the maximum efficacy of existing anthelmintic drugs. One example of this trend is the direct administration of racemic ABZ-SO to animals, marketed as ricobendazole (RBZ). The slightly greater solubility in water of (±)-ABZ-SO than that of the parent drug has allowed the development of an injectable

* Corresponding author. Tel.: +55 16 33518092; fax: +55 16 33518350.
E-mail address: oliveirarv@dq.ufscar.br (R.V. Oliveira).

0039-9140/$ – see front matter © 2008 Elsevier B.V. All rights reserved.
doi:10.1016/j.talanta.2008.02.013

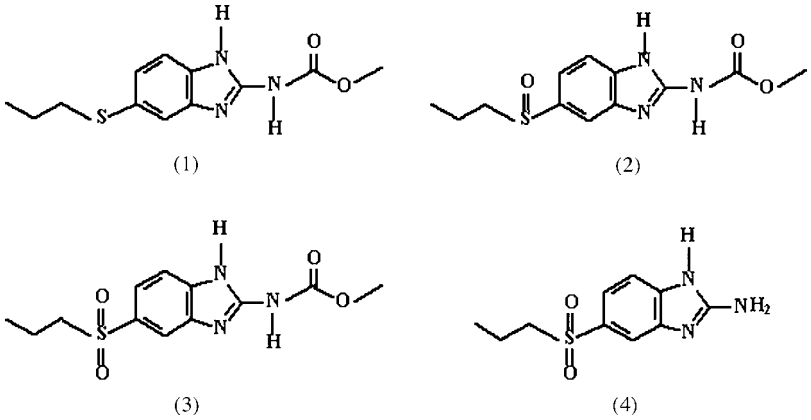

Fig. 1. Chemical structure of albendazole **(1)**, albendazole sulphoxide **(2)**, albendazole sulphone **(3)** and albendazole 2-aminosulphone **(4)**.

aqueous solution for animals. In Brazil, Ricobendazole from Ouro Fino Saúde Animal and Ricover from VetBrands Saúde Animal are examples of injectable products for cattle.

A number of liquid chromatography methods for analyzing benzimidazoles in human [11,12] and sheep plasma [13,14], human serum [15], spermatozoa and seminal plasma [16], animal tissue [17], parasite animal [18] and bovine milk [19] have been developed using achiral or chiral columns [10,14,20–22] and different compositions of mobile phases. Prior to chromatographic analysis, most of these methods used liquid–liquid extraction as a common approach to sample clean-up, usually with aqueous extraction at high pH with partitioning into an immiscible organic solvent [15,16]. Some sample pre-treatments were based on matrix solid-phase dispersion (MSPD) [23], supercritical fluid extraction [24] and multiple stages of liquid–liquid extraction and/or solid-phase extraction clean-ups [10,11,13,18,25]. In addition to these labour-intensive and time-consuming sample treatments, in the enantioselective assays chiral analysis of (±)-ABZ-SO was performed by an indirect method, where the (±)-ABZ-SO fractions were collected, evaporated to dryness and re-chromatographed using a chiral stationary phase, except for studies assayed on Chiralpak AD® column in normal elution mode [26–29].

Therefore, in order to diminish the number of steps during sample treatment and to simultaneously analyze all three major ABZ metabolites in biological matrices we report the development and validation of a fully automated achiral–chiral high performance liquid chromatography (HPLC) method for determination of the enantiomers of albendazole sulphoxide (ABZ-SO), albendazole sulphone (ABZ-SO_2) and albendazole 2-aminosulphone (ABZ-SO_2NH_2) in bovine plasma. The method is based on a restricted access media (RAM) column coupled to a chiral polysaccharide column.

2. Experimental

2.1. General

Acetonitrile (HPLC grade) was purchased from Mallinckrodt Baker (St. Louis, MO, USA) and water was purified by a Milli-Q purification system (Millipore, São Paulo, Brazil). Dihydrogen potassium phosphate was obtained from Cinética Química (São Paulo, SP, Brazil), bovine serum albumin (fraction V powder minimum 98%) from Sigma (St. Louis, MO, USA), glutaraldehyde and sodium borohydride were from Merck (Darmstadt, Germany), and Coomassie brilliant blue G-250 from Mallinckrodt Baker (St. Louis, MO, USA). Forty-seven millimeter diameter, 0.45 μm Nylon membrane used to filter all the mobile phases were also from Millipore. Other reagents were of analytical grade.

Albendazole sulphoxide and albendazole sulphone were synthesized in our laboratory with a purity of more than 99.0%. The compounds were fully characterized by IR, ^{1}H NMR, CHNS-O and ^{13}C NMR analysis. Albendazole 2-aminosulphone (98%) was purchased from Lan Aeser.

IR spectra were recorded on a BOMEM MB-Series spectrometer and are reported in wavenumbers (cm^{-1}). UV–vis spectra were obtained on HP 8452A instrument in a glass cuvette.

^{1}H NMR and ^{13}C NMR spectra were recorded on a Bruker 9.4 T DRX-400 MHz, in a 5 mm probe at 303 K. Samples were dissolved in CF_3COOD and TMS was used as an internal standard. All signals were as ppm downfield from tetramethylsilane used as an internal standard (δ value). Splitting patterns are designated as s (singlet), d (doublet), t (triplet), dd (double doublet), m (multiplet), sext (sextuplet).

Microanalysis were recorded on a Fisons Instruments, model EA 1108—CHNS-O. Melting points were measured using a Microquímica apparatus model MQAPF-310 and are uncorrected.

Enantiomeric elution order was determined by injection of (+)- and (−)-albendazole sulphoxide at the established separation conditions. The enriched enantiomers were obtained by enantioselective separation using an amylose tris(3,5-dimethylphenylcarbamate) coated onto APS-Nucleosil (7 μm particle size and 500 Å pore size, 20% w/w, 200 × 7.0 mm I.D.) as stationary phase using hexane:ethanol (80:20, v/v) as mobile phase at 3 mL min^{-1}. The optical activities of the separated enantiomers were defined using a PerkinElmer Model 241 polarimeter. Under the optimal analytical and semi-preparative conditions the (+)-albendazole sulphoxide was the first enantiomer to elute.

Bovine venous whole blood samples, supplied by Embrapa Pecuária Sudeste—Brazil, were taken by jugular venepuncture into 500 mL citric acid vacutainers. The blood samples were centrifuged at 5000 × *g* for 15 min to separate the bovine plasma. Plasma samples were frozen at −20 °C until analysis.

2.2. Synthesis of (±)-albendazole sulphoxide and albendazole sulphone

The synthesis of (±)-albendazole sulphoxide **(2)** and albendazole sulphone **(3)** in 87% yields were obtained by the oxidation of albendazole **(1)** using aquo(*N*-oxo of pyridine) molybdenum(VI) oxodiperoxo complexes **(5)** (Scheme 1). The protocol of oxidation is described elsewhere [30]. Briefly, molybdenum(VI) oxodiperoxo complex (327.0 mg; 1.13 mmol) was added in small portions, using a solid addition flask, to a 30.0 mL solution of albendazole (300 mg; 1.13 mmol) in methanol:acetonitrile (1:5, v/v), at room

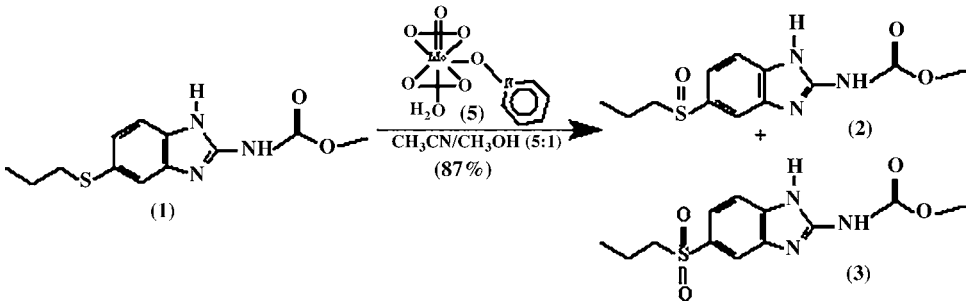

Scheme 1. Reaction scheme used for the synthesis of (±)-albendazole sulphoxide and albendazole sulphone.

temperature, under constant stirring. The reaction was followed by thin layer chromatography (TLC) using as eluent a mixture of dichloromethane:acetone (60:40, v/v). The reaction was stopped when initial reagents were not observed in the reaction mixtures. A saturated solution of sodium hydrogen carbonate (10 mL) was added to the mixture and then was extracted with dichloromethane (3 mL × 10 mL). The organic phase was separated, dried over anhydrous sodium sulphate and concentrated in vaccum. The oxidation products were isolated and purified by column chromatography using dichloromethane:acetone as eluent (60:40, v/v) to yield sulphoxide as a white solid (62%) and sulphone as an yellowish solid (17%).

2.2.1. (±)-Albendazole sulphoxide: $C_{12}H_{15}N_3O_3S$

IR (υ_{max}, KBr, cm^{-1}): 1026.7. ^1H NMR (400 MHz, CF_3COOD, δ): 1.19 (t, 3H); 1.86 (sext, 2H); 3.30 (m, 2H); 4.1 (s, 3H); 7.92 (dd, 1H); 8.01 (d, 1H) and 8.32 (d, 1H). ^{13}C NMR (400 MHz; CF_3COOD, δ): 13.5; 18.4; 57.1; 59.9; 113.7; 117.4; 125.4; 131.1; 133.5; 139.2; 148.2 and 156.0. Calcd. for $C_{12}H_{15}N_3O_3S$: C, 51.19%; H, 5.33%; N, 14.93%; S, 11.37%. Found: C, 51.25%; H, 4.82%; N, 14.65%; S, 12.29%; mp 315–316 °C.

2.2.2. Albendazole sulphone: $C_{12}H_{15}N_3O_4S$

IR (υ_{max}, KBr, cm^{-1}): 1133.6; 1256.0. ^1H NMR (400 MHz, CF_3COOD, δ): 1.10 (t, 3H); 1.87 (sext, 2H); 3.43 (t, 2H); 4.13 (s, 3H); 8.19 (dd, 1H); 8.03 (d, 1H) and 8.47 (d, 1H). ^{13}C NMR (400 MHz; CF_3COOD, δ): 13.8; 18.9; 57.7; 61.0; 117.3; 117.6; 128.6; 131.2; 135.2; 138.0; 149.6 and 156.3. Calcd. for $C_{12}H_{15}N_3O_4S$: C, 48.47%; H, 5.08%; N, 14.13%; S, 10.78%. Found: C, 48.24%; H, 5.41%; N, 13.46%; S, 10.89%; mp 292–293 °C.

2.3. Equipment and chromatographic conditions

The HPLC system consisted of two Shimadzu LC-10ATVP pumps (Kyoto, Japan), with one of the pumps containing a valve FCV-10AL for selecting solvent, an auto injector model SIL 10AVP, a degasser model DGU-14A, a column oven CTO-10A (at 30 °C), a RF 10Axl fluorescence detector (λ_{exc} 290 nm and λ_{em} 320 nm), a SPD-6AV UV–vis detector (at 290 nm) and a SCL 10AVP interface. A sample valve HPLC 7000 Nitronic EA (Supelco, St. Louis, MO, USA) was used for the automated column switching. Data acquisition was done on Shimadzu Class-VP Software. The sensitivity of the detector was set at "low" and the response time, at 1.5 s.

The chiral columns used were as follows: amylose tris (3,5-dimethylphenylcarbamate) (CSP-1); cellulose tris(3,5-dimethylphenylcarbamate) (CSP-2); amylose tris[(*S*)-1-phenylethylcarbamate] (CSP-3) and amylose tris(3,5-dimethoxyphenylcarbamate) (CSP-4) phases coated (20%) onto APS-Nucleosil (7 μm; 500 Å) (150 mm × 4.6 mm I.D.). The chiral columns were prepared as described elsewhere [31]. Restricted access medium C_8-and C_{18}-RAM-BSA columns (50 mm × 0.46 mm I.D.) (Luna Phenomenex® 10 μm; 120 Å) was used for direct injection of bovine plasma. The restricted access media C_8-RAM-BSA column was prepared as previously described [32] and the immobilization of BSA was carried out *in situ* based on Menezes and Felix [33].

2.4. Recovery of bovine plasma proteins by RAM-BSA columns

The conditions used for evaluating bovine plasma protein recovery were the same as described elsewhere for human plasma [32] and milk plasma protein [34] and were based on the Bradford method [35] as follows: Coomassie brilliant blue (CBB) dye solution for protein quantification was prepared by dissolving 100 mg of CBB in 50 mL of ethanol, adding 100 mL of phosphoric acid, then diluting the mixture to 1 L with water. An aliquot of 50.0, 100 or 200 μL of bovine plasma was injected and eluted through the restricted access media column at a flow rate of 1.0 mL min^{-1} using water as mobile phase. The eluent was collected for 5 min in a volumetric flask. A 250 μL portion of the eluent was mixed with 5 mL CBB reagent and after 3 min the UV–vis spectrum recorded from 400 to 800 nm. The increase in absorbance at 596 nm of the protein-dye complex compared to a blank sample, which containing only water was used to estimate the total amount of protein present in the sample mixture.

The recovery of plasma protein was calculated from the absorbance ratio of the proteins of the bovine plasma reference solutions with the solutions of the proteins of the chromatographed-sample bovine plasma.

2.5. Standard solutions for method development

Stock solutions of (±)-ABZ-SO (8000 μg mL^{-1}), ABZ-SO_2 (1000 μg mL^{-1}) and ABZ-SO_2NH_2 (1000 μg mL^{-1}) were individually prepared in 2.0 mL of methanol. Then, two combined stock solutions at the following concentrations were prepared: 160.0; 160.0 and 2560 μg mL^{-1} for ABZ-SO_2NH_2, ABZ-SO_2 and (±)-ABZ-SO and 5.000, 5.000 and 80.00 μg mL^{-1} for ABZ-SO_2NH_2, ABZ-SO_2 and (±)-ABZ-SO, respectively.

Using the appropriated combined stock solution, eight calibration standards were prepared in methanol at the following concentrations: 0.100; 0.150; 0.200; 0.300; 0.400; 0.800; 1.60 and 3.20 μg mL^{-1} for ABZ-SO_2NH_2 and for ABZ-SO_2 and 0.800; 1.20; 1.60; 2.40; 3.20; 6.40; 12.8 and 25.6 μg mL^{-1} for (±)-ABZ-SO.

Quality control solutions were prepared at 0.240, 1.50 and 3.00 μg mL^{-1} for ABZ-SO_2NH_2; 0.120, 1.50 and 3.00 μg mL^{-1} for ABZ-SO_2 and 0.960, 10.0 and 20.0 μg mL^{-1} for (±)-ABZ-SO. Stock, standard and quality control solutions were prepared fresh weekly. The stability of the stock solutions were assessed by analyzing a set of freshly prepared stock solutions and comparing the results

with the analysis of a set of stock solution stored at −20 °C during 1 week.

2.6. Preparation of spiked bovine plasma samples

Calibration standard, quality control and plasma unknown solutions were prepared by aliquoting 50 μL of the appropriate standard solution into a series of culture tubes and the solvent was evaporated under a stream of dry air. The dried analytes were reconstituting using 500 μL of bovine plasma. The solutions were vortex mixed for 15 s and centrifuged for 10 min at 10,000 × *g*. Aliquots of 300 μL were transferred to auto-sampler vials and 200 μL were injected into the column-switching HPLC system.

2.7. Method validation

2.7.1. Calibration curve

Linearity was determined using calibration standards prepared as described in Section 2.5. Using the appropriate standard solution of (±)-ABZ-SO, ABZ–SO_2 and ABZ-SO_2NH_2, eight plasma calibration standard were prepared in triplicate using drug-free plasma at the following concentrations: 10.00; 15.00; 20.00; 30.00; 40.00; 80.00; 160.0 and 320.0 ng mL^{-1} for ABZ-SO_2NH_2; 10.00; 15.00; 20.00; 30.00; 40.00; 80.00; 160.0 and 320.0 ng mL^{-1} for ABZ-SO_2 and 80.00; 120.00; 160.00; 240.0; 320.0; 640.0; 1280.0 and 2560 ng mL^{-1} for (±)-ABZ-SO. The calibration curves were obtained by linear regression analysis of the peak area of the compounds versus the nominal concentration of each analyte.

2.7.2. Selectivity, recovery (extraction efficiency), precision and accuracy

For selectivity purposes, analysis of drug-free bovine plasma and spiked bovine plasma with ABZ-SO_2NH_2, ABZ-SO_2 and (±)-ABZ-SO were assessed daily.

The extraction efficiency of all analytes from spiked plasma by the C_8-RAM-BSA column was determined by analyzing quality control samples at three different concentrations for each analyte: 24.00, 150.0 and 300.0 ng mL^{-1} for ABZ-SO_2NH_2; 12.00, 150.0 and 300.0 ng mL^{-1} for ABZ-SO_2 and 96.00, 1000.0 and 2000 ng mL^{-1} for (±)-ABZ-SO. The peak area of five replicates of each extracted quality control was compared with the area of five replicates injections of quality controls in methanol at the same concentrations to derive a percent extraction.

The precision and accuracy of the method was evaluated by replicates analysis of the three quality controls samples. Quality control samples in plasma were prepared five times for each concentration on three non-consecutive days. Precision was estimated from the coefficients of variation (CV%) and the accuracy was evaluated by back-calculation and expressed as the percent deviation between amount found and amount added at the three concentrations examined. Accuracy was also tested using blinded unknowns, at two different concentrations, which were prepared by a different analyst.

2.7.3. Limits of detection and quantification

The acceptance criterion for the limits of quantification were defined as the precision and accuracy for three extracted sample must be ≤20% [36]. The limit of detection was determined by the lowest concentration of analytes which resulted in a signal-to-noise ratio of 3.

2.7.4. Stability

The stability of all analytes in bovine plasma was assessed by analyzing three aliquots of the quality control samples following storage in different conditions. The stability of (±)-ABZ-SO, ABZ-SO_2 and ABZ-SO_2NH_2 were evaluated under the following conditions: (a) room temperature for 6 h (bench-top stability) and 16 h (auto-sampler stability); (b) after storage at −20 °C and exposed to three freeze–thaw cycles and (c) stored at −20 °C for 15 days. Variations of less than 15% in the concentration of the samples were the criteria for the stability evaluation [36].

3. Results and discussion

3.1. Synthesis of (±)-albendazole sulphoxide and albendazole sulphone

Oxidation of sulphides to sulphoxides or sulphones is an important process in organic chemistry where these compounds are widely used as activating groups in organic synthesis [37]. A number of procedures for this transformation from sulphides have been reported and include treatment with sodium periodate [38], halogens [39], *m*-chloroperbenzoic acid [40] and hydrogen peroxide [41].

Batigalhia et al. [30] reported the oxidation of sulphides to sulphoxides and sulphones using a simple and less expensive method. In the latter approach, molybdenum(VI) oxodiperoxo complex were efficiently used for the oxidation of different sulphides, including aliphatic and aromatic compounds.

The use of this complex showed some advantages over other methods, such as excellent chemoselectivity, high yields, easy manipulation and recovery of complexes used. Furthermore, selective and efficient preparation of sulphoxides were obtained by using the complex adsorbed to silica gel while sulphones were obtained by altering the addition conditions of the adsorbed complex or by using it not coated to silica gel [30]. Thus, based on this study, oxidation of albendazole using molybdenum(VI) oxodiperoxo complex was selected for preparation of (±)-ABZ-SO and ABZ-SO_2 (Scheme 1).

In order to obtain both products of interest in a single reaction procedure, the oxidation reaction was assayed at room temperature, in accordance with procedure described in Section 2.2. The compounds were fully characterized by IR, ^{1}H NMR, ^{13}C NMR and elemental analysis.

3.2. Enantioseparation of albendazole sulphoxide based on polysaccharide chiral phases

Polysaccharide-based chiral phases are among the most widely used chiral stationary phase (CSPs) for enantiomeric separation by HPLC due to their versatility and high-loading capacity [42]. The derivatized polysaccharides are multimodal CSPs and can be used in normal-phase mode; reverse-phase mode (which is preferable for high polar compounds) and polar organic mode using either a binary alcohol mixture or binary acetonitrile–alcohol [43,44].

Previous study in the group proved that these chiral stationary phases are efficient for the resolution of a series of chiral suphoxides, including olefinic and ketosulphoxides, sulphonile acids and esters, aromatic sulphoxides [45,46] and, a series of benzimidazoles: omeprazole; pantoprazole and lanzoprazole [43]. On the basis of the previous results, the use of polysaccharide-based chiral phases was taken into account for the enantioseparation of (±)-ABZ-SO.

The use of reversed-phase mode for chiral separation was preferred as the goal of this work was to develop a multidimensional method for quantification of albendazole metabolites by direct injection of bovine plasma.

Thus, the retention factor (k), enantioselectivity (α), and enantioresolution (Rs) of ABZ-SO was evaluated in reversed-phase elution mode using amylose (CSP-1) and cellulose tris(3,5-dimethylphenylcarbamate) (CSP-2), amylose tris[(*S*)-1-phenylethylcarbamate] (CSP-3) and amylose tris(3,5-dimethoxyphenylcarbamate) (CSP-4) phases. For each chiral phase evaluated, differences were observed in enantioselectivity and resolution when the organic modifiers were changed from methanol to ethanol or acetonitrile. A complete evaluation of the chiral resolution of ABZ-SO using multimodal elution has been carried out and the obtained results will be published elsewhere.

The CSP-1 showed excellent selectivity ($1.86 < \alpha < 2.28$) and resolution ($1.84 < Rs < 2.63$) when ethanol or acetonitrile were used as organic modifier. When methanol was the organic modifier, the resolution obtained was 1.03, although the enantioselectivity was very good ($\alpha = 2.14$). The chiral phase CSP-4 also showed satisfactory selectivity for ABZ-SO when methanol:H_2O (1:1, v/v) ($\alpha = 1.51$ and $Rs = 1.66$) was used as mobile phase.

(±)-ABZ-SO was not enantioresolved in any reverse-phase mode condition used with CSP-2 and CSP-3 phases.

Since the highest enantioselectivity (α) and enantiomeric resolution (Rs) were observed with amylose tris(3,5-dimethylphenylcarbamate) phase using acetonitrile or ethanol as eluent, this chiral column was chosen for method development. Different percentages of organic modifiers, acetonitrile or ethanol, were also evaluated in order to obtain a satisfactory analysis time and separation for all target compounds, (±)-ABZ-SO, ABZ-SO_2 and ABZ-SO_2NH_2, while maintaining enantioselective separation of (±)-ABZ-SO.

3.3. Method development for bovine plasma analysis

There have been several publications describing the quantification of benzimidazoles and its metabolites in different complex matrices by liquid chromatography and were discussed in details in a review by Danaher et al. [47]. In these revisited publications, the most widely used sample preparation methods were liquid–liquid extraction (LLE), using water immiscible organic solvent, and solid-phase extraction (SPE). Multiple stages of liquid–liquid extraction and/or solid-phase extraction clean-ups were also proposed. Nevertheless, these off-line procedures are labor intensive and time consuming when a large number of samples have to be prepared; they also require a large volume of sample, as well as addition of internal standard [48]. Moreover, the extensive sample handling can reduce the accuracy and precision for quantification of the analytes of interest.

In an attempt to overcome these problems, direct injection of biological samples onto HPLC columns has been preferred [32,49]. Meanwhile, the determination of compounds in biological fluids by direct injection of the samples is a challenge due to the high concentration of proteins and endogenous compounds present in this type of sample [50]. The major difficult step is complete removal of macromolecules, which can precipitate leading to backpressure build-up, changes in retention time and decreased column efficiency and capacity [48].

In order to improve analytical process, new approaches for direct injection of biological samples into the chromatographic columns have been reported. Among these, macromolecular sample components can be efficiently removed by RAM that allow direct and repetitive injection of untreated biological fluids [51].

Recently, a wide variety of RAM columns have been reported [49,51–53] and represent a very attractive approach due to automation, simplification and speeding up of the sample treatment process.

The use of restricted access media bovine serum albumin (RAM-BSA) for plasma sample clean-up has been successfully applied to plasma [32,54–57] as well as milk [34,58,59] and, more recently, eggs [60]. When different RAM-BSA columns (C_8, C_{18}, cyano and phenyl) were investigated for milk sample pretreatment, excellent results were achieved (80–100%) for milk's protein exclusion [34].

Building on all these previous results, a C_8 and C_{18} RAM-BSA column were investigated for the on-line bovine plasma sample clean-up. Initially, in order to determine the elution profile and retention times of (±)-ABZ-SO, ABZ-SO_2 and ABZ-SO_2NH_2 in these plasma matrix, the RAM column was directly connected to the ultraviolet detector at 280 nm (maximum wavelength for proteins).

The efficiency of exclusion of the bovine plasma proteins by the C_8- and C_{18}-RAM-BSA columns were measured by Bradford's method [35]. Recoveries of bovine plasma protein from 93.8% to 97.2% with CV ($n = 3$) in the range of 1.89–4.46% were achieved in 5 min using 100% water at a flow rate of 1.0 mL min^{-1} and sample injections of 50, 100 and 200 μL of plasma.

Due to the differences of hydrophobic character between (±)-ABZ-SO, ABZ-SO_2 and ABZ-SO_2NH_2, it was difficult to obtain the precise retention for albendazole 2-aminosulphone, the most hydrophilic metabolite. Thus, it was necessary to evaluate mobile

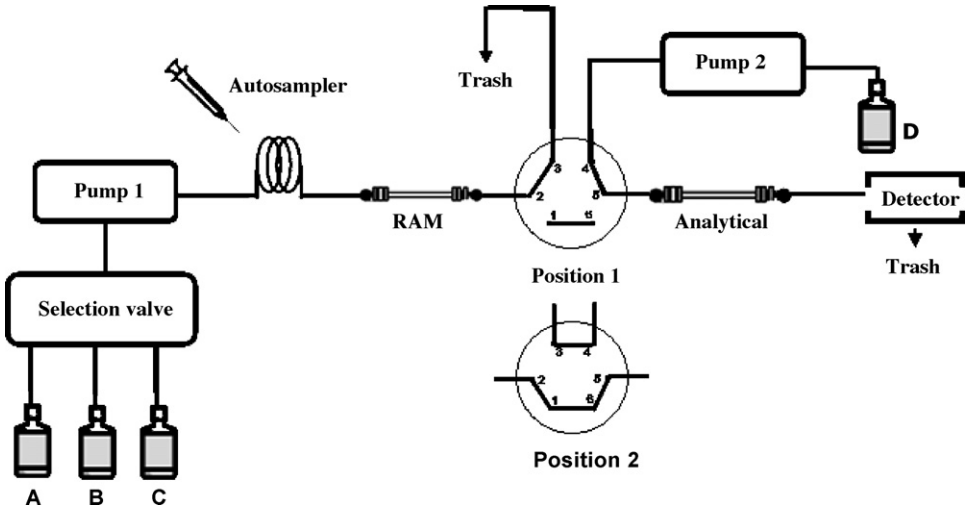

Fig. 2. Schematic diagram of the column-switching system.

Table 1
Time events for the column-switching procedure and mobile phases

Time (min)	Pump (eluent)	Flow rate (mL min^{-1})	Event	Valve position
0.00–5.00	1 (A)	1.0	Plasma proteins are excluded by RAM column	1
5.01–14.00	1 (B)	0.5	Elution of retained analytes from the RAM	1
8.01–14.00	1 (B)	0.5	Analytes are transferred to the analytical column	2
14.01–25.00	1 (C)	1.0	Washing of RAM column	1
25.01–35.00	1 (A)	1.0	Conditioning of RAM column	1
0.00–8.00	2 (D)	0.5	Conditioning of the analytical column	1
8.01–14.00	2 (D)	0.5	Analytes are transferred to the analytical column	2
14.01–35.00	2 (D)	0.5	Analysis of the albendazole metabolites	1

Pump 1 (eluent): (A) 100% KH_2PO_4 10 mmol L^{-1} pH 7.5; (B) KH_2PO_4 10 mmol L^{-1} pH 7.5:CH_3CN (60:40, v/v); (C) H_2O:CH_3CN:2-prOH (75:15:10, v/v/v). Pump 2 (eluent): (D) KH_2PO_4 10 mmol L^{-1} pH 7.5:CH_3CN (60:40, v/v).

phases composed of buffer solution at different pH values. Phosphate buffers at pH 2.5 and 7.5 were evaluated and both results obtained for protein's exclusion were very similar. However, optimal retention time for albendazole 2-aminosulphone and better selectivity for all analytes on the RAM-BSA column was obtained when phosphate buffer pH 7.5 was used. Both RAM-BSA columns evaluated showed satisfactory results for exclusion of plasma proteins as well as for retention capacity, thus allowing them to be used for analyzing of the target compounds.

The composition of mobile phase used with the RAM columns for the transfer of the analytes to the chiral column was also investigated considering pH buffer solutions (pH 7.5) and different percentages of organic modifier, such as ethanol or acetonitrile (40–60%). Optimal chromatographic conditions were obtained using phosphate buffer (10 mmol L^{-1}; pH 7.5): acetonitrile (60:40, v/v) at flow rate of 0.5 mL min^{-1}.

The column-switching system used is illustrated in Fig. 2. Table 1 shows the time-event used for the analytical procedure.

Plasma samples were directly injected onto the RAM column (position 1) and plasma proteins were excluded by the C_8 RAM-BSA using phosphate buffer (10 mmol L^{-1}; pH 7.5). The six-port valve remained in this position for 8.0 min and then the valve changed to position 2, redirecting the flow to the chiral analytical column. Albendazole sulphoxide, albendazole sulphone and albendazole 2-aminosulphone were transferred from 8.0 to 14.0 min using phosphate buffer (10 mmol L^{-1}; pH 7.5): acetonitrile (60:40, v/v) at a flow rate of 0.5 mL min^{-1}. After this time, the valve was switched back to position 1 for cleaning and conditioning the RAM column. The C_8-RAM column was cleaned with a mixture of MeCN:H_2O:2-prOH (75:15:10, v/v/v). In the mean time, albendazole metabolites were analyzed on the amylose tris(3,5-dimethylphenylcarbamate) onto APS-Nucleosil column using phosphate buffer (10 mmol L^{-1}; pH 7.5):MeCN (60:40, v/v). The flow rate of 1.0 mL min^{-1} was used for the RAM column while 0.5 mL min^{-1} was adopted for the chiral column. The detection was measured at 290 and 320 nm, for excitation and emission, respectively. The total analysis was 35 min and, to achieve the necessary sensitivity, an injection volume of 200 μL of bovine plasma was used.

Representative chromatograms of plasma free drug and plasma spiked at 10 μg mL^{-1} (racemic ABZ-SO); 5.0 μg mL^{-1} (ABZ-SO_2) and 5.0 μg mL^{-1} (ABZ-SO_2NH_2) are shown in Fig. 3 (A and B). The comparison of the chromatogram given in Fig. 3A with the one in B highlights that no interferences are observed in the region of interest where the albendazole metabolites eluted.

3.4. Method validation

The method validation was carried out according to internationally accepted criteria [36]. The calibration curves were linear from 20.0 to 320 ng mL^{-1} for ABZ-SO2NH2 , from 40.00 to 1280 ng mL^{-1} for each enantiomer of albendazole sulphoxide and from 10.0 to 320.0 ng mL^{-1} to albendazole sulphone. The following regression equation and correlation coefficient was obtained: ABZ-SO_2NH_2 ($y = -37824.2 + 27752.3x$; $r = 0.998$); (+)-ABZ-SO ($y = -7708.6 + 435.32x$; $r = 0.999$); (−)-ABZ-SO ($y = -2278.9 + 429.25x$; $r = 0.999$); ABZ-SO_2 ($y = 14879.4 + 12724.4x$; $r = 0.999$).

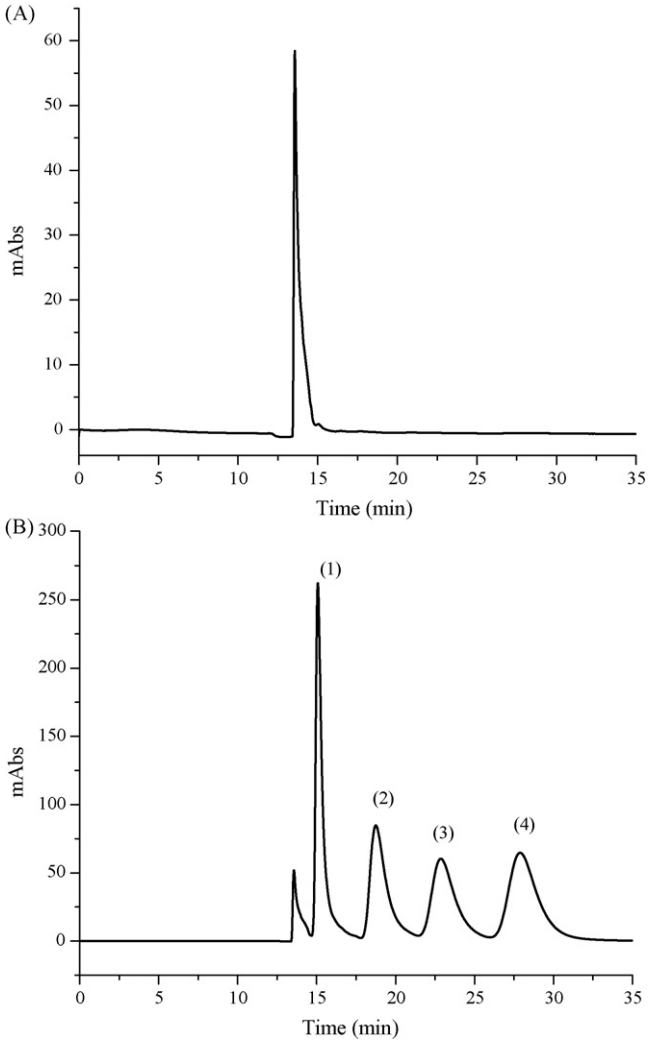

Fig. 3. Representative chromatograms of plasma free drug (A) and plasma spiked with albendazole metabolites (B) using the HPLC multidimensional system. (1) ABZ-SO_2NH_2 5.0 μg mL^{-1}; (2) (+)-ABZ-SO 10 μg mL^{-1}; (3) (−)-ABZ-SO 10 μg mL^{-1}; ABZ-SO_2 5.0 μg mL^{-1}.

Table 2
Accuracy, intra-day ($n = 5$), inter-day ($n = 15$) variability and extraction efficiency ($n = 5$) for the assay of albendazole metabolites in bovine plasma

Analyte (ng mL^{-1})	1st day		2nd day		3rd day		Extraction efficiency (%)
	CV (%)	Accuracy (%)	CV (%)	Accuracy (%)	CV (%)	Accuracy (%)	(mean ± S.D.)
ABZ-SO_2NH_2							
24.00	3.70	114	3.58	112	3.59	112	84.4 ± 3.77
150.0	3.27	114	5.98	98.8	2.56	98.8	98.0 ± 2.95
300.0	4.28	112	5.45	103	1.51	103	95.6 ± 3.13
(+)-ABZ-SO							
48.00	6.96	109	5.48	111	6.65	111	88.4 ± 3.84
500.0	0.760	113	2.66	108	1.39	108	97.1 ± 2.96
1000	5.77	114	2.72	111	4.35	111	92.5 ± 4.69
(−)-ABZ-SO							
48.00	4.19	109	7.99	89.9	2.17	89.9	97.1 ± 3.24
500.0	4.18	105	3.22	104	2.61	104	100 ± 5.00
1000	2.88	114	6.99	108	2.42	108	103 ± 3.73
ABZ-SO_2							
12.00	2.03	104	1.92	99.8	1.31	102	93.7 ± 4.32
150.0	3.92	103	3.42	105	2.51	101	99.7 ± 3.69
300.0	2.97	111	3.87	102	1.97	101	103 ± 2.21

Inter- and intra-day precision and accuracy were established at three quality control samples (high, medium and low concentrations) prepared in five replicates and analyzed on three non-consecutive days. The precision was expressed as coefficient of variation (CV%) and the accuracy was evaluated by back-calculation and expressed as the percent deviation between amount found and amount added at the three concentrations examined.

During intra- and inter-day precision and accuracy evaluation, the columns performed poorly after injection of 15 mL of bovine plasma into them. To circumvent this problem, both columns were replaced by new ones and a sequence of 15 samples were reanalyzed. All precision and accuracy results showed satisfactory intra- and inter-day precision, with coefficient of variation ≤15%. These results obtained are presented in Table 2. Therefore, the use of two different RAM and chiral columns added to the robustness of the method.

The extraction and transfer efficiencies (Table 2) were determined at the same three quality control concentration levels. The results were calculated based on comparison to aqueous analyte solutions at corresponding concentrations. High recoveries were obtained at the three concentrations examined (84.8–103%).

The limit of quantification (LOQ) was 40 ng mL^{-1} for (+)-ABZ-SO, 12 ng mL^{-1} for (−)-ABZ-SO, 20 ng mL^{-1} for ABZ-SO_2NH_2 and 6.0 ng mL^{-1} for ABZ-SO_2. The limit of detection (LOD) was 30 ng mL^{-1} for (+)-ABZ-SO, 10 ng mL^{-1} for (−)-ABZ-SO, 10 ng mL^{-1} for ABZ-SO_2NH_2 and 5.0 ng mL^{-1} for ABZ-SO_2. Two blind samples containing unknown concentrations of all compounds to the analyst produced accuracies in the range of 94.4–114% at concentration levels of 67.2–480 ng mL^{-1} with CV% at the range of 1.07–4.52 for the duplicate analysis of the samples (Table 3)

Table 3
Precision and accuracy for the determination of modafinil enantiomers and their metabolites in blinded bovine plasma samples

Analyte (ng mL^{-1})	CV (%)	Accuracy (%)
ABZ-SO_2NH_2		
67.20	1.63	114
144.0	1.07	114
(+)-ABZ-SO		
224.0	1.25	97.2
480.0	4.05	104
(−)-ABZ-SO		
224.0	4.52	94.4
480.0	3.64	102
ABZ-SO_2		
67.20	3.82	105
144.0	2.78	107

3.5. Stabilities

The long-term storage, short-term storage (bench-top), freeze-thaw stability and auto-sampler stability were evaluated. Analytical standard solutions were stable for 5 days when stored at −20 °C. Plasma samples spiked with ABZ-SO_2 were stable at least for 24 h when kept at −20 °C while plasma samples spiked with ABZ-SO_2NH_2 or (+)-ABZ-SO were stable for 7 days and with (−)-ABZ-SO for 3 days. For short-term storage (bench-top) the samples were prepared and kept at room temperature for 6 h before analysis and all of them proved to be stable. Autosampler stability was also determined and all samples were stable over the 16 h period evaluated. The stability of all compounds in plasma samples during three freeze-thaw cycles was evaluated and the ABZ-SO_2NH_2 was stable for two cycles, ABZ-SO_2 for one cycle, while (−)- and (+)-ABZ-SO were stable for three cycles.

4. Conclusions

A selective method based on column switching technique has been developed for the on line determination of albendazole and its metabolites in bovine plasma by means of a restricted access media column for sample clean-up. The novel method described herein was proved to be simple, sensitive, selective, precise and accurate for a challenging and complex biofluid.

Further, it is the first method described for analyzing, in a single run of 35 min, the enantiomers of albendazole sulphoxide, albendazole sulphona and albendazole 2-aminosulphone making it an attractive alternative to the laborious previously employed sample treatment methods. The method might be considered for enantioselective pharmacokinetics studies of albendazole.

Acknowledgment

The authors acknowledge the financial support from Fundação de Amparo a Pesquisa do Estado de São Paulo (FAPESP). The grants from Conselho Nacional de Desenvolvimento Científico e Tecnológico (CNPq) and Coordenação de Aperfeiçoamento de Nível Superior (CAPES) are also acknowledged.

References

[1] A.D. Dayan, Acta Trop. 86 (2003) 141.
[2] H.C. Rawden, G.O. Kokwaro, S.A. Ward, G. Edwards, Br. J. Clin. Pharmacol. 49 (2000) 313.
[3] E. Lacey, Parasitol. Today 6 (1990) 112.
[4] D.W. Gotschall, V.J. Theorides, R. Wang, Parasitol. Today 6 (1990) 115.
[5] C.E. Lanusse, B. Nare, L.H. Gason, R.K. Prichard, Xenobiotica 22 (1992) 419.
[6] H. Souhaili-El-Amri, O. Mothe, M. Totis, C. Masson, A.M. Batt, P. Delatour, G. Siest, J. Pharmacol. Exp. Ther. 246 (1988) 758.
[7] F. Bolás-Fernández, S. Rama-Iñiguez, J.J. Torrado, J. Parasitol. 90 (2004) 407.
[8] M. Navvaro, L. Canut, A. Carretero, C. Cristòfol, F.J. Pérez-Aparicio, M. Arboix, J. Ruberte, Reprod. Toxicol. 13 (1999) 295.
[9] C. Villaverde, A.I. Alvarez, P. Redondo, J. Voces, J.L. Del Estal, J.G. Pietro, Xenobiotica 25 (1995) 433.
[10] P. Delatour, E. Benoit, S. Besse, A. Boukraa, Xenobiotica 21 (1991) 217.
[11] R. Sarin, A.P. Dash, V.K. Dua, J. Chromatogr. B 799 (2004) 233.
[12] X. Chen, L. Zhao, H. Xu, D. Zhong, J. Pharm. Biom. Anal. 35 (2004) 829.
[13] Z. Wu, N.J. Medlicott, M. Razzak, I.G. Tucker, J. Pharm. Biom. Anal. 39 (2005) 225.
[14] B.P.S. Capece, G. Castells, F. Pérez, M. Arboix, C. Cristòfol, Vet. Res. Commun. 24 (2000) 339.
[15] A. Mirfazaelian, S. Dadashzadeh, M.R. Rouini, J. Pharm. Biom. Anal. 30 (2002) 1249.
[16] G.C. Batzias, E. Theodosiadou, G.A. Delis, J. Pharm. Biom. Anal. 35 (2004) 1191.
[17] B. Shaikh, N. Rummel, R. Reimschuessel, J. Agri. Food Chem. 51 (2003) 3254.
[18] L. Mottier, L. Alvarez, C. Lanusse, J. Chromatogr. A 798 (2003) 117.
[19] D.J. Fletouris, N.A. Botsoglou, I.E. Psomas, A.I. Mantis, Anal. Chem. Acta 345 (1997) 111.
[20] H.D. Solana, J.A. Rodriguez, C. Lanusse, Parasitol. Res. 87 (2001) 275.
[21] A. Goudah, Vet. Res. Commun. 27 (2003) 555.
[22] P. Delatour, F. Garnier, E. Benoit, I. Caude, Res. Vet. Sci. 50 (1991) 134.
[23] S.C. Su, H.H. Chou, P.C. Chang, C.H. Lui, S.S. Chou, J. Food Drug Anal. 12 (2004) 244.
[24] M. Danaher, M. O'Keeffe, J.D. Glennon, Anal. Chim. Acta 483 (2003) 313.
[25] L. Moreno, F. Echevarria, F. Muñoz, L. Alvarez, S. Sanchez Bruni, C. Lanusse, Exp. Parasitol. 106 (2004) 150.
[26] V.L. Lanchote, O.M. Takayanagui, F.H. Mateus, Chirality 16 (2004) 520.
[27] O.M. Takayanagui, P.S. Bonato, S.A.C. Dreossi, V.L. Lanchote, Br. J. Clin. Pharmacol. 54 (2002) 125.
[28] V.L. Lanchote, F.S. Garcia, S.A.C. Dreossi, O.M. Takayanagui, Ther. Drug Monitor. 24 (2002) 338.
[29] M.P. Marques, O.M. Takayanagui, V.L. Lanchote, Br. J. Med. Biol. Res. 35 (2002) 261.
[30] F. Batigalhia, M. Zaldini-Hernades, A.G. Ferreira, I. Malvestiti, Q.B. Cass, Tetrahedron 57 (2001) 9669.
[31] Q.B. Cass, M.E. Tiritan, S.A. Calafatti, S.A. Matlin, J. Liq. Chromatogr. Relat. Technol. 22 (1999) 3091.
[32] N.M. Cassiano, Q.B. Cass, A.L. Degani, I.W. Wainer, Chirality 14 (2002) 731.
[33] M.L. Menezes, G. Felix, J. Liq. Chromatogr. Relat. Technol. 19 (1996) 3221.
[34] R.V. Oliveira, Q.B. Cass, J. Agric. Food Chem. (2006) 1180.
[35] M.M. Bradford, Anal. Biochem. 72 (1976) 248.
[36] U.S., Food and Drug Administration, in: Guidance for Industry, 2001 p. 1.
[37] J. Clayden, N. Greeves, P. Wothers, Organic Chemistry, Oxford University Press, New York, 2001.
[38] J. Otera, T. Sato, Synlett (1995) 365.
[39] M.H. Ali, G.J. Bohnert, Synthesis (1998) 1238.
[40] M. Tajbakhsh, J.M. Lakoura, K. Yadollahzadeh, A.R. Shakeri, M.A. Khalilzadeh, J. Chem. Res. (2005) 796.
[41] K. Kaczorowska, Z. Kolarska, K. Mitka, P. Kowaslski, Tetrahedron 61 (2005) 8315.
[42] E. Yashima, J. Chromatogr. A 906 (2001) 105.
[43] Q.B. Cass, A.L. Degani, N.M. Cassiano, J. Liq. Chromatogr. Rel. Technol. 26 (2003) 2083.
[44] E.P. Sousa, M.E. Tiritan, R.V. Oliveira, C.M.M. Afonso, Q.B. Cass, M.M.M. Pinto, Chirality 16 (2004) 279.
[45] Q.B. Cass, F. Batigalhia, J. Chromatogr. A 987 (2003) 445.
[46] M.L.C. Montanari, Q.B. Cass, A.D. Andricopulo, A. Leitão, A.C. Montanari, Anal. Chim. Acta 545 (2005) 33.
[47] M. Danaher, M. O'Keeffe, J.D. Glennon, J. Chromatogr. B 845 (2007) 1.
[48] D.J. Anderson, Anal. Chem. 65 (1993) 434R.
[49] N.M. Cassiano, V.V.d. Lima, R.V. Oliveira, A.C. De Pietro, Q.B. Cass, Anal. Bioanal. Chem. 384 (2006) 1462.
[50] C. Milsĭanová, M. Hutta, J. Chromatogr. B 797 (2003) 91.
[51] K.S. Boos, A. Rudolphi, LC–GC 15 (1997) 602.
[52] V.V.de. Lima, N.M. Cassiano, Q.B. Cass, Química Nova 29 (2006) 72.
[53] A. Rudolphi, K.S. Boos, LC–GC 15 (1997) 814.
[54] Q.B. Cass, A.L. Degani, N.M. Cassiano, J. Pedrazolli Jr., J. Chromatogr. B 766 (2002) 153.
[55] Q.B. Cass, V.V. Lima, R.V. Oliveira, N.M. Cassiano, A.L. Degani, J. Pedrazzoli, J. Chromatogr. B 798 (2003) 275.
[56] Q.B. Cass, T. Ferreira Galatti, J. Pharmaceut. Biomed. Anal. 46 (2008) 937.
[57] Q.B. Cass, R.F. Gomes, S.A. Calafatti, J. Pedrazolli Jr., J. Chromatogr. A 987 (2003) 235.
[58] R.V. Oliveira, A.C. De Pietro, Q.B. Cass, Talanta 71 (2007) 1233.
[59] A.V. Pereira, Q.B. Cass, J. Chromatogr. B 826 (2005) 139.
[60] F.C.C.R. de Paula, A.C. De Pietro, Q.B. Cass, J. Chromatogr. A 1189 (2008) 221.

Talanta 76 (2008) 49–53

Contents lists available at ScienceDirect

Talanta

journal homepage: www.elsevier.com/locate/talanta

Surface plasmon resonance spectroscopic chiral discrimination using self-assembled leucine derivative monolayer

Hongxia Chen[a], Haiyun Cheng[b], Jaebeom Lee[c], Jae-Ho Kim[d], Myung Ho Hyun[e], Kwangnak Koh[c,*]

[a] College of Pharmacy, Pusan National University, Pusan 609-735, Republic of Korea
[b] K-MAC, Daejeon 305-380, Republic of Korea
[c] College of Nanoscience and Nanotechnology, Pusan National University, Pusan 609-735, Republic of Korea
[d] Department of Molecular Science and Technology, Ajou University, Suwon 442-749, Republic of Korea
[e] Department of Chemistry, Pusan National University, Pusan 609-735, Republic of Korea

ARTICLE INFO

Article history:
Received 19 October 2007
Received in revised form 5 February 2008
Accepted 7 February 2008
Available online 15 February 2008

Keywords:
Chiral differential detection
Leucine
Chiral stationary phase (CSP)
Surface plasmon resonance (SPR)
Self-assembled monolayer (SAM)

ABSTRACT

Pirkle-type chiral stationary phases (CSPs) showed excellent enantiomeric separation for amino acid derivatives by forming energetically different two transient diastereomeric π–π donor–acceptor complexes with two enantiomers. A CSP derived from *N*-(3,5-dinitrobenzoyl) leucine with a thiol ending group for immobilization on Au was synthesized and self-assembled on Au surface as chiral sensing layer. The monolayer characterized by spectroscopic and microscopic methods such as AFM, FTIR reflection absorption spectroscopy (FTIR-RAS) and cyclic voltammetry (CV). The enantiospecific detection onto CSP of the leucine derivative was studied by surface plasmon resonance (SPR). (*S*)-CSP SAM showed high chiral differential detection for (*S*)-analyte in a range of 1.0×10^{-9} to 1.0×10^{-4} M. In combination with the SPR method, the leucine derivative monolayer provided a reliable and simple experimental platform for enantiospecific detection.

1. Introduction

Chiral differential detection is an important subject in the fields of medical and pharmaceutical technologies. Various techniques and methods have been developed of which high-performance liquid chromatography (HPLC) and capillary electrophoresis are the most powerful tools [1,2]. However, the pretreatment is of time consuming for these sensitive methods detection. Electrochemical methods suffer from losing selectivity and interference due to the presence of other components [3].

In order to be useful for routine analysis, a sensor should meet several requirements such as ease of use, speed, reproducibility and the potential for automation. The surface analysis technique of surface plasmon resonance (SPR) spectroscopy has emerged as a powerful method for studying chemical and biological processes due to its non-labeling, real time measurement and high sensitivity. Hofstetter et al. [4] developed SPR immunosensors for the detection of native amino acid enantiomers. Chen et al. [5] developed a multiwavelength surface plasmon resonance (mwSPR) approach to study the chiral discrimination between D- and L-cystine (Cys). Corradini et al. [6] reported a method to probe DNA by SPR with chiral nucleic acid conjugates. Recently, a novel method based on SPR, immobilization by recognition monolayers on noble metals have been utilized to detect target molecules and to obtain better reproducibility [7–9]. These approaches have been proved to increase the sensitivity compared with other techniques.

For chiral differential discrimination at a solid surface modified with a chiral component such as an enantiospecific heterogeneous catalyst, supramolecular assemblies of the modifier are expected to induce enantioselectivity. Our research purpose is an SPR-based fundamental study of chiral differential discrimination using a leucine derivatized chiral stationary phase (CSP). We synthesized Pirkle-type (*S*)-CSP and self-assembled on Au surface as chiral sensing layer. Pirkle-type CSPs have been known to separate two enantiomers by forming energetically different two transient diastereomeric π–π donor–acceptor complexes with two enantiomers [10,11]. The chiral recognition mechanisms that separate chiral solutes having π-donor groups have been investigated by HPLC [12,13], X-ray crystallography [14], Raman spectrometry and computational studies [15,16]. Pirkle and Pochapsky [17] and Kato et al. [18] validated the π–π interaction and hydrogen bonding in the Pirkle-type CSP and amino acid interaction by NMR studies.

* Corresponding author. Tel.: +82 55 350 5294; fax: +82 51 514 2358.
E-mail address: koh@pusan.ac.kr (K. Koh).

0039-9140/$ – see front matter © 2008 Elsevier B.V. All rights reserved.
doi:10.1016/j.talanta.2008.02.001

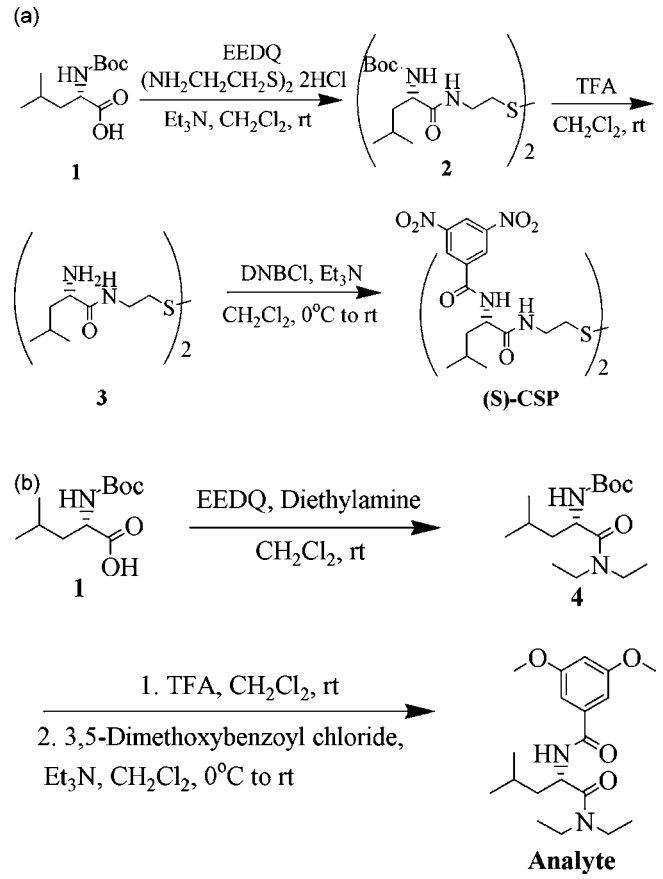

Scheme 1. Scheme of synthesis of (a) (*S*)-CSP and (b) (*S*)-/(*R*)-analyte.

The (*S*)-CSP was designed with a thiol ending group for immobilization on gold surface [19,20]. CSP SAM and the complexes with (*R*)- and (*S*)-analytes were characterized by atomic force microscopy (AFM), Fourier transform infrared reflection absorption spectroscopy (FTIR-RAS) and cyclic voltammetry (CV). The chiral differential discrimination was investigated on the enantioselective leucine derivatized monolayer by SPR. The combination of SPR technique with the construction of CSP SAM is a useful method to the development of efficient chiral differential discrimination sensing interface.

2. Experimental

2.1. Synthesis and characterization of (S)-CSP and (R)-/(S)-analytes

The synthesis scheme of (*S*)-CSP and (*R*)- and (*S*)-analytes was shown in Scheme 1 [19–21].

For synthesis of (*S*)-CSP, 0.64 g of *N*-ethoxycarbonyl-2-ethoxy-1,2-dihydroquinoline (EEDQ) was added to a stirred mixture of 0.55 g of *N*-*t*-Boc-leucine **1** in 35 mL of CH_2Cl_2. After 30 min stirring, 0.29 g of cystamine dihydrochloride and 0.36 mL of triethylamine in 10 mL of CH_2Cl_2 was poured into the reaction mixture. The mixture was stirred for 12 h at room temperature and then washed with 1 N HCl, 0.5 N NaOH and brine solution, respectively. The organic layer was dried over Na_2SO_4 and concentrated under the reduced pressure. The residue was purified by silica gel chromatography to give the product in 61% yield as a colorless solid (acetone:hexane = 2:1). Then, 0.6 mL of trifluoroacetic acid was added to a stirred mixture of 0.44 g of compound **2** in 20 mL of CH_2Cl_2. The reaction mixture was stirred for 12 h at room temperature and concentrated under reduced pressure to remove the excess of trifluoroacetic acid. The residue was dissolved again in 20 mL of CH_2Cl_2 and washed with 0.5 N NaOH and brine solution. The organic layer was dried over Na_2SO_4 and concentrated under reduced pressure to afford the product in 88% yield as a yellowish oily material. The solution of 0.26 g of 3,5-dinitrobenzoyl chloride in 5 mL of CH_2Cl_2 was slowly dropped into a stirred mixture of 0.22 g of compound **3** and 0.16 mL of triethylamine in 30 mL of CH_2Cl_2 at 0 °C. The mixture was stirred at room temperature for 2 h, and washed with NaOH (0.5 N), HCl (1 N) and brine solution, respectively. The organic layer was dried over Na_2SO_4 and concentrated under reduced pressure. The residue was purified by crystallization to give 80% yield of the product as yellow solid (THF:hexane = 1:1). ^{1}H NMR (200 MHz, DMSO-d_6, δ) 9.25 (d, J = 8.06 Hz, 2H), 9.09 (d, J = 2.20 Hz, 4H), 8.93 (t, J = 2.20 Hz, 2H), 8.29 (t, J = 5.50 Hz, 2H), 4.52 (q, J = 7.69 Hz, 2H), 3.35–3.28 (m, 4H), 2.76 (t, J = 6.59 Hz, 4H), 1.73–1.52 (m, 6H), 0.88 (d, J = 8.06 Hz, 6H), 0.85 (d, J = 8.06 Hz, 6H). IR (KBr, cm^{-1}) 3289 (s), 3090, 2957, 1635 (s), 1538 (s), 1344. Element analysis for $C_{30}H_{38}N_8O_{12}S_2$ (C, 46.98; H, 5.00; N, 14.62; S, 8.35) found C, 47.3; H, 4.99; N, 14.34; S, 8.45.

To prepare (*R*)- and (*S*)-analytes, 0.45 g of EEDQ was added to a stirred mixture of 0.35 g of *N*-*t*-Boc-leucine **1** in 20 mL of CH_2Cl_2. After 30 min, 0.2 mL of diethylamine was dropped into the reaction mixture. The mixture was stirred for 12 h at room temperature and then the mixture was washed with 1 N HCl, 1 N NaOH, and brine solution sequentially. The organic layer was dried over Na_2SO_4 and concentrated under reduced pressure. The residue was purified by silica gel chromatography to give 46% yield of the product **4** as a colorless oil (ethylacetate:hexane = 1:5). 0.3 mL of trifluoroacetic acid was added to a stirred solution of 0.2 g of *N*-*t*-Boc-leucine *N*,*N*-diethylamide **4** in 20 mL of CH_2Cl_2. The reaction mixture was stirred for 12 h at room temperature, and concentrated under reduced pressure to remove the excess of trifluoroacetic acid. The residue was dissolved in 20 mL of CH_2Cl_2 and then the solution was washed by 0.5 N NaOH and brine solution. The organic layer was dried over Na_2SO_4 and concentrated under reduced pressure to afford leucine *N*,*N*-diethylamide as a yellowish oily material. Without further purification, leucine *N*,*N*-diethylamide was used for the next reaction. The solution of 0.15 g of 3,5-dimethoxybenzoyl chloride in 5 mL of CH_2Cl_2 was slowly dropped into a stirred mixture of 0.12 g of leucine *N*,*N*-diethylamide prepared above and 0.1 mL of triethylamine in 15 mL of CH_2Cl_2 at 0 °C. The mixture was stirred at room temperature for 2 h, and washed with 0.5 N NaOH, 1 N HCl and brine solution, respectively. The organic layer was dried over Na_2SO_4 and concentrated under reduced pressure. The product was purified by silica gel chromatography to give 70% yield of the product as a white solid (ethylacetate:hexane = 1:1). ^{1}H NMR (200 MHz, $CDCl_3$, δ) 7.00 (d, J = 8.42 Hz, 1H), 6.93 (d, J = 2.20 Hz, 2H), 6.55 (t, J = 2.20 Hz, 1H), 5.15 (m, 1H), 3.80 (s, 6H), 3.63–3.44 (m, 1H), 3.42 (q, J = 7.33 Hz, 2H), 3.32–3.15 (m, 1H), 1.76–1.63 (m, 2H), 1.51–1.37 (m, 1H), 1.28 (t, J = 7.33 Hz, 3H), 1.12 (t, J = 7.33 Hz, 3H), 1.03 (d, J = 6.59 Hz, 3H), 0.93 (d, J = 6.23 Hz, 3H). IR (KBr, cm^{-1}) 3304 (s), 3014, 2962, 1624 (s), 1603 (s), 1540. Element analysis for $C_{19}H_{30}N_2O_4$ (C, 65.10; H, 8.63; N, 8.00) found C, 65.59; H, 7.80; N, 8.45.

2.2. Formation and characterization (S)-CSP SAM on Au

The sensor chip comprises an Au film (50 nm) deposited onto a quadrangular glass prism (18 mm × 18 mm with a refractive index of 1.567, K-MAC, Korea). For the preparation of the SAM of CSP, the chip was freshly cleaned in deionized water, ethanol and then immersed into CSP solution of 0.5 mM in ethanol for 24 h. After

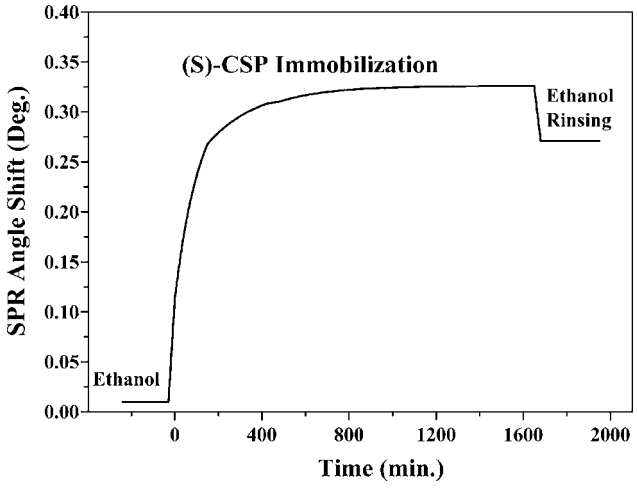

Fig. 1. SPR sensogram of immobilization of (*S*)-CSP.

immobilization, the chip was rinsed rigorously with ethanol and dried in a stream of dry nitrogen gas.

The FTIR-RAS (Magma IR TM 550, Nicdet, USA) spectra were measured with a resolution of 2 cm^{-1}. Incident angle was set at 85° and a p-polarized beam was obtained through a Hitachi Au/AuBr wire-grid polarizer.

An AFM (SPM-LS; Park Scientific Instruments, USA) was used to image the sensor chip surface. The AFM experiments were performed using the contact mode. The nominal force constant of the tip cantilevers was 0.067 N/m.

Cyclic voltammetry was performed with a voltammetric analyzer (BSA 100B; Bioanalytical Systems; USA) at room temperature.

2.3. Chiral differential discrimination by SPR spectroscopy measurement

For investigating the binding between CSP and analytes, (*R*)- and (*S*)-analytes were diluted in nine concentrations with a mixed solvent of isopropanol–hexane (20:80, v/v) in a range of 1.0×10^{-12} to 1.0×10^{-4} M. Each sample was flowed into the SPR cell from low to high concentration, followed rinsing with mixed solvent to remove the physically adsorbed sample. The SPR spectroscopy was used to monitor the chiral differential recognition by analyzing SPR angle shifts. All SPR experiments were carried out in a SpectraBio instrument (SpectraBio2000; K-MAC, Korea). The temperature was kept constant at 25 ± 0.5 °C.

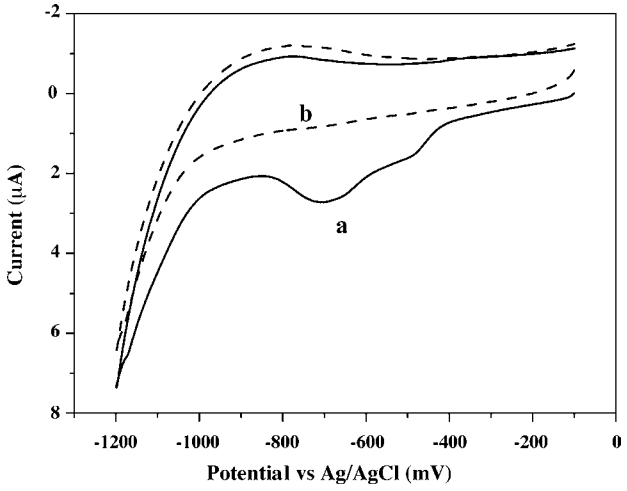

Fig. 2. Voltammetric response for reductive desorption of a CSP SAM modified Au electrode in 0.5 M NaOH with a scan rate of 50 mV s^{-1}. The electrode before (a) and after (b) reductive desorption.

3. Results and discussion

The resonance angle of SPR was increased after injecting (*S*)-CSP solution, which directly indicated the formation of the (*S*)-CSP SAM (Fig. 1). The resonance angle shift indicated the surface modification of the Au coated layer. The strong back-shift of resonance angle at the washing step with ethanol reflected the sensitive response of the quantitative analysis using SPR.

In previous studies, a formation mechanism of alkanethiol monolayers on Au substrates has been proposed [22–24]. The properties of the electrode with CSP SAM can be estimated by submitting the electrode to reductive desorption experiment. Fig. 2 shows the reductive desorption peak of CSP SAM on the Au electrode. The voltammetric response displays a peak at about −0.7 V by scanning from −0.1 to −1.2 V. This peak has been attributed to the reductive desorption of thiolated compounds that are chemisorbed to Au. It is supported that (*S*)-CSP was absorbed onto the gold electrode by the reduction of the S–S bond and forming of the Au–S bond.

After assuming that all thiolated compounds are reduced in the CV experiment, the surface coverage can be determined from the reductive desorption data [23–25]. Accounting for the surface roughness of the Au electrode, the surface coverage (Γ) of the CSP SAM at the Au electrode was calculated from the integrated area under the reduction peak. The surface coverage of CSP SAM was calculated to be 1.13×10^{-10} mol cm^{-2}. These calculated values effectively indicate the relative packing degree of each (*S*)-CSP SAM on the Au surface.

FTIR-RAS was used to characterize the CSP monolayer on an Au thin film and the complex formation with the (*R*)- and (*S*)-analytes. FTIR-RAS spectrum of the CSP SAM exhibits many strong and clear stretching modes that reflect the arrangement of CSP SAM on the Au surface (Fig. 3 and Table 1). A considerable part of the infrared spectra in comparison between CSP and analyte is C=O

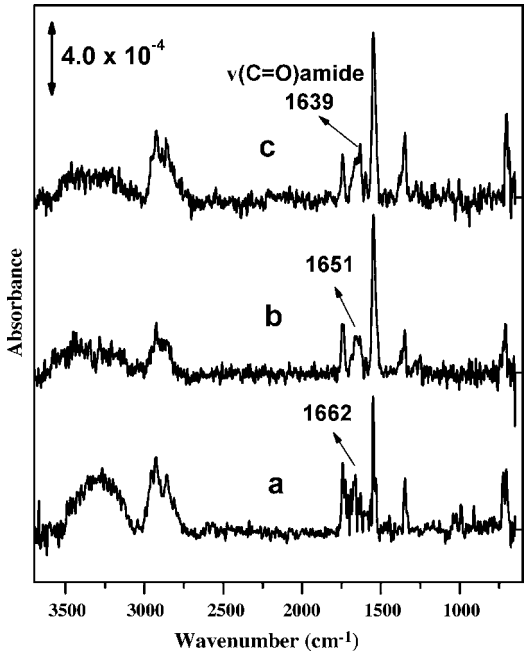

Fig. 3. FTIR-RAS spectra of (*S*)-CSP SAM (a) and after binding with (*R*)-analyte (b) and (*S*)-analyte (c).

Table 1
FTIR-RAS peak assignment of (*S*)-CSP SAM and after binding with (*R*)-/(*S*)-analyte

Vibration mode	Wavenumber (cm^{-1})		
	(*S*)-CSP SAM	(*S*)-CSP SAM + (*R*)-analyte	(*S*)-CSP SAM + (*S*)-analyte
ν(NH)	3299	3284	3287
$\nu_a(CH_3)$	2955	2955	2955
$\nu_a(CH_2)$	2927	2827	2921
$\nu_s(CH_2)$	2859	2849	2859
ν(C=O)	1747	1741	1738
ν(C=O) amide	1662	1651	1639
$\nu_a(NO_2)$	1550	1541	1549
$\nu_s(NO_2)$ aromatic	1346	1352	1352

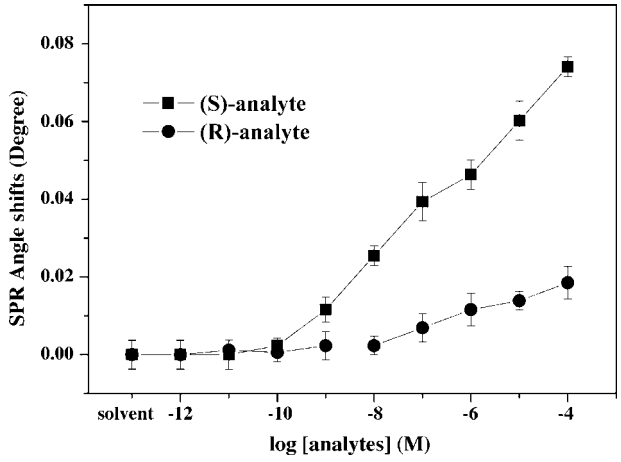

Fig. 4. SPR angle shifts according to CSP SAM binding with various concentrations of (*R*)-/(*S*)-analytes.

stretching vibration from 1662 to 1651 ((*R*)-analyte) and 1639 cm^{-1} ((*S*)-analyte), which caused by hydrogen bonding between CSP and analyte. It indicates that (*S*)-analyte has stronger hydrogen bond with (*S*)-CSP SAM than that of (*R*)-analyte.

In AFM photography, the bare Au substrate, (*S*)-CSP, (*S*)-CSP + (*R*)-analyte and (*S*)-CSP + (*S*)-analyte showed a root mean square (RMS) roughness of 20.6, 16.5, 15.5 and 14.0 Å, respectively. The bare gold surface showed relatively large size domain, whereas CSP SAM surface and after binding with analytes had a remarkably smooth and densely uniform surface characteristics. These changes in RMS roughness of CSP modified Au surface strongly support the formation of SAM. In particular, (*S*)-analyte binding with (*S*)-CSP SAM showed the smaller RMS roughness value than that of (*R*)-analyte. These results suggest that the self-assembled CSP monolayer can provide favorable condition for promoting detection resolution of chiral interaction and the (*S*)-analyte is adsorbed much than that of (*R*)-analyte on CSP SAM.

Stereoselective binding of the analytes to (*S*)-CSP SAM was demonstrated with SPR (Fig. 4). The SPR resonance angle gradually increased as the increase of (*S*)-analyte concentration. In respect of detection limit, CSP SAM was able to detect (*S*)-analyte from 1.0×10^{-9} to 1.0×10^{-4} M by used SPR system. However, the (*R*)-analyte showed less SPR response compare with that of (*S*)-analyte. It exhibits a fairly good chiral enantioselectivity with a ratio of $R_{(S)}/R_{(R)} = 7.5$, where $R_{(S)}$ and $R_{(R)}$ denote the SPR response for (*S*)-analyte and (*R*)-analyte, respectively. The high enantioselectivity may contribute to the well-ordered (*S*)-CSP on Au. (*S*)-CSP and the (*S*)-analyte are proposed to interact through the face-to-face π–π complexation between the 3,5-dinitrophenyl group of the CSP and the 3,5-dimethoxybenzoyl group of the analyte, combining the hydrogen bonding between the carbonyl oxygen of the analyte and the amide N–H hydrogen of the CSP [26–29]. In this instance, the edge of the 3,5-dimethoxybenzoyl group of the (*R*)-analyte confronts the face of the isobutyl group of the (*S*)-CSP, invoking the face-to-edge π–π interaction which has been considered as an associative force between aromatic rings [30]. Therefore, the transient diastereomeric (*S*, *S*)-complex formed between the (*S*)-CSP and the (*S*)-analyte might be more stable than (*S*, *R*)-complex.

4. Conclusion

We have described a chiral monolayer prepared via self-assembling and its use for the chiral differential discrimination of leucine derivatized entantiomers by SPR. (*S*)-CSP SAM showed sensitivity and selectivity for (*S*)-analyte. In combination with the SPR method, this leucine derivative monolayer provided a reliable and simple experimental platform for enantiospecific detection under experimental conditions. This study illuminates a fundamental method of using the SPR technique combined with the construction of appropriate SAM to the development of efficient sensing chiral interface.

Acknowledgement

This work was supported by the Korea Research Foundation Grant funded by the Korean Government (MOEHRD, Basic Research Promotion Fund) (KRF-2007-331-C00140).

References

[1] A. Kaddoumi, T. Mori, M.N. Nakashima, M. Wada, K. Nakashima, J. Pharm. Biomed. 34 (2004) 643.
[2] A.D. Presley, K.M. Fuller, E.A. Arriaga, J. Chromatogr. B 793 (2003) 141.
[3] K. Kerman, Y. Morita, Y. Takamura, E. Tamiya, Electrochem. Commun. 5 (2003) 887.
[4] O. Hofstetter, H. Hofstetter, M. Wilchek, V. Schurig, B.S. Green, Nat. Biotechnol. 17 (1997) 371.
[5] Y. Chen, H. Huang, X. Yu, L. Qi, Carbonhydr. Res. 340 (2005) 2024.
[6] R. Corradini, G. Feriotto, S. Sforza, R. Marchelli, R. Gambari, J. Mol. Recogn. 17 (2004) 76.
[7] M. Lee, T.I. Kim, K.H. Kim, J.H. Kim, M.S. Choi, H.J. Choi, K. Koh, Anal. Biochem. 310 (2002) 163.
[8] Y. Hur, K. Ock, K. Kim, S. Jin, Y. Gal, J. Kim, S. Kim, K. Koh, Anal. Chim. Acta 460 (2002) 133.
[9] H. Chen, Y.S. Kim, S.R. Keum, S.H. Kim, H.J. Choi, J. Lee, W.G. An, K. Koh, Sensors 7 (2007) 1216.
[10] W.H. Pirkle, T.C. Pochapsky, Chem. Rev. 89 (1989) 347.
[11] N. Banno, T. Nakanishi, M. Matsunaga, T. Asahi, T. Osaka, J. Am. Chem. Soc. 126 (2004) 428.
[12] W.H. Pirkle, C.J. Welch, J. Org. Chem. 49 (1984) 138.
[13] W.H. Pirkle, M.H. Hyun, B. Bank, J. Chromatogr. 316 (1984) 585.
[14] E. Horvóth, L. Kocisis, R.L. Frost, B. Hren, L.P. Szabó, Anal. Chem. 70 (1998) 2766.
[15] K.B. Lipkowitz, D.A. Demeter, R. Zegarra, R. Larter, T. Darden, J. Am. Chem. Soc. 110 (1988) 3446.
[16] S. Topiol, M. Sabio, J. Moroz, W.B. Caldwell, J. Am. Chem. Soc. 110 (1988) 8367.
[17] W.H. Pirkle, T.C. Pochapsky, J. Am. Chem. Soc. 109 (1987) 5975.
[18] M. Kato, T. Fukushima, N. Shimba, I. Shimada, Y. Kawakami, K. Imai, Biomed. Chromatogr. 15 (2001) 227.
[19] M.H. Hyun, J.B. Lee, Y.D. Kim, J. High Resol. Chromatogr. 21 (1998) 69.

[20] M. Lee, T.-I. Kim, K.-H. Kim, J.-H. Kim, M.-S. Choi, H.-J. Choi, K. Koh, Anal. Biochem. 310 (2002) 163.
[21] W.H. Pirkle, J.M. Finn, J. Org. Chem. 46 (1981) 2935.
[22] G.M. Whitesides, P.E. Laibinis, Langmuir 6 (1990) 87.
[23] M.A. Bryant, J.E. Pemberton, J. Am. Chem. Soc. 113 (1991) 8284.
[24] A.J. Bard, L.R. Faulkner, Electrochemical Methods, John Wiley & Sons, New York, 2001, pp. 239–243.
[25] M.M. Walczak, D.D. Popenoe, R.S. Deinhammer, B.D. Lamp, C. Chung, M.D. Porter, Langmuir 7 (1991) 2687.
[26] W.H. Pirkle, T.C. Pochapsky, G.S. Mahler, R.E. Field, J. Chromatogr. 348 (1985) 89.
[27] W.H. Pirkle, T.C. Pochapsky, J. Org. Chem. 51 (1986) 102.
[28] W.H. Pirkle, J.E. McCune, J. Chromatogr. 479 (1989) 419.
[29] M.H. Hyun, C.S. Min, Y.J. Cho, M.S. Na, J. Liq. Chromatogr. 18 (1995) 2527.
[30] M.C. Grossel, A.K. Cheetham, D.A.O. Hope, S.C. Weston, J. Org. Chem. 58 (1993) 6654.

Talanta 76 (2008) 154–160

Contents lists available at ScienceDirect

Talanta

journal homepage: www.elsevier.com/locate/talanta

Evaluation of liquid-phase microextraction conditions for determination of chlorophenols in environmental samples using gas chromatography–mass spectrometry without derivatization

Li-Wen Chung, Maw-Rong Lee*

Department of Chemistry, National Chung-Hsing University, Taichung 40227, Taiwan, ROC

ARTICLE INFO

Article history:
Received 15 November 2007
Received in revised form 15 February 2008
Accepted 18 February 2008
Available online 26 February 2008

Keywords:
Without derivatization
Enrichment factor
Chlorophenols
Liquid-phase microextraction
Solid-phase microextraction
Environmental samples

ABSTRACT

Determination of trace chlorophenols (CPs) in environmental samples has been evaluated using liquid-phase microextraction (LPME) coupled with gas chromatography–mass spectrometry (GC–MS) without derivatization. The LPME procedure used to extract CPs from water involved 15 μL 1-octanol as acceptor solution in a 5.0 cm polypropylene hollow fiber with an inner diameter of 600 μm and a pore size of 0.2 μm. Under the optimal extraction conditions, enrichment factors from 117 to 220 are obtained. The obtained linear range is 1–100 ng mL^{-1} with r^2 = 0.9967 for 2,4-dichlorophenol (2,4-DCP); 1–100 ng mL^{-1} with r^2 = 0.9905 for 2,4,6-trichlorophenol (2,4,6-TCP); 5–500 ng mL^{-1} with r^2 = 0.9983 for 2,3,4,6-tetrachlorophenol (2,3,4,6-TeCP), and 10–1000 ng mL^{-1} with r^2 = 0.9929 for pentachlorophenol (PCP). The limits of detection range from 0.08 to 2 ng mL^{-1}, which is comparable with the reported values (12–120 ng mL^{-1}). Recoveries of CPs in various matrices exceed 85% with relative standard deviations of less than 10%, except for PCP in landfill leachate. The applicability of this method was examined to determine CPs in environmental samples by analyzing landfill leachate, ground water and soil. The 2,4-DCP and 2,4,6-TCP detected in the landfill leachate are 6.68 and 2.47 ng mL^{-1}. The 2,4,6-TCP detected in ground water is 2.08 ng mL^{-1}. All the studied CPs are detected in contaminated soil. The proposed method is simple, low-cost, less organic solvent used and can potentially be applied to analyze CPs in complex environmental matrices.

1. Introduction

Extensively used as preservative agents, pesticides, antiseptics and disinfectants, CPs are introduced into water either during manufacturing processes or through the degradation of phenoxyalkanoic acids. They are also formed while the chlorination of municipal drinking water [1]. Chlorophenols are carcinogenic and quite persistent [2]. The National Institutes of Health (NIH) has determined the 2,4,6-trichlorophenol (2,4,6-TCP) to be a carcinogen [3]. Therefore, CPs has been designated priority pollutants by the US Environmental Protection Agency (EPA) [4] and the European Community (EC) [5]. Exposure to large amounts of pentachlorophenol (PCP) leads to damage in the liver, kidneys, blood, lungs, nervous system, immune system and gastrointestinal tract [6–8].

Pentachlorophenol and CPs are frequently present in contaminated soils at wood treatment sites [6,9], and are very difficult to separate from various solid environmental matrices because they are not only firmly attached to the matrices but also soluble in non-aqueous medium. Residues of phenolic contaminants can be extracted qualitatively from solid matrices, using various extraction methods such as supercritical fluid extraction [10], Soxhlet extraction [11], shaking-assisted extraction [9], pressurized liquid extraction [12], ultrasonication-assisted extraction [13], and microwave-assisted extraction [14]. These procedures are time-consuming and require a large amount of organic solvent or expensive pretreatment equipment. Recent efforts have attempted to miniaturize liquid-liquid extraction (LLE) by markedly reducing the amount of organic solvent involved, resulting in the development of liquid-phase microextraction (LPME) methodology. Indeed, LPME reduces 99% less organic solvent than traditional LLE [15]. Since LPME requires micro-volume of solvent, applications of this method have attracted considerable attention and are feasible to environment [16–24].

In addition to minimizing organic solvent, high enrichment is also one factor to validate LPME while extraction. In other way, high enrichment is needed to enhance the sensitivity for CPs when analyzing environmental samples. Recently, determination of CPs by 3-phase LPME coupled with HPLC [17] and aqueous samples were

* Corresponding author. Tel.: +886 422851716; fax: +886 422862547.
E-mail address: mrlee@dragon.nchu.edu.tw (M.-R. Lee).

0039-9140/$ – see front matter © 2008 Elsevier B.V. All rights reserved.
doi:10.1016/j.talanta.2008.02.018

extracted by LPME with high enrichment factors. This provides an opportunity for quantification of the LPME method by implementing the kinetic approach. Otherwise, a derivatization step enhances sensitivity particularly when GC was used for the determination of CPs. The derivatization leads to sharper peaks and hence to better separation and higher sensitivity for the CPs. Different derivatization systems have been used including water-bath derivatization [25,26], in situ derivatization [7,27], injection port-derivatization [28] and microwave-assisted derivatization [29]. Although derivatization is one of the most common procedures to enhance the sensitivity of CPs, it unnecessarily contaminates the GC–MS system, shortens column life and creates a need for additional maintenance. In order to avoid these problems, the method without derivatization is used as modified conditions to get high enrichment factor for trace CPs determination. Therefore, this study explores the potential of procedure without derivatization based on LPME to achieve high enrichment factor. Since LPME is a process dependent on equilibrium [20,30], the objective of this work is to reach high distribution equilibrium in the extraction system. Herein, the optimal conditions were examined systematically to evaluate linearity, limits of detection, limits of quantification and precision. Furthermore, the validity of this method was also applied to determine CPs in contaminated environmental samples and assessed with our previous solid-phase microextraction (SPME) method [31].

2. Experimental

2.1. Chemicals, reagents and materials

2,4-Dichlorophenol (2,4-DCP, 99%), 2,4,6-TCP (97%), 2,3,4,6-tetrachlorophenol (2,3,4,6-TeCP, 80%) were obtained from TCI (Tokyo, Japan). 2,3,4,6-TeCP was further purified by recrystallization from diethyl ether and a final purity of over 99% obtained [31]. 2,4,6-Tribromophenol (99%) as a surrogate standard was obtained from TCI and used without further purification. Pentachlorophenol (neat) was purchased from Supelco (Bellefonte, PA, USA). A stock solution of a mixture of CPs at 100 mg L^{-1} for 2,4-DCP, 100 mg L^{-1} for 2,4,6-TCP, 500 mg L^{-1} for 2,3,4,6-TeCP and 1000 mg L^{-1} for PCP was prepared by dissolving the solid bulk CPs in isopropanol (Merck, Darmstadt, Germany) and storing it at 4 °C. The stock solution was further diluted to yield the appropriate working solutions with water.

1-Octanol (99.5%) and NaCl (99.8%) were purchased from Riedel-deHaën (Seelze, Germany). KCl (99%) and hydrochloric acid (HCl, 37.5%) were ordered from Fisher (Fair Lawn, NJ, USA). Citric acid (99.5%) was bought from Riedel-deHaën. NaOH (98.9%) was from TEDIA (Fairfield, Ohio, USA). The laboratory purified water (18 MΩ) was obtained using a SG-Ultra Clear water purification system (SG, Barsbűttel, Germany). The pH 1 buffer solution was prepared by using 0.1 M KCl and adjusted to pH 1 with 0.2 M HCl. The citrate solution was prepared by adding 200 mL of 1 M NaOH solution to dissolve 21.014 g of citric acid, and diluting to 1000 mL with pure water. To obtain buffer solutions with pH values between 2 and 4, suitable volumes of 0.1 M HCl were added to citrate solution. To obtain buffer solutions with pH values 5 and 6, suitable volumes of 0.1 M NaOH were added to citrate solution.

2.2. GC–MS analysis

Chromatographic analysis was performed using a Hewlett-Packard (HP) MS Engine mass spectrometer (Palo Alto, CA, USA) with an HP 5890 Series II GC through an injector in splitless mode. Separations were carried out using a 30 m × 0.25 mm fused capillary column DB-5MS (J&W Scientific, Folsom, CA, USA) with a stationary phase thickness of 0.25 μm. Helium (99.999%) was used as the carrier gas at a constant flow of 1 mL min^{-1}. In LPME, the temperature of the injector port was maintained at 250 °C. The oven was initially set to 130 °C, programmed to 190 °C at a rate of 30 °C min^{-1}, and then to 230 °C at rate of 10 °C min^{-1}. The total analysis time for a single run took 6 min. The GC–MS temperature of the transfer line was maintained at 250 °C. In SPME, the temperature of the injector port was maintained at 290 °C. The oven was initially set to 60 °C, programmed to 190 °C at a rate of 30 °C min^{-1}, and then to 310 °C at a rate of 10 °C min^{-1}. Here, the total analysis time for a single run was 16 min. The GC–MS temperature of the transfer line was maintained at 310 °C [31]. The ion source and quadrupole temperatures were set to 250 °C and 100 °C, respectively. Mass spectra were obtained using the electron impact (EI) mode. The full scan mode with a mass range of m/z 40–350 was adopted to confirm the CPs and the selected ion monitoring (SIM) mode was applied to quantify the CPs. The most abundant ion was used as the quantification ion and the specific ion was used as the confirmation ion, as indicated in Table 1.

Table 1
Analytical conditions of chlorophenols determined by GC–MS

Compound	Retention time (min)	Quantification ion/confirmation ion (m/z)	Mr
2,4-DCP	2.38	162/164 (3:2)	162
2,4,6-TCP	2.72	196/198 (1:1)	196
2,3,4,6-TeCP	3.50	232/230 (4:3)	230
PCP	4.59	266/264/268 (15:9:10)	264

2.3. Liquid-phase microextraction

The experimental set-up for extraction was described as reported by Pedersen-Bjergaard and Rasmussen [30]. The Accurel® Q3/2 polypropylene hollow fiber (600 μm inner diameter, 200 μm wall thickness, 0.2 μm pore size) was purchased from Membrana (Wuppertal, Germany). Before extraction, the hollow fiber was ultrasonically cleaned in acetone for 30 min to remove contaminant. After it had been dried, the hollow fiber was cut by hand into 5.0 cm lengths. Briefly, a fresh hollow fiber was immersed in 1-octanol for approximately 5 min to impregnate the pores of the fiber with the solvent and then known amounts of 1-octanol (15 μL) as acceptor solution was injected carefully into the hollow fiber by syringe. The hollow fiber filled with 1-octanol was then immersed for extraction into 30 mL of donor solution, which was prepared by mixing 15 mL of pH buffer solution with 15 mL of sample solution (contained 5 μg mL^{-1} surrogate standard). The donor solution was continuously stirred using a magnetic stirrer to facilitate the mass transfer process and reduce the time required to reach equilibrium (80 min). After the extraction time, the acceptor solution in the hollow fiber was withdrawn by the syringe and collected in a 0.7 mL conical vial. A 1 μL of extraction solution was taken to analyze.

2.4. Solid-phase microextraction

The SPME condition was according with our previous work [31]. In briefly, the experiment was conducted using a commercially available polyacrylate fiber with a film thickness of 85 μm, housed in its manual holder (Supelco, Bellefonte, PA, USA). The new polyacrylate fiber was conditioned using the injector port of the GC at 300 °C for 2 h. During extraction, 12.5 mL of the sample was added to 12.5 mL of pH 1 buffer solution saturated with KCl for adsorption 40 min at a stirring rate of 1000 rpm. Then, the extract was

desorbed from the fiber into a GC injector at 290 °C at the maximum length (4.5 cm) of the syringe carriage for 2 min.

2.5. Validation of method

Blank samples were spiked with 2,4-DCP at 1, 25, 50, 75 and 100 ng mL^{-1}, 2,4,6-TCP at 1, 25, 50, 75 and 100 ng mL^{-1}, 2,3,4,6-TeCP at 5, 125, 250, 375 and 500 ng mL^{-1} and PCP at 10, 250, 500, 750 and 1000 ng mL^{-1}, then analyzed by the optimum LPME procedure to generate calibration curves. These curves were obtained by plotting the peak area ratio (analyte to 5 μg mL^{-1} surrogate standard) as a function of the concentration. The limit of detection (LOD) was defined as the concentration in the sample that resulted in a peak with an S/N (signal-to-noise ratio) of three [32]. The limit of quantification (LOQ) was defined as the concentration in the sample that yielded a peak with an S/N of ten [32]. The precision of the assay was evaluated by analyzing the CPs in quality control (QC) samples on the same day. Quality control samples were prepared at three different concentrations of low, medium and high. The low QC concentration sample: 2,4-DCP, 2,4,6-TCP, 2,3,4,6-TeCP and PCP were at 1, 1, 5 and 10 ng mL^{-1}, respectively. The medium QC concentration sample: 2,4-DCP, 2,4,6-TCP, 2,3,4,6-TeCP and PCP were at 50, 50, 250 and 500 ng mL^{-1}, respectively. The high QC concentration sample: 2,4-DCP, 2,4,6-TCP, 2,3,4,6-TeCP and PCP were at 100, 100, 500 and 1000 ng mL^{-1}, respectively.

2.6. Sample preparation

A soil sample was obtained from the CPs-contaminated soil at an abandoned chemical manufacturing site in Tainan (southern of Taiwan). After the soil was shaken through two mesh screens with mesh sizes of 1.981 mm and 2.000 mm, it was collected and stored at 4 °C in a refrigerator. The sample solution was prepared by soaking 30 mg of soil in 15 mL aqueous solution that contained 5 μg mL^{-1} surrogate standard.

Landfill leachate was obtained from a landfill site in Taichung (middle of Taiwan). Ground water was collected from a ground water tap, which was allowed to flow for 10 min. The landfill leachate sample solution was prepared by 15 mL landfill leachate contained 5 μg mL^{-1} surrogate standard. The ground water sample solution was prepared similar to the landfill leachate samples.

3. Results and discussion

3.1. Effect of pH on extraction efficiency

The pH value relates to the equilibrium between the ionized form and the neutral form. Chlorophenols are extracted mainly as neutral molecules in LPME. The results in Fig. 1 indicate that the extraction efficiency increases as the pH value decrease. At low pH, the equilibrium of CPs favors neutral form, which is more soluble in the acceptor solution and has a lower affinity toward donor solution. According to these results, the pH value was adjusted to one in subsequent experiments.

3.2. Effect of salt on extraction efficiency

According to Zhao et al. [33], the effect of salt on extraction can be separated into two simultaneous processes—salting out and electrostatic interactions. The salting out effect increases the amount of extraction at high salt concentration, depending on the solubility of the analytes. The electrostatic interaction method decreases the amount of extraction at high salt concentration, involving attractive forces between charged particles that are dispersed in electrolytes and the analytes. The results in Fig. 2 reveal

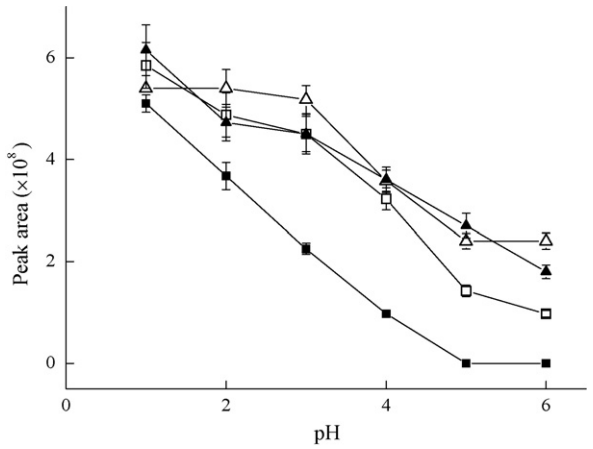

Fig. 1. Effect of pH on peak area of chlorophenols obtained by LPME–GC–MS. Experiment conditions: 100 ng mL^{-1} of 2,4-DCP (△), 100 ng mL^{-1} of 2,4,6-TCP (□), 500 ng mL^{-1} of 2,3,4,6-TeCP (▲) and 1000 ng mL^{-1} of PCP (■); without the addition of NaCl; stirring rate: 550 rpm; extraction time: 30 min.

that the extraction efficiency of the four CPs decreases as the NaCl concentration increases. This phenomenon is explained by the fact that the electrostatic interactions between analytes and the salt ions in the donor solution are stronger than the salting out effect. Hence, no NaCl was added in the following studies.

3.3. Effect of stirring rate on extraction efficiency

Extraction kinetics can be accelerated by agitating samples. Here donor solutions were examined at various stirring rates for 30 min to evaluate the effect of the stirring rates. As shown in Fig. 3, the higher the stirring rate, the better the extraction efficiency for all the studied CPs. This result is consistent with the film theory of convective diffusion [34] that attributes the high extraction efficiency to the continuous exposure of fresh donor solution. Since the extracted amount reached the highest value at 1100 rpm, the same stirring rate was used for ensuing studies.

3.4. Effect of extraction time on extraction efficiency

Liquid-phase microextraction is an equilibrium process between donor solution and acceptor solution [20,30]. Based on

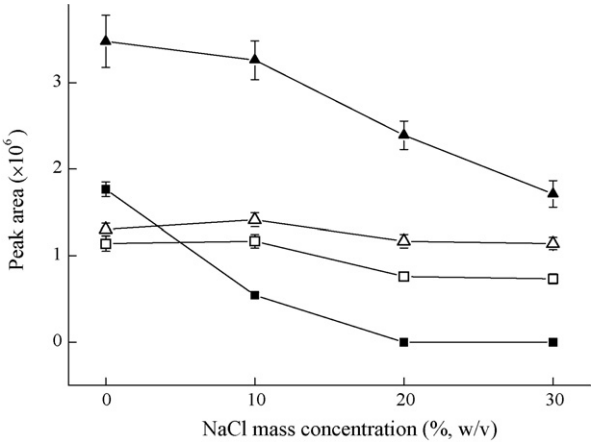

Fig. 2. Effect of salt addition on peak area of chlorophenols obtained by LPME–GC–MS. Experiment condition: 100 ng mL^{-1} of 2,4-DCP (△), 100 ng mL^{-1} of 2,4,6-TCP (□), 500 ng mL^{-1} of 2,3,4,6-TeCP (▲) and 1000 ng mL^{-1} of PCP (■); pH 1 buffer; stirring rate: 550 rpm; extraction time: 30 min.

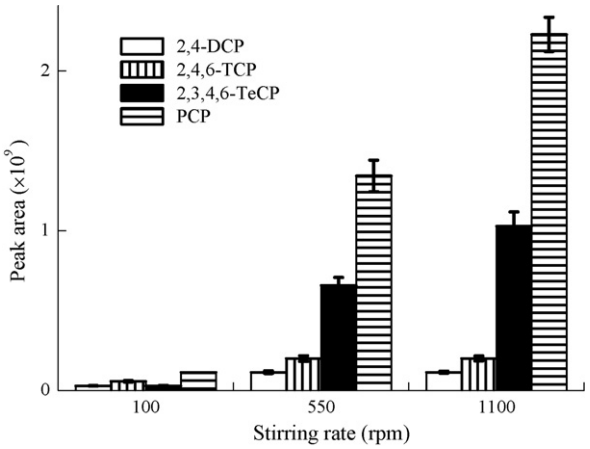

Fig. 3. Effect of stirring rate on peak area of chlorophenols produced by LPME–GC–MS. Experiment condition: 100 ng mL^{-1} of 2,4-DCP, 100 ng mL^{-1} of 2,4,6-TCP, 500 ng mL^{-1} of 2,3,4,6-TeCP and 1000 ng mL^{-1} of PCP; pH 1 buffer; without the addition of NaCl; extraction time: 30 min.

partition coefficient of CPs, this characteristic is particularly beneficial in quantification of the LPME method. It enables substantial portion of the CPs extracted from donor solution to acceptor solution. For this reason equilibrium time was studied herein was 10–180 min. For all studied CPs, the amount extracted increases markedly with the extraction time from 10 to 80 min, as shown in Fig. 4. At 80 min, the amount of extracted CPs reached equilibrium. Therefore, 80 min was used as the optimal extraction time in further analysis. Compared the extraction time with previous literature, which was 30 min [28] and 60 min [17], this developed method is comparatively long may be due to the slow mass transfer for analytes into organic solvent [35].

3.5. Enrichment factor

The enrichment factor can be defined as the ratio of the equilibrium concentration of analytes in the organic phase to the original concentration of analytes in the aqueous phase [36]. Table 2 shows that the enrichment factor in this procedure varies from 117 to 220, depending on the CPs studied. The high enrichment factor is obtained through the optimum conditions, which are mixing 15 mL of pH 1 buffer solution with 15 mL of sample solution with a surrogate standard concentration of 5 μg mL^{-1} at 1100 rpm for 80 min extraction. High enrichment factor is evidence for high partition coefficients of the anlytes and outstanding extraction efficiency in LPME. With the high enrichment factor, this LPME method is capable of reaching low enough detection ranging from 0.08 to 2 ng mL^{-1} and quantification limits between 0.3 and 7 ng mL^{-1}. Compared with other extraction technique, the LOD was 12 ng mL^{-1} for 2,4-DCP by ultrasound-assisted headspace LPME [16], 0.5 μg L^{-1} for 2,4-DCP and 1.0 μg L^{-1} for 2,4,6-TCP by hollow fiber supported ionic liquid membrane extraction [17], and 53 ng g^{-1} for 2,4-DCP, 12 ng g^{-1} for 2,4,6-TCP, 39 ng g^{-1} for 2,3,4,6-TeCP and 120 ng g^{-1} for PCP by focused microwave-assisted micellar extraction combined with SPME [37]. It could be seen that the LODs of the proposed method are fairly better than that obtained by previous works. This result is in agreement with that obtained by Wen et al. [38], which the advantages of high enrichment is capable of achieving lower detection.

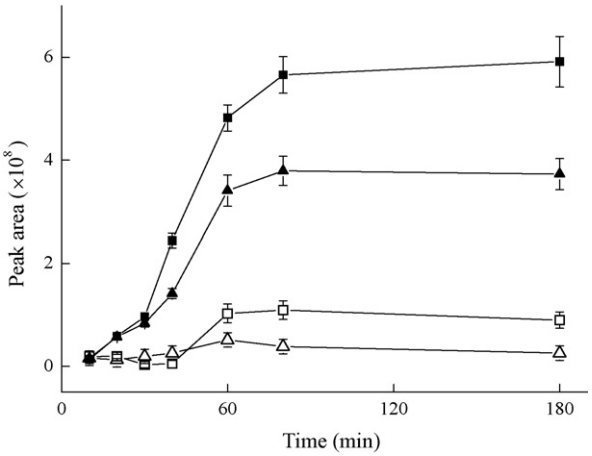

Fig. 4. Effect of extraction time on peak area of chlorophenols produced by LPME–GC–MS. Experiment condition: 100 ng mL^{-1} for 2,4-DCP (△), 100 ng mL^{-1} of 2,4,6-TCP (□), 500 ng mL^{-1} of 2,3,4,6-TeCP (▲) and 1000 ng mL^{-1} of PCP (■); pH 1 buffer; without the addition of NaCl; stirring rate: 1100 rpm.

3.6. Performance of method

The linearity, LOD, LOQ and precision were investigated in water under the aforementioned optimal conditions of LPME coupled to GC–MS procedure, as shown in Tables 2 and 3. The correlation coefficient of each studied analyte is above 0.99 in the range of interest, but correlation coefficient gives insufficient information about the linearity of the curve. A linearity test is performed to give sufficient information about the linearity of curve by comparing the linear calibration function with the nonlinear calibration function. According to DIN 38402 section 51, a test value (TV) was calculated from the residual standard deviation [39]. The TV value was smaller than the *F*-test value as shown in Table 2; therefore the calibration function is linear. The detection response factor (RF) was used to calculate the coefficient of variation (CV). According to Telliard et al. [40], a RF is acceptable if CV < 20%. The CV values calculated are presented in Table 2, where all CVs calculated were less than 10%. Based on the linearity test and considering the small standard error of slope, the analysis of the breakthrough samples was performed using a single calibration curve over the whole concentration range. After generating calibration curves as depicted in Table 2, the linear regression analysis for CPs is observed on the slopes between 0.0035 and 0.0055, intercepts between 0.0483 and 0.1076. With the advantages of high enrichment factor, the obtained LOD and LOQ are in the range of 0.08–2 ng mL^{-1} and 0.3–7 ng mL^{-1}, respectively, competitive with the reported LOD in literature, which were 12–120 ng g^{-1} [37].

Precision in terms of repeatability and reproducibility is expressed as the relative standard deviation (R.S.D.) [41]. Repeatability is the degree of agreement among individual test results when the procedure is applied repeatedly. It was measured from six replicate analyses of the QC samples. As seen in Table 3, the R.S.D.s ranged between 1.15 and 8.87% for repeatability. Even in the low QC concentration, the R.S.D.s are lower than 10% for repeatability. These results for repeatability show the suitability of the LPME–GC–MS technique in the analysis of trace CPs. In the case of reproducibility, six replicates were analyzed for 3 consecutive days at QC samples. The R.S.D.s ranged from 2.92 to 11.63% for reproducibility, as indicated in Table 3. The R.S.D.s of reproducibility are within ±15% for all measurements, it shows the good precision of the method [41].

3.7. Real sample

In order to overcome the difficult extraction from soil, LPME was applied to determine the CPs from the CPs-contaminated soil. This

Table 2
Calibration curve results, limits of detection (LOD), limits of quantification (LOQ) and enrichment factor of chlorophenols in water produced by LPME–GC–MS

Compound	Correlation coefficient	TV	CV (%)	Linear range (ng mL^{-1})	Linear equation	LOD (ng mL^{-1})	LOQ (ng mL^{-1})	Enrichment factor
2,4-DCP	0.9967	0.30	6.29	1–100	$Y = 0.0046X + 0.1018$	0.10	0.33	176
2,4,6-TCP	0.9905	0.05	9.87	1–100	$Y = 0.0055X + 0.1076$	0.08	0.26	117
2,3,4,6-TeCP	0.9983	0.28	3.77	5–500	$Y = 0.0040X + 0.0956$	1.31	4.37	155
PCP	0.9929	0.02	8.91	10–1000	$Y = 0.0035X + 0.0483$	2.01	6.70	220

F-test (0.99, 1, 2) = 98.5.

Table 3
Repeatability and reproducibility for chlorophenols in water spiked at three QC concentrations in water produced by LPME–GC–MS ($n = 6$)

Compound	Repeatability (R.S.D., %)			Reproducibility (R.S.D., %)		
	Low QC concentration	Medium QC concentration	High QC concentration	Low QC concentration	Medium QC concentration	High QC concentration
2,4-DCP	3.28	1.85	1.15	10.39	6.71	2.92
2,4,6-TCP	8.87	1.61	1.34	9.14	3.26	3.21
2,3,4,6-TeCP	7.21	1.51	1.58	11.63	3.06	3.52
PCP	4.05	1.37	1.70	9.26	6.32	6.43

Low QC concentration was spiked 2,4-DCP, 2,4,6-TCP, 2,3,4,6-TeCP and PCP at 1, 1, 5 and 10 ng mL^{-1}, respectively. Medium QC concentration was spiked 2,4-DCP, 2,4,6-TCP, 2,3,4,6-TeCP and PCP at 50, 50, 250 and 500 ng mL^{-1}, respectively. High QC concentration was spiked 2,4-DCP, 2,4,6-TCP, 2,3,4,6-TeCP and PCP at 100, 100, 500 and 1000 ng mL^{-1}, respectively.

method was also utilized to extract CPs from a complex matrix, such as landfill leachate and ground water. Table 4 demonstrates the concentration of CPs determined from the environmental samples by LPME. Two analytes, 2,4-DCP and 2,4,6-TCP were detected in the landfill leachate and the concentrations were 6.68 and 2.47 ng mL^{-1}, respectively. In ground water, only 2.08 ng mL^{-1} of 2,4,6-TCP was detected. In the case of soil samples, all the studied CPs were detected, as seen in Table 4.

To assess quantification analysis, the measured result of LPME is compared with the result obtained by SPME for the environment sample. The SPME condition was according with our previous work [31]. The determined concentrations show no variation, as depicted in Table 4. Furthermore, fewer significant interference peaks in chromatogram (Fig. 5b and c) were obtained than those obtained by using SPME (Fig. 5e and f). Base on the quantification and chromatogram of LPME, it clearly reveals that the LPME–GC–MS technique exactly quantifies CPs and effectively reduces the matrix interference in the environmental samples.

The components of the environmental sample are very complex and the matrix effect reduces the recovery. The environmental samples were spiked with all CPs at medium QC concentration to real samples in order to evaluate the recovery. The recovery is calculated

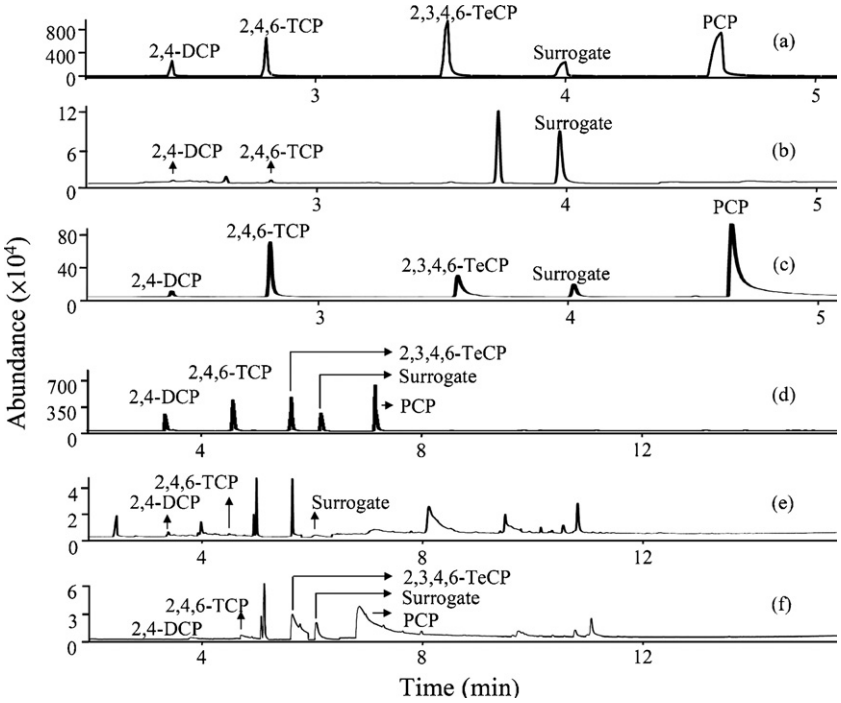

Fig. 5. Mass ion chromatograms (a) 25 ng mL^{-1} of 2,4-DCP, 25 ng mL^{-1} of 2,4,6-TCP, 50 ng mL^{-1} of 2,3,4,6-TeCP and 250 ng mL^{-1} of PCP in water solution produced by LPME–GC–MS; (b) landfill leachate produced by LPME–GC–MS; (c) contaminated soil produce by LPME–GC–MS; (d) 25 ng mL^{-1} of 2,4-DCP, 25 ng mL^{-1} of 2,4,6-TCP, 50 ng mL^{-1} of 2,3,4,6-TeCP and 250 ng mL^{-1} of PCP in water solution produced by SPME–GC–MS (e) landfill leachate produced by SPME–GC–MS; (f) contaminated soil produced by SPME–GC–MS.

Table 4
Comparison of LPME with SPME on environmental samples ($n = 3$)

Compound	SPME							LPME					
	Landfill leachate			Ground water			Soil	Landfill leachate			Ground water			Soil		
	Conc. ($ng\,mL^{-1}$)	Recovery (%)	R.S.D. (%)	Conc. ($ng\,mL^{-1}$)	Recovery (%)	R.S.D. (%)	Conc. ($ng\,mL^{-1}$)	Recovery (%)	R.S.D. (%)	Conc. ($ng\,mL^{-1}$)	Recovery (%)	R.S.D. (%)	Conc. ($ng\,mL^{-1}$)	Recovery (%)	R.S.D. (%)
2,4,-DCP	6.35	58.18	7.44	ND	80.66	5.56	8.19	89.43	4.71	6.68	97.21	10.30	ND	91.39	3.45	7.72	93.02	5.13
2,4,6-TCP	2.72	16.25	6.84	2.39	86.83	5.78	17.08	93.26	6.45	2.47	87.38	3.45	2.08	94.75	9.50	22.93	90.52	1.16
2,3,4,6-TeCP	ND[a]	8.81	9.74	ND	94.22	8.17	38.86	101.88	7.83	ND	89.45	1.24	ND	109.53	4.30	32.16	106.47	4.54
PCP	ND	7.44	11.58	ND	72.74	9.92	48.79	86.86	8.66	ND	65.85	2.84	ND	101.31	4.28	46.90	99.86	3.18

[a] ND: Not detected.

from the ratio of the peak area obtained in environmental sample to that in pure water. In Table 4, the recoveries of SPME were between 7.44 and 58.18% in landfill leachate, 72.74 and 94.22% in ground water, 86.86 and 101.88% in soil. For LPME, the recoveries were between 65.85 and 97.21% in landfill leachate, 91.39 and 109.31% in ground water, 90.52 and 106.47% in soil. In contrast with Peng et al. [17], the recovery was 90.1% for 2,4-DCP and 88.7% for 2,4,6-TCP in ground water. In present study, the recovery in ground water was 91.39% for 2,4-DCP and 94.75% for 2,4,6-TCP. The R.S.D. of SPME was below 11.58% and the R.S.D. of LPME was below 10.30%. Since the LPME recoveries are higher than SPME with smaller R.S.D. value for all environmental samples, it clearly demonstrates that LPME effectively prevent matrix effect from complex environmental matrices.

4. Conclusions

The proposed method is highly successful for determining trace amounts of CPs in environmental samples using LPME coupled with GC–MS without derivatization. Factors that influence the extraction efficiency have been investigated. High enrichment factor is sufficient to establish the outstanding extraction efficiency. The LODs of CPs are 0.08–2 $ng\,mL^{-1}$, revealing the high sensitivity of this method and comparable with the reported value (12–120 $ng\,mL^{-1}$). Under optimal conditions, recoveries of CPs in environmental samples exceed 85% with R.S.D.s of less than 10%, except for PCP in landfill leachate. Liquid-phase microxtraction coupled with GC–MS is favored over SPME and involves no carry-over problem or fewer interference peaks. Based on the simplicity and sensitivity, this method can be recommended to determine CPs in environmental samples.

Acknowledgments

The authors would like to thank the National Science Council of the Republic of China, Taiwan, for financially supporting this research under Contract No. NSC 94-2113-M-005-001. K. David Tau is appreciated for his editorial assistance.

References

[1] R.C.C. Wegman, A.W.M. Hosfstee, Water Res. 13 (1979) 651.
[2] K. Kawamoto, K. Urano, Chemosphere 18 (1989) 1987.
[3] NCI, Bioassay of 2,4,6-Trichlorophenol for Possible Carcinogenicity (CAS No. 88-06-2), Technical Report Series No 155, DHEW (NIH) Publication No. 79-1711, National Institutes of Health, Bethesda, MD, 1979, 131 pp.
[4] Sample and Analysis Procedure for Screening of Industrial Effluents for Priority Pollutants, US Environmental Protection Agency, Environment Monitoring and Support Laboratory, Cincinnati, OH, 1977.
[5] The list of priority substances in the field of water policy and amending directive, Council directive 2455/2001/ECC, Official Journal L331, November 20, 2001, pp. 1–5.
[6] C.C. Lee, Y.L. Guo, C.H. Kuei, H.Y. Chang, J.F. Hsu, S.T. Wang, P.C. Liao, Chemosphere 65 (2006) 436.
[7] M. Kawaguchi, Y. Ishii, N. Sakui, N. Okanouchi, R. Ito, K. Saito, H. Nakazawa, Anal. Chim. Acta 533 (2005) 57.
[8] P. Patnaik, Handbook of Environmental Analysis: Chemical Pollutants in Air, Water, Soil, and Solid Wastes, CRC/Lewis Publishers, Boca Raton, c1997.
[9] A.P. Khodadoust, M.T. Suidan, C.M. Acheson, R.C. Brenner, Chemosphere 38 (1999) 2681.
[10] M.P. Llompart, R.A. Lorenzo, R. Cela, K. Li, J.M.R. Bélanger, J.R.J. Paré, J. Chromatogr. A 774 (1997) 243.
[11] A. Egizabal, O. Zuloaga, N. Etxebarria, L.A. Ferńandez, J.M. Madariaga, Analyst 123 (1998) 1679.
[12] L.J. Fitzpatrick, J.R. Dean, M.H.I. Comber, K. Harradine, K.P. Evans, S. Pearson, J. Chromatogr. A 873 (2000) 287.
[13] A. Buhr, C. Genning, T. Salthammer, Fresenius J. Anal. Chem. 367 (2000) 73.
[14] M.C. Alonso, D. Puig, I. Silgoner, M. Grasserbauer, D. Barcelo, J. Chromatogr. A 823 (1998) 231.
[15] S.P. Huang, S.D. Huang, J. Chromatogr. A 1135 (2006) 6.
[16] H. Xu, Y. Liao, J. Yao, J. Chromatogr. A 1167 (2007) 1.
[17] J.F. Peng, J.F. Liu, X.L. Hu, G.B. Jiang, J. Chromatogr. A 1139 (2007) 165.
[18] K. Reddy-Noone, A. Jain, K.K. Verma, Talanta 73 (2007) 684.

[19] L. Li, B. Hu, Talanta 72 (2007) 472.
[20] J.S. Chiang, S.D. Huang, Talanta 71 (2007) 882.
[21] L. Nozal, L. Arce, B.M. Simonet, Á. Ríos, M. Valcárcel, Electrophoresis 28 (2007) 3284.
[22] N. Vora-adisak, P. Varanusupakul, J. Chromatogr. A 1121 (2006) 236.
[23] P.S. Chen, S.D. Huang, J. Chromatogr. A 1118 (2006) 161.
[24] K.E. Rasmussen, S. Pedersen-Bjergaard, TrAC, Trends Anal. Chem. 23 (2004) 1.
[25] M. Nichkova, M.P. Marco, Anal. Chim. Acta 533 (2005) 67.
[26] T.J. Boyd, J. Chromatogr. A 662 (1994) 281.
[27] N. Campillo, R. Penalver, M. Hernandez-Cordoba, J. Chromatogr. A 1125 (2006) 31.
[28] C. Basheer, H.K. Lee, J. Chromatogr. A 1057 (2004) 163.
[29] M. Ramil Criado, S. Pombo da Torre, I. Rodriguez Pereiro, R. Cela Torrijos, J. Chromatogr. A 1024 (2004) 155.
[30] S. Pedersen-Bjergaard, K.E. Rasmussen, Anal. Chem. 71 (1999) 2650.
[31] M.R. Lee, Y.C. Yeh, W.S. Hsiang, B.H. Hwang, J. Chromatogr. A 806 (1998) 317.
[32] F.Q. Yang, J. Guan, S.P. Li, Talanta 73 (2007) 269.
[33] L. Zhao, L. Zhu, H.K. Lee, J. Chromatogr. A 963 (2002) 239.
[34] K.R. Chitra, A.G. Gaikwad, G.D. Surender, A.D. Damodaran, J. Membr. Sci. 125 (1997) 257.
[35] A. Gjelstad, T.M. Andersen, K.E. Rasmussen, S. Pedersen-Bjergaard, J. Chromatogr. A 1157 (2007) 38.
[36] H.J. Pan, W.H. Ho, Anal. Chim. Acta 527 (2004) 61.
[37] V. Pino, J.H. Ayala, V. Gonzalez, A.M. Afonso, Anal. Chim. Acta 582 (2007) 10.
[38] X. Wen, C. Tu, H.K. Lee, Anal. Chem. 76 (2004) 228.
[39] Deutsches Institut für Normung, DIN 38402 part 51, In Kalibrierung von Analysenverfanhren, Answertung von Analysenergebnissen und lineare Kalibrierfunktionen für die Bestimmung von Verfahrensgrössen, Beuth Verlagm Berlin, Germany, 1986, pp 1–8.
[40] W.A. Telliard, M.B. Rubin, D.R. Rushneck, J. Chromatogr. Sci. 25 (1987) 322.
[41] R. Zanella, E.G. Primel, F.F. Goncalves, A.F. Martins, J. Chromatogr. A 904 (2000) 257.

Talanta 76 (2008) 107–110

Contents lists available at ScienceDirect

Talanta

journal homepage: www.elsevier.com/locate/talanta

Adaptation of a commercial ion selective fluoride electrode to a tubular configuration for analysis by flow methodologies

António C.L. Conceição*, M.M. Correia dos Santos, M.L.S. Simões Gonçalves

Centro de Química Estrutural, Instituto Superior Técnico, Avenida Rovisco Pais, 1049–001 Lisboa, Portugal

ARTICLE INFO

Article history:
Received 19 October 2007
Received in revised form 1 February 2008
Accepted 14 February 2008
Available online 10 March 2008

Keywords:
Fluoride tubular electrode
FIA
SIA
Water analysis

ABSTRACT

The determination of fluoride ions in water samples is accomplished by using a tubular flow through detector constructed by drilling a channel through a commercially available LaF_3 crystal electrode in such a way that the original contacts of the non-modified unit are maintained. Its performance when incorporated in both FIA and SIA systems was evaluated and the results show that the tubular unit retains the characteristics of the non-modified electrode. In SIA conditions an extended linear range of response and lower detection limit were achieved when compared with the electrode performance in FIA conditions. These aspects together with the additional advantage of low sample and reagent consumptions in SIA when compared to FIA, makes the incorporation of the proposed tubular ISE in a SIA system the preferred approach for on line determination and monitoring of fluoride content in natural water samples.

1. Introduction

The fluoride electrode with a LaF_3 membrane is one of the most commonly used ion selective electrodes (ISE) in many analytical applications. Several methodologies based on potentiometric fluoride analysis have been developed and consequently some agencies and associations have adopted fluoride ISE for quantification of fluoride in many different matrices, namely in waters [1]. The reliability of the response characteristics of fluoride ISE makes it suitable to be used as a detector in flowing systems and consequently, the incorporation in such systems has also been the subject of extensive studies. It has been widely used as detector in Flow Injection Analysis (FIA) where the cell types were mainly of the cascade or wall jet design [2–5]. It has also been used in a cell configuration that combines a gradient flow chamber and the electrode as a single unit [6].

Fluoride ion selective electrode is also suitable to be used as detector in Sequential Injection Analysis (SIA) systems though just a few works dealt with the incorporation of fluoride ISE in a SIA manifold [7,8]. This is not surprising since SIA is a much newer technique than FIA [9]. The major advantages of SIA are its versatility and the drastic reduction of sample and reagent volumes used although the sample throughput of SIA is normally less than that of conventional FIA [10].

The performance of flow ISE techniques depends largely on the construction of flow-through potentiometric cells suitable for integration in the flow channels. This study describes the construction of a fluoride ion selective tubular electrode from a commercial unit and its performance when incorporated in both a FIA and SIA system for the determination of fluoride in natural waters. The electrode was constructed by drilling a channel through the LaF_3 crystal of a commercial available solid-state electrode. Recently, the construction of tubular fluoride electrodes to be used in flow systems was reported. The electrodes were constructed from a commercial available LaF_3 membrane by drilling a hole through it. The construction requires several other steps, namely housing the internal reference solution and the electrical contacts [11,12]. To our knowledge this is the first time that a commercial fluoride ISE is used in a tubular configuration, with a user friendly design that makes it possible to use the same internal solution and original contacts of the non-modified commercial unit. In this way the coupling of commercial available fluoride ISE to flow manifolds is achieved with maximum simplicity. The tubular electrode was then used to the determination of fluoride content in mineral waters.

2. Experimental

2.1. Reagents and solutions

The water used in the experiments to rinse and to prepare the solutions was distilled and deionized from a Milli-Q-water purification system. All solutions were prepared with pro-analysis

* Corresponding author. Tel.: +351 21 8419171; fax: +351 21 8464455.
E-mail address: antonio.conceicao@ist.utl.pt (A.C.L. Conceição).

0039-9140/$ – see front matter © 2008 Elsevier B.V. All rights reserved.
doi:10.1016/j.talanta.2008.02.010

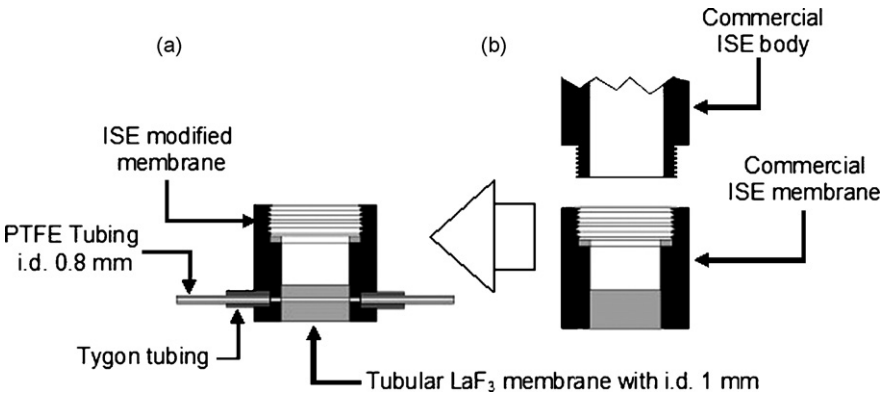

Fig. 1. (a) The structure of the modified commercial fluoride electrode with the tubular LaF_3-membrane. (b) The structure of the commercial fluoride electrode.

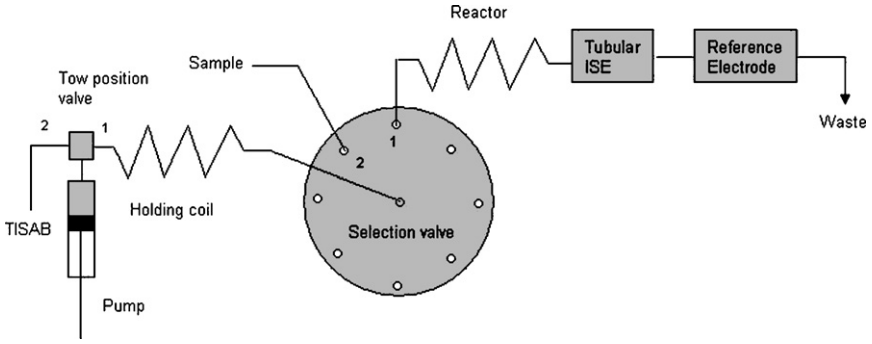

Fig. 2. Sequential injection analysis set-up.

grade reagents. A commercially available sodium fluoride solution (1.8998 g L^{-1}), ORION 940906 (NaF) was used to prepare the standards. In all experiments, a TISAB (Total Ionic Strength Adjustment Buffer) solution was used to adjust the conditions of fluoride analysis. The composition of TISAB was: 0.1M sodium chloride, 0.25M acetic acid, 0.75M sodium acetate and 0.02M sodium citrate [13].

2.2. Construction of the fluoride tubular electrode

The tubular fluoride ion selective electrode was constructed from a commercial available unit (fluoride ISE from Crison, model 9655) that consists of two parts, the commercial ISE body and the ISE membrane, by drilling a channel through the LaF_3 crystal. A 1 mm internal diameter hole was machined with a cobalt drill at 100 rpm, parallel to the crystal surface. Poly(tetrafluoroethylene) (PTFE) tubing (i.d. 0.8 mm) was then connected to the PVC body as shown in Fig. 1.

2.3. Apparatus

All measurements were made in combination with a Metrohm Ag/AgCl (KCl, 3.0 M) reference electrode model 6.0727.000. Both electrodes were incorporated in series in the flow set-ups and connected to a pH/ISE Meter Orion Model 720A. A personal computer was used as a control and data acquisition unit. The interface with the analytical system was made using an Advantech PCL-818L card. A simple computer program was developed for control and data acquisition. Experimental data files (potential vs. time) were then processed using Microsoft Excel spread sheet to obtain relative peak heights in mV.

2.3.1. FIA set-up

The FIA experimental set-up consists of an injection valve (Rheodyne 4 way, RH5020) with a loop of 50 μL, a peristaltic pump Ismatec model Reglo-Digital MS-4/8-100 and a reactor with 0.2 m.

2.3.2. SIA set-up

The manifold used in SIA (Fig. 2), consists of a Valco digital valve, actuated by TTL signals, a Crison model 2031 microburette, with a syringe of 1 mL, used as pump, a reactor with 0.4 m and a holding coil of 0.4 m.

2.4. SIA procedure

The operating sequence used involved the steps detailed in Table 1. In the first step, the two-position valve is directed to position 1, the central communication channel of the selection valve, SV, is directed to port 2 and the holding coil, HC (0.4 m long), is filled with 100 μL of sample. In the second step, the central communication channel of the SV is directed to port 1 (pump is in dispense flow) and the detector is filled with a mixture of sample and buffer coming from the HC and the reactor (0.4 m long). In the third step, the SV is in the same position and the pump is in dispensed flow, the mixture of sample and buffer go to waste. In the fourth step, the

Table 1
Device sequence of one cycle of the SIA system

Step	Two-position valve Position	Selection valve Position	Pump Pick/dispense	Pump Volume handling (μL)
1	1	2	Pick	100
2	1	1	Dispense	205
3	1	1	Dispense	315
4	2	1	Pick	420

Table 2
Relative height of the analytical signal as function of the reactor length in FIA

Reactor length (m)	Relative Height (%)
0.2	99
0.4	100
1	69

Experimental conditions: flow rate, 1 mL min^{-1}, injection volume 50 μL, [F$^-$] = 3.8 mg L^{-1}.

two-position valve is directed to position 2 and pump is in pick flow and the syringe is filled again with the buffer solution. The system is then ready to analyze a new sample. After steps 1, 2 and 4 there was a delay of 5 s and of 10 s for step 3.

The tubing of the manifolds both in FIA and SIA was poly(tetrafluoroethylene) (PTFE) with internal diameter of 0.8 mm.

A low fluoride concentration was always included in the carrier stream (TISAB) to assure a constant conditioning of the electrode surface and contribute to the base line stabilization.

In order to assess the quality of the FIA and SIA results obtained with the tubular electrode configuration, fluoride concentration of the water samples were also determined by the reference method, i.e., direct potentiometric determination with the non-modified commercial fluoride ISE [1].

All experiments were done at room temperature 25 ± 1 °C.

3. Results and discussion

3.1. Flow injection analysis, FIA

Some preliminary studies were performed to optimize the FIA manifold. Injection volume, flow rate and reactor length were varied and optimum values established as a trade-off between the magnitude of the analytical signal and the sampling rate.

The injection volume was set to 50 μL. Larger injection volumes led to an increase in the time of return to the baseline and only slight increase in the signal magnitude while lower injection volumes caused a decrease in the precision of the analysis.

Following this, the length of the reactor was optimized injecting 50 μL of a 3.8 mg L^{-1} standard at a flow rate of 1 mL min^{-1}. Three different coils were tested and the results in terms of relative height of the signal (Table 2) show that a 0.2 m long reactor is the best choice.

A value of 1 mL min^{-1} was adopted for the flow rate as a compromise between sampling frequency and reproducibility. Also, as a stable potential is not achieved in the flow injection measurements, the limit of linearity is reduced at higher flow rates as well as the change in potential over a decadal concentration step [14].

3.1.1. Tubular electrode evaluation

Using the FIA system under the optimized conditions, a study of the tubular electrode functioning characteristics was then carried out. Fluoride standard solutions were analyzed and a graphical output of these determinations is shown in Fig. 3. From the plot of peak potentials vs. logarithms of concentrations of the standards it can be seen that a Nernstian response (slope 2.3RT/F) was

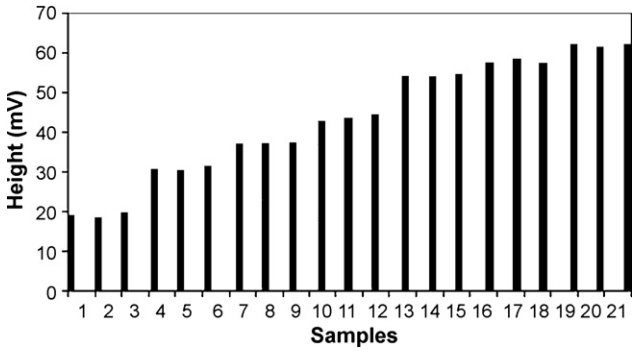

Fig. 3. Recorder output (as height of the analytical signal) of triplicates of seven fluoride standards obtained in FIA with the tubular fluoride ISE. Experimental conditions: fluoride concentration (mg L^{-1}): 0.76; 1.52; 2.28; 3.04; 4.56; 5.32; 6.08, flow rate 1 mL min^{-1}, injection volume 50 μL.

observed for fluoride concentrations above 1.5 mg L^{-1} (Table 3). In the range between 0.5 and 1.5 mg L^{-1} the electrode still exhibits a linear answer thought with a 19 mV slope. Nernstian behavior could be extended over that range using a flow rate lower than 1 mL min^{-1}.

The repeatability of the analytical signal was evaluated by the determination of the relative standard deviation (R.S.D.) values corresponding to consecutive injections of ten standard solutions 1.5 mg L^{-1}. The R.S.D. are expressed as percentage. The limit of detection was calculated as $t \times \sigma$ where σ is the standard deviation of ten independent measurements of the standard 1.5 mg L^{-1} and the t is the student's parameter at 95% confidence level (Table 4).

3.2. Sequential injection analysis, SIA

In SIA experiments the length of the holding coil must be long enough to ensure that the standards and the samples do not fill the syringe while those solutions are being pumped (step 1 in Table 1). For this purpose a 0.40 m long holding coil was selected.

The sample volume and the length of the reactor coil were varied in order to optimize an effective mixing with the TISAB solution, the sensitivity and precision of the procedure. A good volume was found to be 100 μL (Fig. 4) for a 0.40 m long reactor coil. The flow rate (imposed by the syringe volume) was 7 mL min^{-1}.

Table 4
Figures of merit for the methods compared

	FIA	SIA	Batch
Linear range (mg L^{-1})	0.5–1.5 1.5–6.0	0.5–6.0	0.5–6.0
Limit of detection (mg L^{-1})	0.08	0.1	0.05
Reproducibility (%)	6	4	2
Sampling frequency (Sample h^{-1})	65	30	15
TISAB Consumed per determination (μL)	923	420	50000[a]

[a] Estimated value on the basis of the calibration of the ISE and the sample measurement requires 25.0 mL of solution.

Table 3
Features of the calibration graphs

Method	Linear range mg L^{-1}	Linear calibration	r	Standard error
FIA	0.5–1.5	$E = -19(\pm2)\log C_p + 6.6(\pm0.2)$; $n = 5$	0.987	0.51
	1.5–6.0	$E = -56(\pm1)\log C_p + 14.7(\pm0.7)$; $n = 5$	0.999	0.37
SIA	0.5–6.0	$E = -56(\pm3)\log C_p + 52.4(\pm0.6)$; $n = 5$	0.994	1.2
Batch	0.5–6.0	$E = -59.40(\pm0.07)\log C_p + 99.30(\pm0.02)$; $n = 9$	1.00	0.060

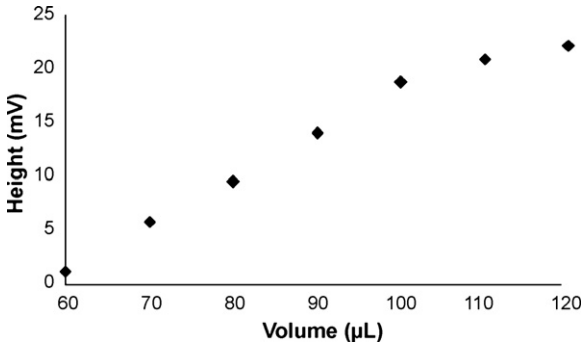

Fig. 4. Height of the analytical signal as a function of the sample volume pumped during step 1 in SIA with a 0.40 m long reactor coil.

Table 5
Recovery of fluoride added to tape water using batch, FIA and SIA methods

	Fluoride determined ($mg\,L^{-1}$)	Fluoride added ($mg\,L^{-1}$)	Fluoride recovery (%)
Batch	0.397	0.380	105
	0.586	0.570	103
FIA	0.903	0.950	95
	1.10	1.14	96
SIA	0.848	0.950	89
	1.59	1.52	105

Table 6
Comparison of the results obtained with the fluoride ISE tubular electrode in FIA and SIA with those from the non-modified fluoride ISE in the reference procedure

Sample	Batch Concentration ($mg\,L^{-1}$)	FIA Concentration ($mg\,L^{-1}$)	SIA Concentration ($mg\,L^{-1}$)
Mineral water Pedras	1.20 (±0.01)	1.39 (±0.08)	1.30 (±0.08)
Mineral water Vidago	0.67 (±0.01)	0.83 (±0.08)	0.76 (±0.08)
Mineral water Carvalhelhos	0.44 (±0.01)	0.49 (±0.08)	0.47 (±0.08)
Water Fontenova	1.52 (±0.01)		1.54 (±0.08)

3.2.1. Tubular electrode evaluation

The response characteristics of the fluoride tubular electrode were evaluated for the proposed SIA configuration using different standards as in the FIA experiments. The resulting data (peak potentials vs. logarithms of concentrations of the standards) are summarized in Table 3. The figures of merit of the method, determined as above, can be seen in Table 4.

For comparison the analytical parameters of the conventional fluoride ISE were also evaluated in batch configuration.

The results presented for the performance of the tubular fluoride electrode, show that the intrinsic response characteristics of the commercial fluoride ISE used to construct the tubular unit are maintained. Throughout the experiments the tubular electrode incorporated in the flowing systems showed a very good response with average slopes close to the theoretical value (Table 3). In terms of linearity the incorporation of the tubular ISE in the SIA manifold shows a better performance leading to a lower limit with Nernstian response when compared to the FIA configuration.

3.3. Analysis of samples

The performance of the fluoride tubular electrode in both FIA and SIA was further evaluated by its application to the determination of fluoride in tap and mineral waters. In the analysis of tap water samples, fluoride additions were made since no fluoride was detected. The quality of the results obtained was evaluated by comparing them with those of the reference method.

Recoveries of fluoride added to tap water samples are presented in Table 5 and as can been seen average recoveries of 99 ± 6% were obtained. Application to fluoride analysis in mineral waters is shown in Table 6. The regression analysis established between the results obtained by the flow methodologies C_F and by the conventional procedure C_c (7 data points) obeys the relationship $C_c = -0.05\ (\pm 0.07) + 0.96\ (\pm 0.06) C_F$ with a correlation coefficient of $r = 0.989$ and a standard error of $\sigma = 0.068$. The results provide by the ISE tubular electrode in the flowing systems compared quite well with those obtained by the reference procedure using a conventional fluoride ISE.

4. Conclusion

The widespread of flow ISE techniques largely depends on the availability of user friendly tubular electrodes that can be easily incorporated in a flow manifold. The construction procedure here reported for the tubular detector is simple and easy to establish in most laboratories. For the first time, a fluoride ion-selective electrode in a tubular design was easily constructed using a commercial unit by drilling a channel with internal diameter compatible with the diameter of tubing used in flow systems while using the same internal contacts of the original unit. This design renders the tubular ISE suitable for its incorporation in both FIA and SIA manifolds. Characterization of the tubular electrode performance in both type of flowing systems shows that it retains the characteristics of the non-modified unit, namely a Nernstian type behavior. In SIA conditions an extended linear range of response was achieved, when compared with the electrode performance in FIA conditions, with a slope according to Nernst type equation. This aspect together with the additional advantage of low sample and reagent consumption in SIA when compared to FIA, makes the incorporation of the proposed tubular ISE in a SIA system suitable for on line determination of fluoride content in natural water samples. The detection limit obtained is suitable for fluoride control in potable waters where current EU legislation stipulates that the maximum level should be 1.5 $mg\,L^{-1}$ [15].

Acknowledgment

The authors thank FCT for financial support.

References

[1] U.S. Environmental Protection Agency, Methods for Chemical Analysis of Water and Wastes, Method 340.2, Environmental Monitory and Support Laboratory Office of Research and Development, U.S.EPA, Cincinnati, OH, 1991.
[2] W. Frenzel, P. Bratter, Anal. Chim. Acta 338 (1986) 127.
[3] H. Hara, K. Yabuuchi, M. Higashida, M. Ogawa, Anal. Chim. Acta 364 (1998) 117.
[4] R.I. Stefan, J.F. van Staden, H.Y. Aboul-Enein, Pharma. Acta Helv. 73 (1999) 307.
[5] K. Itai, H. Tsunoda, Clin. Chim. Acta 308 (2001) 163.
[6] A.C. Lopes da Conceição, M.M. Correia dos Santos, M.L. Simões Gonçalves, F.J.V. Santos, Talanta 50 (2000) 1245.
[7] J. Alpizar, A. Crespi, A. Cladera, R. Forteza, V. Cerdà, Electroanalysis 8 (1996) 1051.
[8] J.F. van Staden, R.I. Stefan, S. Birghila, Talanta 52 (2000) 3.
[9] J. Ruzicka, G.D. Marshall, Anal. Chim. Acta 237 (1990) 329.
[10] J. Ruzicka, Anal. Chim. Acta 261 (1992) 3.
[11] M. Bralic, E. Generalic, S. Krka, Anal. Lett. 33 (2000) 1811.
[12] J.R. Santos, R.A.S. Lapa, J.L.F.C. Lima, Anal. Chim. Acta 583 (2007) 429.
[13] M.S. Frant, J.W. Ross Jr., Anal. Chem. 40 (1968) 1169.
[14] E. Lindner, K. Tóth, E. Pungor, Pure Appl. Chem. 58 (1986) 469.
[15] European Drinking Water Directive, 98/83/CE.

Talanta 76 (2008) 200–205

Contents lists available at ScienceDirect

Talanta

journal homepage: www.elsevier.com/locate/talanta

Ripening and geographical characterization of Parmigiano Reggiano cheese by ^{1}H NMR spectroscopy

R. Consonni*, L.R. Cagliani

Istituto per lo Studio delle Macromolecole, Lab. NMR, CNR, v. Bassini 15, 20133 Milan, Italy

ARTICLE INFO

Article history:
Received 30 October 2007
Received in revised form 15 February 2008
Accepted 20 February 2008
Available online 4 March 2008

Keywords:
Parmigiano Reggiano
PCA
PLS-DA
O-PLS
^{1}H NMR

ABSTRACT

Samples of Italian Parmigiano Reggiano cheese of different ripening stages (14, 24 and 30 months) were analyzed by ^{1}H NMR spectroscopy and the water-soluble metabolites content compared with samples of "Grana type" cheese from east Europe countries. Different multivariate statistical protocols were examined to build up a stable model for both ripening and geographical discrimination among the samples. The discriminant approach revealed a larger metabolite content increasing with ripening process; in particular younger samples were characterized by a higher content in leucine and isoleucine, while 30 months samples by a larger extent of threonine.

The use of a classification approach resulted in a better discrimination of geographical samples. Foreign "Grana type" samples resulted well differentiated with respect to all Italian samples of Parmigiano Reggiano cheese. Foreign samples were characterized by a large amount of leucine and isoleucine, compounds that typified young Italian samples (14 months), and also by lactate, butanoate and acetate, thus suggesting short ripening for foreign samples. Parmigiano Reggiano samples were instead characterized by a large amount of all other compounds, in particular by threonine, which typified old samples (30 months), and other amino acids.

1. Introduction

Parmigiano Reggiano is probably the most appreciated Italian cheese all over the world and several studies have been devoted in the last years to both this and Grana Padano cheese, by the use of different analytical techniques. During the ripening period, which implies several modifications of different complexities, the cheese components undergo important chemical/physical and enzymatic modifications. The biochemical transformations give rise to flavour, taste and appearance, which are characteristic and unique, ensuring typicalness and the quality of the product. The enzymes play a dominant role during ripening: they are of different origins and give rise to protein pre-digestion to oligopeptides, peptides, peptones and free amino acids. Oligopeptides have been identified and quantified in both Grana Padano and Parmigiano Reggiano cheese [1,2] as well as free amino acids [3,4] with the purpose of ripening correlation. The concentration of these fractions are very high in "Grana type" with respect to other "hard" cheeses: in particular free amino acids are the most dominant and important metabolites in the final product. As a matter of fact free amino acids content, expressed as percentage of the total proteins is the index for solubility and digestibility for caseins and for product, respectively [5,6], β-casein being the primary source of free amino acids production.

Particular attention has been devoted to pyroglutamic acid, present in high amount in different cheese varieties [7–9]; it has been suggested that its content can be used as an index for assessing the ripening of Parmigiano Reggiano and Grana Padano cheese [10,11]. Very recently, combined use of solid state NMR spectroscopy and chemometrics has been used for characterization of Parmigiano Reggiano cheese; the evolution in time of the metabolic profile has been monitored in order to assess the ripening time [12], limited to samples up to 24 months of ripening. The authors, on the basis of their results, suggested aspartic acid, methionine and serine as the most abundant amino acids characterizing 18 months samples while citrulline and tyrosine showed lower content for longer ripening time of Parmigiano Reggiano samples (24 months). These results were somehow different from that found originally [3]: high level of serine and ornithine and low concentration of glutamine and arginine with increasing the ripening process.

The sensory quality of Parmigiano Reggiano cheese has been suggested to be affected by free amino acids and fatty acids content, contributing to distinctive taste features. In particular short chain fatty acids contribute directly to cheese flavour, while free amino acids contribute indirectly to cheese flavour by acting as a precursors for the production of volatile compounds, as a secondary

* Corresponding author. Tel.: +39 02 23699578; fax: +39 02 23699620.
E-mail address: roberto.consonni@ismac.cnr.it (R. Consonni).

0039-9140/$ – see front matter © 2008 Elsevier B.V. All rights reserved.
doi:10.1016/j.talanta.2008.02.022

event, through a series of reactions. Extensive studies have been focused on the characterization of aroma and volatile compounds by the use of chromatographic techniques [13–17]: a recent work [18] indicated some aldehydes and acids as key components to the aroma of Parmigiano Reggiano on the basis of odor activity values calculated on the sensory threshold present in the literature.

In the present study, the water-soluble metabolites content of Parmigiano Reggiano cheese was related to ripening (14, 24 and 30 months) by the use of different multivariate statistical protocols in combination with high resolution NMR spectroscopy. Furthermore, a geographical discrimination among Parmigiano Reggiano cheeses and other analogue "Grana type" cheeses from east Europe countries present on the Italian market was evaluated.

2. Experimental

2.1. Sample preparation and NMR experiments

A total number of 33 samples have been used for NMR analysis. Among them 25 were Italian Parmigiano Reggiano cheeses of 14, 24 and 30 months of ripening (10, 8 and 7 samples, respectively), from both hill and plain sites; 8 were "Grana type" cheeses coming from east Europe countries, whose ripening stage was unknown. Each Italian sample was originally consisting of a single small cube packed derived from the middle of the mould. Samples from east Europe countries were bought directly. pH values were measured for all samples and resulted between 5.48 and 5.73. For this reason we did not add any buffer, also to preserve the compound ratio in the water solution.

100 mg of Parmigiano Reggiano samples were dissolved into 600 μL of D_2O and after centrifugation only 500 μL of supernatant were used as NMR sample. All spectra were acquired at 11.7 T on Bruker DMX 500 spectrometer operating at 500.13 MHz proton frequency. Spectra were recorded at 300 K, with a spectral width of 7500 Hz and 32K data points, 90° pulse of 9 μs at 2 db of attenuation, acquisition time of 2.8 s, relaxation time of 2 s and 128 scans, and referenced to sodium trimethylsilyl [2.2.3.3-$^2H_4$] propionate (TSP). Solvent suppression was achieved by applying a presaturation scheme with low power radiofrequency irradiation for 1.2 s. Standard pulse sequences were employed for bi-dimensional TOCSY, HSQC and HMBC experiments, acquired to solve signal overlapping of particularly crowed regions, with the use of WATERGATE module for solvent suppression [19] and with TOPSPIN software package (version 1.3. Bruker GmbH). Heteronuclear experiments were acquired with a spectral width of 25150 Hz, 256 scans and optimized for a long range coupling of 4 Hz. In addition, selective 1D TOCSY experiments were employed to further improve the signal assignment (shaped Gaussian 90° pulse of 40 ms and standard Bruker pulse sequence were used). ^{1}H NMR spectra were analyzed and processed automatically with ACD/Spec Manager (ACD Labs, version 8.12) software. The spectra were scaled to TSP signal for quantitative evaluation.

3. NMR data processing and multivariate analysis

Spectral intensities were calibrated to TSP reference signal and reduced to integrated regions (buckets) of equal width over spectral region from 0.4 to 10.5 ppm with the exclusion of the water region: the complete spectra resulted splitted into 485 buckets of 0.02 ppm each. No significant resonance shifts were observed for all signals that could justify a different bucket size. Bucket centred at 1.32 ppm (1.31–1.33) labelled as threonine, was quantified by subtraction of the following bucket (1.33–1.35), constituted only by one resonance of lactate doublet. The generated files, containing the "buckets" of equal width, were imported into SIMCA-P program (version 11 UMETRICS, Umea, Sweden) and subjected to "mean centering" before statistical analysis [20]. In some cases, even though small sized buckets were considered, single bucket contains resonances from different amino acids. In many areas of life science and especially in food science, classification problem is often counter parted by regression approach. This in terms of discrimination between groups and interpretation of group differences in meaningful ways. Several linear regression approaches exist, like Partial Least Square (PLS) [21], which is largely applied to spectroscopic data. In a typical setting, with n samples (X_i, Y_j matrix) PLS builds a linear relationship between X and Y that is then used to predict Y for new X data. The regression algorithm of PLS, searches for the direction adequate to explain the maximum variance among variables but weighting the variables upon their higher or lower correlation with the response variable. Data pre-treatment like Orthogonal Signal Correction (OSC) sometimes greatly improves the calibration model when the signal contains large systematic variation in the X block not related to the responses Y (buckets and ripening, respectively, in our case). Recently, a further development of OSC has been reported [22,23]. This approach, called Orthogonal PLS (O-PLS), consists of a new way to decompose the PLS solution into two components: (a) components orthogonal to Y and (b) components correlated to Y. We used this procedure to enhance the relevant information while decreasing or eliminating any structured noise in the data. As a matter of fact all structured variations from X (e.g. spectral data) that are not related (Y-orthogonal or pseudo-orthogonal components) to Y are removed thus optimizing the linearity correlation between X and Y (t_1/u_1 plot).

4. Results and discussion

4.1. Ripening sample analysis

^{1}H NMR spectrum of Parmigiano Reggiano aqueous extract is largely dominated by the presence of free amino acids in combination with small quantities of fatty acids and organic acids. The high quality of the spectra enables the identification and attribution of the most of the water-soluble components (Fig. 1); standard TOCSY, HSQC and HMBC spectra lead to unambiguous assignment (proton and carbon chemical shifts) of 23 amino and organic acids spin systems while other 6 spin systems of unknown compounds have been detected. Chemical shift values were found largely in according to the values reported in the literature [24]. In particular, spectra were dominated by large amount of lactate (Lac) for all samples in contrast with relatively small amounts of butanoate (But) and formiate (For). Table 1 summarized all the observed systems. In case of ambiguous spin system assignment, addition of single compound was performed for comparison.

Preliminarily statistical analysis with unsupervised technique like Principal Component Analysis (PCA) was performed on all Italian samples (25) used for NMR determination, to detect possible samples differentiation derived from NMR data of the water-soluble fractions. Spectra of aged samples of 14, 24 and 30 months were subjected to the "bucket" integration, as described in the previous section, and imported into SIMCA-P program to compute PCA analysis. Four PC's adequately explained 93.5% of the variance, with PC1 = 55.6%, PC2 = 23.1% and Q^2 = 0.83. The scatter 3D plot in Fig. 2 showed that clear separation among samples according to different ripening stage is feasible: only two samples of 30 months (highlighted by a circle) resulted different with respect to the other samples of the same ripening, most likely due to sample imperfection. For this reason these two samples were not considered

Table 1
Resonance assignment of Parmigiano Reggiano cheese water solution: ^{1}H and ^{13}C chemical shifts are reported on the basis of TOCSY, HSQC and HMBC experiments

Compound	Assignment	^{1}H ppm	^{13}C ppm
Acetate	α-CH_3	1.93	23.62
Acetoacetate	γ-CH_3	2.45	33.58
	α-CH_2	3.21	54.7
Alanine	β-CH_3	1.47	16.81
	α-CH	3.76	51.22
	γ-CH_2	1.63	25.16
	γ′-CH_2	1.69	25.16
Arginine	β,β′-CH_2	1.89	28.35
	δ,δ′-CH_2	3.23	41.24
	α-CH	3.75	55.25
	β-CH_2	2.85	35.1
Asparagine	β′-CH_2	2.95	35.1
	α-CH	4	52.01
	β-CH_2	2.68	37.11
Aspartic acid	β′-CH_2	2.81	37.11
	α-CH	3.89	52.87
	γ-CH_3	0.88	13.68
Butanoate	β-CH_2	1.57	n.d.
	α-CH_2	2.18	n.d.
Citrulline	γ,γ′-CH_2	1.59	25.55
	β,β′-CH_2	1.88	28.31
	δ,δ′-CH_2	3.13	39.89
	α-CH	3.75	55.25
Formic acid	HCOO	8.64	166.15
	β,β′-CH_2	2.09	27.44
Glutamic acid	γ,γ′-CH_2	2.35	33.87
	α-CH	3.75	55.2
Glycine	α-CH_2	3.55	42.16
Isoleucine	δ-CH_3	0.93	11.74
	γ-CH_3	1	15.25
	γ-CH_2	1.25	25.23
	γ′-CH_2	1.46	25.23
	β-CH	1.98	36.59
	α-CH	3.66	60.26
Lactate	β-CH_3	1.32	20.76
	γ-CH	4.13	69.35
Leucine	δ,δ′-CH_3	0.95	21.61/22.58
	β,β′-CH_2	1.69	40.37
	γ-CH	1.69	24.84
	α-CH	3.72	54.39
	γ,γ′-CH_2	1.46	21.96
	δ,δ′-CH_2	1.72	26.95
Lysine	β,β′-CH_2	1.89	30.57
	ε,ε′-CH_2	3.01	39.69
	α-CH	3.75	55.2
Methionine	ε-CH_3	2.12	14.58
	β,β′-CH_2	2.12	30.62
	γ,γ′-CH_2	2.63	29.57
	α-CH	3.86	54.65
Phenylalanine	β-CH_2	3.12	37.01
	β′-CH_2	3.29	37.01
	αCH	3.98	56.81
	2,6-CH	7.33	130.24
	3,5-CH	7.42	129.99
	4-CH	7.37	128.55
Proline	γ,γ′-CH_2	1.99	24.45
	β-CH_2	2.06	29.73
	β′-CH_2	2.35	29.73
	δ-CH_2	3.32	46.76
	δ′-CH_2	3.41	46.76
	α-CH	4.12	62
Pyroglutamic acid	γ,γ′-CH_2	2.05	29.74
	β-CH_2	2.4	26.05
	β′-CH_2	2.49	26.05
	α-CH	4.17	58.86
Serine	α-CH	3.84	57.13
	β,β′-CH_2	3.96	60.75
Threonine	γ-CH_3	1.32	19.91
	α-CH	3.58	61.11
	β-CH	4.25	66.62
	β-CH_2	3.08	36.28
	β′-CH_2	3.19	36.28
Tyrosine	α-CH	3.93	56.86
	3,5-H	6.89	116.67
	2,6-H	7.18	131.68
Valine	γ-CH_3	0.98	17.37
	γ′-CH_3	1.03	18.57
	β-CH	2.26	29.74
	α-CH	3.6	61.1
Unknown A		1.5	n.d.
		3.29	26.83
		3.48	n.d.
		4.01	54.5
		3.54	63.19
Unknown B		3.63	63.19
		3.77	72.8
Unknown C		4.15	64.27
Unknown D		1.46	n.d.
		3.77	n.d.
Unknown E		2.39	30.32
Unknown F		2.12	27.47

in the following statistical protocols. The corresponding "loading plot" (data not shown) indicated that samples with different ripening stage were characterized by different amount of amino acids. In particular oldest samples (30 months) were characterized by larger content of threonine (Thr, bucket at 1.31–1.33 ppm) and valine (Val, bucket at 0.97–0.99 ppm); medium aged samples (24 months) by other amino acids, like proline (Pro, buckets from 1.97 to 2.07 ppm, from 2.31 to 2.39 ppm and from 4.09 to 4.15 ppm), glutamic acid (Glu, buckets from 2.01 to 2.15 ppm, from 2.31 to 2.39 ppm and bucket at 3.73–3.75 ppm), lactate (Lac, buckets from 1.33 to 1.35 ppm and from 4.09 to 4.17 ppm), citrulline (Cit, buckets from 1.53 to 1.57 ppm, from 1.85 to 1.91 ppm, bucket at 3.13–3.15 ppm and buckets from 3.73 to 3.77 ppm), arginine (Arg, buckets from 1.67 to 1.73 ppm, from 1.87 to 1.91 ppm and from 3.73 to 3.77 ppm), serine (Ser, bucket at 3.83–3.85 ppm and buckets from 3.93 to 3.99 ppm), alanine (Ala, buckets from 1.45 to 1.49 ppm and from 3.73 to 3.79 ppm), lysine (Lys, buckets from 1.39 to 1.53 ppm, from 1.67 to 1.73 ppm, from 1.85 to 1.91 ppm, from 2.99 to 3.03 ppm and from 3.73 to 3.77 ppm), pyroglutamic acid (Pyr, buckets from 2.03 to 2.09 ppm, from 2.37 to 2.41 ppm, from 2.45 to 2.51 ppm and bucket at 4.15–4.17 ppm), glycine (Gly, buckets from 3.53 to 3.57 ppm) and by acetate and acetoacetate signals (Ace and Ac ace, buckets at 1.93–1.95 ppm and at 2.45–2.47 ppm, respectively). Young samples (14 months) were characterized by larger content of leucine (Leu, bucket at 0.95–0.97 ppm) and isoleucine (Ile, bucket at 0.99–1.01 ppm).

To investigate the possible relationship between a descriptor matrix *X* and a response matrix *Y* we applied an improved regression method, O-PLS, which enables the elimination of strong systematic orthogonal variation with respect to *Y* from a given dataset *X*, like the so called "structured noise". As a matter of fact, NMR signals could be affected by several sources of noise

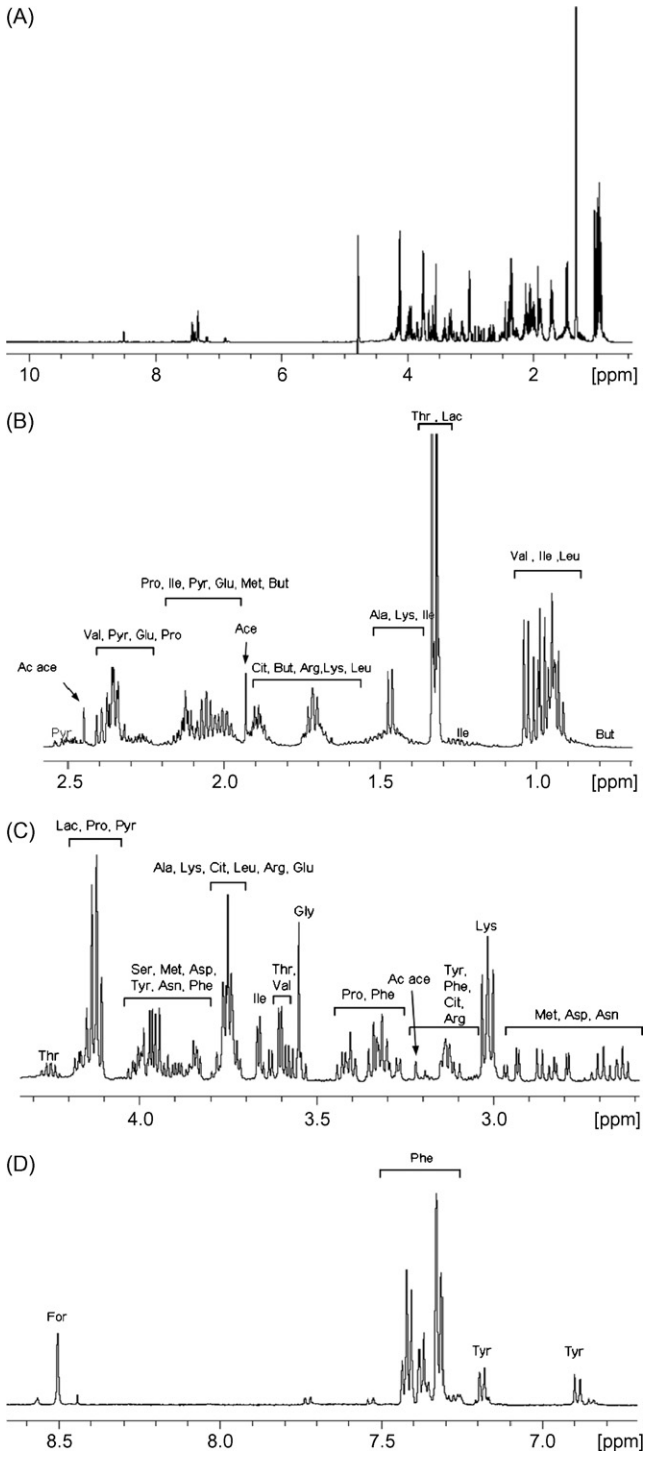

Fig. 1. ^{1}H NMR spectrum of "Parmigiano Reggiano" aqueous extract sample. Complete spectrum (A) and expanded regions (B, C, D) with principal spin system assignments indicated.

information, such as temperature, pH and electronic instabilities and the use of O-PLS could improve this source of "noise" information with further advantage of improved detection limit for outliers in the scores, predictions and simplification of data interpretation.

O-PLS score plot in Fig. 3

performed on the 23 samples revealed that two PC's accounted for 71.8% of the total variance (PC1 = 57.6%, PC2 = 14.2% and

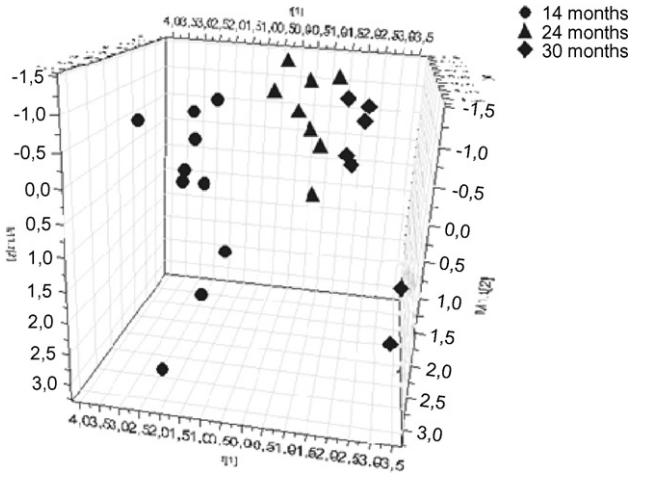

Fig. 2. PCA scatter 3D plot obtained by using all Italian samples: PC1 = 55.6%, PC2 = 23.1%. R^2 = 0.94 and Q^2 = 0.83. Filled symbols represent samples of 14 (circle), 24 (triangle) and 30 (diamond) months of ripening, respectively.

Q^2 = 0.89). Validation of the model was performed by distance to model in the *X* space and showed no strong outliers for this model. Score contribution plots for the analyzed samples (Fig. 4) represented the buckets contribution for samples differentiation and can be used to compare the metabolite content that differentiated the ripening process of samples. They substantially revealed a generally larger amino acids content increasing with ripening

Table 2
Most relevant Variable Importance in the Projection (VIP) relative to the O-PLS model

ppm	Compounds	VIP
0.95...0.97	Leu	7.47027
1.31...1.33	Thr	6.92123
0.97...0.99	Val	5.45549
2.35...2.37	Pro_Glu	5.35368
3.73...3.75	Ala_Glu_Lys_Arg_Cit	4.59369
3.53...3.55	Gly	4.43548
2.37...2.39	Pyr_Pro_Glu	4.34932
3.95...3.97	Ser	4.27027
3.01...3.03	Lys	4.12795
2.33...2.35	Pro_Glu	3.84061
2.05...2.07	Glu_Pro_Pyr	3.69884
1.87...1.89	Lys_Cit_Arg	3.25946
1.93...1.95	Ace	3.25168
2.01...2.03	Pro_Glu	2.90093
2.99...3.01	Lys	2.8566
1.45...1.47	Lys_Ile_Ala	2.74338
1.89...1.91	Lys_Cit_Arg	2.69711
3.75...3.77	Ala_Glu_Lys_Arg_Cit	2.55078
2.03...2.05	Glu_Pro_Pyr	2.39458
4.11...4.13	Lac_Pro	2.37454
1.47...1.49	Lys_Ile_Ala	2.33798
2.45...2.47	Ac ace_Pyr	2.2385
2.39...2.41	Pyr	2.21037
1.29...1.31	Ile_Thr	2.18316
1.71...1.73	Lys_Leu_Arg	2.10311
1.97...1.99	Pro_Ile	2.04325
0.93...0.95	Leu_Ile	1.97721
1.99...2.01	Pro_Ile	1.97349
3.31...3.33	Pro_Phe	1.96206
4.13...4.15	Lac_Pro	1.90822
2.07...2.09	Glu_Pro_Pyr	1.90256
2.11...2.13	Met_Glu	1.89945
3.83...3.85	Ser	1.78806
3.93...3.95	Ser_Tyr	1.71895
1.03...1.05	Val	1.69048
3.33...3.35	Pro	1.64321
2.09...2.11	Met_Glu_Pro	1.63439
0.99...1.01	Ile	1.6073

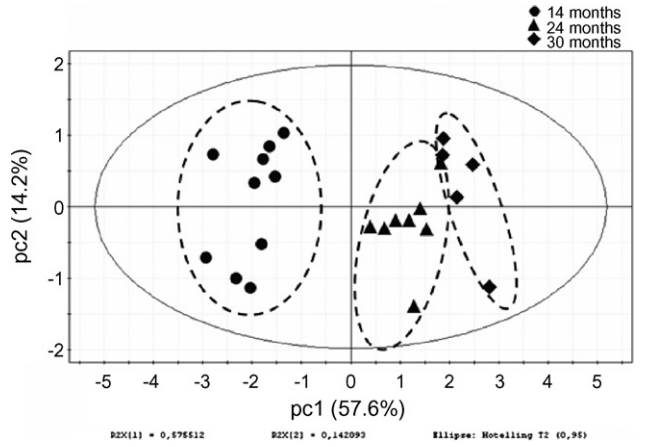

Fig. 3. Score plot of O-PLS model obtained by considering 23 Italian samples. Filled symbols represent samples of 14 (circle), 24 (triangle) and 30 (diamond) months of ripening. PC1 = 57.6%, PC2 = 14.2%, $R^2X = 71.8\%$, $R^2Y = 92.7\%$ and $Q^2 = 0.89$.

process, highly evident for Thr, while further specific differences can be observed. Youngest samples (14 months of ripening) showed a higher content in Leu and Ile with respect to the oldest samples (30 months of ripening). By comparing 30 and 24 months of ripening samples, the larger extent of Thr for the oldest samples was evident, while Ile seemed more abundant in 24 months samples. The comparison between 24 and 14 months samples indicated globally larger amino acids content for older samples while younger ones resulted Leu reach. This increase in amino acids content is in according to previous results [3] that indicated also how the amino acids content could be largely influenced by the production site (mountain or hill or plain). Our results are not in agreement with previously published data [12] most likely due to the differences in both ripening and origin of the samples considered. The Leu lack in older samples resulted in agreement with the well-known catabolism of the branched amino acids, where Leu, Ile and Val were degraded by a number of pathways into volatile compounds, important for cheese flavour.

In order to establish the importance of each *X* variable we calculated the VIP (Variable Importance in the Projection) parameter [25]. This parameter measures the influence on the *Y* variable of all *X* variables in the model. Terms with largest VIP (up to 1.6) were the most relevant for explaining the response. In particular, Table 2 showed the largest VIP: from the list it was evident that the most affecting variables was Leu, followed by other amino acids like Thr, Val, Pro and Glu.

4.2. Geographical discrimination

A classification approach, like Projection to Latent Structures Discriminant Analysis, PLS-DA, could be better used to correlate spectral data and samples origin in an unbiased way recognizing the compounds playing the main role in the geographical samples discrimination. In this respect, PLS-DA was performed on all samples, with two classes approach: Italian and foreign samples. Two PC's adequately explained 72.5% of the variance, with PC1 = 35.1%, PC2 = 37.4% and $Q^2 = 0.76$. For each class we evaluated the correct classification rate by means of misclassification test; 93.5% of samples resulted correctly classified. The

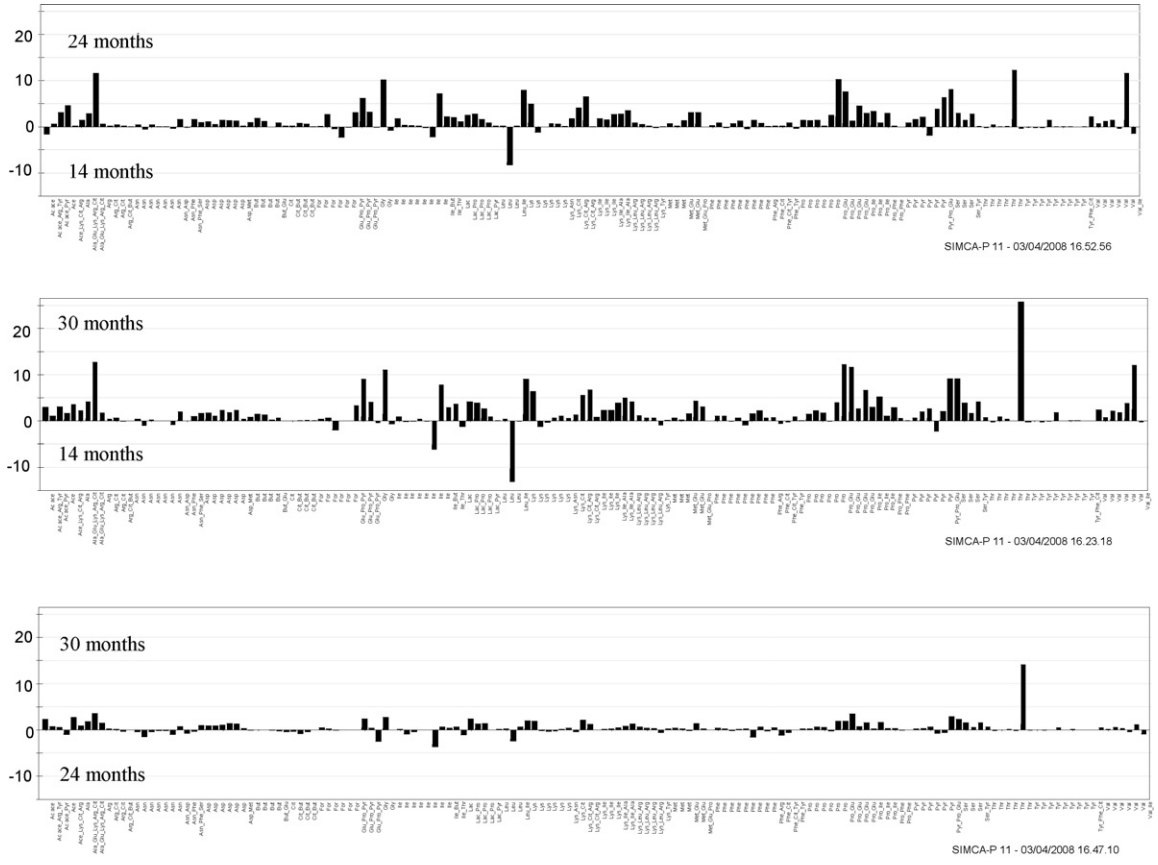

Fig. 4. Score contribution plots from O-PLS model comparing different aged samples of Parmigiano Reggiano cheese.

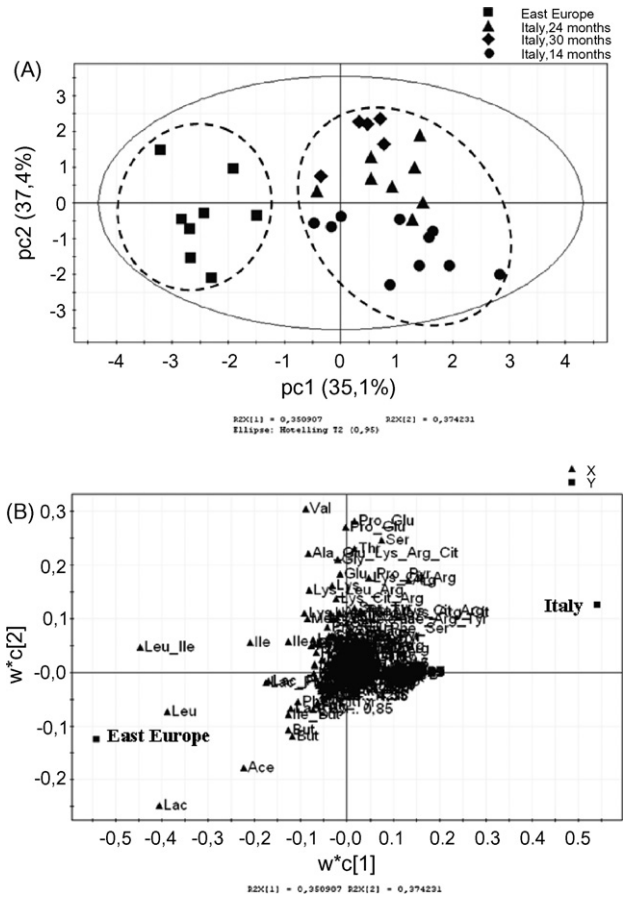

Fig. 5. PLS-DA score (A) and loading (B) plots obtained by using 23 Italian samples and all east Europe countries samples. In the score plot filled symbols represent samples of 14 (circle), 24 (triangle), 30 (diamond) months of ripening for Parmigiano Reggiano cheese while filled square east Europe cheese. PC1 = 35.1%, PC2 = 37.4%, $R^2X = 72.5\%$, $R^2Y = 82\%$ and $Q^2 = 0.76$. In the loading filled triangles represent the variables while filled squares the sample classes.

score plot in Fig. 5A showed like Italian and east European countries samples were in opposite regions of the hotelling plot demonstrating that a geographical differentiation is possible. Furthermore, the loading plot in Fig. 5B highlighted that foreign samples were characterized by a large amount of Leu and Ile, and also by Lac, But and Ace. Italian Parmigiano Reggiano aqueous extract samples were instead characterize by a large amount of all other compounds, in particularly by Thr, which typified old samples (30 months), Val, Pro, Glu, Lys, Ala, Ser, Arg and Cit.

Our previous data concerning ripening differentiation indicated that Leu content would characterize young Parmigiano Reggiano samples, while Thr the older ones. Interestingly, high Leu content was found for east Europe countries samples, thus suggesting that short ripening process took place; moreover the Leu content for foreign samples, resulted higher with respect to all Italian samples, even more than younger Italian samples.

5. Conclusions

Our results indicated that this rapid analysis of water-soluble fraction of Parmigiano Reggiano cheese constitutes a valid approach for sample characterization. In this case, sample preparation is extremely easy without any need of sample stabilization or derivatization. Amino acids and simple metabolites were found to be the most relevant compounds characterizing the aqueous extract cheese samples. NMR and statistical approach confirmed to be a valid tool in food analysis, as already highlighted in the literature. Ripening differentiation of Parmigiano Reggiano cheese is particularly important from the economical point of view and this method can be applied successfully with reasonably good reliability.

A geographical discrimination of Emmenthal cheese from different regions was recently obtained by means of MAS NMR spectroscopy combined with chemometric methods [26]. In that case detection of amino acids, lipids and fatty acids content led to samples discrimination. In our studies, the geographical differentiation between Parmigiano Reggiano samples and east Europe samples was achieved by using high resolution NMR spectroscopy combined with multivariate statistical protocols performed on aqueous extract of cheese; our methodology revealed the capability to obtain samples discrimination simply based on amino acids content, providing a reliable analytical method.

Acknowledgments

Parmareggio spa and particularly Dr. B. Cartinazzi are acknowledged for samples gifted.

References

[1] S. Sforza, L. Ferroni, G. Galaverna, A. Dossena, R. Marchelli, Eur. J. Mass. Spectrom. 10 (2004) 421.
[2] S. Sforza, L. Ferroni, G. Galaverna, A. Dossena, R. Marchelli, J. Agric. Food Chem. 51 (2003) 2130.
[3] P. Resmini, L. Pellegrino, J. Hogenboom, M. Bertuccioli, Gli amminoacidi liberi nel formaggio Parmigiano Reggiano stagionato in Ricerca Triennale sulla Composizione e su alcune peculiari caratteristiche del formaggio Parmigiano Reggiano, Consorzio del Formaggio Parmigiano-Reggiano, Ed. Reggio Emila, Italy, 1988, p. 41.
[4] S. de Angelis Curtis, R. Curini, M. Delfini, E. Brosio, S. D'Ascenzo, B. Bocca, Food Chem. 71 (2000) 495.
[5] C. Choisy, M.J. Desmazeaud, J.C. Gripon, G. Lamberet, J. Lenoir, C. Tourner, Les phénomènes microbiologiques et enzymatiques et la biochimie de l'affinage, A. Eck., Le Fromage, Technique et Documentation, Ed. Lavoisier, Paris, 1984, p. 62.
[6] D. Hemme, C. Bouillanne, F. Metro, M.J. Desmazeaud, Sci. des Aliments 2 (1982) 113.
[7] S. Skeie, J.A. Narvhus, Y. Ardo, K. Thorvaldsen, R.K. Abrahamsen, Lait 77 (1997) 575.
[8] E. Tschager, H. Jager, Milkwirtsch. Ber. 95 (1988) 79.
[9] G. Panari, Milchwissenschaft 41 (1986) 214.
[10] G. Panari, Sci. Tecn. Latt. Casear. 36 (1985) 98.
[11] G. Mucchetti, F. Locci, M. Gatti, E. Neviani, F. Addeo, A. Dossena, R. Marchelli, J. Diary Sci. 83 (2000) 659.
[12] L. Shintu, S. Caldarelli, J. Agric. Food Chem. 53 (2005) 4026.
[13] R.C. Lindsay, Dairy Field 166 (1983) 20.
[14] A.H. Woo, R.C. Lindsay, J. Dairy Sci. 67 (1984) 960.
[15] E. Meinhart, P. Schreier, Milchwissenschaft 41 (1986) 689.
[16] J.K. Ha, R.C. Lindsay, J. Food Sci. 56 (1991) 1241.
[17] G. Barbieri, L. Bolzoni, M. Careri, A. Mangia, G. Parolai, S. Spagnoli, R. Virgili, J. Agric. Food Chem. 42 (1994) 1170.
[18] M. Qian, G.A. Reineccius, J. Diary Sci. 86 (2003) 770.
[19] M. Piotto, V. Saudek, V. Sklenar, J. Biomol. NMR 2 (1992) 661.
[20] S. Wold, N. Kettaneh, K. Tjessem, J. Chemom. 10 (1996) 463.
[21] S. Wold, A. Ruhe, H. Wold, W.I. Dunn, SIAM J. Sci. Stat. Comput. 5 (1998) 735.
[22] S. Wold, M. Sjöström, L. Eriksson, in: R. von Schleyer, N.L. Allinger, T. Clark, J. Gasteiger, P.A. Kollman, H.F. Schaefer, P.R. Schreiner (Eds.), Encyclopedia of Computational Chemistry, vol. 3, Wiley, Chichester, England, 1999, p. 2006.
[23] J. Trygg, S. Wold, J. Chemom. 16 (2002) 119.
[24] T.W.M. Fan, Prog. Nucl. Magn. Res. Spectrosc. 28 (1996) 161.
[25] L. Eriksson, E. Johansson, N. Kettaneh-Wold, S. Wold, Multi- and Megavariate Data Analysis, Principles and Applications, Appendix I, Umetrics AB, Umeå, 2001.
[26] L. Shintu, S. Caldarelli, J. Agric. Food Chem. 54 (2006) 4148.

Talanta 76 (2008) 134–137

Contents lists available at ScienceDirect

Talanta

journal homepage: www.elsevier.com/locate/talanta

Determination of trace phosphorus in zirconium–niobium alloy and Zircaloy by UV–vis spectrophotometry

S.M. Dhavile, R. Shekhar, S. Thangavel, S.C. Chaurasia, J. Arunachalam*

National Centre for Compositional Characterisation of Materials, Bhabha Atomic Research Centre, ECIL Post, Hyderabad 500062, India

ARTICLE INFO

Article history:
Received 3 December 2007
Received in revised form 14 February 2008
Accepted 14 February 2008
Available online 4 March 2008

Keywords:
Phosphorus
Spectrophotometry
Glow Discharge-Quadrupole Mass Spectrometry
Zirconium–niobium alloy

ABSTRACT

A spectrophotometric method has been developed for the determination of traces of phosphorus in zirconium based alloys (Zr–2.5Nb and Zircaloy). It is achieved by selective fluoride complexation controlled by boric acid. The samples were dissolved in HF and fluoro-complexes of the matrices were formed by maintaining the concentration of HF while the excess HF was controlled by boric acid. After the formation of phosphomolybdate, extracted into *n*-butyl acetate, ion-associated with crystal violet and the absorbance was measured at 582 nm. The results obtained by this procedure were in close agreement with the certified reference material (CRM) values and further these values were compared with the values determined by Glow Discharge-Quadrupole Mass Spectrometry (GD-QMS). The potential interferences like fluoride, silicon, arsenic(V), niobium, titanium, tantalum, etc., were tolerable to large level. LOD (3 s) was found to be 0.055 mg kg^{-1} with a precision (R.S.D.) of 2–3% and molar absorptivity was 2.7×10^5 L mol^{-1} cm^{-1}.

1. Introduction

Zirconium alloys find many applications due to their excellent corrosion resistant properties and high mechanical strength [1,2]. These alloys are used as coolant and fuel cladding tubes in pressurized heavy water nuclear reactors [3]. Phosphorus affects fracture toughness when its concentration exceeds its specification limit of 10 mg kg^{-1} [4]. Therefore, accurate determination of phosphorus at trace levels in these alloys is very essential. Accurate determination of phosphorus at low levels is difficult even with very sensitive analytical techniques like Inductively Coupled Plasma Mass Spectrometry (ICP-MS) or Graphite Furnace Atomic Absorption Spectrometry (GFAAS) [5]. Glow Discharge-Quadrupole Mass Spectrometry (GD-QMS) methods [6,7] require certified reference materials (CRMs) and specialized sample preparation techniques and therefore have limitation on their applicability to variety of samples. Hence, there is a need to develop a spectrophotometric method due to its simplicity, low cost, sample flexibility and due to its prominence in many chemical laboratories.

Generally, spectrophotometric methods such as molybdophosphovenadate and heteropolyblue were employed for the determination of phosphorus [8,9]. Due to lack of sensitivity of these methods it difficult to analyse at desired level (<10 mg kg^{-1}). To increase the sensitivity, heteropoly acid has been extracted with basic dyes into *n*-butyl acetate in nitric acid [9] and sulfuric acid medium [10]. In all these methods silicon, arsenic, titanium, zirconium, niobium and fluoride ions interfered very strongly [11–14]. Since hydrofluoric acid is the most suitable acid for the dissolution of zirconium matrix, it is difficult to analyse phosphorus due to the presence large amount of zirconium and fluoride. Separation and preconcentration procedures involving ion-exchange [15] and co-precipitation [16] are difficult to apply in this matrix due to high salt concentration and non-availability of suitable co-precipitating agent, respectively. Selective fluoride complexation using heteropolyblue method has been employed for the determination of phosphorus in chromium based alloys with tedious chemical manipulation [16]. But the real potential of this method was not investigated for interring matrices like Nb, Zr, Ti, etc. Pakalns determined phosphorus in these matrices [17], but due to insensitive of this method ($\varepsilon = 3000$) it cannot be applied for trace level determination. In this paper, we have developed a simple, reliable spectrophotometric method using crystal violet to determine trace level of phosphorus (<0.5 mg kg^{-1}) in zirconium based alloys (Zr–2.5Nb and Zircaloy). This method can also be applied to determine phosphorus in various other interfering matrices (Ta, Nb, Ti, etc.). To the best of our knowledge, no paper has been cited in the literature at such low level determination of phosphorus using

* Corresponding author. Fax: +91 40 27125463.
E-mail address: aruncccm@rediffmail.com (J. Arunachalam).

0039-9140/$ – see front matter © 2008 Elsevier B.V. All rights reserved.
doi:10.1016/j.talanta.2008.02.036

spectrophotometry in the presence of strong interfering element matrices (Nb, Zr, Ta, etc.).

2. Experimental

2.1. Instrumentation

A Hitachi-U-3210 double beam UV–vis spectrophotometer was used for spectrophotometric measurements. GD-QMS, Model GQ230 (VG Elemental, Wins ford, Cheshire, U.K.), was used for the analysis. This instrument was located in ultra-trace analysis laboratory inside a clean room of class 200. Discharge was generated in constant current mode where the discharge voltage was adjusted by changing the flow rate of discharge gas (argon) of purity 99.9999%. The dual detector system (Model: 4870 V, Galileo, Electro-Optics Corp., USA) utilizes an electron multiplier for ion counting for trace and ultra-trace elements and a Faraday cup for measurement of matrix and minor elements. The detector system provides dynamic range of more than eight orders of magnitude. The peak jump mode was used for the data acquisition. A flat sample holder was used for the analysis. The detector's calibration factor was adjusted to be 2610 ± 100 by adjusting the HT voltage to the electron multiplier.

2.2. Reagents

HF (40%) and H_3BO_3 were of supra-pure grade (Merck, Darmstadt, Germany). HNO_3 (69%), *n*-butyl acetate, acetone and $KMnO_4$ were of A.R. grade (E-Merck, India). Crystal violet (E-Merck, India) 0.008% was prepared in water and acidified when required. Standard stock solution of phosphorus (0.5 mg mL^{-1}) was prepared by dissolving potassium hydrogen phosphate (K_2HPO_4) (S.D. Fine Chem., India) in water and made up to the required volume. Ammonium molybdate (Feran, Berlin, AR grade) 2.5% in 3% HNO_3 was prepared by dissolving 2.5 g of reagent in hot water and cooled to which 3 mL of HNO_3 was added and made up to 100 mL. All solutions were prepared using high purity water obtained from milli-Q system (Millipore, Bedford, MA, USA).

2.3. Procedure

About 0.25 g of sample was taken in a plastic container, 4 mL of HNO_3 and 2 mL of HF were added, after complete dissolution of the sample, it was made up to 50 mL with water. A suitable aliquot corresponding to 0.1–1 μg of phosphorus was taken in a plastic container, 0.1 mL of 0.02 M $KMnO_4$ was added and heated over an Infra Red lamp. After cooling it was taken in a 125 mL capacity separating funnel containing 40 mL of 4% boric acid, acidity was adjusted to around 0.5 M using nitric acid and then mixed with 2 mL of ammonium molybdate solution. Five milliliter of *n*-butyl acetate was added to this mixture and was vigorously shaken for 1 min, to extract the phosphomolybdate complex into the organic phase. After discarding the aqueous phase, 10 mL of acidified dye solution (9 mL of 0.008% crystal violet solution + 1 mL of 5 M HNO_3) was equilibrated with the organic phase for the formation of ion-pair associate of phosphomolybdate with crystal violet. The aqueous phase was discarded and the organic phase containing the ion-pair was washed twice with 5 mL of 0.5 M HNO_3. The organic phase was drained into a dry 10 mL standard flask and inner wall of the separating funnel was washed with a few mL of acetone to collect back any traces of the ion-pair complex sticking to the funnel wall and finally the solution was made up to 10 mL with acetone. The spectrophotometric measurements were carried out using 1 cm cell at a wavelength of 582 nm after filtering the organic layer through Whatmann 540 filter paper to remove any aqueous traces.

Table 1
Stability constants (*K*) of some fluorocomplexes

Equilibrium	log *K*
$Zr^{4+} + 6F^- \leftrightarrow ZrF_6^{2-}$	38.4
$H_4SiO_4 + 6HF \leftrightarrow SiF_6^{2-} + 2H^+ + 4H_2O$	26.3
$H_3BO_3(s) + 3H^+ + 4F^- \leftrightarrow BF_4^- + 3H_2O$	20.0
$H_2MoO_4 + 4F^- \leftrightarrow MoO_2F_4^{2-} + 2H^+$	10.6

2.4. GD-QMS sample preparation

The surface of the sample was cleaned by isopropanol using ultra sonic cleaner. The cleaned sample was dried under infrared lamp. After loading the sample, it was cooled to near liquid nitrogen temperature in the GD system to reduce contaminations from gaseous elements (C, N, O). The discharge parameters were optimized to obtain maximum counts per second (500 Kcps) for $^{90}Zr^+$ ion. The discharge voltage and current were 1.2 kV and 3.0 mA, respectively. The sample surface was etched with GD plasma for nearly 60 min in order to eliminate the surface contaminants such as C, N, O and hydrocarbon materials. The analytical measurements were carried out at a mass step of 0.01 amu with 140 points in peak scan. Single scan for Faraday cup (for matrix elements, Zr and Nb) and 20 scans for electron multiplier (for phosphorus) were used for the scanning.

3. Results and discussion

3.1. Interference study and optimization of fluoride complexation

It is widely known that the spectrophotometric determination of phosphorus, especially at the trace level, by molybdenum heteropoly acid method is prone to extensive interferences from the presence of silicon, arsenic, and refractive metals, such as titanium, zirconium, niobium, etc. [11,12]. It has been found that the above interferences can be eliminated by fluoride complexation [16]. With the exception of arsenic, all the interfering elements form stable fluoro-complexes [18–21] neither of which take part in the heteropoly acid formation nor retain phosphorus. To suppress the formation of fluoride complex of molybdenum, boric acid was added to the sample solution. However, this addition of boric acid does not affect the stability of Zr, Nb and Si fluorocomplexes [14]. This is in fact due to the larger stability constant (*K*) for these complexes compared to the stability constant of BF_4^-, which in turn is larger than the stability constant for molybdenumfluoride complex (Table 1). The addition of boric acid additionally removes the excess fluoride. The concentration of boric acid required for eliminating free fluoride present in the sample solution containing 0.2 μg of phosphorus was studied by varying 0–0.64 M H_3BO_3 during extraction with *n*-butyl acetate (Fig. 1). It shows that the absorbance values reaches maximum at 0.05 M beyond this concentration of boric acid no change in absorbance was observed. However, it is essential to use higher concentration of boric acid when analysing the samples containing low level of phosphorus due to large sample size to be taken for analysis.

The interference study was carried out by adding known amount of interfering elements to the standard solution containing 0.5 μg of phosphorus (Table 2). It shows that none of these elements interfered in the present spectrophotometric method. Since, even very large amount (50 mg) of refractory metals (Ta, Ti, W and V) caused no interferences, this method can also be applied for analyzing phosphorus in these matrices. The interference due to arsenic(V) was eliminated by optimizing time duration between the addition of ammonium molybdate and extraction into *n*-butyl acetate (within 1 min). Because, the kinetics of formation of molybdoarsenic complex has been reported to be slow, while the

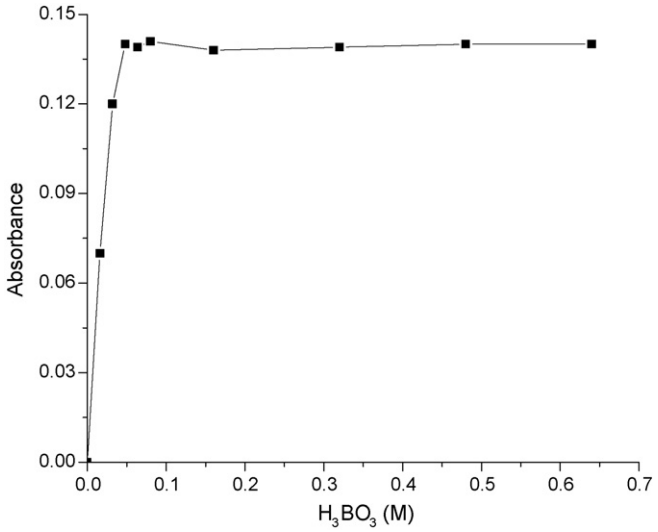

Fig. 1. Effect of concentration of boric acid on absorbance value of phosphorus (0.2 μg).

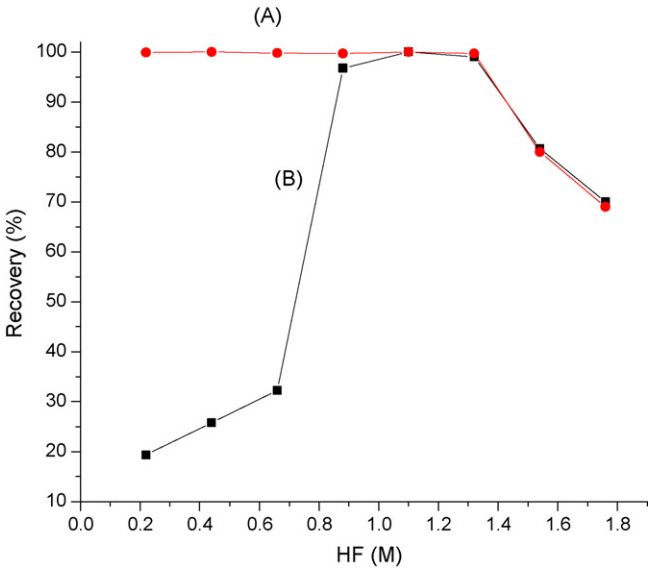

Fig. 2. Effect of concentration hydrofluoric acid in the sample solution on recovery of phosphorus (A) Zircaloy and (B) Zr–2.5Nb alloy.

formation of phosphomolybdate is complete within a few seconds [8], it can be seen from Table 2.

3.2. Optimization of HF concentration and total acidity on extraction

The effect of concentration of HF in the sample solution (Zircaloy and Zr–2.5Nb alloy) for the release of phosphorus from the matrix to enable the formation of phosphomolybdate and its extraction into *n*-butyl acetate was studied. Around 0.25 g of sample was dissolved separately by varying 0.5–4.0 mL of 22 M HF and made upto 50 mL (corresponds to 0.22–1.76 M HF). A suitable aliquot (0.1–1.0 μg of phosphorus) from the sample solution was taken to study the recovery of phosphorus against the concentration of HF (Fig. 2). In Zircaloy the recovery of phosphorus was around 100% irrespective of a concentration of HF (0.22–1.32 M) (Fig. 2(A)). In the case of Zr–2.5Nb alloy, at lower concentration of HF, the recovery of phosphorus was poor (Fig. 2(B)). It may be due to the formation of niobiophosphomolybdate [12], which could not be extracted into *n*-butyl acetate [11]. Hence, in the case of Zr–2.5Nb alloy excess HF was needed to release phosphorus from niobiophosphomolybdate. Fig. 2 shows that when the concentration of HF was more than 1.32 M, the recovery of phosphorus was declined in both the cases (Zr–2.5Nb alloy and Zircaloy). It may be attributed to the formation of fluoride complex with phosphorus, because the free fluoride has strong complexing affinity with phosphorus [22].

Acidity of the solution during the extraction of phosphomolybdate into *n*-butyl acetate should be ≈0.5 M of total mineral acids present. The optimum acidity has to be calculated by considering total acids used to dissolve the sample. The hydrofluoric acid present in the sample solution exists in two forms, one as H_2ZrF_6 and another as free hydrofluoric acid. Each millilitre of free concentrated 22 M hydrofluoric acid only contributes to approximately 7 mmol of acid due to its eventual conversion to fluoroboric acid, presumably the $H[BF_3(OH)]$ [11]. This was confirmed by titrating HF in 4% boric acid against standard alkali solution using methyl orange indicator.

Table 2
Interference study of various ions in spectrophotometric determination of phosphorus (0.5 μg)

Ion	Added as	Amount of ion (mg)	Absorbance
–	–	–	0.350
Fluoride	HF	300	0.345
Silicon	SiO_2	2	0.350
Arsenic(V)	Na_3AsO_4	0.8[a]; 1.6	0.345 (0.431[b]); 0.581(0.613[b])
Chromium(III)	$Cr_2(SO_4)_3{\cdot}6H_2O$	2	0.350
Niobium	Nb metal	2	0.345
Nickel	Ni metal	2	0.350
Iron	Fe metal	2	0.355
Tin	Sn metal	2	0.357
Boron	H_3BO_3	283	0.350
Tantalum	Ta metal	50	0.352
Titanium	Ti metal	50	0.350
Tungsten	W metal	50	0.354
Zirconium	Zr metal	50	0.347
Vanadium	V metal	50	0.356

Added salts/metals were dissolved in HF–HNO_3.
[a] Maximum permissible amount above which the interference do exist.
[b] Time duration between ammonium molybdate added and extracted into *n*-butyl acetate was 10 min.

3.3. Sample analysis, accuracy, precision and limit of detection

Quantification of analyte was carried out using external calibration curve, which was linear ($R^2 > 0.991$,) in the concentration ranging from 0.1 to 1 μg of phosphorus per 10 mL and the linear regression equation of the calibration plot was $Y = 0.712[x] - 0.00142$, where Y is absorbance, $[x]$ is the concentration of the phosphorus (μg). To validate the developed spectrophotometric method, this procedure was applied to certified reference materials of Zircaloy (Teledyne Wachang standard USA, X867-16D and X869-25B) and the results were in close agreement (Table 3). The entire sequence of the analytical spec-

Table 3
Determination of phosphorus (mg kg^{-1} ± s) in Zircaloy (CRM) obtained by the proposed method and comparison with CRM values

CRM	Found value ($n = 5$)	Certified value
Zircaloy, X867-16D	100 ± 5[a]	102 ± 7
Zircaloy, X869-25B	48 ± 6[b]	49 ± 8

[a] Sample size and dilution: 0.25 g → 50 mL, 1 mL taken for extraction.
[b] Sample size and dilution: 0.25 g → 50 mL, 2 mL taken for extraction.

Table 4
Determination of phosphorus (mg kg^{-1} ± s) in Zr–2.5Nb alloy obtained by the proposed method and comparison with GD-QMS values

Zr–2.5Nb samples	Proposed method[a] (n = 5)	GD-QMS value (n = 5)
1	7.23 ± 0.20	7.60 ± 0.32
2	9.35 ± 0.22	9.56 ± 0.87
3	6.98 ± 0.19	7.29 ± 0.78
4	8.78 ± 0.18	8.50 ± 0.32
5	5.34 ± 0.15	5.35 ± 0.35
6	4.70 ± 0.11	4.33 ± 0.18
7	5.20 ± 0.13	5.59 ± 0.34
8	6.71 ± 0.22	5.97 ± 0.32

[a] Sample size and dilution: 0.25 g → 50 mL, 10 mL taken for extraction.

trophotometric procedure (same sample size) was followed for CRMs. As the concentration of phosphorus in the CRMs is high, 1 mL (for X868-16D) and 2 mL (for X869-25B) aliquots from the 50 mL sample solution were taken for analysis. In the absence of CRM for Zr–Nb alloy, the result obtained by the spectrophotometric method was compared to those found by GD-QMS values (Table 4). The paired t-test was applied to examine whether the results by spectrophotometry and GD-QMS differed significantly at the 95% confidence limit. The pooled standard deviation was used for calculating the precision of the two sets of data in the t-test. As the calculated values of t were less than the critical t-value of 2.776 (Degree of freedom = 4), it follows that there is no statistical difference between the results. The limit of detection (3 s) was found to be 0.055 mg kg^{-1}, which was determined by measuring absorbance of process blank (n = 5) and its standard deviation (s) and was calculated based on dilution factor 20 (0.25 g → 50 mL, 10 mL). The molar absorptivity was found to be 2.7×10^5 L mol^{-1} cm^{-1}.

3.4. Quantification by GD-QMS

The raw counts of analyte (phosphorus) and matrix elements were normalized to 100% from their relative abundances. The ion beam ratio (IBR) values were generated by taking the ratio of abundance corrected raw counts of each element to the total sum of normalized raw counts of all the elements including the matrix zirconium isotope. The relative sensitivity factor (RSF) value is generated by taking the ratio of certified concentration of analyte to its ion beam ratio.

In GD-QMS it is preferable to use matrix matched reference materials to obtain accurate results. Zr–Nb solid reference materials certified for phosphorus are not available for the analysis of other Zr–Nb samples by GD-QMS. Generally, GD-QMS shows minimal matrix effects due to the decoupling of atomization and ionization process in the plasma and thereby minimizing the stringent need for matrix matched solid standards for the analysis. However it is required to verify whether the relative sensitivity factors generated on various solid standards for a particular element are indeed independent of matrix or matrix composition. Hence earlier we have made an extensive study on the use of Zircaloy standards (X867-16D and X869-25B) for the analysis of zirconium metals, Zircaloys, Zr–Nb alloys for various elements including phosphorus [6,7]. The study indicated that the RSF value of phosphorus generated using the Zircaloy standard is quite applicable to the zirconium metals, Zircaloys, Zr–Nb alloys for the determination of their phosphorus content. In the present study, therefore, the above Zircaloy reference materials (867 and 869) were used for the determination of phosphorus in Zr–Nb alloys by GD-QMS.

4. Conclusion

The developed spectrophotometric method in the presence of hydrofluoric acid leads to one of most sensitive and selective procedure for the determination of traces of phosphorus in complex matrices. Selectivity in the proposed method has been achieved by masking metal ions (Ti, Zr, Nb, etc.) with fluoride that generally forms insoluble phosphate and by selective demasking with boric acid to facilitate the formation of heteropoly acid of molybdenum and phosphorus.

Acknowledgements

We thank Dr. S.V. Narasimhan, Associate Director, Dr. Tulsi Mukhurjee, Director, Chemistry Group, BARC for their support and encouragement for this work.

References

[1] J.R. Theaker, R. Choubey, G.D. Moan, S.A. Aldridge, L. Davis, R.A. Graham, C.E. Coleman, Proceedings of the X International Symposium on ASTM STP 1245, 1994, p. 221.
[2] C.E. Ells, C.E. Coleman, C.K. Chow, Can. Met. Quart. 24 (1985) 215.
[3] M.P. Go'mez, G. Domizzi, M.I. Lo'pez Pumarega, J.E. Ruzzante, J. Nucl. Mater. 353 (2006) 167.
[4] K.N. Choo, Y.H. Kang, S.I. Pyun, V.F. Urbanic, J. Nucl. Mater. 209 (1994) 226.
[5] D.M. Hughes, D.C. Gregoire, H. Naka, C.L. Chakrabarti, Spectrochim. Acta Part B 53 (1998) 1079.
[6] R. Shekhar, J. Arunachalam, G. Radha Krishna, H.R. Ravindra, B. Gopalan, At. Spectrosc. 25 (2004) 157.
[7] R. Shekhar, J. Arunachalam, G. Radha Krishna, H.R. Ravindra, B. Gopalan, J. Nucl. Mater. 340 (2005) 284.
[8] E.B. Sandell, Hiroshi Onishi, Photometric Determination of Traces of Metals. Part-1, vol. 3, A Wiley-Interscience Publication, 1978.
[9] A.K. Babko, A.T. Pilipenko, Photometric Analysis Methods of Determining Non-Metals, Mir Publisher, Moscow, 1976, p. 103.
[10] S. Thangavel, K. Dash, S.C. Chaurasia, Talanta 55 (2001) 501.
[11] K. Murata, Y. Yokoyama, S. Ikeda, Anal. Chim. Acta 48 (1969) 349.
[12] G. Norwitz, M. Codell, Anal. Chem. 26 (1954) 1230.
[13] D.F. Boltz, J.A. Howell, Colorometric Determination of Nonmetals, second ed., Wiley, New York, 1978, p. 337.
[14] W.J. Williams, Handbook of Anion Determination, Butterworth, London, 1979, p. 471.
[15] T. Taniai, M. Sukegawa, A. Sakuragawa, A. Uzawa, Talanta 61 (2003) 905.
[16] V.J. Zatka, N. Zelding, Anal. Chem. 56 (1984) 1734.
[17] P. Pakalns, Anal. Chim. Acta 50 (1970) 103.
[18] L.G. Sillen, A. Martell, Stability Constants of Metal—Ion Complexes, second ed., Chemical Society, London, 1964 (Special publication no. 17).
[19] L.G. Sillen, A. Martell, Stability Constants of Metal—Ion Complexes Supplement 1, (Special publication no. 25), Chemical Society, London, 1971.
[20] E. Hogfeldt, Stability Constants of Metal—Ion Complexes, part A (IUPAC chemical data Ser. No. 21), Pergamon Press, Oxford, 1982.
[21] A.E. Martell, R.M. Smith, Critical Stability Constants, vol. 5, First Supplement, Plenum Press, New York and London, 1982, p. 416.
[22] J.W. Mellor, Comprehensive Treaties on Inorganic and Theoretical Chemistry, Longman Group Ltd., London, 1971.

Available online at www.sciencedirect.com
ScienceDirect
Talanta 76 (2008) 29–33
Talanta
www.elsevier.com/locate/talanta

Green synthesis of silver nanoparticles for ammonia sensing

Stephan T. Dubas [a,b,*], Vimolvan Pimpan [b]

[a] *Metallurgy and Materials Science Research Institute, Chulalongkorn University, Bangkok, Thailand*
[b] *Department of Materials Science, Faculty of Science, Chulalongkorn University, Bangkok, Thailand*

Received 14 January 2008; received in revised form 28 January 2008; accepted 29 January 2008
Available online 13 February 2008

Abstract

Silver nanoparticles synthesized by a reagent less method involving only UV radiation have been used in colorimetric assay for the detection of ammonia in solution. The silver nanoparticles were synthesized by the exposure of a silver nitrate solution to a low-power UV source in the presence of poly(methacrylic acid) (PMA), which acted both as reducing and capping agent. The synthesis of the silver nanoparticles was studied by monitoring the changes in position and amplitude of the localized plasmon resonance (LSPR) band using UV–vis spectroscopy. The morphology of the particles was studied using transmission electron microscopy which confirmed the formation of spherical particles with an average particle size around 8 nm. Interestingly, the silver nanoparticles solution was found to display a strong color shift from purple to yellow upon mixing with increasing concentration of ammonia ranging from 5 to 100 ppm. Hence, the nanoparticles prepared with this method could be used as colorimetric assay for sensing applications of ammonia in water.

Keywords: Ammonia; Silver nanoparticles; Sensor

1. Introduction

Ammonia is produced in very large quantity (2.1–8.1 Tg/year) by the chemical industry to be used as fertilizers and in refrigeration systems [1]. Because of its toxicity, ammonia presents serious health hazards, and the monitoring of its concentration in air and liquid is of major importance. Concentration control of ammonia not only interest environmental agencies but also, for example, the automotive industry as ammonia has been found in exhaust systems with concentrations up to 8 ppm [2,3]. There are also medical interests in measuring ammonia in the body, as it can be an indicator of disorder or disease. For instance, breath ammonia level can be a diagnostic for urea imbalance as a result of kidney disorder or stomach bacterial infection [4,5].

To this end, a wide range of sensors have been designed with detection limit lower than part per million (ppm). Sensors have been commercialized with detection mechanisms often based on metal-oxide or organic conducting films, whose electrical properties are perturbed upon the adsorption of ammonia molecules [6,7]. Films based on SnO_2 or WO_3 demonstrated good response to NH_3 with a detection limit down to 1 ppm [8]. Films from conjugated polymer such as polypyrrole or polyaniline have also been used to detect ammonia by changes of their conduction properties [7]. All of these techniques display extremely good reproducibility and low detection limit but only work for ammonia gas and cannot be used to measure ammonia dissolved in water. For the detection of ammonia in solution, spectrophotometric methods based on the change in color of a reagent in the presence of ammonia have been developed. The best-known reaction is probably the Nessler reaction based on the color change of potassium tetraiodomercurate (II) in a dilute alkaline solution which has the inconvenience to produce a toxic precipitate [9]. Another coloration method is the Berthelot reaction that displays a blue color in the presence of ammonia with a detection limit of 90 ppb but has a very slow kinetic of reaction [10]. Recent report of low detection of ammonia in drinking water was made using carbon nanotube/copper composite paste coating for electrochemical electrode [11]. In their experiment, Valentini et al. reported sub ppm detection of ammonia with fast response time but the experimental setup is more complex and can be difficult to adapt for on-site measurements.

Silver nanoparticles have already been extensively studied for their unique optical and sensing properties [12,13]. Solutions of

* Corresponding author at: Metallurgy and Materials Science Research Institute, Chulalongkorn University, Bangkok, Thailand. Tel.: +66 2 218 4234.
E-mail address: Stephan.d@chula.ac.th (S.T. Dubas).

0039-9140/$ – see front matter © 2008 Elsevier B.V. All rights reserved.
doi:10.1016/j.talanta.2008.01.062

spherical silver nanoparticles are known to have a strong yellow color and an extinction UV–vis spectrum featuring a sharp peak at 400 nm [14,15]. The color of silver nanoparticles solutions is due to the so-called localized surface plasmon absorption (LSPR) which arises from the coupled oscillations of the conduction electron in the metallic nanoparticles induced by the incident light electric field [16]. The position, shape and intensity of the LSPR are the function of factors such as morphology, dielectric constant of the environment as well as inter-particle coupling [17]. The properties of nanoparticles the most often used in sensing application are based on changes in dielectric constant of the surrounding medium by changing the solvent quality or by complex formation at the surface of the nanoparticles. It is well known that less polar surrounding medium induces a shift of the LSPR toward higher wavelength [16,17]. Silver nanoparticles present therefore great interest for sensing applications in both gas and liquid phase [18,19].

In this article a very simple method is presented for the synthesis of silver nanoparticles to be used in colorimetric sensors for ammonia. Silver nitrate salts are reduced using an 8-W UV lamp in the presence of poly-methacrylic acid which acts as capping and reducing agent. Commonly used reducing agents such as hydrazine or sodium borohydride are replaced by a more environmental friendly method based on mild UV-light illumination. The low power of the UV lamp provides a very slow kinetic of reaction which allows the preparation of purple solution of silver nanoparticles. UV–vis spectroscopy was used to monitor the kinetic of nanoparticles synthesis while their size and morphology were confirmed by transmission electron microscopy (TEM). Finally, the sensing properties of the nanoparticles solution were tested against increasing ammonia concentration in the range of 5–100 ppm by monitoring the changes in LSPR position and amplitude with a UV–vis spectrophotometer.

2. Experimental method

2.1. Chemicals

Poly(methacrylic sodium salt) (PMA) and sodium borohydride were purchased from Aldrich and AR grade silver nitrate was purchased from Mallinckrodt, Thailand. The pH of the solution was adjusted in all experiments to a value of 4 using a 100 mM acetic-acetate buffer. Ammonia diluted from a 30% solution was used in the sensing experiments to prepare solutions with a final concentration ranging from 5 to 100 ppm. Double distilled water was used in all experiments.

2.2. Nanoparticles synthesis

Silver nanoparticles were prepared by the reduction of silver nitrate solutions under exposure to UV light in the presence of poly(methacrylic). PMA which acts both as a reducing and capping agent can stabilize the silver nanoparticles in solution by electrostatic repulsion and steric hindrance. The synthesis steps of the silver nanoparticles can be summarized as follow: 25 ml of a 10 mM solution of PMA was mixed with 25 ml of a 10 mM silver nitrate solution and stirred for 5 min. All solution had a pH of 4, which was fixed by a 100 mM acetic-acetate buffer. The solution was then exposed to the UV light and the solution slowly turned pink before finally acquiring a purple color within an hour. After 1 h exposure time, the solutions were stored in a dark bottle. Under storage conditions, the purple solution was stable for several months.

2.3. Characterization of the nanoparticles

The position and amplitude of the LSPR of the silver nanoparticles solutions were analyzed using a UV–vis spectrophotometer (SPECORD S 100, Analytikjena) in the wavelength range of 350–700 nm. The morphology and particles size of freshly synthesized silver nanoparticles were evaluated using a transmission electron microscope model (Jeol JEM 100SX). For the sample preparation, a drop of diluted silver nanoparticles solution was dropped on the grid and left to dry overnight in a desiccator. The samples were measured without any further treatment the following day.

3. Results and discussion

3.1. Synthesis of the silver nanoparticles

In contrast with conventional methods used in the synthesis of silver nanoparticles (e.g. sodium borohydride or hot sodium citrate), this experiment uses a low intensity (8 W) UV lamp. The choice of a low intensity UV lamp was dictated by the need of a reduction method which would have a very slow kinetic of reaction. UV–vis spectroscopy was used to monitor the changes in λ_{max} absorbance and amplitude of the LSPR band during the reduction reaction. By recording the changes in absorbance as a function of time, the kinetic of formation of silver nanoparticles solution was monitored and the compilation of the absorbance spectra is shown in Fig. 1. The increase in absorbance at 515 nm as a function of time can be seen. The final absorbance peak of the nanoparticles solution contrasts strongly with the expected absorbance maximum at 400 nm, which is commonly presented as the characteristic of successful silver nanoparticles synthesis. For reference, are shown in Fig. 2, spectra and pictures of nanoparticles solutions prepared by two methods. The experiment A represents the typical silver nanoparticles synthesis from $NaBH_4$ which leads to a characteristic yellow color solution with an absorbance maximum at 400 nm. In contrast, the solution prepared with the UV lamp had a deep purple color with a maximum absorbance at 515 nm. The author speculates that the difference in spectral absorbance is due to the incomplete reduction of the silver ions which perturb the dielectric surround of the nanoparticles. The unreacted silver ions can interact with the COO^- carboxylic groups present at the surface of the nanoparticles and form an Ag^+/COO^- complex. The color shift is then justified by the less hydrophilic environment due to the complex formation as it displaces the water molecules and modifies the dielectric constant of the medium in the vicinity of the nanoparticles surface. Less hydrated and less polar surrounding medium have been demonstrated to induce a red shifted absorbance spectrum [17].

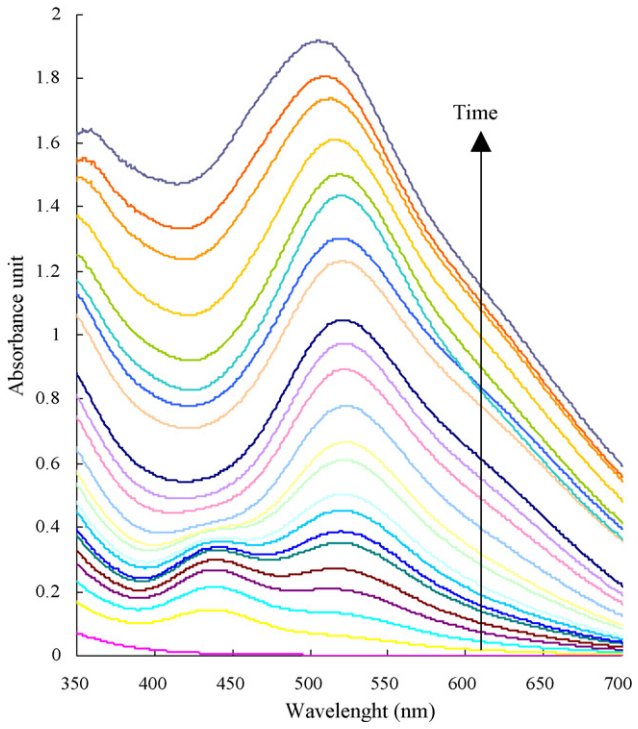

Fig. 1. Changes in absorbance as a function of reaction time of a 10 mM silver nitrate solution mixed with a 10 mM PMA solution exposed to an 8-W UV lamp. The spectra were recorded every 5 min.

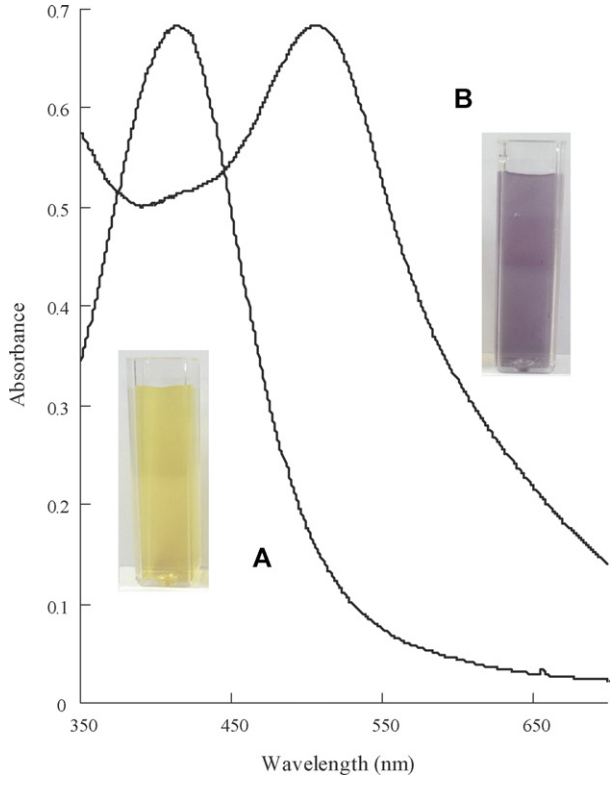

Fig. 2. UV–vis spectrums and pictures of silver nanoparticles solution produced by reduction of $AgNO_3$ with sodium borohydride (A) and by exposure to an 8-W UV lamp (B). In both experiments PMA was used as capping agent.

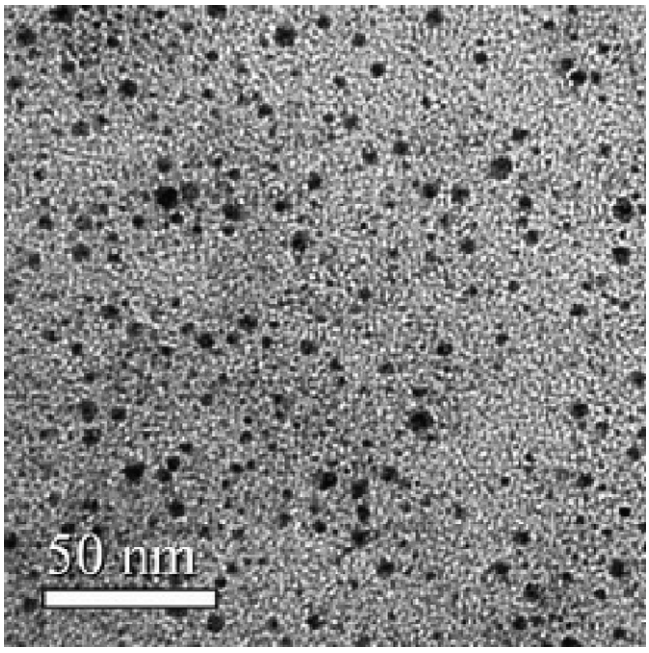

Fig. 3. TEM image of silver nanoparticles prepared by exposure of a 10 mM silver nitrate and 10 mM PMA solution at pH 4 under an 8-W UV lamp for 1 h.

The morphology of produced silver nanoparticles using this method was monitored by TEM. The nanoparticles seen in Fig. 3 appear spherical and have a narrow particles size distribution with the largest having a diameter of 10 nm. TEM analysis confirms thus the formation of spherical nanoparticles and not nanorods as it might have been though since silver nanorods solution would also posses a purple/red color. Although the polymer coating cannot be seen on the TEM image, the carboxylic groups from the PMA can interact with the silver metals surface as a protective coating and prevent Ostwall ripening of the nanoparticles by electrostatic repulsion and stearic hindrance.

3.2. Ammonia sensing

The spectral absorbance of the nanoparticles in solution was found to display a strong shift upon adjunction of ammonia and the color of solution changed from purple to yellow. Using UV–vis spectroscopy the changes in absorbance can be monitored as a function of the ammonia content. Shown in Fig. 4 is the plot of changes in spectral absorbance as a function of ammonia concentration increasing from 0, 5, 15, 40, 60, 75, 85 and 100 ppm. It can be seen that the initial absorbance peak intensity at 515 nm decreases and is replaced by another peak appearing at 460 nm while the ammonia content is increased. The presence of an isosbectic point at 490 nm indicates the presence of two species in equilibrium. Considering the already reported association of ammonia with Ag^+ ions to form $Ag(NH_3)_2^+$ coordination complex, the two species in our case are the silver nanoparticles with and without excess silver ions. Spectral shifts of LSPR band are usually explained by a combination of changes in interparticles distance and by a shift of the dielectric constant of the surrounding medium. Upon the addition of ammonia in solution,

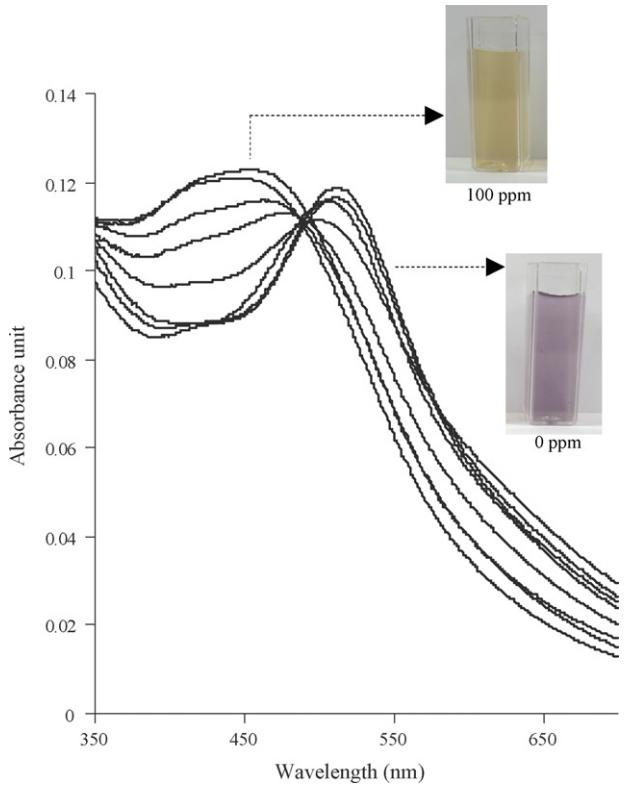

Fig. 4. UV–vis spectrum of a silver nanoparticles solution exposed to various concentration of ammonia (0, 5, 15, 40, 60, 75, 85, and 100 ppm).

a $Ag(NH_3)_2^+$ complex is formed between ammonia and silver ion which increases the surface charge of the particles and allows the repulsion between the particles as well as increase the water content in the surrounding of the particles. This results in more hydrophilic and isolated particles with a blue shifted spectrum. Similarly, the addition of sodium chloride was found to also induce the color shift between purple to yellow but in this case the AgCl complex is non-soluble and leads to the appearance of a turbid yellow solution. These results confirm that the excess of unreacted silver ions which are responsible for the purple color can be removed by any complexing agent.

For the design of optical sensors, the monitoring of changes in absorbance at specific wavelengths instead of the entire UV–vis spectrum is preferred. The choice of the wavelengths is usually dictated by the area of the spectrum which displays the largest variation in absorbance during the sensing experiment. The two wavelengths of interest here are 460 and 515 nm as they display the increase and decrease in absorbance respectively upon mixing of the solution with dilute ammonia solutions as it can be seen from Fig. 4. Shown in the cartouche Fig. 5 is a plot of the absorbance for these wavelengths across the isosbectic point as a function of the ammonia content which displays a linear relationship. Further improvement is possible by data processing and taking the ration of these two values (abs_{460}/abs_{515}). This has for effect to provide a less scattered plot as it can be seen in Fig. 5 which displays a linear relationship as a function of ammonia concentration with a correlation factor R^2 equal to 0.988. The kinetic of color shift was found to be extremely

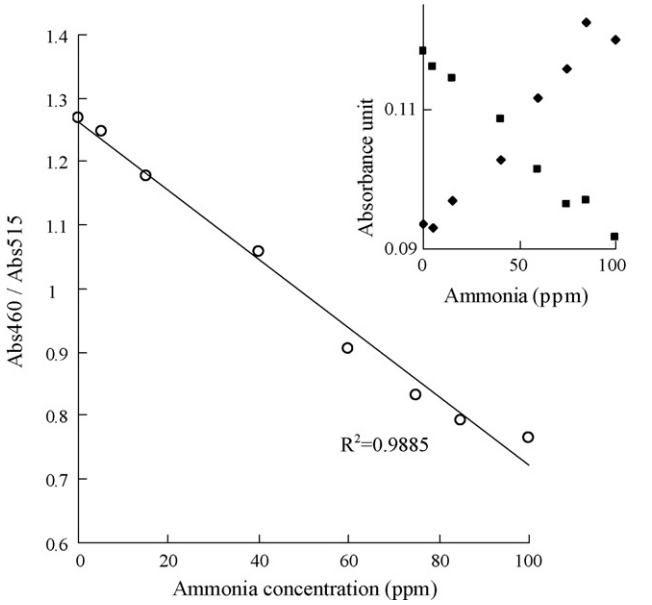

Fig. 5. Ratio of the absorbance peak at 460 and 515 nm for a silver nanoparticles solution exposed to increasing ammonia content (5–100 ppm). In the cartouche the detailed changes in absorbance for each wavelength are given (square = absorbance at 515 nm; diamonds = absorbance at 460 nm).

fast and it only took a few seconds for the color change to occur.

4. Conclusion

We have presented a new method for the synthesis of silver nanoparticles based on the incomplete reduction of silver ions when exposed to a weak UV light and capped by PMA. The nanoparticles solution displays an absorbance maximum at 515 nm instead of the 400 nm usually expected for spherical silver nanoparticles. The unreacted silver is thought to be responsible for the color shift by forming an Ag^+/COO^- complex with the PMA stabilizing polyelectrolyte. The resulting solution displays a purple color which can be reversed to yellow upon adjunction of ammonia. Based on this mechanism, an ammonia sensor has been proposed and shows a linear response in the range of 5–100 ppm.

Acknowledgement

This research was funded by the Chulalongkorn University through the Center for Innovative Nanotechnology (CIN).

References

[1] P. Warneck, Chemistry of the Natural Atmosphere, Academic Press Inc., 1998.
[2] C. Pijolat, C. Pupier, M. Sauvan, G. Tournier, R. Lalauze, Sens. Actuators B 59 (1999) 195.
[3] T.D. Durbin, R.D. Wilson, J.M. Norbeck, J.W. Miller, T. Huai, S.H. Rhee, Atmos. Environ. 36 (2002) 1475.
[4] W. Ament, J.R. Huizenga, E. Kort, T.W. Van Der Mark, R.G. Grevink, G.J. Verkerke, Int. J. Sports Med. 20 (1999) 71.

[5] L.R. Narasimhan, W. Goodman, N. Patel, Proc. Natl. Acad. Sci. U.S.A. 98 (2001) 4617.
[6] K. Zakrzewska, Thin Solid Films 391 (2001) 229.
[7] M. Sahm, A. Oprea, N. Barsan, U. Weimar, Sens. Actuators B 127 (2007) 204.
[8] X. Wang, N. Miura, N. Yamazoe, Sens. Actuators B 66 (2000) 74.
[9] A.I. Vogel, Vogel's Qualitative Inorganic Analysis, Longman Scientific & Technical, 1987.
[10] P.L. Saerle, Analyst 109 (1984) 549.
[11] F. Valentini, V. Biagiotti, C. Lete, G. Palleschi, J. Wang, Sens. Actuators B 28 (2007) 326.
[12] Y. Shen, P.N. Prasad, Appl. Phys. B: Lasers Opt. 74 (2002) 641.
[13] H. Guo, S. Tao, Sens. Actuators B 123 (2007) 578.
[14] K.L. Kelly, E. Coronado, L.L. Zhao, G.C. Schatz, J. Phys. Chem. B 107 (2003) 668.
[15] J. Perez-juste, I. Pastoriza-Santos, L. Liz-Marzan, P. Mulvaney, Coordin. Chem. Rev. 249 (2005) 1870.
[16] U. Kreibig, M. Vollmer, J.P. Toennies, Optical Properties of Metal Clusters, Springer-Verlag, Berlin, 1995.
[17] S. Link, M.A. El-Sayed, Int. Rev. Phys. Chem. 19 (2000) 409.
[18] H.Y. Wang, Y.F. Li, C.Z. Huang, Talanta 72 (2007) 1698.
[19] C.S. Cheng, Y.Q. Chen, C.J. Lu, Talanta 73 (2007) 358.

Talanta 76 (2008) 183–188

Contents lists available at ScienceDirect

Talanta

journal homepage: www.elsevier.com/locate/talanta

Non-destructive analysis of cultural heritage artefacts from Andalusia, Spain, by X-ray diffraction with Göbel mirrors

A. Duran*, L.K. Herrera, M.C. Jimenez de Haro, A. Justo, J.L. Perez-Rodriguez

Materials Science Institute of Seville (CSIC-Seville University), Avda Americo Vespucio, s/n. 41092 Seville, Spain

ARTICLE INFO

Article history:
Received 30 July 2007
Received in revised form 14 February 2008
Accepted 20 February 2008
Available online 4 March 2008

Keywords:
Göbel mirrors
Low fixed incidence angles
Depth profile
Cultural heritage
Bronze
Organ pipe

ABSTRACT

The characterization of the phases present in artefacts has been normally carried out using XRD (Bragg–Brentano geometry) that requires sampling from artworks, being a destructive technique. However, X-ray diffraction with Göbel mirrors permits directly to study rough artefacts without sampling. Grazing incidence attachments can be used to characterize as much the superficial layer as the underlying ones in flat samples to obtain information about the depth profile of some samples. The combination of Göbel mirrors and measure at low fixed incidence angles allow to obtain information about the depth profile of bent samples.

This work reports the alteration processes on the surface of the following cultural heritage artefacts: a rivet and a nail extracted from Pardon Gateway, located in the North façade of Mosque-Cathedral of Cordoba; a Roman arrow and a button from a Roman jacket obtained from an excavation in Baena (Cordoba); organ pipe from Cathedral of Zaragoza; lead seals from Seville City Hall collection.

The main objective of this paper is the study through a totally non-destructive analytical method, X-ray diffraction with Göbel mirrors, of the superficial alteration of some metallic artefacts from cultural heritage. This knowledge allows us the election of appropriate methods to carry out the restoration of these artefacts.

1. Introduction

Several techniques have been used to characterize the materials and its products of alteration, but many of them only give chemical composition and frequently require the sampling and the destruction of the material (grinding, solution, heating, etc.). Also, the material is altered during the analysis, being important to use techniques that give information of the phases present without any destruction (non-destructive techniques) or sampling.

Conventional techniques of X-ray diffraction requires necessary sampling from artworks and grinding of the extracted samples, being, in this form, destructive analytical methods.

Parafocusing Bragg–Brentano geometry leads to a 2θ-shift of the X-ray reflection, if the sample is not precisely positioned on the focusing circle. A sample displacement can occur if the sample has an uneven surface, as frequently happens in samples coming from archaeology or cultural heritage [1].

Graded Multilayer Optics ("Göbel-Mirrors") have proved as very useful beam conditions for parallel-beam diffraction without sampling [2–4]. Grazing incidence reflectometry can be also used in flat samples without sampling. High-resolution XRD and XRD using capillary are used more frequently to study samples from cultural heritage but in these cases, sampling is necessary.

The Göbel Mirrors are a device, based on a layered crystal, which, mounted on a D-5000 Siemens diffractometer, transforms the primary divergent X-ray beam into a highly brilliant, parallel beam. If dimensions of an object are adequate (up to 60 cm in bulk), it can be directly analyzed by XRD, without sampling. Even a rough, irregular surface, both on flat and bent objects, is suitable for the analysis. The XRD analysis using Göbel mirrors is therefore, totally non-destructive and very useful to study artefacts from Cultural Heritage [5–7]. It can be obviously very adaptable to study the surfaces of these artefacts, giving information of degradation and corrosion processes and information about pigments, ceramics, metals, patinas, crusts, etc., used to manufactured artworks.

All the samples studied in this work belong to historic metals of Spanish Cultural Heritage.

Simply stated, metal corrosion is a process of chemical dissolution. Cations migrate from the metal substrate and react with available anions to form the metal salts that constitute tarnish layers and corrosion crusts. The character and chemical makeup of the corrosion products depend on the nature of the substrate and the

* Corresponding author. Tel.: +34 4489532; fax: +34 4460665.
E-mail address: adrian@icmse.csic.es (A. Duran).

0039-9140/$ – see front matter © 2008 Elsevier B.V. All rights reserved.
doi:10.1016/j.talanta.2008.02.025

environment to which it is exposed. Analyses are necessary to study the alterations imposed on an artifact in order to contribute to the development of adequate conservation and restoration treatments. The study of the alteration products formed in the surface can be realized using conventional XRD technique (powder diffraction measurements) that requires sampling of external products from metal artefact or XRD with Göbel mirrors, which permits directly the study of metal surfaces without sampling.

Most frequently used copper alloys are brasses (Cu–Zn), copper–nickel (Cu–Ni 70:30 or 90:10) and bronzes (Cu with Sn, Al or Si). Bronzes are used for the construction of different types of artworks, statues and monuments of cultural relevance, due to its high stability to environmental corrosion [8]. The corrosion of bronze monuments has been studied by several workers [9–13]. This interest is mainly due to the increasing awareness of air pollution damages to the cultural heritage. Some works have contributed to a better understanding on the reaction mechanisms of environmental deterioration [10].

Frequently, the first reaction that takes place is the oxidation of the metallic base exposed to the atmosphere to produce cuprous ions. In a chloride polluted atmosphere, cuprous chloride is formed. This is an unstable compound that in the presence of oxygen and environmental humidity turns into basic copper chloride with simultaneous production of hydrochloric acid. The presence of this acid will induce a new cyclic reaction of copper until the total consumption of the metal. Only if the cuprous chloride is eliminated, these damaging cyclic processes ("bronze disease") would be stopped [8,14,15].

Environmental conditions produce iron oxides and other compounds derived, such as oxyhydroxides or hydroxides in iron implements. The most common compound formed is goethite, which gives the brown and dark reddish brown colours to monuments. In poorly drained zones, lepidocrocite, an isomer of goethite, has been frequently reported [16]; it gives a bright orange colour. Vesuvianite, calcium magnesium iron aluminium silicate hydroxide ($Ca_{10}(Mg,Fe)_2Al_4(SiO_4)_5(Si_2O_7)_2(OH,F)_4$), named after its discovery locality, Mount Vesuvius (Campania, Italy) is rarely found in iron artefacts that have been buried during long time. This mineral is produced by the reaction between iron from artefacts and silicates present in the soil.

Other metals, such as lead employed in alloys were also widely used in antiquity, especially in organ pipes and lead seals manufacturing. Depending on the characteristic of the environment to which it is exposed, lead is quite reactive, forming anglesite ($PbSO_4$), cerussite ($PbCO_3$), hydrocerussite ($Pb_3(CO_3)_2(OH)_2$) or plumbonacrite $Pb_5O(CO_3)_3(OH)_2$. The presence of lead carbonate compounds is responsible for the unsightly, white and powdery "white rust" of lead and can be localised on the surface in the form of pits [17]. The carboxylic acids formic, propanoic, tannic and acetic acids formed by cellulose hydrolysis from woods or parchment paper used for storing lead artefacts in museums or that support organ pipes can convert the lead surface of artefacts in voluminous corrosion compounds, and in some cases, the artefacts may be corroded in bulk through a progressive peeling of the corrosion layer [18–20].

The main objective of this work is the use of a totally non-destructive analytical method, X-ray diffraction with Göbel mirrors, for the study of the superficial alteration of some metallic artefacts, so much bent as flat ones, proceeding from important artworks, since in most of the cases cannot be taken samples for the study by conventional method of powder diffraction. Grazing incidence X-ray diffraction is offering the possibility of depth profiling studies; it is possible to record normal X-ray diffraction patterns as a function of X-ray penetration depth. The penetration depth of X-ray is affected by the diffraction geometry, sample absorption and reflectance of X-rays. In this case, measures using Göbel mirrors and low fixed incidence angles were done to study superficial and underlying layers of metallic samples.

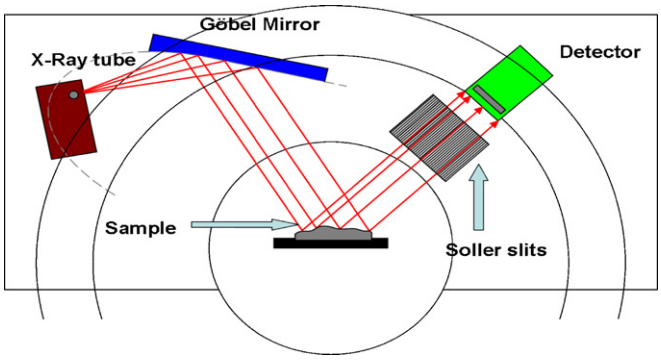

Fig. 1. Experimental procedure for non-destructive analysis by X-ray diffraction with Göbel mirrors of artefacts belonging to cultural heritage.

2. Materials and methods

The phases formed during the alteration processes on the surface of the following cultural heritage artefacts have been studied:

(a) A Rivet extracted from the Pardon Portico, located in the North façade of the Mosque-Cathedral of Cordoba (Spain). The gateway leaves (dated on March 1377) were made with pine wood covered with bronze plates. From the same Portico, studies were carried out in two other places.
(b) A piece of bronze with a high degree of alteration in its surface.
(c) An altered piece containing nails used for knocking the bronzes to the wood. All these pieces were extracted by experts and restorators using physical methods. Artefacts were not scraped to obtain powders, analysis were realized directly over the pieces. After adequate study and restoration, artefacts will be returned to its original places.

Other samples for the research were:

(d) A Roman arrow and a button from a Roman jacket obtained from an archaeological excavation in Baena (Cordoba, Spain).
(e) Organ pipes from the Cathedral of Zaragoza (Spain).
(f) Lead seals from Seville City Hall collection.

The crystalline phases on the surfaces of samples were characterized by X-ray diffraction (XRD) using a Siemens diffractometer model Kristalloflex D-5000 with Göbel mirrors. Graded multilayer optics creates a highly parallel incident beam while suppressing Kβ-radiation. By capturing a large solid angle, the mirror turns otherwise unusable radiation into a useful parallel beam. The Göbel mirror enables the investigation of irregularly shaped samples surfaces and reduces the requirement for the exact sample position (Fig. 1). Also, low fixed incidence angles X-ray were used in complement with Göbel mirrors.

To calculate the depth of the layer that is analyzed by X-ray diffraction is used ABSORBDX which is a program belonging to the software suite DIFFRACplus evaluation package [21,22].

The scanning electron microscopy (SEM) study was carried out with a JEOL JSM5400 microscope equipped with energy dispersive X-ray analyzer.

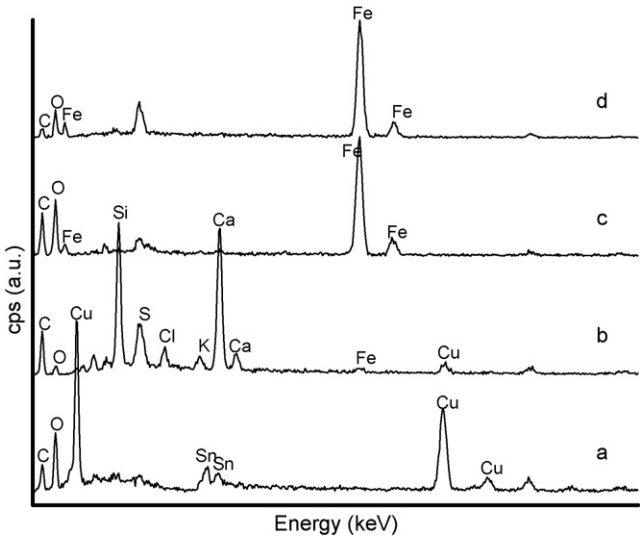

Fig. 2. EDX analysis of: (a) a rivet from the Pardon Portico of the Mosque-Cathedral of Cordoba and of a zone corresponding to a Roman jacket button from Baena's archaeological excavation, where surface crust was removed, showing the presence of Cu and Sn. (b) Superficial products formed on the piece of bronze from Pardon Portico, showing the presence of Cu, Cl, Si, S, Ca, Fe, K and O. (c) Powder taken from the nail, that shows the presence of Fe and O. (d) A Roman arrow from Baena's archaeological excavation, after removing the surface crust, showing the presence of Fe.

3. Results and discussion

3.1. Pardon-Portico of the Mosque-Cathedral of Cordoba

The elemental analysis of the rivet (sample a) from the Pardon Portico shows that the original material is constituted by copper and tin (Fig. 2a). The X-ray diffraction pattern (obtained using Göbel mirrors) of this sample shows the presence of the diffractions at values 42.8° and 49.7° of angle 2θ (Fig. 3a), corresponding to alpha bronze (B), according with the file 44-1477 of JCPDS. This piece was cleaned by restorators before studying and no degradation products are detected.

The elemental analysis of the superficial products formed on the bronze (sample b) shows the presence of copper, chlorine, silicon, sulphur, calcium, iron, potassium and oxygen (Fig. 2b). The XRD pattern measured with Göbel mirrors shows that the surface of the sample is constituted by atacamite [$Cu_2Cl(OH)_3$] (At), gypsum [$Ca(SO_4)2H_2O$] (Gy), quartz (SiO_2) (Q) and weddellite [$Ca(C_2O_4)2H_2O$] (We) (Fig. 3b). Atacamite has been detected previously in copper and copper alloys exposed outdoors due to environmental contamination [8,14]. This environmental contamination is also responsible of the presence of gypsum and other compounds. The weddellite, also present, may be formed by reaction between environmental gypsum and rests of calcite with oxalate ions from the dissolved acid. In urban areas oxalic acid is abundant in rain and mists [23] or it may be secreted by microorganisms, such as fungi and liquens [24].

The punctual chemical analysis of the nail (sample c) shows the presence of iron and oxygen (Fig. 2c). X-ray diffraction on the surface of the nail using Göbel mirrors confirms the presence of goethite [α-$Fe^{3+}O(OH)$] (Goe), lepidocrocite [γ-$Fe^{3+}O(OH)$] (Lep) and [FeO(OH)] (Fig. 4). These iron oxyhydroxides or hydroxides are frequently formed in the surface of iron artefacts due to environmental contamination. Also, gypsum (Gy) and quartz (Q) are present in the sample due to this factor.

3.2. Roman samples

Elemental analysis of a zone corresponding to a Roman arrow, where surface crust was removed, shows the presence of iron. Punctual chemical analysis carried out by EDX in the arrow is shown in Fig. 2d. X-ray diffraction analysis carried out with Göbel mirrors on the superficial covered area of crust shows the presence of calcite (Calc) and quartz (Q), deposited during the burial in the soil. Also

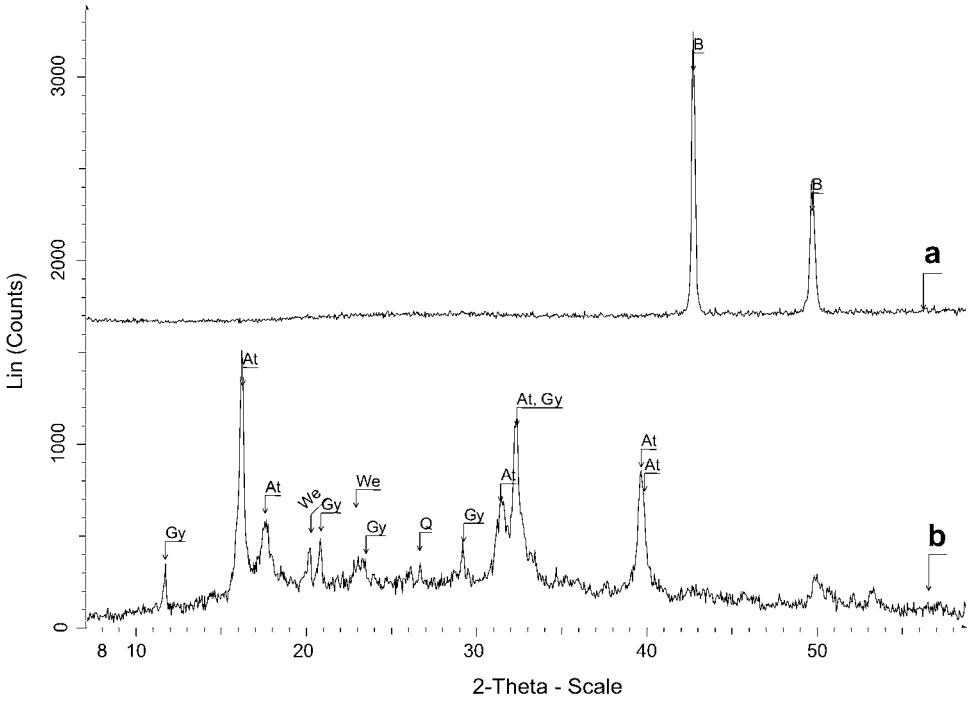

Fig. 3. X-ray diffraction pattern with Göbel mirrors of: (a) a rivet extracted from the Pardon Portico of the Mosque-Cathedral, corresponding to alpha bronze. (b) Superficial product on the altered bronze of the Portico, corresponding to atacamite (At), gypsum (Gy), quartz (Q) and weddellite (We).

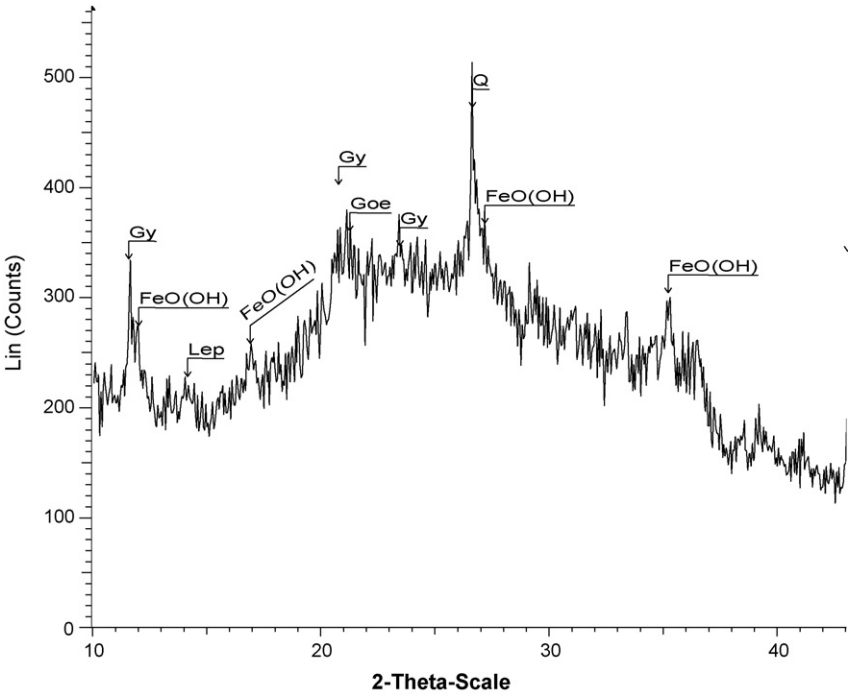

Fig. 4. X-ray diffraction pattern with Göbel mirrors of the altered iron nail of the Mosque-Cathedral of Cordoba, showing the presence of goethite (Goe), lepidocrocite (Lep), [FeO(OH)], gypsum (Gy) and Quartz (Q).

vesuvianite (Ves) was found (Fig. 5). Vesuvianite (calcium, magnesium, iron, aluminium, silicate hydroxide) is rarely found in iron artefacts that have been buried during long time. This mineral is produced by the reaction between iron from artefacts and silicates present in the soil.

Elemental analysis of a punctual zone corresponding to a Roman jacket button, where surface crust was removed similarly to the arrow sample cited before, shows the presence of copper and tin (similar to Fig. 2a). Studies realized on the surface of the sample by X-ray diffraction with Göbel mirrors only shows the

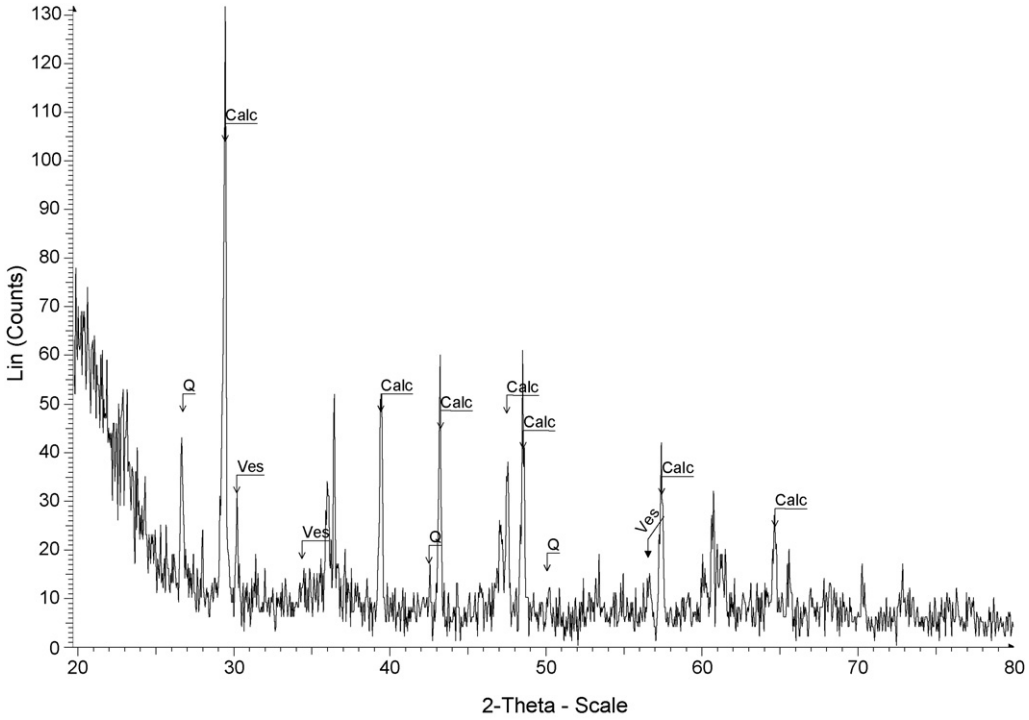

Fig. 5. X-ray diffraction patterns of the superficial covered area of crusts of a Roman arrow, using Göbel mirrors, showing the presence of calcite (Calc), quartz (Q) and vesuvianite (Ves).

presence of calcite, quartz (figure not shown) that were deposited from the soil. The crusts deposited on the surfaces of arrow and button are very thick and, except in punctual areas cited before, do not permit the study of the underlying material (bronze) and its alteration products.

3.3. Organ pipes and lead seals

3.3.1. Organ pipes

The atmospheric corrosion of lead-rich organ pipes in Spanish church has recently attracted the attention of organ builders. Organ pipe corrosion leads to the gradual development of cracks and holes which destroy the function of the pipes. When this occurs, the historic lead organ pipes have to be replaced by new ones, and a part of the sounding cultural heritage is lost forever. It is not clear why these organs are corroding. However, the church environment to which these organs are exposed is characterized by relatively low temperature and high relative humidity.

Another characteristic is the presence of large amounts of wood structures around organs. The studied pipe organ is enclosed in wood furniture. The humidity in combination with alteration products of wood (organic vapors acid, such as acetic or formic, and aldehydes produced by the hydrolysis of the hemicellulose during aging) can react with lead forming corrosion products, mainly lead carbonates. In extreme cases, they can cause a complete destruction of the artefact.

Crystalline corrosion products were analyzed; the diffractometer was equipped with Göbel mirrors and the measures were realized at low fixed incidence angles, which can be used to characterize as much the superficial layer as the underlying ones without any effect of the roughness and obtain information in the depth profile of the sample.

The organ pipes are not flat, it is necessary to use a parallel X-ray beam; the beams diffracted by the sample are collimated using a parallel slit analyzer and not a divergent beam that obtained with Bragg–Brentano geometry. The alteration layer of the organ pipes is very thin. When the study is realized using coupled θ–2θ angles diffraction, the peaks of bulk components (lead-rich organ pipe) are very intense compared to the alteration products (figures not shown). The employment of a fixed low incidence angle (θ) increases path length through the sample and decreases X-ray penetration into the bulk. This method provides better sample peak detection for the attempt of analyzing more superficial layers and of trying to observe products of alteration, such as lead carbonates (hydrocerussite and cerussite), phases that were observed in analysis of other organ pipes [25,26].

This procedure is new in this work and can be employed for study of artefacts belonging to cultural heritage. In organ pipes samples, the application of low incidence angle offers many information without scrapping into the corrosion thin layer.

The diffraction profiles of the sample was acquired under fixed incidence angles, at 1° (θ) and 5° (θ), all the other parameters were kept constant. Fig. 6 shows the diffraction patterns of the same sample belongs to organ pipe at two incidence angles, 1° (θ) and 5° (θ). The XRD patterns of the 1° incident angle (θ) gives information about the more external layer. The crystalline phases detected can be attributed to tin (Sn), lead (Pb) and hydrocerussite (HC) (Fig. 6a).

However, it is also evident that there is a certain evolution of the diffractogram from the surface to the depth of the sample. In particular, the pattern taken at 5° (θ) (Fig. 6b) shows higher intensity of the peaks corresponding to tin (Sn). In the organ pipe's surface is possible to detect the alteration process because the pattern at 1° (θ) shows some conversion of lead to hydrocerussite;

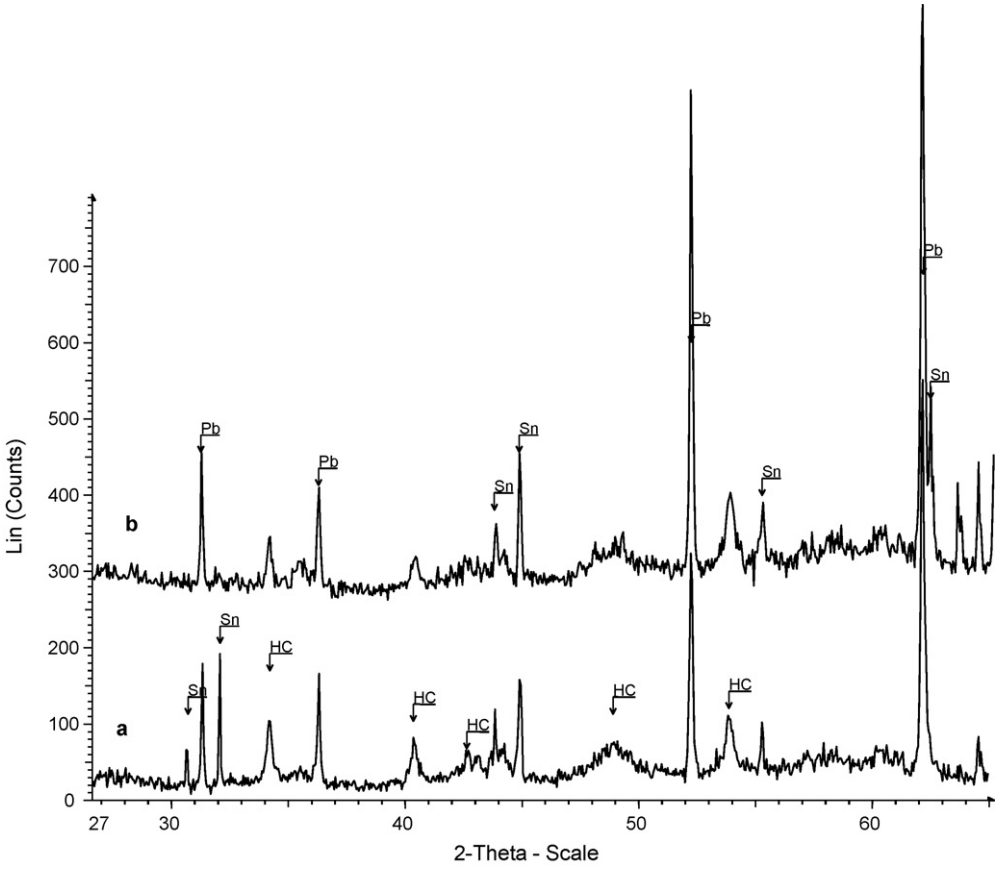

Fig. 6. (a) XRD pattern at 1° incident angle of an organ pipe, tin (Sn), lead (Pb) and hydrocerussite (HC). (b) XRD pattern at 5° incident angle of the same pipe.

Table 1
The depth for 90% contribution of the measured intensity for 1° and 5° in the study of organ pipes

	Pb (μm)	Sn (μm)	$Pb_3(CO_3)_2(OH)_2$ (μm)
$\theta = 1°$	0.149	0.211	0.306
$\theta = 5°$	0.645	0.912	1.350
θ–2θ couple	1.195	1.657	2.655

peaks of lead decrease and peaks corresponding to hydrocerussite increases.

In order to get the depth of the analyzed layer of the organ pipe, it is considered the global chemical composition (lead, tin and hydrocerussite), the density of these phases, the wavelength of X-ray radiation ($\lambda = 1.54$ Å), the diffraction angle for each compound (strongest peak, Pb $2\theta = 31.28°$, Sn $2\theta = 30.73°$, $Pb_3(CO_3)_2(OH)_2$ $2\theta = 34.15°$), and finally the incidence angle. The depth for 90% contribution of the measured intensity for these angles is described in Table 1.

Due to the studied organ pipe has a curved and rough surface, obtained information cannot be comparable with that it would obtain in case of thin layers. With employment of fixed low incidence angles (1° and 5°), although it obtains major information about superficial layers, we cannot obviate that X-ray beam gets also in the bulk of the sample.

In another sonorous organ pieces, alloy composition is about 50% of lead and 50% of tin [27]. However, in the case of the samples studied in this work, the composition is about 90% of lead and 10% of tin, determined by X-ray diffraction semiquantitative analysis, what is corroborated by the presence of alteration products of lead (hydrocerussite) and no presence of alteration products of tin, such as cassiterite or romarchite [25,26]. In this form, the depth for 90% contribution of the measure intensity of the alloy layer would be, according with Table 1, approximately of $x = 0.155$ μm at $\theta = 1°$ and $x = 0.671$ μm at $\theta = 5°$.

3.3.2. Lead seals

Lead seals from the Seville City Hall collection had suffered significant alterations, losing not only the external figurative prominence, but also some of them were corroded in bulk through a progressive peeling of the corrosion layer. This represents an alteration in the entire sample, showing superficial powdery "white rust", composed of lead, hydrocerussite and cerussite, whose study was carried out by X-ray diffraction with Göbel mirrors.

Lead seals were stored in a hole made in cardboard and we suggested that the superficial alteration might be due to the storage in enclosures in the museum for a long period [28]. To check this suggestion, the following experiment was performed. In a beaker containing water and CO_2 was introduced a rectangular piece of lead whose length was longer than the water. On this piece of exposed lead, a piece of cardboard was put and the beaker was covered. After 3 months, the stored lead layer was covered with a white powder that the X-ray diffraction shows as hydrocerussite and cerussite. The same experiment was repeated without using cardboard and in this case, white powders did not appear after 3 months of treatment.

The cellulose hydrolysis has provided carboxylic acid (mainly acetic acid) that dissolves the PbO of the surface forming lead carbonate after reaction with CO_2 and humidity of the atmosphere.

4. Conclusions

The data obtained in this work show that X-ray diffraction with Göbel mirrors is a good method for the characterization of the irregular surfaces from artefacts belonging to cultural heritage because allow non-destructive study (without sampling) of them. The combination of Göbel mirrors attachment and measure at fixed low incidence angles allow to obtain information about the depth profile of sample, being a very important application in the artworks.

Bronze in the rivet from Pardon Portico of Mosque-Cathedral of Cordoba was detected using X-rays diffraction with Göbel mirrors, and on the surface of the bronze, wedellite, atacamite and gypsum were detected as alteration products. Goethite, lepidocrocite and FeO(OH) appeared on an iron nail proceeding of this Portico too.

The study demonstrated that metallic point of a Roman arrow was composed of iron. On the surface, it was found calcite, quartz and vesuvianite. The Roman button was covered with a thick crust, formed by calcite and quartz. The surface of these materials is affected by environmental and soil in which they were buried.

Lead from seals and organ pipes were altered to hydrocerussite by the method used for storing these materials in the museums and in the churches where they were.

Acknowledgment

This work was supported by the project MAT 2007-63234.

References

[1] M. Gross, S. Haaga, H. Fietzek, M. Herrmann, W. Engel, Mater. Sci. Forum 278–281 (1998) 242–247.
[2] H. Göbel, 43rd Annual Denver X-Ray Conference, August 1–5, 1994, Paper D-63.
[3] M. Schuster, H. Göbel, J. Phys. D: Appl. Phys. 28 (1995) A270–A275.
[4] M. Schuster, H. Göbel, Adv. X-ray Anal. 39 (1996) 57–71.
[5] G. Chiari, A. Giordiano, G. Menges, Sci. Technol. Cult. Heritage 5 (1) (1996) 21–36.
[6] G. Chiari, R. Compagnoni, R. Giustetto, M. Ricq-de-Bouard, Le vie della pietra verde, Omega, 1996, pp. 35–53.
[7] G. Chiari, R. Compagnioni, M. Ricq-de-Bouard, XII Congress UISPP, Forli, 1996.
[8] L. Uller, H. Videla, L.K. Herrera, Patinas naturales y artificiales y su importancia en la preservación de piezas de cobre del patrimonio cultural, Latincorr, Brasil, 2006.
[9] E. Mattson, R. Holm, Atmos. Corros. (1982) 365–382.
[10] P. Eriksson, L. Johansson, J. Gullman, Corros. Sci. 34 (1993) 1083–1097.
[11] J.D. Meakin, D.L. Amest, D.A. Dolske, Atmos. Environ. 26B (1992) 207–215.
[12] G. Lanterna, Thermochim. Acta 269/270 (1995) 729–742.
[13] L.S. Selwyn, N.E. Binnie, J. Poitras, M.E. Laver, D.A. Dowham, Stud. Conserv. 41 (1996) 205–228.
[14] A.E. Cepero, Principios científicos del deterioro de los objetos de arte metálicos y de sus tratamientos de conservación, Cencrem, La Habana, Cuba, 2002.
[15] M. Morcillo, M. Almeida, in: M. Morcillo et al. (Eds.), Corrosión y protección de metales en las atmósferas de Iberoamérica, 1998, pp. 547–590.
[16] U. Schwertman, J. Neues, J. Miner. 93 (1959) 67–86.
[17] E. Rocca, C. Rapin, F. Mirambet, Corros. Sci. 46 (2004) 653–665.
[18] J. Tetrault, IIC-CG17, 1992.
[19] N.H. Tennent, J. Tate, L. Cannon, SSCR (1993), J.4,8.
[20] C. Degrigny, R. Le Fall, E. Geuilmoint, Papers in: ICOM Committee for conservation 11th Triennal Meeting, Edinburgh, 1986, pp. 865–870.
[21] ABSORBDX, software DIFFRACplus evaluation package.
[22] J. Leroux, T.P. Thinh, Revised Tables of X-rays Mass Attenuation coefficients, Corporation Scientifique Claisse Inc., Quebec, 1977.
[23] S. Steinberg, K. Kawamura, I.R. Kaplam, Int. J. Environ. Anal. Chem. 19 (1985) 251–260.
[24] M. del Monte, C. Sabbioni, G. Zappia, Sci. Total Environ. 67 (1987) 17–39.
[25] L.K. Herrera, A. Duran, M.C. Jiménez de Haro, J.L. Perez-Rodriguez, Á. Justo, "Study of baroque artworks by non-destructive techniques" in Coalition. CSIC Thematic Network on Cultural Heritage (Electronic Newsletter), vol. 14, 2007, pp. 10–14.
[26] A. Justo, M.C. Jiménez, M.B. Sigüenza, A. Durán, J.L. Pérez-Rodríguez. Internal report "Estudio científico de muestras procedentes del Órgano de la Catedral de Zaragoza", CSIC, 2004, p. 40.
[27] A. Justo, J.M. Martinez, A. Cea, J.L. Pérez-Rodríguez, E. Jiménez, Estudio científico de los tubos sonoros de metal del órgano Francisco Pérez de Valladolid (s. XVIII), Alcalá de los Gazules (Cádiz), III Congreso Nacional de Arqueometría, 2001, pp. 571–578.
[28] A. Duran, M.C. Jimenez de Haro, A. Justo, L.K. Herrera, M.L. Franquelo, Estudio del proceso de degradación en la colección de sellos de plomo del Ayuntamiento de Sevilla, Procceedings of VII Iberic Congress of Archaeometry, History Institute (CSIC), National Archeologic Museum and SAPaC, Madrid, november 2007, in press.

Talanta 76 (2008) 138–145

Contents lists available at ScienceDirect

Talanta

journal homepage: www.elsevier.com/locate/talanta

Determination of catechin isomers in human plasma subsequent to green tea ingestion using chiral capillary electrophoresis with a high-sensitivity cell

Deia Abd El-Hady*, Nagwa Abo El-Maali

Department of Chemistry, Faculty of Science, Assiut University, 71516 Assiut, Egypt

ARTICLE INFO

Article history:
Received 15 October 2007
Received in revised form 14 February 2008
Accepted 15 February 2008
Available online 29 February 2008

Keywords:
Catechin isomers
Chiral capillary electrophoresis
High-sensitivity cell
Green tea
Human plasma

ABSTRACT

A simple and reliable analytical electrophoretic method using chiral capillary electrophoresis (CCE) with a high-sensitivity cell of special design has been established for simultaneous determination of (+)-catechin (C) and (−)-epicatechin (EC) in aqueous and human plasma media. The application of a capillary with high-sensitivity cell has led to an improvement of 10-fold and 5-fold time-corrected peak area over a standard cell and a capillary with bubble cell, respectively. Analysis has involved the electrophoretic separation of C and EC in less than 4.0 min at 210 nm. The running buffer consist of 50.0 mmol L^{-1} borate buffer with 1.0 mmol L^{-1} β-cyclodextrin at pH 8.5. CCE system has been proved for its intended use by applying procedure starting from calibration of CE instrument into validation of all experimental parameters. The resolution between catechin isomers under optimal conditions has been found to be more than 3.0. The detection limits of C and EC have been calculated to be 3.2 and 1.0 ng mL^{-1}, respectively. Good linearity has been obtained with correlation coefficient (r^2) ranging between 0.995 and 0.996 at 99% confidence level (CL). Application of the proposed method to human plasma after ingestion of green tea has successfully been achieved and has statistically been proved. The unchanged amounts of C and EC in plasma were about 17.4 and 1.8% of the administered dose after 2 h of starting tea ingestion. The detection limits of C and EC in human plasma at 210 nm were 4.1 and 1.5 ng mL^{-1}, respectively.

1. Introduction

Many of the common foods found in grocery stores or organic markets contain cancer-fighting properties, from the antioxidants that neutralize the damage caused by free radicals to the powerful phytochemicals that scientists are just beginning to explore. Epidemiological studies indicated that catechins from some commercial drinks like green tea have prophylactic properties that are beneficial to the health of humans [1]. A lower relative risk for stomach [2], esophageal [3] and lung cancer [4] was shown with increased tea consumption. Increased tea consumption was also associated with a decreased incidence of stroke [5], lower atherogenic index [6] and improved liver function [7]. (+)-Catechin (C) and (−)-epicatechin (EC) (Fig. 1) are the main catechins widely distributed in plant-derived foods [8,9].

Further knowledge on the absorption, bioavailability, and metabolism of catechins after normal dietary intakes was considered essential for our understanding of their mechanisms of action. Several analytical methods, commonly used for the analysis of polyphenols in food [10,11], lacked specificity and sensitivity when applied to plasma [12–14]. The concentration of C in rabbit plasma was determined by fluorescent detection [15], although a few liquid chromatography–mass spectrophotometry (LC–MS) methods for the analyses of catechins in biological fluids were developed [16,17]. The actuality of the low-concentration problem and the lack of high-quality data for the determination of C and EC in human plasma gave us a ground to study their determination in human plasma. Capillary electrophoresis (CE) became useful and powerful separation technique that exhibited higher resolution and shorter analysis time. In addition, the most significant features that made CE a successful tool in clinical laboratories were low cost, small sample volume, increased selectivity, automation, and versatility. The application of CE to the field of chiral analysis was exploded because the chiral selector (e.g. cyclodextrin) dissolved in the running buffer rather than bound to a stationary phase in HPLC [1]. Several trials were achieved to illustrate analytical approaches for significant increasing of CE sensitivity in clinical analysis [18–21]. Recently, the sensitivity of enantiomers in pharmaceutical and clinical samples was improved by column coupling electrophoresis with fiber-based diode-array detection [22–24] and the high sensitivity of weak electrolytes was achieved by dynamic pH junction and/or large-volume sample stacking for on-line preconcentration technique coupled with CE [25–27]. Mrestani et al. [28,29] used high-sensitivity cell (Z-cell) for the

* Corresponding author. Tel.: +20 882412392; fax: +20 882373799.
E-mail address: deiaabdelhady@yahoo.com (D.A. El-Hady).

0039-9140/$ – see front matter © 2008 Elsevier B.V. All rights reserved.
doi:10.1016/j.talanta.2008.02.026

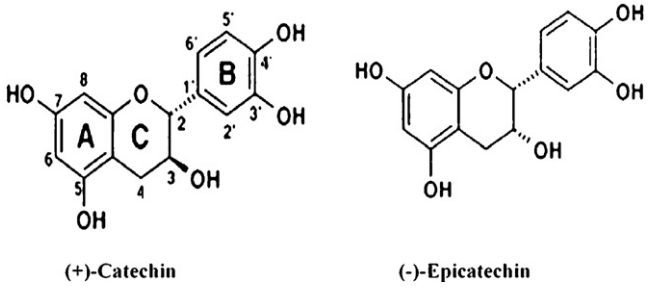

Fig. 1. Chemical structure of (+)-catechin (C) and (−)-epicatechin (EC).

sensitive determination of meropenem and thiamine in biological media.

Nowadays, Agilent Technology fabricated a high-sensitivity detection cell with special design to simple and reliable the achievement of CE sensitivity in complex media like body fluids. To the best of our knowledge, no chiral capillary electrophoresis (CCE) system coupled with such high-sensitivity cell dealt with the simultaneous determination of C and EC in human plasma. Therefore, our work was devoted to improve the CE sensitivity for the simultaneous determination of C and EC in human plasma by coupling chiral capillary electrophoresis with a high-sensitivity cell (special design) after the precipitation of protein component in order to avoid the capillary wall–protein interaction.

2. Experimental

2.1. Apparatus

All separations were carried out using a 1600 CE system (Agilent Technologies, Germany), equipped with a photodiode-array detector from 190 to 600 nm. CE ChemStation software was used for instrument control, data acquisition and data analysis. A standard fused-silica capillary (Agilent Technologies of 64.5-cm total length (56.0-cm effective length), 650-μm outer diameter and 50.0-μm internal diameter), a capillary with bubble cell (optical path length is 150 μm) and a capillary with high-sensitivity cell with special design obtained from Agilent (8,5-cm outlet, 56.0-cm effective length × 50.0-μm internal diameter) were used. The detection cell was constructed from silica parts, which were fused together, and had an area of 100 μm^2 with a path length of 1.2 mm. The light path through the cell was entirely made of black fused silica to minimize stray light and to define the aperture for diode-array detection. In addition the reflective interior functions as a light pipe ensuring almost 100% transmission of the light when entering the detection cell. The detection cell was flanked by flat clear windows. All these properties enhanced the spectral analysis by diode-array detection as well as the flared and beveled capillaries maintained peak shape of analytes by ensuring proper alignment and coupling to the cell body. The schematic picture of the high-sensitivity detection cell for Agilent-CE systems was illustrated in Fig. 2.

The applied voltage was maintained at 30.0 kV (anodic detection) with controlled temperature at 25.0 °C to give current value of 25.0 μA. The CE sampling was performed by hydrodynamic injection at 25.0 mbar for 5.0 s; the detection wavelength was 210 nm. Before injection into the CE system, each solution (running buffer and sample solutions) was subjected to filtration through a 0.22-μm membrane filter. Flushing procedure was optimized to give precise analysis by the following: at the beginning of day, procedure was 10.0 min of 0.1 mol L^{-1} NaOH, 10.0 min H_2O and 10.0 min running buffer; between runs it was 1.0 min of 0.1 mol L^{-1} NaOH, 2.0 min H_2O and 4.0 min running buffer; at the end of day it was 5.0 min of 1.0 mol L^{-1} NaOH and 15.0 min H_2O.

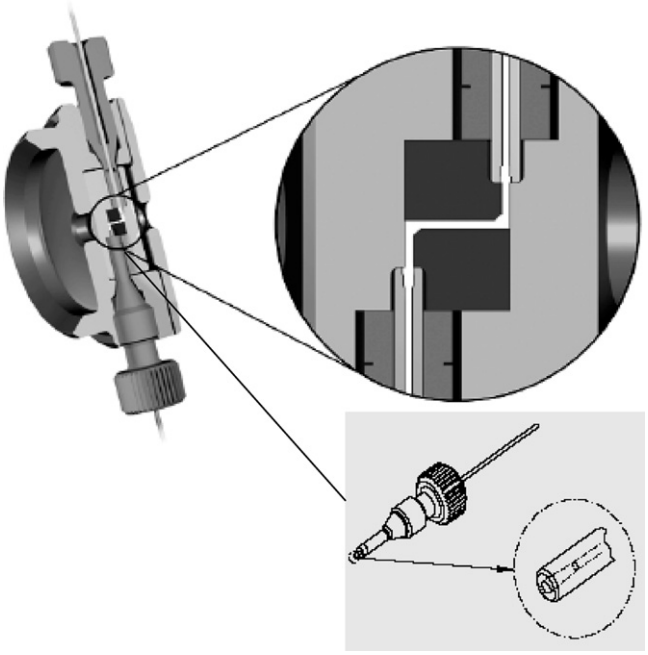

Fig. 2. Schematic of the high-sensitivity detection cell for Agilent ^{3D}CE systems and of capillary connection.

The pH measurements carried out with the Fisher Scientific Accument pH Meter Model 810 equipped with a combined glass electrode, which was calibrated regularly with buffer solutions (pH 4.0 and 7.0) at 22.0 ± 1.0 °C. V3 series HTL micropipettes (Germany) were used to pipette microlitre volumes of solutions.

The MiniTab software package (USA statistical software) was used to perform the statistical analysis of data.

2.2. Chemicals and reagents

(+)-Catechin (*trans*-3,3′,4′,5,7-pentahydroxyflavan) reference material (C) and (−)-epicatechin (*cis*-3,3′,4′,5,7-pentahydroxyflavan) reference material (EC) were obtained from Sigma (St. Louis, MO, USA). Sodium dodecyl sulfate (SDS), β-cyclodextrin (β-CD), hydroxypropyl-β-cyclodextrin (HP-β-CD) and succinyl-β-cyclodextrin (succinyl-β-CD) were from Fluka (Buchs, Switzerland). Boric acid, sodium borate and sodium hydroxide were purchased from Sigma (St. Louis, MO, USA). Water used for the preparation of solutions and running buffers, was purified by a Milli-Q apparatus (Millipore, Milford, MA, USA) to give ultra pure water (type I) having the following specifications: conductivity 0.056 μs, resistivity 18.2 MΩ cm at 25.0 °C, total organic compounds (TOC) 2.0 μg L^{-1}, bacteria <1 cfu mL^{-1}, Na 1.0 μg mL^{-1}, K 1.0 μg mL^{-1}, particulates >0.22 μm (P mL^{-1}) and well irradiated at 185 and 254 nm.

The borate background electrolyte was prepared at a concentration of 50.0 mmol L^{-1} by weighing an appropriate amount of sodium borate and adjusting pH to 8.5 using boric acid. The running buffer was daily prepared by dissolving β-CD (1.0 mmol L^{-1}) in borate background electrolyte. For validation experiments stock solutions of standard (+)-C and (−)-EC were prepared at 150 and 100 μg mL^{-1}, respectively.

2.3. Samples

2.3.1. Preparation of ingestion samples

Commercial samples of green tea were collected from the local market (Assiut, Egypt). Solutions were prepared by immersing a packet of green tea (2.0 g dry weight) in boiled water (40.0 mL) at 95 °C for 3 min. If necessary, dilutions were done in order to give the concentration of analytes within the proposed linearity range.

2.3.2. Preparation of plasma samples

Plasma samples were obtained from a single healthy male adult volunteer (34 years old, 63 kg body weight and nonsmoker) who was orally ingested with green tea solution. These samples were mixed with acetonitrile (1:3, v/v) in order to precipitate protein component. These mixtures were centrifuged at 4000 rpm for 10 min. The supernatant was filtered through a 0.45-μm syringe filter and was stored at −20 °C until analysis.

2.4. Method validation procedure

Method validation has received considerable attention in literature and from industrial committees and regulatory agencies. The Guidance on the interpretation of the EN 45000 Series of Standards and ISO/IEC Guide 25 included a chapter on the validation of methods [30] with a list of nine validation parameters. The International Conference on Harmonization (ICH) of Technical Requirements for the Registration of Pharmaceuticals for Human Use [31] developed a consensus text on the validation of analytical procedures. The United States Environmental Protection Agency (US EPA) prepared guidance for methods development and validation for the Resource Conservation and Recovery Act (RCRA) [32]. The United States Food and Drug Administration (US FDA) proposed guidelines on submitting samples and analytical data for methods validation [33]. The United States Pharmacopoeia (USP) published specific guidelines for method validation for compound evaluation [34]. Depending on the above guidelines, it was satisfied to valid our proposed system in biological fluids by the following parameters.

2.4.1. Calibration of CE system

Before an instrument was used to validate a method, its performance should be verified using generic standards. Special attention should be paid to the equipment characteristics that are critical like baseline noise, detector response, etc. Operational qualification/performance verification (OQ/PV) kit (traceable to NIST) was used to perform a comprehensive test of the complete system using established conditions and known sample characteristics.

2.4.2. Selectivity, accuracy and precision

Selectivity of the proposed method was demonstrated by the use of pure reference materials. The peak identity was confirmed by the spectra recorded using the diode-array detector. The peak purity was estimated from the calculated peak symmetry of each analyte using the ChemStation software.

Accuracy of the method was investigated by recovery studies achieved by spiking a blank sample matrix of interest with known concentration of analytes (Pure reference materials). After that, recovery was obtained by calculating the concentration of analytes in sample matrix and comparing to the actual ones.

Precision tests were performed to determine both intra-day and inter-day variations in migration time and peak area. Intra-day precision test was carried out by repeating 10 runs within the same day and inter-day precision test was carried out by repeating measurements within three consecutive days (eight runs per day).

2.4.3. Sensitivity and method limits

Sensitivity was measured from the slope of calibration graphs. The linearity range was investigated for (+)-C and (−)-EC by selecting the concentrations according to their amounts in the investigated samples. Duplicate injections were made for each solution. The calibration graph was obtained by plotting the time-corrected peak areas against the concentrations of each analyte.

Limit of detection (LOD) was calculated by the equation [35]: $S/N = 2H/h_n$, where H is the height of the measured signal related to the average base signal. The value h_n describes the maximum spread of the baseline signal within 10 signal (peak)-width at half height at both edges of the peak. The LOD was calculated easily by this equation due to the achievement of high-resolution factors (more than 3.0) between analytes.

Limit of quantification (LOQ) was the injected amount of analyte that resulted peak height 10 times higher than the baseline noise.

2.5. Application

The commercial green tea sample was treated as described in Section 2.3. After that, the proposed procedure was applied to determine C and EC in tea solutions. In order to determine C and EC in plasma, a healthy volunteer was orally ingested with 40.0 mL of green tea. Plasma samples were treated as described in Section 2.3. 50 μL of serum sample was filtered through a 0.22-μm membrane and then was injected into the CE system. Recovery was studied by determining the concentration of both C and EC in this complex matrix and comparing the obtained time-corrected peak areas with that in aqueous media at the same concentrations.

3. Results and discussion

3.1. Method optimization

3.1.1. Type of background electrolyte (BGE)

Since catechin and epicatechin ($pKa_1 = 8.16$, $pKa_2 = 9.20$) are weak bases [36], a weak basic buffer system is preferred. The most familiar alkaline buffers like Briton-Robinson, borate and phosphate buffers were tested and the most promising results were obtained in borate buffer. The latter had a good-buffering capacity in quite a large pH interval making it possible to increase the buffer concentration and to add sufficient amounts of additives without an excessive rise in measured current. In addition, borate buffer offered the best selectivity due to that the large possibility for the formation of chelate bonds between borate ions and hydroxide radicals of analytes which could increase the negative charge and the resolution between analytes [37]. Buffer concentration was tested in the range of 25.0–75.0 mmol L^{-1}; best resolution between catechin and epicatechin (resolution factor <1.2) with shorter analysis time and acceptable generated current (less than 20 μA) were achieved in the presence of 50.0 mmol L^{-1}. Therefore, borate buffer with concentration of 50.0 mmol L^{-1} at pH 8.5 was chosen as the BGE.

3.1.2. Type of additives in the BGE

It was interesting to see a little separation between C and EC (resolution factor <1.2) in the presence of borate ions (CZE) and absence of chiral selector (Fig. 3). The reason could be due to the possibility for the formation of chelate bonds between borate ions and hydroxide radicals of C and/or EC which could increase unequally the intensity of analytes negative charges and then could increase the resolution between analytes. This resolution is very weak to apply the proposed method in biological conditions and it is necessary to modify the resolution by adding suitable additives. Cyclodextrins (CDs) and their derivatives are the most commonly used chiral selectors in CCE at the present time due to the possible stereoselective inclusion-complexation of the chiral analytes into CDs [1]. In addition, on the basis of the molecular size of analytes, it is better to work with β-cyclodextrin or its derivatives than α- or γ-cyclodextrins. On the basis of this rational, the borate buffer was supplemented with different neutral and charged β-CDs and the effect on analysis time, separation of analytes and enantioseparation of C and EC was evaluated. Among the tested CDs, β-cyclodextrin (β-CD) resulted the more effective in improving the chiral resolution of C and EC (Figs. 3 and 4) compared to succinyl-β-CD and hydroxypropyl-β-CD (Fig. 4).

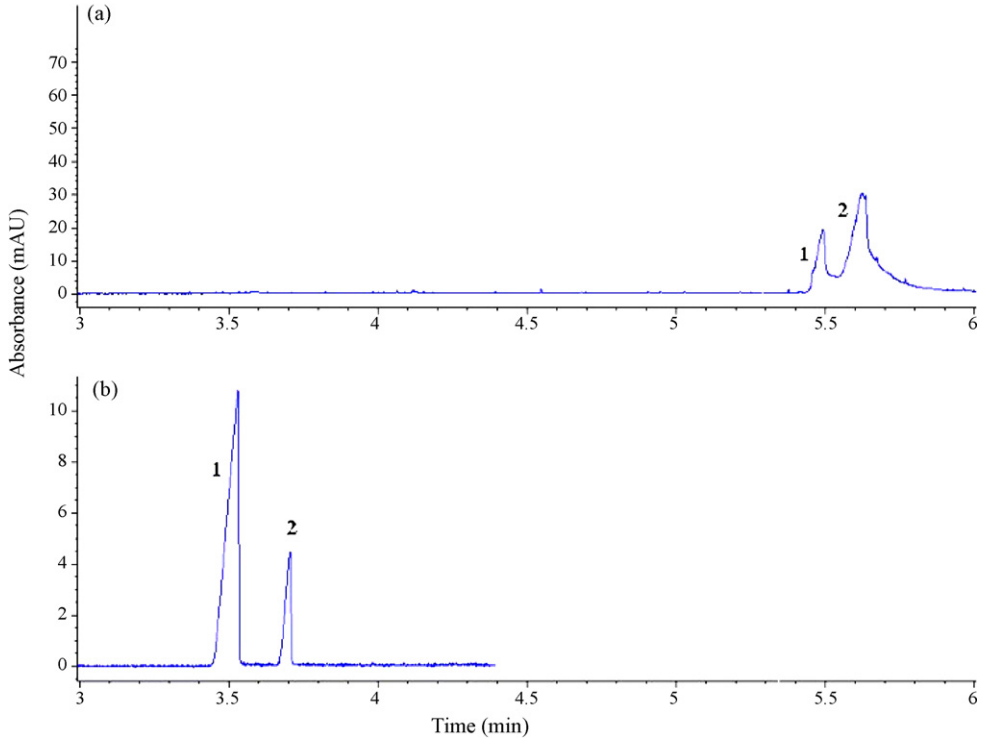

Fig. 3. Comparison between the separation of C(1) and EC(2) in the presence of 50.0 mmol L^{-1} borate buffer at pH 8.5 without additives (CZE, a) and with 3.0 mmol L^{-1} β-cyclodextrin (CCE, b) under the electrophoretic conditions as described in the text.

The effect of β-CD concentration on the separation of analytes with attention to the enantioseparation between C and EC was tested in the range of 1.0–11.0 mmol L^{-1}. A β-CD concentration of 1.0 mmol L^{-1} gave the best resolution factor of ≈3.0 with quite shorter analysis time (Fig. 4) while further increase of β-CD concentration led to a general slower migration with decrease in resolution factor between C and EC. Therefore, 50.0 mmol L^{-1} borate buffer supplemented with 1.0 mmol L^{-1} β-cyclodextrin at pH 8.5 was used as a running buffer for further analysis.

3.1.3. Modification of the fused silica capillary

In this paper we studied the separation and determination of C (200.0 ng mL^{-1}) and EC (100.0 ng mL^{-1}) in aqueous and biological media. The determination of analytes was performed in aqueous solution using a standard fused silica capillary, a capillary with bubble cell and a capillary with a high-sensitivity cell (special design, Fig. 2). The results showed that the application of a capillary with a high-sensitivity cell led to an approximately 10-fold time-corrected peak area improvement compared to standard cell and fivefold improvement compared to capillary with bubble cell (Table 1).

Cyclodextrin-chiral capillary electrophoresis is very suitable and simple technique for the analysis of catechin isomers in aqueous solutions due to their UV absorption and solubility in water. This is also the case in biological fluids but it is needed to increase the sensitivity to a level suitable for the analysis of analytes. The fused silica capillary with a high-sensitivity cell (special design) achieved this aim in human plasma as depicted in Table 1.

Table 1
Comparison between the sensitivity of three different types of fused silica capillaries for the analysis of catechin (200.0 ng mL^{-1}) and epicatechin (100.0 ng mL^{-1})

Type	Sensitivity as time-corrected peak area	
	Aqueous	Plasma
Standard fused silica capillary	C 5.50; EC 3.40	C 5.10; EC 3.30
Capillary with bubble cell	C 11.0; EC 6.90	C 13.0; EC 7.80
Capillary with high-sensitivity cell	C 55.0; EC 34.0	C 52.0; EC 32.0

3.1.4. Applied voltage, temperature, injection and wavelength

The effect of experimental parameters on the separation of analytes, sensitivity and analysis time was investigated. The applied voltage and temperature were studied in the range of 5.0–30.0 kV and ±10 °C of ambient temperature (22 °C), respectively. The best resolution between catechin isomers (≈3.0) and quiet rapid analysis time were achieved at voltage of 30.0 kV (anodic detection) with controlled temperature at 25.0 °C giving current value of 25.0 μA. The effect of injection system and wavelength on sensitivity of simultaneous determination of C and EC was studied. Hydrodynamic injection at 25.0 mbar for 5.0 s and the detection wavelength at 210 nm gave the best sensitivity for the simultaneous determination of analytes in aqueous and biological media.

3.2. Method validation

The optimized CCE method was validated in a list of nine parameters as described below.

3.2.1. Selectivity, accuracy and precision

Selectivity was evaluated by comparing the migration time of each reference material of C and EC with that obtained by analyzing real extracts of green tea as well as in plasma. In addition, the peak identity of analytes was confirmed by spiking different volumes of C and EC reference solutions in the studied matrix.

The method accuracy in aqueous solutions was evaluated by recovery studies (each measurement replicated 10 times) performed under the optimized analytical approach at three different concentration levels for each of analytes covering their working

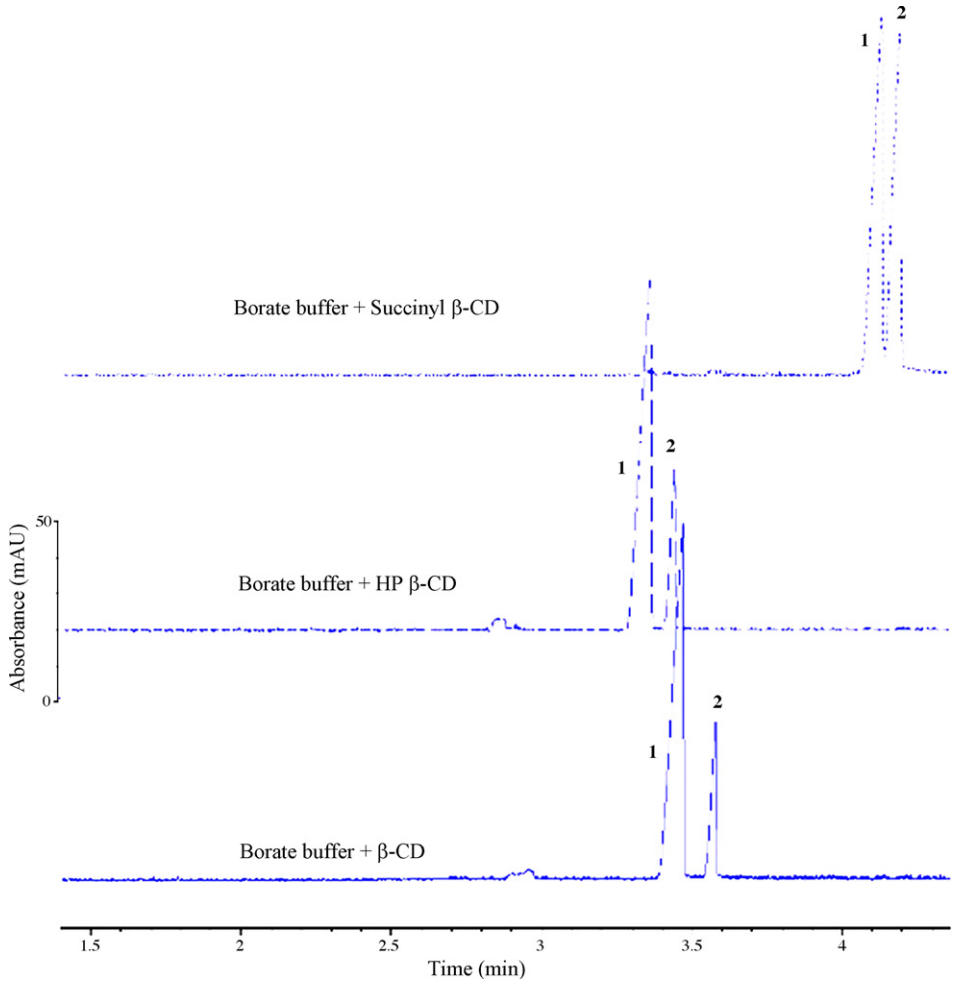

Fig. 4. Effect of chiral selector type (1.0 mmol L^{-1}) on the resolution between C(1) and EC(2) under the electrophoretic conditions as described in the text.

Table 2
Method accuracy data in aqueous solutions (n = 10) at three different concentration levels of analytes

Analyte	Added amount (ng mL^{-1})	Measured amount (ng mL^{-1})	Recovery (%)
Catechin	15.0; 150.0; 300.0	15.0; 156.0; 310.0	100; 104; 103
Epicatechin	7.0; 60.0; 100.0	7.0; 58.0; 98.0	100; 97; 98

concentration range as indicated in Table 2. The recovery ranged between 97 and 104%. The accuracy was also determined by recovery studies in plasma media and the obtained results were indicated in application section.

The method precision was tested by replicating measurements of reconstituted mixture containing C and EC reference materials at concentrations of 130.0 and 50.0 ng mL^{-1}, respectively within the same day (repeatability, intra-day precision) and three consecutive days with different analysts (reproducibility, inter-day precision) in aqueous media under the optimized conditions. The obtained results as relative standard deviation (R.S.D.) were collected in Table 3. Results indicated that the null hypothesis that R.S.D. belong to the same population is accepted; there is no a significant difference in precision at 99% confidence level. Therefore, our proposed method is considered precise and accurate for the determination of C and EC.

3.2.2. *Linearity, sensitivity and method limits*

The linearity to the detector was investigated at the wavelength of 210 nm by linear regression analysis of the response (y) defined as the time-corrected peak area (area/migration time) ratio against the concentration of analytes (x) in ng mL^{-1}. (+)-C up to 300.0 ng mL^{-1} and (−)-EC up to 100.0 ng mL^{-1} were obtained linearly with good correlation coefficient (0.995–0.996) at 99% confidence level (CL). Table 4 indicates the calibration data of C (A) and EC (B) with the results of regression analysis using MiniTab software. It was obvious from the same table that method was sensitive for the determination of C 1.3 times more than EC.

Table 3
Method precision data in aqueous solutions

Analyte	Concentration (ng mL^{-1})	Migration time		Time-corrected peak area	
		Inter-days R.S.D. (n = 8)	Intra-day R.S.D. (n = 24)	Inter-days R.S.D. (n = 8)	Intra-day R.S.D. (n = 24)
Catechin	130.0	1.20	1.85	2.12	3.10
Epicatechin	50.0	1.53	2.12	3.20	4.11

Table 4
Calibration graphs data of catechin and epicatechin: $Y = mX + q$ with slope (m) and intercept (q), $n = 5.0$

Analyte	Concentration range (ng mL^{-1})	m	q	r^2 (%)[a]	s[b]	CL (%)[c]
Catechin	25.0–300.0	0.289	−0.754	99.5	2.803	99
Epicatechin	5.0–100.0	0.339	−0.163	99.6	1.015	99

[a] Correlation coefficient percent.
[b] Standard deviation of calibration plot.
[c] Confidence level.

Table 5
Detection limits and sensitivity of catechin (C) and epicatechin (EC) by various methods

Method	LOD (ng mL^{-1})	Sensitivity (ng mL^{-1} area^{-1})	References
CLC-EC	1.76 (C) and 2.16 (EC)	N/A	[38]
LC–LC–MS	2.00 (C) and 2.00 (EC)	N/A	[39]
HPLC–ESIMS	0.22 (C) and 0.21 (EC)	15853 (C) and 15433 (EC)	[40]
HPLC-SPE	2.89 (C) and 2.89 (EC)	N/A	[41]
HPLC-EC	2.97 (C) and 1.72 (EC)	N/A	[42]
HPLC-EC	3.00 (C) and 3.00 (EC)	N/A	[43]
HPLC-FL	4.97 (C) and 4.97 (EC)	N/A	[44]
HPLC-FL	5.00 (C) and 5.00 (EC)	N/A	[43]
HPLC-FL	5.00 (C)	995 (C)	[45]
HPLC-CA	5.00 (C)	N/A	[46]
HPLC-DAD	17.40 (C)	N/A	[47]
HPLC-UV	1000 (C)	1300 (C)	[45]
HPLC-UV	22.00 (C) and 23.00 (EC)	N/A	[43]
CE	50.00 (C)	N/A	[48]
CE-HSC	3.20 (C) and 1.00 (EC)	0.289 (C) and 0.339 (EC)	Current

CA = coulometric array detection; CE = capillary electrophoresis; CLC = capillary liquid chromatography system; DAD = diode-array detection; EC = electrochemical detection; ESIMS = electrospray ionization mass spectrometry; FL = fluorescence detection; HPLC = high-performance liquid chromatography; HSC = high-sensitivity cell; LC = liquid chromatography; MS = mass spectrophotometry; SPE = solid-phase extraction; UV = ultraviolet.

The limit of detection (LOD) was estimated and found to be 3.2 and 1.0 ng mL^{-1} for (+)-C and (−)-EC, respectively. The limit of quantification (LOQ) was similarly estimated and found to be 10.1 and 3.1 ng mL^{-1} for (+)-C and (−)-EC, respectively.

Sensitivity and detection limits of (+)-C and (−)-EC were compared with other alternative techniques proposed to increase sensitivity of analytes in human plasma as shown in Table 5. The LOD of (+)-C in the present work was higher than or about equal others except CLC-EC [38], LC–LC–MS [39] and HPLC–ESIMS [40]. Although, the LOD of (+)-C in these techniques was lower than the present method, whereas the proposed system gave lower LOD of (−)-EC than CLC-EC and LC–LC–MS. In addition, it was more sensitive than HPLC–ESIMS [40], HPLC-FL [45] and HPLC-UV [45]. Therefore, the present system modified the sensitivity of analytes in plasma matrix.

3.2.3. Robustness, stability and completeness

The robustness test was done with the so-called "Youden–Steiner partial factor design" where in only five replicate analysis four factors (temperature, applied voltage, pH and β-CD concentration) were varied in a narrow range around the optimized ones. Good values (R.S.D. ranged between 0.08 and 1.40%) were obtained proving that our proposed method is quite robust.

The system stability was checked by injecting concentrations corresponding to the quantitation limits of analytes in biological matrix during 48 h and comparing the collected results with data collected from freshly prepared standard mixtures. The R.S.D. was found to be 3.56–5.30%, indicating that our system is stable for a long-analysis time.

The completeness of our proposed method was checked by applying in the following equation: $\%C = 100 \times V/n$, where $\%C$ = percent completeness, V = number of measurement judged valid and n = total number of measurements necessary to achieve at 99% confidence level. It was found that our proposed method achieved 101.2% completeness ($n = 20$) in aqueous extracted media and 98.0% in plasma media at 99% confidence level.

3.3. Application

The described method was found to be suitable for the determination of C and EC in green tea and human plasma media. Fig. 5 indicates a representative electropherogram for the determination of C and EC in green tea solution after dilution in water (1:8,

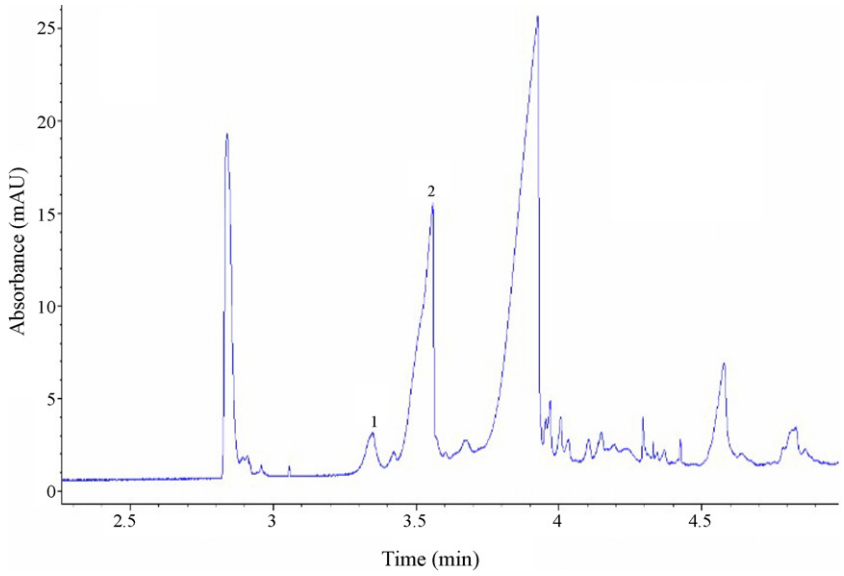

Fig. 5. Representative electropherogram for the determination of C(1) and EC(2) in green tea (2.0 g/40 mL) solution after dilution in water (1:8, v/v) under the optimal conditions—running buffer: 50.0 mmol L^{-1} borate buffer + 1.0 mmol L^{-1} β-CD at pH 8.5 with high-sensitivity cell with Agilent special design (8.5-cm outlet, 58.0-cm effective length × 50.0-μm internal diameter); 30 kV; 25 °C; pressure injection: 5 s at 25 mbar; detection: 210 nm.

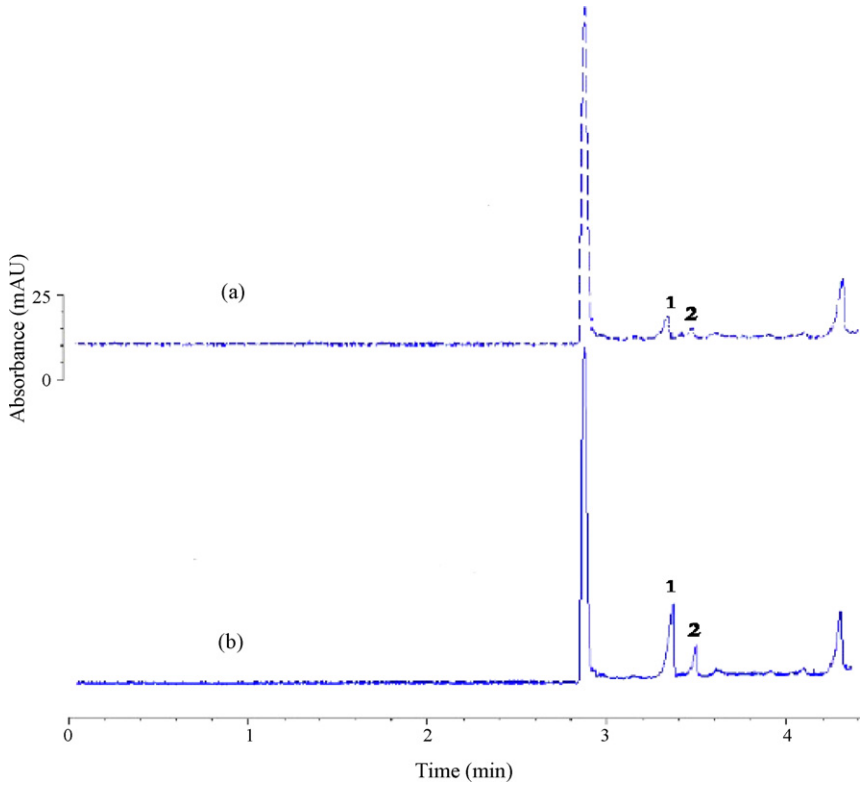

Fig. 6. Electropherogram of a plasma sample (a) and of a blank plasma standard addition of 50 ng mL^{-1} of C(1) and EC(2) (b) under optimal conditions as described in Fig. 5.

Table 6
Method precision data in plasma media

Analyte	Concentration (ng mL^{-1})	Migration time		Time-corrected peak area	
		Inter-days R.S.D. (n = 3)	Intra-day R.S.D. (n = 10)	Inter-days R.S.D. (n = 3)	Intra-day R.S.D. (n = 10)
Catechin	32.0	3.15	5.23	4.20	6.50
Epicatechin	11.0	4.33	5.93	5.10	7.31

v/v). The concentrations of C and EC were found to be 184.0 and 608.0 ng mL^{-1}, respectively.

To determine the unchanged amounts of C and EC in plasma, the samples of healthy volunteer were withdrawn after 2 h of administered dose and treated as described in Section 2. C and EC were determined in plasma after protein precipitation in order to increase the precision and reproducibility of measurements. Fig. 6 shows electropherograms of a blank plasma sample and of a plasma sample containing 50.0 ng mL^{-1} of analytes at pH 8.5. The electropherograms demonstrated that the C and EC peaks were completely separated from plasma components. The concentrations of C and EC in plasma were found to be 32.0 and 11.0 ng mL^{-1}, respectively. Therefore, unchanged C and EC amounted to about 17.4 and 1.8% of the administered dose in the 2 h plasma collection. The proposed method achieved mean recoveries in plasma ranging between 95 and 105%. To monitor the repeatability and reproducibility of the peak areas and the migration times in human plasma, three injections of plasma samples containing analytes within three consecutive days were made. Inter- and intra-day precisions of the peak areas and the migration times gave good R.S.D. values as declared in Table 6. Due to the high resolution between catechin isomers and their separation from plasma components, the detection limits of C and EC were determined by two equations as described elsewhere [28,35] in this complex media using high-sensitivity cell and they were found to be 4.1 and 1.5 ng mL^{-1}, respectively.

4. Conclusion

A simple and reliable chiral capillary electrophoresis (CCE) coupled with a high-sensitivity cell (special design) has been developed for the improvement of (+)-C and (−)-EC sensitivity in tea solutions and human plasma. This technique has been easy to handle and has showed good robustness. The high sensitivity and the relatively short analysis time have been the main advantages of the current work. Therefore, our modified system together with the biological activity of catechin isomers has accounted for the importance of the proposed system for clinical analysis.

References

[1] B. Chankvetadze, Capillary Electrophoresis in Chiral Analysis, John Wiley & Sons Ltd., UK, 1997.
[2] G. Yu, C. Hsieh, L. Wang, S. Yu, X. Li, T. Jin, Cancer Control 6 (1995) 532.
[3] Y.T. Gao, J.K. McLaughlin, W.J. Blot, B.T. Ji, Q. Di, J.F. Fraumeni Jr, J. Natl. Cancer Inst. 86 (1995) 855.
[4] G. Axelsson, T. Liljeqvist, L. Andersson, B. Bergman, R. Rylander, Int. J. Epidemiol. 25 (1996) 32.
[5] S.O. Keli, M.G.L. Hertog, E.J.M. Feskens, D. Kromhout, Arch. Intern. Med. 156 (1996) 637.
[6] T. Yokozawa, E. Dong, T. Nakagawa, D.W. Kim, M. Hattori, H. Nakagawa, Biosci. Biotech. Biochem. 62 (1998) 44.
[7] K. Imai, K. Nakachi, Br. Med. J. 310 (1995) 693.
[8] N.C. Cook, S. Samman, J. Nutr. Biochem. 7 (1996) 66.
[9] J.B. Harborne, The Flavonoids. Advances in Research Since 1986, Chapman & Hall, London, UK, 1994.
[10] A. Finger, S. Kuhr, U.H. Engelhardt, J. Chromatogr. A 624 (1992) 293.

[11] W.E. Bronner, G.R. Beecher, J. Chromatogr. A 805 (1998) 137.
[12] F.R. Montreau, Connaissance Vigne Vin 24 (1972) 397.
[13] H.Y. He, C. Kies, Plant Foods Hum. Nutr. 46 (1994) 221.
[14] G.A.A. Kivits, J.P. Frans, F. van der Sman, L.B.M. Tijburg, Int. J. Food Sci. 48 (1997) 387.
[15] Y. Ho, Y.L. Lee, K.Y. Hsu, J. Chromatogr. B: Biomed. Appl. 665 (1995) 383.
[16] P. Cremin, S. Kasim-Karakas, A.L. Waterhouse, J. Agric. Food Chem. 49 (2001) 1747.
[17] C. Li, X. Meng, B. Winnik, M.J. Lee, H. Lu, S. Sheng, B. Buckley, C.S. Yang, Chem. Res. Toxicol. 14 (2001) 702.
[18] A. Alnajjak, A.M. Idris, M. Multzenberg, B. McCord, J. Chromatogr. B 856 (2007) 62.
[19] A. De Rossi, C. Desiderio, J. Chromatogr. B 839 (2006) 6.
[20] N. Anastos, N.W. Barnett, S.W. Lewis, Talanta 67 (2005) 269.
[21] B.M. Simonet, A. Rios, M. Valcarcel, TrAc Trends Anal. Chem. 22 (2003) 605.
[22] J. Marak, P. Mikus, K. Marakova, D. Kaniansky, I. Valaskova, E. Havranek, Electrophoresis 28 (2007) 2738.
[23] P. Mikus, K. Marakova, J. Marak, D. Kaniansky, I. Valaskova, E. Havranek, J. Chromatogr. A 1179 (2008) 9.
[24] P. Mikus, P. Kubacak, I. Valaskova, E. Havranek, Talanta 70 (2006) 840.
[25] J. Horakova, J. Petr, V. Maier, J. Znaleziona, A. Stanova, J. Marak, D. Kaniansky, J. Sevcık, J. Chromatogr. A 1155 (2007) 193.
[26] R.-L. Chien, Electrophoresis 24 (2003) 486.
[27] P. Britz-McKibbin, D.D.Y. Chen, Anal. Chem. 72 (2000) 1242.
[28] Y. Mrestani, R. Neubert, J. Chromatogr. A 871 (2000) 351.
[29] Y. Mrestani, R. Neubert, F. Nagel, J. Pharm. Biomed. 20 (1999) 899.
[30] EURACHEM Guidance Document No. 1/WELAC Guidance Document No. WGD 2: Accreditation for Chemical Laboratories: Guidance on the Interpretation of The EN 45000 Series of Standards and ISO/IEC Guide 25, 1993.
[31] International Conference on Harmonization (ICH) of Technical Requirements for the Registration of Pharmaceuticals for Human Use, Validation of Analytical Procedures, ICH-Q2A, Geneva 1995.
[32] US EPA, Guidance for Methods Development and Methods Validation for The Resource Conservation and Recovery Act (RCRA) Program, Washington, 1995.
[33] US FDA Technical Review Guide: Validation of Chromatographic Methods, Center for Drug Evaluation and Research (CDER), Rockville, MD, 1993.
[34] General Chapter <1225>, Validation of Compendial methods, United States Pharmacopeia XXIII, National Formulary, XVIII, Rockville, MD, The United States Pharmacopeial Convention Inc., 1995, pp. 1710–1612.
[35] Ph. Eur/DAB (German Pharmacopoeia) Official Edition. Deutscher Apotheker Verlag, Stuttgart 1996, Methoden: 2.2.28 und.29.
[36] N.P. Slabbert, Tetrahedron 33 (1977) 821.
[37] H. Horie, K. Kohata, J. Chromatogr. A 881 (2000) 425.
[38] A. Kotani, K. Takahashi, H. Hakamata, S. Kojima, F. Kusu, Anal. Sci. 23 (2007) 157.
[39] M. Takino, S. Daishima, K. Yamaguchi, T. Nakahara, Analyst 128 (2003) 46.
[40] Y. Masukawa, Y. Matsui, N. Shimizu, N. Kondou, H. Endou, M. Kuzukawa, T. Hase, J. Chromatogr. B 834 (2006) 26.
[41] T. Unno, Y.M. Sagesaka, T. Kakuda, Agric. Food Chem. 53 (2005) 9885.
[42] A. Bolarinwa, J. Linseisen, J. Chromatogr. B 823 (2005) 143.
[43] J.L. Donovana, D.L. Luthriaa, P. Strempleb, A.L. Waterhouse, J. Chromatogr. B 726 (1999) 277.
[44] D.J. Jones, C.K. Lim, D.R. Ferry, A. Gescher, Biomed. Chromatogr. 12 (1998) 232.
[45] S. Carando, P. Teissedre, J. Cabanis, J. Chromatogr. B 707 (1998) 195.
[46] M.-J. Lee, S. Prabhu, X. Meng, C. Li, C.S. Yang, Anal. Biochem. 279 (2000) 164.
[47] H.Y. Pan, D.L. Liu, P.P. Xu, M.L. Lu, Acta Pharm. Sin. 26 (1991) 371.
[48] B.L. Lee, C.N. Ong, J. Chromatogr. A 881 (2000) 439.

Talanta 76 (2008) 128–133

Contents lists available at ScienceDirect

Talanta

journal homepage: www.elsevier.com/locate/talanta

Flow injection analysis using carbon film resistor electrodes for amperometric determination of ambroxol

Fabiana S. Felix[a], Christopher M.A. Brett[b], Lúcio Angnes[a,*]

[a] Instituto de Química, Universidade de São Paulo, 05508-000 São Paulo, Brazil
[b] Departamento de Química, Universidade de Coimbra, 3004-535 Coimbra, Portugal

ARTICLE INFO

Article history:
Received 29 November 2007
Received in revised form 12 February 2008
Accepted 14 February 2008
Available online 19 February 2008

Keywords:
Flow injection analysis
Carbon film electrodes
Ambroxol
Amperometry
Pharmaceutical products

ABSTRACT

Flow injection analysis (FIA) using a carbon film sensor for amperometric detection was explored for ambroxol analysis in pharmaceutical formulations. The specially designed flow cell designed in the lab generated sharp and reproducible current peaks, with a wide linear dynamic range from 5×10^{-7} to 3.5×10^{-4} mol L^{-1}, in 0.1 mol L^{-1} sulfuric acid electrolyte, as well as high sensitivity, 0.110 A mol^{-1} L cm^{-2} at the optimized flow rate. A detection limit of 7.6×10^{-8} mol L^{-1} and a sampling frequency of 50 determinations per hour were achieved, employing injected volumes of 100 μL and a flow rate of 2.0 mL min^{-1}. The repeatability, expressed as R.S.D. for successive and alternated injections of 6.0×10^{-6} and 6.0×10^{-5} mol L^{-1} ambroxol solutions, was 3.0 and 1.5%, respectively, without any noticeable memory effect between injections. The proposed method was applied to the analysis of ambroxol in pharmaceutical samples and the results obtained were compared with UV spectrophotometric and acid–base titrimetric methods. Good agreement between the results utilizing the three methods and the labeled values was achieved, corroborating the good performance of the proposed electrochemical methodology for ambroxol analysis.

1. Introduction

Ambroxol, *trans*-4-[(2-amino-3,5-dibromobenzyl)amino]cyclohexanol or 2-amino-3,5-dibromo-*N*-[*trans*-4-hydroxycyclohexyl]-benzylamine, is an expectorant agent which leads to bronchial secretion due to its mucolytic properties. It is administered as the hydrochloride in daily doses of 30–120 mg and is available commercially as syrups, granules, tablets, or in solutions, utilized in the injectable form or for inhalation [1].

Several analytical methods for ambroxol quantification in biological fluids and pharmaceutical formulations are described in the literature. These include (TLC) densitometry [2], high performance liquid chromatography [3–12], capillary electrophoresis [13–15], Raman-spectroscopy [16,17], UV-spectrophotometry [18,19], gas chromatography [20], voltammetry [21,22] and chromatography with amperometric detection [23]. The British Pharmacopoeia recommends potentiometric titration as the official method [24]. Only a few automated analytical procedures for the quantification of this drug have been reported, including liquid chromatography coupled with sequential injection analysis (SIA) [25,26], spectrophotometry with flow injection analysis (FIA) [27] and potentiometry under flow conditions [28]. Some of the reported methods require time-consuming sample preparation or expensive instrumentation.

Flow injection methodology in association with amperometric detection has provided a means of automation in routine analyses with good selectivity and sensitivity. To our knowledge, FIA using amperometric detection for ambroxol determination has still not been explored.

In this work, carbon film electrodes have been employed as sensors in the electrochemical determination of ambroxol in different pharmaceutical samples, without any sample pretreatment. Cyclic voltammetry and flow injection analysis with amperometric detection were performed employing carbon films as working electrodes. These electrodes have a wide potential window, particularly after electrochemical pretreatment by cycling in acid media [29]. They have been characterized by electrochemical impedance spectroscopy [30] and have already been used in different applications such as trace metal analysis [31,32], biosensors [33–39] and pharmaceutical formulations analysis [40]. We will describe the

* Corresponding author. Tel.: +55 11 3091 3828; fax: +55 11 3815 5579.
E-mail address: luangnes@iq.usp.br (L. Angnes).

0039-9140/$ – see front matter © 2008 Elsevier B.V. All rights reserved.
doi:10.1016/j.talanta.2008.02.005

application of these electrodes to the direct analysis of ambroxol in pharmaceutical products.

2. Experimental

2.1. Reagents and solutions

Sulfuric acid, sodium mono-hydrogen phosphate, potassium di-hydrogen phosphate, orthophosphoric acid, citric acid, benzoic acid, sodium sulfate and hydrochloric acid were acquired from Merck (Darmstadt, Germany). Ambroxol hydrochloride in its pure form was received as a gift from Arvensis Manipulation Pharmacy (São Paulo, Brazil), and was used without further purification. Ambroxol solutions were freshly prepared by dissolving the solid salt in supporting electrolyte. Two different supporting electrolytes were used during cyclic voltammetric experiments, phosphate buffer (0.1 mol L^{-1}, pH 2–12, in the preliminary experiments) and sulfuric acid/sodium sulfate solution (0.1 mol L^{-1}, pH 1–4). The phosphate buffer solutions (0.1 mol L^{-1}) were prepared by mixing solutions of sodium mono-hydrogen phosphate, potassium di-hydrogen phosphate, orthophosphoric acid or sodium hydroxide to give the desired pH. Sulfuric/sodium sulfate solutions were prepared by mixing the required amounts of $H_2SO_4 + Na_2SO_4$, both 0.1 mol L^{-1}. All solutions were prepared with ultra pure water from a Millipore Milli-Q system (resistivity $\geq$18 MΩ cm). The pharmaceutical products analyzed were purchased in a local drugstore.

2.2. Electrode preparation

Electrodes were made from carbon film resistors of 2 Ω nominal resistance. These resistors (built for electronic applications) are fabricated from ceramic cylinders with 4–6 mm length and 1.5 mm external diameter by pyrolytic deposition of carbon [29]. The resistor has two metal caps with wires as external contact placed over each end. One of the two caps was removed and the other was covered with epoxy resin. In this way the exposed cylindrical area of the electrode was ~0.17 cm^2. Before use, each electrode was electrochemically pretreated in 1.0 mol L^{-1} perchloric acid. This conditioning treatment is essential to ensure a good performance of the electrode [29,30].

2.3. Apparatus

Voltammetric measurements were carried out with an Eco-Chemie Autolab PGSTAT 20 potentiostat (EcoChemie, The Netherlands). Cyclic voltammetry studies were done in a conventional 10 mL cell. The FIA/amperometric experiments were performed using the flow cell previously described [40] using a carbon film resistor as working electrode, an $Ag/AgCl_{sat}$ (sat. KCl) as reference electrode and a stainless steel tube (positioned in the exit of the flow channel) as the auxiliary electrode. A peristaltic pump (Ismatec, Zurich, Switzerland) was used for fluid propulsion during the analyses. The standard solutions and ambroxol samples were introduced into the stream through a manually operated injection valve.

Spectrophotometric measurements were performed with a Hitachi U-2001 UV–vis spectrophotometer with a conventional quartz cell (optical path length 1.00 cm and total volume of 4 mL). Potentiometric titration measurements were carried using a pH-meter (Quimis-model 400 M1S) with a combined glass electrode. All pH measurements were performed at room temperature, maintained at 25 ± 2 °C.

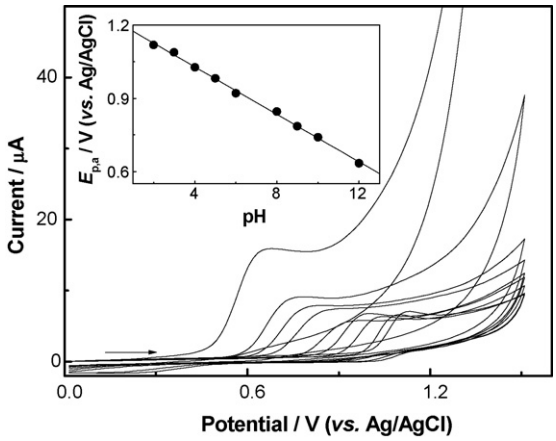

Fig. 1. Cyclic voltammograms of 2.0×10^{-4} mol L^{-1} ambroxol in 0.1 mol L^{-1} phosphate buffer solution at different pH (from 2 to 12). Carbon film electrode area = 0.17 cm^2. Scan rate 100 mV s^{-1}.

2.4. Preparation of the samples and standard solution

For amperometric studies, aliquots of 120 μL or 240 μL of ambroxol samples (for syrups containing 30 and 15 mg of drug, respectively) were transferred to a volumetric flask of 100 mL and filled with 0.1 mol L^{-1} sulfuric acid solution. Standard solutions of ambroxol were prepared daily in a similar way, in the same supporting electrolyte.

For the spectrophotometric studies, aliquots of 200 μL and 400 μL of ambroxol syrup (for samples containing 30 and 15 mg, respectively) were appropriately diluted in 0.1 mol L^{-1} hydrochloric acid solution, in accordance with the methodology described in the literature [21]. The calibration curve was done for ambroxol concentrations ranging from 1.0 to 5.0×10^{-5} mol L^{-1} in 0.1 mol L^{-1} hydrochloric acid solution. The absorbances were measured at 307 nm [22].

The acid–base titration of the pharmaceutical formulation samples was done following the procedure described in the British Pharmacopoeia [24]. A known amount of hydrochloric acid was added to a chosen volume of syrup. The mixture was then titrated with a standardized (0.1 mol L^{-1}) sodium hydroxide solution. Two equivalence points were observed, the first corresponding to the neutralization of the excess of hydrochloric acid and of the other acidic excipients such as citric, tartaric and benzoic acids. The second equivalence point was due to neutralization of the protonated ambroxol. The difference of titrant volume between these two equivalence points was then used to calculate the concentration of ambroxol (pK_2 = 7.16) [7].

3. Results and discussion

3.1. Voltammetric studies

The electrochemical behavior of ambroxol on the carbon film electrode was initially explored in phosphate medium, due to the ease of preparation of phosphate buffer solutions over a wide range of pH. Fig. 1 shows cyclic voltammograms of 2.0×10^{-4} mol L^{-1} ambroxol in 0.1 mol L^{-1} phosphate buffer over the pH range from 2 until 12. In all these conditions, the compound was oxidized presenting just one oxidation peak in the potential region studied, corresponding to an irreversible process. The peak potential for ambroxol oxidation showed a linear variation with increase of pH and shifted towards to a less positive potential. A slope of 49 mV pH^{-1} (correlation coefficient of 0.998) was found over the whole

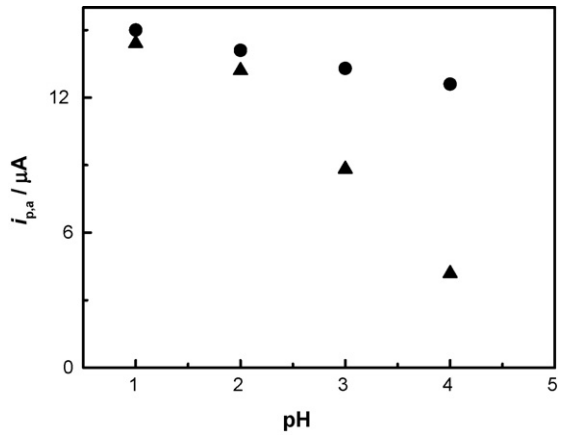

Fig. 2. Oxidation peak current, i_{pa}, measured by cyclic voltammetry in sulfuric acid/sodium sulfate (0.1 mol L^{-1}, pH 1–4) in a solution containing 5.0×10^{-4} mol L^{-1} ambroxol: (●) 1st cycle and (▲) 11th cycle.

pH range from 2 to 12, demonstrating that the oxidation potential is strongly pH-dependent, see inset of Fig. 1. The corresponding value of the anodic transfer coefficient α_a of 0.72 ± 0.09 calculated from the slope of this plot is very close of that value found by Habib and Zayed [21] of 0.76 ± 0.04 for an irreversible reduction process involving the transfer of one electron and one proton in Britton–Robinson buffer solution.

From voltammetric studies of ambroxol and the electrochemical oxidation of clenbuterol (which has a structure very similar to ambroxol) [41,42], Demircigil et al. [22] proposed a mechanism for the oxidation process of ambroxol. According to these authors, this process involves the oxidation of the amine group to form a radical cation, two of which react head to head to form a dimer. This dimer is more easily oxidized than ambroxol during the second cycle of the potential sweep. Tamba and Torreggiani [43] investigated the chemical properties of ambroxol under irradiation. They demonstrated that ambroxol is a good scavenger of water radicals, especially of e_{aq} and •OH species. In their studies it was verified that •OH radical attack was preferentially addressed to the ring positions occupied by bromine atoms, generating hydroxycyclohexadienyl radicals.

Our experiments showed higher anodic currents when the pH is increased and at less positive oxidation potentials. Unfortunately, in alkaline medium the irreproducibility of the measurements was very high and the response for successive cyclic voltammograms decreased very rapidly. In acidic medium, more reproducible results were obtained but a very narrow linear range of response was observed. This behavior made us search for different supporting electrolytes, based on sulfuric, acetic and hydrochloric acids. Amongst them, experiments performed in sulfuric acid medium lead to the most favorable results. To evaluate the best working pH, experiments involving sulfuric acid/sodium sulfate were performed.

Fig. 2 shows the results of cyclic voltammetry experiments carried out using 5.0×10^{-3} mol L^{-1} ambroxol in sulfuric acid/sodium sulfate solution (pH 1–4) at a carbon film working electrode. Only a slight decrease of the peak current values was observed after 11 cycles at pH 1. However at pH 4 the decrease of the signal was significant (~33%) compared with the initial current value. The reason for this decrease of signal is not obvious, but probably at this pH, the products generated during the oxidation process remain on the electrode, partially blocking its surface.

Based on the results presented in Fig. 2, as well as on other experiments not shown here, and considering mainly the good reproducibility and the linear response range obtained in 0.1 mol L^{-1} H_2SO_4, this condition was selected for all the experiments performed in the following experiments.

Fig. 3 presents cyclic voltammograms corresponding to increasing additions of ambroxol in 0.1 mol L^{-1} sulfuric acid solution at scan rate 100 mV s^{-1} on carbon film electrode. The signal obtained for each concentration of ambroxol was very stable and reproducible. A very good linear relationship between anodic current and ambroxol concentration ($1.0 \times 10^{-4} - 2.0 \times 10^{-3}$ mol L^{-1}) was observed, as can be seen in the inset of Fig. 3. These results confirmed the usefulness of sulfuric acid as supporting electrolyte in the analysis of ambroxol.

The variation of anodic current with scan rate, from 0.01 to 0.9 V s^{-1} was investigated in the same medium. As the scan rate was increased, the peak potential shifted towards more positive values, confirming the irreversibility of the process. The oxidation current values varied linearly with the square root of the scan rate ($\nu^{1/2}$), with a slope of 0.38 (correlation coefficient of 0.999), suggesting a diffusion-controlled process. Moreover the variation of logarithm between the oxidation current and the scan rate presented a slope of 0.47 (correlation coefficient of 0.999) because of the diffusive component, close to the theoretical value of 0.5 for a diffusion-controlled process [44]. The slope values obtained in the present study are in very good agreement with those found by Demircigil et al. [22]: 0.37 (plot of anodic current with square root of the scan rate) and 0.46 (variation of logarithm between the anodic current and the scan rate) in Britton–Robinson buffer solution.

The electrochemical oxidation of ambroxol was also investigated using two other electrode materials in the presence of 2.0×10^{-4} mol L^{-1} ambroxol in 0.1 mol L^{-1} sulfuric acid solution. Results obtained for carbon film, glassy carbon and platinum electrodes are shown in Fig. 4. For platinum electrodes, it was not possible to obtain a well-defined anodic peak. For both carbon film and glassy carbon electrodes an anodic wave was observed during the forward sweep, corresponding to ambroxol oxidation (around +1.1 V *vs.* Ag/AgCl) and a cathodic process in the reverse sweep was also observed. The magnitude of the anodic current density at the carbon film electrode was greater than at glassy carbon. This is a clear indication that a more favorable electrochemical performance for the oxidation of ambroxol is achieved on the carbon film surface.

3.2. Flow injection parameters

To establish the best conditions for flow injection analysis of ambroxol, the influence of parameters such as flow rate and injected sample volume on the amperometric signal was evaluated using

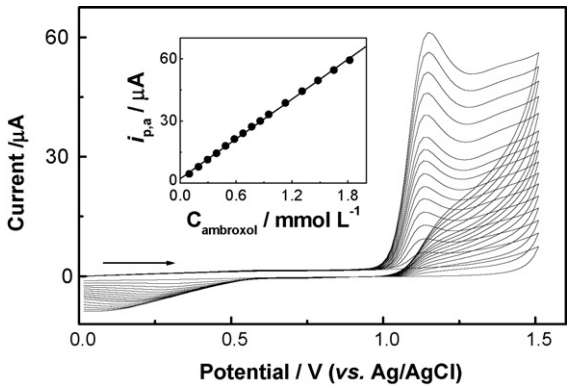

Fig. 3. Cyclic voltammograms measured with the carbon film electrode ($A = 0.17$ cm^2) in 0.1 mol L^{-1} sulfuric acid for increasing concentrations of ambroxol (from 1.0×10^{-4} to 2.0×10^{-3} mol L^{-1}). Scan rate: 100 mV s^{-1}.

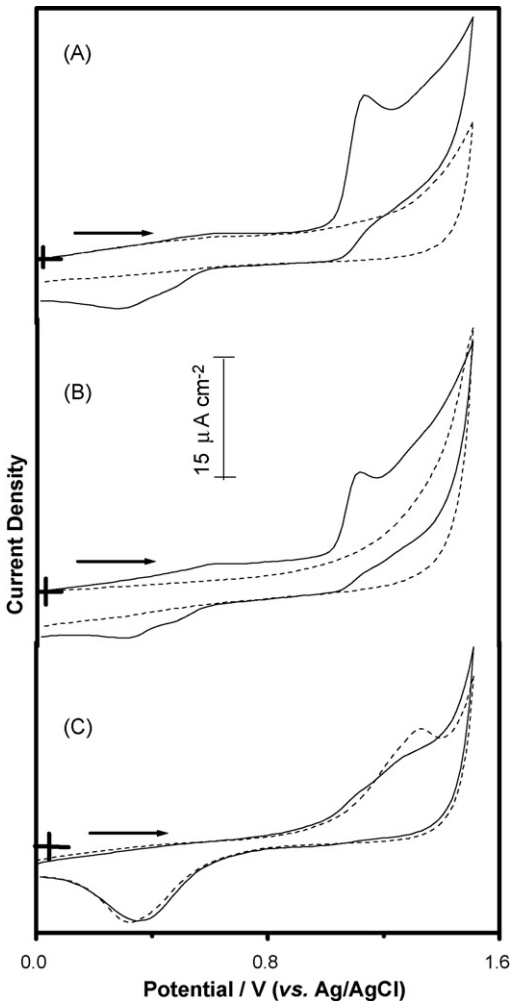

Fig. 4. Cyclic voltammograms at different electrodes: carbon film (A), glassy carbon (B) and platinum (C) in 0.1 mol L^{-1} sulfuric acid solution (dashed line) and in the presence of 2.0×10^{-4} mol L^{-1} ambroxol (solid line). Electrode areas: (A) 0.17 cm^2, (B) 0.18 cm^2 and (C) 0.07 cm^2. Scan rate, 100 mV s^{-1}.

a solution containing 5.0×10^{-6} mol L^{-1} of the analyte diluted in 0.1 mol L^{-1} sulfuric acid. Taking into account the cyclic voltammetric studies (Fig. 3) and hydrodynamic experiments (not showed), an applied potential of +1.15 V (*vs.* Ag/AgCl) was selected for all FIA experiments.

The effect of flow rate (from 1.0 to 5.0 mL min^{-1}) on the analytical signal was evaluated, utilizing a sample volume of 100 μL. The current increased with flow rate until 4.0 mL min^{-1} and remained virtually constant for higher values. When the flow rate was

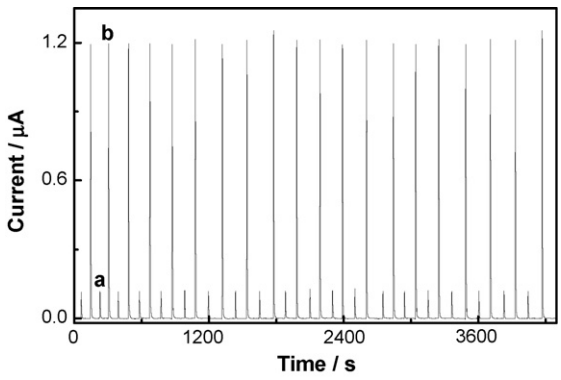

Fig. 5. FIA results for alternate injections of (a) 6.0×10^{-6} mol L^{-1}, (b) 6.0×10^{-5} mol L^{-1} ambroxol in 0.1 mol L^{-1} sulfuric acid supporting electrolyte. Applied potential +1.15 V *vs.* Ag/AgCl, flow rate 2.0 mL min^{-1}, sample loop 100 μL.

increased above 2.0 mL min^{-1} there was a decrease in repeatability, the relative standard deviation (R.S.D.) was 1.0% for 2.0 mL min^{-1} compared with 2.5% for 3.0 mL min^{-1}. The R.S.D. did not significantly improve at flow rates below 2.0 mL min^{-1}. Taking into account these aspects, a flow rate of 2.0 mL min^{-1} was selected as the most favorable due to its good repeatability and satisfactory sampling rate (50 determinations per hour).

The effect of sample volume injected in the stream was also evaluated using volumes from 50 up to 300 μL. The amperometric signal increased linearly with sampling loops from 50 until 150 μL. A volume of 100 μL was adopted because it represented the minimum sample volume that gave good repeatability and was the most favorable taking into account the sampling frequency.

3.3. Analytical characteristics

In order to establish the linear working range, a series of experiments was performed with a standard solution of ambroxol. All ambroxol standard solutions were prepared by dilution from a 1.0×10^{-2} mol L^{-1} stock solution. This study showed a wide linear range from 5.0×10^{-7} to 3.5×10^{-4} mol L^{-1}, with calibration plot intercept at 0.025 ± 0.011 μA and a slope of 18.76 ± 0.11 μA/mmol, with a correlation coefficient of 0.999. The estimated detection limit was 7.61×10^{-8} mol L^{-1} (three times the blank standard deviation/slope) and the quantification limit was calculated as 2.53×10^{-7} mol L^{-1}.

Fig. 5 presents the FIA–amperometric responses for 40 successive and alternated injections of ambroxol solutions containing 6.0×10^{-6} and 6.0×10^{-5} mol L^{-1} of ambroxol. A very good repeatability of the current peaks for both concentrations is seen in this experiment. In this series of injections, relative standard deviations (R.S.D.) of 3.0 and 1.5% for 6.0×10^{-6} and 6.0×10^{-5} mol L^{-1}

Table 1
Results obtained after analyses of ambroxol in four commercial pharmaceutical samples by FIA, UV spectrophotometry (307 nm) [21,22] and potentiometric titration [23]

Sample	Composition	Labeled value (mg/5 mL)	Amperometry ± S.D.[a] (mg/5 mL)	Spectrophotometry ± S.D.[a] (mg/5 mL)	Titration ± S.D.[a] (mg/5 mL)
1	Ambroxol hydrochloride, sorbitol, glycerol, essence, benzoic acid, menthol, sacarine, propylene glycol	30	30.6 ± 0.2	30.4 ± 0.4	31.4 ± 0.8
2	Ambroxol hydrochloride, sorbitol, citric acid, glycerol, methylparaben, essence, propylparaben	30	30.1 ± 0.3	29.8 ± 0.3	29.7 ± 0.4
3	Ambroxol hydrochloride, sorbitol, glycerol, benzoic acid, menthol, propylene glycol, aroma, tartaric acid	15	15.3 ± 0.2	14.8 ± 0.3	15.5 ± 0.4
4	Ambroxol hydrochloride, citric acid, aroma, methylparaben, propylparaben, sorbitol, glycerol	15	15.5 ± 0.3	15.1 ± 0.2	15.2 ± 0.2

[a] Average ± standard deviation for three determinations.

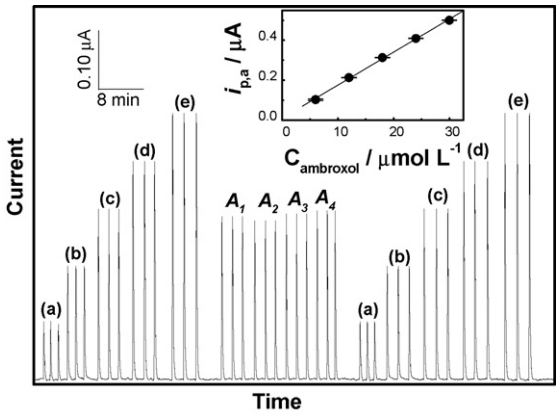

Fig. 6. Analyses of ambroxol samples A_1–A_4 using carbon film electrode in 0.1 mol L^{-1} sulfuric acid supporting electrolyte. Inset: calibration curve obtained from injections of (a) 6.0, (b) 12, (c) 18, (d) 24, (e) 30 μmol L^{-1} ambroxol standard solutions. Applied potential +1.15 V *vs.* Ag/AgCl, flow rate 2.0 mL min^{-1}, sample volume 100 μL.

ambroxol solutions, respectively, were obtained. These results demonstrate that there is no memory effect between successive injections, as well as the good performance of the working electrode under these conditions, since no decrease of the signal of the carbon film electrode was observed after 40 injections.

To estimate the effect of potentially interfering species present in the syrup constitution, the full composition of the studied syrups was accessed; the composition of each syrup is listed in Table 1. Citric acid and benzoic acid excipients in the pharmaceuticals investigated are the most likely to cause interferences. To evaluate their effects, a solution containing 1.0×10^{-5} mol L^{-1} ambroxol (in 0.1 mol L^{-1} sulfuric acid supporting electrolyte) was utilized. For benzoic acid, addition of 1.0×10^{-5} mol L^{-1} to the ambroxol solution (ratio 1:1) does not cause any change and a second addition corresponding to 1.0×10^{-4} mol L^{-1} (10-fold more benzoic acid than ambroxol) causes an increase of only 2%. The same strategy was used for citric acid: the first addition does not show almost any effect, but when 1.0×10^{-4} mol L^{-1} was added, an increase of ~7% in the current was verified. However, such a high concentration of citric acid cannot be found in any pharmaceutical formulation of ambroxol. The titration curves shown clearly that for all the samples, the volume of HCl consumed to neutralize citric acid ($pK_{a_1} = 3.14$; $pK_{a_2} = 4.77$) + benzoic acid ($pK_a = 4.19$) was smaller than the volume consumed until attain the equivalence point corresponding to ambroxol ($pK_{a_1} = 6.84$) neutralization. Additional tests were done with almost all the other constituents listed in Table 1 and do not lead to any change in response.

3.4. Analyses of ambroxol samples

To demonstrate the applicability of the proposed method, four different commercial syrup formulations containing ambroxol were analyzed. The results obtained using FIA–amperometry were compared with those from the spectrophotometric procedure [21,22] and with the potentiometric acid/base titration. Potentiometric titration is the methodology recommended in the British Pharmacopoeia for ambroxol quantification [24].

Fig. 6 shows a series of typical results (amperometric signals) obtained for syrup samples, preceded and followed by a series of injections of ambroxol standard solutions (from 6.0×10^{-6} to 3.0×10^{-5} mol L^{-1}). The concentration of ambroxol in the syrup samples was evaluated using the calibration plot shown in the inset of Fig. 6.

The results of the analyses of all syrup samples obtained for amperometry, spectrophotometry and potentiometric titration methods are summarized in Table 1, together with the corresponding standard deviations, calculated from three independent measurements for each sample. The composition of each pharmaceutical product is also included in order to show the components present, as well as the amount of ambroxol expected for each sample. Relative differences of the mean values between −0.4 and +2.7% were calculated by comparison of the results found employing the three methodologies, but agreement between the proposed method and the other two methods is very good.

4. Conclusion

The results obtained in this work demonstrate the potentiality of flow injection analysis combined with amperometric detection for the rapid quantification of ambroxol in pharmaceutical formulations. The proposed method allows simple and precise analyses without any sample pretreatment, such as filtration, extraction or derivatization. The carbon film sensor shows a better performance for determination of this analyte, compared to other electrodes, such as glassy carbon and platinum electrodes. Moreover, the carbon film sensor provides a low detection limit, good selectivity and good reproducibility. Other additional advantages that make this new sensor attractive for quality control applications are its low cost, ease of preparation and the fact that it can be used as a disposable sensor.

Acknowledgements

The authors gratefully thank the financial support from Brazilian Foundation (CNPq-proc. 141530/2004-9 and 304031-85-2) and Fundação para a Ciência e Tecnologia (FCT) Portugal, ICEMS (Research Unit 103). The donation of pure ambroxol by Arvensis from Brazil is acknowledged. This work was partially supported by the Renami, Sanmuti and IM^2C projects.

References

[1] W.H. Martindale, in: J.E.F. Reynold (Ed.), The Extra Pharmacopoeia, 29th ed., The Pharmaceutical Press, London, 1989, p. 904.
[2] E. Sumarlik, G. Indrayanto, J. Liq. Chromatogr. Related Technol. 27 (2004) 2047.
[3] M.L. Qi, P. Wang, R.H. Cong, J.J. Yang, J. Pharmaceut. Biomed. 35 (2004) 1287.
[4] G. Bazylak, L.J. Nagels, J. Pharmaceut. Biomed. 32 (2003) 887.
[5] H. Kim, J.Y. Yoo, H.J. Lee, K.R. Lee, J. Pharmaceut. Biomed. 32 (2003) 209.
[6] A. Zarzuelo, M.L. Sayalero, F.G. López, J.M. Lanao, J. Liq. Chromatogr. Related Technol. 24 (2001) 1007.
[7] M. Heinanen, C. Barbas, J. Pharmaceut. Biomed. 24 (2001) 1005.
[8] J.E. Koundourellis, E.T. Malliou, T.A. Broussali, J. Pharmaceut. Biomed. 23 (2000) 469.
[9] B.D. Kiss, K.B. Nemes, I. Urmos, J. Szunyog, I. Klebovich, Chromatographia 51 (2000) S217.
[10] M. Nobilis, J. Pastera, D. Svoboda, J. Kvetina, K. Macek, J. Chromatogr.-Biomed. 581 (1992) 251.
[11] V. Brizzi, U. Pasetti, J. Pharmaceut. Biomed. 8 (1990) 107.
[12] M.H.A. Botterblom, T.J. Janssen, P.J.M. Guelen, T.B. Vree, J. Chromatogr.-Biomed. 421 (1987) 211.
[13] M. Pospisilova, M. Polasek, V. Jokl, J. Pharmaceut. Biomed. 24 (2001) 421.
[14] T. Perez-Ruiz, C. Martinez-Lozano, A. Sanz, E. Bravo, J. Chromatogr. B 742 (2000) 205.
[15] T. Perez-Ruiz, C. Martinez-Lozano, A. Sanz, E. Bravo, J. Chromatogr. B 692 (1997) 199.
[16] M.S. Hwang, S. Cho, H. Chung, Y.A. Woo, J. Pharmaceut. Biomed. 38 (2005) 210.
[17] R. Szostak, S. Mazurek, J. Mol. Struct. 704 (2004) 229.
[18] Z. Dincer, H. Basan, N.G. Goger, J. Pharmaceut. Biomed. 31 (2003) 867.
[19] G. Indrayanto, R. Handajani, Drug Dev. Ind. Pharm. 20 (1994) 1639.
[20] L. Colombo, F. Marcucci, M.G. Marini, P. Pierfederici, E. Mussini, J. Chromatogr.-Biomed. 530 (1990) 141.
[21] I.H.I. Habib, S.I.M. Zayed, Pharmazie 60 (2005) 193.
[22] B.T. Demircigil, B. Uslu, Y. Ozkan, S.A. Ozkan, Z. Senturk, Electroanalysis 15 (2003) 230.

[23] F.J. Flores-Murrieta, C. Hoyo-Vadillo, E. Hong, G. Castañeda-Hernandez, J. Chromatogr.-Biomed. 490 (1989) 464.
[24] British Pharmacopoeia, vol. I, The Stationery Office, London, 2005, pp. 106– 107.
[25] D. Satinsky, J. Huclova, R.L.C. Ferreira, M.C.B.S.M. Montenegro, P. Solich, J. Pharmaceut. Biomed. 40 (2006) 287.
[26] D. Satinsky, L.M.L. Dos Santos, H. Sklenarova, P. Solich, M.C.B.S.M. Montenegro, A.N. Araujo, Talanta 68 (2005) 214.
[27] J.L.M. Santos, A. Clausse, J.L.F.C. Lima, M.L.M.F.S. Saraiva, A.S. Rangel, Anal. Sci. 21 (2005) 461.
[28] N.T. Abdel-Ghani, S.H. Hussein, Farmaco 58 (2003) 581.
[29] C.M.A. Brett, L. Angnes, H.D. Liess, Electroanalysis 13 (2001) 765.
[30] O.M.S. Filipe, C.M.A. Brett, Electroanalysis 16 (2004) 994.
[31] O.M.S. Filipe, C.M.A. Brett, Talanta 61 (2003) 643.
[32] C. Gouveia-Caridade, R. Pauliukaite, C.M.A. Brett, Electroanalysis 18 (2006) 854.
[33] M. Florescu, C.M.A. Brett, Talanta 65 (2005) 306.
[34] M.E. Ghica, C.M.A. Brett, Anal. Chim. Acta 532 (2005) 145.
[35] R. Pauliukaite, M.E. Ghica, C.M.A. Brett, Anal. Bioanal. Chem. 381 (2005) 972.
[36] M.E. Ghica, C.M.A. Brett, Electroanalysis 18 (2006) 748.
[37] R. Pauliukaite, M. Florescu, C.M.A. Brett, J. Solid State Electrochem. 9 (2005) 354.
[38] M. Florescu, C.M.A. Brett, Anal. Lett. 37 (2004) 871.
[39] M.E. Ghica, C.M.A. Brett, Anal. Lett. 38 (2005) 907.
[40] F.S. Felix, C.M.A. Brett, L. Angnes, J. Pharmaceut. Biomed. 43 (2007) 1622.
[41] S. Moane, J.R.B. Rodriguez, A.J.M. Ordieres, P.T. Blanco, M.R. Smyth, J. Pharmaceut. Biomed. 14 (1995) 57.
[42] G.J. McGrath, E. O'Kane, W.F. Smyth, F. Tagliaro, Anal. Chim. Acta 322 (1996) 159.
[43] M. Tamba, A. Torreggiani, Radiat. Phys. Chem. 60 (2001) 43.
[44] D.K. Gosser Jr., Cyclic Voltammetry: Simulation and Analysis of Reaction Mechanisms, VCH Publishers Inc., New York, 1993.

Available online at www.sciencedirect.com
ScienceDirect
Talanta 76 (2008) 21–28
Talanta
www.elsevier.com/locate/talanta

An extraction/concentration procedure for analysis of low-level explosives in soils

D.R. Felt [a,*], S.L. Larson [a], L. Escalon [b]

[a] U.S. Army Engineer Research and Development Center, 3909 Halls Ferry Road, Vicksburg, MS 39180, United States
[b] SpecPro Inc., 3532 Manor Drive, Vicksburg, MS 39180, United States

Received 19 December 2007; received in revised form 28 January 2008; accepted 29 January 2008
Available online 8 February 2008

Abstract

The methods traditionally used for explosives analysis in soil matrices have inherent data quality limitations for low-level samples. The traditional methods employ a soil-dilution extraction of the sample prior to analysis by high performance liquid chromatography with UV absorption detection. Another concern with the traditional analysis is that energetics contamination in environmental samples is often very heterogeneous in nature, usually requiring a large number of samples and multiple testing. The technique presented here addresses these data quality limitations by using a concentrative extraction procedure which produces a small volume of extract from a large soil sample. A concentration factor of 60-fold is achieved in this manner and energetics detection limits for soils are lowered by two orders of magnitude. The larger soil sample size also helps reduce the error associated with sample heterogeneity. The ability to detect explosive-based contaminants at levels of environmental interest enables a more accurate assessment of the transport pathways and treatment options for explosives contamination.

Keywords: Explosives; Extraction; High-performance liquid chromatography; Salting-out; Soil; Training ranges

1. Introduction

Most explosives-contaminated soils found on training ranges, impact areas, and firing points, contain a mixture of energetic compounds distributed heterogeneously in the soil. Hexahydro-1,3,5-trinitro-1,3,5-triazine (RDX) is the primary explosive found on training ranges, but other munitions constituents (MCs) such as 2,4,6-trinitrotoluene (TNT) and 2,6-dinitrotoluene (2,4 DNT) are also present in range soils. Jenkins et al. [1] and Pennington et al. [2,3] have shown there is a large degree of variability in contamination type, concentration and spatial distribution, both across a single range and among different ranges. This heterogeneous energetic contamination poses a possible environmental risk due to the compounds' toxicity and mutagenicity [4–7]. Energetic-contaminated soil can also act as a source zone for ground and surface water contamination due to the compounds' soil partition coefficients and dissolution rate [8–12]. The ability to detect explosive-based contaminants at values of environmental interest would enable an accurate assessment of the explosives contamination in the soil and measure the efficiency of treatment systems if warranted.

In order to accurately assess explosive concentrations in soils, an analytical method with lower detection limits for energetic compounds is required. Currently, two methods for the determination of explosives in soil samples have been promulgated by the United States Environmental Protection Agency (USEPA): SW-846 as Methods 8330 and 8095 [13]. The most widely used analytical method is 8330 that analyzes samples using reverse-phase high-performance liquid chromatography (HPLC) with UV detection [14]. The detection limit for RDX in soils is 20 μg/kg using USEPA Method 8330, but soil concentrations below this value can still act as source zones for ground and surface water contamination. USEPA Method 8330 B, a variation on the traditional USEPA Method 8330 that was approved in November 2006, addresses the question of sample heterogeneity from range soils through combining numerous samples into one composite sample from a given field site [15–20]. A larger sample (10 g) is extracted in a larger volume (50 mL acetonitrile)

* Corresponding author at: U.S. Army Engineer Research and Development Center, 3909 Halls Ferry Road, Vicksburg, MS 39180, United States.
Tel.: +1 601 634 3576; fax: +1 601 634 3518.
E-mail address: Deborah.Felt@usace.army.mil (D.R. Felt).

0039-9140/$ – see front matter © 2008 Elsevier B.V. All rights reserved.
doi:10.1016/j.talanta.2008.01.059

as compared to the traditional 8330 Method, but the rest of the extraction procedure is the same.

The proposed extraction technique addresses both of the current problems facing explosive analysis in soil; a need for lower detection limits and sample heterogeneity. Using the current method, two grams of soil are extracted into 10 mL of extraction solvent, which represents a fivefold dilution of the analyte concentration in the extract. The proposed method involves extracting a large mass of soil (150 g) and producing a small volume of extract (10 mL). This allows the detection limits for soil sample analysis to be decreased by two orders of magnitude compared to the detection limits achieved using the traditional USEPA Method 8330 or 8330 B.

The proposed technique also addresses sample heterogeneity by increasing the mass of soil extracted. The small sample size (2 g) used in the traditional methods is problematic for range soils, as the distribution and concentration of MC residues found on range soils can vary a great deal within a small area [3]. Collecting numerous composite samples would be necessary in order to correct for this variability, but it can be difficult to thoroughly homogenize such composites [3]. The need for representivity has been recently addressed by the USEPA Method 8330 B [15]. In this new method collection of large sample masses, drying, grinding, mixing, and sub-sampling to produce a 10 g sample is preferred to minimize heterogeneity of extracted soil. This 10 g is then extracted in the same manner as Method 8330. The larger sample mass used in the proposed procedure reduces the need for multiple tests or labor-intensive sample homogenization required by the current methods. A larger sample mass would reduce the laboratory error associated with multiple testing and increase the accuracy of the estimated energetics concentrations.

The proposed procedure utilizes the same laboratory instrumentation used for performing the traditional explosives methods with some additional types of standard glassware. The increased method performance together with a nominal capital outlay will make this technique economically attractive, while the increased sensitivity will allow for a better understanding of the fate of contaminants in solid matrixes.

2. Experimental

2.1. Analytical system

The HPLC system consisted of a Waters 610 Fluid Unit pump capable of achieving 6000 psi, a Waters 717 plus Autosampler including a 200 μL loop injector, a Waters 486 Tunable UV Absorbance detector monitored at 245 nm and Millenium 2.1 Chromatography Software. A Supelco LC-18 reverse phase HPLC column 25 cm × 4.6 mm (5 μm), was used as the primary column and a Supelco LC-CN reverse phase HPLC column 25 cm × 4.6 mm (5 μm), was used as a confirmation column. The appropriate pre-column, Novapak C-18 or Novapak CN, was used. A column heater set at 30 °C was used to reduce retention time shifts due to changes in room temperature.

Sonication extractions were performed using a temperature-controlled ultrasonic bath set at 4 °C. Reagent grade inorganic chemicals were used in all tests. Unless otherwise indicated, all reagents conform to the specifications of the Committee on Analytical Reagents of the American Chemical Society. The solvent, acetonitrile, used in this method was HPLC grade. The water used was organic-free reagent water (18.2 Ω). The HPLC mobile phase for both columns was 1:1 (v/v) methanol/reagent water.

Table 1
Target compounds listed in USEPA Method 8330

Compound	Abbreviation	CAS No.
Octahydro-1,3,5,7-tetranitro-1,3,5,7-tetrazine	HMX	2691-41-0
Hexahydro-1,3,5-trinitro-1,3,5-triazine	RDX	121-82-4
1,3,5-Trinitrobenzene	TNB	99-35-4
1,3-Dinitrobenzene	DNB	99-65-0
Methyl-2,4,6-trinitrophenylnitramine	Tetryl	479-45-8
Nitrobenzene	NB	98-95-3
2,4,6-Trinitrotoluene	TNT	118-96-7
4-Amino-2,6-dinitrotoluene	4-A-DNT	1946-51-0
2-Amino-4,6-dinitrotoluene	2-A-DNT	355-72-78-2
2,4-Dinitrotoluene	2,4-DNT	121-14-2
2,6-Dinitrotoluene	2,6-DNT	606-20-2
2-Nitrotoluene	2-NT	88-72-2
3-Nitrotoluene	3-NT	99-08-1
4-Nitrotoluene	4-NT	99-99-0

2.2. Sample preparation

Reference soil samples were dried and homogenized in preparation for the method detection limits study. Prior to extraction, each homogenized sample (300 g) was amended with 2 mL of each of two solutions: one containing 2.0 mg/L HMX, RDX, TNB, DNB, NB, TNT, and 2,4-DNT, and the other solution containing 2.0 mg/L Tetryl, 4-A-DNT, 2-A-DNT, 2,6-DNT, 2-NT, 3-NT, and 4-NT (abbreviations defined in Table 1). This corresponds to a simulated concentration in the soil matrix of 13.3 μg/kg for each of the 14 analytes in the soil. The amended soil was then extracted as described in USEPA Standard Method [13] or with the concentrative technique as described in the next section.

2.3. Concentrative extraction procedure

The concentrative extraction technique used aliquots (150 g) of air-dried soil samples that were mixed with 1 L of extraction solvent (175 mL acetonitrile and 825 mL of distilled and deionized water) (V_1 in Eq. (1)) in amber bottles. The amber bottles were placed in a temperature-controlled sonic bath at 4 °C and extracted for 18 h. The solids in the bottles were re-suspended by shaking the bottles for 5 min at three different times during the extraction: after 1 h, after 2 h, and after 17 h. Saturated, aqueous calcium chloride solution (10 mL) was added to each amber bottle after extraction to flocculate any clay particles and the slurries were mixed and allowed to settle for 10 min. The supernates were poured from the amber bottles into 1 L centrifuge bottles and the remaining solids were discarded. The centrifuge bottles were centrifuged at 1800 rpm for 15 min and the resulting supernates were transferred to 1 L graduated cylin-

ders and the volume of the supernates was recorded (V_2 in Eq. (1)).

The supernates in the graduated cylinders were poured into flasks containing 250 g solid sodium chloride and stirred for 1 h. The salt solution was then allowed to settle for 30 min to allow phase separation and the acetonitrile layer (upper layer) was transferred to a glass 20 mL centrifuge tube. Fresh acetonitrile, 5 mL, was added to the flask to re-extract the soil/salt mixture, and the solution was vigorously stirred for 30 min. After another 30 min settling period, the acetonitrile layer was removed from the flask and combined with the previous acetonitrile layer in the centrifuge tube. The combined acetonitrile solution was then centrifuged for 10 min at 1000 rpm, pipetted into a 25 mL graduated cylinder, and brought up to volume (16.4 mL) with acetonitrile.

The 16.4 mL acetonitrile extract was placed in a 100 mL volumetric flask and brought up to volume with an aqueous sodium chloride solution (325 g NaCl/L). A stir bar was added to the acetonitrile/salt solution and the contents of the flask were mixed vigorously for 10 min. The solution was allowed to settle for 30 min and the supernate was removed and placed in a 20 mL centrifuge tube. One milliliters fresh acetonitrile was added to the volumetric flask to re-extract the remaining solids. The solution was mixed for 10 min and allowed to settle for 30 min. The supernatant was removed and combined with the acetonitrile solution in the 20 mL centrifuge tube. The acetonitrile solution was then centrifuged for 10 min at 1000 rpm. The acetonitrile layer was carefully removed from the centrifuge tube, placed in a 10 mL graduated cylinder, and the volume adjusted to 5 mL with fresh acetonitrile.

The acetonitrile extract was then cleaned up using an acetonitrile-rinsed chromatographic clean-up column. The column consisted of a cotton plug, 0.5 g florisil, and 0.5 g of alumina in a 10 mL disposable glass pipette and was conditioned with 100% acetonitrile. The 5 mL concentrated extract was added to the clean-up column and the filtrate was collected in a 20 mL glass vial. An additional 5 mL of acetonitrile was passed through the column and collected in the same vial to yield a final extract volume of 10 mL (volume of final extract in Eq. (1)).

A portion (2 mL) of the final extract was diluted with distilled-deionized water (2 mL), filtered through a 0.45 μm Teflon filter, and analyzed according to USEPA Method 8330.

2.4. Analytical method

The analytical method described in USEPA Standard Method 8330 [13,14] was used for the detection of the 14 compounds listed in this standard analytical method. A list of these analytes is shown in Table 1. The USEPA Method 8330 was the analytical method used in this study because it is a widely used method for explosives determination.

3. Results and discussion

This paper describes a soil sample preparation technique that:

- Uses a large sample mass.
- Produces a concentrated extract without heat or evaporation steps.

3.1. Concentration techniques

The preparation of concentrated extracts from liquid and solid environmental matrixes is a common practice in analytical chemistry. Analyses for stable organic contaminants such as semi-volatile organics (USEPA Method 8250), chlorinated herbicides (USEPA Method 8151), and dioxins and furans (USEPA Method 8290) are accomplished using heat or evaporation steps [13]. Production of concentrated extracts from explosives using these techniques is problematic because of the unique molecular characteristics of the explosive compounds. The energetic nature of these compounds makes them thermally and photochemically labile. As a result, extensive contaminant transformation has been shown to occur during such evaporative processes, even at relatively low temperatures [14]. In the latest version of 8330, 8330 B, no concentrative procedure for soil samples was incorporated [15].

There are concentrative methods that can be used to extract energetic compounds from water without contaminant transformation. Two concentrative techniques have been described in USEPA Method 8330 concerning the preparation of water samples for explosives analysis. One method involves passing 1 L of water through a solid phase extraction cartridge and eluting the trapped contaminants with a small volume of organic solvent. The second technique, a low-level salting-out method, involves the concentration of analytes of interest using acetonitrile, sodium chloride, and water, with no evaporation steps [13,21]. A significant reduction (up to 500-fold) of the detection limits for explosives in water is realized when such concentration steps are used. Salting-out methods have also been developed for other sample media and organic contaminants [22–24] and a salting-out procedure is the basis for the proposed soil extraction technique described in this paper.

3.2. Method detection limit determination

Studies were performed using freshly amended reference soils in order to determine the method detection limits (MDLs) for the 14 analytes listed in Table 1 using the concentrative extraction technique. Table 2 contains the results of seven replicate runs at a known concentration for each analyte as well as the statistical interpretation of those results. As can be seen, good precision was obtained for the replicate analysis. The USEPA SW846 Method criterion [13] for determination of MDL (three times the standard deviation of seven replicates) was used. Method detection limits ranged from 1 μg/kg to 23 μg/kg depending on the specific analyte. The results presented in Table 2 show a reduction in detection limits by two orders of magnitude compared to the soil-dilution extraction currently used in USEPA Method 8330. This increase in sensitivity is also expected to be noted between the concentrative technique described here and the recent Method 8330 B that retains the same extraction steps from the original 8330.

Table 2
Results of soils amended with 0.013 μg/kg of 14 contaminants prior to extraction ($n = 7$) using concentrative procedure

Analyte	Average μg/kg ($n = 7$)	Method detection limit (3 × S.D.)	Laboratory reporting limit (3 × MDL)	%Recovery
HMX	0.0118	0.010	0.046	87.98
RDX	0.0082	0.005	0.015	64.53
TNB	0.0127	0.004	0.011	98.34
DNB	0.0137	0.02	0.069	106.42
Tetryl	0.0125	0.004	0.012	95.82
NB	0.0121	0.006	0.019	96.71
TNT	0.0112	0.02	0.048	82.14
4-A-DNT	0.0127	0.003	0.010	98.73
2-A-DNT	0.0143	0.01	0.035	109.71
2,4-DNT	0.0118	0.006	0.017	90.41
2,6-DNT	0.0145	0.01	0.029	114.10
2-NT	0.0128	0.001	0.0030	98.19
4-NT	0.0124	0.004	0.013	95.40
3-NT	0.0126	0.003	0.0081	95.96

The recoveries of the freshly amended analytes used in the MDL study were seen to be in the range of 64–114% (Table 2). These recoveries are similar to the recoveries indicated in the USEPA Method 8330 for soils, which range from 58% to 98% [13]. Recoveries of greater than 100% obtained from the analysis of concentrated extracts such as those seen for the analytes DNB, 2-A-DNT, and 2,6-DNT are not uncommon. The salting-out extraction technique for water samples described in USEPA Method 8330 also reports results of a precision and accuracy study in which recoveries over 100% were reported for 7 of the 11 analytes studied and an overall range of recoveries between 93% and 119% [13].

All extracts prepared throughout this study were analyzed using HPLC equipped with a UV detector according to the USEPA Method 8330. The USEPA Method 8095, that employs gas chromatography with an electron capture detector (GC-ECD), could also have been used to analysis this extract. Other analytical techniques that may benefit from this concentrative preparation method are gel permeation chromatography, nuclear magnetic resonance, spectroscopic analyses, or any technique that requires a concentrated analyte.

3.3. Analysis of five site soils using Method 8330 and the concentrative technique

Recoveries for the freshly amended soils used throughout the MDL determinations were generally close to 100% (Table 2). However, contamination of most soils that are analyzed in the laboratory generally occurred through a combination of contact with contaminated water, solids disposal, or the use of explosives-containing munitions over periods of months to years. These extended time periods provide for extensive weathering of the contamination and allow natural processes such as microbial action and contaminant sorption to occur. For this reason, analyses of weathered (aged) soils generally show significantly reduced recoveries compared to freshly amended soils. In order to compare extraction recoveries of weathered compounds using both procedures, several site soils were extracted following the USEPA 8330 extraction method and the concentrative extraction technique.

Five site soils were used for the comparative analysis of the traditional USEPA Method 8330 for soil and the concentrative technique evaluated during this study. Two site soils were collected from military sites where the use and manufacture of explosives had occurred (Soils 1 and 2). The other three site soils were soil composites collected at training ranges or testing areas (Soils 3, 4, and 5). Explosives concentrations and the standard deviations for the five site soils derived using both USEPA Method 8330 and the soil concentration technique are listed in Table 3. Target compounds listed in Table 1 but not shown in Table 3 were below the detection limits using both extraction techniques. Mean concentrations were identified with a "J" label when one or more of the repetitions resulted in non-detection.

Analysis of the concentrated extracts of the site soils yielded quantification of low-level contamination by explosives that were not detected using the traditional method. In total, 30 positive identifications of USEPA Method 8330 analytes were detected in the five soils using the concentration method. Of the 30 positive indications, 14 compounds were detected above the laboratory reporting limit using the concentrative method that were not detected using the traditional soil-dilution method and two compounds were detected below the concentrative method's laboratory reporting limit that were not detected using the soil-dilution method. Two compounds marked as a "J" value using the traditional soil-dilution method were detected above the laboratory reporting limit using the concentration method. Seven compounds were detected above the reporting limit by both methods and two were flagged with a "J" value by both methods.

Standard deviations (sample variability) generally decreased when using the concentrative procedure for Soils 1 and 2. The standard deviations could not be compared for Soils 3, 4, and 5 as all these samples were below the detection limit using USEPA Method 8330. The largest percent standard deviations for both procedures were observed when analyte concentrations were low, below 250 μg/kg for Method 8330 and 50 μg/kg for the concentration technique. It is expected that the smaller standard deviations noted here for the concentrative technique relative to the Method 8830 would not be noted for Method 8330 B [15].

The method detection limits measured using freshly amended soils suggested the ability to detect analytes at concentrations

Table 3
Results of explosives analysis of site soil extracts using concentrative procedure and traditional extraction method in μg/kg

Soil	Method	Statistic	HMX	RDX	TNB	TNT	4-A-DNT	2-A-DNT	2,4 -DNT
Soil 1	Concentrative	Mean	1.068	0.546	J0.008	0.178	0.155	0.303	0.0261
		S.D.	0.020	0.015	0.002	0.008	0.005	0.006	0.003
	EPA 8330	Mean	J1.490	J0.990	J0.005	0.273	0.245	0.587	nd
		S.D.	0.182	0.120	0.005	0.104	0.015	0.016	nd
Soil 2	Concentrative	Mean	1.706	8.063	J0.008	0.034	0.090	0.149	J0.005
		S.D.	0.051	0.351	0.003	0.004	0.005	0.004	0.001
	EPA 8330	Mean	3.79	21.40	J0.01	J0.07	0.155	0.247	nd
		S.D.	0.583	1.325	0.002	0.008	0.009	0.012	nd
Soil 3	Concentrative	Mean	1.217	10.850	0.195	0.032	0.067	nd	J0.197
		S.D.	0.559	2.689	0.013	0.009	0.013	nd	0.140
	EPA 8330	Mean	nd	nd	nd	nd	nd	nd	nd
		S.D.	nd	nd	nd	nd	nd	nd	nd
Soil 4	Concentrative	Mean	0.454	46.190	1.855	0.624	0.100	1.203	12.100
		S.D.	0.030	4.469	2.296	0.466	0.008	1.144	14.090
	EPA 8330	Mean	nd	nd	nd	nd	nd	nd	nd
		S.D.	nd	nd	nd	nd	nd	nd	nd
Soil 5	Concentrative	Mean	nd	11.700	0.668	2.114	nd	nd	nd
		S.D.	nd	5.696	0.373	1.010	nd	nd	nd
	EPA 8330	Mean	nd	nd	nd	nd	nd	nd	nd
		S.D.	nd	nd	nd	nd	nd	nd	nd

J values denote one or more of the replicates in this matrix resulted in a non-detect. S.D.: standard deviation; nd: non-detect.

two orders of magnitude below the current USEPA Method 8330 (Table 2). This increased analytical capability was also noted during the analysis of the aged site soils. This indicates that the decreased detection limits allowed by the concentrative extraction technique when compared to the results from the traditional method for the same soil may be independent of soil type.

3.4. Relative recovery of the concentrating method to the soil-dilution method

Determination of recoveries from aged, site-contaminated soils is not possible due to the unknown nature of the contamination, but a comparison of the concentrations determined using the two techniques discussed can provide a means of specifying a recovery of one technique relative to the other. Relative recoveries on the five soils from contaminated sites are presented in Table 4. Relative recoveries (%RR) were determined by dividing the mean concentration value of the concentrative method by the mean value derived from the EPA 8330 method and multiplying by 100.

The mean concentrations resulting from the traditional USEPA Method 8330 were actually higher than those yielded by the concentrative method for Soils 1 and 2, but with higher standard deviations as shown in Table 3. The calculated % relative recoveries were therefore less than 100%, with average relative recoveries detected in extracts from Soil 1 and Soil 2 of 77.7% and 51.7%, respectively (Table 4). This indicates that different soils extract differently and specific soil types appear to play a role in the extractability of the energetics analytes. The relative recoveries for the other three soils could not be calculated, as these soils yielded non-detection values using USEPA Method 8830.

Of note are the much higher concentrations for HMX and RDX for Soil 2 using the USEPA Method 8330 compared to the concentrative extraction procedure. The large amount of interfering peaks and noise observed in analysis of Soils 2 extracts, and to some degree in Soil 1, using USEPA Method 8330 appears to have resulted in over-quantification of these two compounds. This interference contributed to the larger standard deviations for these samples. Extracts from Soils 1 and 2 may have benefited from a clean-up step, not unlike the column used in the concentrative technique.

After comparing the recovery results of the concentrative method to the current method, two unambiguous observations can be stated about the concentrative method:

(1) The method detection limits were decreased considerably from the current technique allowing quantification of contaminants that would be missed using the traditional extraction method for soils.
(2) The standard deviations obtained at these low concentrations were lower than those obtained when using the traditional extraction procedure (Method 8330 not Method 8330 B).

3.5. Comparison of the two methods for two aged soils: reproducibility

The standard deviations and percent relative standard deviation for the analytical results from Soils 1 and 2 are presented in Table 5. The percent relative standard deviation is calculated by dividing the standard deviation by the mean concentration and multiplying by 100, which yields a normalized measure of error for each sample. Of the 12 analytes detected in the both

Table 4
Relative recoveries of analyte quantification for USEPA 8330 and the concentrative extraction techniques

Soil sample	Method	HMX (μg/kg)	RDX (μg/kg)	TNB (μg/kg)	TNT (μg/kg)	4-A-DNT (μg/kg)	2-A-DNT (μg/kg)
Soil 1	EPA 8330	J1.49	J0.998	J0.005	0.273	0.245	0.587
	Concentrative	1.068	0.546	J0.008	0.178	0.155	0.303
	%RR	71.66	54.67	160.	65.28	63.06	51.55
Soil 2	EPA 8330	3.79	21.398	J0.013	J0.067	0.155	0.247
	Concentrative	1.706	8.063	J0.008	0.034	0.090	0.149
	%RR	45.02	37.68	58.46	50.75	57.81	60.32
Soil 3	EPA 8330	nd	nd	nd	nd	nd	nd
	Concentrative	1.217	10.850	0.195	0.032	0.067	J0.197
	%RR	nd	nd	nd	nd	nd	nd
Soil 4	EPA 8330	nd	nd	nd	nd	nd	nd
	Concentrative	0.454	46.190	1.855	0.624	0.100	12.100
	%RR	nd	nd	nd	nd	nd	nd
Soil 5	EPA 8330	nd	nd	nd	nd	nd	nd
	Concentrative	nd	11.700	0.668	2.114	nd	nd
	%RR	nd	nd	nd	nd	nd	nd

Relative recoveries (%RR) were determined by dividing the mean concentration value of the concentrative method by the mean value derived from the EPA 8330 method and multiplying by 100. J values denote one or more of the replicates in this matrix resulted in a non-detect. nd: non-detect

site soils, the %R.S.D. for the three replicates using the concentrative method was lower than the %R.S.D. for the traditional method in eight cases. In two of the cases where the traditional method had a lower %R.S.D., both extraction techniques yielded low explosives concentration. In the other two cases, the explosives concentrations yielded by both procedures were above the laboratory reporting limits. This comparison suggests that, depending on the contaminant levels in a particular soil and the detection limits required for the specific study, both analytical techniques can play a role in assessing the environmental impact of explosives contamination.

Two factors affect the increased reproducibility of analyte concentration determinations using the concentrative procedure. First, higher analyte concentrations in the concentrated extract produce significantly more signal at the detection wavelengths than those from the traditional soil-dilution extract for the same soil sample. This increased signal reduces the impact of random noise on the size of the chromatographic peak and increases the repeatability of quantification.

The second factor that affects the increased reproducibility of the proposed technique is the larger sample size used, which increases the uniformity of each replicate. Analytes may be dissolved, suspended, or in a particulate form in an individual soil sample. These factors contribute to sample heterogeneity and possible lack of method reproducibility. The increased soil mass used in the concentrative technique results in averaging these variances in analyte distribution and contributes to improved reproducibility. Method 8330 B may reduce the variability associated with this factor. The use of numerous samples combined in one composite sample would increase the uniformity of each extracted sample, but 8330 B still involves a dilution of the sample extract. Therefore, the proposed technique would still yield

Table 5
Comparison of mean, standard deviation (S.D.), and % relative standard deviations (%R.S.D.) of analyte concentrations for three replicates by USEPA 8330 and the concentrative extraction techniques

Soil sample	Method	HMX (μg/kg)	RDX (μg/kg)	TNB (μg/kg)	TNT (μg/kg)	4-A-DNT (μg/kg)	2-A-DNT (μg/kg)	2-4-DNT (μg/kg)
Soil 1	EPA 8330	J1.490	J0.998	J0.005	0.273	0.245	0.587	nd
	S.D.	0.182	0.120	0.005	0.104	0.02	0.016	nd
	%R.S.D.	12.27	12.08	100.00	3.81	6.12	2.74	nd
	Concentrative	1.068	0.546	J0.008	0.178	0.155	0.303	0.026
	S.D.	0.020	0.015	0.002	0.008	0.005	0.006	0.003
	%R.S.D.	1.91	2.76	25.00	4.26	3.29	5.14	11.51
Soil 2	EPA 8330	3.790	21.398	J0.013	J0.067	0.155	0.247	nd
	S.D.	0.583	1.325	0.002	0.008	0.009	0.012	nd
	%R.S.D.	15.39	6.19	21.65	11.46	5.59	4.68	nd
	Concentrative	1.706	8.063	J0.008	0.034	0.090	0.149	J0.005
	S.D.	0.051	0.351	0.003	0.004	0.005	0.004	0.001
	%R.S.D.	3.00	4.35	33.07	11.75	5.03	2.41	21.53

J values denote one or more of the replicates in this matrix resulted in a non-detect. nd: non-detect

higher detector responses (signal) which would reduce random noise and increase repeatability of quantification.

3.6. Calculations

The analyte in the dried soil can be calculated by using two key volumes that were noted during the extraction. Since the amount of extraction solvent adsorbed to the solid material during the extraction is variable, the initial volume of extraction solution (V_1) and the volume of extract solution that can be decanted following centrifugation (V_2) are used for this calculation. A simplifying assumption is made in this process: the concentrations of the analytes in the extraction solution are constant irrespective of how well the solution can be decanted. The calculation, described in Eq. (1), determines a correction factor to be used in the calculation of the mass of analyte in the original solid matrix.

$$\frac{\text{sample mass(g)}\,(V1_{(\text{mL})}/V2_{(\text{mL})})}{\text{volume of final extract(mL)}} = \text{grams extracted per mL of extract.} \quad (1)$$

For example, if a dried soil sample of 150 g was extracted with 950 mL of extraction solution (acetonitrile/water) and 850 mL solution was decanted following centrifugation, and the final volume of extract was 5 mL, a correction factor of 33.53 would be used.

The mass of analyte in the original soil sample can then be calculated

$$\frac{\text{mg analyte}}{1\text{ L extract}} \times \frac{1\text{ L extract}}{1000\text{ mL extract}} \times \text{inverse of result from Eq. (1)} = \frac{\text{mg analyte}}{\text{g soil}} \quad (2)$$

using the inverse of the result from Eq. (1), as illustrated in Eq. (2). The mg analyte per L extract is the concentration experimentally derived from the HPLC.

3.7. Interferences

To this point in time, no single significant interference has been identified for the determination of explosives in soils by the concentrative technique. Analysis of explosives from concentrated extracts containing large amounts of extractable compounds, which absorb at 245 nm, may result in high background absorbance or unidentified interfering peaks. Many of these interferences can be kept to a minimum, however, through the use of rigorously cleaned reagents and sample processing equipment and the use of a clean-up column as the final extraction step.

3.8. Advantages of the concentrative technique for environmental professionals

The increased repeatability afforded by the concentrative technique directly impact the accuracy of site assessments as well as evaluations of remediation effectiveness. The fact that small samples collected from areas separated by a few inches may have drastically varied explosives concentrations can result in significant over- or underestimations of a given site's level of contamination. The current technique requires extensive sampling of a number of locations at a single site which results in increased analytical costs. The larger samples used with the concentrative technique allow field workers to collect more representative samples from a single location or batch smaller samples from a given area suspected of explosives contamination.

Improved sample representivity can also avoid potential problems during the assessment of novel remediation techniques. An apparent 10% reduction in contaminant concentration between two subsequent analyses might indicate the treatment is effective, especially when dealing with low-level contamination. With the current extraction technique, the apparent reduction may instead be due to a lack of sample uniformity, not a result of a successful treatment strategy. This discrepancy could prolong the use of an ineffective treatment and delay remediation goals.

4. Conclusions

A means of extraction and concentration of explosives from a soil matrix has been developed and shown to produce results that are statistically significant and viable for potentially low-level or heterogeneous contamination. The proposed concentrative extraction procedure was shown to detect explosives in freshly amended and weathered soils at lower detection levels and with higher repeatability than the traditional soil-dilution method. Sample reproducibility for low-level samples was also increased using the proposed technique in comparison to the current method. The concentrative extraction procedure could provide environmental professionals with an improved tool to assess the fate of explosive-based contamination in order to understand the source of low-level surface and ground water. Remediation and management approaches could then be applied to these locations if warranted.

Acknowledgements

Funding this research was provided by the U.S. Department of Defense Installation Restoration Research Program (IRRP) and the U.S. Army Environmental Quality Technology Research Program. The authors gratefully acknowledge Jane W. Adams and Richard A. Price, U.S. Army Corps of Engineers, Engineer Research and Development Center (ERDC), for providing exposed soil samples and Toy S. Poole and Robert P. Jones, U.S. Army Corps of Engineers, ERDC, for helpful discussion. This report does not reflect the policy, practices, programs, or doctrine of the U.S. Army or the Government of the United States. The contents of this report are not to be used for advertising or promotional purposes. Citation of brand names does not constitute endorsement or approval of the use of such commercial products.

Appendix A. Supplementary data

Supplementary data associated with this article can be found, in the online version, at doi:10.1016/j.talanta.2008.01.059.

References

[1] T.F. Jenkins, J.C. Pennington, T.A. Ranney, T.E. Berry, Jr., P.H. Miyares, M.E. Walsh, A.D. Hewitt, N.M. Perron, L.V. Parker, C.A. Hayes, E.G. Wahlgren, MAJ. ERDC/CRREL TR-01-5, U.S. Army Engineer Research and Development, 2001.

[2] J.C. Pennington, T.F. Jenkins, J.M. Brannon, J. Lynch, T.A. Ranney, T.E. Berry, C.A. Hayes, P.H. Miyares, M.E. Walsh, A.D. Hewitt, N. Perron, J.J. Delfino, ERDC/EL TR-01-13, U.S. Army Engineer Research and Development Center, Vicksburg, MS, 2001.

[3] J.C. Pennington, T.F. Jenkins, G. Ampleman, S. Thiboutot, J.M. Brannon, J. Lynch, T.A. Ranney, J.A. Stark, M.E. Walsh, J. Lewis, C.A. Hayes, J.E. Mirecki, A.D. Hewitt, N. Perron, D. Lambert, J. Clausen, J.J. Delfino, ERDC/EL TR-01-13, U.S. Army Engineer Research and Development Center, Vicksburg, MS, 2002.

[4] U.S. Environmental Protection Agency (USEPA), Drinking water standards and health advisories, Office of Water, Washington, DC, 2004 (EPA 822-R-04-005).

[5] United States Environmental Protection Agency, Integrated risk information system (IRIS): 2,4,6-trinitrotoluene (TNT), http://www.epa.gov/iris, 2005.

[6] United States Environmental Protection Agency, Integrated risk information system (IRIS): hexahydro-1,3,5-trinitro-1,3,5-triazine (RDX), http://www.epa.gov/iris, 2005.

[7] United States Environmental Protection Agency, Integrated risk information system (IRIS): octahydro-1,3,5,7-tetranitro-1,3,5,7-tetrazocine (HMX), http://www.epa.gov/iris, 2005.

[8] N. Adrian, K. Sutherland, USACERL TR-99-15, Construction Engineering Research Laboratory, Champaign, IL, 1999.

[9] P.R. Binks, S. Nicklin, N.C. Bruce, Appl. Environ. Microbiol. 61 (4) (1995) 1318–1322.

[10] J.M. Brannon, J.C. Pennington, ERDC/EL TR-02-10, U.S. Army Environmental Research and Development Center, Vicksburg, MS, 2002.

[11] S.B. Funk, D.J. Roberts, D.L. Crawford, R.L. Crawford, Appl. Environ. Microbiol. 59 (7) (1993) 2171–2177.

[12] T. Gorontzy, O. Drzyzga, M.W. Kahl, D. Bruns-Nagel, J. Breitung, E. von Loew, K.H. Blotevogel, Crit. Rev. Microbiol. 20 (4) (1994) 265–284.

[13] United States Environmental Protection Agency (USEPA), Test Methods for Evaluating Solid Waste, Physical/Chemical Methods SW-846, third edition, 1998 (Proposed Update IV. U.S. Environmental Protection Agency, Office of Solid Waste and Emergency Response, Washington, DC).

[14] T.F. Jenkins, Development of an Analytical Method for the Determination of Extractable Nitroaromatics and Nitramines in Soils, Ph.D. dissertation, University of New Hampshire, Durham, New Hampshire, 1989.

[15] United States Environmental Protection Agency, Method 8830 B, http://www.epa.gov/epaoswer/hazwaste/test/pdfs/8330b.pdf, 2006.

[16] T.F. Jenkins, A.D. Hewitt, M.E. Walsh, T.A. Ranney, C.A. Ramsey, C.L. Grant, K.L. Bjella, J. Environ. Forensics 6 (2005) 45–55.

[17] M.E. Walsh, C.A. Ramsey, T.F. Jenkins, Chemosphere 49 (2002) 1265–1271.

[18] M.E. Walsh, D.J. Lambert, Extraction kinetics of energetic compounds from training range and army ammunition plant soils: platform shaker versus sonic bath methods, ERDC/CRREL TR-06-6, 2006.

[19] M.E. Walsh, C.A. Ramsey, C.M. Collins, A.D. Hewitt, M.R. Walsh, K. Bjella, D. Lambert, N. Perron, Collection methods and laboratory processing of samples from donnelly training area firing points Alaska 2003, ERDC/CRREL TR-05-6, 2005.

[20] M.E. Walsh, D.J. Lambert, Extraction kinetics of energetic compounds from training range and army ammunition plant soils, ERDC/CRREL TR06-6, 2006.

[21] T.F. Jenkins, P.H. Miyares, K.F. Myers, McCormick, A.B. Strong, Anal. Chim. Acta 289 (1994) 69–78.

[22] N. Ni, S. Yalkowsky, Int. J. Pharm. 254 (2003) 167–172.

[23] A. Turner, M.C. Rawling, Sci. Total Environ. 312–316 (2003) 599–612.

[24] J.C. Means, Mar. Chem. 51 (1995) 3–16.

Talanta 76 (2008) 172–182

Contents lists available at ScienceDirect

Talanta

journal homepage: www.elsevier.com/locate/talanta

Effect of long-term storage and use on the properties of reversed-phase liquid chromatographic columns

Erik Haghedooren[a], Edit Farkas[b], Ágnes Kerner[c], Sanja Dragovic[a], Béla Noszál[d], Jos Hoogmartens[a], Erwin Adams[a,*]

[a] Katholieke Universiteit Leuven, Laboratorium voor Farmaceutische Analyse, O&N, 2, PB 923, Herestraat 49, B-3000 Leuven, Belgium
[b] Semmelweis University, Department of Pharmaceutics, Hőgyes E. u. 7, H-1092 Budapest, Hungary
[c] National Institute of Forensic Toxicology, Varannó u. 2-4, H-1146 Budapest, Hungary
[d] Semmelweis University, Department of Pharmaceutical Chemistry, Hőgyes E. u. 9, H-1092 Budapest, Hungary

ARTICLE INFO

Article history:
Received 20 April 2007
Received in revised form 8 February 2008
Accepted 20 February 2008
Available online 4 March 2008

Keywords:
Reversed-phase liquid chromatography
Column characterisation
Chromatographic tests
Column classification
Long-term usage
Storage

ABSTRACT

In order to study column deterioration as a result of long-term storage and/or usage in liquid chromatography analyses, 55 pairs (same batch) of different commercial reversed-phase C_{18} columns were examined using an already existing column characterisation system. After initial testing, one column was stored and the other was used to analyse different pharmaceuticals. All columns were characterized by four chromatographic parameters reflecting hydrophobicity, silanol activity, metal impurity and steric selectivity at the beginning and at the end of the test. An *F*-value was calculated to express the change of column properties with one single number. After performing analyses, higher *F*-values were obtained as compared to the non-used, stored columns. Although the time during which the columns were used to perform analyses was relatively short, an obvious influence was noticed, mainly resulting from small changes in silanol activity and hydrophobicity. Most of the affected columns have no endcapping and/or no base deactivation, making them more vulnerable for degradation, resulting in higher silanol activity and faster ageing. This effect is observed less with columns equipped with polar-embedded groups and/or polar endcapping, protecting the column by blocking the silanol groups and attracting a shielding water layer. Also columns with higher coverages and bulky or long chains show more resistance towards degradation.

1. Introduction

The variety of available stationary phases provide different selectivities and as a consequence, the search for a suitable column for a particular reversed-phase liquid chromatographic (RP-LC) separation may be complicated [1]. Although many silica gel-based RP columns can be considered as nominally identical, previous studies demonstrated significant differences between them [2–4]. Since there is a lack of unified, exact information from the manufacturers, which allows easy classification of RP-LC phases, several column characterisation tests were developed based on destructive, spectroscopic or chromatographic methods. Subtle differences, which may have decisive impact on the separation process, can be measured principally by a chromatographic characterisation method [4–10].

After selecting the suitable type of stationary phase, the lifetime of the RP column is an important parameter for analysts, which is often expressed in number of injections performed under a certain condition of analysis. In the literature, accelerated stability tests to study column ageing are described [11,12]. It was shown earlier that aqueous mobile phases above pH 8 could markedly enhance degradation of the silica support. High pH mainly attacks the silica backbone, whereas the hydrolysis of the bonded phase is not considerable. Further investigation proved that the degradation is strongly affected by the type and purity of the silica support and also influenced by the nature of the bonded silane [13]. Enhanced column stability was observed with certain endcapped and densely bonded phase columns, where double endcapping appeared to be superior to single endcapping. Deterioration of stationary phase also depends on the nature of both the buffer salts and the organic modifier. The addition of an organic modifier to the aqueous buffer solution can result in a change of the apparent pH. The lifetime of the column can be influenced by the usage of organic buffers instead of inorganic ones [14,15]. Also, when the mobile phase contains a high percentage of organic solvent (70–80%) the dissolution of silica at high pH is lower [16]. At low pH, enhanced hydrolysis of the siloxane bond between the organosilane and the silica surface was observed. The ligand chain length, functionality and bonding

* Corresponding author. Tel.: +32 16 323444; fax: +32 16 323448.
E-mail address: erwin.adams@pharm.kuleuven.be (E. Adams).

0039-9140/$ – see front matter © 2008 Elsevier B.V. All rights reserved.
doi:10.1016/j.talanta.2008.02.020

Table 1
Description of the methods used to characterise columns

Method	Mobile phase	Sample	Column parameter
A	Methanol–water–0.2 mol/l KH_2PO_4 at pH 2.7 (34:90:10 w/w)[a]	Benzylamine, phenol	$rk'_{\text{benzylamine/phenol}}$
B	Methanol–water–0.2 mol/l KH_2PO_4 at pH 6.5 (34:90:10 w/w)[a]	2,2′-Dipyridyl	$k'_{2,2'-\text{dipyridyl}}$
C	Methanol–water (317:100 w/w)	Uracil, amylbenzene, *o*-terphenyl, triphenylene	$k'_{\text{amylbenzene}}$ $rk'_{\text{triphenylene/}o\text{-terphenyl}}$

[a] The pH adjustments were performed before adding the organic compound of the mixture.

density of the organic phase was shown to remarkably influence the stability. Analyses performed at high temperature have many advantages, but due to lower stability of the traditional silica, the use of other types of backbone-like zirconia was recommended [17,18].

A chromatographic column characterisation method was developed in this laboratory based on the determination of four parameters, representing different properties: the retention factor of amylbenzene (hydrophobicity), the relative retention factor benzylamine/phenol at pH 2.7 (silanol activity), the relative retention factor triphenylene/*o*-terphenyl (steric selectivity) and the retention factor of 2,2′-dipyridyl (silanol activity and metal impurity). This procedure was developed based on earlier work where 36 chromatographic parameters were selected from the literature. Of these 36 parameters, 24 could be measured in a repeatable and reproducible way and further selection of the final 4 parameters out of these 24 was performed using principal component analysis. After that, the correlation was examined between these test parameters and the suitability of columns for a number of separations [19–27].

In the present study, 55 different commercial stationary phases were involved and from each type, two columns of the same batch were tested. One of them was used for performing several separations while the other one was stored. In order to examine the effect of performed analyses and storage on the properties of RP-LC columns, all columns were characterised by four parameters, determined at the beginning of the test and after storage or performance of the separations.

2. Experimental

2.1. Reagents and samples

Uracil was purchased from Janssen Chimica (Geel, Belgium) and *o*-terphenyl from Aldrich (Bornem, Belgium). Amylbenzene, benzylamine, 2,2′-dipyridyl, phenol and triphenylene were acquired from Acros Organics (Geel, Belgium).

All solvents and reagents were of European Pharmacopoeia (Ph. Eur.) quality. Methanol (Prolabo, Paris, France) was of LC grade, other chemicals were of AR grade. Potassium dihydrogen phosphate was obtained from Fluka (Buchs, Switzerland) and phosphoric acid from Sigma–Aldrich (Seelze, Germany). Water was purified by a Milli-Q water-purification system (Millipore, Milford, MA, USA).

2.2. Instrumentation and liquid chromatographic conditions

The LC apparatus consisted of a Varian (Walnut Creek, CA, USA) 9010 LC pump, a 9100 autosampler equipped with a 20-μl loop and a 9050 UV–vis detector, set at 254 nm. ChromPerfect 4.4.0 software (Justice Laboratory Software, Fife, UK) was used for data acquisition. The column temperature was maintained by immersion in a water bath heated by a Julabo EC thermostat (Julabo, Seelbach, Germany) at 40 °C while the laboratory was air-conditioned at 25 °C. The buffers were calibrated using a Consort C831 pH meter (Consort, Turnhout, Belgium) equipped with a Hamilton (Bonaduz, Switzerland) combination glass electrode.

2.3. Column characterisation

To characterise the columns, three chromatographic methods were carried out in a defined order (A–B–C) to determine the four column parameters. The flow rate was 1 ml/min and the conditions are shown in Tables 1 and 2. A 0.2-mol/l KH_2PO_4 solution was brought at pH 2.7 and 6.5 with 0.2 mol/l phosphoric acid and 0.2 mol/l K_2HPO_4, respectively. As compared to the originally proposed chromatographic methods, some of the conditions were slightly adapted, as was explained elsewhere [27]. The relative retention factor benzylamine/phenol at pH 2.7 ($rk'_{\text{ba/ph pH 2.7}}$) from method A, the retention factor of 2,2′-dipyridyl ($k'_{2,2'\text{-dip}}$) from method B, the retention factor of amylbenzene (k'_{amb}) and the relative retention factor triphenylene/*o*-terphenyl ($rk'_{\text{tri}/o\text{-ter}}$) from method C were calculated using the dead volume obtained in method C with uracil. All measurements were executed in triplicate, resulting in R.S.D. values lower than 1%.

For the determination of the four parameters, the first column was conditioned with the mobile phase of method A after which $rk'_{\text{ba/ph pH 2.7}}$ was determined in triplicate. Then, method B was performed on that column and finally method C. Next, the column was conditioned with the storage solution prescribed by the manufacturer. After that, the second and subsequent columns were characterised. For the determination of the parameters after storage or performance of the separations (retest), the same chromatographic equipment was used as the first time.

Autoscaling of the data was performed to proceed in further calculations with four parameters with the same magnitude and range. After the calculation of an averaged value from the three chromatograms and a S.D. for each parameter, each single value was autoscaled:

$$\frac{x_{ij} - \bar{x}_j}{s_j} \tag{1}$$

where x_{ij} is the value of parameter j on column i, $\bar{x}_j$ is the mean of parameter j on all tested columns and s_j is the S.D. of parameter j.

An *F*-value was used to express the difference between columns with one single number, calculated from the four column parameters as follows:

$$F = (k'_{\text{amb}},\ \text{ref}^{-k'}_{\text{amb}},\ i)^2 + (rk'_{\text{ba/ph pH 2.7}},\ \text{ref}^{-rk'}_{\text{ba/ph pH 2.7}},\ i)^2 + (k'_{\text{dip}},\ \text{ref}^{-k'}_{\text{dip}},\ i)^2 + (rk'_{\text{tri}/o\text{-ter}},\ \text{ref}^{-rk'}_{\text{tri}/o\text{-ter}},\ i)^2 \tag{2}$$

Table 2
Description of the samples analysed in the column characterisation methods

Method	Sample composition
A	5 mg of benzylamine and 5 mg of phenol in 10 ml of mobile phase A
B	3 mg 2,2′-dipyridyl in 10 ml of mobile phase B
C	0.1 mg uracil, 7 mg amylbenzene, 0.2 mg *o*-terphenyl and 0.02 mg triphenylene in 10 ml mobile phase C

The *F*-value of a column *i* equals the sum of squares of the differences between each parameter value of the reference column and of column *i*. The smaller the *F*-value, the more similar is column *i* to the reference column.

2.4. Chromatographic conditions of separations

All mobile phases were degassed by sparging with helium. The stationary phase was kept at the right temperature by immersion in a water bath. For a particular analysis, the mobile phase, even the gradient, was the same for all columns. So, no adaptation was made in order to obtain similar retention times on all columns.

2.4.1. Analysis of tetracycline

The mobile phase consisted of acetonitrile, 0.3 mol/l tetrabutyl ammonium (TBA) pH 7.5, 0.3 mol/l ethylenediaminetetraacetic acid (EDTA) pH 7.5, water for the mobile phases: (A) (12:35:35:18 v/v) and (B) (30:35:35:0 v/v). Gradient program used 0–15 min, 5% of B (isocratic); 15–45 min, 5–75% of B (linear gradient); 45–65 min, 75% of B (isocratic) and 65–80 min, 75–5% of B (linear gradient). The EDTA and TBA solutions were adjusted to the required pH with concentrated ammonia before bringing up to volume. Since a small change in the temperature within a sufficiently wide range around the selected operating conditions does not affect the separation of the critical pair of tetracycline (TC) and 2-acetyl-2-decarboxamidotetracycline, the temperature was lowered from 40.0 °C to 35.0 °C, to protect the columns. On the other hand, as the run time for TC on all the columns could not be predicted, the last isocratic step was prolonged to 65 min instead of the prescribed 45 min. Other chromatographic conditions were kept the same as published [28]. A flow rate of 1.0 ml/min was used and UV-detection was performed at 280 nm.

2.4.2. Analysis of erythromycin

The mobile phase consisted of acetonitrile, 0.2 mol/l potassium phosphate pH 7.5 and water (35:5:65 v/v). The flow rate was 1.0 ml/min. The detector was set at 210 nm and the column was kept at 65.0 °C [29].

2.4.3. Analysis of fluoxetine hydrochloride

The Ph. Eur. method prescribes a mobile phase consisting of methanol–tetrahydrofuran–triethylammonium phosphate buffer (8:30:62 v/v). The buffer was prepared by adding 980 ml of water to 10 ml of triethylamine, adjusting to pH 6.0 with phosphoric acid and diluting to 1000 ml with water. The flow rate was 1.0 ml/min. The detector was set at 215 nm and the column was kept at 30.0 °C [30].

2.4.4. Analysis of gemcitabine hydrochloride

The United States Pharmacopeia (USP) method was applied with some slight modifications since the mixing of a pure organic solvent with an aqueous solution can cause problems. So, premixed eluents were prepared as follows: eluent A consisted of 97% of solution A (a filtered and degassed solution containing 13.8 g of anhydrous monobasic sodium phosphate and 2.5 ml of phosphoric acid in 1000 ml of water) and 3% of solution B (filtered and degassed methanol). Eluent B was pure methanol. The pH of solution A was checked to be 2.45–2.55 (2.4–2.6 was prescribed). The gradient program was adapted as follows: 0–8 min, 100% eluent A; 8–13 min, from 100% eluent A to 50% eluent A; 13–20 min, 50% eluent A; 20–25 min, from 50% eluent A to 100% eluent A. The flow rate was 1.2 ml/min. The detector was set at 275 nm and the column was kept at 25.0 °C [31].

2.5. Column examination

A set of 55 RP-LC columns was investigated. Specifications of the different columns examined are given in Table 3. It must be noted that Zirchrom (51) is a zirconia-based column whereas all other columns are silica based. All columns were gifts from either the manufacturer or the supplier. Two columns of each type and of the same batch were available and they were characterised as described under Section 2.3. While one column of each pair was used for four different, subsequent separations of drug substances from their respective impurities, the other column was stored at room temperature, according to the prescriptions of the manufacturer. If nothing was prescribed, pure acetonitrile was used as a storage solvent. Tetracycline, erythromycin, fluoxetine hydrochloride and gemcitabine hydrochloride were analysed on one column of each pair. The respective chromatographic procedures are described in Section 2.4. The first substance was analysed on all the columns before a next substance was analysed.

Each analysis was repeated three times, except for erythromycin, which was analysed twice since the total analysis time then could reach 400 min. For erythromycin, the average passed column volume of all columns was estimated to be about 350 ml. For tetracycline, fluoxetine and gemcitabine, it was about 320 ml, 210 ml and 250 ml, respectively. It must be noted that the total analysis time fluctuated slightly amongst columns.

Immediately after finishing the analysis of a compound each column was washed with acetonitrile:water:1 mol/l phosphoric acid (50:45:5 v/v) followed by acetonitrile:water (50:50 v/v) and finally by the storage mixture, as prescribed by the company, or by pure acetonitrile if nothing was prescribed, all with a flow rate of 1 ml/min for 30 min. When the first analysis was performed on all columns, the second analysis was started keeping the same order of the columns. This means that the time difference between the performed separations was the same for each column and during this period columns were stored in the same way as the second one of the pair. Since the analyses were performed over a period of 15 months (time consumed for doing analyses on the complete set of columns), this was also the storage period for the second column of each pair. However, it must be noticed that each column that was selected to perform analyses was only used effectively four times for 1 day. Each time half a day was used for column stabilization and the other half for proper analysis.

2.6. Data treatment

After completion of the analyses, the stored and used columns were characterised again. The deviations between the final and initial four parameter values of the columns were calculated and plotted in function of the initial parameter value. Also, four different *F*-values were determined: start, storage, storage + usage and usage alone. F_{start} was calculated using the initially determined parameters of the two columns of one batch. $F_{storage}$ was based on the difference of the parameter values for columns before and after storage and $F_{storage+usage}$ on the difference of the parameter values for columns before and after the analyses. Finally, F_{usage} was based on the difference between the parameter values for columns from the same batch, where one column was stored and the other was used for analyses. To clearly show these data, plots were drawn whereby the *X*-axes represent each parameter value for one of a pair of two columns to be compared. For each column type and each of the four parameters, the percentage deviation (*Y*-axis) of the parameter obtained for the second column was calculated with reference to the value obtained for the first column. As mentioned in the introduction, the four parameters were tested earlier for their repeatable and reproducible character. The repeatability R.S.D. was

Table 3
Characteristics of C_{18} columns examined in this study

No.	Name of the column (250 mm × 4.6 mm i.d., 5 mm, spherical particles)	Manufacturer supplier	Substrate (type of silica)	Type of bounded phase, polar group in bonded phase	Endcapping/base-deactivation	Pore size (A)	Surface area (m^2/g)	Carbon loading (%)	Storage
1	ACE5C18	Achrom	B		Yes/yes	100	300	15.5	MeOH–water (85:15 v/v)
2	Alltima AQ	Alltech	B	Polar endcapping	Yes/no	100	450	20	ACN–water (58:42 v/v)
3	Alltima C18	Alltech	B		Yes/no	100	340	16	ACN–water (58:42 v/v)
4	BravaBDSC18	Alltech	B		Yes/no	145	185	8.5	ACN–water (58:42 v/v)
5	CapcellPakC18ACR	Shiseido F. Ch.	B		Yes/yes	80	340	18	ACN–water (70:30 v/v)
6	CapcellPakC18AQ	Shiseido F. Ch.	B		Yes/yes	80	300	11	ACN–water (70:30 v/v)
7	CapcellPakC18MG	Shiseido F. Ch.	B		Yes/yes	90	280	15	ACN–water (70:30 v/v)
8	CapcellPakC18UG120	Shiseido F. Ch.	B		Yes/yes	120	290	15.1	ACN–water (70:30 v/v)
9	Chromolith Performance RP-18e	Merck	B		Yes/no	20000/130[a]	300	18	ACN 100%
10	Discovery C18	Supelco	B		Yes/no	180	200	12	MeOH 100%
11	Discovery HS C18	Supelco	B		Yes/no	120	300	20	MeOH–water (70:30 v/v)
12	Exsil ODS 5Lim	SGE	B		Yes/no	80	138	12	ACN–water (70:30 v/v)
13	Hamilton HxSilC18	Hamilton	B		Yes/–	312	17.9	15	ACN–water (65:35 v/v)
14	HydrospherC18	YMC	B		Yes/yes	120	335	12.5	ACN–water (70:30 v/v)
15	HyPURITY Advance	Thermo E. C.	B	Polar-embedded group	No/yes	190	200	10	ACN–water (80:20 v/v)
16	HyPURITYAquastar	Thermo E. C.	B	Polar endcapping	Yes/yes	190	200	10	ACN–water (80:20 v/v)
17	HyPURITY C18	Thermo E. C.	B		Yes/yes	190	200	13	ACN–water (80:20 v/v)
18	Inertsil ODS-2	GL Sci. Inc.	B	Intermediate bonded C18	Yes/yes	150	320	18.5	ACN 100%
19	Inertsil ODS-3	GL Sci. Inc.	B		Yes/yes	100	450	15	ACN 100%
20	Inertsil ODS-80A	GL Sci. Inc.	B		Yes/yes	80	450	17.5	ACN 100%
21	Inertsil ODS-P	GL Sci. Inc.	B	Polymeric bonded C18	No/no	100	450	29	ACN 100%
22	KromasilKR100-5C18	EKA Chem.	B		Yes/yes	100	340	19	MeOH–water (90:10 v/v)
23	LiChrosorb RP-18 irregular particle	Merck	A	Polymeric bonded C18	Yes/no	100	300	17	ACN 100%
24	LiChrospher 100 RP-18	Merck	A		No/no	100	350	21	ACN 100%
25	MP-Gel ODS-5	OmniChrom	B		Yes/–	120	340	13.3	MeOH–water (75:25 v/v)
26	Omnispher5C18	Varian	B		No/no	110	320	20	ACN–water (70:30 v/v)
27	Platinum C18	Alltech	B		Yes/no	100	200	6	ACN–water (58:42 v/v)
28	Platinum EPS C18	Alltech	B		No/no	100	200	5	ACN–water (58:42 v/v)
29	Polaris 5iim	Varian	B		Yes/yes	180	180	14	ACN 100%
30	Prevail Amide	Alltech	B	Polar-embedded group	No/no	190	200	12	ACN–water (58:42 v/v)
31	Prevail C18	Alltech	B	Hydrophylic endcapping	Yes/no	110	350	15	ACN–water (58:42 v/v)
32	Prevail Select C18	Alltech	B	Polar-embedded group	No/no	110	350	17	ACN–water (58:42 v/v)
33	Prontosil 120-5-ace-EPS	Bischoff	B	Polar-embedded group	Yes/yes	120	300	18.5	ACN–water (85:15 v/v)
34	Prontosil 120-5-C18AQ	Bischoff	B		Yes/yes	120	300	15	ACN 100%
35	Prontosil 120-5-C18 AQ PLUS	Bischoff	B	Polar endcapping	Yes/yes	120	300	17	ACN 100%
36	Prontosil 120-5-C18-H	Bischoff	B		Yes/yes	120	300	17	ACN–water (85:15 v/v)
37	Prontosil 120-5-C18-SH	Bischoff	B		Yes/yes	120	300	19	ACN–water (85:15 v/v)
38	Prontosil 60-5-C18 H	Bischoff	B		Yes/yes	60	450	18.5	ACN–water (85:15 v/v)
39	PurospherRP18e	Merck	B		Yes/no	90	350	18	ACN 100%
40	Purospher Star RP-18	Merck	B		Yes/yes	120	330	17	ACN 100%
41	Pursuit 5uC18	Varian	B		Yes/no	180	180	14	ACN 100%
42	Supelcosil LC-18	Supelco	A		Yes/no	100	170	11	MeOH–water (70:30 v/v)
43	Supelcosil LC-18 DB	Supelco	A		Yes/yes	100	170	11	MeOH–water (70:30 v/v)
44	Superspher 100 RP-18	Merck	B		Yes/no	100	350	21	ACN 100%
45	Uptisphere 5 HDO-25QS	Interchrom	B		Yes/–	120	310	16.2	MeOH 100%
46	Uptisphere 5 ODB-25QS	Interchrom	B		Yes/–	120	330	17.6	MeOH 100%
47	WakosilII5C18RS	SGE	B		Yes/yes	120	136	17	ACN–water (70:30 v/v)
48	YMC-Pack Pro C18 3Lim	YMC	B		Yes/yes	120	325	16	ACN–water (70:30 v/v)
49	YMC-Pack Pro C18 5Lim	YMC	B		Yes/yes	120	332	16	ACN–water (70:30 v/v)
50	YMC-Pack Pro C18RS	YMC	B	Polymeric bonded C18	Yes/yes	80	501	22.1	ACN–water (70:30 v/v)
51	Zirchrom PS	ZirChrom	B	Polystyrene coating	No/no	300	30	1	ACN–water (50:50 v/v)
52	Zorbax Eclipse XDB-C18	Agilent	B		Yes/yes	80	180	10	MeOH–water (85:15 v/v)
53	Zorbax Extend-C18	Agilent	B	Bidentate	Yes/–	80	180	12.5	MeOH–water (85:15 v/v)
54	Zorbax SB–Aq	Agilent	B		No/–	80	180	10	MeOH–water (70:30 v/v)
55	Zorbax SB-C18	Agilent	B		No/–	80	180	10	MeOH–water (85:15 v/v)

This information, when given, was supplied by the manufacturer and/or supplier; –: unknown.

[a] Macropore/mesopore.

less than 2% and the reproducibility R.S.D. in three different laboratories was found to be less than 10% [19].

In this study the experimental error of the test measurements was also determined. Experimental error was examined on three of the columns on the same instrument. The procedure for the determination of four test parameters was performed on each column by injecting the samples (see Table 1) three times and then the procedure was repeated twice in the same way, each time using freshly prepared mobile phase. The values obtained for the S.D. of *D*% were not more than 1% for $rk'_{\text{tri/o-ter}}$, not more than 2% for k'_{amb} and $k'_{2,2'\text{-dip}}$ and not more than 5% for $rk'_{\text{ba/ph pH 2.7}}$. This means that the various conclusions in the present paper are based on reliable data, which are not subjected to large experimental errors.

3. Results and discussion

3.1. Column characterisation in relation to the intra-batch deviations

Among the packings, listed in Table 3, high purity silica type B is better represented than type A silica. With exception of the Chromolith and Zirchrom, all stationary phases of the studied columns contain C_{18} chains, showing different types of bonding: monomeric, polymeric or intermediate. The presence of a polar-embedded group and deactivation and/or endcapping can be responsible for the differences of the column properties. Base deactivation is the process to obtain a stationary phase with a decreased interaction with basic compounds. Endcapping was not considered here as base deactivation. Fig. 1 represents the intra-batch deviations for each pair of columns as a function of the original, non-autoscaled parameter value. The 2,2′-dipyridyl test hereby gives the highest deviations, as can be seen in Fig. 1c. The *k*-values of six columns (23, 28, 42, 46, 51 and 52) differ more than 20% in the intra-batch test. This phenomenon could point towards inhomogeneity of metal traces in the column packing. In this test, peak tailing was often observed and could lead to a less accurate measurement resulting in higher differences for the retention factor of 2,2′-dipyridyl.

According to previous observation, $k'_{2,2'\text{-dip}}$ may not only characterise metal impurities but also silanol activity [20]. Three of these columns (23, 28 and 42) also show higher $rk'_{\text{ba/ph pH 2.7}}$ values ($rk'_{\text{ba/ph pH 2.7}} > 0.3$) (Fig. 1b), which refer to the silanol activity of the columns [19]. The intra-batch difference in silanol activity of column 28 can also contribute to the higher deviation of $k'_{2,2'\text{-dip}}$. Column 23 contains type A silica, which is less purified

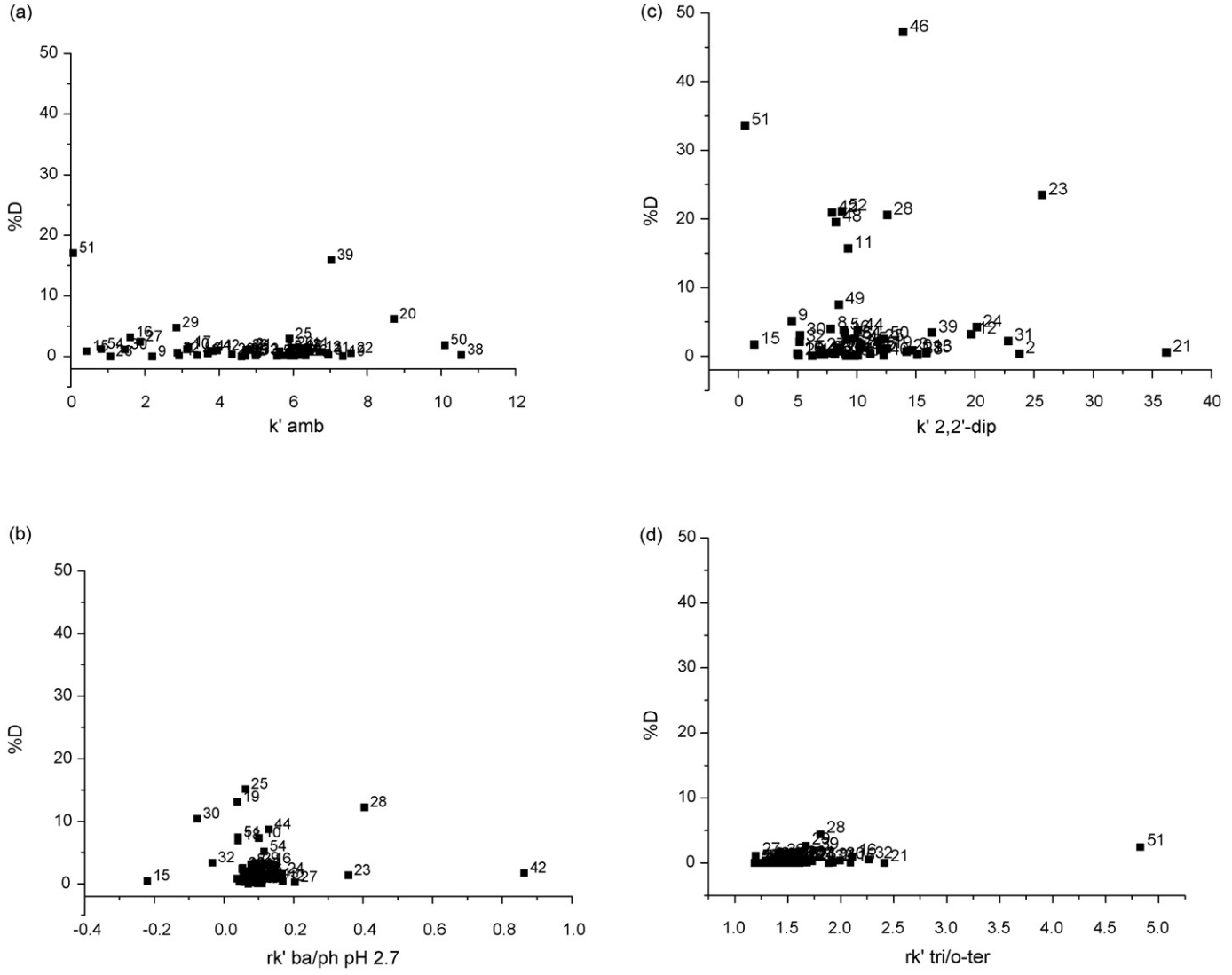

Fig. 1. Percentage deviation (*%D*) between parameter values for two new columns of the same batch. The value of the reference column of each pair is indicated by the *X*-axis.

than the type B silica. Nine columns (10, 18, 19, 25, 28, 30, 44, 51 and 54) have a difference in silanol activity within the same batch between 5% and 20% while only three columns (20, 39 and 51) deviate in this range for the hydrophobicity value (Fig. 1a). The deviation of the parameter measuring the steric selectivity is always less than 5% (Fig. 1d). Since the retention time of benzylamine was small, usually close to the t_0 of uracil, the parameter of the silanol activity can be less precise than the other parameters. Three columns (15, 30 and 32) gave even less retention for benzylamine than for uracil. All three were non-endcapped columns with a polar-embedded group. These polar-embedded columns probably provide a kind of shielding towards the silanol groups on the column surface, leading to less interaction possibilities with the benzylamine and to lower values. Moreover, an incorporated polar group attracts a water layer, preventing the interaction of benzylamine with the silanol groups located below this strongly bound water layer [32]. Zirchrom (51), a column which possesses porous zirconia particles coated with polystyrene, shows of course a low silanol activity and the 2,2′-dipyridyl parameter is equal to 0.56. The value for the other Zirchrom column is 0.84. These small numbers result in a high percentage (33%) of difference, which can be explained by the fact that Zirchrom columns have no silanol groups and a very low amount of metal impurities in comparison with other columns, leading to relatively low values for the 2,2′-dipyridyl parameters. The smaller the values, the higher the possibility of large percentage differences. Higher parameters for metal impurity and silanol activity (Fig. 1c, $k'_{2,2'-\mathrm{dip}} > 17$) were measured on columns that were either non-base deactivated (2, 12 and 31) or non-endcapped (21, 23 and 24). Other type A columns (42 and 43), which are endcapped, show smaller parameter values. Fig. 1a indicates that certain 'Aqua columns' (16 and 54), not or not fully endcapped stationary phases (27 and 28), columns with a polar-embedded group (15 and 30) and a Zirchrom column (51), which have a reduced carbon loading (5–12%) possess low parameter values for hydrophobicity ($k'_{amb} < 2$). It was found earlier that columns prepared by polymeric silanization exhibit greater shape discrimination than monomeric phases [33]. Zirchrom (51) is known to be not as hydrophobic as a typical C_{18} column, which can clearly be seen in Fig. 1a. Fig. 1d shows an increased steric selectivity ($rk'_{\mathrm{tri/o\text{-}ter}} > 1.7$) for some typical columns containing polar-embedded groups (15, 30, 32 and 33) or a polar endcapping (2, 16 and 31) and for only one column (21) with polymeric bonded C_{18}. The highest value was observed for the Zirchrom column (51).

The column with the starting *F*-values in Table 4 shows the ranked *F*-values of the new columns studied using the other new column from the same batch as reference. A small *F*-value points towards good similarity between the columns of the same batch. Only six columns have an *F*-value higher than 0.1, most belong to a group with salient deviation of $k'_{2,2'\text{-dip}}$ and one column, the Purospher RP 18e (39) with a very high value for k'_{amb}. 17 out of the 55 columns have a value higher than 0.01.

Concerning column-to-column and batch-to-batch variability of stationary phases, a study was carried out previously by Kele and Guiochon. Different brands of commercially available C_{18} packings

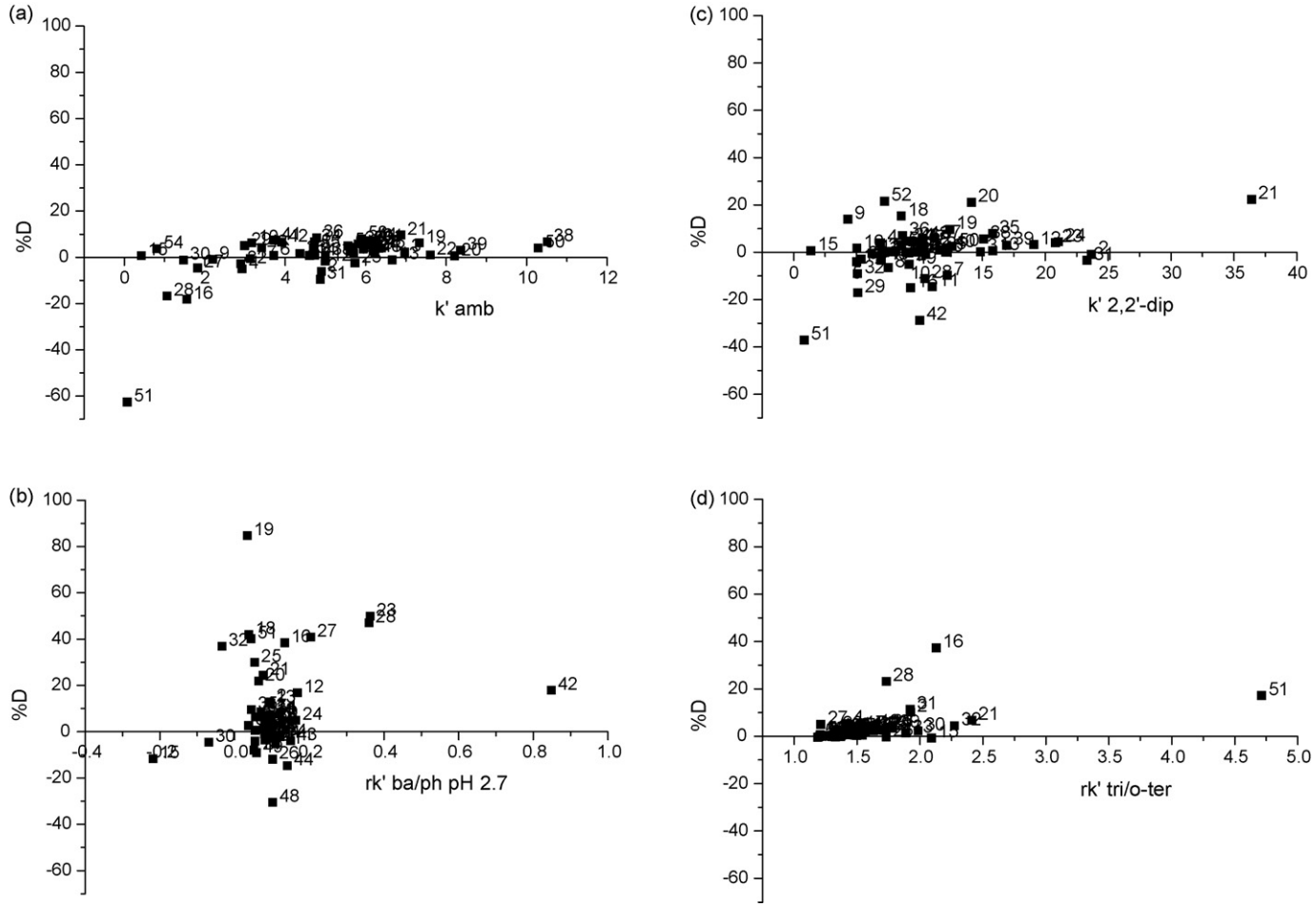

Fig. 2. Percentage deviation (%*D*) between the parameter values for the same stored and unused column, measured at the beginning and at the end of the study.

were examined as well as the short-term and long-term repeatability of chromatographic data, acquired on a single column and on different columns of the same batch or of different batches [34–38]. The parameters under investigation were characteristic for the retention, the hydrophobic interaction selectivity, the steric selectivity, the relative retention of basic and neutral compounds, the column efficiency and the peak asymmetry. Kele and Guiochon reported R.S.D. values below 0.02 for relative retention times of different solutes [36]. In this study, 55 different stationary phases were checked whereas Kele and Guiochon applied their test method onto four different packings only. In our study, 43 out of the 55 columns (or almost 80%) have a percentage difference value below 0.02.

3.2. Stability of columns after storage and after usage

Not only new columns should be characterised. Columns can also be retested to monitor changes in column properties as a function of time or of the samples analysed [39].

The percentage deviation between the parameter values at the beginning and at the end of the study, as calculated for each stored and used column is shown in Figs. 2 and 3. Positive or negative changes may be observed. The deviation between the characteristics of the used column and the stored column at the end of the study was also calculated to deduce the influence of the separations. The latter results can be seen in Fig. 4. Previous comparison of the column parameters at the start of the study (Fig. 1) was necessary to verify in how far the difference between parameters measured on two columns from the same batch can be due to intra-batch differences.

3.2.1. Change of column parameters after storage

Differences between the chromatographic parameters caused by storage can be seen in Fig. 2. For most of the columns there is only little influence on the hydrophobicity (Fig. 2a). This indicates that storage mostly does not lead to extended hydrolytic degradation followed by a decrease of the number of alkyl chains.

Most of the column pairs show only small shifts ($D < 20\%$) for each parameter. However, some columns have greater deviations. The silanol activity (Fig. 2b) of columns 16, 18, 19, 20, 21, 23, 25, 27, 28, 32 and 51 increased by more than 20% after storage, which may influence their retention properties for basic substances. It has already been reported that absolute and relative retention as well as peak shape of neutral solutes hardly are affected by storage, whereas the elution sequence and more pronouncedly the peak shape of basic solutes are subjected to alternations [40]. The new active silanol site can originate from the hydrolytic loss of only a few bonded groups (endcapping). The changes in Fig. 2c are spread, although more columns show a slight increase. This could be explained by an increase in the amount of free silanols, rather than to an increase in the metal impurities, due to the interaction of the mobile phase with the backbone of the column, since an overall positive value for $rk'_{\mathrm{ba/ph\,pH\,2.7}}$ can be seen in Fig. 2b, representing the silanol activity. The changes in Fig. 2d are almost always positive. It was not possible to find a plausible explanation for the

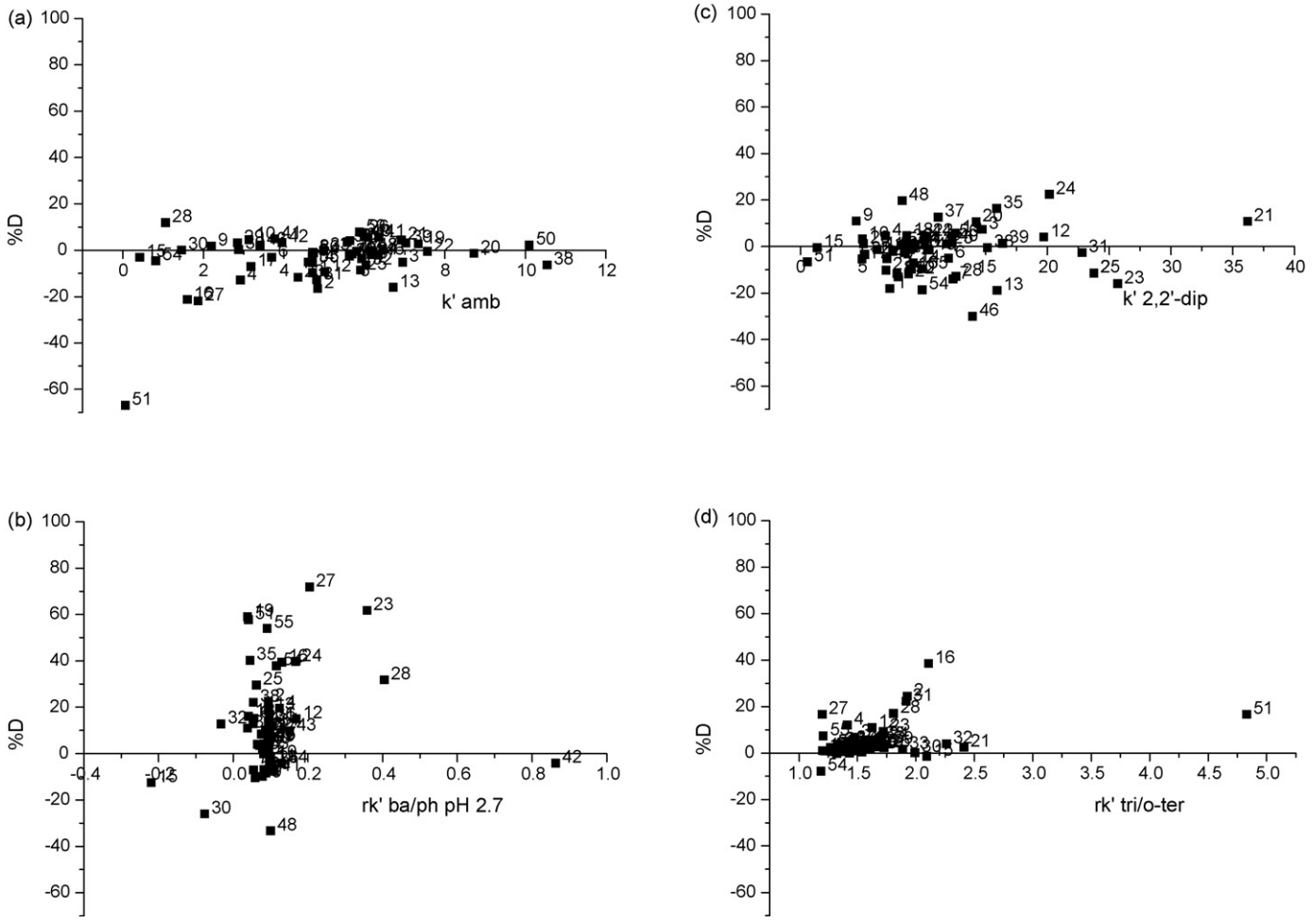

Fig. 3. Percentage deviation (%D) between the parameter values for the same used column, measured at the beginning and at the end of the study.

Table 4
F-values of columns at the beginning of the test (start), of stored columns (storage), of used columns at the end of the test (storage + usage) and of used columns without storage effect (usage), based on the ranking of the *F*-values of start

No.	Column	*F*-values			
		Start	Storage	Storage + usage	Usage
23	LiChrosorb RP 18	0.544	0.437	3.352	0.909
46	Uptisphere 5 ODB	0.513	0.007	0.422	0.012
39	Purospher RP 18e	0.359	0.019	0.028	0.176
28	Platinum EPSC18	0.208	0.596	1.080	0.558
42	Supelcosil LC 18	0.126	0.267	0.093	0.005
48	YMCPackPro 3	0.115	0.084	0.150	0.014
11	Discovery HS C18	0.091	0.087	0.044	0.031
20	Inertsil ODS-80A	0.066	0.135	0.052	0.147
52	Zorbax Eclipse XDB	0.062	0.081	0.039	0.072
24	LiChrospher 100 RP-18	0.042	0.034	0.661	0.694
21	Inertsil ODS-P	0.030	0.452	0.325	0.192
31	Prevail C18	0.025	0.246	0.252	0.091
44	Superspher 100 RP-18	0.017	0.086	0.047	0.031
49	YMCPackPro 5	0.015	0.008	0.002	0.003
29	Polaris 5	0.014	0.014	0.025	0.031
25	MP Gel ODS 5	0.013	0.056	0.072	0.024
16	HyPURITYAquastar	0.010	0.947	1.010	0.033
50	YMCPackPro RS	0.009	0.003	0.024	0.010
51	Zirchrom PS	0.006	0.034	0.058	0.004
32	Prevail Select C18	0.005	0.049	0.068	0.021
2	Alltima AQ	0.004	0.150	0.595	0.239
54	Zorbax SB-Aq	0.004	0.023	0.189	0.235
15	HyPURITY Advance	0.003	0.443	0.191	0.097
9	Chromolith	0.003	0.041	0.035	0.005
12	Exsil ODS 5	0.003	0.023	0.087	0.114
3	Alltima C18	0.003	0.019	0.048	0.070
10	Discovery C18	0.003	0.016	0.026	0.006
5	Capcell Pak ACR	0.003	0.014	0.024	0.016
38	Prontosil 60-5-C18-H	0.003	0.009	0.090	0.121
8	Capcell Pak UG120	0.003	0.004	0.012	0.005
7	Capcell Pak MG	0.002	0.062	0.068	0.013
19	Inertsil ODS-3	0.002	0.055	0.059	0.006
13	Hamilton Hx Sil	0.002	0.035	0.453	0.242
26	Omnispher5	0.002	0.032	0.065	0.049
36	Prontosil 120-5-C18-H	0.002	0.026	0.022	0.037
6	Capcell Pak AQ	0.002	0.004	0.011	0.007
27	Platinum C18	0.001	0.100	1.346	0.703
30	Prevail Amide	0.001	0.075	0.105	0.016
18	Inertsil ODS-2	0.001	0.057	0.043	0.028
41	Pursuit 5	0.001	0.029	0.023	0.008
22	Kromasil KR100 5	0.001	0.016	0.024	0.028
37	Prontosil 120-5-C18-SH	0.001	0.014	0.062	0.048
40	Purospher Star RP-18	0.001	0.011	0.044	0.021
17	HyPURITYC18	0.001	0.011	0.008	0.013
55	Zorbax SB-C18	0.001	0.009	0.176	0.215
35	Prontosil 120-5-C18AQPL	0.001	0.007	0.163	0.111
45	Uptisphere 5 HDO	0.001	0.006	0.005	0.015
14	Hydrosphere	0.001	0.005	0.011	0.015
43	Supelcosil LC 18 DB	0.000	0.041	0.019	0.093
33	Prontosil 120-5-ace-EPS	0.000	0.036	0.042	0.010
4	Brava BDSC18	0.000	0.022	0.097	0.075
34	Prontosil 120-5-C18AQ	0.000	0.022	0.013	0.047
53	Zorbax Extend C18re	0.000	0.018	0.066	0.023
1	ACE	0.000	0.017	0.055	0.100
47	Wakosil II 5 RS	0.000	0.005	0.003	0.002
	Average	0.042	0.093	0.220	0.107
	S.D.	0.11	0.17	0.51	0.19

relatively large changes found for columns 16, 28 and 51. These three columns also show a relatively high change in silanol activity (Fig. 2b).

The *F*-values of stored columns at the end of the study are also listed in Table 4. Although the average *F*-value is low (F_{av} = 0.093), it is more than two times higher than the F_{av} (F = 0.042) of the intra-batch deviation. The highest *F*-values in the ranking (columns 16, 28, 21, 15 and 23) were in the range of 0.4–1, which is considerably higher than the *F*-values for the first five ranked columns (23, 46, 39, 28 and 42) of the intra-batch test ($0.1 < F < 0.6$). These results indicate that characteristics of at least some columns may change considerably upon storage. Previously, small changes in retention factors and in column properties like hydrophobicity and steric resistance were also reported over a 2-year period [41].

The data of Table 4 were also retreated by eliminating the non-standard C_{18} columns (embedded polar, type A, etc). With the remaining 38 columns, the average $F_{storage}$-value was 0.053 (S.D. = 0.097) which is considerably smaller than the difference reported in Table 4, but seen the large S.D. not important.

Endcapped columns were also examined more in detail. It is generally accepted that endcapping is much more easily removed

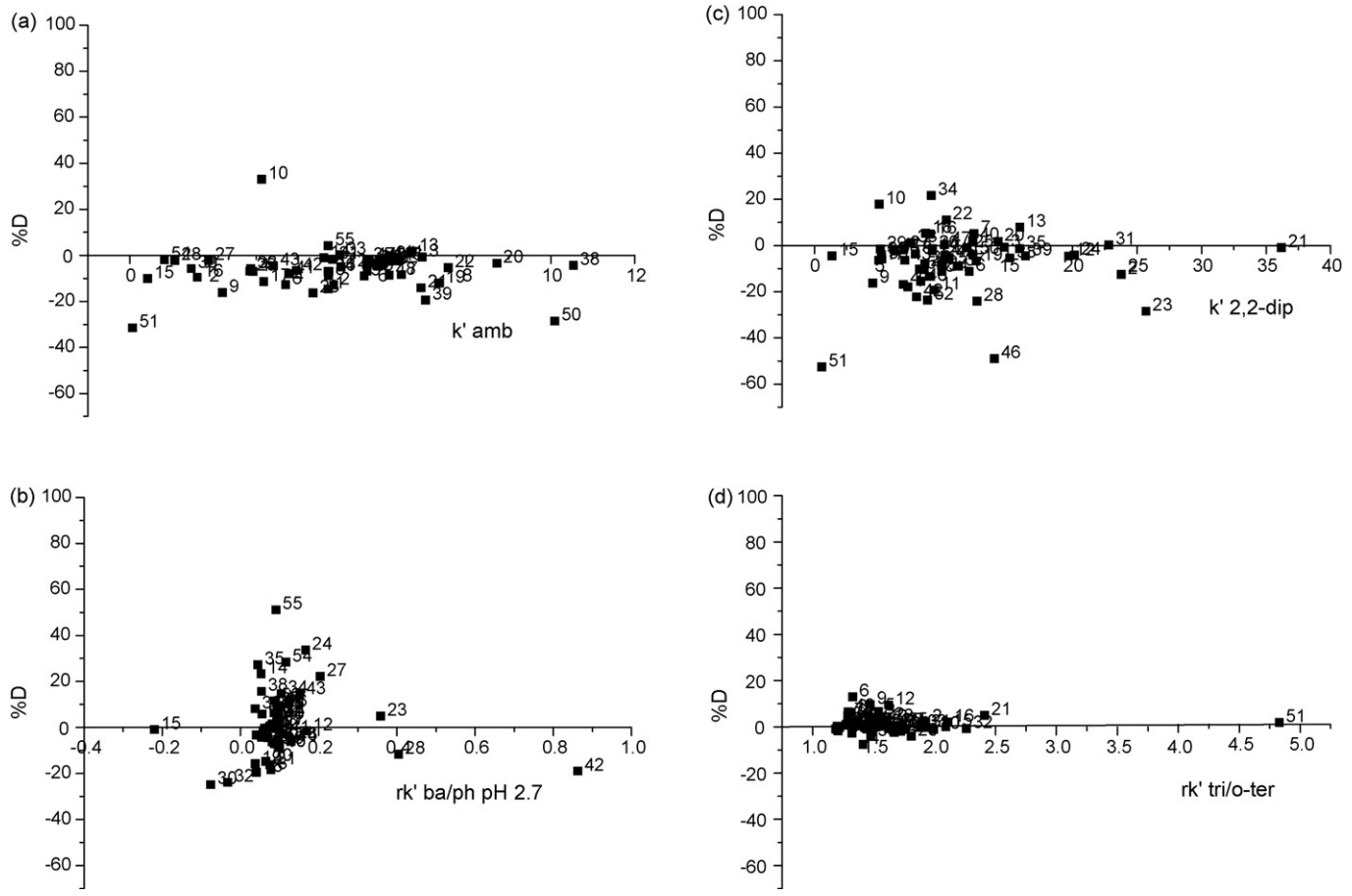

Fig. 4. Percentage deviation (%*D*) between the parameter values determined at the end of the study for two columns of the same batch, where one column was just stored while the other was used to analyse samples.

during storage than the C_{18} ligands. This was confirmed since the average $F_{storage}$-value amounted to 0.175 for the endcapped columns compared to 0.079 for the non-endcapped.

3.2.2. Change of column parameters after performing analyses combined with storage

Fig. 3 represents the change of columns, induced by the combined effect of analyses and storage. In Fig. 3a–d, it can be observed that columns giving the highest *F*-values ($F > 0.5$) (2, 16, 23, 24, 27 and 28) possess relatively low hydrophobicity, high silanol activity, high metal content/silanol activity and high steric selectivity. These columns, altering the most, have no endcapping and/or no base deactivation. Other columns, developed with polar-embedded groups (15, 30, 32 and 33), or polar-endcapped phases with further stabilization (column 54 is sterically protected) have similar characteristics but they do not change that much. These additional features provide the column surface with an additional shielding towards outside influences and give protection to the silanol groups present. *F*-values of the columns used for several analyses (*F*-value for storage + usage) can be seen in Table 4. The average *F*-value for storage + usage is considerably higher than the respective *F*-value of the stored columns, which is probably due to the performed separations. Taking into account that the four analyses took each 1 day, columns were only used for 1% of the time between the first and the second characterisation. Checking the differences between the *F*-values for storage ($F_{av} = 0.093$) and for storage + usage ($F_{av} = 0.220$), it can be concluded that the influence of the performed analyses is not negligible at all.

3.2.3. Change of column parameters after performing analyses

Fig. 4 represents the differences of the column characteristics only caused by the separation procedures. Each difference was determined by calculating the *F*-value between two columns of the same batch, after storage and after performing analyses, respectively. Since a percentage difference was also observed between two columns of a batch, this intra-batch deviation was subtracted from the percentage deviation calculated here.

Fig. 4a shows that the hydrophobicity almost always has decreased upon usage, as can be expected. When the pH of the mobile phase is low, acid-catalyzed hydrolysis of the siloxane bond may occur, resulting in continuous loss of the bonded phase and concomitant loss of chromatographic retention. The analysis of gemcitabine was performed with a mobile phase containing a phosphate buffer of pH 2.5. This condition could facilitate the above-mentioned process causing the change of the column parameter. It was reported earlier that the improvement in bonding chemistry, including high coverage, the use of multi-reactive silanes and/or bulky groups or long chain silane groups, could show a significant stabilizing effect [42]. Few columns (11, 22, 24, 26 and 44) are known to have a higher surface coverage (value $\geq 3.5\ \mu mol/m^2$). They show only small (−1.2% to −5.4%) deviations of the hydrophobicity parameter. The functionalities of Prontosil columns were made available by the manufacturer. The monofunctional bonded C_{18} columns (34, 36 and 38) show a deviation of hydrophobicity of −4.0% to −7.0% whereas the bifunctional bonded phases (columns 33, 35 and 37) have a decrease of 0% to −3.4%. Note that there is some difference in the surface coverage of the

mono-C_{18} columns (the values for columns 34, 36 and 38 are 2.0 μmol/m^2, 3.2 μmol/m^2 and 3.0 μmol/m^2) and bi-C_{18} columns (the value for columns 33, 35 and 37 is 3.2 μmol/m^2). Among the Zorbax columns, the deviation of Eclipse (52) with extra-dense bonding is −3.3%, the sterically protected diisobutyl-ODS phases (columns 54 and 55) give −1.9% and 4.1% and finally, the bidentate-C_{18} phase (column 53) has a values of −4.0%, pointing out their stability.

Fig. 4b demonstrates that the number of silanol sites increases after usage, mostly for endcapped columns. For non-endcapped columns, this phenomenon can be assigned to the loss of bonded phase. On "shielded phases", where a neutral polar group has been introduced close to the surface, the silanol groups are blocked by strong hydrogen bonds. The polar group also attracts a water layer, preventing the interaction of analytes with the silanol groups located below this strongly bound water layer [32]. The polar-embedded phases ensure low silanol activity (columns 15, 30, 32 and 33). No increase of the silanol sites could be observed after usage of these columns. If silanols were formed, they were probably also shielded by the polar group.

The $k'_{2,2'\text{-dip}}$ value of the columns differs over a quite broad range after usage (Fig. 4c). A number of the columns show an increased value after use. This can be explained by the fact that most of these columns have also increased values for the $rk'_{\text{ba/ph pH 2.7}}$ value, pointing towards increased silanol activity. On the other hand, it can also be observed in Fig. 4c, that the majority of the columns lose metal ions during analyses, which is attributable to the chromatographic conditions used. For one separation, the mobile phase contained the chelating agent EDTA, which can be responsible for partial removal of metal ions.

Fig. 4d shows the differences in steric selectivity of the different columns. This parameter does not deviate in the same manner as the other three parameters, confirming that the bonding chemistry does not change.

When looking at the *F*-values (Table 4), the average for usage is slightly higher than that of storage alone. It must be noted that the *F*-value of the intra-batch deviation ($F_{\text{av}} = 0.042$) could be considered to be partially included in the F_{usage}-value. Moreover, it has to be mentioned that the chromatographic circumstances used were not very aggressive. Also, the columns were used for a total of only 4 days. It can therefore be concluded that changes due to use do occur already after a short period of time.

4. Conclusion

In this paper, 55 pairs of RP columns were examined in order to study the influence of storage and usage on their properties. For each column, four parameters were measured to assess hydrophobicity, silanol activity, metal impurity and steric selectivity at the beginning and at the end of the test. The deviation between the parameters revealed changes of different column properties during the test. The *F*-value was calculated to express the change of four column parameters within a single value.

Most unused RP columns from the same batch show very good similarity. However, for those characterised by a high silanol activity, greater differences were observed.

After long-term storage, small changes of the column characteristics occur for most of the columns, producing slightly increased *F*-values. A few columns differed by a greater extent and showed considerable changes in silanol activity and hydrophobicity. Most of these columns have no endcapping and/or no base deactivation, making these stationary phases more vulnerable towards degradation. This effect is observed less with columns with polar-embedded groups and/or polar endcapping, protecting the column by blocking the silanol groups and attracting a shielding water layer. Also columns with higher coverages and bulky or long chains show more resistance towards degradation.

When columns were used to perform analyses, about two times higher *F*-values were obtained compared to the non-used, stored columns. The difference can be attributed to the analyses performed. Loss of bonded phase and increase of the silanol sites were observed.

Considering the short analysis time (about 1% analysis time versus a storage time of 15 months), it can be concluded that changes in the stationary phases do occur. With the analytical conditions used here the influence of use was about 100 times more important than that of storage.

Acknowledgements

The authors thank the manufacturers and the suppliers for the gift of columns. E. Farkas, A. Kerner and K. Kóczián thank the Ministry of the Flemish Community for financial support. E. Adams is a post-doctoral fellow of the Fund for Scientific Research (FWO)—Flanders, Belgium. Financial support to this project is given by a Research Grant of the Fund for Scientific Research—Flanders (Belgium).

References

[1] H. Engelhardt, R. Grüner, Int. Lab. (1999) 34.
[2] E. Cruz, M.R. Euerby, C.M. Johnson, C.A. Hackett, Chromatographia 44 (1997) 151.
[3] Á. Sándi, Á. Bede, L. Szepesi, G. Rippel, Chromatographia 45 (1997)206.
[4] L.R. Snyder, J.W. Dolan, P.W. Carr, J. Chromatogr A 1060 (2004) 77.
[5] M.R. Euerby, P. Peterssonn, J. Chromatogr. A 1088 (2005) 1.
[6] U.D. Neue, J.E. O'Gara, A. Méndez, J. Chromatogr. A 1127 (2006) 161.
[7] D. Visky, Y. Vander Heyden, T. Iványi, P. Baten, J. De Beer, B. Noszál, E. Roets, D.L. Massart, J. Hoogmartens, Pharmeuropa 14 (2002) 288.
[8] K. Kimata, K. Iwaguchi, S. Onishi, K. Jinno, R. Eksteen, K. Hosoya, M. Araki, N. Tanaka, J. Chromatogr. Sci. 27 (1989) 721.
[9] H.A. Claessens, TrAC 20 (2001) 563.
[10] H.A. Claessens, M.A. van Straten, J. Chromatogr. A 1060 (2004) 23.
[11] M.J.J. Hetem, J.W. de Haan, H.A. Claessens, C.A. Cramers, A. Deege, G. Schomburg, J. Chromatogr. 540 (1991) 53.
[12] J.J. Kirkland, M.A. van Straten, H.A. Claessens, J. Chromatogr. A 691 (1995)3.
[13] J.J. Kirkland, J.W. Henderson, J.J. DeStefano, M.A. van Straten, H.A. Claessens, J. Chromatogr. A 762 (1997) 97.
[14] H.A. Claessen, M.A. van Straten, J.J. Kirkland, J. Chromatogr. A 728 (1996) 259–270.
[15] J.J. Kirkland, J.W. Henderson, J.J. DeStefano, M.A. van Straten, H.A. Claessen, J. Chromatogr. A 762 (1997) 97–112.
[16] B. Law, P.F. Chan, J. Chromatogr. 467 (1990) 267.
[17] B.C. Trammell, C.A. Boissel, C. Carignan, D.J. O'Shea, C.J. Hudalla, U.D. Neue, P.C. Iraneta, J. Chromatogr. A 1060 (2004) 153.
[18] S.J. Marin, B.A. Jones, W.D. Felix, J. Clark, J. Chromatogr. A 1030 (2004) 255.
[19] D. Visky, Y. Vander Heyden, T. Iványi, P. Baten, J. De Beer, Zs. Kovács, B. Noszál, E. Roets, D.L. Massart, J. Hoogmartens, J. Chromatogr. A 977 (2002) 39.
[20] T. Iványi, Y. Vander Heyden, D. Visky, P. Baten, J. De Beer, I. Lázár, D.L. Massart, E. Roets, J. Hoogmartens, J. Chromatogr. A 954 (2002) 99.
[21] D. Visky, Y. Vander Heyden, T. Iványi, P. Baten, J. De Beer, Z. Kovács, B. Noszál, P. Dehouck, E. Roets, D.L. Massart, J. Hoogmartens, J. Chromatogr. A 1012 (2003) 11.
[22] P. Dehouck, D. Visky, G. Van den Bergh, E. Haghedooren, E. Adams, A. Kerner, Y. Vander Heyden, D.L. Massart, Zs. Kovács, B. Noszál, J. Hoogmartens, LC–GC Europe 17 (2004) 592.
[23] P. Dehouck, D. Visky, Y. Vander Heyden, E. Adams, Z. Kovács, B. Noszál, D.L. Massart, J. Hoogmartens, J. Chromatogr. A 1025 (2004) 189.
[24] D. Visky, E. Haghedooren, P. Dehouck, Zs. Kovács, K. Kóczián, B. Noszál, J. Hoogmartens, E. Adams, J. Chromatogr. A 1101 (2006) 103.
[25] E. Haghedooren, J. Diana, B. Noszál, J. Hoogmartens, E. Adams, Talanta 71 (2007) 31.
[26] E. Haghedooren, D. Visky, P. Dehouck, K. Kóczián, Zs. Kovács, B. Noszál, J. Hoogmartens, E. Adams, LC–GC Europe 20 (2007) 82.
[27] E. Haghedooren, A. Kerner, B. Noszál, J. Hoogmartens, E. Adams, J. Pharm. Biomed. Anal. 44 (2007) 634.
[28] R. Capote, J. Diana, E. Roets, J. Hoogmartens, J. Sep. Sci. 25 (2002) 399.
[29] H.K. Chepkwony, P. Dehouck, E. Roets, J. Hoogmartens, Chromatographia 53 (2001) 159.

[30] Council of Europe, European Pharmacopoeia, 1615, 5th edition, Council of Europe, Strasbourg, France, 2005.
[31] United States Pharmacopeial Convention, The United States Pharmacopeia, 892, 28th edition, United States Pharmacopeial Convention, Rockville, USA, 2005.
[32] U.D. Neue, Y.-F. Cheng, Z. Lu, B.A. Alden, P.C. Iraneta, C.H. Phoebe, K. Van Tran, Chromatographia 54 (2001) 169.
[33] L.C. Sander, M. Pursch, S.A. Wise, Anal. Chem. 71 (1999) 4821.
[34] M. Kele, G. Guiochon, J. Chromatogr. A 830 (1999) 41.
[35] M. Kele, G. Guiochon, J. Chromatogr. A 830 (1999) 55.
[36] M. Kele, G. Guiochon, J. Chromatogr. A 855 (1999) 423.
[37] M. Kele, G. Guiochon, J. Chromatogr. A 869 (2000) 181.
[38] M. Kele, G. Guiochon, J. Chromatogr. A 913 (2001) 89.
[39] C.F. Poole, The Essence of Chromatography, Elsevier, Amsterdam, 2003.
[40] H. Engelhardt, M. Jungheim, Chromatographia 29 (1990) 59.
[41] J.J. Gilroy, J.W. Dolan, L.R. Snyder, J. Chromatogr. A 1000 (2003) 757.
[42] N. Sagliano, T.R. Floyd, R.A. Hartwick, J.M. Dibussolo, N.T. Miller, J. Chromatogr. A 443 (1988) 155.

Talanta 76 (2008) 72–79

Contents lists available at ScienceDirect

Talanta

journal homepage: www.elsevier.com/locate/talanta

Multisyringe flow injection analysis coupled to capillary electrophoresis (MSFIA–CE) as a novel analytical tool applied to the pre-concentration, separation and determination of nitrophenols

Burkhard Horstkotte[a], Olaf Elsholz[b], Víctor Cerdà Martín[a,*]

[a] Department of Chemistry, University of the Balearic Islands, Carreterra de Valldemossa km 7.5, 07122 Palma de Mallorca, Spain
[b] Research Center of Bioprocess Engineering and Analytical Techniques, Hamburg University of Applied Sciences, Lohbrügger Kirchstraße 65, Hamburg 21033, Germany

ARTICLE INFO

Article history:
Received 2 November 2007
Received in revised form 24 January 2008
Accepted 8 February 2008
Available online 10 March 2008

Keywords:
Nitrophenols
Capillary electrophoresis
Multisyringe flow injection analysis
Pre-concentration

ABSTRACT

For the first time, a multisyringe flow injection analysis capillary electrophoresis system is described. The potential of the hyphenation for sample treatment including analyte pre-concentration is demonstrated by its successful application to the determination of *mono*-nitrophenols (NPs) in different water samples.

The analytical system was used to automate in-line sample acidification, analyte pre-concentration, elution, hydrodynamic injection, electrophoretic separation, and detection as well as the maintenance and re-conditioning of the solid-phase extraction (SPE) column and the separation capillary.

A pre-concentration factor of better than 115 and detection down to 0.11 μmol L^{-1} were achieved. Detection was carried out at visible wavelength using a blue LED as a low baseline-noise light source. High repeatability was obtained each for migration times and for peak heights with relative standard deviations typically below 2.5 and 6% including the pre-concentration procedure, respectively.

Three injections per hour were achieved by running in parallel the pre-concentrating and the electrophoretic separation procedures. Instrumental control and data registration and evaluation were carried out with the software package AutoAnalysis, allowing autonomous operation of the analytical system.

1. Introduction

In the present work, the hyphenation of multisyringe flow injection analysis (MSFIA) [1] with capillary electrophoresis (CE) is firstly described. The flow system was used for solid-phase extraction (SPE) pre-concentration of *mono*-nitrophenols (NPs) from water samples on a reverse phase (C18) mini-column, elution, and injection in a home-made CE system [2] as well as for all re-conditioning and cleaning procedures.

CE is a powerful tool in biomolecular, pharmaceutical, and environmental analysis and one of the fastest-growing analytical technique nowadays. Its advantageous characteristics are excellent separation efficiencies with up to several 100,000 theoretical plates, a simple instrumentation, and its versatility and applicability even to neutral analytes due to a variety of operation modes and detection techniques developed up-to-now [3,4]. Since the first works on CE [5,6], considerable investigation work was done to overcome the relatively low sensitivity derived from small sample and detection volumes as a main drawback of this technique, which also limits its applicability for trace analysis. Although these efforts have led to ingenious on-capillary concentration techniques such as sample stacking, focusing or sweeping techniques [7,8], SPE presents one of the most applied techniques for analyte enrichment. This is due to the variety of commercially available SPE products, handling simplicity and the simultaneous removal of sample matrix components, which might affect the CE separation. However, the SPE procedures are labor-intensive, time-consuming and the cartridges are relatively costly.

Flow techniques such as flow injection analysis (FIA) [9], sequential injection analysis (SIA) [10], Lab-on-valve technique [11] or MSFIA have been multiply applied for the automation of SPE pre-concentration [12–19]. The ability of these techniques to handle small liquid volumes precisely and reproducibly allow the minimization of the required sorbent and solvent quantity and improvement of sample frequency and reproducibility. On-line coupling of flow techniques and CE is an excellent supplementation combining the benefits of both techniques [20]. Apart from the potential of sensitivity improvement by automated pre-concentration [21–23], coupled flow systems can be used for the automation of sampling and injection protocols [24–27], required sample pre-treatment as mixing with required additives [28], ana-

* Corresponding author. Tel.: +34 971 173 260; fax: +34 971 173 426.
E-mail address: victor.cerda@uib.es (V.C. Martín).

0039-9140/$ – see front matter © 2008 Elsevier B.V. All rights reserved.
doi:10.1016/j.talanta.2008.02.014

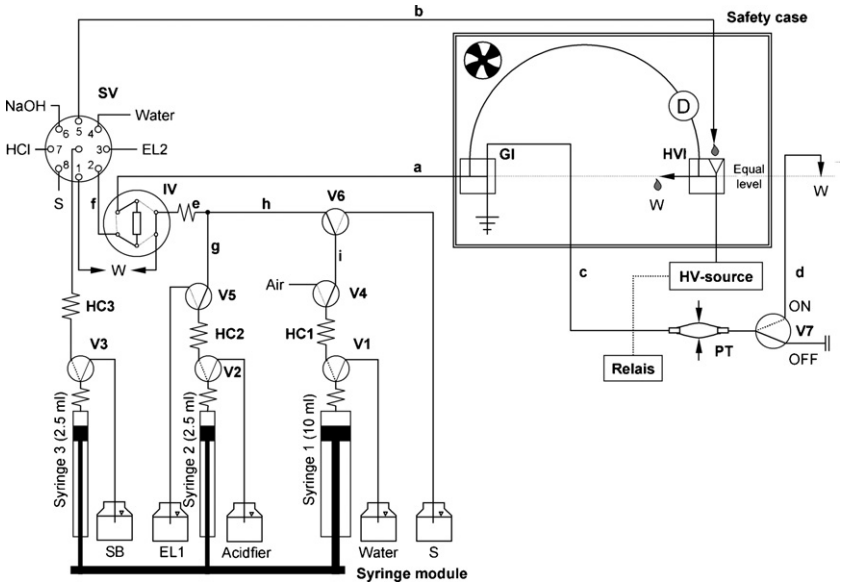

Fig. 1. Scheme of the MSFIA–CE system. GI: grounded interface, HVI: high-voltage interface, IV: injection valve with SPE column, SV: selection valve (Pos1: waste, Pos2: IV, Pos3: EL2, Pos4: water, Pos5: HVI, Pos6: HCl 10 mmol L^{-1}, Pos7: NaOH 10 mmol L^{-1}, Pos8: S, and V1–V7: solenoid valves with normally closed position (ON, activated, dotted) and normally open; position (OFF) straight; V3 and V7 of enhanced pressure stability, D: photometric detector cell, PT: pressure tube, and HC: holding coils (1: 500 cm, 1.5-mm i.d., 2: 150 cm, 0.8-mm i.d., 3: 175 cm, 0.8-mm i.d., a: tube 40 cm, 0.5-mm i.d., b: tube 50 cm, 0.5-mm i.d., c: tube 40 cm, 0.8-mm i.d., d: tube 20 cm, 0.8-mm i.d., e: 20 cm, 0.8-mm i.d., knotted, f and g: 10 cm, 0.8-mm i.d., h and i: PVC tubes 4 cm, 0.8-mm i.d., SB: separation buffer, W: waste, S: sample, EL1: 10 mmol L^{-1} NaOH with 40% MeOH, and EL2: 10 mmol L^{-1} NaOH with 10% acetonitrile.

lyte derivatization [29,30] or sample clean-up [31,32]. The fully automation of the analytical procedure using flow techniques further allows the application of CE for monitoring purposes [33]. A review of coupling flow techniques to CE has been published lately [34]. An overview about interfacing modes and resulting instrumental limitations can be found elsewhere [2].

MSFIA comprises advantages of SIA, such as a programmable syringe pump, high pressure and solvent robustness, low consumption of sample and reagents, and easy adaptation of the analytical procedure by software control as well as of FIA, such as multichannel manifolds, implementation of multicommutation using additional solenoid valves and a high-sample frequency due to parallel execution of flow operations. MSFIA instrumentation, flow-network configurations, and analytical applications have been reviewed lately [35].

Phenolic derivates such as NP are substances of considerable toxicity showing mutagenic, cyto- and phyto-toxic effects and are regarded as priority pollutants [36]. They are widely used in plastic, textile, pharmaceutical, armaments, paper, and dye-fabricating industry. Further anthropogenic sources are pesticide degradation and combustion processes [37,38]. They also present secondary pollutants generated by nitration of phenolic compounds in the atmosphere [39,40]. Consequently, they can be found in different environmental compartments such as atmosphere, precipitation, surface, and ground water or leaching water from land areas of former-mentioned industries [41]. Analytical techniques with the ability to monitor NPs including automated pre-concentration and quantification of the different species are therefore of high interest.

Former analytical flow technique applications for nitrophenols are based on multivariant regression using absorbance spectra data in order to achieve the quantification of the single compounds [42–44]. Although limits of detection (LOD) in the range of 0.5–0.04 μmol L^{-1} were achieved applying liquid–liquid extraction (LLE) or SPE for analyte pre-concentration and even down to 3 nmol L^{-1} applying reflectometry [45], the precision of species quantification of separation techniques can hardly be achieved.

With separation techniques such as HPLC and CE, a resolution between the analytes and absorbing matrix components is ideally achieved, by this allowing the application of less selective but more sensitive spectrometric detection at deep ultraviolet. In combination with CE using a capillary of either 75-μm i.d. [46] or 300-μm i.d. [47], including sample stacking [48] or SPE [49], or with HPLC with prior LLE [50], LOD in the range of 1.4 mg L^{-1}, 27, 0.7, and 2 μg L^{-1} were obtained, respectively. Electrochemical detection on HPLC in combination with SPE pre-concentration allowed the detection of even 10 ng L^{-1} [51].

In this paper we demonstrate the advantages of coupling MSFIA and CE as an alternative analytical tool to the former approaches for the fully automation of sample treatment (acidification, pre-concentration, and elution) and electrophoretic separation on the analytes NP with visible wavelength spectrometry.

2. Material and methods

2.1. Reagents

Distilled water and chemicals of analytical-reagent grade were used throughout. All stock solutions and water for dilution were filtered through 0.45 μm nylon membrane filters prior to use.

Stock solutions of *mono*-NP (each 600 mg L^{-1}) were prepared by accurate weighting using 10 mmol L^{-1} NaOH. An intermediate stock solution containing *p*-NP, *o*-NP, and *m*-NP in the concentrations of 30, 60, and 120 mg L^{-1}, respectively, was prepared and used for all experiments applying CE. Both stock solutions were stored in the dark. Standard working solutions were prepared daily by proper dilutions. For the optimization experiments on the pre-concentration and elution procedures applying a flow cuvette instead of the CE apparatus, a solution of *p*-NP of 0.3 mg L^{-1} was used.

All CE separations were carried out using a borate separation buffer (SB) of pH 9.7 of a final concentration of 40 mmol L^{-1} containing 10% (v/v) methanol as organic modifier. It was prepared daily from a stock solution of 1 mol L^{-1} sodium borate. HCl

0.1 mol L^{-1} was used for the in-line acidification of the sample and to rinse the SPE column for conditioning. Prior to the conditioning, NaOH 10 mmol L^{-1} containing 40% (v/v) methanol (EL1) was passed through to elute all eventually still absorbed acidic components. NaOH 10 mmol L^{-1} containing 10% (v/v) acetonitrile (EL2) was used for the elution of the retained analytes from the polymeric resin.

2.2. Pre-concentration flow system

The implemented hyphenated MSFIA–CE system is shown in Fig. 1. A valve module VA1 + 1 equipped with a rotary 8-port selection valve (SV) and a 6-port injection valve (IV) and a syringe module Bu4S, both from Crison Instruments S.A. (Allela, Spain), were used. The syringe module was equipped with three syringes, one polypropylene syringe of 10 mL (S1) from Sciware S.L. (Palma de Mallorca, Spain) and two glass syringes of 2.5 mL (S2, S3) from Hamilton Bonaduz AG (Bonaduz, Switzerland).

As a basic characteristic of the syringe module, all syringe pistons are mounted on a common steel bar and move simultaneously, driven by a single step motor (16,000 steps). The head outlet of each syringe was connected to a multicommutation solenoid valve (V1–V3) in order to enable the connection either to the manifold or to the solution reservoir for refilling. S1 and S2 were used for column conditioning, in-line sample acidification and analyte preconcentration, whereas S3 was used for analyte elution from the column and for all operations on the CE apparatus. Each syringe was connected via a holding coil (HC) to the tubing manifold.

Additional supply ports of the syringe module were used to power and control auxiliary solenoid valves for pickup of sample (V6), solutions for conditioning of the SPE column (V5) or air (V4) to reduce the sample dispersion or to close the outlet of one of the implemented capillary flow interfaces (see Section 2.2) for pressure build-up temporarily at the capillary inlet (V7). The syringe module has been described in detail including possible manifold configurations and analytical applications in a comprehensive review [35].

All solenoid valves were purchased from Takasago Electric Inc. (Nagoya, Japan). V3 and V7 had a nominal pressure stability of up to 600 kPa (MTV-3-1/4UKGH), the remaining up to 200 kPa (MTV-3-1/4UKG). Excessive valve heating was prevented by using protection circuits from Sciware S.L. Remote control was accomplished by the connection of both modules in series via RS232C serial interface to a PC using the software AutoAnalysis [52].

All liquid contacted parts of the instruments and the tubing manifold were made of plastic materials ETFE, PEEK, and PTFE, PVC, or PMMA. Tubing dimensions are indicated in Fig. 1. The indicated tubes a–d and f–i were used as short as possible. Tube e was knotted in order to improve mixing of sample and acid.

2.3. Capillary electrophoresis system

All experiments were performed with a HCP 35-35,000 high-voltage (HV) supply (F.u.G. Elektronik GmbH, Rosenheim, Germany). Voltage application was controlled via the analog interface of the source. The safety circuit included a relay powered by the supply port 6 of the syringe module, allowing remote control via software instructed activation of port 6.

All separations were carried out in a fused-silica capillary of 75-μm inner diameter (i.d.) × 65-cm total length (55 cm effective length) from Polymicro technologies LLC (Phoenix, USA). On-capillary photometric detection was carried out using a home-made detection cell (see Fig. 2). After preparation of an optical window by removing the polyimide coating on a length of about 0.5 cm, the capillary was fixed into a groove on the light entering

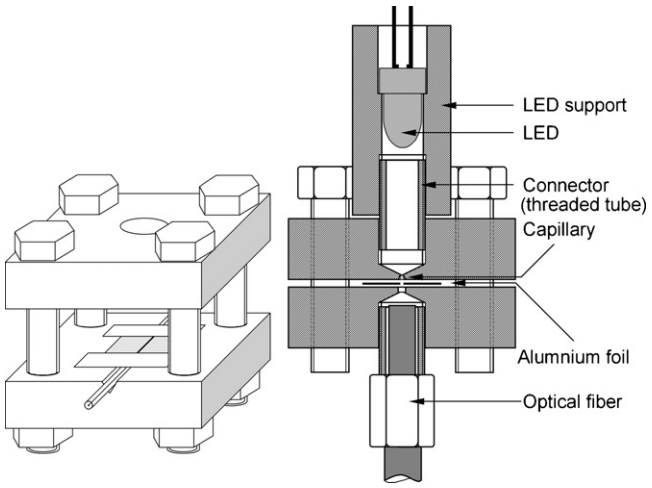

Fig. 2. Montage of the home-made on-capillary detection cell with optical fiber, LED, and respective support.

part of the cell with two drops of black nail polish. The required small aperture was obtained by masking the optical window with two small pieces of aluminium foil leaving open a gap of only 70 μm. The aluminium foil pieces were fixed with black nail polish and protected with adhesive film. Afterwards, the cell was assembled and connected to an USB-2000 miniature spectrophotometer via a QP450-1-XSR optical fiber of 455-μm core diameter (both from Ocean Optics Inc., Dunedin, USA). An ultra-bright blue LED was used as a low baseline-noise light source. Using a home-made adaptor, it was plugged directly onto the detection cell and powered by a constant current supply (Sciware S.L.). All measurements were performed at the emission maximum 401 nm with a detection frequency of 2 Hz, intensity averaging over 35-times 12 ms and wavelength integration interval of 4 nm.

Two former described flow interfaces were used to connect the grounded as well as the HV side of the capillary to the flow system [2]. Injection was done at the tubular grounded interface, which was directly connected to the tubing manifold. To avoid galvanic contact to the HV side of the capillary during buffer exchange, the SB was dripped into the HV interface from 2.5 cm above and the corresponding tube 5 on the selection valve was emptied afterwards. This principle was former described as falling drop interface [53]. Capillary, interfaces and detector were housed in a home-made ventilated safety box made of PMMA.

A silicone rubber tube (length 3.5 cm, 5.5-mm o.d., 1.5-mm i.d.) connected the grounded interface and V7. Propelling of liquid towards the grounded interface with V7 in position OFF (interface outlet closed) caused the inflation of the silicone rubber tube and pressure increase as the result of the silicone tube wall tension. As a consequence, the tube acted as a pressure reservoir for capillary flushing or to generate a reproducible pressure for hydrodynamic injection. No loss of reproducibility was observed due to tube stretching even after 6 months.

For optimization the pre-concentration and elution procedures, the CE apparatus was substituted by a flow cuvette, type 75.15 SOG from Starna (Essex, UK), placed into a cuvette support CUV-UV (Ocean Optics Inc.) and connected by a tube of 25 cm in length and 0.8-mm i.d. to the MSFIA system.

2.4. Solid-phase extraction column

The solid-phase extraction (SPE) column used for the analyte pre-concentration was turned of a PMMA cylinder (25 mm, Ø

20 mm). The inner volume of the column was 7.5 mm in length and 4.5-mm i.d.

Polymeric reversed phase resin (C18) from commercial solid-phase extraction tubes (strata-X 33 μm from Phenomenex, Aschaffenburg, Germany) was used throughout. For filling of the column, the resin was handled as a slurry in 50% (v/v) ethanol. The polypropylene frits from the former named solid-phase extraction tubes were used to tap both sides of the column. The frits discs were cleaved to half to reduce their flow resistance and die-cut to a diameter of 5.5 mm. Slices of silicon rubber tube were used to obtain finger tight sealing between column and 1/4″-28-UNF-connectors. The column was mounted via 0.8-mm i.d. PTFE tubing (8 cm in length) to the 6-port injection valve IV. This configuration allowed incorporating the column either into the pre-concentration part of the system for conditioning and loading or into the CE part of the system for analyte elution afterwards. Loading and elution were performed in counter-direction to obtain a sharper elution peak profile and higher maximal concentrations of the analytes and to avoid the compaction of the resin.

2.5. Software

Instrumental control, data acquisition and processing were done on the software platform AutoAnalysis 5.0 (http://www.sciware-sl.com) [52]. The program allows the execution of instruction protocols, the definition and usage of variables, loops, waiting steps, and the execution of repeating protocols defined as procedures. Using procedures, a library of program modules instructing the conditioning of the capillary or the SPE column, injection, cleaning of the manifold or SB exchange in both flow interfaces was created, which were assembled and activated as required to generate the instruction protocol for the entire analytical method. Especial advantage of the program's versatility was taken during optimization work, as the applied analytical method could be varied easily in respect of the interesting parameter.

Table 1
Injection procedure without sample pre-concentration

No.	Description of step
1	Aspiration of 100 μL of sample into holding coil 3
2	Insertion 50 μL into the selection valve position 2 with SPE column by-passed (injection valve in position LOAD)
3	Discharge of redundant sample from the holding coil 3
4	Propulsion of sample segment to the capillary entrance with open grounded interface outlet (solenoid valve 7 in position ON)
5	Dispense of 10 μL to inflate the pressure reservoir with closed grounded interface outlet with 1.5 mL min^{-1} (solenoid valve 7 in position OFF)
6	Holding for 800 ms
7	Release of the hydrodynamic pressure by aspiration of 5 μL from the grounded interface and opening of outlet 1.5 mL min^{-1} (solenoid valve 7 in position ON)
8	Flushing of grounded interface with 200 μL of separation buffer (solenoid valve 7 in position ON)

2.6. Analytical procedures

Prior to use, the capillary was pretreated with 0.1 mol L^{-1} HCl, 0.01 mol L^{-1} NaOH, and distilled water, each for 15 min and flushed with SB for 30 min. In situ flushing of the capillary with former listed solutions for each 5 min was done every day as described below.

Sample injection omitting the pre-concentration step was performed according the protocol summarized in Table 1. To include analyte pre-concentration, the protocol given in Table 2 was followed including cleaning of the SPE column, pre-concentration, elution, and injection. For each analysis, the column was rinsed with 200 μL EL1, 400 μL HCl 0.1 mol L^{-1} (only S2 activated) and 1 mL HCl 20 mmol L^{-1} (S2 and S1 activated).

Prior to sample uptake into HC1, an air segment of 100 μL was aspirated (V4 in position ON) to diminish the dispersion of the 6 mL sample aspired in the following step. A reduced flow rate of 5 mL min^{-1} had to be used for both steps to avoid the rupture of the segmentation air bubble. By dispense form S1 and S2 and

Table 2
Procedure used for SPE column cleaning, sample pre-concentration, elution and injection

No.	Procedure	Description of step
1	Conditioning of SPE column (150 s)	Pickup of 200 μL cleaning eluent (EL1, into holding coil 2)
2		Dispense of 600 μL from holding coil 2 through SPE column in order to eliminate acid as well as basic components
3		Dispense of 200 μL from syringe 2 and 800 μL from syringe 1 for conditioning SPE column with diluted hydrochloric acid
4		Pickup of 200 μL from solution reservoirs for syringes refilling
5	SPE column load and washing (800 s)	Aspiration of 100 μL of air to minimize sample dispersion in the holding coil 3
6		Aspiration of 6.1 mL de sample with syringe 1 into the holding coil 1
7		Dispense of 6 mL sample with syringe 1 with in-line acidification by dispense of hydrochloric acid with syringe 2
8		Syringe refilling
9		Discharge of redundant sample and air segment (800 μL, from holding coil 1 into waste with SPE column by-passed (injection valve in position INJECT)
10		Dispense of 800 μL water by syringe 1 to wash SPE column (injection valve in position LOAD)
11	Elution and injection (70 s)	Pickup of 200 μL of EL2 from selection valve into holding coil 3
12		Dispense of 260 μL by syringe 3 through SPE column for elution of analyte and propulsion to the capillary entrance (injection valve in position INJECT)
13		Change of injection valve position to LOAD
14		Dispense of 5 μL to inflate the pressure reservoir with closed grounded interface outlet with 0.5 mL min^{-1} (solenoid valve 7 in position OFF)
15		Holding for 800 ms
16		Release of the hydrodynamic pressure by aspiration of 5 μL from the grounded interface and opening of outlet with 0.5 mL min^{-1} (solenoid valve 7 in position ON)
17		Flushing of grounded interface with 250 μL of separation buffer (solenoid valve 7 in position ON)

activation of V2 and V5, the sample was acidified in-line as it was propelled through the SPE column. Since in acidic medium the analytes are un-dissociated and show a hydrophobic character, they were retained on polymeric sorbent. Afterwards, the rest of sample and the segmentation air bubble were discharge to waste completing the loading procedure. Finally, the SPE column was rinsed with water from S1.

For elution, 200 μL of the auxiliary eluent EL2 were picked up into HC3 to improve matching of the elution profiles of the three analytes and an optimized volume 260 μL was propelled with IV in position "inject" through the SPE column for elution. By this, the maximal analyte concentration of the elution was positioned at capillary entrance in the grounded interface. For injection, the SPE column was disconnected by turning IV to position "load". Hydrodynamic pressure for injection was built up by a dispense of 5 μL towards the grounded interface with V7 in position "closed" and pressure was released after 800 ms by opening V7. After injection, the grounded interface was flushed with SB and HV was turned on by software command (see Section 2.2). During the electrophoretic separation, V7 remained in open position to ensure atmospheric pressure on both capillary ends.

In situ flushing of the capillary with SB was done prior to each analysis for 1 min likewise the hydrodynamic injection but with a higher pressure build-up volume of 300 μL. Since the silicone tube acted as a pressure reservoir, flushing of the HV interface to eliminate stacked air bubbles caused by electrolysis was possible in the meantime. Conditioning of the SPE column, loading with sample and washing (Table 2, 1–8) were done during the electrophoretic separation step (background operation), by this reducing the required time for analysis about 9 min.

3. Results and discussion

3.1. Electrophoretic procedure

The electrophoretic procedure had been described in a former work [2]. Although a new capillary and a modern power source were used, renewed optimization of SB composition, voltage and conditioning and injection procedures omitting pre-concentration were proved to be unnecessary since the separation characteristics were analog and baseline separation of all analytes was achieved throughout. The injection procedure was modified slightly utilizing a lower pressure pulse volume of only 5 μL.

The retention times of *m*-NP, *p*-NP and *o*-NP were 453 ± 9, 494 ± 11, and 508 ± 11 s with a theoretical plate number of up to 12,000. Electrophoretic separation runs of on-line pre-concentrated aqueous standards of concentrations between 0.22 and 4.35 μmol L^{-1} are shown in Fig. 3.

Peak heights were used instead of peak areas for data evaluation, since a better repeatability was obtained. Elution and loading flow rates, elution volume and composition, volume for interface flushing after injection as well as sample loading, and elution conditions were optimized. All measurements were done at least in triplicate.

3.2. Sample loading and in-line acidification

The influence of HCl used for in-line acidification of the sample during the loading procedure was studied for the following concentration 0.05, 0.1, 0.2, 0.4, 0.75, and 1 mol L^{-1}, corresponding to final acid concentrations in the sample of 0.01–0.2 mol L^{-1}. No significant effect on the peak height was observed, and a concentration of 0.1 mol L^{-1} was finally chosen.

The influence of the flow rate used for sample loading was studied at 715, 750, 875, 1000, and 1125 μL min^{-1}. Results are shown in Table 3. For elution, a flow rate 300 μL min^{-1} was applied. A lower flow rate applying the required syringe 1 (10 mL) for sample handling and S2 (2.5 mL) for acidification was not achievable, whereas a higher flow rate led to considerably backpressure increase. Elution peaks of *p*-NP (0.75 mg L^{-1}) were slightly lower at higher flow rates with a total decrease of 9% over the studied flow rate range. As a compromise between time consumption and peak height, 750 μL min^{-1} were finally applied, corresponding to a flow rate of 600 μL min^{-1} for syringe 1 and 150 μL min^{-1} for S2.

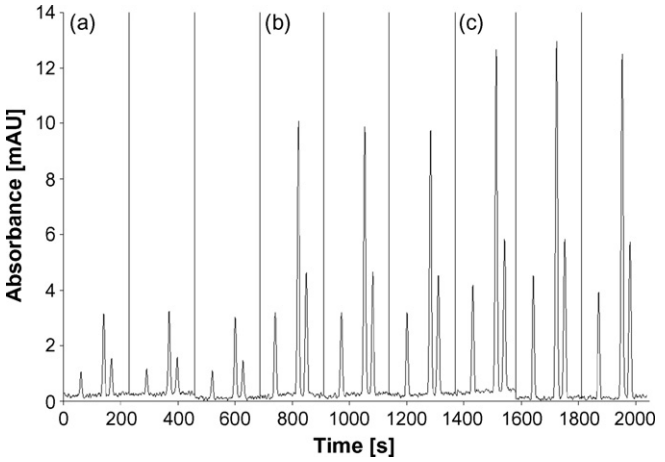

Fig. 3. Electrophoretic separations in triplicate of aqueous standards, pre-concentrated according the proposed method. Concentrations of *o*-NP, *m*-NP and *p*-NP in μmol L^{-1}: (a): 0.43, 0.87, 0.22; (b): 1.74, 3.48, 0.87; (c): 2.17, 4.35, 1.09. The time scale refers to time of data acquisition. Separation conditions: borate buffer 40 mmol L^{-1}, pH 9.7 with 10% (v/v) MeOH, 25 kV.

3.3. SPE column washing

After loading, the SPE column was rinsed with water from S1. The influence of the applied volume for rinsing was studied and 50, 100, 150, 200, and 250 μL were tested as well as omitting the rinsing step. No significant influence on the height of the elution peak of *p*-NP (0.75 mg L^{-1}) was observed. However, occurrence of baseline disturbances as a consequence of eluted gas bubbles were considerably reduced applying a rinsing volume of at least 200 μL. Therefore, a rinsing volume of 200 μL was finally applied since the entrance of gas bubbles into the separation capillary would interrupt the galvanic connection between both sides of the capillary and interfere the electrophoretic separation. Elution peaks of about 30%

Table 3
Results of optimization of flow rates for loading and elution

Loading flow rate (μL min^{-1})	Peak height (mAU)[a]
715	138 ± 6
750	137 ± 3
875	127 ± 3
1000	134 ± 2
1125	126 ± 9
Elution flow rate (μL min^{-1})	**Peak height (mAU)[a]**
200	199 ± 8
300	181 ± 4
400	163 ± 9
500	159 ± 7
600	149 ± 6
750	144 ± 5
1000	140 ± 7

[a] Results are expressed as the mean of three determinations with standard deviation.

reduced height were obtained when the rising step was performed with syringe 3 in counter direction to loading.

3.4. Analyte elution and injection

The influences of the elution flow rate as well as the eluent type were studied with the objective to obtain maximal and reproducible peak heights and an equal elution profile for all analytes. Apart from the possibility to concentrate selectively hydrophobic compounds, the SPE column permitted the elution of the analytes with the alkaline SB used for the electrophoretic separation. By this, ideally, the influence of the ionic strength of the sample can be eliminated totally.

Thus, optimization of the elution conditions was started using the normal SB (40 mmol L^{-1} borate, pH 9.7, 10% (v/v) MeOH). Aspiration of a short segment of SB containing methanol in higher content of 20% (v/v) as an auxiliary eluent (EL2) prior to elution resulted into a narrower and higher elution peak for *p*-NP. However, the higher methanol content led to gas bubble formation in the eluent flow of the SPE column, even after ultrasonic degasification. Applying an auxiliary eluent of the same composition as the SB but containing 10% (v/v) acetonitrile instead of methanol as a less polar solvent and of lower vapor pressure than methanol led to an improvement of 50% of peak heights. Besides, the gas bubble formation was considerably reduced using acetonitrile instead of methanol. However, a higher content of acetonitrile was not practicable as gas bubble formation was observed likewise.

During optimization of the elution volume before performing the hydrodynamic injection on the CE system we observed, that the elution of *m*-NP was delayed in respect of *o*-NP and *p*-NP, which led to an apparent loss of sensitivity for *m*-NP of 71% when hydrodynamic injection on the CE system was performed when the maximum of the elution peak of *p*-NP and *o*-NP passed the capillary entrance.

Altering of the pH, salt content or flow rate during elution did not improve the overlap of the elution profiles of the three analytes. The use of a sodium hydroxide solution of 10 mmol L^{-1} containing 10% acetonitrile for EL2 instead of the modified borate buffer led to a satisfying overlapping of the elution profile when a volume of 200 μL was used. The former observations suggest, that the difference in the elution characteristics was to interaction of the borate ion and the absorbed meta-nitrophenol [54,55].

The influence of the elution flow rate was studied for 0.2, 0.3, 0.4, 0.5, 0.6, 0.75, and 1 mL min^{-1}. Results are shown in Table 3. The peak height decreased exponentially with increasing flow rate with a loss of 30% of peak height for 1 mL min^{-1} compared to 0.2 mL min^{-1}. As a compromise between elution time and peak height, a flow rate of 0.3 mL min^{-1} was finally applied. Incorporation of a waiting step

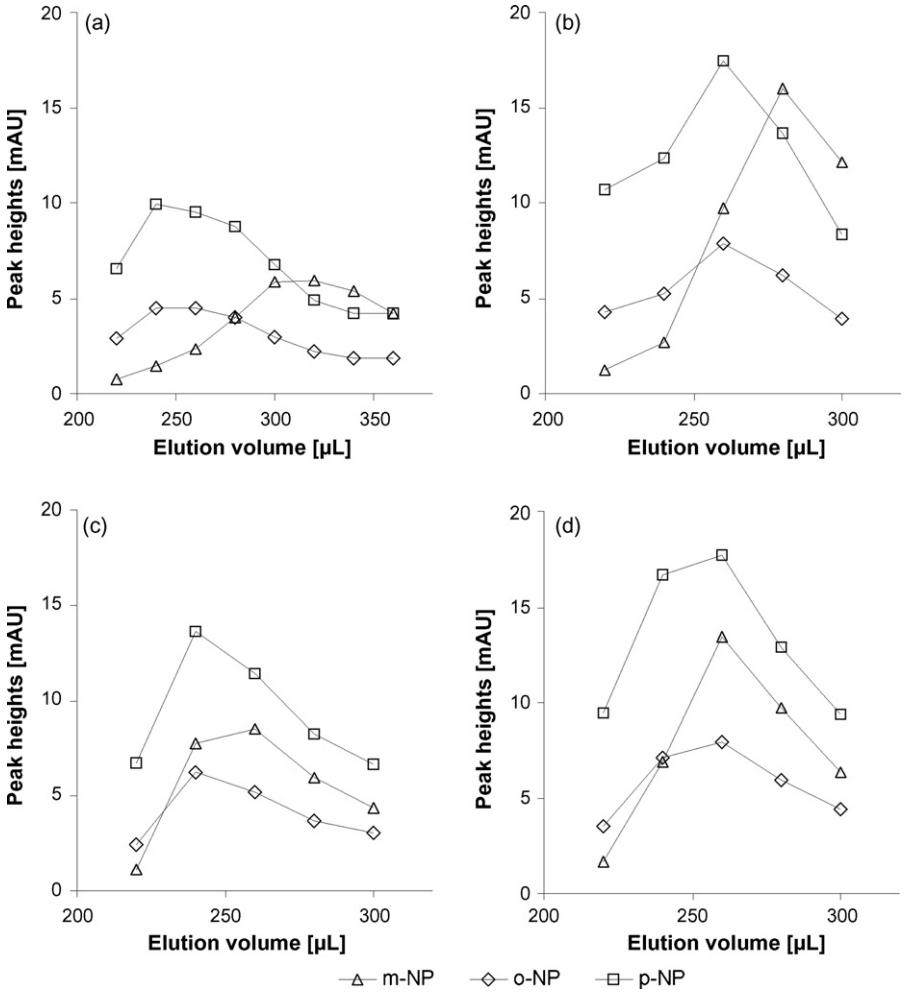

Fig. 4. Optimization of analyte elution using auxiliary eluent EL2 of following composition and volume: (a): borate 40 mmol L^{-1}, pH 9.7, 10% (v/v) acetonitrile, 100 μL, (b): NaOH 10 mmol L^{-1}, 10% (v/v) acetonitrile, 100 μL, (c): NaOH 20 mmol L^{-1}, 10% (v/v) acetonitrile, 100 μL, and (d): NaOH 10 mmol L^{-1}, 10% (v/v) acetonitrile 200 μL. All measurements were done in triplicate including pre-concentration of 6 mL of aqueous standard 1.1 μmol L^{-1} *p*-NP, 2.2 μmol L^{-1} *o*-NP, and 8.7 μmol L^{-1} *m*-NP and separation on the CE system.

into the elution procedure caused lower repeatability without any positive effect on the elution peak heights.

The elution volume prior to the pressure pulse for hydrodynamic injection was optimized and results are shown in Fig. 4. The highest peaks were obtained for all three analytes applying an elution volume of 260 μL before injection. To shorten the duration of the procedure, the injection valve was turned into position "load" after the dispense of the optimized elution volume and the SPE column was cleaned first with the alkaline eluent EL1 and afterwards with acid from S2.

3.5. SPE column length

Two different columns of 4.5-mm i.d. but different lengths (7.5 and 15 mm) were tested in order to minimize the required resin volume and consequently backpressure and dispersion. The required loading capacity of the SPE column was estimated considering a pre-concentration factor of at least 30, a sample volume of 6 mL for pre-concentration and the quantification limit of *m*-NP as the analyte of less absorptivity from the former reported CE method without analyte pre-concentration to be in the order of 30 nmol. Fifteen times higher loading capacity was found for both columns and no significant change in the peak height was observed. Therefore, the shorter SPE column was used in this work.

4. Characteristic of quantitative analysis

4.1. Calibration range and detection limit

Using aqueous standards containing *o*-NP, *m*-NP, and *p*-NP in a concentration ratio of 2:4:1, a linear response was found for up to 43, 17, and 22 μmol L^{-1}, respectively, including pre-concentration (see Fig. 5). The SPE column permitted a load of at least 450 nmol of the analytes. The pre-concentration factors were calculated from the analysis of a sample measured according the protocol in Table 1 omitting the pre-concentration procedure containing 86.9, 173.9, and 43.5 μmol L^{-1} of *o*-NP, *m*-NP, and *p*-NP and the calibration data from the quantification including the pre-concentration procedure to be 123, 124, and 117, respectively.

The baseline amplitude was typically below 0.2 mAU due to the low noise of the LED used as light source. The detection limits, calculated as the concentration resulting in a peak height of three times the noise amplitude were 0.11 μmol L^{-1} (*o*-NP), 0.35 μmol L^{-1} (*m*-NP), and 0.03 μmol L^{-1} (*p*-NP), respectively. A sample containing 0.22 μmol L^{-1} (*o*-NP), 0.44 μmol L^{-1} (*m*-NP), and 0.11 μmol L^{-1} (*p*-NP) was used as the lowest concentrated standard solution in this work.

The found LOD were similar or even lower than former achieved by spectrophotometric detection on flow technique systems including pre-concentration [42–44] although the light path was much smaller in the present work. Besides, a separation procedure was accomplished, which is adaptable to the analysis of further nitrated phenols. Lowering of LOD is achievable by repeated execution of the pre-concentration procedure before elution as former done for the determination of total phenolic compounds with MSFIA [19], however, a lower sample frequency would result. Electrokinetic sample stacking [48] or detection at deep UV spectral range, where the absorptivity of the NPs is multiply higher [46] give way for further detection improvement. However, for want of a sufficient intense deep-UV source or polarity switch, these possibilities were not possible to accomplish.

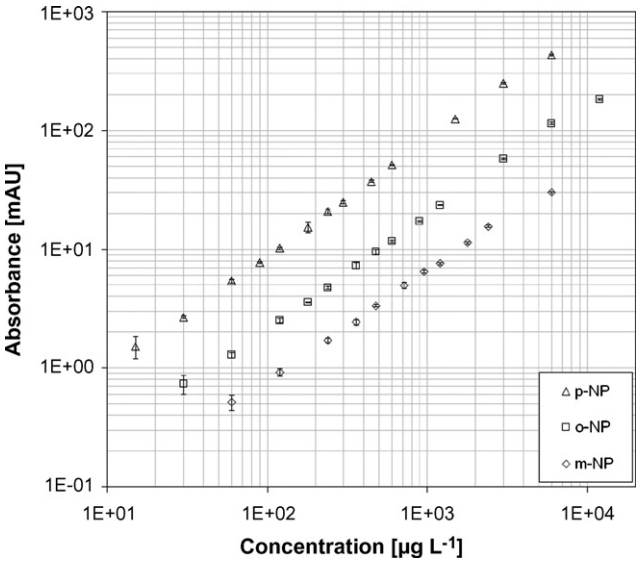

Fig. 5. Calibration results using aqueous standards of *o*-NP, *m*-NP, and *p*-NP in ratio 2:4:1 applying on-line pre-concentration with 6 mL of sample and followed separation with conditions as given in Fig. 3.

4.2. Repeatability and sample frequency

The method showed satisfying repeatabilities regarding migration times with a mean relative standard deviation of <0.5% for the same sample and <2.5% for different standards and samples as well as regarding peak heights with mean relative standard deviations <6% (*m*-NP) and <3% (*o*-NP, *p*-NP) for three replicates. Relative standard deviation using peak area was generally higher than the corresponding value using peak heights for calibration and quantification.

The entire pre-concentration procedure (Table 2, 1–10) including SPE column conditioning required about 16 min. The required time for flushing of the capillary and both interfaces was 70 s, refilling of the syringe about 40 s and for elution and injection 70 s. The electrophoretic separation was completed after 500 s. By performing the SPE column conditioning and pre-concentration during the electrophoretic separation of the former injected sample, the duration of the entire analytical method was considerably reduced from about 27 to 19 min between two injections.

4.3. Real samples

For the evaluation of matrix influences, leachate, tap water, and groundwater samples were spiked each with 2.17 μmol L^{-1} *o*-NP, 4.35 μmol L^{-1} *m*-NP, and 1.09 μmol L^{-1} *p*-NP, afterwards filtered through 0.45-μm nylon membrane filters and directly analysed. The blank concentrations of all samples were below the detection limit. Analytical results and recovery values, calculated using peak height data compared to aqueous standards are given in Table 4. The recovery values were between 91 and 111%, mean values for all samples were 102% (*o*-NP), 97.7% (*m*-NP), and 101% (*p*-NP), respectively. The results were satisfying considering the generally problematic reproducibility of capillary electrophoresis and the implementation of analyte pre-concentration. The incorporation of a solid-phase extraction resin led to a considerably improvement of the sensitivity but as well allowed to diminish the negative effects of the ionic strength of the sample and matrix components as metal ions or basic components, which will not retain on the applied resin. Nevertheless, the retention and elution profile of the analytes might be influenced by the buffering capacity of the sample.

Table 4
Results of the determination of nitrophenols in spiked wastewater samples

Spiked samples[a]	Found nitrophenols (μmol L^{-1})			Recovery (%)		
	o-NP	*m*-NP	*p*-NP	*o*-NP	*m*-NP	*p*-NP
Deposit leachate 1	2.38 ± 0.06	4.49 ± 0.39	1.19 ± 0.05	109.3	103.3	109.8
Deposit leachate 2	2.04 ± 0.06	4.01 ± 0.40	1.01 ± 0.02	103.4	91.2	104.4
Deposit leachate 3	2.25 ± 0.11	3.96 ± 0.36	1.13 ± 0.07	110.9	111.0	108.4
Ground water	2.41 ± 0.08	4.82 ± 0.29	1.18 ± 0.04	93.9	91.1	91.2
Tap water	2.04 ± 0.07	3.96 ± 0.07	0.99 ± 0.05	93.7	92.2	92.6

[a] Spiked concentration: 2.17 μmol L^{-1} *o*-NP, 4.35 μmol L^{-1} *m*-NP, and 1.09 μmol L^{-1} *p*-NP. Results are expressed as the mean of three determinations with standard deviation.

5. Conclusion

The proposed hyphenated system of multisyringe flow technique and capillary electrophoresis (MSFIA–CE) worked autonomously and proved to be robust, reliable and applicable to real samples. In combination with the applied control software, it presents a versatile and easy adaptable instrumentation for analysis and potentially for monitoring purposes. The system shows the advantageous automation of the total analytic procedure including in-line sample modification (acidification) and pre-concentration and of the entire CE apparatus maintenance and control of all injection parameters. By utilizing other solid phases for pre-concentration or retention of matrix components affecting the electrophoretic separation as well as other modifying reagents, the systems offers a promising potential for further analytical applications. The application of the multisyringe technique allowed background operations and thus, higher sample frequencies. The advantage of the employment of a pressure robust and multichannel syringe pump allowed the use of a very fine sorbent material, and parallel operations which would not have been possible with a single syringe pump (SIA) or multichannel peristaltic pump (FIA) with the same obtained analytical performance, and robustness. Satisfyingly high repeatability and low limits of detection were achieved with concentration factors of about 120 for all analytes.

Acknowledgements

The authors acknowledge the grant from the Conselleria de Economia, Hisenda i Innovació Govern Balear.

This work is part of the project CTQ2004-01201, “Desarrollo de métodos automáticos en flujo para la monitorización y control de bioreactores y depuradoras de aguas residuales” supported by the Spanish Ministry of Science and Technology.

References

[1] V. Cerdà, J.M. Estela, R. Forteza, A. Cladera, E. Becerra, P. Altimira, P. Sitjar, Talanta 50 (1999) 695.
[2] B. Horstkotte, O. Elsholz, V. Cerdà, Int. J. Environ. Anal. Chem. 87 (2007) 797.
[3] B.L. Karger, Nature 339 (1989) 641.
[4] K.D. Altria, J. Chromatogr. A 856 (1999) 443.
[5] S. Hjerten, Chromatogr. Rev. 9 (1967) 122.
[6] J.W. Jorgenson, K.D. Lukacs, Anal. Chem. 53 (1981) 1294.
[7] Z.K. Shihabe, J. Chromatogr. A 902 (2000) 107.
[8] J.P. Quirino, J.-B. Kim, S. Terabe, J. Chromatogr. A 965 (2002) 357.
[9] J. Ruzicka, E.H. Hansen, Anal. Chim. Acta 78 (1975) 145.
[10] J. Ruzicka, G. Marshall, Anal. Chim. Acta 237 (1990) 329.
[11] J. Ruzicka, Analyst 125 (2000) 1053.
[12] W. Frenzel, S. Krekler, Anal. Chim. Acta 310 (1995) 437.
[13] M.A. Crespın, M. Gallego, M. Valcarcel, J. Chromatogr. B 773 (2002) 89.
[14] Z.-L. Zhi, A. Rios, M. Valcárcel, Analyst 121 (1996) 1.
[15] W.-L. Song, Z.-L. Zhi, L.-S. Wang, Talanta 44 (1997) 1423.
[16] M. Miró, E.H. Hansen, Trends Anal. Chem. 25 (2006) 267.
[17] E.H. Hansen, M. Miró, X. Long, Anal. Lett. 39 (2006) 1243.
[18] J. Wang, E.H. Hansen, J. Anal. At. Spectrom. 16 (2001) 1349.
[19] H.M. Oliveira, M.A. Segundo, S. Reis, J.L.F.C. Lima, Microchim. Acta 150 (2005) 187.
[20] B.M. Simonet, A. Rios, M. Valcárcel, Trends Anal. Chem. 22 (2003) 605.
[21] L. Nozal, L. Arce, B.M. Simonet, A. Rios, M. Valcárcel, Anal. Chim. Acta 517 (2004) 89.
[22] P. Hinsmann, L. Arce, A. Rios, M. Valcárcel, J. Chromatogr. A 866 (2000) 137.
[23] J.R. Veraat, H. Lingeman, U.A.Th. Brinkman, J. Chromatogr. A 856 (1999) 483.
[24] H.-W. Chen, Z.-L. Fang, Anal. Chim. Acta 355 (1997) 135.
[25] P. Kubáň, A. Engström, J.C. Olsson, G. Thorsén, R. Tryzell, B. Karlberg, Anal. Chim. Acta 337 (1997) 117.
[26] C.-H. Wu, L. Scampavia, J. Ruzicka, Analyst 127 (2002) 898.
[27] P. Kubáň, R. Pirmohammadi, B. Karlberg, Anal. Chim. Acta 378 (1999) 55.
[28] S. Kulka, G. Quintas, B. Lendl, Analyst 131 (2006) 739.
[29] C.-H. Wu, L. Scampavia, J. Ruzicka, Analyst 128 (2003) 1123.
[30] R.M. Latorre, J. Saurina, S. Hernández-Cassou, J. Chromatogr. A 976 (2002) 55.
[31] L. Bao, P.K. Dasgupta, Anal. Chem. 64 (1992) 991.
[32] A.G. Lista, L. Arce, A. Ríos, M. Valcárcel, Anal. Chim. Acta 438 (2001) 315.
[33] H. Sirén, S. Rovio, T. Työppönen, P. Vastamäki, J. Sep. Sci. 25 (2002) 1136.
[34] M. Valcárcel, L. Arce, A. Ríos, J. Chromatogr. A 924 (2001) 3.
[35] B. Horstkotte, O. Elsholz, V. Cerdá, J. Flow Injection Anal. 22 (2005) 99.
[36] National Recommended Water Quality Criteria, Environmental Protection Agency, USEPA, Washington, DC, 2006.
[37] Roempp Chemie Lexikon, Georg Thieme, Stuttgart, 1995.
[38] Y. Ni, L. Wand, S. Kokot, Anal. Chim. Acta 431 (2001) 101.
[39] M.A.J. Harrison, S. Barra, D. Borghesi, D. Vione, C. Arsene, R.I. Olariu, Atmos. Environ. 39 (2005) 231.
[40] M. Kohler, N.V. Heeb, Anal. Chem. 75 (2003) 3115.
[41] W. Schüssler, L. Nitschke, Chemosphere 42 (2001) 277.
[42] A. Cladera, M. Miró, J.M. Estela, V. Cerdà, Anal. Chim. Acta 421 (2000) 155.
[43] M. Miró, A. Cladera, J.M. Estela, V. Cerdà, Anal. Chim. Acta 438 (2001) 103.
[44] M. Manera, M. Miró, J.M. Estela, V. Cerdà, Anal. Chim. Acta 582 (2007) 41.
[45] M. Manera, M. Miró, J.M. Estela, V. Cerdà, M.A. Segundo, J.L.F.C. Lima, Anal. Chim. Acta 600 (2007) 155.
[46] X. Guo, Z. Wang, S. Zhoum, Talanta 64 (2004) 135.
[47] D. Kaniansky, E. Krčmova, V. Madajova, M. Masar, J. Marak, F.I. Onuska, J. Chromatogr. A 772 (1997) 327.
[48] P. Kubáň, M. Berg, C. García, B. Karlberg, J. Chromatogr. A 912 (2001) 163.
[49] C.-W. Whang, J. Pawliszyn, Anal. Commun. 35 (1996) 353.
[50] L. Zhu, L. Zhu, H.K. Lee, J. Chromatogr. A 924 (2001) 407.
[51] N. Cardellicchio, S. Cavalli, V. Piangerelli, S. Giandomenico, P. Ragone, Fresen. J. Anal. Chem. 358 (1997) 749.
[52] E. Becerra, A. Cladera, V. Cerdà, Lab. Robot. Automat. 58 (1999) 131.
[53] S.L. Wang, X.J. Huang, Z.-L. Fang, Anal. Chem. 73 (2001) 4545.
[54] Y.-C. Wang, Y.-R. Zeng, C.-H. Xie, N. Guan, E.-Q. Fu, J.-K. Cheng, Chromatographia 54 (2001) 475.
[55] R.A. Wallingford, A.G. Ewing, Anal. Chem. 61 (1989) 98.

Talanta 76 (2008) 161–165

Contents lists available at ScienceDirect

Talanta

journal homepage: www.elsevier.com/locate/talanta

Highly sensitive and selective electrochemical detection of sub-ppb level chromium(VI) using nano-sized gold particle

Bikash Kumar Jena, C. Retna Raj*

Department of Chemistry, Indian Institute of Technology, Kharagpur, West Bengal 721302, India

ARTICLE INFO

Article history:
Received 22 November 2007
Received in revised form 15 February 2008
Accepted 18 February 2008
Available online 29 February 2008

Keywords:
Au nanoparticle
Silicate network
Chromium(VI)
Electrochemical detection

ABSTRACT

Gold nanoparticle based nanostructured electrode has been developed for the amperometric detection of ultratrace amount of toxic Cr(VI). The nano-sized Au particles have been grown on a conducting substrate modified with sol–gel-derived thiol functionalized silicate network and used for the electroanalysis of Cr(VI). The nanostructured interface show well-defined voltammetric peak for the reduction of Cr(VI) at ~0.4 V. The voltammetric behavior of Cr(VI) strongly depends on the coverage of nanoparticle on the electrode surface. Constant potential amperometry has been used for the detection of Cr(VI) at well below the guideline value set by World Health Organization (WHO). This electrode is highly sensitive (30 ± 0.2 nA/ppb) and the detection limit (S/N = 9) was 0.1 ppb. Cr(III) and coexisting other metal ions and surface active agent present in water do not interfere with the amperometric measurement of Cr(VI). This nanostructured electrode is highly stable and it can be used for continuous measurement of Cr(VI) without using any pretreatment or activation procedures. The accuracy of the measurement has been validated by measuring the concentration of Cr(VI) in the certified reference material (CRM).

1. Introduction

The development of highly sensitive analytical methodology for the detection of trace level of toxic chromium species is of significant interest in analytical chemistry. In solution, chromium exists in two oxidation states (Cr(III) and Cr(VI)) and Cr(VI) is reported to be the second most inorganic contaminant in groundwater at hazardous waste site [1]. Cr(VI) is highly toxic and carcinogenic [2,3]. Cr enters into the environment via plating, steel, and paint industries [4]. The chromate anion easily crosses the cell membrane and reduced inside the cell to Cr(III) that binds to DNA more efficiently than Cr(VI) and damage the cellular components [5]. According to the International Agency for Research on Cancer (IARC) reports on the human carcinogenicity study, exposure to Cr(VI) cause lung and sinonasal cancer [6]. Cr(VI) has been classified by US Environmental Protection Agency (EPA) as human carcinogen in Group A [7]. WHO has set the provisional guideline value of Cr(VI) in ground water as 50 ppb [8].

Several methodologies including spectral, chromatographic and electrochemical techniques have been developed for the detection of Cr(VI) [2,3,8–21]. The selective detection of Cr(VI) is a challenging task because it suffers from interference due to Cr(III), which exists in relatively high concentration in natural water [13]. Most of the electrochemical techniques are based on the preconcentration of Cr(VI) species on the electrode surface using complexing agent [14–18]. Turyan and Mandler have successfully used the pyridinium-based self-assembled monolayer for the detection of Cr(VI) [13]. The electrochemical methods based on preconcentration suffer either from the interference or it requires regeneration procedures for the repeated use of the same electrode. Recently, Compton and coworkers demonstrated the utilization of polycrystalline Au electrode for the voltammetric detection of Cr(VI) in the micromolar level and it has been shown that Au electrode is highly sensitive for the detection of Cr(VI) [8]. The common interfering other metal ions does not interfere in the measurement at this electrode [8]. Polyaniline-based electrode has been used for the flow injection detection of Cr(VI) at sub-ppb level. This electrode suffers from the interference due to other metal ions and the stability of the electrode has not been tested [19]. The pyridinium-based sol–gel film [20] and monolayer [13] modified electrode has been used for the detection of Cr(VI) using preconcentration procedures. Bismuth-coated electrodes have been used for the detection of Cr(VI) in the sub-nanomolar level [17]. However, this method requires the complexing agent diethylenetriamine pentaacetic acid [17]. The enzyme-based amperometric sensor could detect Cr(VI) at the level of 0.2 mg L^{-1} [21].

Metal nanoparticles have been extensively used in recent years for the development of highly sensitive nanodevices because of their unusual physical and chemical properties. The Au nanoparticles are of great interest for analytical and bioanalytical applications

* Corresponding author. Tel.: +91 3222 283348; fax: +91 3222 282252.
E-mail address: crraj@chem.iitkgp.ernet.in (C.R. Raj).

0039-9140/$ – see front matter © 2008 Elsevier B.V. All rights reserved.
doi:10.1016/j.talanta.2008.02.027

[22–24]. Willner and coworkers have successfully utilized the nano-sized Au particles in the development of versatile biosensors [23]. The electrodeposited Au nanoparticles have been used for the detection of arsenic [25]. However, Au nanoparticles have not been used for the detection of carcinogenic Cr. Our group is interested in utilizing Au nanoparticle for the development of electrochemical sensors and biosensors [26–30]. Because Au is known to be very sensitive towards Cr(VI), it would be promising to investigate the electrochemical behavior of Cr(VI) on the nanostructured Au particle modified electrode. Considering the importance of the measurement of Cr(VI) in groundwater, in the present investigation we have utilized the Au nanoparticles for the amperometric detection of Cr(VI). Herein we describe the electrochemical behavior and amperometric detection of Cr(VI) using Au nanoparticle based electrode for the first time.

2. Experimental

2.1. Materials

3-(Mercaptopropyl)trimethoxysilane (MPTS), $K_2Cr_2O_7$ and $HAuCl_4$ (99.9%) were obtained from Aldrich and used as received. All other chemicals (Merck), unless mentioned otherwise, used in this investigation were of analytical grade (99%). All the solutions were prepared with Milli-Q (Millipore) A-10 gradient (18 MΩ cm) deionised water. Freshly prepared solutions were used in all experiments. Certified reference material (CRM) (ICP standard, Cr(VI) content: 100 mg L^{-1}) was obtained from Merck. The CRM was diluted and used for the analysis.

2.2. Instrumentation

Electrochemical measurements were performed using nanoparticle-modified Au working electrode (geometrical surface area: 0.031 cm^2), a Pt wire auxiliary electrode and Ag/AgCl (3 M NaCl) reference electrode. Cyclic voltammograms were recorded using a computer controlled CHI643B electrochemical analyzer (CHI, Austin, TX). Scanning electron microscopic measurements were performed with JEOL JEM 6700 field emission scanning electron microscope (FE-SEM).

2.3. Procedure

The Au electrodes were first functionalized with sol–gel silicate network containing –SH groups derived from MPTS according to our earlier procedures [26,27]. Briefly, MPTS sol was prepared by mixing 1:3:3 molar ratio of MPTS, methanol and water in the form of 0.1 M HCl and stirring the mixture vigorously for 30 min. Then a cleaned Au electrode was soaked in MPTS sol for 10 min. MPTS self-assembles on the Au electrode and exists as 3D silicate network [31]. The colloidal Au nanoseeds (GNS) were synthesized using citrate as stabilizing agent [27]. The MPTS-modified electrode was soaked in colloidal GNS for 18 h. The size of GNS on the silicate network was enlarged by seed-mediated growth approach. The GNS self-assembled electrode was soaked in a solution containing 0.3 mM NH_2OH and 0.3 mM $HAuCl_4$ and the solution was shaken constantly for 20 min. The nanoparticle grown by the seed-mediated growth approach will be referred as gold nanoelectrode ensemble (GNE).

3. Result and discussion

The schematic illustration for the preparation of GNE electrode and the FESEM image of GNEs on the silicate network are shown in Scheme 1. The nanoparticles on the silicate network were characterized by X-ray diffraction (XRD), UV–vis spectral, FESEM and electrochemical measurements according to our previous reports [27,28]. Briefly, the GNEs have the size ranging from 70 to 100 nm

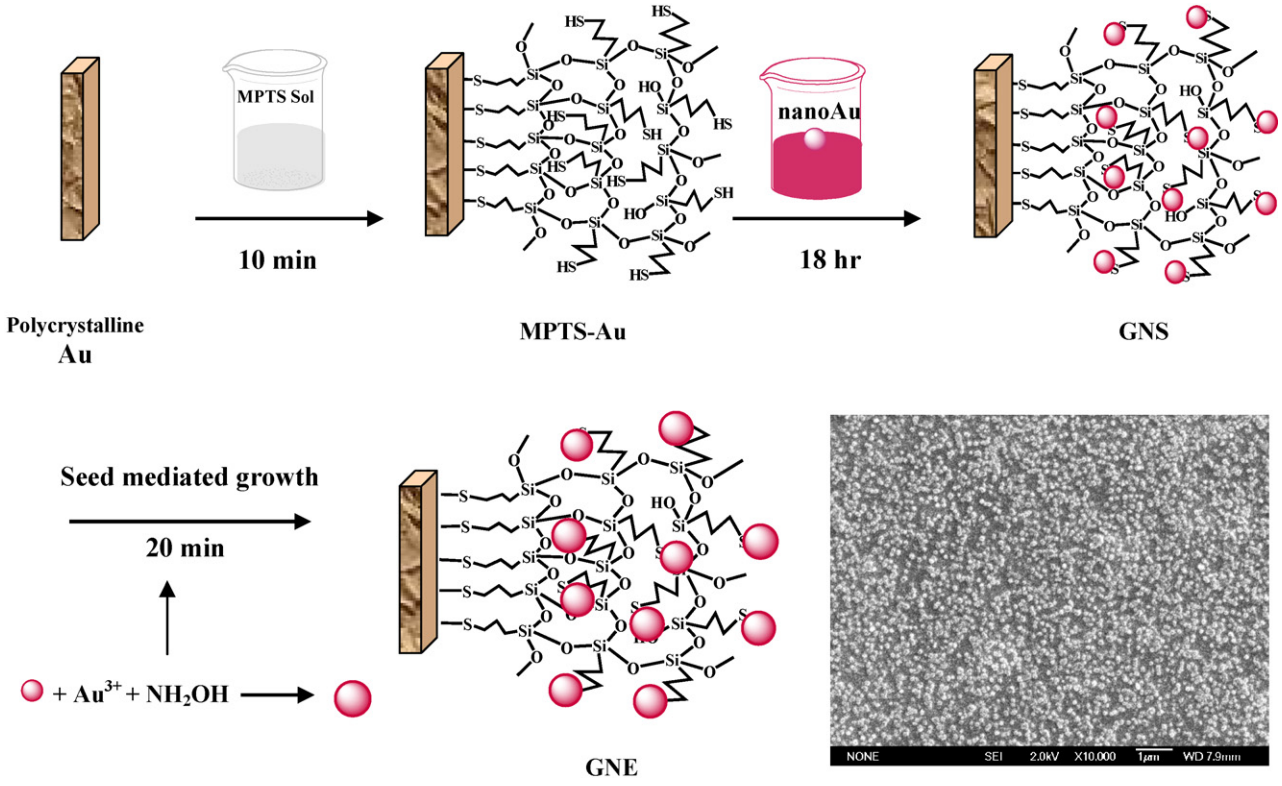

Scheme 1. Scheme illustrating the preparation of GNE electrode and the FESEM image of GNE on the silicate network.

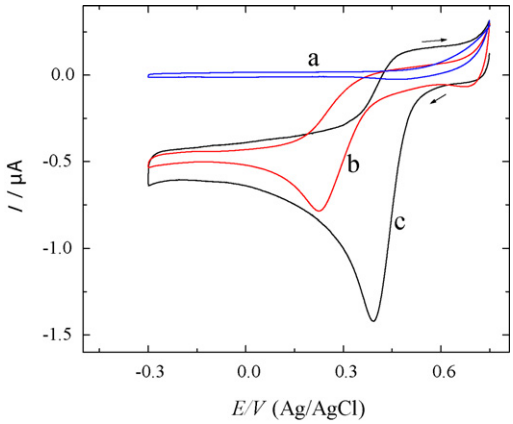

Fig. 1. Voltammetric response of (a) MPTS, (b) GNS and (c) GNE electrodes toward 10.4 ppm Cr(VI) in 0.1 M HCl. Scan rate: 10 mV/s.

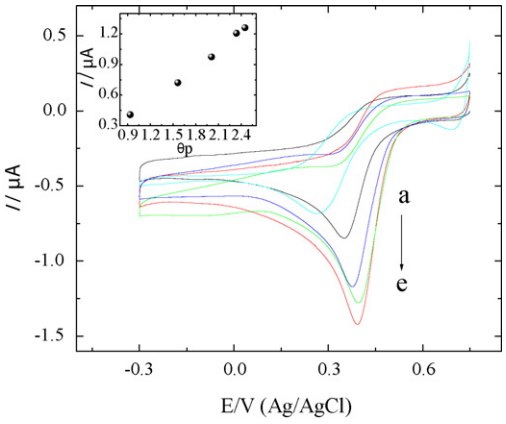

Fig. 2. Cyclic voltammograms obtained for the reduction of Cr(VI) (10.4 ppm) at different θ_p, other experimental conditions are same as Fig. 1. θ_p: (a) 0.93, (b) 1.56, (c) 2, (d) 2.33, and (e) 2.45.

and are almost spherical in shape. The distance between the particles is very small and GNEs are closely packed (Scheme 1 inset) and it can be considered as ensemble of nanoelectrodes. Au nanoparticles are known to exhibit characteristic surface plasmon resonance (SPR) band. The band position depends on the shape and size of the particle. GNS on the sol–gel network displays the characteristic SPR band at 522 nm whereas GNE shows the band at 540 nm (supporting information, Fig. 1S). The red shift in the SPR band for GNE is ascribed to the increase in size of the particle.

3.1. Electroreduction of Cr(VI)

The ability to the reduction of Cr(VI) on the GNS and GNE electrodes has been first investigated using cyclic voltammetry. Fig. 1 depicts the typical cyclic voltammetric response obtained for Cr(VI) in 0.1 M HCl. The MPTS-modified polycrystalline Au electrode does not show any characteristic response (Fig. 1a) for the reduction of Cr(VI) in the potential window used. The MPTS network on the electrode surface hinder the electron transfer for the reduction of Cr(VI). However, the nanoparticle-modified electrodes exhibit typical voltammetric response for Cr(VI). The GNS and GNE electrodes show well-defined voltammetric peaks for Cr(VI) at ~0.25 and ~0.4 V, respectively. The voltammetric response obtained is ascribed to the three-electron reduction of Cr(VI) to Cr(III) [8]. The unmodified Au electrode shows a reduction peak at ~0.11 V, which is in close agreement with the reported value [8]. The large shift in the reduction potential and increase in the peak current with respect to the unmodified electrode implies that the nano-sized particles on the electrode surface efficiently catalyze the reduction of Cr(VI). Close examination of the voltammograms obtained for the reduction of Cr(VI) reveals that the reduction potential on the GNE electrode is ~150 mV more positive than that on the GNS electrode; the peak current on the GNE electrode is twofold higher than that on the GNS electrode. The facilitated reduction process on the GNE electrode explains different surface morphology and area of GNE and GNS.

The surface morphology and area of GNE is largely different from GNS. The XRD pattern obtained for GNE shows that the (1 1 1) plane is the predominant orientation (supporting information Fig. 2S). It suggests that the surface morphology plays a key role in facilitating the reduction of Cr(VI). The electrochemically accessible surface area [28] of GNS and GNE was calculated by electrochemical measurements. The surface area of GNE is ~2.5 times larger than GNS. The peak potential for the reduction of Cr(VI) slightly shifts to negative potential as the scan rate is increased and the peak current scales approximately linear with $\upsilon^{1/2}$ at lower scan rate. The voltammetric response obtained for Cr(VI) on the nanoparticle-modified electrodes is highly stable; the peak current and peak position do not change in the subsequent sweeps.

The voltammetric response of Cr(VI) on the nanostructured electrode depends on the coverage of the nanoparticles on the electrode surface. The nanoparticle coverage (θ_p) was calculated by taking the ratio of the surface area of nanoparticles on the network to the geometrical surface area of the underlying electrode surface [32]. Fig. 2 displays the voltammetric response at different θ_p. Gradual positive shift in the peak potential and significant increase in the peak current has been observed while increasing the θ_p. For instance, ~150 mV positive shift in the peak potential and twofold increase in the magnitude of the reduction current were noticed when the θ_p was increased from 0.93 to 2.45. These results can be explained conveniently by considering the nanoelectrode ensemble behavior of the GNE electrode [30]. θ_p controls the electrocatalytic activity of the nanoparticles on the silicate network.

3.2. Amperometric detection of Cr(VI)

The analytical performance of the nanostructured electrode was evaluated by constant potential amperometry. Fig. 3 displays the amperometric response obtained for Cr(VI) on the GNE electrode. The GNE electrode was polarized at 0.4 V and sub-ppb level of Cr(VI)

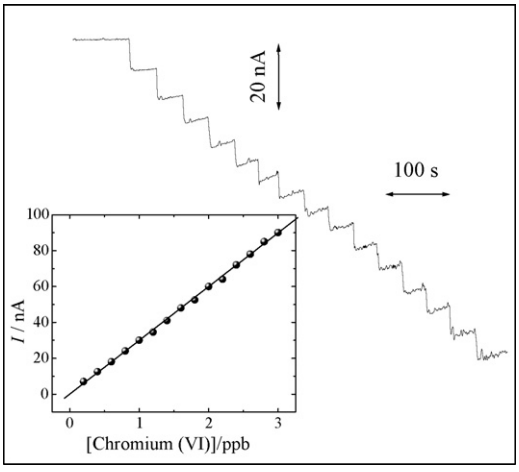

Fig. 3. Amperometric trace obtained on GNE electrode for the detection of Cr(VI) (0.2 ppb) in 0.1 M HCl. Inset shows the corresponding calibration plot. The electrode was polarized at the potential of 0.4 V.

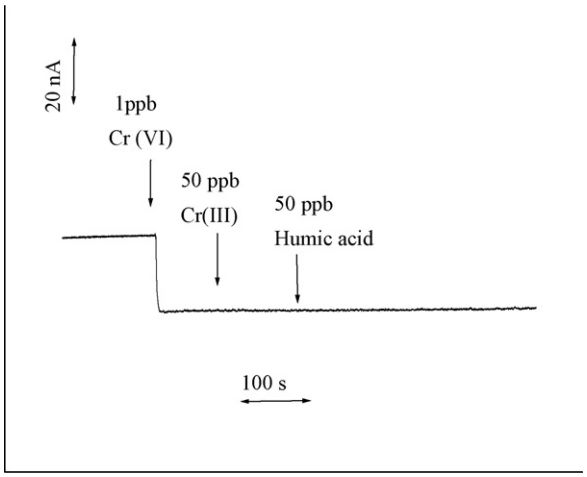

Fig. 4. Amperometric response illustrating the detection of Cr(VI) (1 ppb) without any interference from 50-fold excess of Cr(III) and humic acid in 0.1 M HCl.

was injected into a stirred supporting electrolyte solution. Rapid increase in the current was noticed after each addition of Cr(VI). Linear response was obtained over a wide range of concentration (0.2–3 ppb). The sensitivity and limit of detection (S/N = 9) was found to be 30 ± 0.2 nA/ppb and 0.1 ppb, respectively. The excellent sensitivity can be conveniently explained by considering the ensemble behavior of the GNE electrode. It is well recognized that analytical detection limit at an ensemble electrode will be much lower than that at the analogous macrosized electrode [33,34]. In the present case, the excellent sensitivity of the GNE electrode in the detection of Cr(VI) can be ascribed to the (i) existence of ensemble of nanoelectrodes and (ii) high surface area of the nanoparticles on the silicate network. The accuracy of the measurement was verified with CRM. Diluted CRM was injected repeatedly into the supporting electrolyte at regular interval and the amperometric current was measured after attaining the steady state. The sensitivity of the electrode towards CRM was calculated to be 31 ± 2 nA/ppb, which is in close agreement with the sensitivity of the electrode towards Cr(VI) (Fig. 3), indicating that the GNE electrode can be successfully used for the accurate measurement of Cr(VI).

3.3. Interference

The detection of Cr(VI) in real sample without any interference is a challenging task, as the concentration of Cr(III) is normally 100-fold excess of the Cr(VI). To evaluate the performance of the GNE electrode toward Cr(VI) in the presence of the interfering Cr(III), amperometric measurement has been performed. The amperometric response of the GNE electrode towards 1 ppb of Cr(VI) was first measured. Fiftyfold excess of Cr(III) was subsequently injected into the same supporting electrolyte. As shown in Fig. 4, no observable change in the amperometric response of Cr(VI) was noticed after the addition of 50-fold excess of Cr(III), indicating that GNE electrode does not suffer from the interference due to Cr(III). Cr(III) is electrochemically inert at the experimental condition used in our investigation. Groundwater may contain surface active compound and it can interfere the measurement by deactivating the electrode surface. Amperometric measurements have been performed in the presence of humic acid (Fig. 4) to examine such interference. The amperometric response for Cr(VI) does not change upon the addition of humic acid (Fig. 4), demonstrating that surface active compound has no influence on the measurement. Cu(II), Ni(II), Fe(III), Hg(II), Zn(II) and Pb(II) are the other potential electroactive interferents present in the real sample. The concentration of these metal ions is relatively high in groundwater [35–37]. The amperometric signal for Cr(VI) was recorded in the absence of these interfering metal ions and excess of the interfering metal ions was injected subsequently at regular interval (supporting information, Fig. 3S). The amperometric response obtained for Cr(VI) does not change upon the addition of the interfering metal ions, indicating that the GNE electrode can detect the trace of Cr(VI) without any interference from other coexisting metal ions.

3.4. Stability

For the practical application of any sensor, the long-term stability of the electrode is very essential. The stability of the GNE electrode was evaluated by using the same GNE electrode for 20 repetitive voltammetric measurements in a supporting electrolyte solution containing 5 ppm of Cr(VI). The electrode used in this measurement was kept in deionised water and subjected to another 20 repetitive measurements after 24 h. No appreciable change in the peak potential and peak current for the reduction of Cr(VI) was noticed. The coefficient of variation in the peak current for both sets of experiments was calculated to be 0.23%, confirming that the electrode is stable and can be used for the repeated measurement. In order to further ascertain the operational stability of the present electrode, voltammetric measurement in a supporting electrolyte solution containing 5 ppm of Cr(VI) has been performed with GNE electrode and the peak current for the reduction of Cr(VI) was measured at regular interval (4–6 h) over a period of 25 h. The magnitude of the peak current did not change appreciably during the whole set of experiments (25 h), demonstrating that GNE electrode is very stable (Fig. 5A). The long-term storage stability was

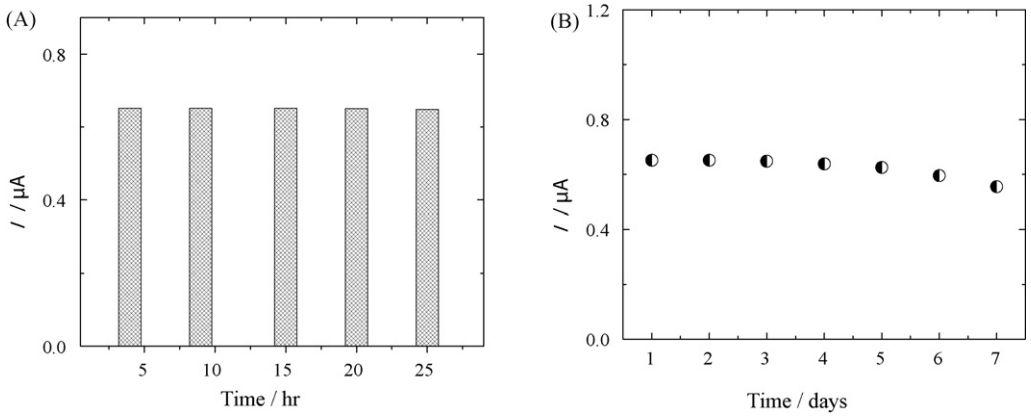

Fig. 5. (A) Operational and (B) long-term storage stability of GNE electrode towards Cr(VI). Voltammetric current was measured at the scan rate of 10 mV/s. [Cr(VI)]: 5 ppm.

tested by measuring the electrode response (peak current) for a period of 1 week (Fig. 5B). The response did not change appreciably in the first 3 days and only 14% loss of activity was noticed after a storage time of 1 week in deionised water at room temperature, demonstrating the long-term storage and operational stability. To check the reproducibility of the results, four different GNE electrodes were used for the voltammetric measurement of a solution containing 5 ppm of Cr(VI). All the four electrodes exhibited identical voltammograms for the reduction of chromium(VI), confirming that the results are highly reproducible. The standard deviation in the peak current and peak potential was calculated to be 0.02 μA and 3 mV, respectively.

The practical utilization of the GNE electrode in the detection of Cr(VI) has been tested by spiking the unfiltered river water with Cr(VI). The voltammetric measurements have been performed before and after spiking. The spiked river water sample displays typical voltammogram for Cr(VI), indicating that GNE electrode can be successfully used for the Cr(VI) contaminated real samples. To further evaluate the performance of the electrode towards Cr(VI), voltammetric measurement has been performed in air saturated solution. Identical voltammetric response has been obtained (supporting information, Fig. 4S) in the presence and absence of air, demonstrating that dissolved oxygen does not interfere the voltammetric measurement of Cr(VI) and measurements can be performed without deaeration.

The analytical performance of present nanostructured electrode is superior to the existing Cr(VI) sensors. (i) The nanostructured electrode can detect sub-ppb of Cr(VI) amperometrically without any interference from other coexisting metal ions and surface active compound. (ii) It is highly stable and does not undergo deactivation. (iii) This electrode does not require any pretreatment or activation procedure or any complexing agent and it can be used for the repeated measurements. (iv) The detection limit is well below the regulatory standard for Cr(VI) in drinking water.

4. Conclusions

In conclusion, the nanostructured Au particle based electrode has been successfully used for the amperometric detection of trace level of Cr(VI). The nanostructured electrode is highly sensitive and selective towards Cr(VI) and it can detect sub-ppb level of Cr(VI) without any interference from coexisting other metal ions and surface active compounds. This electrode is highly stable and can be used for the repeated measurements. The nanoparticles on the silicate network behave as ensemble of nanoelectrodes. The ultrasensitivity of the electrode towards Cr(VI) is ascribed to (i) enhanced mass transport to the electrode, (ii) high catalytic activity of the nanoparticles and (iii) the large surface area of the nanoparticles on the electrode surface. Because the electrode shows excellent sensitivity, selectivity and stability, it may find application in the analysis of real sample. Our investigation demonstrates that the Au nanoparticle-modified electrode can be successfully used for the electroanalysis of environmentally toxic metal ions.

Acknowledgements

This work was supported by grants from Department of Science and Technology (No. SR/S5/NM-80/2006), New Delhi. BKJ acknowledges research fellowship from Council of Scientific and Industrial Research (CSIR), New Delhi.

Appendix A. Supplementary data

Supplementary data associated with this article can be found, in the online version, at doi:10.1016/j.talanta.2008.02.027.

References

[1] D. Blowes, Science 295 (2002) 2024.
[2] (a) R.M. Cespon-Romero, M.C. Yebra-Biurrun, M.P. Bermejo-Barrera, Anal. Chim. Acta 327 (1996) 37;
(b) M.C. Kavanaug, Alternatives for Ground Water Cleanup, National Academy Press, Washington, DC, 1994.
[3] M. Pantsar-Kallio, P.K.G. Manninen, Anal. Chim. Acta 318 (1996) 335.
[4] R.J. Kieber, J.D. Willey, S.D. Zvalaren, Environ. Sci. Technol. 36 (2002) 5321.
[5] S.D. Flora, Carcinogenesis 21 (2000) 533.
[6] International Agency for Research on Cancer, IARC monographs on the evaluation of carcinogenic risks to humans, vol. 49, IARC Scientific Publications, IARC, Lyon, 1990.
[7] USEPA, Integrated Risk Information System (IRIS), US Environmental Protection Agency, Environmental Criteria and Assessment Office, Cincinnati, OH, June 2, 1992.
[8] C.M. Welch, O. Nekrassova, R.G. Compton, Talanta 65 (2005) 74.
[9] K. Wrobel, K. Wrobel, P.L. Lopez-de-Alba, L. Lopez-Martinez, Talanta 44 (1997) 2129.
[10] R. Milacic, J. Stupar, Analyst 119 (1994) 627.
[11] A. Padarauskas, A. Judzentiene, E. Naujalis, V. Paliulionyte, J. Chromatogr. A 808 (1998) 193.
[12] M. Derbyshire, A. Lamberty, P.H.E. Gardiner, Anal. Chem. 71 (1999) 4203.
[13] I. Turyan, D. Mandler, Anal. Chem. 69 (1997) 894.
[14] N.A. Malakhova, A.V. Chernysheva, K.Z. Brainina, Electroanalysis 3 (1991) 803.
[15] M. Korulczuk, M. Grabarczyk, Talanta 49 (1999) 703.
[16] J. Golimowski, P. Valenta, H.W. Nurnberg, Fresenius Z. Anal. Chem. 322 (1985) 315.
[17] L. Lin, N.S. Lawrence, S. Thongngamdee, J. Wang, Y. Lin, Talanta 65 (2005) 144.
[18] J. Wang, J. Lu, C. Olsen, Analyst 117 (1992) 1913.
[19] Y.-J. Yang, H.-J. Huang, Anal. Chem. 73 (2001) 1377.
[20] N.A. Carrington, L. Yong, Z.-L. Xue, Anal. Chim. Acta 572 (2006) 17.
[21] C. Michel, A. Ouerd, F. Battaglia-Brunet, N. Guigues, J.-P. Grasa, M. Bruschi, I. Ignatiadis, Biosens. Bioelectron. 22 (2006) 285.
[22] A.N. Shipway, E. Katz, I. Willner, ChemPhysChem 1 (2000) 18.
[23] (a) M. Zayats, R. Baron, I. Popov, I. Willner, Nano Lett. 5 (2005) 21;
(b) V. Pavlov, Y. Xiao, B. Shlyahovsky, I. Willner, J. Am. Chem. Soc. 126 (2004) 11768.
[24] M.-C. Daniel, D. Astruc, Chem. Rev. 104 (2004) 293.
[25] (a) X. Dai, G.G. Wildgoose, C. Salter, A. Crossley, R.G. Compton, Anal. Chem. 78 (2006) 6102;
(b) E. Majid, S. Hrapovic, Y. Liu, K.B. Male, J.H.T. Luong, Anal. Chem. 78 (2006) 762.
[26] C.R. Raj, B.K. Jena, Chem. Commun. (2005) 2005.
[27] B.K. Jena, C.R. Raj, Chem. Eur. J. 12 (2006) 2702.
[28] B.K. Jena, C.R. Raj, Anal. Chem. 78 (2006) 6332.
[29] B.K. Jena, C.R. Raj, Electroanalysis 19 (2007) 816.
[30] B.K. Jena, C.R. Raj, J. Phys. Chem. C 111 (2007) 6228.
[31] J. Wang, P.V.A. Pamidi, D.R. Zanette, J. Am. Chem. Soc. 120 (1998) 5852.
[32] S. Kumar, S. Zou, J. Phys. Chem. B 109 (2005) 15707.
[33] (a) H. Reller, E. Kirowa-Eisner, E. Gileadi, J. Electroanal. Chem. 161 (1984) 247;
(b) J. Cassidy, J. Ghoroghchian, F. Sarfarazi, J.J. Smith, S. Pons, Electrochim. Acta 31 (1986) 629.
[34] (a) V.P. Menon, C.R. Martin, Anal. Chem. 67 (1995) 1920;
(b) K.R. Wehmeyer, M.R. Deakin, R.M. Wightman, Anal. Chem. 57 (1985) 1913.
[35] Y. Liu, Y. Guo, S. Meng, F. Feng, X. Chang, Microchim. Acta 157 (2007) 209.
[36] I.A. Katsoyiannis, A.I. Zouboulis, Water Res. 38 (2004) 1922.
[37] S.H. Jadhav, S.N. Sarkar, G.C. Ram, H.C. Tripathy, Arch. Environ. Contam. Toxicol. 53 (2007) 450.

Talanta 76 (2008) 60–65

Contents lists available at ScienceDirect

Talanta

journal homepage: www.elsevier.com/locate/talanta

Optode for uranium(VI) determination in aqueous medium

J.M. Joshi [a], P.N. Pathak [b], A.K. Pandey [b,*], V.K. Manchanda [b]

[a] Chemical Engineering Division, Bhabha Atomic Research Centre, Trombay, Mumbai 400 085, India
[b] Radiochemistry Division, Bhabha Atomic Research Centre, Trombay, Mumbai 400 085, Maharashtra, India

ARTICLE INFO

Article history:
Received 5 December 2007
Received in revised form 31 January 2008
Accepted 7 February 2008
Available online 15 February 2008

Keywords:
Uranium(VI)
Membrane optode
2-(5-Bromo-2-pyridylazo)-5-diethylaminophenol
Visual colorimetry
Spectrophotometry

ABSTRACT

A colorimetric method for simultaneous preconcentration and determination of uranium(VI) anions from aqueous samples was developed using a membrane optode formed by physical inclusion of a chromophore 2-(5-bromo-2-pyridylazo)-5-diethylaminophenol (Br-PADAP) into a plasticized cellulose triacetate matrix. The optode was tested for uranium uptake in bicarbonate/carbonate medium ($\sim 10^{-4}$ M) at pH 7–8 in the presence of triethanolamine buffer. The inclusion of an anion-exchanger tricaprylylmethyl ammonium chloride (Aliquat-336) was found to be necessary for the formation of U(VI)–Br-PADAP complex in the optode matrix, resulting into distinct color change of the optode from yellow to magenta after uranium sorption. The composition of the optode was optimized by varying the amounts of different plasticizers and Aliquat-336 to obtain minimum response time towards U(VI) in aqueous bicarbonate medium. The proportionality in intensity of the magenta color of the optode samples loaded with varying amounts of U(VI) suggested its potential applications for screening of U(VI) in aqueous samples by visual colorimetry. The effects of experimental parameters involved in the detection and quantification of U(VI) using optode were optimized. The optode analytical performance was evaluated in terms of interference of cations and anions, equilibration time, reusability, detection limit, etc. and compared with the conventional spectrophotometric method for U(VI) using same chromophore Br-PADAP. The optode developed in the present work was tested in real alkaline $Mg(NO_3)_2$ effluent sample obtained from uranium extraction process.

1. Introduction

Uranium is one of the contaminants that can be found in natural waters at ultra-trace concentration as a result of anthropogenic activities, weathering effects and erosion of rocks and soil. In addition, the increased nuclear power production, predominantly based on the uranium fuel cycle, leads to the possibility of release of uranium and other radionuclides during different stages in the life history of uranium fuel. The uranium fuel cycle begin with mining of uranium ore, followed by its extraction and purification, fuel fabrication, irradiation in the reactor, spent fuel reprocessing, recycling of separated plutonium and uranium back into the reactor, and ending with the management of nuclear waste produced. U(VI) is known to be nephrotoxic as a heavy metal ions and radiologically harmful as a radionuclide. Although radiological impact is determined by its total concentration, the chemical toxicity of uranium is dependent on chemical form of its species that interacts with bio-molecules [1,2]. The WHO, Health Canada, and Australian drinking water guidelines have fixed the maximum U(VI) concentration in drinking waters to be less than 9, 20, and 20 μg/L, respectively [3]. Therefore, it is desirable to have a analytical method that can determine a specific U(VI) species present in the aqueous medium at trace level. The comparison of different conventional analytical methods like spectrophotometry, laser fluorimetry, liquid scintillation (LSC), gamma spectrometry, and alpha spectrometry has been carried out for estimating waterborne uranium concentration [4]. In order to enhance the detection limits of these methods, the chemical procedures applied were preconcentration, liquid extraction, chromatographic resin extraction and precipitation. However, these methods require multi-steps sample manipulation, which are time consuming and possible in the laboratory only.

Membrane-based preconcentration method can be tailor-made for a specific analytical application. The analyte selective membrane can be converted to optical chemical sensor (optode) by immobilizing the indicator that responds to analyte in a concentration dependent manner [5–7]. The membrane optodes have been prepared by immobilizing the indicator (ionophores, chromoionophores, and fluoroionophores) with or without extractant in the solid matrix using highly diversified methods [8–11]. These optodes are based on the preconcentration of the analyte as a chomogenic species on a solid substrate and subsequent measurement of the absorbance/reflectance of the solid phase, without

* Corresponding author. Tel.: +91 22 25590641; fax: +91 22 25505150/1.
E-mail address: ashokk@barc.gov.in (A.K. Pandey).

0039-9140/$ – see front matter © 2008 Elsevier B.V. All rights reserved.
doi:10.1016/j.talanta.2008.02.003

stripping the chromogenic species. The presence of extractant provides an increase in selectivity and sensitivity of optodes as compared to the corresponding solution spectrophotometry using same chromophore. The applicability of a fiber-optic-based laser-induced luminescence sensor for uranium (10^{-9}–10^{-4} M) estimation in different samples has been studied [12]. Collins et al. have developed a remote optical fiber flow-cell with Nafion-117 membrane and capillary electrophoresis method, both using Arsenazo III as an indicator, for sensing U(VI) in the ground water [13,14]. However, these designs have not yet proven as a viable method for field applications due to complicated hardware and lower selectivity. The color changeable optode for uranium and thorium have been reported using non-specific Alizarin Red S [15] and 4-(*p*-nitrophenylazo)-pyroctachol (NAP) [16], respectively. The applications of these optodes require a careful evaluation of possible interferences in actual applications. Hexyphyrin (1.0.1.0.0.0) (isometyrin) has been found to give significant color change in the presence of UO_2^{2+}, PuO_2^{2+}, and NpO_2^{2+}, which can be used for developing actinide sensor [17]. However, isometyrin requires a week for complexation with actinides in dark.

In present work, a colorimetric method for simultaneous preconcentration and determination of U(VI) anions from aqueous samples has been developed using a membrane optode formed by physical inclusion of a chromophore 2-(5-bromo-2-pyridylazo)-5-diethylaminophenol (Br-PADAP) into a plasticized cellulose triacetate matrix. The choice for Br-PADAP was based on its high sensitivity and selectivity for uranium estimation by the spectrophotometry [18–21]. Two different plasticizers such as tris(2-ethylhexyl)phosphate (TEHP), and 2-nitrophenyloctyl ether (NPOE) have been used to plasticize cellulose triacetate. The dinonylnaphthalene sulphonic acid (DNNS), tri-*iso*-octyl amine (TiOA), and tricaprylylmethyl ammonium chloride (Aliquat-336) have been evaluated as the carriers for facilitating transfer of U(VI) from aqueous to the optode matrix. The carrier in the optode is necessary as immobilized Br-PADAP does interact with U(VI) present in the aqueous medium. The experimental parameters such as composition of optode, pH, interference of cations and anions on the determination of uranium, range of uranium concentration, response time, and detection limit have been studied and compared with the conventional spectrophotometry. Finally, the optode has been tested for quantitative determination of U(VI) in the real effluent sample.

2. Experimental

2.1. Reagents and apparatus

Br-PADAP, 2-nitrophenyloctyl ether, Aliquat-336, DNNS, TiOA, triethanolamine (TEA), and cellulose triacetate were obtained from Sigma–Aldrich (Steinheim, Switzerland), and tris(2-ethylhexyl) phosphate was obtained from Koch-Light Laboratories (Coinbrook Bucks, England). Uranyl nitrate, chloroform, and dichloromethane were obtained from Merck (Mumbai, India). A stock solution of uranium (10^{-2} M) was prepared by dissolving suitable quantities of $UO_2(NO_3)_2{\bullet}6H_2O$ in distilled water and the concentration of uranium was determined by Davies and Gray method [22]. Working standard stock solutions of uranium were prepared by suitable dilution in the desired medium. Triethanolamine buffer was prepared by dissolving it in distilled water and neutralizing with perchloric acid (pH 7.8).

A microprocessor-based pH meter model PHAN from Lab India (Mumbai, India) was used for pH measurements. The thickness of the optode was measured by a digital micrometer (Mitutoy, Japan) with an accuracy of ±0.001 mm. UV–vis spectrophotometer model V 53 from JASCO (Tokyo, Japan) was used for recording the spectra and the absorbance measurements. The absorbance measurements were done by mounting the optode samples (3 cm × 1 cm) inside a quartz cuvette. The absorbance measurements of the optode samples were carried out with respect to air as well as blank optode sample.

2.2. Preparation of membrane optode

The membrane optodes were prepared by using the chromorphore (Br-PADAP), extractant (DNNS/TiOA/Aliquat-336), plasticizer (TEHP/NPOE), and matrix forming polymer (CTA). Desired quantities of CTA, extractant, Br-PADAP and plasticizer were dissolved separately in CH_2Cl_2. After complete dissolution, the casting solution was prepared by mixing the required volumes of the solutions containing known amounts of the components. The resulting casting solution was homogenized by ultrasonication for 5–10 min. The casting solution was poured in a Petri dish to allow the slow evaporation of CH_2Cl_2 and the formation of the homogeneous transparent membrane.

2.3. Uptake experiments

The optode strips (3 cm × 1 cm) were equilibrated in sample solutions of desired medium (~10^{-4} M bicarbonate/carbonate solution in TEA buffer) and agitated with magnetic stirring bar at a rate of 250 rpm. TEA buffer (3.0 mL) was added in 15 mL (sample volume) to maintain a pH of 7.8 ± 0.2 unless stated otherwise. It should be noted that uranium precipitation was observed in the absence of bicarbonate medium. The membrane strips were taken out of the sample solutions and washed with a jet of distilled water. The color of optode strips changed from yellow to magenta depending on the uranium concentration in the sample solution. The change in absorbance of U(VI)–Br-PADAP complex was monitored at λ_{max} = 578 nm under different experimental conditions. The uranium uptakes by the optode were obtained by the spectrophotometric analyses [18] of sample solutions before and after equilibration with the optode.

3. Results and discussion

3.1. Composition of optode

Various combinations of the matrix forming polymer, plasticizer (TEHP/NPOE), chromophore (Br-PADAP), and the carrier (DNNS/TiOA/Aliquat-336) were studied to optimize the uranium uptake in the optode matrix from aqueous samples having pH range of 7–8. Table 1 lists different optodes having Br-PADAP with or without carrier. It is seen from Table 1 that Br-PADAP immobilized in the optode could not form complex with U(VI) in absence of a carrier in the optode matrix. This seems to suggest that Br-PADAP itself does not act as a carrier to facilitate the transfer of U(VI) from equilibrating solution to the optode matrix. Among the different carriers studied, Aliquat-336 was found to be efficient for facilitating the transfer of U(VI) from equilibrating solution to optode matrix. This may be attributed to the fact that the presence of bicarbonate/carbonate anions in the equilibrating solution helps in the formation of anionic uranium carbonate complex species. This anionic form of U(VI) could interact with the liquid anion-exchanger Aliquat-336 present in the optode matrix to form an ion-pair. In addition, the Aliquat-336 may also be responsible to prevent leaching of U(VI)–Br-PADAP anionic complex formed in the optode matrix.

Table 1
Response of optode samples after 3 h equilibration with well-stirred aqueous solution containing U(VI) and ~10^{-3} M $NaHCO_3$ at pH 7–8

Composition	Response
CTA (49 wt.%) + TEHP (49 wt.%) + Br-PADAP (2 wt.%)	No color change
CTA (44 wt.%) + TEHP (44 wt.%) + Br-PADAP (2 wt.%) + DNNS (10 wt.%)	No color change
CTA (44 wt.%) + TEHP (44 wt.%) + Br-PADAP (2 wt.%) + TiOA (10 wt.%)	No color change
CTA (44 wt.%) + TEHP (44 wt.%) + Br-PADAP (2 wt.%) + Aliquat-336 (10 wt.%)	Color changes from yellow to magenta

3.2. Spectral characteristics

Br-PADAP is one of the most sensitive reagents for the spectrophotometric analysis of uranium present in various aqueous/organic phase samples. It forms 1:1 stable complex with U(VI) in pH range of 7–8 [23–26]. The comparison of UV–vis spectra of optode samples equilibrated with different aqueous matrix having same concentration of U(VI) (3.6 μg/mL) is shown in Fig. 1. It is seen from this figure that TEA buffer (pH 7–8) in the equilibrating solution enhanced the color change in optode sample corresponding to the formation of U(VI)–Br-PADAP complex. In seawater matrix, the optode response towards U(VI) was significantly lower as compared to other aqueous matrices, and may not be useful for the detection and quantification of U(VI) in seawater. The change in absorbance spectra of optode samples, equilibrated with solutions having varying concentrations of U(VI) in TEA buffer, is shown in Fig. 2. The comparison of spectra given in Fig. 2 indicated that there was large bathochromic shift in absorbance of optode samples from 450 nm (blank) to 541 and 578 nm with an isobestic point at 505 nm on equilibration with buffer solutions having U(VI) concentration ranging from 0.7 to 3.6 μg/mL. The double absorbance maxima λ_{max} at 541 and 578 nm are reported in the literature as a characteristic of U(VI)–Br-PADAP complex [23–26]. This indicated that the optode is responsive towards change in the uranium concentrations in the equilibrating solution. It is seen from Fig. 2 that the change in absorbance of optode at λ_{max} 578 nm was higher than that at 541 nm. At 578 nm wavelength, the absorbance of the blank optode sample (without uranium) is lower as compared to that at 541 nm. Therefore, the change in the absorbance at 578 nm can be used for quantitative detection of U(VI) in the aqueous samples. It was also observed that magenta color of U(VI)-loaded optode sample changes back to yellow on immersing this optode in well-stirred

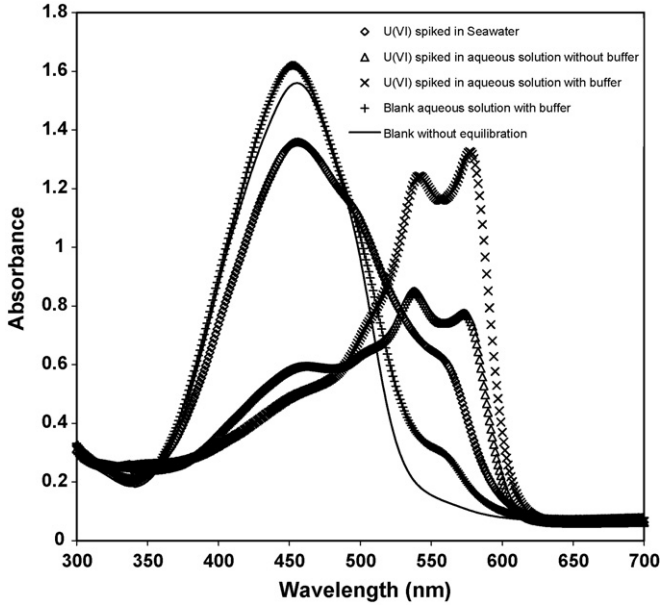

Fig. 1. UV–vis spectra of optode samples (1 cm × 3 cm) equilibrated with 15 mL of different aqueous samples spiked with 54 μg of U(VI) in bicarbonate medium.

Table 2
Effect of cations/anions on absorbance data of UO_2^{2+}–Br-PADAP complex at λ_{max} = 578 nm; [UO_2^{2+}] = 8.7 μM; sample volume = 15 mL; pH 7–8 (TEA buffer in carbonate medium); duration = 3 h; [cation] = 1×10^{-4} M; [anion] = 2×10^{-4} M

Cation	Absorbance	Anion	Absorbance
UO_2^{2+}	1.88	$F^- + UO_2^{2+}$	1.59
$Fe^{3+} + UO_2^{2+}$	1.11	$CO_3^{2-} + UO_2^{2+}$	1.27
$Nd^{3+} + UO_2^{2+}$	2.07	$C_2O_4^{2-} + UO_2^{2+}$	1.67
$Th^{4+} + UO_2^{2+}$	1.39		

0.01 M HNO_3 for 10–15 min. This indicated that U(VI)–Br-PADAP complex formed in the optode is broken at pH 2 to regenerate the Br-PADAP in the optode.

3.3. Optimization

The optode response depends on the rate of diffusion of anionic uranyl-carbonato species ($UO_2(CO_3)(HCO_3)^-$, $UO_2(CO_3)_2^{2-}$, or $UO_2(CO_3)_3^{4-}$) existing in the aqueous phase to the optode interface, and then to form complex with the Br-PADAP molecule present in the optode matrix. The primary role of Aliquat-336 appears to mediate the transfer of U(VI) from aqueous medium to optode matrix. In order to understand the effects of Aliquat-336, the optode samples having varying amounts of Aliquat-336 were prepared by keeping same initial amounts of CTA, TEHP, and Br-PADAP. The amount of Br-PADAP in the optode was fixed to obtain the absorbance at 450 nm not exceeding 2. The high amount of Br-PADAP was found to degrade the optical quality of the optode. The amounts of Br-PADAP and CTA used in preparation of the optodes are given in Table 1. The variation of U(VI) as a function of Aliquat-336 amounts is shown in Fig. 3. As can be seen from Fig. 3, the U(VI) uptake in the optode samples was increased from 14 to 83% with

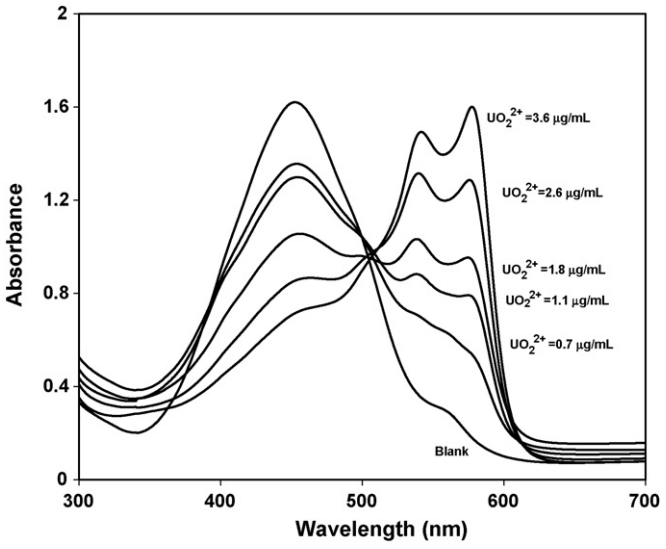

Fig. 2. Absorbance spectra of the optode samples equilibrated with well-stirred 15 mL of blank solution and solutions containing varying amounts of U(VI) in TEA buffer.

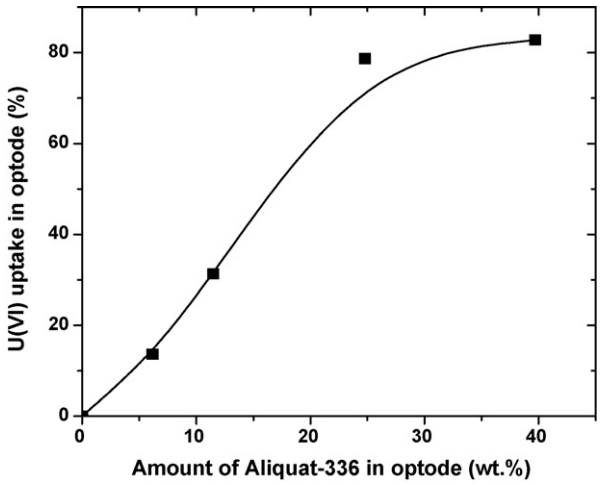

Fig. 3. Variation of uranium uptake with Aliquat-336 concentration in the optode; U_{total} = 31 μg; sample volume = 15 mL; duration = 17 h; pH 7–8 (TEA buffer).

increase in the Aliquat-336 concentration from 6.2 to 39.7% under identical conditions of the equilibrating solution. The optode samples were equilibrated for 17 h in well-stirred 15 mL buffer solution having U(VI) concentration 2.11 μg/mL. The increase in U(VI) with increase in Aliqaut-336 concentration in the optode seems to suggest that the Aliquat-336 enhances the U(VI) loading capacity of the optode. However, the kinetics of uranium uptake (17 h) was too slow to allow its use as a chemical sensor for wide ranging applications. In this context, the properties of plasticizer and their relative concentrations in the optode matrix are also important. It was reported that increase in amount of plasticizer increases the diffusion rate of anions in the plasticized membranes [27]. Therefore, the optode samples having varying amounts of two different plasticizers (e.g., TEHP and NPOE) were prepared and tested for their response time towards U(VI) ions in buffered carbonate aqueous medium.

The variation in absorbance of the optode samples, plasticized with varying amounts of TEHP and NPOE, was studied by equilibrating these with well-stirred 15 mL buffered sample solutions having 2.11 μg/mL U(VI) concentrations in bicarbonate/carbonate medium. The optode samples were taken out at regular time intervals to monitor the absorbance of U(VI)–Br-PADAP complex at 578 nm as a function of equilibration time. The variations of absorbance at 578 nm in the optode samples as a function of equilibration time are shown in Fig. 4. This graph indicates the kinetics of sorption of anionic U(VI) species in the optode. As can be seen

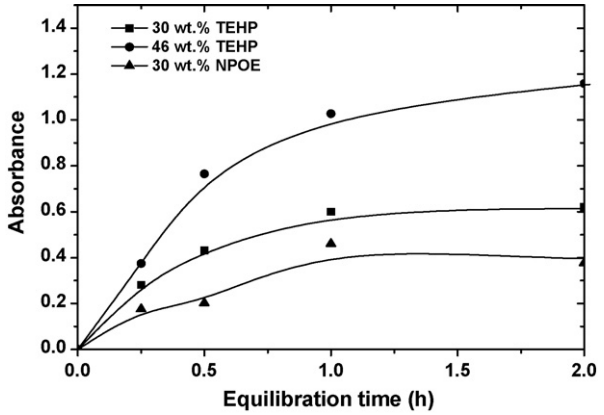

Fig. 4. Uranium uptake kinetics as a function of plasticizer amount in the optode; U_{total} = 31 μg; sample volume = 15 mL; pH 7–8 (TEA buffer).

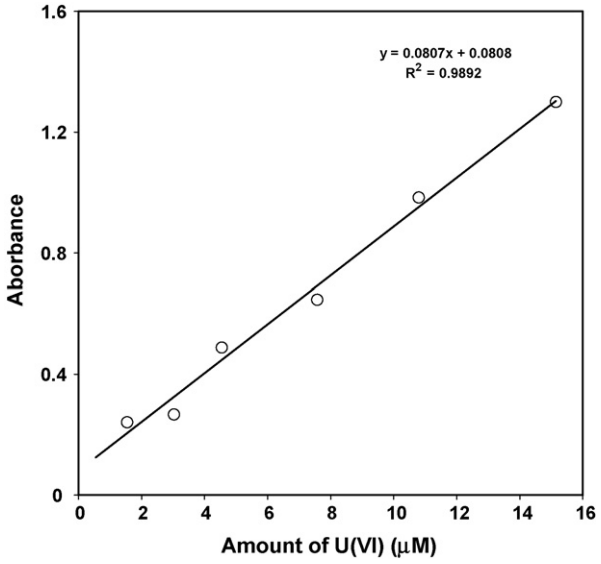

Fig. 5. Change in absorbance of the optode sample at 578 nm as a function of U(VI) concentration after equilibration for 2 h in well-stirred 15 mL sample solution with TEA buffer (pH 7–8).

from Fig. 4, the rate of sorption of uranium anionic species increases with increase in amount of plasticizer in the optode. The matrix forming CTA chains in the liquid fraction of optode (plasticizer) matrix produces obstruction in the path of the moving ion-pair. This obstruction is reduced with increase in the liquid fraction of the optode. Hence, the plasticizer, which is the major component of liquid phase, acts as a medium for diffusional transport of ions in the optode. The optode could not be plasticized more than 46 wt.% of the plasticizer as mechanical strength of the optode was not enough to use it in well-stirred solution. Out of two plasticizer used in the preparation of optode, the optode sample with 46 wt.% TEHP gave faster increase in absorbance corresponding to U(VI)–Br-PADAP complex than the optode formed by NPOE. Though the equilibration time required for almost complete U(VI) sorption is longer than 3 h, the shorter equilibration time could be used for quantitative analysis of U(VI) as % uptake remains constant at fixed equilibration time. The equilibration time of 30 min could be used for constructing calibration graph for aqueous sample containing U(VI) greater than 1 μg/mL. However, the detection limit for uranium would be better after 3 h equilibration of the optode sample as more than 80% of U(VI) sorption in the optode is achieved. Finally, the composition of optode was kept as: 23 wt.%CTA + 30 wt%Aliquat-336 + 46 wt.%TEHP + 0.09 wt.%Br-PADAP for uranium uptake studies with an equilibration time of 3 h.

The absorbance signals at 578 nm monitored for a long period over 24 h did not show the evidence of leaching of U(VI)-Br-PADAP complex from the optode sample to equilibrating bicarbonate aqueous medium with TEA buffer. There was no drift in the absorbance signal when the film used for uranium uptake was exposed to light. No appreciable change in the optode absorbance value was observed when the film was dipped in de-ionized distilled water overnight. These observations suggest that the optode film was quite stable under the conditions of present studies.

3.4. Calibration and reproducibility

The response of the optode, in the form of change in absorbance at 578 nm, towards uranium concentration up to 15 μM is shown in Fig. 5 after correcting for the blank. The blank absorbance at 578 nm was measured after equilibrating optode sample with blank

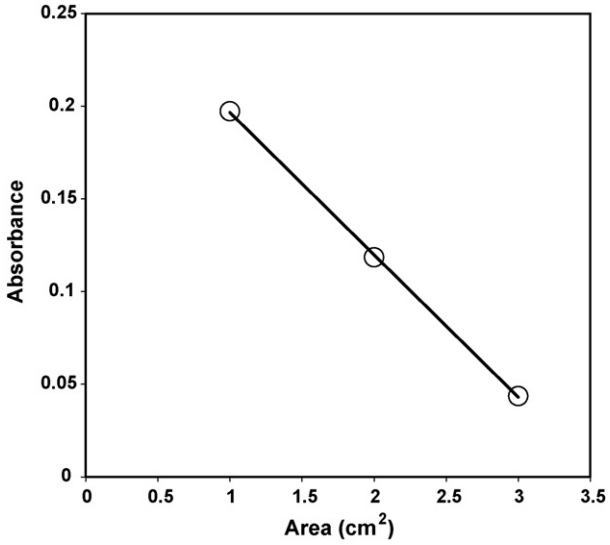

Fig. 6. Variation in absorbance of the optode samples at 578 nm equilibrated with buffered solution containing 24 μg of U(VI). The area of optode was varied by changing length and keeping same breadth 1 cm.

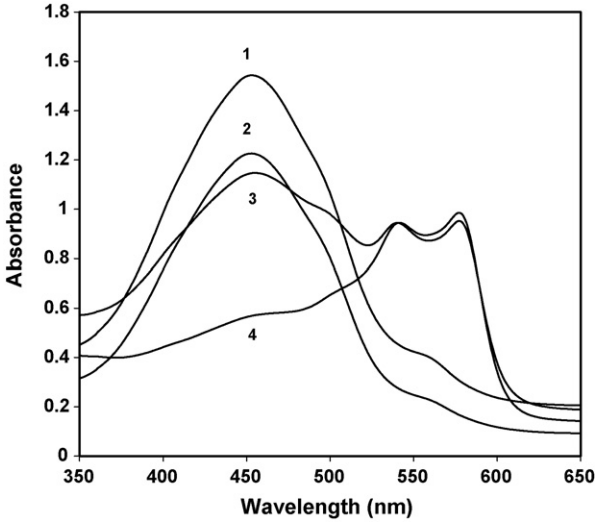

Fig. 7. UV–vis spectra of optode samples equilibrated with (i) blank solution with buffer (curve-1), (ii) buffer solution containing 25 μg of Th(IV) (curve-2), (iii) buffer solution containing 5 μg of Th(IV) and 24 μg of U(VI) (curve-3), and (iv) buffer solution containing 100 μg of Th(IV) and 24 μg of U(VI) (curve-4).

solution at pH 7–8, without uranium. It is seen from this figure that the absorbance linearly varies as a function of U(VI) concentration range of 1.5–15 μM. However, the calibration line did not pass through the zero. This may be due to the chemical changes produced on sorption of U(VI) in the matrix that might have changed the absorbance. These chemical changes may be counterions or water content in the optode matrix. The water contents before and after U(VI) sorption in optode sample were found to be within 2 wt.%. The minimum concentration of U(VI) required in the 15 mL equilibrating solution to produced distinct color change of optode (dimensions 3 cm × 1 cm) was found to be 0.33 μg/L. However, this detection limit of U(VI) concentration can be further enhanced by using larger volume of aqueous sample.

The reproducibility of the optode membrane was determined using standard uranium solution (1000 μg/mL from Merck). Suitable aliquots were spiked from standard uranium solution in to the medium of uptake experiments, e.g., pH 7–8, TEA buffer, volume = 15 mL; and [U] = 8.7 μM. The optode sample was taken out for the absorbance measurements after equilibration for 3 h. The mean absorbance values with the relative standard deviation were found to be 1.8 ± 0.1 (n = 6). The small deviations in absorbance values suggest that optode membrane responses are reproducible under the conditions of this study.

In order to enhance the change in absorbance at 578 nm in the optode, the optode samples of different dimensions were equilibrated with buffered solutions having 24 μg of U(VI) in 15 mL in bicarbonate medium. As can be seen from Fig. 6, the absorbance increases from 0.05 to 0.2 by decreasing area of optode samples from 3 to 1 cm^2. This can be attributed to increase in U(VI) concentration in the unit volume of the optode. Therefore, the possibility exist to improve U(VI) detection limit of optode by decreasing its volume.

3.5. Interfering ions

The selectivity of the optode was tested by equilibrating optode samples with solutions containing different cations (Fe^{3+}, Eu^{3+}, and Th^{4+}) and anions (NO_3^-, F^-, I^-, CO_3^{2-}, and $C_2O_4^{2-}$). As shown in Fig. 7, the absorbance spectra of optode samples did not change on its equilibration with solution containing 5–100 μg of Th^{4+}. However, some of these ions were found to affect the U(VI) sorption in the optode. In order to examine the effects of these ions on U(VI) sorption in the optode, the uptake studies were carried out in the presence of micro-molar concentrations of cations such as Fe^{3+}, Nd^{3+}, Th^{4+}, and anions such as F^-, $C_2O_4^{2-}$ at pH 7–8 in TEA buffer with 2.11 μg/mL U(VI) concentration. In all cases except $C_2O_4^{2-}$, the absorbance variations in the optode samples were within ±10%, suggesting that these cations/anions in the micro-molar concentrations can be tolerated in the uranium sample solutions. The tolerance limit was taken as 10% deviations in the mean absorbance values in U(VI)–Br-PADAP complex at 578 nm in the absence of the competing cations/anions. In case of $C_2O_4^{2-}$, the absorbance was reduced to 15% which indicated that $C_2O_4^{2-}$ ions interfere in the sorption of U(VI) in the optode.

In order to study the interference at higher concentration, the optode samples were equilibrated with solution containing 8.7 μM of U(VI) with 10-time excess of a interfering cations (Fe^{3+}, Nd^{3+}, and Th^{4+}) and 20-time excess of a interfering anions (CO_3^{2-}, F^-, and $C_2O_4^{2-}$). The choice of interfering anions was based on the fact that optode contains Aliquat-336 for transferring U(VI) from aqueous to the optode matrix, and presence of anions may affect the sorption of U(VI) in the optode matrix. Fe^{3+}, Nd^{3+}, and Th^{4+} are representative cations that are likely to be present in the aqueous samples of ground water. The absorbance of U(VI) was suppressed by 30 and 15% in presence of 0.2 mM of CO_3^{2-} and F^- ions, respectively. This may be related to fact that U(VI) species are highly dependent on strong complexing CO_3^{2-} ions. The Nd^{3+} ions were found to enhance the absorbance at 578 nm by 11%. In presence of Fe^{3+} and Th^{4+} in the solution, the absorbance of the optode at 578 nm was reduced by 40 and 25%, respectively. The decrease in absorbance of optode at 578 nm in presence of U(VI) with Fe^{3+} and Th^{4+} could not be understood. There is a possibility that U(VI) may be sorbed in the hydroxides of these ions. It is evident form Table 2 that Fe^{3+}, Th^{4+}, F^-, and CO_3^{2-} can lead to negative bias of uranium concentration in the sample. By contrast, the presence of Nd^{3+} type metal ions may give rise to positive bias in estimated concentration of uranium in the samples.

3.6. Comparison with solution spectrophotometry

The comparison of uranium determination by optode and spectrophotometry [18] using chromophore Br-PADAP is given in Table 3. Unlike solution spectrophotometry, the presence of F^- ions

Table 3
Comparison of spectrophotometry and optode for the U(VI) determination in the aqueous sample

Characteristics	Solution spectrophotometry[a]	Optode
Complexing solution comprising of (1,2-cyclohexylenedinitrilo) tetraacetic acid + NaF	Required	Not required
U(VI)–Br-PADAP complex absorbance	Observed at 541 and 578 nm	Observed 541 and 578 nm
Stability of U(VI)–Br-PADAP complex	24 h	Can be stored for 1 month
Absorbance of solution sample containing 30 μg U	0.9 ± 0.1 (in 10 mL)	1.8 ± 0.1 for optode equilibrated with 15 mL solution
Equilibration time required for color development	2 h	3 h
Detection limit of U(VI)	0.8 μg/mL	0.3 μg/mL
Reuse	Not possible	Possible

[a] Ref. [18].

was not found to affect the formation of U(VI)–Br-PADAP complex. Only bicarbonate/carbonate medium was found to necessary for good response of optode towards U(VI). It is evident that the detection limit of U(VI) is significantly enhanced by using optode (0.3 μg/mL) than that can be achieved with spectrophotometry (0.8 μg/mL). The uranium determination by optode appears to be simple as it involves less sample manipulation and can be reused. Apart from this, the optode samples can be stored for longer period. This would be useful for preparation of standards for calibration plot or for visual colorimetric analysis of U(VI).

3.7. Applications to real samples

Alkaline $Mg(NO_3)_2$ effluent sample was obtained from Uranium Extraction Division, BARC, to evaluate the applicability of the optode for real samples. Uranium concentration in the sample was determined by conventional Br-PADAP-based spectrophotometric method as 66 ± 1 ppm [18]. The uptake experiment was done under specified experimental conditions such as pH 7–8 (with TEA buffer) and volume = 15 mL, using 0.5 mL of the effluent sample containing ~33 μg U. The optode film (3 cm × 1 cm) was taken out for the absorbance measurements after exposure for 3 h. The mean absorbance values were found to be 1.23 ± 0.1. The calibration plot constructed by adding known amount of U(VI) in buffered bicarbonate solution as described above. The amount of uranium obtained by optode was found to be 10% less than that expected in the $Mg(NO_3)_2$ effluent sample by solution spectrometry [18]. This was due to the presence of higher nitrate concentration (~2 M) in the sample solution that may affect uptake of U(VI) in optode sample by ion-exchange mechanism. However, the response of the optode with the sample solution was highly reproducible indicating that the calibration curve should be prepared in the aqueous matrix likely to be encountered in the real sample.

4. Conclusions

A CTA-based optode has been developed for uranium preconcentration and its determination. The optode changes color due to uranium uptake in bicarbonate/corbonate medium (~10^{-4} M) at pH 7–8 in the presence of TEA buffer. The intensity of color in the optode sample was found to be dependent on the uranium uptake from the sample solution as well as the composition of membrane. The composition of the optode was optimized as: 23 wt.%CTA + 30 wt.%Aliquat-336 + 46 wt.%TEHP + 0.1 wt%Br-PADAP, for uranium uptake studies with an equilibration time of 3 h. The detection limit of the optode film (dimension: 3 cm × 1 cm) was determined to be ~0.3 μg/mL U(VI) for a 15 mL sample at pH 7–8 (in TEA buffer). The presence of micro-molar concentrations of cations such as such as Fe^{3+}, Nd^{3+}, Th^{4+}, and of anions such as NO_3^-, F^-, I^-, and CO_3^{2-}, etc. can be tolerated during uranium estimation at pH 7–8 in TEA buffer. At higher concentration of these ions, the negative bias was observed in the most cases except for Nd^{3+} ions. This indicated that performance of the optode is dependent on the concentrations of ions in aqueous samples. The optode film was quite stable under the conditions of present studies. The response of the optode towards U(VI) was found to be highly reproducible in real effluent $Mg(NO_3)_2$ sample obtained from uranium extraction process.

Acknowledgement

J.M. Joshi is thankful to Shri M.R.K. Shenoi, Head, Laboratory Services Section, Chemical Engineering Division, Bhabha Atomic Research Centre, Trombay, Mumbai, for his keen interest in the present work.

References

[1] D.C. Kocher, Health Phys. 57 (1989) 9.
[2] S.J. Markich, Sci. World J. 2 (2002) 707.
[3] (a) WHO, Guidelines for drinking water quality, in: Health Criteria and Other Supportive Information, Addendum to vol. 2, 2nd ed., WHO/EOS/98.1, Geneva, 1998, p. 283;
(b) WHO, Guidelines for Drinking Water Quality, 3rd ed., WHO, 2003.
[4] Z. Toshova, K. Stoyanova, L. Nikolchev, J. Environ. Radioact. 72 (2004) 47.
[5] E. Bakker, P. Bühlmann, E. Pretsch, Chem. Rev. 97 (1997) 3083.
[6] E. Pretsch, P. Bühlmann, E. Bakker, Chem. Rev. 98 (1998) 1593.
[7] O.S. Wolfbeis, Anal. Chem. 78 (2006) 3859.
[8] Y.M. Scindia, A.K. Pandey, A.V.R. Reddy, S.B. Manohar, Anal. Chim. Acta 515 (2004) 311, and references therein.
[9] S. Sodaye, R. Tripathi, A.K. Pandey, A.V.R. Reddy, Anal. Chim. Acta 514 (2004) 159.
[10] M. Plaschke, R. Czolk, H.J. Ache, Anal. Chim. Acta 304 (1995) 107.
[11] O.S. Murkovic, Wolfbeis, Sens. Actuators B 38–39 (1997) 246.
[12] P.T. Varineau, R. Duesing, L.E. Wangen, Appl. Spectrosc. 45 (1991) 165.
[13] G.E. Collins, Q. Lu, S. Abubeker, E. Vajs, Appl. Spectrosc. 56 (2002) 464.
[14] G.E. Collins, Q. Lu, Anal. Chim. Acta 436 (2001) 181.
[15] A. Safavi, M. Bagheri, Anal. Chim. Acta 530 (2005) 55.
[16] A. Safavi, M. Sadeghi, Anal. Chim. Acta 567 (2006) 184.
[17] J.L. Sessler, P.J. Melfi, D. Seidel, A.E.V. Gordon, D.K. Ford, P.D. Palmer, C.D. Tait, Tetrahedron 60 (2004) 11089.
[18] A. Suresh, D.K. Patre, T.G. Srinivasan, P.R. Vasudeva Rao, Spectrochim. Acta A 58 (2002) 341.
[19] S.J. Lyle, M. Tamizi, Anal. Chim. Acta 108 (1979) 267.
[20] L. Sommer, E. Šamlotová, Can. J. Chem. 66 (1988) 401.
[21] S. Abe, M. Endo, K. Ozaki, J. Radioanal. Nucl. Chem. Lett. 154 (1991) 41.
[22] W. Davies, W. Gray, Talanta 11 (1964) 1203.
[23] D.A. Johnson, T.M. Florence, Anal. Chim. Acta 53 (1971) 73.
[24] S.D. Hartenstein, Anal. Chim. Acta 228 (1990) 279.
[25] N. Rawat, P.K. Mohapatra, V.K. Manchanda, Sol. Chem. 35 (2006) 803.
[26] C. Moulin, S. Rougeault, D. Hamon, P. Mauchien, Appl. Spectrosc. 47 (1993) 2007.
[27] S. Sodaye, G. Suresh, A.K. Pandey, A. Goswami, Radiochim. Acta 94 (2006) 347.

Talanta 76 (2008) 1–8

Contents lists available at ScienceDirect

Talanta

journal homepage: www.elsevier.com/locate/talanta

Review

Analytical applications of Raman spectroscopy

Andrzej Kudelski*

Department of Chemistry, University of Warsaw, Pasteur 1, 02-093 Warsaw, Poland

ARTICLE INFO

Article history:
Received 16 November 2007
Received in revised form 26 February 2008
Accepted 29 February 2008
Available online 6 March 2008

Keywords:
Resonance Raman
Surface-enhanced Raman scattering
CARS
Tip-enhanced Raman spectroscopy
Biomedical diagnostics
DNA sequencing

ABSTRACT

During the last decade, the analytical capabilities of Raman spectroscopy have changed fundamentally. Due to the technical development, relatively cheap, portable Raman devices for onsite analysis can be now constructed. Moreover, for some molecules in special metal nano-resonators, the efficiency of Raman scattering (in so-called surface-enhanced Raman scattering—SERS) is so high, that, when using SERS-sensors, a limit of detection even of the order of 10^{-18} mol dm^{-3} can be achieved for some analytes. Therefore, dramatically increased usage of SERS spectroscopy for analysis of industrial, biological, medical and environmental samples has recently been observed. The aim of this mini-review is thus to illustrate the main analytical applications of Raman spectroscopy—especially SERS spectroscopy. We mainly focus on the applications developed within the period from 2004 up to now. Future perspectives in this field are also discussed.

Contents

1. Introduction

For many decades Raman spectroscopy has not been considered a useful analytical tool because of very low efficiency of "normal" Raman scattering. Typical total Raman scattering cross-section is *ca.* 10^{-29} cm^2 per molecule, whereas typical cross-sections for absorption in ultraviolet and infrared are *ca.* 10^{-18} and 10^{-21} cm^2 per molecule, respectively [1]. Therefore, to record conventional Raman spectra, analytical concentrations greater than 0.01 M are usually required. Moreover, Raman spectrometers constructed in the previous decades were expensive and were not suitable for onsite analysis. Both these limitations of Raman spectroscopy have been, however, overcome. By utilizing special resonators constructed from metal nano-clusters the Raman scattering cross-sections can be significantly increased, e.g., to 2×10^{-14} cm^2 per molecule [2] (i.e., about 15 orders of magnitude in comparison to the normal Raman scattering), making possible observation of Raman spectra even of a single molecule [2–4]. Raman spectrometers have significantly profited from technical development and now it is possible to construct low-cost, battery-powered, portable Raman spectrometers, which have many of the spectral capabilities of laboratory-based systems [5]. The resent spectacular improvements in the construction of Raman spectrometers are well illustrated by the mass of the prototype Raman spectrometer for next Mars missions (low mass Raman spectroscope is considered as one of the fundamental instruments in the future NASA and

* Tel.: +48 228220211x278; fax: +48 228225996.
E-mail address: akudel@chem.uw.edu.pl.

0039-9140/$ – see front matter © 2008 Elsevier B.V. All rights reserved.
doi:10.1016/j.talanta.2008.02.042

ESA Mars missions [6–8]). The mass of this shock-resistant device is only 1.5 kg [9].

All these above-mentioned methodical and technical developments caused that, in the last few years, one observes dramatically increased usage of Raman spectroscopy for the analytical purposes. In this article some analytical applications of Raman spectroscopy are reviewed, with special emphasis on the resent developments. We mainly focus on analytical applications of resonator-enhanced Raman scattering (for the historical reasons called surface-enhanced Raman scattering—SERS). Future perspectives in this field, i.e., Raman analysis with nanometers spatial resolution achieved by the coupling of the Raman spectroscope with the STM or AFM device, are also discussed.

2. Raman scattering

When monochromatic radiation of frequency ν_0 is incident on a sample, some of the radiation is scattered. In the scattered radiation, in addition to radiation with the same frequency as the incident radiation (elastically scattered radiation—Rayleigh radiation), radiation of different frequencies (inelastically scattered radiation—Raman radiation) is also observed. The basic idea of the inelastic scattering may be described as follows: the interaction of the photon of energy $h\nu_0$ with the molecule may lead to the annihilation (virtual absorption) of the initial photon and simultaneous creation of a new photon of energy $h(\nu_0 - \nu_M)$, accompanied by the transition of the molecule on which scattering occurs, to a state with energy higher by $h\nu_M$ (usually an excited vibrational state). When the molecule is initially in the excited vibrational state, it is also possible to observe scattering that leads to the annihilation of the initial photon of energy $h\nu_0$ and creation of a new photon of energy $h(\nu_0 + \nu_M)$ accompanied by the transition of the molecule, on which scattering occurs, to a state with energy lower by $h\nu_M$. Since molecular energy is quantized, losses of photon energy are also quantized (similarly like quantization of energy of photons absorbed during recording of the infrared (IR) spectrum). Briefly put, the information included in the vibrational Raman spectrum is analogous to the information included in the IR spectrum, however, due to different selections rules, both spectra are often significantly different in details. In practical analytical applications scattered radiation with frequencies lower than the incident frequency is usually analyzed. However, in some analytical Raman measurements (e.g., in experiments utilizing coherent anti-Stokes Raman scattering—CARS) the radiation with frequencies higher than the incident frequency is analyzed. For detailed description of the theory of Raman scattering see Ref. [10].

2.1. Analytical applications of "normal" Raman scattering

Analogously to spectra obtained with other vibrational techniques (e.g., infrared absorption, vibrationally resonant sum frequency generation, high resolution electron energy loss spectroscopy), Raman spectrum can be treated as a compound's fingerprint. This makes Raman spectroscopy a useful technique for the identification of many compounds. For example, de Veij et al. have recently showed that Raman spectroscopy is a promising and reliable method for fast detection and identification of some counterfeit medicines [11]. Since many blister package materials provide suitable spectral window for both excitation and scattering radiations (both often lie in a comparably narrow spectral interval, e.g., for the excitation radiation of 514.5 nm, the scattered radiation with the Raman shift of 1600 cm^{-1} has the wavelength of 560.7 nm) the tablet components can be often analyzed through the packaging [11]. This is different from IR, where the absorption of both packaging and sample stretch over the same spectral range. As other example of pharmaceutical/criminological Raman analysis it is worth to note very quick (lasting only a few seconds) identification of cocaine, heroin, ecstasy and various other phenethylamine ecstasy analogues [12–14]. Bell et al. have showed that from Raman composition profiling of ecstasy tablets it may be possible to distinguish the tablets prepared by various major manufacturers, and hence, to track the illegal distribution of ecstasy [13].

In the field of research dealing with cultural heritage, each art object is usually unique, and sampling is generally prohibited even if it requires detachment of only minute specimens with dimensions of the order of few hundreds of microns (or less). Raman spectroscopy does not usually require any sample preparation (it is in principle a non-destructive technique), and therefore, Raman spectroscopy has become an important tool in the surface analysis of works of art (especially identification of used pigments). Moreover, when Raman spectrometer is combined with the microscope, analysis is spatially refined, and by carrying out Raman measurements at various places of the sample (mapping the sample) it is possible to obtain detailed information regarding the distribution of specific compounds. The study and characterization of pigments on art objects may provide information regarding the technique implemented in their construction, their authentication and possible restoration undertaken in earlier times, as well as it may help to designate appropriate procedures for future restoration and conservation [15]. In the last few years many reports have been published dealing with Raman spectroscopy analysis of pigments in ancient manuscripts [16], paintings [17] including prehistoric rock paintings [18], ancient pottery [17] and ancient glass [19]. In such studies, to facilitate measurements of spectra from various places of the sample (it would be rather difficult to get a large object under a conventional Raman microscope), one can use small probe head linked by the optical fibers to the portable micro-Raman apparatus [20]. Possibility of easy separation of the probe head from the main part of the spectroscope is unique for devices utilizing visible radiations (as Raman spectroscopes with VIS excitation sources) since waveguides for other parts of the electromagnetic spectrum are not so simple and flexible.

Of great practical importance is Raman non-destructive analysis of various biological samples [21,22]. For example, Reitzenstein et al. showed that on the basis of the measured Raman spectra it is possible to distinguish rapeseed (*Brassica napus*) seedlings from the classic line 'Drakkar' from the new genetically modified line 't-mix' [21]. Moreover, the seedlings were not affected from the Raman spectroscopic measurements and it was possible to cultivate each of them afterwards [21]. Using Raman mapping technique it is also possible to determine detailed information regarding the distribution of specific compounds, e.g., secondary metabolites [22–24]. Fig. 1 shows distribution of polyacetylenes and carotenoids in the chamomile (*Chamomilla recutita*) inflorescence obtained on the basis of the Raman measurements (for details see the Figure caption) [23]. It is worth to note that water, which content in the biological samples is usually above 50%, is a weak Raman scatterer and usually does not interfere with Raman measurements (in contrary to the IR absorption measurements).

Another important biological applications of Raman spectroscopy are distinguishing cancerous from normal tissue and detection of precancerous cells. For example, Kast et al. showed that Raman spectroscopy can differentiate malignant tumors from normal breast tissue and can detect early neoplastic changes in a mouse model [25]. Jess et al. showed that Raman spectroscopy can become a useful tool in the early detection of cells exposed to human papillomavirus (HPV) [26]. HPV (particularly HPV16) infection can lead to the development of uterine cervical neoplasia, and therefore, the identification in clinical samples of the effects of HPV infection may have clinical value [26].

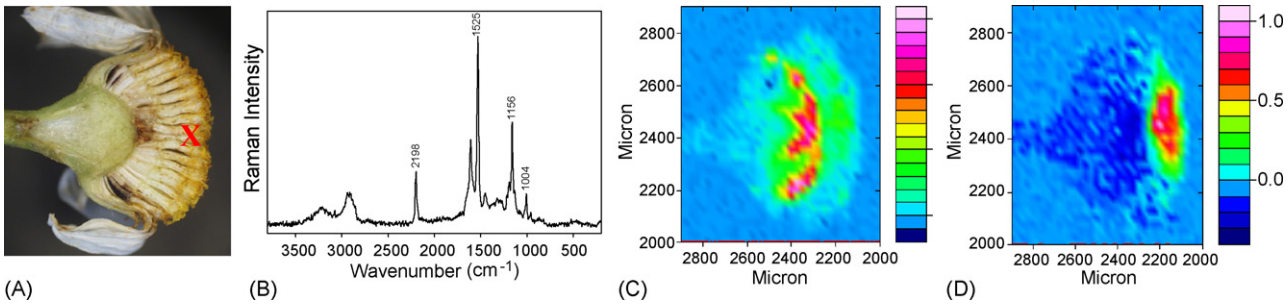

Fig. 1. Microscopic image of chamomile (*Chamomilla recutita*) inflorescence (A), FT-Raman spectrum (B) (a cross in the image (A) shows where the Raman spectrum was measured) and Raman mapping showing the distribution of polyacetylenes (C) and carotenoids (D). The relative concentration of polyacetylenes was determined according to the intensity of the acetylene band at 2198 cm^{-1} whereas carotenoids were identified based on the signal at 1525 cm^{-1} ([23], Reproduced by permission of The Royal Society of Chemistry).

When the sample is transparent (or semi-transparent) to the excitation and scattered radiation, it is possible to analyze parts of the sample which are not exposed at the sample's surface [19,27,28]. The possibility of the non-destructive subsurface analysis is often a significant advantage of the Raman spectroscopy, since in many standard surface analysis techniques the signal is collected only from a few outermost atomic layers of the sample. As examples of Raman subsurface measurements one can mention: identification of counterfeit pharmaceutical tablets and capsules through different types of packaging using of so-called spatially offset Raman spectroscopy (SORS) [27] and analysis with high spatial resolution of single microcrystallites enclosed in the glass matrix [19].

2.2. Analytical applications of resonance Raman scattering

About 50 years ago Shorygin realized that if one tunes the frequency of the excitation radiation to the absorption band of an analyte, the intensity of measured Raman spectrum increases significantly (e.g., by a factor of 10^6) [29]. Therefore, resonance Raman spectra can be recorded for sample concentration as low as 10^{-8} M. The electronic excitation increases the Raman scattering probability of vibrational normal modes in the spatial vicinity of the chromophore, hence enhancing these signals in the resulting spectrum. Resonance Raman scattering has been extensively exploited in the analysis of various chromophoric biological samples (e.g., enzymes). In many cases, one can tune the excitation radiation to the specific absorption of the active part of an enzyme, and hence, from resonance Raman measurements one can selectively determine its structure [30–32]. Moreover, using different excitation radiations one can obtain spectra dominated by the vibrations localized on various parts of studied biomolecules [32].

The resonance Raman spectroscopy is an exceptionally selective analytical tool (effectively interfering species must both absorb excitation radiation and have Raman band with the Raman shift similar to the analyte) allowing for analysis of very complex mixtures. For example, Ward et al. determined the hemoglobin oxygen saturation in living tissue by the measurement of the ratio of intensities of resonance Raman bands due to the oxygenated and de-oxygenated hemoglobin [33].

It is worth to note that now the excitation radiation is commercially available in a wide range (from near IR to far UV), and by proper tuning of the experimental conditions strong resonance Raman spectra may be obtained for a wide range of compounds, even for species transparent in the visible part of the spectrum. Using 204 and 229 nm excitation radiation Ianoul et al. recorded strong resonance Raman spectra of nitrite and nitrate [34]. Further investigations showed that resonance Raman spectroscopy can be applied for on-line monitoring of NO_2^-/NO_3^- in wastewater (using such excitation radiation practically eliminates fluorescence from other species present in the wastewater) with the detection limits below 200 ppb for both NO_2^- and NO_3^- [34].

As mentioned above, Raman spectrum can be treated as a compound's fingerprint. Therefore, Raman spectroscopy can be also used for qualitative analysis of atypical samples. When resonance Raman spectrum is obtained for an analyte, on the basis of measured Raman spectrum it is possible to identify analyte at a very low concentration (for the identification purposes Raman spectrum is significantly better than the UV–vis absorption spectrum). An interesting example of possible application of resonance Raman spectroscopy for the analysis of atypical samples is on site search for photopigments from possible Mars habitats in the future NASA and ESA Mars missions (photosynthetic organisms must contain a compound adsorbing solar radiation) [6–8]. Antarctic trials of a miniature Raman spectrometer showed that resonance Raman scattering is ideal for detection of productive and protective pigments of photosynthetic organisms [6–8]. Moreover, even if searching for traces of pigments failed, "normal" Raman spectroscopy should allow for the identification of Martian minerals [9], and therefore, low mass Raman spectroscope is considered as one of the fundamental instruments in the future NASA and ESA Mars missions [6–8].

3. Nonlinear Raman techniques

When a sample is illuminated with radiation which has an adequately large irradiance some nonlinear optical processes may appear. For example, when the incident radiation has consisted of one monochromatic wave of frequency ω_0, the scattered radiation may include additional frequencies of the type $2\omega_0$ (hyper-Rayleigh radiation), $2\omega_0 \pm \omega_M$ (hyper-Raman radiation), $3\omega_0$ (second hyper-Rayleigh radiation), $3\omega_0 \pm \omega_M$ (second hyper-Raman radiation), etc. Analytical applications of such nonlinear Raman techniques (for example, possible analytical application of hyper-Raman scattering see Ref. [35]) are still rare and have been slow in coming, due largely to the complexity of the instrumentation. Nonlinear Raman scattering can be also realized when the incident radiation consists of two or more overlapping coherent monochromatic beams, as in the case of coherent anti-Stokes Raman scattering (CARS). CARS has become the most extensively used nonlinear Raman technique. In a typical CARS experiment, the incident radiation consists of two overlapping coherent monochromatic beams of frequencies ω_1 and ω_2, with $\omega_1 > \omega_2$. When $\omega_1 - \omega_2 = \omega_M$, where ω_M is a molecular frequency that can be observed in "normal" Raman scattering, the intensity of the scattering of the radiation with the frequency $2\omega_1 - \omega_2$ increases dramatically. In the resonance condition $\omega_1 - \omega_2 = \omega_M$, the produced frequency $\omega_s = 2\omega_1 - \omega_2 = \omega_1 + (\omega_1 - \omega_2) = \omega_1 + \omega_M$ has the form of an anti-

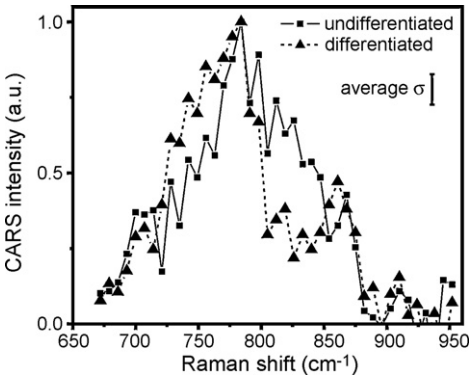

Fig. 2. Averaged CARS intensities over 675–950 cm^{-1} Raman shift region for undifferentiated and differentiated mouse embryonic stem cells. Each point represents the average intensity of six measurements, each of which was normalized to the intensity of the 788 cm^{-1} (DNA) band; the vertical bar in the legend shows the magnitude of the standard deviation (σ) averaged over all points. Reprinted with permission from Ref. [37], Copyright (2007) American Chemical Society.

Stokes Raman frequency relative to ω_1. CARS, however, differs in many important respects from the "normal" Raman process considered in Section 2. CARS radiation forms coherent, highly directional beam with small divergence.

CARS spectroscopy has two important advantages: strong signal level and high spatial resolution (laser pulses are tightly focused into a sample and a signal is generated in a small excitation volume <1 μm^3) [36]. A recent application of CARS spectroscopy, which well illustrates its advantages over conventional Raman techniques, is non-destructive analysis of embryonic stem cells within a growing culture [37]. CARS cell analysis has been developed by Konorov et al. and is based on the measurement of CARS signals due to some specific molecular vibrations (mainly due to the vibrations giving "normal" Raman bands at 788 and 811 cm^{-1} assigned to DNA- and RNA-specific backbone vibrations, respectively, as well as several protein vibrations), which are believed to be spectroscopic markers indicating the differentiated *vs.* undifferentiated states of studied cells (see Fig. 2) [37]. CARS permits imaging with sub-cellular resolution (see Fig. 3) for natural concentration of analyzed compounds (nuclear acids, proteins), potentially offering a method by which chemical changes accompanying the early stages of differentiation

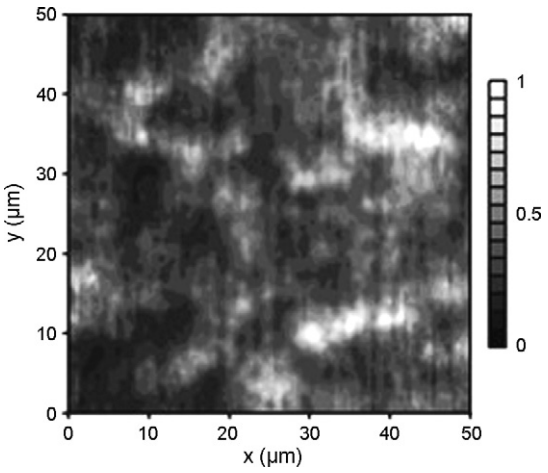

Fig. 3. CARS signal distribution over a colony of differentiating mouse embryonic stem cells at 800 cm^{-1} in femtosecond mode (150 cm^{-1} resolution) showing regions rich in nucleic acid and protein. The most intense regions were re-measured in picosecond mode, scanning from 675 to 950 cm^{-1}. Reprinted with permission from Ref. [37], Copyright (2007) American Chemical Society.

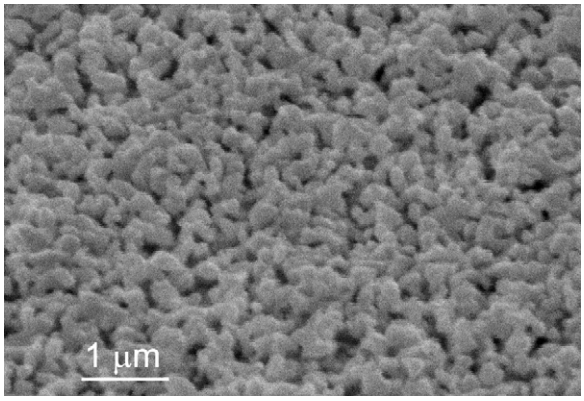

Fig. 4. Scanning electron microscope micrograph of the electrochemically roughened SERS-active silver substrate. The roughening was carried out by three successive positive–negative cycles in a 0.1 M KCl aqueous solution. (Reproduced with permission from Ref. [48].)

may be associated with certain intracellular compartments (e.g., nucleus, cytoplasm, membranes). Another interesting example of CARS analysis is non-invasive determination of the blood oxygenation (precisely oxygenation state of hemoglobin) in individual vessels inside bulk tissue [38]. Achieved 3D imaging capability and tolerance to scattering was sufficient for practical biomedical applications [38].

Beadie et al. showed that CARS measurements may be used for detection of bacterial spores of anthrax [39]. As in other Raman-based methods of anthrax detection (see Section 4.1), the analysis is based on the detection of dipicolinic acid (DPA), since calcium salt of DPA is unique to the bacterial spores and is a major component of spores—up to 15% by weight [39].

Majority of analytical applications of Raman spectroscopy is based on the measurement of Raman vibrational spectra. However, in some cases, also Raman rotational and electronic transitions may be used. For example, Seeger et al. reported using CARS rotational spectra for the determination of relative concentrations of O_2/N_2 and CH_4/N_2 in a fuel-rich, CH_4/air flames [40].

4. Surface-enhanced Raman scattering (SERS)

Large increase of the Raman cross-section of an analyte (up to 15 orders of magnitude in comparison to the "normal" Raman scattering) can be observed in so-called surface-enhanced Raman scattering (SERS) measurements. SERS spectra are measured for molecules placed in resonators formed from some (e.g., Ag, Au, Cu) metal nano-clusters (such resonators can be found, for example, in metal sols or at electrochemically roughened metal electrodes). Increase of Raman intensity due to the SERS effect is mainly a result of the enhancement of the electric field at the metal surface. However, a part of the SERS enhancement is due to the so-called charge transfer enhancement that resembles the ordinary resonance Raman process occurring in metal–ligand complexes. For more detailed discussion of the SERS phenomena the reader is referred to Refs. [1,41–43].

Metal substrates for SERS measurements must be nanostructured. Fig. 4 shows the scanning electron microscope picture of the silver surface after the electrochemical roughening (such substrates are among the most widely used in SERS measurements). In the earliest applications of SERS spectroscopy, electrochemically roughened metal electrodes (see Fig. 4) or metal sols have been usually used. It is worth to note that these highly active SERS substrates can be obtained at a cost of a few cents apiece using equipment costing about 100–1000 euros. In the last decade, in order

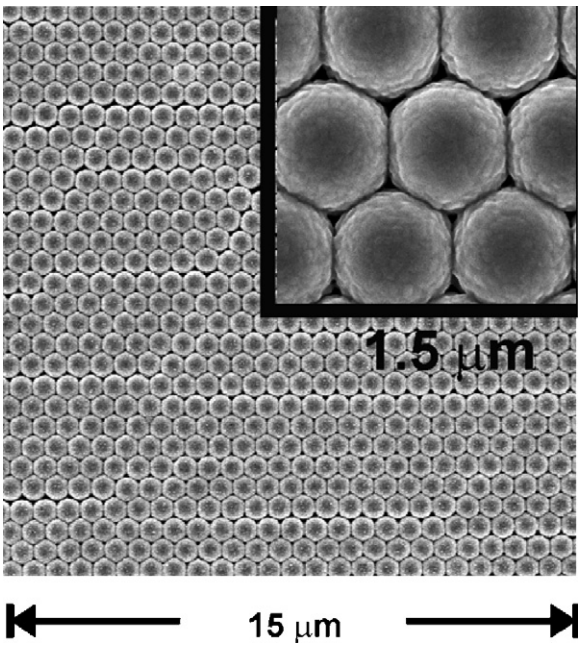

Fig. 5. Scanning electron microscope images of alumina-modified silver film-over-nanosphere (AgFON) substrate. The substrate was obtained by the vapor deposition of the 200 nm layer of silver on the monolayer of surfactant-free white carboxyl-functionalized polystyrene latex nanospheres with diameters of 590 nm. Then, the layer of alumina with the average thickness of 2 Å was deposited. Reprinted with permission from Ref. [44], Copyright (2006) American Chemical Society.

to improve stability and reproducibility of SERS substrates and to increase the achievable SERS enhancement factors, more shape-controlled and shape-reproducible metallic nano-resonators on solids substrates have been introduced (e.g.: metal film-over-nanosphere substrates, metal-coated alumina nanoparticles) [44,45]. Fig. 5 shows scanning electron microscope images of alumina-modified silver film-over-nanosphere (AgFON) substrate [44]. The substrate was obtained by the vapor deposition of the 200 nm layer of silver on the monolayer of surfactant-free white carboxyl-functionalized polystyrene latex nanospheres with diameters of 590 nm [44]. Then, to increase temporal stability of the substrate (at least to about 9 months) the layer of alumina with the average thickness of 2 Å was deposited [44]. The overview of many commonly used SERS substrates can be found in Ref. [45].

4.1. SERS analysis on substrates containing large number of active areas

As mentioned in the introduction, the efficiency of the generation of SERS signal is, in same cases, so high, that it is possible to observe Raman spectrum even of a single molecule (moreover, such measurements can be carried out in a dense media as water or methanol) [2–4]. Since, for a large system, single analyte molecule would seldom adsorb at the highly active part of the resonator, "simple" single molecule SERS spectroscopy (in contrary to TERS—see the Section 4.2) cannot be treated as a reliable single molecule analytical technique (SERS signal from a single molecule reveals strong temporal fluctuations and is not reproducible). However, for some analytes, even when only about 50–100 analytes molecules are contained in the sample, reproducible SERS signal can be measured. Therefore, SERS is one of the most sensitive analytical tools with the limit of detection for some analytes of the order of 10^{-18} mol dm^{-3} [46].

The simplest SERS analysis is based on the measurement of the Raman signal of an analyte. For example, Vo-Dinh and coworkers showed that anthraquinone dyes can be detected by the deposition of an analyte solution on the SERS-active metal substrate and the successive recording of the SERS spectrum of adsorbed species [47]. The limit of detection of alizarin (one of the studied dyes) was estimated to be 7×10^{-15} g [47]. Instead of deposition of an analyte on the SERS-active substrate, metal clusters can be deposited on the analyzed sample. Such approach has been applied by Leona et al. to detect dyes in textiles [48]. In the first step, silver clusters were deposited on the analyzed single fiber (Leona et al. analyzed 1 mm by approximately 50 μm wool fiber from a sixteenth-century Dutch tapestry [48]). After this procedure Leona et al. were able to record SERS spectra with high signal-to-noise ratio, which allowed to recognize clearly, in the obtained spectra, the bands characteristic to alizarine, and hence, to prove the presence of this dye in the analyzed sample [48]. Since measured SERS spectra are very characteristic of scattering molecules, SERS analysis is recommended for atypical samples, for which unexpected species present in the sample could seriously interfere the result of analysis carried out with other methods, e.g., UV/visible spectroscopy or electrochemical techniques.

An interesting example of the analytical application of SERS spectroscopy is the analysis of complex mixtures by the measurement of many SERS spectra from only a few semi-randomly chosen molecules in the sample. This technique illustrates well both the extremely low detection limit of SERS measurements and the fingerprint-like character of recorded spectra. "A few molecules" SERS measurements can be applied to the analysis of mixtures without separation of the individual compounds, even when the contribution from the individual compounds could be hardly identified in the averaged spectrum of the analyzed sample [49–52]. The measurement of SERS spectra dominated by the contribution from only "a few molecules" randomly chosen in the sample can be often easily realized due to the large differences in the enhancement factors at different places of the SERS-active substrate (e.g., Shalaev and coworkers presented calculations according to which the local SERS electromagnetic enhancement differs more than 10^{10} [53]). Very large SERS enhancements are accomplished with a rather high spatial confinement. In other words, when SERS substrate is covered with the monolayer of the analyte, only a very small part of adsorbed molecules (e.g., 0.01% [54]) effectively contribute to the measured SERS signal (this statement is not valid for a low coverage of the analyte, since adsorbates often preferentially occupy highly SERS-active parts of the substrate [55]). Therefore, even when in the focal area of the Raman microscope (minimal focal area is of the order of 1 μm^2) there is a very large number of analyte molecules, in many cases, when short accumulation time is used, it is possible to measure SERS spectrum dominated by the contribution from only a few semi-randomly chosen molecules (clusters) of the analyte [49–52]. As mentioned above, this opens possibility for easy identification of various species present in the complex mixture, without its previous decomposition on fractions. For example, on the basis of the analysis of many SERS spectra dominated by the contribution from only a few molecules of the analyte, Itoh et al. identified in the products of the photo-chemical carbonization of 10,12-pentacosadiynoic acid the following carbon species: polyenes, graphite sheets with various sizes, carbon nanotubes and fullerenes [51]. Recently, we have used this method to analyze the composition of the carbon material formed on the surface of the copper catalyst during the electrochemical reduction of CO_2 [52]. Fig. 6 illustrates an example differences in the SERS spectra measured for various small groups of carbon clusters (in the spectrum measured from a large number of clusters any narrow Raman band could not be identified). By the analysis of these spectra, we identified in the analyzed sample large graphite-like rings and polyenes with various lengths [52].

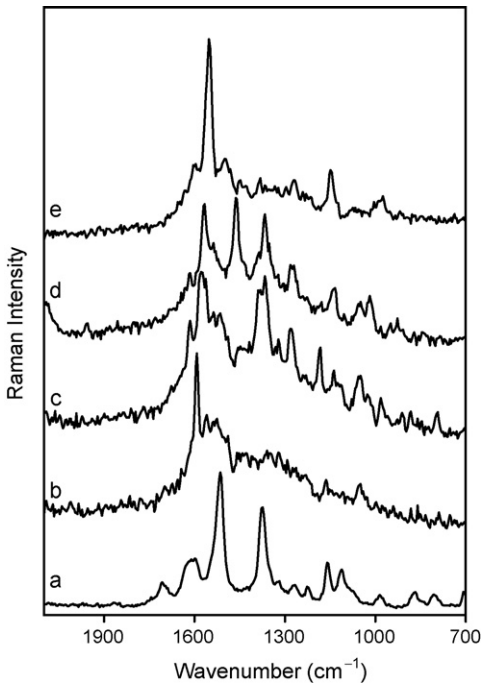

Fig. 6. Five SERS spectra of the carbon materials deposited on the copper-modified silver electrode. Raman spectra have been recorded with Raman spectrometer equipped with an optical microscope with a 50 × long distance objective (the focal area of the Raman microscope was a few μm^2). Accumulation time 1 s. Excitation radiation λ_{exc} = 514.5 nm. Carbon material was formed on the surface of copper-modified silver electrode during the electrochemical reduction of CO_2 in a 0.1 M $KHCO_3$ aqueous solution saturated with CO_2 at p_{CO2} = 1 bar (the electrode potential was −2.1 V *vs.* Ag/AgCl (0.1 M KCl) electrode).

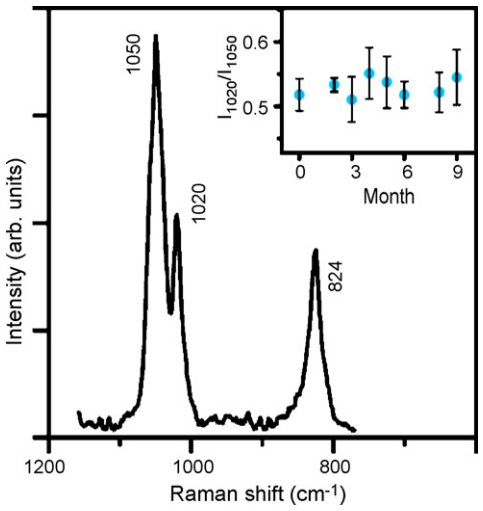

Fig. 7. SERS spectrum of 3.0×10^{-14} M *Bacillus subtilis* spores (3.6×10^3 spores in 0.2 μL of 0.02 M HNO_3) on a 9-month-old alumina-modified AgFON substrate. The inset shows the intensity ratio (I_{1020}/I_{1050}) variation with time (for substrates of different ages). Laser excitation, 785 nm; laser power, 50 mW; acquisition time, 10 s. Reprinted with permission from Ref. [44], Copyright (2006) American Chemical Society.

To facilitate adsorption of the analyte, SERS-active metal substrates (as those presented in Fig. 4) are often modified with various adlayers. For example, when metal substrate used as a SERS-sensor is hydrophobized by the covering with an alkanethiol monolayer, the detection limit of aromatic hydrocarbons in aqueous solutions is significantly decreased [56,57]. Larger increase of the selectivity and decrease of the detection limit of SERS-sensors can be achieved by covering of the SERS-active metal substrate with the monolayer of species forming specific complexes with the analyte. For example, on SERS-active substrates modified with substituted calixarenes only aromatic molecules that fit into the cavities in calixarenes are adsorbed, and therefore, contribute to the measured SERS spectrum. As a result, such molecules can be selectively detected [58]. Even when interfering molecules strongly interact with the metal substrate, proper modification of the SERS-active metal surfaces makes possible detection of molecules that have little natural binding affinity for the metal surface. An example of such sensor is, very promising from the practical point of view, glucose SERS-sensor developed by van Duyne and coworkers, which allows for a continuous, real-time, quantitative detection of glucose in the physiological range (0–25 mM) under physiological conditions (presence of interfering proteins) [59–61]. SERS glucose sensors can be probably safely implanted into the human body (the sensor will be connected to the ultra-miniature Raman spectrometer via the optical fiber), and in the near future van Duyne et al. plan to implant such sensors into the body of an animal to test in vivo glucose sensing, and to cross-calibrate SERS-sensors with the qualified hospital laboratory equipment [59]. Determination of glucose using SERS-sensors well illustrates advantages of the detection techniques based on the direct measurement of the spectrum (signal) characteristic for the analyzed compound. Numerous studies have been performed in recent years toward developing in vivo, minimally invasive, biologically compatible, and quantitative real-time glucose sensors. Among many extensively studied techniques are: electrochemical method relying on the detection of hydrogen peroxide produced by the enzymatic oxidation of glucose, fluorescence technique exploiting the reversible glucose-binding characteristics of fluorophore-labeled concanavalin A, diffraction method exploiting the binding of glucose to boronic acid embedded in a polymerized crystalline colloidal array, polarimetry method based on the rotation of polarized light caused by glucose, etc. [60]. However, all these indirect glucose detection methods seriously suffer from the presence of many interfering species in blood (for details see [60]). Therefore, if reliable and portable SERS glucose sensing will be developed and miniature and relatively cheap Raman devices will be commercially available, one can expect large market for in vivo SERS glucose sensors.

SERS analysis can be also carried out for analytes that do not (or nearly do not) give any SERS signal. For example, determination of alkali metal ions can be based on the measurement of the SERS spectrum of immobilized crown ethers that form complexes with the metal ions present in the ambient solution [62]. Carron and coworkers have showed that the average conformation of immobilized crown ethers, and hence measured SERS spectrum, changes in a regular fashion in the presence of alkali metals in the surrounding medium [62]. Moreover, the crown ether responds differently to dissimilar alkali metal ions, and therefore, for example, K^+ ions can be determined in the solution containing Li^+ ions.

Detection of various biological agents (viruses, fungi, bacteria and bacterial spores) is another possible application of SERS spectroscopy. Rapid and accurate identification of bioagents is important in order to facilitate timely and appropriate actions in the event of a biological attack. Of particular concern is detection of *Bacillus anthracis* spores, a dangerous pathogen for the disease anthrax [5,44,63]. SERS procedures for the detection of these spores are usually based on the detection of calcium dipicolinate, which exists in the protective layer of the spore and accounts for ∼10% of the spore's dry weight [5,44,63]. Zhang et al. have showed that calcium dipicolinate can be extracted from spores by the sonication in nitric acid and after that detected with SERS-sensor (Fig. 7 shows an example of measured SERS spectrum) [5]. The whole procedure took 11 min (the period of acquisition of Raman spectrum was only

a few seconds) and the achieved limit of detection is $\sim 2.6 \times 10^3$ spores (further decreased to $\sim 1.4 \times 10^3$ spores [44]), below the anthrax infectious dose of 10^4 spores [5]. It is worth to note that in the anthrax detection with the SERS spectroscopy both the limit of detection and the time of the analysis are acceptable from the practical point of view. Usually, when the anthrax determination is fast the limit of detection of bacillus spores is high, whereas techniques having low limits of detection are time-consuming (especially, the time required for the sample preparation is often long).

Interesting approach in the identification of microorganisms (bacteria, viruses) is measurement of the whole-organism SERS spectrum [64–71]. Due to the specific enhancement mechanism, SERS probe only these parts of microorganisms those are near the surface of metal clusters (usually metal clusters are not introduced into the body of the microorganism, and hence, SERS probe only its outermost parts: the cell wall of a bacterium or the shell of a virus). Since bacterial cell walls differ more between various species than the composition of bacteria's bulk, SERS spectra of bacteria exhibit greater species differentiation than their corresponding non-SERS (bulk) Raman spectra [66]. Recently, many groups have proved that the identification of the wide variety of bacteria can be based on their SERS spectra [65–71]. In other words, SERS can be considered a label-free whole-organism fingerprinting technique.

Intensively developing group of SERS-sensors are sensors used for the detection of certain DNA targets, as specific gene sequences or bacteria and viral DNA [72–75]. The first efficient SERS procedure for the DNA analysis involved the following steps: (i) replication of the DNA sample in such a way that very strong Raman scatterers (e.g., rhodamine 6G, cresyl fast violet) were bonded to the developed DNA chains; (ii) adsorption of the labeled DNA fragments on the SERS-active substrate previously modified with known DNA chains; (iii) recording of SERS spectrum [72,73]. When a labeled gene sequence finds a complementary fragment on the surface, it is bonded, and Raman signal of the dye is enhanced via the SERS mechanism. In this fashion a strong Raman signal of the label dye suggests presence of the searched gene sequence in the analyzed DNA material [72,73]. SERS DNA sequencing can be also carried out without any replication and modification of the initial DNA material [75]. Wabuyele and Vo-Dinh used plasmonics nanoprobe containing a metal nanoparticle and a stem-loop DNA molecule tagged with a Raman label [75]. In the absence of target DNA, the stem-loop configuration maintains the Raman label in proximity to the metal cluster allowing for observation of intense SERS signal. When searched DNA material is present in the surrounding medium, the stem-loop configuration is disrupted (searched DNA molecules bond to the DNA molecules attached to the metal surface), causing separation of the Raman label from the metal cluster, thus quenching the SERS signal [75]. Raman bands are relatively narrow in comparison to the spectral region that can be utilized, and therefore, Raman bands of many different dyes recorded in a single experiment can be usually easily distinguished. Thus, when different gene sequences are labeled with distinct dyes, multiple gene targets can be identified in a single SERS measurement.

4.2. Tip-enhanced Raman spectroscopy (TERS)

The spatial resolution of standard SERS measurements, as in other purely optical techniques, is restricted by the Abbe's diffraction limit to $\lambda/2$, where λ is the wavelength of the incident radiation [76]. This diffraction limit may be, however, overcome. In 2000, Zenobi and coworkers [77] and Anderson [78] showed that it is possible to couple Raman spectroscopy and scanning probe microscopy (STM or AFM), forming a new spectroscopic–microscopic tool, so-called tip-enhanced Raman spectroscopy (TERS). In TERS measurements a sharp AFM (or STM) tip made of SERS-active metal is moved towards the sample under investigation and illuminated with the laser radiation (see Fig. 8) [79]. The Raman scattering from the sample underneath the tip is enhanced. For example, Neacsu et al. experimentally achieved the tip-induced enhancement of the Raman scattering of about 5×10^9 [80]. In this way, TERS allows on recording Raman spectra with high spatial resolution (TERS lateral resolution achieved today is about 10 nm, whereas laser beam focal radius is about 500 nm [76]).

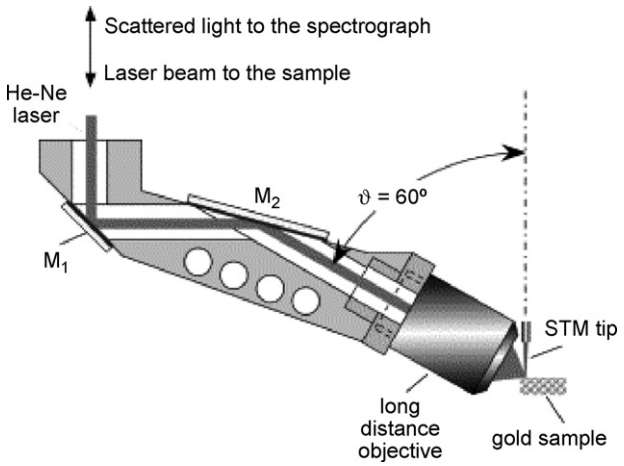

Fig. 8. Schematic diagram of the 60° configuration for TERS measurements. Reprinted with permission from Ref. [79].

TERS measurements are relatively complex, and therefore, only a few practical applications of TERS technique have been described so far. The main efforts of groups developing TERS are still focused on the improvement of TERS sensitivity—for example, TERS detection of single molecules [80,81]. From some already existing applications of TERS spectroscopy, it is worth to mention local characterization of the bacterial shell developed by Popp and coworkers [82]. Recently, this group reported Raman spectra from various parts of the shell of a single bacteria [82]. Measured spectra (significantly different for various parts of the shell) allowed for local analysis of polysaccharide and peptide components of the bacterial shell. In the near future, one can expect development of many similar analytical TERS techniques, such as, for example, identification of a single virus (or a bacteria) by determination of the chemical composition of its shell or TERS measurements of a single DNA chain allowing its direct local analysis (the first step towards this process – TERS measurements of DNA bases [83] – has been already made).

5. Conclusions

Recent developments of Raman spectroscopy have made this technique one of the most sensitive analytical tools. In contrary to the luminescence techniques, which also achieve very low detection limits, Raman measurement gives the vibrational spectrum of the analyte that can be treated as its "fingerprint" and allows for its easy identification. Since measured Raman signals are often characteristic for analyzed compounds, Raman spectroscopy allows for analysis of very complex samples, including, for example, in vivo analysis of live tissues. Non-destructive character of many Raman measurements is also of significant practical importance, especially for biological samples and objects of cultural heritage. Raman signal can be collected with a small probe head linked to the (portable) Raman apparatus by the optical fiber. Therefore, Raman analysis can be comfortably carried out at different locations of even very large objects. Moreover, it is also possible to

implant Raman sensors into the body of an animal. Wide potential field of application for various Raman techniques (especially in the medical diagnostic) suggests that the number of applications of Raman spectroscopy in analytical science will significantly increase as the technical development continues and lasers and Raman spectrometers become smaller, less expensive, easier to use and more reliable.

Acknowledgement

This work was supported financially by Ministry of Science and Higher Education (Poland) funds through the Department of Chemistry, the University of Warsaw.

References

[1] R. Aroca, Surface-Enhanced Vibrational Spectroscopy, John Wiley & Sons Ltd., Chichester, 2006.
[2] A.M. Michaels, M. Nirmal, L.E. Brus, J. Am. Chem. Soc. 121 (1999) 9932.
[3] K. Kneipp, Y. Wang, H. Kneipp, L.T. Perelman, I. Itzkan, R.R. Dasari, M.S. Feld, Phys. Rev. Lett. 78 (1997) 1667.
[4] S. Nie, S.R. Emory, Science 275 (1997) 1102.
[5] X. Zhang, M.A. Young, O. Lyandres, R.P. van Duyne, J. Am. Chem. Soc. 127 (2005) 4484.
[6] D.L. Dickensheets, D.D. Wynn-Williams, H.G.M. Edwards, C. Schoen, C. Crowder, E.M. Newton, J. Raman Spectrosc. 31 (2000) 633.
[7] D.D. Wynn-Williams, H.G.M. Edwards, Planet. Space Sci. 48 (2000) 1065.
[8] H.G.M. Edwards, D.D. Wynn-Williams, S.E. Jorge Villar, J. Raman Spectrosc. 35 (2004) 470.
[9] F.R. Perez, J. Martinez-Frias, Spectrosc. Eur. 18 (2006) 18.
[10] D.A. Long, The Raman Effect: A Unified Treatment of the Theory of Raman Scattering by Molecules, John Wiley & Sons Ltd., Chichester, 2002.
[11] M. de Veij, P. Vandenabeele, K.A. Hall, F.M. Fernandez, M.D. Green, N.J. White, A.M. Dondorp, P.N. Newton, L. Moens, J. Raman Spectrosc. 38 (2007) 181.
[12] A.G. Ryder, G.M. O'connor, T.J. Glynn, J. Forensic Sci. 44 (1999) 1013.
[13] S.E.J. Bell, L.J. Barrett, D.T. Burns, A.C. Dennis, S.J. Speers, Analyst 128 (2003) 1331.
[14] S.E.J. Bell, D.T. Burns, A.C. Dennis, L.J. Matchett, J.S. Speers, Analyst 125 (2000) 1811.
[15] K.S. Andrikopoulos, S.X. Daniilia, B. Roussel, K. Janssens, J. Raman Spectrosc. 37 (2006) 1026.
[16] D. Bersani, P.P. Lottici, F. Vignali, G. Zanichelli, J. Raman Spectrosc. 37 (2006) 1026.
[17] C. Sandalinas, S. Ruiz-Moreno, A. Lopez-Gil, J. Miralles, J. Raman Spectrosc. 37 (2006) 1146.
[18] A. Hernanz, J.M. Gavira-Vallejo, J.F. Ruiz-Lopez, J. Raman Spectrosc. 37 (2006) 1054.
[19] N. Welter, U. Schussler, W. Kiefer, J. Raman Spectrosc. 38 (2007) 113.
[20] D. Bersani, P.P. Lottici, F. Vignali, G. Zanichelli, J. Raman Spectrosc. 37 (2006) 1012.
[21] S. Reitzenstein, P. Rösch, M.A. Strehle, D. Berg, M. Baranska, H. Schulz, E. Rudloff, J. Popp, J. Raman Spectrosc. 38 (2007) 301.
[22] B. Schrader, H. Schulz, M. Baranska, G.N. Andreev, C. Lehner, J. Sawatzki, Spectrochim. Acta 61A (2005) 1395.
[23] M. Baranska, H. Schulz, P. Rösch, M.A. Strehle, J. Popp, Analyst 129 (2004) 926.
[24] M. Baranska, H. Schulz, R. Baranski, T. Nothnagel, L.P. Christensen, J. Agric. Food Chem. 53 (2005) 6565.
[25] R.E. Kast, G.K. Serhatkulu, A. Cao, A.K. Pandya, H. Dai, J.S. Thakur, V.M. Naik, R. Naik, M.D. Klein, G.W. Auner, R. Rabah, Biopolymers 89 (2008) 235.
[26] P.R.T. Jess, D.D.W. Smith, M. Mazilu, K. Dholakia, A.C. Riches, C.S. Herrington, Int. J. Cancer 121 (2007) 2723.
[27] C. Eliasson, P. Matousek, Anal. Chem. 79 (2007) 1696.
[28] P. Matousek, M.D. Morris, N. Everall, I.P. Clark, M. Towrie, E. Draper, A. Goodship, A.W. Parker, Appl. Spectrosc. 59 (2005) 1485.
[29] P.P. Shorygin, T.M. Ivanova, Doklady Akad. Nauk USSR 121 (1958) 70.
[30] C. Johannessen, P.C. White, S. Abdali, J. Phys. Chem. A 111 (2007) 7771.
[31] J. Belyea, C.M. Belyea, S. Lappi, S. Franzen, Biochemistry 45 (2006) 14275.
[32] T.G. Spiro, T.C. Strekas, J. Am. Chem. Soc. 96 (1974) 338.
[33] K.R. Ward, R.W. Barbee, P.S. Reynolds, I.P. Torres-Filho, M.H. Tiba, L. Torres, R.N. Pittman, J. Terner, Anal. Chem. 79 (2007) 1514.
[34] A. Ianoul, T. Coleman, S.A. Asher, Anal. Chem. 74 (2002) 1458.
[35] W. Leng, A.A. Yasseri, S. Sharma, Z. Li, H.Y. Woo, D. Vak, G.C. Bazan, A.M. Kelley, Anal. Chem. 78 (2006) 6279.
[36] J.R. Baena, B. Lendl, Curr. Opin. Chem. Bio. 8 (2004) 534.
[37] S.O. Konorov, C.H. Glover, J.M. Piret, J. Bryan, H.G. Schulze, M.W. Blades, R.F.B. Turner, Anal. Chem. 79 (2007) 7221.
[38] H.A. Rinia, M. Bonn, E.M. Vartiainen, C.B. Schaffer, M. Muller, J. Biomed. Opt. 11 (2006) 050502.
[39] G. Beadie, M. Bashkansky, J. Reintjes, M.O. Scully, J. Mod. Optic. 51 (2004) 2627.
[40] T. Seeger, J. Jonuscheit, M. Schenk, A. Leipertz, J. Mol. Struct. 661 (2003) 515.
[41] A. Kudelski, Vib. Spectrosc. 39 (2005) 200.
[42] Z.Q. Tian, B. Ren, D.Y. Wu, J. Phys. Chem. B 106 (2002) 9463.
[43] A. Otto, J. Raman Spectrosc. 22 (1991) 743.
[44] X. Zhang, J. Zhao, A.V. Whitney, J.E. Elam, R.P. van Duyne, J. Am. Chem. Soc. 128 (2006) 10304.
[45] T. Vo-Dinh, TRAC: Trend. Anal. Chem. 17 (1998) 557.
[46] P. Etchegoin, R.C. Maher, L.F. Cohen, H. Hartigan, R.J.C. Brown, M.J.T. Milton, J.C. Gallop, Chem. Phys. Lett. 375 (2003) 84.
[47] K. Chen, M. Leona, K.C. Vo-Dinh, F. Yan, M.B. Wabuyele, T. Vo-Dinh, J. Raman Spectrosc. 37 (2006) 520.
[48] M. Leona, J. Stenger, E. Ferloni, J. Raman Spectrosc. 37 (2006) 981.
[49] A. Kudelski, B. Pettinger, Chem. Phys. Lett. 321 (2000) 356.
[50] A. Kudelski, J. Phys. Chem. B 110 (2006) 12610.
[51] K. Itoh, I. Kudryashov, J. Yamagata, T. Nishizawa, M. Fujii, N. Osaka, J. Phys. Chem. B 109 (2005) 271.
[52] A. Kudelski, J. Solid State Electr. 12 (2008) in press, doi:10.1007/s10008-007-0487-x.
[53] V.A. Markel, V.M. Shalaev, P. Zhang, W. Huynh, L. Tay, T.L. Haslett, M. Moskovits, Phys. Rev. B 59 (1999) 10903.
[54] K. Kneipp, Y. Wang, H. Kneipp, I. Itzkan, R.R. Dasari, M.S. Feld, Phys. Rev. Lett. 76 (1996) 2444.
[55] A. Kudelski, Chem. Phys. Lett. 414 (2005) 271.
[56] K.T. Carron, B.J. Kennedy, Anal. Chem. 67 (1995) 3353.
[57] B.J. Kennedy, R. Milofsky, K.T. Carron, Anal. Chem. 69 (1997) 4708.
[58] W. Hill, B. Wehling, C.G. Gibbs, C.D. Gutsche, D. Klockow, Anal. Chem. 67 (1995) 3187.
[59] O. Lyandres, N.C. Shah, C.R. Yonzon, J.T. Walsh Jr., M.R. Glucksberg, R.P. van Duyne, Anal. Chem. 77 (2005) 6134.
[60] C.R. Yonzon, C.L. Haynes, X. Zhang, J.T. Walsh Jr., R.P. van Duyne, Anal. Chem. 76 (2004) 78.
[61] C.L. Haynes, C.R. Yonzon, X. Zhang, R.P. van Duyne, J. Raman Spectrosc. 36 (2005) 471.
[62] J.B. Heyns, L.M. Sears, R.C. Corcoran, K.T. Carron, Anal. Chem. 66 (1994) 1572.
[63] S.E.J. Bell, J.N. Mackle, N.M.S. Sirimuthu, Analyst 130 (2005) 545.
[64] V.P. Drachev, V.M. Shalaev, Topics Appl. Phys. 103 (2006) 351.
[65] R. Jarvis, S. Clarke, R. Goodacre, Topics Appl. Phys. 103 (2006) 397.
[66] W.R. Premasiri, D.T. Moir, M.S. Klempner, N. Krieger, G. Jones, L.D. Ziegler, J. Phys. Chem. B 109 (2005) 312.
[67] R.M. Jarvis, R. Goodacre, Anal. Chem. 76 (2004) 40.
[68] M. Harz, P. Rosch, K.D. Peschke, O. Ronneberger, H. Burkhardt, J. Popp, Analyst 130 (2005) 1543.
[69] R.M. Jarvis, A. Brooker, R. Goodacre, Anal. Chem. 76 (2004) 5198.
[70] P. Rosch, M. Harz, M. Schmitt, K. Peschke, O. Ronneberger, H. Burkhardt, H. Motzkus, M. Lankers, S. Hofer, H. Thiele, J. Popp, Appl. Environ. Microbiol. 71 (2005) 1626.
[71] R.M. Jarvis, A. Brooker, R. Goodacre, Faraday Discuss. 132 (2006) 281.
[72] T. Vo-Dinh, K. Kouck, D.L. Stokes, Anal. Chem. 66 (1994) 1572.
[73] N.R. Isola, D.L. Stokes, T. Vo-Dinh, Anal. Chem. 70 (1998) 1352.
[74] M. Culha, D.L. Stokes, L.R. Allain, T. Vo-Dinh, Anal. Chem. 75 (2003) 6196.
[75] M.B. Wabuyele, T. Vo-Dinh, Anal. Chem. 77 (2005) 7810.
[76] B. Pettinger, Topics Appl. Phys. 103 (2006) 217.
[77] R.M. Stockle, Y.D. Suh, V. Deckert, R. Zenobi, Chem. Phys. Lett. 318 (2000) 131.
[78] M.S. Anderson, Appl. Phys. Lett. 76 (2000) 3130.
[79] B. Pettinger, G. Picardi, R. Schuster, G. Ertl, J. Electroanal. Chem. 554 (2003) 293.
[80] C.C. Neacsu, J. Dreyer, N. Behr, M.B. Raschke, Phys. Rev. B 73 (2006) 193406.
[81] W. Zhang, B.S. Yeo, T. Schmid, R. Zenobi, J. Phys. Chem. C 111 (2007) 1733.
[82] U. Neugebauer, U. Schmid, K. Baumann, W. Ziebuhr, S. Kozitskaya, V. Deckert, M. Schmitt, J. Popp, Chem. Phys. Chem. 8 (2007) 124.
[83] A. Rasmussen, V. Deckert, J. Raman Spectrosc. 37 (2006) 311.

Talanta 76 (2008) 54–59

Contents lists available at ScienceDirect

Talanta

journal homepage: www.elsevier.com/locate/talanta

Mechanically immobilized nickel aquapentacyanoferrate modified electrode as an amperometric sensor for the determination of BHA

S. Senthil Kumar, S. Sriman Narayanan*

Department of Analytical Chemistry, School of Chemical Sciences, University of Madras, Guindy Campus, Chennai 600025, India

ARTICLE INFO

Article history:
Received 30 November 2007
Received in revised form 31 January 2008
Accepted 7 February 2008
Available online 15 February 2008

Keywords:
Nickel aquapentacyanoferrate
Mechanical immobilization
Electrocatalytic oxidation
Butylated hydroxy anisole
Cyclic voltammetry

ABSTRACT

Nickel aquapentacyanoferrate (NAPCF), a novel transition metal complex has been prepared and its ability to act as an electrocatalyst for BHA oxidation has been demonstrated. The cyclic voltammetric behaviour of the NAPCF modified electrode prepared by mechanical immobilization on the graphite electrode was well defined. A pair of redox peaks corresponding to the electrochemical behaviour of the NAPCF was observed at 0.35 V and 0.31 V, corresponding to the anodic and cathodic peaks respectively, with a formal potential of 0.33 V. The NAPCF modified electrode favoured electrocatalytic oxidation of BHA to occur at a greatly minimized overpotential of 0.48 V. Experiments were performed to characterize the electrode as an amperometric sensor for the determination of BHA. The anodic peak current was linearly related to BHA concentration in the range of 6.24×10^{-7} M to 2.19×10^{-4} M with a detection limit of 2.49×10^{-7} M and a correlation coefficient of 0.9979. Amperometry in stirred solution exhibited quick and sensitive response to BHA, showing the possible application of the modified electrode in flow system analysis. The modified electrode retained its initial response for more than 2 months when stored in supporting electrolyte, owing to the chemical and mechanical stability of the NAPCF mediator. This modified electrode was also quite effective in the determination of BHA in commercial samples.

1. Introduction

Antioxidant compounds play a vital role in many biological processes where the free radicals are present [1]. They are widely used in the food and pharmaceutical industries in order to prevent the decomposition of organic compounds present in the prepared products [2]. They are either used alone or together in commercial mixtures as additives. Among the artificial antioxidants used, butylated hydroxy anisole (BHA) is a commonly used preservative with broad biological activities, including protection against acute toxicity of chemicals, modulation of macromolecule synthesis and immune response, and for its potential tumor-promoting activities. Also, BHA is an effective chemopreventive agent [3]. Recently, it has been found that these artificial phenolic antioxidants may cause a loss of nourishment, and even produce toxic effects [4]. In many countries, the use of BHA is limited and consequently the analytical control of BHA in food samples is of great significance. Current analytical methods for the determination of BHA such as spectrophotometry [5], spectroflourometry [6], gas chromatography [7], liquid chromatography [8] and micellar electrokinetic chromatography [9] are highly sensitive and reliable. But they are accompanied with the drawbacks such as expensiveness, complicated procedures, time consuming and non-suitability in field use. Therefore, easy and fast analytical tools are the pressing need to effectively determine BHA in different samples.

Electrochemical sensors present promising alternative to classical approaches due to their relatively low cost of operation, potential of miniaturization, rapid and sensitive detection procedures suitable for faster analysis [10,11]. Amperometric detection methods are one among the most commonly employed. Unfortunately, because of the large overpotential required for BHA oxidation at conventional electrodes, it is not well suited for quantitation via conventional electrochemical approaches. One promising approach for minimizing overvoltage effects and facilitating the determination is through the use of an electrocatalytic process at chemically modified electrodes. Electrocatalysis involves modifying the overall rates of electrochemical reactions so that selectivity, yield and efficiency are maximized.

The chemical modification of inert substrate electrodes with redox active thin films offers significant advantages in the design and development of electrochemical sensors. In operation, the redox active sites shuttle electrons between the analyte and the electrodes with significant reduction in activation overpotential. A

* Corresponding author. Tel.: +91 44 22351269; fax: +91 44 22352494.
E-mail address: sriman55@yahoo.com (S.S. Narayanan).

0039-9140/$ – see front matter © 2008 Elsevier B.V. All rights reserved.
doi:10.1016/j.talanta.2008.02.002

further advantage of the chemically modified electrodes is that they are less prone to surface fouling and oxide formation when compared to inert substrate electrodes. A wide variety of compounds have been used as electron transfer mediators for modification of electrode surfaces [2,12–15]. Among them metal hexacyanoferrates are important classes of redox mediators showing interesting redox chemistry [16,17]. These polynuclear inorganic compounds have attracted great attention due to their potential application in variety of fields such as electrochromism [18], ion-exchange selectivity [19] and ability to mediate or catalyze electrochemical reactions [20–22]. Although there have been considerable reports on the preparation and application of various metal hexacyanoferrates and their analogues, no reports are available in the literature on metal aquapentacyanoferrates for sensor applications.

For the development of an efficient chemical sensor, good electrocatalysis, sensitivity and selectivity are the factors of great importance. Hence, the detection potential of the analytes is an important aspect in determining the selectivity of the sensor, since higher detection potentials would invite interference from other electroactive species that would alter the response signal of interest. We have reported our preliminary studies on the novel mediator, nickel aquapentacyanoferrate (NAPCF) for the electrocatalysis of several biologically and environmentally significant analytes [23]. The oxidation potential of the NAPCF modified electrode was found to be 50 mV less than the oxidation potential of a nickel hexacyanoferrate modified electrode which was fabricated exactly following the same procedure and consequently the NAPCF complex assumed significance as a better electrocatalyst than the corresponding hexacyanoferrate derivative. The key factor in the report is that the detection of these analytes occurred at a notably lower potentials compared to the bare electrode, favouring interference free determinations.

Thus, the present work demonstrates our attempt to fabricate a highly stable and sensitive sensor for BHA based on the novel mediator NAPCF. The mediator was first prepared chemically and characterized using X-ray photoelectron spectroscopy (XPS). The NAPCF modified electrode was prepared by mechanical immobilization, a technique developed by Scholz et al. [24,25]. The electrochemical characterization of the modified electrode was done using cyclic voltammetry and then the electrode was used for the electrocatalytic oxidation of BHA. Amperometric determinations were carried out to develop the modified electrode as a sensor for BHA. The practical utility of the sensor was tested by applying the sensor for the determination of BHA in commercial food samples.

2. Experimental

2.1. Chemicals and reagents

Sodium ammine pentacyanoferrate was purchased from Aldrich, USA. Butylated hydroxy anisole (BHA) was obtained from Himedia Laboratories, India. All other chemicals employed were of analytical grade and used as received. All the solutions were prepared using doubly distilled water. The stock solution of BHA was prepared freshly in 10% methanol before use. Phosphate buffer (0.05 M) was used to maintain the pH of the solution. For pH adjustment, 0.1 M HNO_3 and 0.1 M NaOH solutions were used. Solutions were deoxygenated by purging high purity nitrogen for 15 min before the commencement of experiment.

2.2. Apparatus

XPS experiments were carried out on a Physical Electronics 5600 spectrometer equipped with a concentric hemispherical analyzer using an Al Kα 945 X-ray source (15 KeV, filament current 20 mA). The samples were investigated under high vacuum conditions: 10^{-9} to 10^{-8} mbar. Electrochemical measurements were carried out on a CHI 400 A electrochemical analyzer (CH Instruments, USA) coupled to an IBM personal computer for data acquisition and processing. A three-electrode system was used, consisting of the NAPCF modified electrode as the working electrode, a platinum wire auxiliary electrode and a saturated calomel reference electrode (SCE), to which all potentials in this paper are referred. pH measurements were carried out using a Elico pH meter model LI 120.

2.3. Fabrication of the modified electrode

The fabrication of the NAPCF modified electrode has been reported already in our previous study [23]. The mediator nickel aquapentacyanoferrate ($NaNi[Fe(CN)_5H_2O]$) was prepared by mixing equimolar (20 ml of 50 mM) solutions of $NiSO_4$ and $Na_3[Fe(CN)_5H_2O]$ (obtained by dissolving $Na_3[Fe(CN)_5NH_3]$ in water at pH 4). Paraffin impregnated graphite electrodes (PIGEs) with a diameter of 6 mm were used for modification. The PIGEs were prepared as reported [24,25] by immersing the graphite rods into molten wax under vacuum until air bubble cease to evolve from the rods. After re-establishing atmospheric pressure, the graphite rods were removed before the solidification of paraffin. The PIGEs were then polished to a mirror like finish by rubbing over a finest quality of emery paper. The polished surface was then washed with methanol and rinsed thoroughly in double distilled water. The mediator was mechanically immobilized on the surface of a paraffin impregnated graphite electrode (PIGE) by pressing and uniform rubbing.

2.4. Determination of BHA in commercial samples

Three different types of packed instant cereals (purchased from local market) spiked with BHA were used for the commercial sample analysis. The extraction was done following the procedure reported earlier [26]. About 10 g of the sample was weighed, ground to a fine powder and then the sample was added with 100 mg of BHA. The spiked sample (1 g) was mixed with 10 ml of 10% methanol solution. After shaking for 20 min, this mixture was centrifuged at 500 rpm for 15 min and the supernatant was collected. The extraction was repeated thrice with 10% methanol solution. The extracts were collected together and concentrated to one third of its volume. The concentrate was then diluted with 0.1 M NaCl to the desired volume and then analyzed by the cyclic voltammetry technique using standard addition method.

3. Results and discussion

3.1. XPS characterization of the mediator

The NAPCF complex was characterized using XPS technique in order to confirm the presence of different elements and their oxidation states. Fig. 1 presents the XPS spectrum of the NAPCF complex. The peak at 710.4 eV could be assigned to Fe 2p corresponding to that of Fe(III) species [27]. No peak was observed at 708 eV showing the absence of Fe(II) species in the as synthesized NAPCF complex. The Ni 2p peak was observed at 858.2 eV confirming the presence of Ni(II) species [28]. The XPS spectrum also showed the presence of C 1s, N 1s and O 1s peaks at 282.1, 398.8 and 532.1 eV respectively [28].

3.2. Electrochemical behaviour

The electrochemical behaviour of the NAPCF modified electrode has already been reported [23]. The formal potential of the mod-

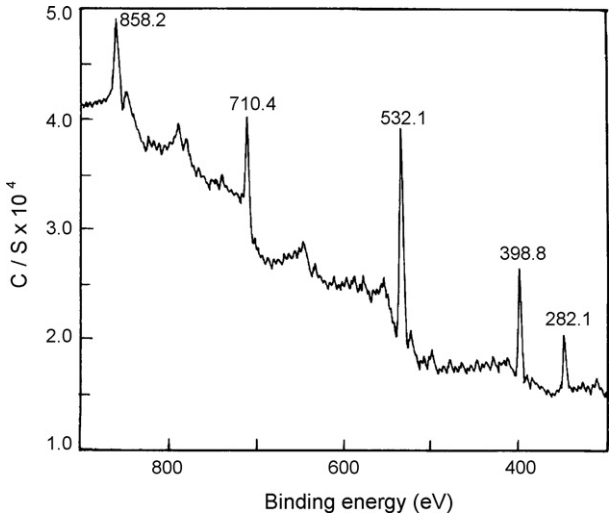

Fig. 1. XPS spectrum of the nickel aquapentacyanoferrate complex.

ified electrode was found to be 0.33 V in 0.1 M $NaNO_3$ at a scan rate of 20 mVs^{-1}. The performance of the modified electrode was tested in different supporting electrolytes. In the redox reaction of the metal hexacyanoferrates, transfer of an electron is always accompanied by the simultaneous motion of a counter cation in order to maintain the charge balance. The insertion of a counter cation into the film during reduction and its exclusion upon oxidation have been verified by Kulesza et al. [29]. Thus the size of the counter cation along with its mobility play a key role in determining the voltammetric response of the NAPCF modified electrode. Fig. 2 compares the cyclic voltammetric responses of the NAPCF modified electrode in the respective 0.1 M $LiNO_3$, $NaNO_3$, KNO_3, NH_4NO_3, $Ca(NO_3)_2$ and $Ba(NO_3)_2$ solutions. From the figure, it is clear that the lower formal potential along with higher peak currents for NAPCF modified electrode could be achieved in presence of Na^+ ions. Anions were found not to alter the electrochemical behaviour of the modified electrode and hence 0.1 M $NaNO_3$ was chosen as the suitable supporting electrolyte for further experiments.

Voltammetric response of the NAPCF modified electrode in different concentrations of $NaNO_3$ was studied. The formal potential of the modified electrode shifted towards less positive potential from 0.39 V to 0.27 V, on decreasing the concentration of $NaNO_3$ from 1.0 M to 0.01 M. The plot of logarithm of Na^+ ion concentration versus formal potential was found to be linear, with an increase of 60 mV per decade change in Na^+ concentration, which indicates that the electrode exhibited a near Nernstian behaviour in Na^+ based on the equation:

$$E = E^0 + \left(\frac{RT}{nF}\right) \ln \left[\frac{a_{NAPCF(ox)} a_{Na^+}}{a_{NAPCF(red)}}\right]$$

The shift in the formal potential is attributed to the change in the activity of Na^+ ions, which is well in agreement with the behaviour of Prussian blue and its analogues [30]. The effect of pH on the electrochemical behaviour of the NAPCF modified electrode was studied in the pH range of 2–10. The voltammetric response of the NAPCF modified electrode remained unaffected in the pH range of 2–8. A further increase in the pH resulted in the lowering of the peak current, which might be due to the hydroxylation of NAPCF in alkaline medium. Hence a neutral pH was chosen for subsequent studies.

3.3. Electrocatalytic oxidation of BHA

In order to assess the electrocatalytic ability of the NAPCF modified electrode towards the oxidation of BHA, cyclic voltammograms were recorded in the presence and absence of BHA in 0.1 M $NaNO_3$ (pH 7.0; 0.05 M phosphate buffer). As shown in Fig. 3 (curve d), upon the addition of 4.75×10^{-6} M BHA, there was a dramatic enhancement in the anodic peak current at the modified electrode whereas a slight increase in the anodic current was observed at the bare PIGE. Also, the anodic potential for oxidation of BHA at the NAPCF modified electrode is at 0.48 V, whereas at the bare electrode BHA undergoes oxidation at about 0.62 V. This decrease in overpotential and enhancement of anodic peak current for BHA oxidation indicates the strong electrocatalytic effect of the NAPCF modified electrode. The mechanism of sensing BHA at the modified electrode can be visualized from Scheme 1. The mechanically immobilized NAPCF at the electrode surface gets oxidised at its oxidation poten-

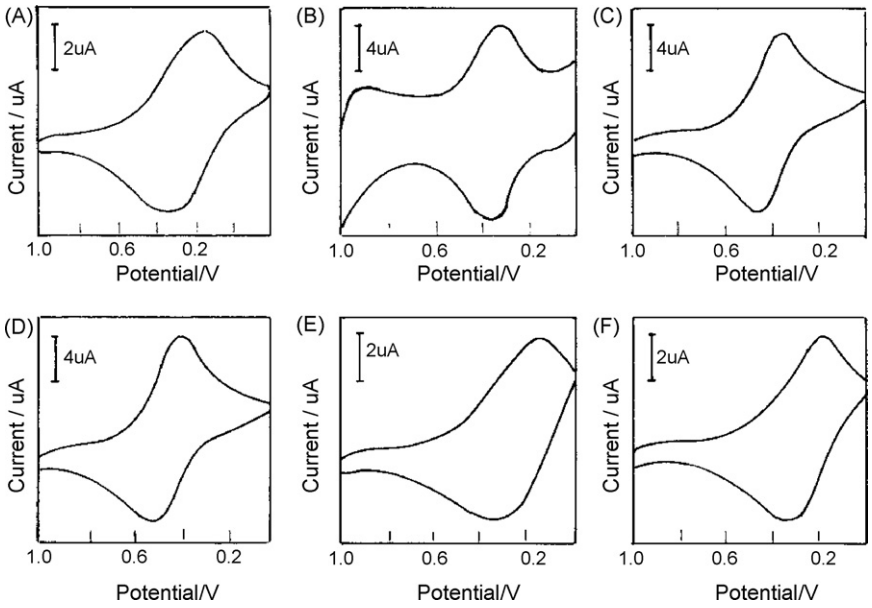

Fig. 2. Cyclic voltammogram of the NAPCF modified electrode in 0.1 M solutions of (A) $LiNO_3$ (B) $NaNO_3$ (C) KNO_3 (D) NH_4NO_3 (E) $Ca(NO_3)_2$ (F) $Ba(NO_3)_2$.

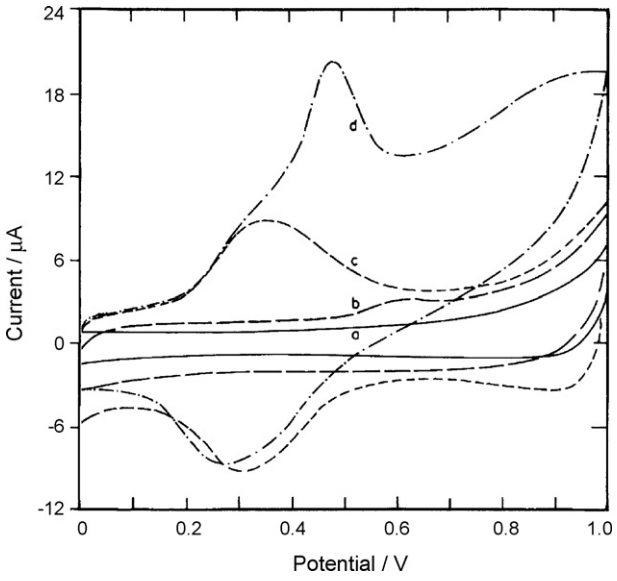

Fig. 3. Cyclic voltammograms in 0.1 M $NaNO_3$ (pH 7.0; 0.05 M phosphate buffer) at a scan rate of 20 mVs^{-1} (a) bare PIGE in the absence of BHA (b) bare PIGE in the presence of 4.75×10^{-6} M BHA (c) NAPCF modified electrode in the absence of BHA (d) NAPCF modified electrode in the presence of 4.75×10^{-6} M BHA.

tial during the forward scan. This oxidised form of the mediator in turn oxidises BHA to *t*-butyl quinone and gets reduced. The reduced form of NAPCF again gets oxidised at the electrode surface producing the oxidation current at the same time. Thus an enhanced anodic current was observed for every addition of BHA.

The influence of pH on the electrocatalytic oxidation of BHA at the NAPCF modified electrode was studied in the pH range from 2 to 10. Catalytic oxidation of BHA at pH 7.0 was found to give better response. The poor response in the acidic pH range might be due to the fact that the oxidation of BHA by NAPCF is suppressed by the common ion effect, as H^+ is one of the products of the oxidation reaction. In the alkaline pH range, the decrease in the oxidation current might be due to the hydroxylation of the mediator. Hence pH 7.0 was chosen as the optimum pH for the determination of BHA.

The quantification of BHA was carried out by measuring the catalytic current as a function of BHA concentration. The linear regression equation of catalytic current versus concentration of BHA is obtained from the experimental data and is given as Ip (μA) = 2.38 [BHA] (μM) + 2.68 μA. The catalytic current was found to increase linearly with the concentration of BHA in the range from 6.24×10^{-7} M to 2.19×10^{-4} M with a correlation coefficient of 0.9979. Thus the sensor could be used to determine the concentration of BHA in this linear range. The detection limit was found to be 2.49×10^{-7} M. Table 1 shows that the linear working range and detection limit obtained with the present sensor are better than or comparable with those of the previously reported electrochemical sensors for the determination of BHA [31–34].

3.4. Hydrodynamic voltammetry and chronoamperometry

In amperometric detection, the potential applied to the working electrode directly affects the sensitivity, detection limit and stability of the detection method. Therefore, hydrodynamic voltammetric experiment was conducted in the potential range from 0 V to 1.0 V to obtain the optimum operating potential. The current response was measured as a function of potential in the presence of 4.00×10^{-6} M BHA in a stirring solution of 0.1 M $NaNO_3$ (pH 7.0; 0.05 M phosphate buffer). Fig. 4 (curves a and b) shows the hydrodynamic voltammograms recorded with bare PIGE and NAPCF modified electrode respectively, in the presence of BHA. From the figure, it could be observed that the response current for the oxidation of BHA was very poor and less significant at the bare PIGE. However, at the NAPCF modified electrode, the current response was found to increase gradually from 0 V to 0.25 V and then rose sharply till 0.5 V with a near equivalent response beyond that. Thus, a working potential of 0.5 V was selected during the amperometric studies for BHA determination.

Amperometric experiments were implemented in stirred solution of 0.1 M $NaNO_3$ (pH 7.0; 0.05 M phosphate buffer). The potential

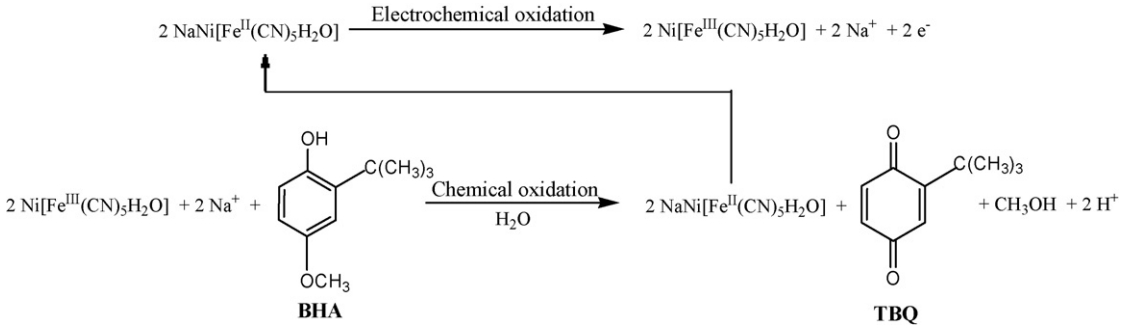

Scheme 1. Electrocatalytic oxidation of BHA at the NAPCF modified electrode.

Table 1
Comparison of linear range and detection limit of various electrodes for the determination of BHA

S.No.	Working electrode	Linear range ($mg\,l^{-1}$)	Detection limit ($mg\,l^{-1}$)	Reference
1	Glassy carbon electrode in micellar media	0.18–1.80	0.23	[31]
2	Glassy carbon electrode in emulsified media	1.80–9.00	0.15	[31]
3	Cylindrical carbon fibre microelectrode	1.80–18.00	0.07	[32]
4	Glassy carbon electrode	0.50–15.00	–	[4]
5	Poly(vinyl chloride) graphite composite electrode	0.10–35.00	0.61	[33]
6	Graphite-wax composite electrode with silver hexacyanoferrate	1.33–150.00	0.67	[34]
7	Nickel aquapentacyanoferrate modified electrode	0.11–39.50	0.05	Present work

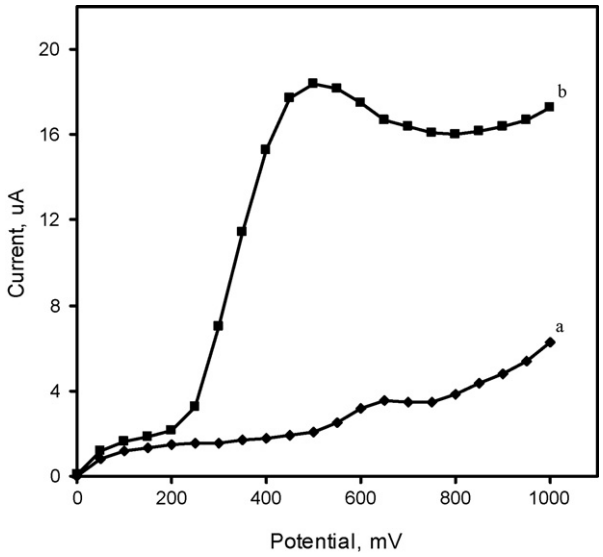

Fig. 4. Hydrodynamic voltammograms obtained with (a) bare PIGE and (b) NAPCF modified electrode in the presence of 4.00×10^{-6} M BHA. Electrolyte: 0.1 M $NaNO_3$ (pH 7.0; 0.05 M phosphate buffer); stirring rate: 300 rpm.

of the NAPCF modified electrode was kept at 0.5 V during successive addition of 0.5 ml of 0.1 mM BHA. The resulting current versus time curve for a series of replicate additions of BHA at a lower concentration range of 5.84×10^{-7} M to 5.03×10^{-6} M is shown in Fig. 5. The corresponding calibration plot with a correlation coefficient of 0.9982 is shown as inset to Fig. 5. The amperogram recorded clearly shows that the current response increases steeply on increasing the concentration of BHA in the solution. Under the optimum conditions, the electrode response was linear to BHA concentration from 5.84×10^{-7} M to 5.03×10^{-4} M. The good linearity observed reveals that the modified electrode could be used as an amperometric sensor for BHA.

3.5. Interference

In order to evaluate the selectivity of the NAPCF modified electrode towards BHA, the interference by other substances such as butylated hydroxy toluene (BHT), ascorbic acid, citric acid, lactic acid, propyl gallate, potassium sorbate and propylene glycol, which are usually present in commercial food products were tested. Under the optimized experimental conditions described above, the influence of the excipients for the determination of 4.00×10^{-6} M BHA was carried out. BHT, citric acid, lactic acid, potassium sorbate and propylene glycol did not affect the current response of BHA even if they were present in 100-fold excess. However, ascorbic acid and propyl gallate were found to interfere in the determination of BHA even when they present in 1:1 ratio. The current response for the determination of 4.00×10^{-6} M BHA was altered by 12% in the presence of ascorbic acid and 9% in the presence of propyl gallate. However, higher concentrations of ascorbic acid influences the current signal for the determination of BHA significantly. Such an influence by ascorbic acid can be eliminated by coating the surface of the sensor with nafion as reported elsewhere [35]. As nafion is an anionic polymer it repels ascorbic acid, an anionic species and can provide a transport channel only for BHA. Further investigation in improving the selectivity of the sensor is under progress. From the above results, it could be ascertained that majority of the excipients do not interfere with the determination of BHA and hence the selectivity of the NAPCF modified electrode towards the determination of BHA is found to be adequate.

3.6. Stability and reproducibility

The stability of the modified electrode was studied both during operation and on long-term storage. The modified electrode did not show any variation in the peak height or peak separation upon subjecting to 100 consecutive cycles, which has been shown in our previous report [23]. The response of the modified electrode in the presence of 4.00×10^{-6} M BHA under hydrodynamic condition for 8 h was found to be unaffected (inset to Fig. 6). The day-to-day response of the modified electrode in the absence (curve a) and presence (curve b) of 4.00×10^{-6} M of BHA during 60 days study is shown in Fig. 6. The modified electrode retained 95% of its response towards 4.00×10^{-6} M BHA, showing that the long-term stability of the modified electrode is not diminished by chemical or mechanical deterioration of the mediator. The intra day precision was established by repeated determination of BHA at the concentration of 4.00×10^{-6} M. The relative standard deviation obtained for 6 deter-

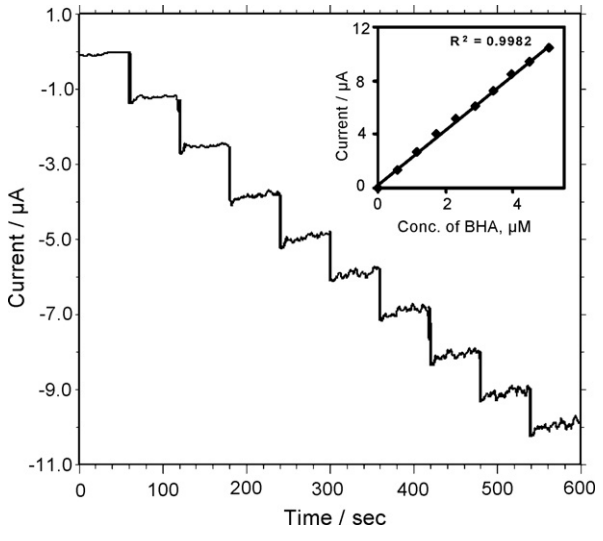

Fig. 5. Chronoamperometric response at NAPCF modified electrode for each addition of 0.5 ml of 0.1 mM BHA to 0.1 M $NaNO_3$ (pH 7.00; 0.05M phosphate buffer); stirring rate: 300 rpm; potential: 0.5 V. Inset: Calibration graph for BHA measurement.

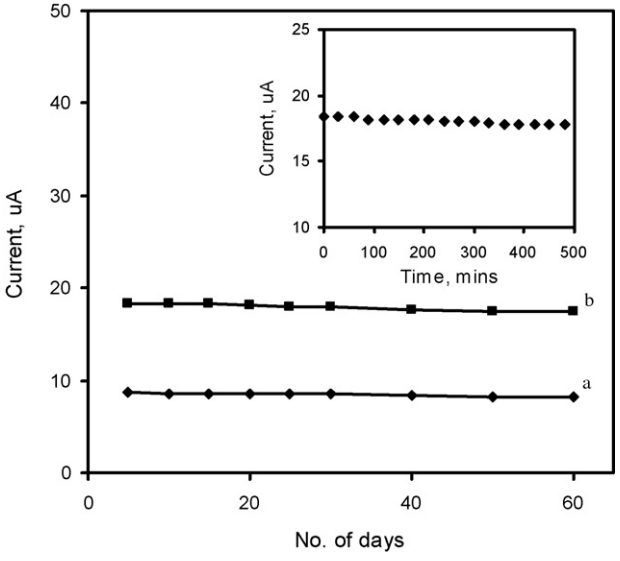

Fig. 6. Plot of day-to-day current response of the NAPCF modified electrode (a) in the absence of BHA (b) in the presence of 4.00×10^{-6} M BHA. Inset: Modified electrode response towards 4.00×10^{-6} M BHA versus time.

Table 2
Determination of BHA in spiked Cereal samples

Packed cereal samples	Concentration of BHA (μM)		Recovery (%)
	Added	Found[a]	
Sample I	20	19.62 ± 0.74	99.2
	40	40.22 ± 0.62	100.4
	60	59.46 ± 0.90	98.4
Sample II	20	20.04 ± 0.44	100.1
	40	39.60 ± 0.58	99.4
	60	59.54 ± 1.00	98.6
Sample III	20	19.28 ± 1.04	98.2
	40	39.80 ± 0.48	98.0
	60	60.12 ± 0.87	100.2

[a] Average of five replicate experiments ± R.S.D.

minations was 2.2% and this infers the good reproducibility of the modified electrode towards the determination of BHA. Thus the modified electrode showed stable and reproducible response for BHA determination.

3.7. Analysis of commercial food samples

The practical utility of the proposed sensor was tested by applying it for the determination of BHA in commercial samples such as packed instant cereal as described in Section 2 using cyclic voltammetry technique. A blank analysis with unspiked sample showed no significant current response, which confirms that the tested samples do not contain any appreciable amount of BHA. Standard addition method was applied for the determination of BHA and the results obtained for the spiked samples are listed in Table 2. A satisfactory recovery in the range of 98.0% to 100.4% was obtained for the determination of BHA.

4. Conclusion

The present work demonstrates the construction of a chemical sensor for BHA based on a novel electrocatalyst, NAPCF for the first time. The fabrication of the modified electrode was done through a simple, convenient and inexpensive route. The graphite rod immobilized with the novel mediator NAPCF enabled the electrooxidation of BHA to proceed effectively at a significant low potential of 0.48 V. Moreover, owing to the linear dependence of BHA oxidation current to its concentration in a wide dynamic range, the possibility of BHA quantitation in stirred and unstirred solutions was shown using amperometry and voltammetry respectively. The fabrication of the modified NAPCF electrode though simple, exhibited good stability for long term use. The application of the modified electrode for the determination of BHA in commercial food samples show the practical usefulness of the sensor. Further work in the development of other aquapentacyanoferrates using different metal ions and applying them for the measurement of chemically and biologically significant substances is underway.

Acknowledgement

One of the authors (SSK) wishes to acknowledge the Indian Council of Medical Research (ICMR), New Delhi for the financial assistance in the form of Senior Research Fellowship.

References

[1] E. Mariani, M.C. Polidori, A. Cherubini, P. Mecocci, J. Chromatogr. B 827 (2005) 65.
[2] C. de la Fuente, J.A. Acuna, V.D. Vazquez, M.L. Tascon, P.S. Batanero, Talanta 49 (1999) 441.
[3] Y.-S. Keum, Y.-H. Han, C. Liew, J.-H. Kim, C. Xu, X. Yuan, M.P. Shakarjan, S. Chong, A.-N. Kong, Pharm. Res. 23 (2006) 2586.
[4] Y. Ni, L. Wang, S. Kokot, Anal. Chim. Acta 412 (2000) 185.
[5] C.S. Sactry, K.E. Rao, U.V. Prasad, Talanta 29 (1982) 917.
[6] C.C. –Blanco, A.S. Caretto, E.M. Boyle, A.F. Gutierrez, Talanta 50 (1999) 1099.
[7] M.-H. Yang, H.-J. Lin, Y.-M. Choong, Food Res. Int. 35 (2002) 627.
[8] C. Perrin, L. Meyer, Food Chem. 77 (2002) 93.
[9] M.M.D. –Zamarreno, I.G. –Maza, A.S. –Parez, R.C. Martinez, Food Chem. 100 (2007) 1722.
[10] D. Ravi Shankaran, N. Uehera, T. Kato, Sens. Actuators B 87 (2002) 442.
[11] S.A. Wring, J.P. Hart, Analyst 117 (1992) 1215.
[12] R. Pauliukaite, C.M.A. Brett, Electrochim. Acta 50 (2005) 4973.
[13] S.-M. Chen, J.-Y. Chen, V.S. Vasantha, Electrochim. Acta 52 (2006) 455.
[14] M. Pandurangappa, N.S. Lawrence, L. Jiang, G. Timothy, J. Jones, R.G. Compton, Analyst 108 (2003) 473.
[15] K. Thenmozhi, S. Sriman Narayanan, Anal. Bioanal. Chem. 387 (2007) 1075.
[16] S. Sriman Narayanan, F. Scholz, Electroanalysis 11 (1999) 465.
[17] S. Senthil kumar, S. Sriman Narayanan, Chem. Pharm. Bull. 54 (2006) 963.
[18] P.J. Kulesza, M.A. Malik, S. Zamponi, M. Berrettoni, R. Marassi, J. Electroanal. Chem. 397 (1995) 287.
[19] H. Dussel, A. Dostal, F. Scholz, Fresenius J. Anal. Chem. 355 (1996) 21.
[20] P. Wu, C.X. Cai, J. Solid State Electrochem. 8 (2004) 538.
[21] D. Ravi Shankaran, S. Sriman Narayanan, Sens. Actuators B 86 (2002) 180.
[22] X. Zhou, S. Wang, Z. Wang, M. Jiang, Fresenius J. Anal. Chem. 345 (1993) 424.
[23] S. Senthil kumar, S. Sriman Narayanan, Electrochem. Commun. 8 (2006) 815.
[24] F. Scholz, B. Meyer, Chem. Soc. Rev. 23 (1994) 341.
[25] F. Scholz, B. Lange, Tr. Anal. Chem. 11 (1992) 359.
[26] W.P. King, K.T. Joseph, P.T. Kissinger, J. Assoc. Off. Anal. Chem. 63 (1980) 137.
[27] T.R.I. Cataldi, G.E.D. Benedetto, A. Bianchini, J. Electroanal. Chem. 448 (1998) 111.
[28] T. Akitsu, Y. Einaga, Inorg. Chim. Acta 360 (2007) 497.
[29] P.J. Kulesza, M.A. Malik, M. Berrettoni, M. Giorgetti, S. Zamponi, R. Schmidt, R. Marassi, J. Phys. Chem. B 102 (1998) 1870.
[30] D. Eillis, M. Eckhoff, V.D. Neff, J. Phys. Chem. 85 (1981) 1225–1231.
[31] A. González, M.A. Ruiz, P. Yáñez-Sedeño, J.M. Pingarrón, Anal. Chim. Acta 285 (1994) 63.
[32] M.L. Agüí, A.J. Reviejo, P. Yáñez-Sedeño, J.M. Pingarrón, Anal. Chem. 67 (1995) 2195.
[33] M. Luque, A. Rios, M. Valcarcel, Anal. Chim. Acta 395 (1999) 217.
[34] D. Jayasri, S. Sriman Narayanan, Sens. Actuators B 119 (2006) 135.
[35] D. Ravi Shankaran, N. Uehera, T. Kato, Biosens. Bioelectron. 18 (2003) 721.

Talanta 76 (2008) 34–39

Contents lists available at ScienceDirect

Talanta

journal homepage: www.elsevier.com/locate/talanta

Study on spectroscopic characterization of Cu porphyrin/Co porphyrin and their interactions with ctDNA

Jun Li, Yanli Wei, Limin Guo, Caihong Zhang, Yong Jiao, Shaomin Shuang, Chuan Dong*

Research Center of Environmental Science and Engineering, Institute of Molecular Science, Shanxi University, Taiyuan, Shanxi 030006, China

ARTICLE INFO

Article history:
Received 10 August 2007
Received in revised form 30 January 2008
Accepted 31 January 2008
Available online 10 March 2008

Keywords:
Cu(II)TMPyP
Co(II)TMPyP
UV–vis
Fluorescence
Resonance light scattering

ABSTRACT

The luminescence behaviors of Cu(II) *meso*-tetrakis (4-*N*-methyl-pyridiniumyl) porphyrin (Cu(II)TMPyP) and Co(II) *meso*-tetrakis (4-*N*-methyl-pyridiniumyl) porphyrin (Co(II)TMPyP) are investigated, and their interactions with calf thymus DNA (ctDNA) are studied by UV–vis, fluorescence and resonance light scattering (RLS) and based on the changes of UV–vis spectra, fluorescence and RLS spectra, the intrinsic binding constants of Cu(II)TMPyP/Co(II)TMPyP with ctDNA are obtained in the case of phosphate buffer solution (pH 7.2), respectively. According to the experimental results, it can be inferred that the interaction model of Cu(II)TMPyP with ctDNA is intercalative binding, while Co(II)TMPyP is the long-range assembly on the molecular surface of ctDNA.

1. Introduction

As the hardcore of biomacromolecules, research interests in cationic porphyrin have been steadily increasing in the past several years [1]. Symmetrically extended porphyrins, such as the *meso*-tetrakis (4-*N*-methyl-pyridiniumyl) porphyrin (H_2TMPyP), exhibit strong absorption bands in the visible region and possess interesting non-linear optical properties, suggesting application in biomedicine and various branches of optical technology [2]. Studies on supramolecular interactions of cationic porphyrins with biological molecules are significant to understand the structures and functions of biomacromolecules [3,4]. Generally, the interactions of cationic porphyrins with DNA involve three binding modes: intercalation, groove binding and long-range assembly on the molecular surfaces of nucleic acids [5]. The studies on the supramolecular interacting system can be made by investigating the binding characteristics of cationic porphyrins through resonance Raman spectra [6], circular dichroism (CD) [7], solid substrate room temperature phosphorescence (SS-RTP) [8], fluorescence [9] and resonance light scattering (RLS) [10] spectra.

DNA has a hydrophilic coat/hydrophobic core structure, thus, aromatic ligands stacking between nucleic base pairs is the main driving force for the binding of an intercalator into double-stranded DNA. The metal derivatives of H_2TMPyP including palladium(II), manganese(III), iron(III) and zinc(II) had been investigated based on the circular dichroism and other techniques [11]. Cobalt porphyrin derivative is the major components of Vitamin B_{12}, which can be used as a fluorescence probe to investigate the structure of DNA and construct a sensitive assay of DNA [12]. Copper is in the same period with cobalt. To study the interaction of cobalt/copper porphyrins with calf thymus DNA (ctDNA) is very significantly useful in the rational design of new and efficient DNA targeted molecules for application in chemotherapy. To the best of our knowledge, there are few studies focused on the interaction of Co(II)/Cu(II) derivatives of H_2TMPyP with biomacromolecules by fluorescence and RLS. In this study, the interactions of Cu(II)TMPyP/Co(II)TMPyP with ctDNA were investigated by UV–vis, fluorescence and RLS. Through comparing the differences, the conclusion is obtained that Cu(II)TMPyP is intercalative binding to ctDNA, while Co(II)TMPyP is the long-range assembly on the molecular surface of ctDNA.

2. Experimental

2.1. Reagents and materials

Calf thymus DNA was purchased from Sigma Chemical Co. and used without further purification. Stock solution of ctDNA was prepared by dissolving the solid ctDNA in 0.1 mol/L NaCl solution with occasionally gentle shaking stored below 4 °C in the dark and the active lifetime was not more than 2 weeks. The base pairs concentration of ctDNA was obtained via absorbance measurements using $\varepsilon = 1.32 \times 10^4\,L\,mol^{-1}\,cm^{-1}$ at the maximum near 260 nm

* Corresponding author.
E-mail address: dc@sxu.edu.cn (C. Dong).

0039-9140/$ – see front matter © 2008 Elsevier B.V. All rights reserved.
doi:10.1016/j.talanta.2008.01.065

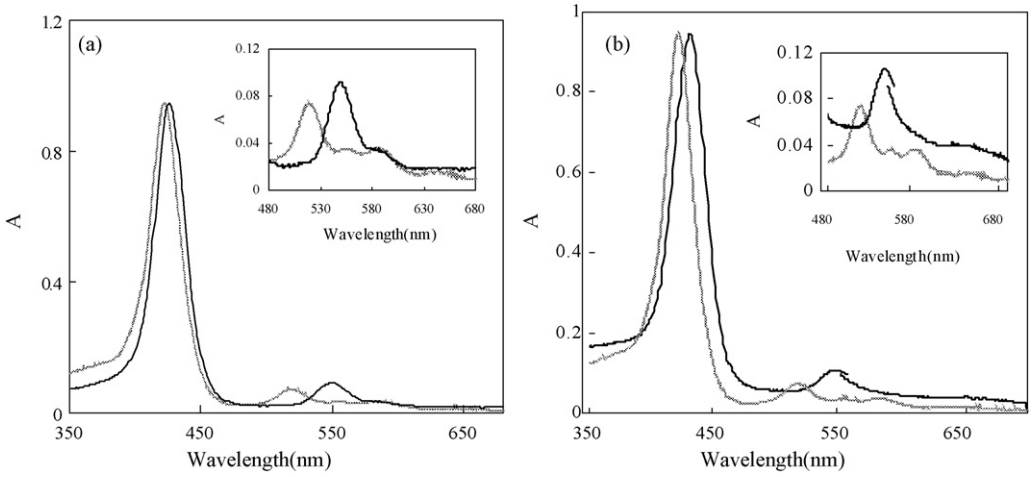

Fig. 1. The absorption spectra of Cu(II)TMPyP(—): (a) (4.20×10^{-6} mol/L)/Co(II)TMPyP (—) and (b) (4.20×10^{-6} mol/L) and H_2TMPyP (——) (4.20×10^{-6} mol/L).

after establishing that the absorbance ratio A_{260}/A_{280} in the range of 1.80–1.90 [13].

The *meso*-tetrakis (4-*N*-methyl-pyridiniumyl) porphyrin (H_2TMPyP) was obtained as the tosylate from Fluka Chemical Co. and then diluted to 1×10^{-4} mol/L with double distilled water. The copper chloride ($CuCl_2$) and cobalt chloride ($CoCl_2$) were obtained from Beijing Chemical Factory (China) and their stock solutions were both 1×10^{-3} mol/L.

Phosphate buffer solution was used to control the pH of the media (pH 7.2). All other reagents were of analytical grade without further purification and double distilled deionized water was used throughout the experiments.

2.2. Apparatus

The fluorescence and RLS spectra were carried out on F-4500 fluorescence spectrophotometer (Hitachi, Japan), equipped with a fluorescence polarization attachment. A 150 W Xenon arc lamp was used as the excitation light source. A standard 1 cm quartz cell was used. A 5 μL microsyringe (Shanghai Medical Laser Instrument Factory, China) was used for introducing samples and ctDNA solution. The absorbance spectra were recorded with a TU-1901 UV–vis spectrophotometer (Beijing Puxi Instrument Factory, China). pH values were measured using a Model pHS-3C pH-meter (Shanghai Rex Instrument Factory, China). All experiments were carried out at 20 ± 1 °C.

2.3. Procedures

2.3.1. Synthesis of Cu(II)TMPyP and Co(II)TMPyP

10.0 mL stock solution of H_2TMPyP and 10.0 mL stock solution of $CuCl_2$ or $CoCl_2$ were mixed with appropriate phosphate buffer (pH 7.2). Then allowed to reflux at 80 °C in the water bath for about 4 h. According to the literature [14], the formation of the complex was supported by the UV–vis spectrum. The maximum absorption of Cu(II)TMPyP and Co(II)TMPyP were 424 nm ($\varepsilon_{424} = 2.31 \times 10^5$ L mol^{-1} cm^{-1}) and 434 nm ($\varepsilon_{434} = 2.15 \times 10^5$ L mol^{-1} cm^{-1}), respectively.

2.3.2. UV–vis, fluorescence and RLS measurements

The absorption, fluorescence and RLS titrations were performed by keeping the concentration of Cu(II)TMPyP/Co(II)TMPyP constant while varying the concentration of ctDNA.

The excitation slit and emission slit were both 5 nm. The excitation/emission wavelengths of Cu(II)TMPyP and Co(II)TMPyP are at 426/629 nm and 438/626 nm, respectively. By scanning both the

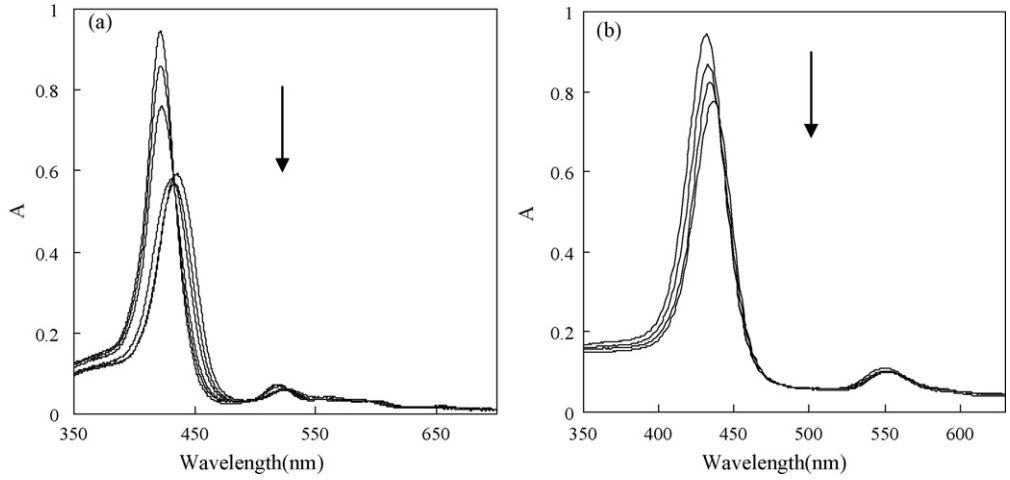

Fig. 2. The absorption spectra of Cu(II)TMPyP: (a) (6×10^{-6} mol/L)/Co(II)TMPyP and (b) (6×10^{-6} mol/L) in different concentration of ctDNA at pH 7.2. DNA concentration (from top to bottom): 0, 1.08×10^{-6} mol/L, 2.70×10^{-6} mol/L, 3.45×10^{-6} mol/L, 4.50×10^{-6} mol/L and 5.40×10^{-6} mol/L for (a); 0, 1.08×10^{-6} mol/L, 2.70×10^{-6} mol/L and 5.40×10^{-6} mol/L for (b).

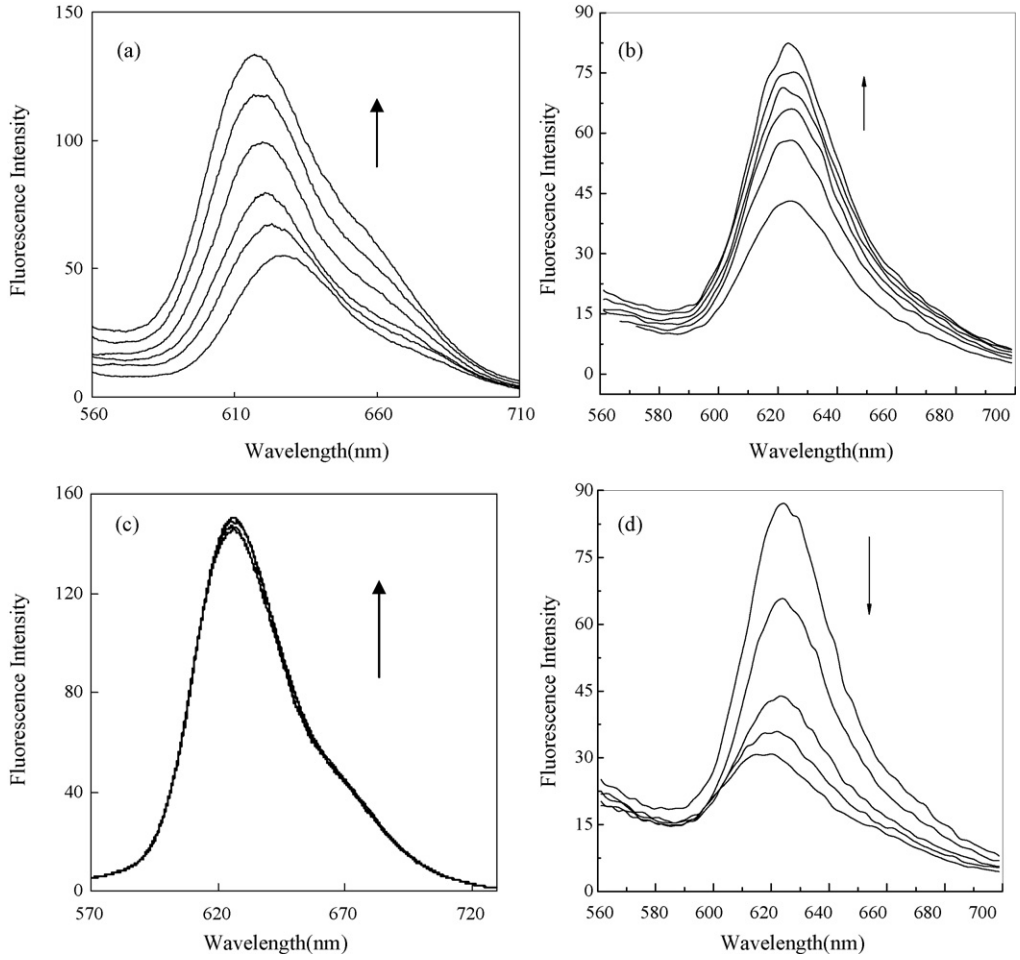

Fig. 3. The fluorescence spectra of Cu(II)TMPyP/Co(II)TMPyP in the presence of ctDNA ((a) Cu(II)TMPyP (4.20×10^{-6} mol/L); (c) Co(II)TMPyP (4.20×10^{-6} mol/L)) or ss-DNA ((b) Cu(II)TMPyP (3.50×10^{-6} mol/L); (d) Co(II)TMPyP (3.70×10^{-6} mol/L)) at pH 7.2. DNA concentration (from bottom to top): 0, 0.67×10^{-6} mol/L, 1.08×10^{-6} mol/L, 2.70×10^{-6} mol/L, 3.45×10^{-6} mol/L and 5.40×10^{-6} mol/L for (a); 0, 0.62×10^{-6} mol/L, 1.24×10^{-6} mol/L, 1.86×10^{-6} mol/L, 4.96×10^{-6} mol/L and 5.58×10^{-6} mol/L for (b); 0, 1.08×10^{-6} mol/L, 3.45×10^{-6} mol/L and 5.40×10^{-6} mol/L for (c); 3.10×10^{-6} mol/L, 2.48×10^{-6} mol/L, 1.24×10^{-6} mol/L and 0.62×10^{-6} mol/L, 0 for (d).

excitation and emission monochromators of a common spectrofluorometer with $\Delta\lambda = 0$ nm, a RLS spectrum can be developed which has been proved to be able to investigate the aggregation of small molecules and the long-range assembly of organic dyes on biological templates [15].

3. Results and discussion

3.1. Formation of Cu(II)TMPyP and Co(II)TMPyP

Fig. 1 shows the UV–vis spectra changes before and after forming Cu(II)TMPyP and Co(II)TMPyP. The maximum absorption of Cu(II)TMPyP is 424 nm (Fig. 1a), which is only 2 nm red shifts and its intensity has unobvious change. But Cu(II)TMPyP has two visible bands while H_2TMPyP has four visible bands. Similarly, Co(II)TMPyP has 12 nm red shifts and two visible bands spectra (Fig. 1b), which confirmed the formation of Cu(II)TMPyP or Co(II)TMPyP [14].

3.2. Interaction of Cu(II)TMPyP/Co(II)TMPyP with ctDNA

The dependence of UV–vis spectra of Cu(II)TMPyP/Co(II)TMPyP in the presence of ctDNA are shown in Fig. 2. With the increasing of ctDNA concentration, the UV–vis spectra of Cu(II)TMPyP shows clear hypochromicity at the Soret maximum and large red shifts (Fig. 2a), which implies the intercalative binding of the porphyrin to the DNA bases. Whereas, the UV–vis spectra of Co(II)TMPyP also has hypochromicity (25%) and small red shifts (6 nm) (Fig. 2b), which indicates Co(II)TMPyP is likely to aggregate on the surface of DNA [16]. In addition, DNA has a weak absorption at 260 nm, with the increasing of Cu(II)TMPyP/Co(II)TMPyP, absorption changes of DNA around 260 nm cannot be observed. It can be inferred that porphyrin complexes have not destroyed the natural base pairing between pyrimidine and purine.

The fluorescence spectra of Cu(II)TMPyP and Co(II)TMPyP in different concentration of ctDNA are shown in Fig. 3. Upon the addition of ctDNA, the maximum emission of Cu(II)TMPyP has 4 nm blue shifts and its intensity increases clearly (Fig. 3a), which may result from that Cu(II)TMPyP intercalates into ctDNA bases and is protected from collision quenching between porphyrin and ctDNA.

Denatured ctDNA is produced by incubation of a native ctDNA solution at 100 °C for 10 min and immediately cooling in ice-water, then, ctDNA splits into two string-like softer polynucleotide chains from original rigid double-helix structure. The fluorescence of Cu(II)TMPyP enhances with the increasing of single-strand DNA (ss-DNA), but the degree of the fluorescence increment is much weaker than that from double-strand DNA (ds-DNA) (Fig. 3b). Highly organized double-helix structure of native DNA seems not to be the necessary condition for the interaction with Cu(II)TMPyP into native DNA base pairs. And this provide another powerful evidence that Cu(II)TMPyP can intercalate into ctDNA bases.

The fluorescence of Co(II)TMPyP enhances only a little with the increasing of ctDNA and it has no shifts at maximum emission wavelength (Fig. 3c). It can be assumed that the Co(II)TMPyP is not intercalative but surface binding to DNA. In contrast, ss-DNA can quench the fluorescence of Co(II)TMPyP shown in Fig. 3d. ss-DNA is incompact clew-shape and PO_4^{3-} functional group is thoroughly exposed, which is in favor of Co(II)TMPyP aggregating on the outside of DNA. In addition, the experiment of the interaction between PO_4^{3-} and Co(II)TMPyP shows that PO_4^{3-} has a similar quenching effect with that from ss-DNA. All the experiments indicate that Co(II)TMPyP can make long-range assembly on the surface of DNA by electrostatic interaction.

An anion quencher such as $Fe(CN)_6^{4-}$ can be used to deducing the interaction pattern of the fluorescence probe with DNA from the variation of Stern–Volmer K_{SV}. It is measured according to the Stern–Volmer equation:

$$\frac{I_0}{I} = 1 + K_{SV}[Q] \quad (1)$$

where I_0 and I are the fluorescence intensities in the absence and in the presence of quencher [Q], respectively.

The Stern–Volmer plots are linear with the slope decreasing in the absence and presence of ctDNA. It is obvious that the K_{SV} of the bound Cu(II)TMPyP is less than that of the free Cu(II)TMPyP. K_{SV} values for the free Cu(II)TMPyP and the bound Cu(II)TMPyP with ctDNA are 9.14×10^4 L/mol and 3.26×10^4 L/mol, respectively, which also supports the intercalation of Cu(II)TMPyP to the ctDNA bases [17]. While, the K_{SV} of the bound Co(II)TMPyP is much large than that of the free Co(II)TMPyP. K_{SV} value of free and bound Co(II)TMPyP are 6.23×10^4 L/mol and 4.81×10^5 L/mol, respectively, which suggests that the presence of ctDNA quickened the anion quenches the fluorescence of Co(II)TMPyP [18], due to it is exposed to the solution [19] and its surface binding.

Fluorescence polarization can provide an effective parameter for investigating dynamic characteristics of fluorescence probe in different microenvironments. And the fluorescence polarization can be obtained from the following equation:

$$P = \frac{I_{VV} - GI_{VH}}{I_{VV} + GI_{VH}} \quad (2)$$

where I_{VV} is the vertical polarization intensity vertical with excitation; I_{VH} is the horizontal polarization intensity vertical with excitation. $G = I_{HV}/I_{HH}$, I_{HV} is the vertical polarization intensity parallel with excitation; I_{HH} is the horizontal polarization intensity parallel with excitation.

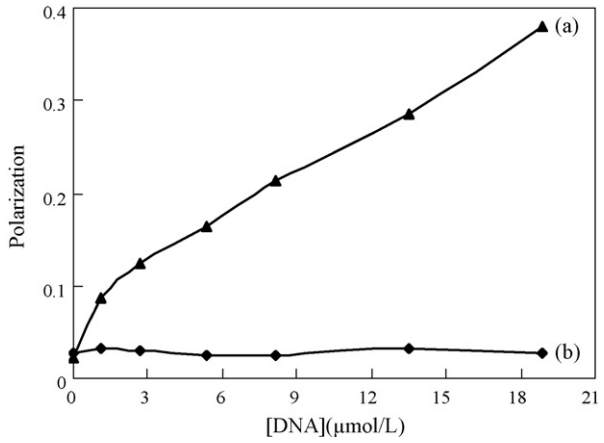

Fig. 4. The fluorescence polarization of Cu(II)TMPyP: (a) (4.20×10^{-6} mol/L) and Co(II)TMPyP and (b) (4.20×10^{-6} mol/L) in the different concentration of DNA at pH 7.2.

Fig. 4 shows the fluorescence polarization of Cu(II)TMPyP/Co(II)TMPyP with the increasing concentration of ctDNA. As shown in Fig. 4, the fluorescence polarization of Cu(II)TMPyP is increased obviously with the increasing concentration of ctDNA. The results above are evidence that Cu(II)TMPyP indeed intercalates into the helix and the ctDNA provides a rigid microenvironment for Cu(II)TMPyP. However, the concentration of ctDNA almost has no effect on the fluorescence polarization of Co(II)TMPyP. That is to say, Co(II)TMPyP is non-intercalative to DNA [20].

Fig. 5 describes Cu(II)TMPyP/Co(II)TMPyP has two weak RLS peaks in the range of 400–700 nm. We have proved that ctDNA has very weak RLS signals in this medium even if its concentration reaches 10^{-3} mol/L. As the increasing of ctDNA, the scattering signal of Cu(II)TMPyP enhances only a little (Fig. 5a) which may be due to the increasing of ctDNA concentration. Whereas, the scattering signal of Co(II)TMPyP increases significantly (Fig. 5b), which further indicates that Co(II)TMPyP aggregated on the outside of ctDNA.

Pasternack [13] reported that the central atoms could influence the binding mode to DNA. From a structural point of view, the thin square planar Cu(II) derivatives of H_2TMPyP are capable of intercalation, because it is not ligated at its vacant axial site by aquo ligands and can intercalate into the pocket between two adjacent, closely spaced base pairs of ctDNA. On the other hand, the presence of axial

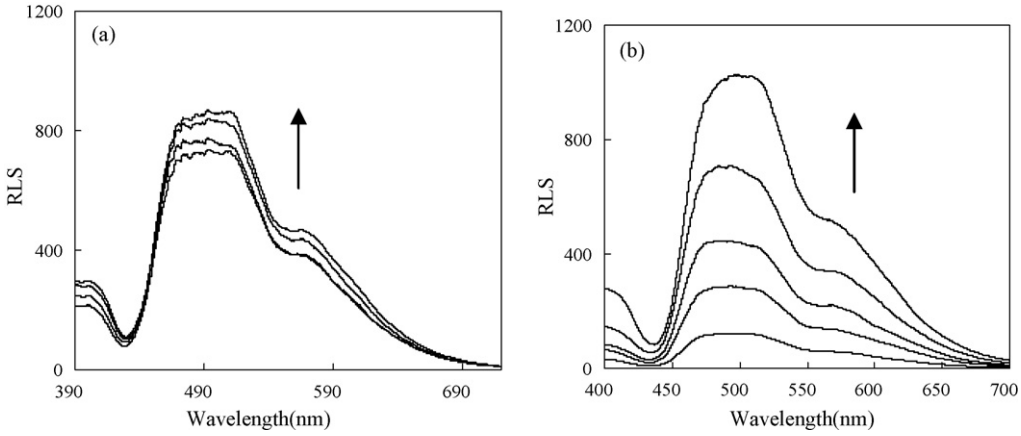

Fig. 5. The resonance light scatter spectra of Cu(II)TMPyP: (a) (4.2×10^{-6} mol/L)/Co(II)TMPyP and (b) (4.2×10^{-6} mol/L) in the absence and presence of DNA at pH 7.2. DNA concentration (from bottom to top): 0, 0.67×10^{-6} mol/L, 2.70×10^{-6} mol/L and 4.5×10^{-6} mol/L for (a); 0, 0.67×10^{-6} mol/L, 2.70×10^{-6} mol/L, 4.5×10^{-6} mol/L and 5.40×10^{-6} mol/L for (b).

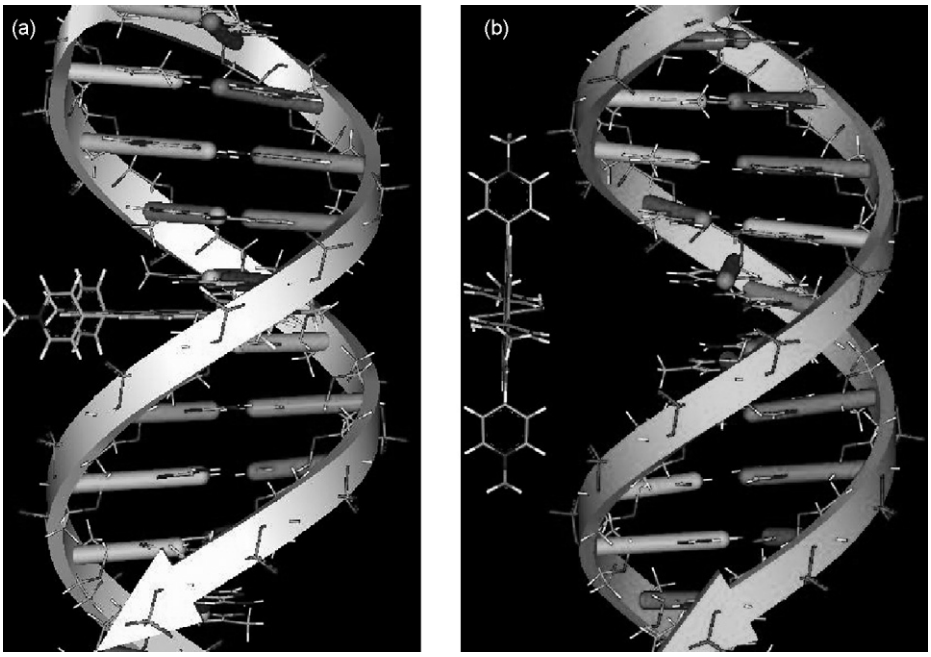

Fig. 6. Binding model of Cu(II)TMPyP (a)/Co(II)TMPyP (b) to DNA.

ligands may limit the metalloporphyrins largely to an electrostatic type of bonding to the phosphate backbone and minimal interaction with the bases of the polynucleotide. Co(II)TMPyP is likely to be the long-range assembly on the molecular surface of ctDNA due to the axial aquo ligands.

To testify the experimental results, the interaction models of Cu/Co(II)TMPyP and the standard B-type DNA are generated and optimized by the Builder module and the Biopolymer module of Insight II 2000 software package (Accelrys), respectively. By monitoring the docking energy of Cu(II)TMPyP and Co(II)TMPyP with DNA, respectively, it is indicated that the former is prone to interacting with DNA in the intercalative model, and the latter in the long-range assembly model on the DNA surface, which is consistent with the above experiment results. All interaction models (Fig. 6) are built on a Silicon Graphics O2 workstation.

3.3. Binding constant of ctDNA and Cu(II)TMPyP/Co(II)TMPyP

For the interaction of small molecules with macromolecules, the McGhee–von Hippel plot is commonly used to characterize the binding properties in terms of measuring the binding constant. The data for this analysis are based on the measurements of absorbance of interaction system [13,21]. The binding constant of DNA to Cu(II)TMPyP/Co(II)TMPyP is estimated from their absorption data by the following equation [13]:

$$\frac{r}{m} = K_{\text{app}}(1 - nr)\left[\frac{1 - nr}{1 - (n-1)r}\right]^{n-1} \quad (3)$$

where r is defined as the number of moles of bound porphyrin per mole of total base pairs; m is the molar concentration of free porphyrin; n is the number of consecutive lattice residues made inaccessible by the binding of a single drug molecule; K_{app} is the apparent affinity constant for the porphyrin binding to a site on the nucleic acid. Values of r and m necessary for the analysis were calculated by the method of Peacocke and Sherrett [22].

In the limit of low r, the value of K can be obtained more precisely from the derivative of the following equation [13]:

$$\lim_{r\to 0}\frac{\mathrm{d}(r/m)}{\mathrm{d}r} = -K_{\text{app}}(2n-1) \quad (4)$$

This limiting slope line intercepts the abscissa at a value of $(2n-1)^{-1}$ and has a slope of $-K_{\text{app}}(2n-1)$. The binding constants of DNA to Cu(II)TMPyP and Co(II)TMPyP are calculated to be 4.29×10^5 L/mol and 3.65×10^5 L/mol, respectively, which indicates that Cu(II)TMPyP/Co(II)TMPyP has intense affinity to ctDNA.

4. Conclusion

Based on the measurements of molecular absorption, fluorescence and RLS, the binding nature of Cu(II)TMPyP and Co(II)TMPyP are characterized. The binding mode of Cu(II)TMPyP involved intercalative binding to ctDNA, while Co(II)TMPyP is long-range assembly on the ctDNA surfaces. Furthermore, according to the binding constants, we can conclude that Cu(II)TMPyP and Co(II)TMPyP have the close affinity with ctDNA. These investigations are of potential importance in understanding the mechanism of interaction and recognition of compounds in living body.

Acknowledgements

Financial supports from the National Natural Science Foundation of China (Grant No. 20575037), the Key Project of National Natural Science Foundation of China (No. 50534100) and the Youth Science Foundation of Shanxi Province (No. 2007021007) are acknowledged.

References

[1] H.Y. Luo, J.H. Jiang, X.B. Zhang, C.Y. Li, G.L. Shen, R.Q. Yu, Talanta 72 (2007) 575–581.
[2] C.Q. Zhu, S.J. Zhuo, Y.X. Li, L. Wang, D.H. Zhao, J.L. Chen, Y.Q. Wu, Spectrachim. Acta Part A 60 (2004) 959–964.
[3] M. Sirish, H.J. Scheider, Chem. Commun. (1999) 907–908.
[4] E.D. Mauro, R. Saladino, P. Tagliatesta, R. Negri, J. Mol. Biol. 282 (1998) 43–57.

[5] D.H. Tjahjono, T. Akutsu, N. Yoshioka, H. Inoue, Biochim. Biophys. Acta 1472 (1999) 333–343.
[6] R.F. Pasternack, S. Ewen, A. Rao, A.S. Meyer, M.A. Freedman, P.J. Collings, S.L. Frey, M.C. Ranen, J.C. de Paula, Inorg. Chim. Acta 317 (2001) 59–71.
[7] J.S. Trommel, L.G. Marzilli, Inorg. Chem. 40 (2001) 4374–4383.
[8] L.M. Guo, W.J. Dong, X.F. Tong, C. Dong, S.M. Shuang, Talanta 70 (2006) 630–636.
[9] W.T. An, X.L. Guo, S.M. Shuang, C. Dong, J. Photochem. Photobiol. A: Chem. 173 (2005) 36–41.
[10] C.Z. Huang, X.B. Pang, Y.F. Li, Y.J. Long, Talanta 69 (2006) 180–186.
[11] R.F. Pasternack, E.J. Gibbs, J.J. Wilafranca, Biochemistry 22 (1983) 5409–5417.
[12] B. Jin, J.S. Shin, C.H. Bae, J.M. Kim, S.K. Kim, Biochim. Biophys. Acta 1760 (2006) 993–1000.
[13] R.F. Pasternack, E.J. Gibbs, J.J. Villagranca, Biochemistry 22 (1983) 2406–2414.
[14] A.M. Brun, A. Harriman, J. Am. Chem. Soc. 116 (1994) 10383–10393.
[15] R.F. Pasternack, C. Bustamante, P.J. Collings, A. Giannetto, E.J. Gibbs, J. Am. Chem. Soc. 115 (1993) 5393–5399.
[16] J.E. McClure, L. Baudouin, D. Mansuy, L.C. Marzilli, Biopolymers 42 (1997) 203–217.
[17] L.S. Lerman, J. Mol. Biol. 3 (1961) 18–30.
[18] C.V. Kumar, R.S. Turner, J. Photochem. Photobiol. A: Chem. 74 (1993) 231–238.
[19] H.M. Berman, P.B. Young, Ann. Rev. Biophys. Bioeng. 10 (1981) 87–114.
[20] C.V. Kumar, E.H. Asuncion, J. Am. Chem. Soc. 115 (1993) 8547–8553.
[21] A.T. Tong, L. Lin, L. Liu, L.D. Li, Fresen. J. Anal. Chem. 370 (2001) 1023–1028.
[22] A.R. Peacoke, J.N.H. Sherrett, Trans. Faraday Soc. 52 (1956) 261–279.

Talanta 76 (2008) 91–95

Contents lists available at ScienceDirect

Talanta

journal homepage: www.elsevier.com/locate/talanta

Determination of detergents in washing machine wastewater with a voltammetric electronic tongue

J. Olsson*, P. Ivarsson, F. Winquist

Division of Applied Physics and Swedish Sensor Centre (S-SENCE), Linköpings Universitet, Se-581 83 Linköping, Sweden

ARTICLE INFO

Article history:
Received 27 August 2007
Received in revised form 1 February 2008
Accepted 14 February 2008
Available online 29 February 2008

Keywords:
Detergents
Surfactants
Electronic tongue
HPLC

ABSTRACT

A voltammetric electronic tongue (ET) and a conductivity meter were used to predict amounts of detergents in process water from washing machines. The amount of detergent in over sixty samples was also determined by a HPLC reference method. Prediction was more accurate for the electronic tongue, but both techniques could be used. The composition of the detergent, e.g. supporting electrolyte, is an important factor for the ability to predict the detergent quantity by conductivity. Also two different surfactants, alkyl benzyl sulfonate (ABS) and etoxylated fatty alcohol (EOA), were fingerprinted by the HPLC. Their behaviour during the wash cycle differs from each other, ABS rinses away in the same proportions as the supporting electrolyte, but EOA appears to stay within the machine and laundry. Prediction models for ABS are accurate both with ET and conductivity meter, mostly due to the correlation with supporting electrolyte. The behaviour of EOA, with almost no correlation to the supporting electrolyte makes it difficult to predict using conductivity but ET prediction models give promising indications of its capabilities.

1. Introduction

Due to increasing awareness concerning environmental issues, consumers are asking for "green products", that is products that contribute to a sustainable society; this is not an exception for household washing machines. In recent years, the development of energy and environmental friendly washing machines has progressed. Since a few decades water consumption has decreased from around 200 l to about 50 l for a normal washing program. This is especially important in areas with limited water reserves, such as the inland of Australia, where water consumption is one of the main concerns. However, lower water consumption has side effects such as lower energy consumption and rinsing performance. Lower energy consumption is beneficial, but decreasing performance of rinsing could leave residue detergent left in the garments. Rest of the detergents within the garments could cause skin irritations or in severe cases even induce allergic reactions [1].

The remarkable increase in washing efficiency had not been possible without the increased use of sensors to control the process parameters involved during a normal washing cycle. Simple sensors such as temperature sensors to turn on and off heaters, pressure and weight sensors for controlling water levels in the machine, have been used for sometime, but more sophisticated sensor systems that enable the machine to make decisions are becoming more available due to decreasing prices on sensors and microprocessors. Use of adaptive algorithms and sensor systems for controlling the wash process will undoubtedly lead to safer and user friendlier washing machines. In the future the 'one button machine' will perhaps be realized, a machine that simply measure and analyses what is needed to be done, accomplishes and controls the outcome in the best and most environmental efficient way. Towards the realization of the 'one button' washing machines, concentration and effort are put on making better sensors that can be used to measure the residue detergent and if possible even surfactants. Such a sensor could be the main source for decisions regarding rinsing and the dispensing of detergents. If sensors could measure the residue detergent or surfactants, the machine could decide if further rinses are necessary, resulting in both saved water and safe levels of residue detergent in the laundry.

Measurements of rest of the detergent are normally done by alkali-titration of residue water within the textiles after a completed wash program [2]. The surfactant, usually sulfonated alkyls or other anions of long carbon backbones, gives rise to basic buffering properties. The amount of acid used to neutralize the pH is a measurement of residue detergent. Although this method is simple to use and does not require expensive laboratory equipment, it is limited to those residues that buffer pH and overlooks other residues, such as non-ionic surfactants. If the residue composition would be the same, this would not cause any problems, but the chemical adsorption factors of the different surfactants in a detergent are normally different. Separation and quantification of different surfactants in water samples could be accomplished by

* Corresponding author. Tel.: +46 13 28 89 04.
E-mail address: john@ifm.liu.se (J. Olsson).

0039-9140/$ – see front matter © 2008 Elsevier B.V. All rights reserved.
doi:10.1016/j.talanta.2008.02.028

liquid chromatography with optical detection [3]. Conversely, liquid chromatography is more complex and expensive compared to the simpler titration as previously described, but has the possibility to fingerprint several components in a detergent. To measure the residue detergent with its components, chromatography appears to be a better technique than alkali titration.

Neither titration nor chromatography systems are convenient to integrate within a washing machine to supervise the rinse process, but other sensor techniques such as electronic tongues (ET) [4,5] or conductivity meters [6] could offer a possibility. Both these sensor types require similar hardware, but the electronic tongue utilizes a more complex signal evaluation compared to that of a conductivity meter. ET signal generation and recording are done by a potentiostat; voltage is applied between working and counter electrodes and current is recorded as a function of time and potential. A relay can be used to connect several different electrodes with different electrochemical properties to increase the information recorded. Signal processing is normally done by multivariable data analysis, such as principal component analysis (PCA) or partial least squares (PLS) modeling. Conductivity meters also measure the current flowing through the solution due to an alternating potential, the hardware required is similar to the electronic tongue except the multielectrode relays and the post-signal processing. A drawback using conductivity is the lack of fingerprinting ability.

2. Experimental

2.1. Chemicals

Distilled water and analytical grade methanol was used as HPLC eluent. The detergent used is a standard detergent IEC-A [7] purchased from WFK Institute, Germany.

Surfactants: alkyl benzyl sulfonate (ABS) and etoxylated fatty alcohol (EOA) of technical grade was used for HPLC identification and in the pretrials.

2.2. Instruments

2.2.1. HPLC system

Agligent system 1100 with diode array detector tuned to 205 nm, flow of 0.5 ml/min, eluent. The HPLC pumps were programmed to pump 30% methanol in water in the beginning of the sample run, 3 min after sample injection the amount of methanol increased to reach 100% 8 min after injection. Peaks from the surfactants were detected within 15 min and system was rinsed with methanol for another 10 min. Separation was performed on an Agligent hypersil ODS 5 μm 4.6 mm × 100 mm colon.

2.2.2. The voltammetric electronic tongue

The voltammetric electronic tongue consists of a potentiostat with a multiplexer to connect to four working electrodes and pattern recognition system. The four working electrodes were of gold, iridium, platinum and rhodium; all with the purity of 99.9% and 1-mm diameter housed inside a stainless steel tube that also worked as a counter and reference electrode. Isolation between the counter electrode and the working electrode was provided by plastic dental material. Potentiostat and multiplexer were built at the lab and controlled by a computer. A fixed set of potentials was applied to the electrodes while the current response was recorded as in Fig. 1. The potential pulses used were 0, 0.8, −0.8, −0.8, 0, 0, 0, 0, 0.6, 0, 0.5, 0, 0.4, 0, −0.2, 0, −0.4 and 0 V relative to the counter electrode with duration of 40 ms. The current signals recorded every meter second was further imported to Matlab and analysed by pattern recognition techniques [8], e.g. PLS.

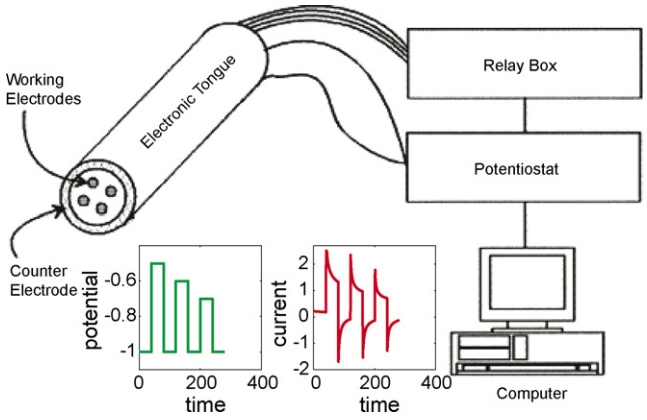

Fig. 1. The electronic tongue system and signals.

2.2.3. Conductivity meter

RS 180-7127 from RS Electronics Comp. GB. The conductivity cell was dipped into the samples, conductivity readings recorded from the display.

2.2.4. The washing machine

The washing machine in which all the samples are made is an Asko W650 (Asko Cylinda AB, Sweden). It is a front-loaded household washing machine with a maximum load of 5 kg. Water intake is through the detergent compartment, and samples were taken through a rubber tube fitted in the bottom of the washing cylinder housing.

2.3. Samples

All samples were taken from a washing machine in different stages in the washing cycles, water intake, main wash and rinses, and put into plastic beakers with lids. The samples were then stored at 8 °C. Small volumes, about 1.5 ml, were put into glass screw cap vials, specially made for the HPLC sample tray, from each sample just before the final analysis. Standards were made from deionised water and standard detergent.

2.4. Measurement and analysis procedure

A method for the separation of the two main surfactants in the detergent was developed, using samples of technical grade surfactants and detergents. This method was then used to measure the amount of detergent and surfactants in the samples. The entire batch of chromatograms was saved for later computer analysis. Conductivity and electronic tongue measurement were completed in parallel to the chromatograms, due to the HPLC auto sampler. The conductivity cell was placed into the plastic beaker and the reading was recorded from the display by hand. Directly after the conductivity measurement, the electronic tongue was immersed into the plastic beaker and 30 sequences were recorded for every sample.

2.5. Computer analysis

Multivariate data analysis is used to treat the raw signals obtained from the sensors and the information from the chromatograms. Since the electronic tongue produce a signal vector with hundreds of variables for every recorded set of pulses, it will be essential to use a multivariate analysis method to predict the samples. Principal component analysis is one of the MVDA methods that explain the variance of a dataset [8,9]. Partial least squares (PLS) are an example of a multivariate linear regression method for

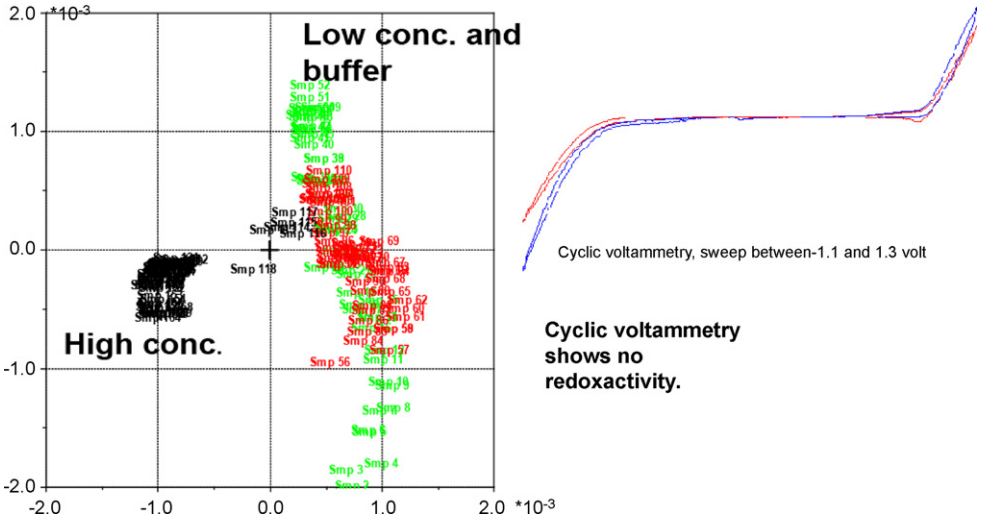

Fig. 2. A distinct difference is shown between measurements with surfactant concentration well above micelle formatting concentration and measurements on no or low surfactant concentration.

finding a mathematical model describing predictable variables in terms of observed variables [8,9].

Calibration was done by using the known standard samples and their chromatograms, for the levels of detergent the whole chromatogram was used as a signal, for ABS and EOA their specific signal in the chromatograms was extracted. These calibrations were then used to predict the concentrations of the surfactants in the washing machine samples. Due to the amount and variation of complexity of the samples, cross-validation was used to evaluate the sensors when predicting the measured sample concentrations from the signals recorded from the conductivity meter or electronic tongue.

All data analysis was performed with Matlab (Mathworks, Inc.) and PLS-toolbox for Matlab (Eigenvector Research, Inc.).

3. Results and discussion

3.1. Initial experiments

To verify that it would be possible to detect changes in surfactant concentrations electrochemically, a few surfactants commonly used in household detergents were tested for redox activity. The tests were performed in phosphate buffer solution using cyclic voltammetry. The potential of a platinum-working electrode was swept between the oxidation and reduction of water. At low concentrations of the surfactants no evident redox activity was observed, also at higher concentrations, well over micelle formation concentrations, no specific redox current was observed. Indicating that the surfactants are not redox active. The currents from the reduction and oxidation of water were affected by the increased concentration of surfactants. This change was not noticeable in the beginning but observed when treating the cyclic voltammograms with PCA. Thus PCA scores show a clear difference between very high concentration and buffer solution, using data collected from cyclic voltammetry as shown in Fig. 2. The shift seen in the score plot is explained by the decrease in reduction and oxidation current at the turn points in the cyclic voltammogram. At these potentials −1.1 and 1.3 V (vs. NHE) reduction and oxidation of water is the major contribution to the current measured. But with high concentrations of surfactant this reduction and oxidation of water is slowed down, and current is decreased. This verification is encouraging but not enough to say if surfactants concentration is measurable by voltammetry.

During the cyclic voltammetry experiments, it was discovered that the equilibrium potential for the electrode changed when the surfactant concentration was altered. A potentiometric examination of a solution where the concentration of surfactant was changed, increased by the addition of more surfactant and decreased by the addition of buffer, showed a concentration-dependent signal that also were reversible (see Fig. 3).

Due to the discovery that the potential could give an estimation of the concentration of surfactant in the solution, it is suggested that the surfactant affects the closest vicinity of the electrode by displacing water molecules and other species that affect the equilibrium potential at the working electrode. Since surface potential depends on many causes like pH, electrolyte composition, etc. it would be very complicated to correlate the electrode potential to the surfactant concentration. But if the surfactant affects the surface of the electrode displacing other species and hindering them from reaching the electrode in normal fashion to be oxidised or reduced, voltammetry could be used as an indirect way to detect the concentration of surfactant. Earlier reports on such phenomenon by Anson [10] demonstrate that neutral molecules like alcohols displace water and other species from

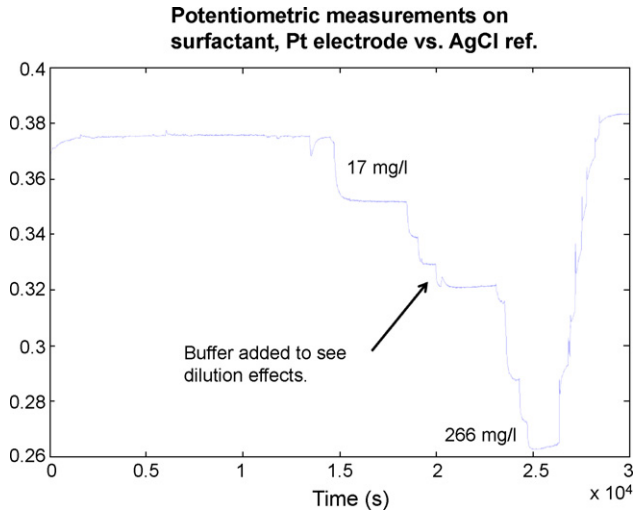

Fig. 3. Potentiometric examination of surfactant concentration.

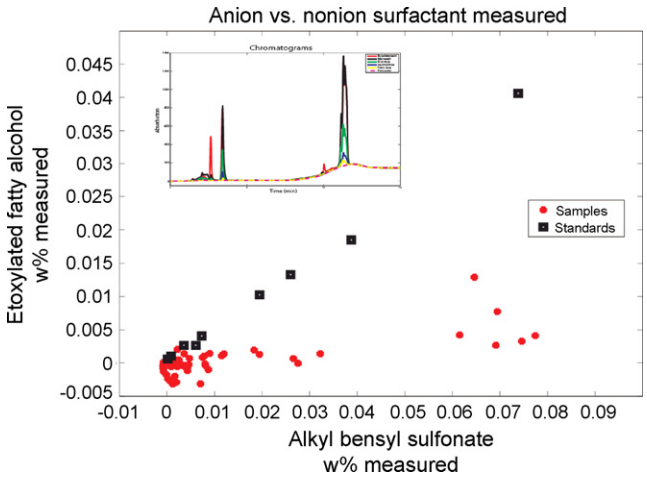

Fig. 4. Chromatograms shows that EOA is present at low concentration in the samples, but ABS varies according to the levels of detergent.

uncharged surfaces and hindering other molecules to reach the surface.

The charging of the double layer will be an important part in the indirect detection of the surfactants. The initial current flow, when shifting potentials depends strongly on the charging of the species close to the electrode surface, could easily be measured by potential step methods such as square wave pulse voltammetry. Together with multivariate data analysis, the wanted information should be possible to be sieved out.

3.2. Washing machine experiments

When attempting to build a multivariate data model for prediction surfactants or detergents in real samples it is essential to use a reference method, such as HPLC. Considering the background matrix within the washing machine samples, a filter or chromatography step is necessary to arrange the different analytes in a measurable way. Since the samples were taken from different stages in the washing cycle (main-wash, first rinse, second rinse, etc.), they contained remains of dirt, textile particles and detergent to different levels.

The calibration of the three unknown species (the amount of detergent, the concentration of ABS and EOA) in the samples was done by mixing artificial standards with known composition from the basic detergent and using the chromatograph for the prediction of all three analytes in the samples. These predicted amounts were later used as the measured analytes.

The behaviour of the samples, from the later parts of the wash cycle shows decreasing levels of detergent compared with the initial starting levels of the washing cycle, mostly due to dilution from the following rinses, as expected. However, when individual surfactants are studied, another behaviour is noticed. The ABS surfactant is rinsed away accordingly to our assumption, but EOA appears to be at a constant low level in the samples. This might be explained by two different phenomena; the surfactant did not dissolve or the surfactant adsorbs to laundry or exposed surfaces in the washing machine. Since the ratio between ABS and EOA concentration is constant in the standards, that was never exposed to dirty textiles or the washing machine, solvent problems can probably be excluded. Higher EOA concentrations are confirmed in a few samples, mainly those overloaded with detergent. In Fig. 4, the concentration of EOA and ABS is shown, for the standards (squares) the ratio EOA/ABS is stable. The sample from the washing machine shows a varied concentration of ABS but a fairly low constant level of EOA.

Unfortunately, most of the EOA lies outside our calibration range and we suspected the two surfactants to perform differently, but not to such a degree that one of them sticks permanently to the load inside the washing machine. This also makes the performance of rinse sensors more important to avoid residue surfactants left on the clothes and textiles.

3.3. Detergent predictions by the electronic tongue and conductivity meter

The amount of detergent in the samples was measured by HPLC, and prediction models were made from the signals recorded by the electronic tongue and conductivity meter. Both the sensors performed well, probably due to the composition of the detergent. The detergent consists of about 50% supporting electrolyte and buffering compounds, which has a great influence on the ability conduct current, when diluted in the rinses the conductivity decreases, which is measurable both for the conductivity meter and the electronic tongue. The conductivity meter is able to predict detergent concentration with less precision than the electronic tongue, but can handle the task reasonable for process control use.

3.4. Surfactant predictions

The main surfactant in the standard detergent used is ABS, at about 7.5% of the dry weight of the detergent. In initial experiments the surfactants were tested for redox activity, which was not found inside the water redox window. However, open circuit potentials showed a potential change due to increasing surfactant concentration, this change was also reversible (see Fig. 3). The experiment showed that even if the surfactant did not have redox activity, it still affects the electrode surface in a measurable way. Since the surfactants are likely to replace water and other small counter-charged species on or near the electrode surface, the effect would be seen as an artefact in the charging of the double layer or even as an increased diffusion resistance, since the surfactants hinder redox active spices to reach the electrode [10]. In the real samples, the prediction of the surfactant ABS is achieved by both sensors because the concentration of the surfactant ABS is following the concentration of detergent with supporting electrolyte and buffer. Due to this, there is a statistic correlation between the ABS surfactant concentration and the supporting electrolyte or buffer concentration,

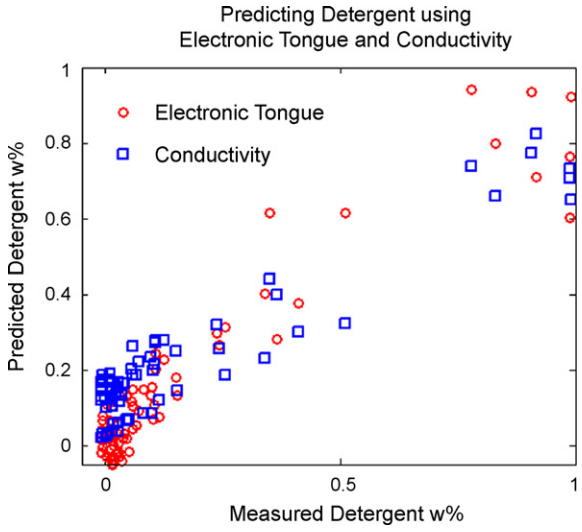

Fig. 5. Detergent predictions by the electronic tongue and conductivity measurements .

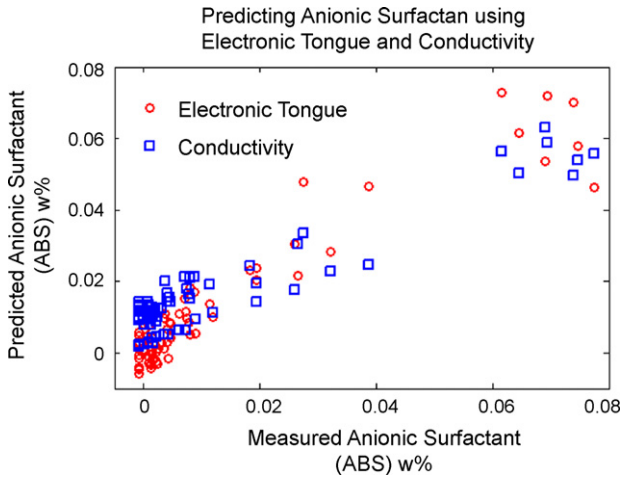

Fig. 6. Prediction of alkylbenzyl sulfonate by conductivity and electronic tongue measurements.

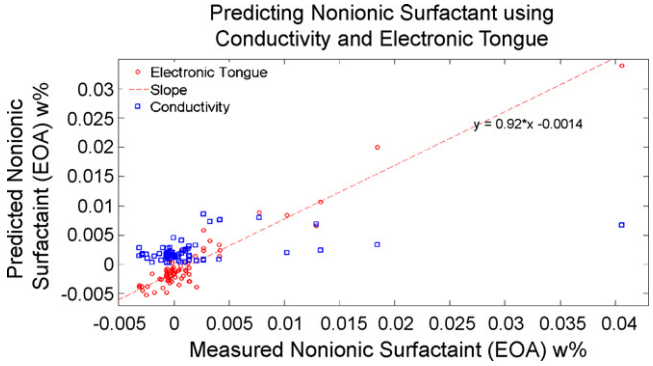

Fig. 7. Prediction of etoxylated fatty acids with conductivity and the electronic tongue, calculated slopes are 0.15 and 0.92, respectively.

thus, ABS concentration can be predicted by both the sensors, as shown in Figs. 5 and 6.

Because of the correlation to the supporting electrolyte, there are no ways to distinguish between supporting electrolytes or the anionic surfactant, ABS, with the electronic tongue. Thus, for process control the simpler conductivity meter will perform equally well.

The non-ionic surfactant EOA has a strong indication of not behaving as the other components in the detergent. EOA appears to have a tendency to stick to the textiles or to the inside of the washing machine then follow the rinses dilution path. Just a few samples, mainly those with low dirt and high detergent concentrations have elevated levels of EOA. Also, since EOA does not behave as the other components in the detergent, it could be predicted with less interference and correlation from other species from the detergent. As pointed out previously, the measured levels of EOA are very low in the calibration, therefore the precision of the measured can be questionable.

In Fig. 7, a model to predict EOA is suggested for the electronic tongue and conductivity meter. Even if the number of observations of high concentration of EOA is low, this model gives a clear indication of the electronic tongue ability. Due to the lack of interference from conducting species in the detergent, the conductivity meter fails to predict the concentration of EOA. The ET predictions are not without error, but one can clearly notice a positive trend in the prediction of EOA. To achieve better EOA predictions a recalibration of the HPLC method is necessary, where a more adequate dynamic range should be measured to give higher resolution of the EOA chromatograms within the actual calibration range. Even though the prediction of the ET has shortcomings, the results indicate its possibilities.

4. Conclusion

If the future bears an automatic washing machine, it will definitively use sensors to control the rinse procedure to leave clothes and textiles without dangerous residues from the detergents. However, as it was shown, some of the residues rinses away differently from others and making it a delicate task to correlate the signals from the sensors with the measured analyte. The conductivity meter is able to give reasonable good predictions of the detergent as a mixture of species, but is lacking performance when predicting non-conducting surfactants, as EOA. The electronic tongue manages to predict both levels of detergent and the anionic surfactant ABS with better precision compared to the conductivity meter. The prediction of the non-ionic surfactant EOA is difficult because its behaviours differ from the rest of the detergent. Thus, it has a very high affinity towards the textiles inside the washing machine, leaving very low levels of EOA in the rinsed water. The few elevated observations are enough to show that the electronic tongue has the potential to predict this surfactant. The missing correlation to other conducting species makes the conductivity meter fail to predict EOA. This work shows that sensors like the electronic tongues can be used for measuring surfactants inside a washing machine, but more thoroughly investigations are needed. The effects of different brands and formulations of detergents and even addition of fabric softeners, usually containing cationic surfactants, need to be explored before there can be an automatic washing machine.

References

[1] L.K. Poulsen, S.K. Clausen, C. Glue, A. Millner, G. Damgaard Nielsen, T. Jinquan, Toxicology 152 (1–3) (2000) 79–85.
[2] Metod för mätning av sköljeffekt, Nordiska Ministerrådet, Ämbetsmannakommitén för Konsumentfrågor, December 2003.
[3] S. Wangkarn, P. Soisungnoen, M. Rayanakorn, K. Grudpan, Talanta 67 (15 October (4)) (2005) 686–695.
[4] P. Ivarsson, M. Johansson, N.-E. Höjer, C. Krantz-Rülcker, F. Winquist, I. Lundström, Sens. Actuators B: Chem. 108 (1–2) (2005) 851–857.
[5] F. Winquist, P. Wide, I. Lundström, Anal. Chim. Acta 357 (1–2) (1997) 21–31.
[6] T.K. Ericson, M. Wilson, Sci. Honeyweller Sens. Issue (1996) 16–20.
[7] IEC60456, Clothes Washing Machines for Household Use—Methods for Measuring the Performance, Geneva, 1998.
[8] P. Geladi, B. Kowalski, Anal. Chim. Acta 185 (1986) 1–17.
[9] S. Wold, K. Esbensen, P. Geladi, Chemometr. Intelligent Lab. Syst. 2 (1987) 37–52.
[10] F.C. Anson, Acc. Chem. Res. 8 (1975) 400–407.

Talanta 76 (2008) 233

Contents lists available at ScienceDirect

Talanta

journal homepage: www.elsevier.com/locate/talanta

Letter to the Editor

Comments on "The determination of tungsten, molybdenum, and phosphorus oxyanions by high performance liquid chromatography inductively coupled plasma mass spectrometery" by Bednar et al.

Dear Editor,

We read with great interest the article by Bedar et al. [1] describing an enhanced analytical technique for detecting the various species of tungsten in environmental media. We concur with the authors that the analytical speciation of tungsten (as well as other oxyanions) is important to understanding their geochemical and toxicological properties.

In describing the impetus for this research, the authors stated "[r]ecently, interest in tungsten geochemistry and occurrence in groundwater has increased due to specific human toxicological events, specifically the cancer cluster in Fallon, NV, and suspected cases in Sierra Vista, AZ, and Elk Grove, CA, all related to natural deposits of tungsten ore. The authors further state that "[t]he potential impact to human health has made the Center for Disease Control investigate the link to human health in impacted areas."

While the underlying technical discussion regarding the HPLC–ICP-MS technique appears to be scientifically sound, we are concerned about the commentary regarding the "toxic properties of tungsten compounds" and the implication that tungsten is the cause of reported cancer clusters in the western U.S.

We note with some dismay that none of the documents cited by the authors include the Centers for Disease Control and Prevention (CDC) reports regarding the Fallon leukemia cluster or the purported Sierra Vista cluster.

Following an extensive study of the Fallon community, the CDC [2] stated "[u]sing conditional logistic regression and limiting our analysis of tungsten exposure to case families, excluding siblings, and their matched comparison families, we found no relation between leukemia and tungsten exposure."

In its final report on the Sierra Vista community, the CDC [3] concluded "[s]ome individual study participants had elevated levels of tungsten, styrene, and a few of the low-numbered PCB congeners. However, this finding most likely indicates individual variation, not community-wide environmental exposure. The number of children with leukemia who participated in the study was small ($n = 4$), thus any attempt to measure associations between environmental exposure and disease would be inherently suspect and not statistically appropriate."

While the CDC was unable to identify a likely source of the increased incidence of leukemia (and numerous agents were investigated), clearly tungsten was not implicated as the cause.

Seiler et al. [4] noted that "residents of the Carson Desert, Nevada are exposed to high levels of W and this prompted an investigation of W [tungsten] in aquifers used as drinking water sources." The Seiler article further states that "[t]he principal sources of W in groundwater are natural ..." Consistent with the findings of naturally occurring tungsten in groundwater, CDC [2] observed that elevated levels of tungsten were found in urine sample from the residents of Fallon when compared to other populations (primarily based on studies of residents in the eastern portion of the U.S.).

Even though no causal association was found between the cases of leukemia and tungsten exposure, the CDC nominated tungsten to the National Toxicology Program for additional study. The basis of this recommendation was to develop additional toxicological data to assess the human health implications of elevated urinary levels of tungsten (68 FR (July (136)) (2003) 42068–42071).

Research on tungsten continues at a high rate, and new studies are being reported on virtually a monthly basis. However, to date none of this research has implicated tungsten in any "human toxicological events, specifically the cancer cluster" as was stated by Bednar.

We are not questioning the quality of the work presented by these authors on the enhanced analytical technique for quantifying oxyanions in environmental media. Rather, we recommend that the authors remain focused on their efforts to further refine this important analytical method. Suggesting that childhood leukemia is related to exposure to environmental tungsten is both inappropriate and misleading.

The author acknowledges that they provide consulting services for Kennametal Inc., a company with a production facility in Fallon, NV.

References

[1] A.J. Bedar, J.E. Mirecki, L.S. Inouye, L.E. Winfield, S.L. Larson, D.B. Ringelberg, Talanta 72 (2007) 1828.
[2] CDC, Cross-Sectional Exposure Assessment of Environmental Contaminants in Churchill County, Nevada, Final Report, February 6, 2003.
[3] CDC, Biosampling Case Children with Leukemia (Acute Lymphocytic and Myelocytic Leukemia) and a Reference Population in Sierra Vista, Arizona, Final Report, November 30, 2006.
[4] Ralph L. Seiler, Kenneth G. Stollenwerk, John R. Garbarino, Appl. Geochem. 20 (2005) 423–441.

M. Pardus*
ARCADIS, 600 Waterfront Drive, Pittsburgh, PA 15222, United States

*Tel.: +1 412 231 6624x561; fax: +1 412 231 6147.
E-mail address: michael.pardus@arcadis-us.com

Available online 26 February 2008

doi:10.1016/j.talanta.2008.02.015

Talanta 76 (2008) 102–106

Contents lists available at ScienceDirect

Talanta

journal homepage: www.elsevier.com/locate/talanta

Microwave-assisted extraction of decabromodiphenylether from polymers

Andreas Ranz [a], Eveline Maier [a], Christian Trampitsch [b], Ernst Lankmayr [a,*]

[a] Institute of Analytical Chemistry and Radiochemistry, Graz University of Technology, Technikerstrasse 4, 8010 Graz, Austria
[b] Anton Paar GmbH, Anton-Paar-Strasse 20, 8054 Graz, Austria

ARTICLE INFO

Article history:
Received 5 October 2007
Received in revised form 8 February 2008
Accepted 14 February 2008
Available online 10 March 2008

Keywords:
Microwave-assisted extraction
Polymers
Decabromodiphenylether
Brominated flame retardants

ABSTRACT

Contrary to its lower brominated congeners, the flame retardant decabromodiphenylether (DecaBDE) is not banned by the decision 2005/717/EG of the European Union. But the question of the bioavailability and bioaccumulation of this second most used flame retardant worldwide becomes subject of more intense research. In the present study, we developed a microwave-assisted method for the extraction of DecaBDE from polymers. Owing to its main use in electrical and electronic appliances and according to the fire safety standard UL94 V-0, the extraction procedure was carried out for the model compounds polyethylene and polystyrene. Special emphasis has been given to an accurate optimization by an experimental response surface design. Quantification was performed by means of HPLC-DAD. In order to achieve comparable data, extraction was also performed with classic Soxhlet extraction. To compare these results with an independent technique, microwave-induced oxygen combustion and ion chromatography complete this study.

1. Introduction

Firstly, the European Union (EU) prohibited the use of polybrominated diphenyls and polybrominated diphenyl ethers including decabromodiphenyl ether (DecaBDE) with the Directive on the Restriction of the Use of Certain Hazardous Substances in Electrical and Electronic Equipment (RoHS) 2002/95/EC. But already 1 year before it took effect on July 2006 the European Commission lifted parts of the ban against the wishes of the European Parliament (2005/717/EG). Presently this debate is ongoing, also at the Court of European Justice [1].

DecaBDE is used as an additive flame retardant mainly in plastics (75%) and textile (25%) applications. Each year, more than 7500 tonnes of DecaBDE are imported into the EU [2]. Contrary to lower brominated diphenylethers like PentaBDE or OctaBDE, which are banned (the maximum tolerated concentration for these chemicals is 0.1%, as set in Commission Decision 2005/618/EC), the use of DecaBDE is still allowed. This decision is reasoned by the assumption that DecaBDE is inert, due to its high molecular weight and its hydrophobicity [3]. But the question, how bioavailable and bioaccumulative it is, becomes subject of more intense research. Recent publications indicate a certain amount of risk [4–9]. A second important point of interest seems to be the possibility of a debromination of DecaBDE [10]. Debromination can result in products, which are potentially toxic and therefore need to be banned [11–14]. Thirdly, The EU Risk Assessment Report (RAR) under Regulation (EEC) 793/93 on Existing Substances (ESR) describes the production of DecaBDE and the impurities issue, mainly the Non-aBDE content [2].

Thus, the necessity of a monitoring of DecaBDE needs to be pointed out, but not only in environmental samples. Especially due to the fact, that it is the second most used brominated flame retardant [15]. Mainly used in electrical and electronic appliances, a determination directly in these materials according also due to the Waste Electrical and Electronic Equipment Directive (WEEE Directive, 2002/96/EC) is necessary.

In the present study, a method for the determination of DecaBDE in polymers has been developed, optimized and validated. Since the concentration at which DecaBDE has to be measured in polymers is high (above 100 ppm), special emphases have been given to an accurate extraction. The challenge in polymer extraction is not only to reach high recoveries of investigated analytes, but also to create an easy-to-handle method.

Due to the fact that more and more studies are published indicating time trend increasing of concentrations in different environmental matrices and also in humans [16], it is astonishing that no standard analytical procedures have been set for these analytes [17]; especially the determination directly from the main originator, from the relevant polymers. Analytical procedures have typically been based on protocols previously established for trace persistent organic pollutants (POPs), such as polychlorinated biphenyls (PCBs) or organochlorine pesticides. This can cause problems,

* Corresponding author. Tel.: +43 316 873 8301; fax: +43 316 873 8304.
E-mail address: lankmayr@tugraz.at (E. Lankmayr).

0039-9140/$ – see front matter © 2008 Elsevier B.V. All rights reserved.
doi:10.1016/j.talanta.2008.02.009

especially if somebody draws comparisons between the molecular mass of bromine and chlorine. This applies mainly for the decabromodiphenylether. Its high molecular mass and its high boiling point make it not easily amenable to a determination with standard gas chromatography. Some papers dealing with this subject are published, thus HPLC was used as the method for separation and quantification [18–21]. HPLC affords a sample preparation without any steps between extraction and injection. The composition of the extracts allows to inject the extracts directly after centrifugation, of course a simple clean up with solid phase extraction with C 18 materials is possible, this additional step can be abandoned however. A very critical and error-prone step and a challenge for analytical chemists is the extraction from the polymers. In recent years, besides the classic Soxhlet extraction and the ultrasonic extraction also alternative techniques have been proposed. Representative examples of these new extraction techniques are supercritical fluid extraction, pressurized liquid extraction and microwave-assisted extraction (MAE). For the extraction of polymers MAE is a promising technique, particularly owing to its technical and safety features. It is possible to control temperature, pressure and microwave energy, as well as to perform serial extractions simultaneously, etc. Since the efficiency is dependent on several parameters, a careful investigation of potentially influential factors is necessary and it needed to be emphasized in this work. Factors of interest in this study are extraction temperature, hold-up time and the addition of methanol as necessary polar component for microwave absorption. In order to identify the statistical influential parameters and also to optimize these factors, a Box-Behnken design was chosen. A comparison between this design and other response surface designs has demonstrated that the Box-Behnken is more efficient than three-level full factorial designs. It allows an estimation of the optimum conditions as a part of a quadratic model, the detection of lacks of the fit, as well as the use of blocks [22,23].

For verification of the performance of the extraction method and in order to obtain meaningful data, a comparison with the classic Soxhlet technique was accomplished. Owing to the well-known composition of the quality control material and due to the fact that DecaBDE is the only brominated additive in the polymers investigated, reference concentrations were determined by analysis of the amount of bromine. Therefore, the polymers were combusted and bromine was quantified by means of ion chromatography.

Thus, microwave extraction has shown to be an efficient, reliable and high throughput method for the determination of DecaBDE from polymers.

2. Experimental

2.1. Sample

Two masterbatch samples of polyethylene (PE) and polystyrene (PS) containing 53.3% and 42.0% DecaBDE as the sole brominated flame retardant were compounded with pure polyethylene or polystyrene.

As a result, polyethylene and polystyrene pellets with a diameter of 2–3 mm and a final concentration of approximately 2% of DecaBDE were obtained. In order to support the recovery data, an additional Laboratory Reference Sample containing 0.5% of DecaBDE was prepared. Pellets from both materials were used for further experiments without any additional pre-treatment.

2.2. Reagents and chemicals

Flame retardant standard decabromodiphenylether (also described as bis(pentabromophenyl)ether or DecaBDE, CAS: 1163-19-5) was supplied by Alfa Aesar (Karlsruhe, Germany) (purity: 99.0%). A stock standard solution was prepared by dissolving in THF of the appropriate weighed solid compound and stored at 4 °C protected from light. Toluene and methanol were supplied by Baker (Deventer, The Netherlands) (purity: ultra resi-analyzed) and THF was acquired from Merck (Darmstadt, Germany) (purity: ultra resi-analyzed). Sodium carbonate (Na_2CO_3, p.a.) and sodium hydrogen carbonate ($NaHCO_3$, p.a.) were purchased from Merck. Ammonium nitrate (NH_4NO_3, p.a.) was purchased from Roth (Karlsruhe, Germany). Sulphuric acid (H_2SO_4, p.a. 95–97%) was also purchased from Merck. Nitrogen (99.9990%) and oxygen (99.9990%) were obtained from Air Liquide (Graz, Austria). A bromide standard for ion chromatography was purchased from Merck as 1000 mg L^{-1} solution of NaBr in H_2O (SRM of NIST). Ultra pure water purified by Milli-Q Gradient system (Millipore, Bedford, USA) was used for all experiments (resistivity > 18 MΩ cm).

2.3. Microwave-assisted extraction

Extraction experiments were carried out with a Multiwave 3000 microwave reaction system (Anton Paar GmbH, Graz, Austria) equipped with a 16-position extraction rotor. Aliquots of 250 mg of polymer sample were weighed into 100 mL extraction vessels made of TFM-PTFE.

The total amount of solvent was kept constantly at 20 mL, the composition of the extraction solvent was changed as indicated by the experimental design. The vessels were closed with lip-type seals made of TFM-PTFE.

Extractions were performed in temperature-controlled mode by measuring pressure and temperature in one reference vessel. After a heating ramp of 10 min, temperature and hold time were set according to the experimental design. Immediately after the temperature program had finished, all vessels were cooled down to ambient temperature. All extractions were performed with magnetic stirring.

After extraction an aliquot was taken and centrifuged for 5 min with 4000 × *g*.

2.4. Soxhlet extraction

In order to achieve comparable data with a reference procedure, a classic Soxhlet extraction had been performed. Therefore, 1 g sample was transferred into an extraction thimble and inserted into a 100 mL Soxhlet extractor. Extraction was accomplished according to the Federal Institute for Materials Research and Testing (BAM) with 70 mL toluene for 6 h resulting in more than 100 extraction cycles. Since extraction thimbles are potential contamination sources they were pre-extracted before use under reflux with 70 mL toluene for 2 h. Raw extracts and washing solution from the rinsing the sample flask were added to an 100 mL volumetric flask and filled up to exactly 100 mL. Two milliliter-portions were centrifuged for 5 min with 3500 rpm and finally transferred into HPLC autosampler vials for measurement.

2.5. Experimental design

Due to the novelty of this procedure, a careful investigation of influential parameters had been essential. To get this information, a Box-Behnken design was performed. This design is a combination of two-level factorials and incomplete block designs. It results in a three-level design used for quantitative factors and is designed to estimate all the main, quadratic and two-way interaction effects. The effect of the parameters, composition of extraction solvent (mixtures of methanol and toluene), extraction temperature and extraction time were considered to obtain optimum conditions. The limits of the three factors are shown in Table 1. The sequence

Table 1
Parameter setting for the optimization

Parameter	Minimum	Intermediate	Maximum
Amount of methanol (%)	25	37	50
Temperature (°C)	100	120	140
Hold-up time (min)	10	25	40

of the experiments has been fully randomized to provide protection against the effect of lurking variables. All experiments were repeated three times. For statistical calculations the software package STATGRAPHICS PLUS Version 3 for Windows (Manguistics, Rockville, USA) was used to create experimental designs and to analyze experimental data.

2.6. High performance liquid chromatography

Analysis was carried out by high performance liquid chromatography. Separation and quantification was performed by using an Agilent 1100 series chromatograph equipped with a diode array detector (HPLC-DAD, Sig = 210,4 Ref = 360,100). An injection volume of 5 μL was selected for all analyses. The column used was a GraceSmart RP 18, 5 μm, 150 mm × 4.6 mm standard reversed phase column. The mobile phase consisted of methanol and water (methanol:water, 95:5, v/v). Separation was accomplished in isocratic mode within a runtime of 10 min. Proper peak purity has been verified by means of comparison of the individual DAD UV-spectra in the range of 200–400 nm of the relevant chromatographic peaks with that from the pure reference component.

Validation was accomplished to verify the performance of the HPLC method. Therefore, a sixfold repetition at six concentration levels (between 2 and 420 μg/mL) was measured. Aim of the validation was to determine the linearity of the method as well as the limit of detection and the limit of quantification. Calculation of LOD, LOQ and linearity was performed by the calibration method with the Excel Macro Validata Version 3.02.54ger (Wegscheider-Rohrer-Neuboeck, Leoben, Austria) at the 95.0% confidence interval, following the Eurachem/CITAC Guide [28]. LOD was determined at 2.40 μg mL^{-1}, LOQ at 8.60 μg mL^{-1} and linearity was proofed within 2.10 and 420 μg mL^{-1} (Fig. 1).

2.7. Microwave-induced oxygen combustion

Combustion of organic samples under (pressurized) oxygen atmosphere has been widely accepted as an effective method for subsequent determination of both metals and non-metals.

The same principle is applied during microwave-induced oxygen combustion, which was performed in a Multiwave 3000 microwave reaction system (Anton Paar GmbH, Graz, Austria) equipped with an 8-position digestion rotor and oxygen combustion accessories. This technique has been already successfully applied to biological materials [24].

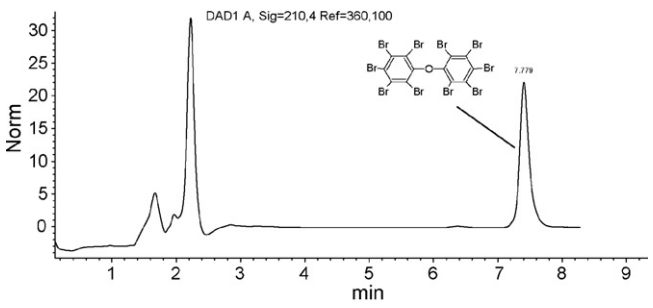

Fig. 1. HPLC chromatogram of DecaBDE.

Up to 8 quartz vessels with a volume of 80 mL were filled with 10 mL of absorption solution (8 mmol L^{-1} Na_2CO_3 and 1 mmol L^{-1} $NaHCO_3$ in water). 50–250 mg of polymer pellets were placed on a special sample holder made of quartz, which contained a piece of ash-free filterpaper, impregnated with 50 μL of NH_4NO_3-solution (50%, m/v).

The sample holders were put into the quartz vessel, which were closed with a lip-type seal made of TFM-PTFE. The vessels were placed into the digestion rotor and pressurized with up to 20 bar of oxygen.

The samples were ignited by means of microwave irradiation. Combustion took place within less than 1 min; microwave power was applied for a total of 15 min to obtain a homogeneous solution.

After cooling down for 60 min, the vessels were vented and an aliquot of the absorption solution was taken for subsequent measurement by ion chromatography.

2.8. Ion chromatography

All measurements were accomplished with a Dionex (Sunnyvale, USA) DX-120 ion chromatograph (IC) with suppressor system (anion self-regenerating suppressor ASRS-II 4 mm) and conductivity detector. Separation was performed using an AS14A IonPac column (4 mm × 250 mm) combined with an AG14A guard (4 mm × 50 mm). The carbonate eluent consisting of 8.0 mmol L^{-1} Na_2CO_3 and 1.0 mmol L^{-1} $NaHCO_3$ was prepared by dissolution of the appropriate standard components. The eluent flow was constant at 1.0 mL min^{-1} and pressurized by nitrogen. Analyses were carried out at 20 °C within 32 min. An injection volume of 25 μL was selected for all analyses. The suppressor module was regenerated with 5 mM H_2SO_4. Analytes were quantified by linear calibration within a range between 10 and 100 mg L^{-1}.

3. Results and discussion

3.1. Sample determination with microwave-induced oxygen combustion-IC

Combustion of organic samples in oxygen-pressurized systems is widely used and also implemented into standards methods of ISO or ASTM [25,26], especially for the subsequent determination by ion chromatography. Beside the conventional techniques, microwave-induced combustion as used in the present study, is a rather new approach with some advantages. So the ignition has been carried out by microwave radiation without the use of additional devices, the microwave system including vessels, rotor parts or pressure control device is the same as used for extraction.

The concentration range of bromide after combustion constitutes between 10 and 150 mg L^{-1}.

The actual content of DecaBDE in PS and PE as determined from these measurements is listed in Table 2. These concentrations were set as 100% and used as target concentration for computation of recovery data as they were obtained from all further experiments (Fig. 2).

Due to the fact, that the generation of elemental bromine resulting from the combustion of the sample is possible, standards with

Table 2
Content of DecaBDE in polyethylene (PE) and polystyrene (PS) with $n = 2$ after determination with microwave-induced oxygen combustion-IC

	PE (%)	PS (%)
2% material	1.83 ± 0.03	2.01 ± 0.03
0.5% material	0.50 ± 0.01	0.44 ± 0.02

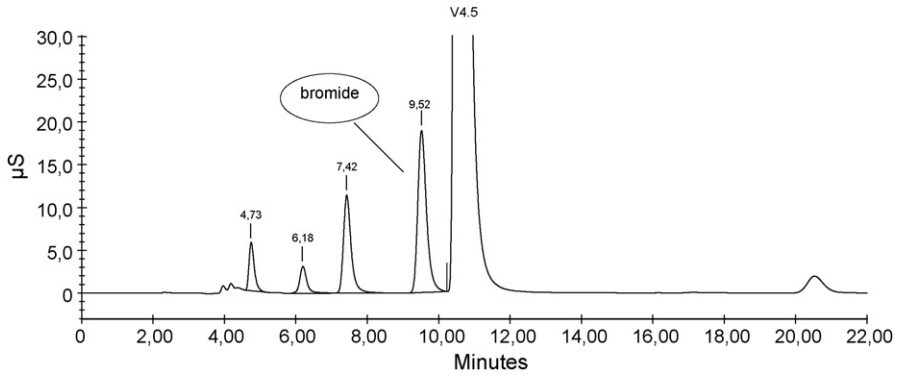

Fig. 2. Chromatogram after microwave-induced combustion and IC-separation.

Table 3
Optimum conditions and recovery for the microwave-assisted extraction of polyethylene (PE) and polystyrene (PS)

Factor	PE	PS
Hold-up time (min)	40	40
Temperature (°C)	124	111
Amount of methanol (%)	25	25

a known DecaBDE concentration (between 50 and 120 mg L^{-1}) were determined to avoid a measurement of too low concentrations. The result of (98.8 ± 0.4)% with $n = 3$ shows only a negligible degradation and allows the usage of the determined values as a reference.

3.2. Experimental design

The optimization of an extraction procedure by means of a Box Behnken design is a process for locating optimum conditions. An optimum parameter setting was investigated for the factors hold-up time, extraction temperature and extraction time. Maximum recovery of DecaBDE was chosen as the target function for the response surface design. All experiments were performed for PE as well as for PS and were repeated three times. By means of the computational calculation with the software package STATGRAPHICS PLUS Version 3 for Windows, optimum conditions were defined [27]. The results are listed in Table 3.

Furthermore, the response surface design allows also a determination of the significance of each factor. Therefore, the influence of the factors on the extraction efficiency is reported by an Analysis of Variance (ANOVA) table. A key component of this ANOVA table is the *p*-value as an indicator for statistical significance. The computationally obtained data are indicated in Table 4. Bold numbers are reflecting significant effects as identified by *p*-values less than 0.05, which means these parameters are significant at 95.0% confidence level. As can be seen from the table, the hold-up time exhibits the biggest influence on the reaction. Temperature and amount of methanol are also identified as statistically significant factors for the extraction from polyethylene. For polystyrene not just the factor hold-up time is influential, also the interaction with the temperature is not negligible, since these reaction variables are not independent from each other.

Table 4
Results of the ANOVA for the response surface design expressed as *p*-values

	p-Values	
	Polyethylene	Polystyrene
A: temperature	**0.001**	0.177
B: hold-up time	**0.009**	**0.000**
C: amount of MeOH	**0.005**	0.059
AA	0.770	0.868
AB	0.609	**0.003**
AC	0.053	0.332
BB	0.065	0.241
BC	0.278	0.817
CC	**0.023**	0.985

Bold numbers are indicating statistically significant factors.

These results are graphically displayed in pareto charts (Fig. 3). The length of each bar in these charts is proportional to the effect divided by its standard deviation. The bars are listed in order of the size of the effect, with the largest effects on top. Factors overpassing the vertical line exert a statistically significant influence on the methylation within the 95.0% confidence level. Interaction factors like AA or BB are just part of the mathematical model without any physical relevance.

Computationally calculated recoveries are about 100%. Both, PE as well as PS is showing similar results, especially for extraction

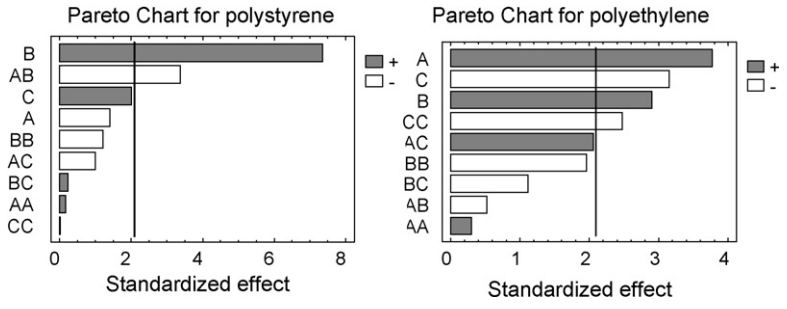

Fig. 3. The pareto charts display not only the influence of the factors temperature A, amount of methanol B, and hold-up time C but also the interactions between these factors.

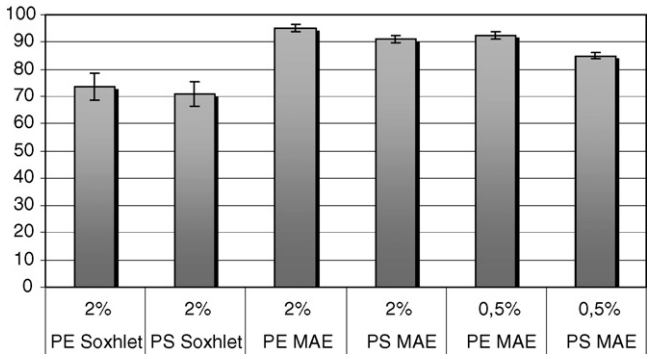

Fig. 4. Comparison of the recoveries between Soxhlet extraction and microwave-assisted extraction (MAE) for the extraction of PE and PS ($n = 4$).

time and temperature. The use of a mixture of solvents is necessary. Toluene with low microwave absorption, but high solubility for DecaBDE requires the addition of methanol with high absorption for microwave radiation. Maximum recovery was obtained for the blend toluene: methanol 75:25 (v/v). The addition of methanol avoids the need of an additional heating element to the reaction vessel. A big advantage of microwave-assisted extraction is the low solvent consumption. The extraction procedure need in total just 20 mL of solvent.

3.3. Comparison with standard Soxhlet extraction

Since Soxhlet extraction has been a standard procedure for the extraction of different kinds of additives from polymers, this technique has been compared to the microwave-assisted extraction. Therefore, MAE experiments were performed four times at the optimum conditions as indicated by the experimental design.

The recovery of DecaBDE in the investigated concentration range was $95.1 \pm 1.3\%$ for PE and $91.1 \pm 1.3\%$ for PS for the 2% material and $92.4 \pm 1.4\%$ for PE and $84.5 \pm 1.1\%$ for PS for the 0.5% material. These values are not as high as those computationally obtained from the optimization, but higher than observed with the standard Soxhlet procedure (as can be seen in Fig. 4).

Another advantage of MAE besides lower solvent consumption is the exact reaction control by temperature and pressure sensoring. Compared to Soxhlet extraction the time is much shorter, not just owing to the better extraction kinetics, but also due to a higher sample throughput.

4. Conclusion

DecaBDE is mainly used to provide flame retardancy to polystyrene, but also to polyolefins like polyethylene in TV back casings, in printers, scanners, fax machines and similar applications. Therefore, a microwave-assisted method was developed to extract DecaBDE from polymers. The microwave-assisted extraction provides an efficient, fast and low solvent consuming method. The extraction from polymers points out the advantages of the microwave better than the extraction from other matrices. The efficiency for polyethylene and polystyrene is very high, especially in a comparison to the standard techniques. As could be shown, the extraction of DecaBDE shows recoveries nearly 100%. This will be reason to continue these results for other polymers and in particular for different blends.

References

[1] UBA (Federal Environment Agency, Germany), Fachpapier, 02/2007.
[2] S. Pakalin, T. Cole, J. Steinkellner, R. Nicolas, C. Tissier, S. Munn and S. Eisenreich, Review on Production Process of Decabromodiphenylether, European Chemicals Bureau, EUR 22693 EN, 2007.
[3] IPCS (International Program on Chemical Safety), Environmental Health Criteria, vol. 162, International Programme on Chemical Safety, World Health Organization, Geneva, 1994.
[4] E. Eljarrat, A. Labandeira, G. Marsh, D. Raldúa, D. Barceló, Chemosphere 70 (2008) 1182.
[5] D.C. Rice, E. Reeve, A. Herlihy, R.T. Zoeller, W.D. Thompson, V.P. Markowski, Neurotoxicol. Teratol. 29 (2007) 511.
[6] X.-Z. Hu, Y. Xu, D.-C. Hu, Y. Hui, F.-X. Yang, Toxicol. Lett. 171 (2007) 19.
[7] I. Watanabe, T. Kashimoto, R. Tatsukawa, Chemosphere 16 (1987) 2389.
[8] U.S. Environmental Protection Agency, Polybrominated Diphenyl Ethers (PBDEs) Project Plan, March 2006.
[9] U.S. Environmental Protection Agency, Tracking progress on U.S. EPA's Polybrominated Diphenyl Ethers (PBDEs) Project Plan: Activity-by-Activity Status Report, March 2007.
[10] E.V.-d. Steen, A. Covaci, V.L.B. Jaspers, T. Dauwe, S. Voorspoels, M. Eens, R. Pinxten, Environ. Pollut. 148 (2007) 648.
[11] K. Hayakawa, H. Takatsuki, I. Watanabe, S. Sakai, Chemosphere 57 (2004) 343.
[12] Y. Wang, G. Jiang, P. Lam, A. Li, Environ. Int. 33 (2007) 963.
[13] M.H. Wong, S.C. Wu, W.J. Deng, X.Z. Yu, Q. Luo, A.O.W. Leung, C.S.C. Wong, W.J. Luksemburg, A.S. Wong, Environ. Pollut. 149 (2007) 131.
[14] J. Regueiro, M. Llompart, C. Garcia-Jares, R. Cela, Anal. Bioanal. Chem. 388 (2007) 1095.
[15] L. Tseng, M. Li, S.-S. Tsai, C.-W. Lee, M.-H. Pan, W.-J. Yao, P.-C. Hsu, Chemosphere 70 (2008) 640.
[16] H.M. Stapleton, J.M. Keller, M.M. Schantz, J.R. Kucklick, S.D. Leigh, S.A. Wise, Anal. Bioanal. Chem. 387 (2007) 216.
[17] A. Covaci, S. Voorspoels, L. Ramos, H. Neels, R. Blust, J. Chromatogr. A 1153 (2007) 145.
[18] M. Schlummer, L. Gruber, A. Mäurer, G. Wolz, R. van Eldik, Chemosphere 67 (2007) 1866.
[19] M. Schlummer, F. Brandl, A. Mäurer, R. van Eldik, J. Chromatogr. A 1064 (2005) 39.
[20] M. García, I. Rodríguez, R. Cela, J. Chromatogr. A 1152 (2007) 280.
[21] Z. Xie, R. Ebinghaus, R. Lohmann, O. Heemken, A. Caba, W. Püttmann, Anal. Chim. Acta 584 (2007) 333.
[22] S.L.C. Ferreira, R.E. Bruns, H.S. Ferreira, G.D. Matos, J.M. David, G.C. Brandão, E.G.P. da Silva, L.A. Portugal, P.S. dos Reis, A.S. Souza, Anal. Chim. Acta 597 (2007) 179.
[23] S.L.C. Ferreira, R.E. Bruns, E.G. Paranhos da Silva, W.N.L. dos Santos, C.M. Quintella, J.M. David, J. Bittencourt de Andrade, M.C. Breitkreitz, I.C. Sales, F. Jardim, B.B. Neto, J. Chromatogr. A 1158 (2007) 2.
[24] M.F. Mesko, D.P. de Moraes, J.S. Barin, V.L. Dressler, G. Knapp, É.M. de Moraes Flores, Microchem. J. 82 (2006) 183.
[25] ASTM D 3566-03 Standard Practice for Rubber—Determination of Bromine in the Presence of Chlorine by Oxygen Combustion, ASTM International, 2003.
[26] ISO 7725, Rubber and rubber products—Determination of Bromine and Chlorine Content: Oxygen Flask Combustion Technique, International Organization for Standardization, Geneva, Switzerland, 1991.
[27] A. Ranz, E. Lankmayr, J. Biochem. Biophys. Methods 69 (2006) 3.
[28] Eurachem/CITAC Guide: Quantifying Uncertainty in Analytical Measurement, second ed., 2000, www.eurachem.org.

Talanta 76 (2008) 206–210

Contents lists available at ScienceDirect

Talanta

journal homepage: www.elsevier.com/locate/talanta

Label-free DNA electrochemical sensor based on a PNA-functionalized conductive polymer

S. Reisberg[a], L.A. Dang[b], Q.A. Nguyen[b], B. Piro[a], V. Noel[a], P.E. Nielsen[c], L.A. Le[b], M.C. Pham[a,*]

[a] Laboratoire Interfaces-Traitements-Organisation et Dynamique des Systèmes (ITODYS), Université Paris 7-Denis Diderot, associé au CNRS, UMR 7086, 1 rue Guy de la Brosse, Paris 75005, France
[b] Institut de Chimie – VAST, 18 Av. Hoang Quoc Viet, Cau Giay, Hanoi, Viet Nam
[c] Department of Cellular and Molecular Medicine, The Panum Institute, Blegdansvej 3C, Copenhagen DK-2200, Denmark

ARTICLE INFO

Article history:
Received 13 November 2007
Received in revised form 8 February 2008
Accepted 20 February 2008
Available online 8 March 2008

Keywords:
PNA
Electrochemical biosensor
DNA sensor

ABSTRACT

An electrochemical hybridization biosensor based on peptide nucleic acid (PNA) probe is presented. PNA were attached covalently onto a quinone-based electroactive polymer. Changes in flexibility of the PNA probe strand upon hybridization generates electrochemical changes at the polymer–solution interface. A reagentless and direct electrochemical detection was obtained by detection of the electrochemical changes using square wave voltammetry (SWV). An increase in the peak current of quinone was observed upon hybridization of probe on the target, whereas no change is observed with non-complementary sequence. In addition, the biosensor is highly selective to effectively discriminate a single mismatch on the target sequence. The sensitivity is also presented and discussed.

1. Introduction

Several technological approaches were followed until now to develop DNA sensors. Optical systems are certainly the most frequent. Two of them are already commercialized, based on fluorescence or surface plasmon resonance spectroscopies. However, electrochemical systems have great potentialities because of their low cost, simplicity, and obvious compatibility with miniaturization [1].

Among the electrochemical methods, the most used is based on redox labels which generate a signal change upon hybridization. However, the main drawback of this technique is the need for a redox label to be added in solution, or grafted on DNA strands. To solve this problem, the redox indicator can be covalently grafted onto the electrode. Following this scheme, electrochemical methods like cyclic voltammetry (CV) [2–14], differential pulse voltammetry (DPV) [15–19] or electrochemical impedance spectroscopy (EIS) [20–28] have been successfully used.

Peptide nucleic acids (PNA) are DNA mimics with a pseudopeptide backbone (see Scheme 1). PNA oligomers are able to form very stable duplex structures with complementary DNA (or PNA) oligomers [29–31]. Conversely to DNA, PNA strands are neutral, i.e. the electrostatic repulsion is absent between two hybridized PNA or PNA–DNA strands. As a consequence, PNA–PNA as well as PNA–DNA duplexes have a higher association constant and a better thermal stability than corresponding DNA–DNA duplexes. Moreover, single-base mismatches are more selectively discriminated in a PNA–DNA context [29,32]. This would make PNA-based hybridization sensors more selective than classical DNA-based homologues. For these reasons, these molecules are of interest in many areas.

The aim of this article is to focus on the peculiar property of PNA strands to change their flexibility upon hybridization. Indeed, single-stranded PNA have flexible backbones, whereas double-stranded PNA or mixed PNA–DNA duplexes have a very rigid structure. It was recently reported that PNA oligomers have even more flexible chains than equivalent DNA strands [33,34], which therefore increases the hybridization impact on the probe neighbourhood, and justifies the use of PNA as probes.

Several works have already explored the strong PNA flexibility changes after DNA–PNA duplexes formation, mainly based on optical (fluorescence quenching) characterization of hybridization [35–37]. Some electrochemical sensors based on PNA probes have been reported, using redox indicators to be added in solution [38–40] or ferrocene-modified PNA probe to transduce directly the hybridization event [41,42]. In the latter case, the label-free sensor gives a "signal-off" (signal decrease) detection.

In this paper, we present a label-free and direct electrochemical system based on a quinone-containing conducting polymer and demonstrate that hybridization of a complementary DNA target onto the PNA-modified electrode generates electrochemical

* Corresponding author. Tel.: +33 1 5727 7223; fax: +33 1 5727 7263.
E-mail address: mcpham@univ-paris-diderot.fr (M.C. Pham).

0039-9140/$ – see front matter © 2008 Published by Elsevier B.V.
doi:10.1016/j.talanta.2008.02.044

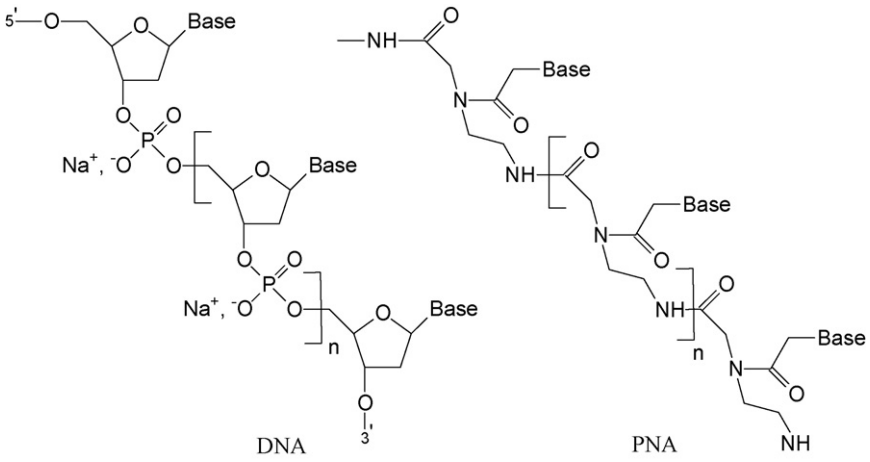

Scheme 1. Comparison between DNA and PNA structures.

changes at the polymer–solution interface. These electrochemical changes are detectable using square wave voltammetry (SWV) and lead to a "signal-on" (current increase). The sensor is very selective as non-complementary or single mismatch strand do not lead to significant change. The sensor electrode can be re-used after a simple dehybridization step in pure water.

2. Experimental

2.1. Chemicals

N′-(3-Dimethylaminopropyl)-*N*-ethylcarbodiimide hydrochloride (EDC) and *N*-hydroxysuccinimide (NHS) were provided by Sigma. Phosphate buffer saline solution (PBS, 0.137 M NaCl; 0.0027 M KCl; 0.0081 M Na_2HPO_4; 0.00147 M KH_2PO_4, pH 7.4) was from Sigma. Aqueous solutions were made with bi-distilled or ultrapure (Millipore) water. Juglone (5-hydroxy-1,4-naphthoquinone, JUG) and 1-naphthol (1-NAP) were purchased from Fluka. 5-Hydroxy-3-thioacetic acid-1,4-naphthoquinone (JUGA) was synthesized in our laboratory. Acetonitrile (ACN) was supplied by *Aldrich* (HPLC grade). All other reagents used were of analytical grade. Oligonucleotides were synthesized by Eurogentec (Belgium). Peptide nucleic acids (PNA) were synthesized in the Department of Cellular and Molecular Medicine, Panum Institute, Denmark.

Probe grafting was performed as follows. The poly(5-hydroxy-1,4-naphthoquinone-*co*-5-hydroxy-3-thioaceticacid-1,4-naphthoquinone)-coated glassy carbon (GC) electrodes were dipped into a solution containing 0.1 μM of PNA probe (pPNA, presenting a free terminal amine group, see Table 1), 1.5×10^{-2} M EDC (3.10^{-5} mol, 1 equiv.) and 3×10^{-2} M NHS (6.10^{-5} mol, 2 equiv.) in distilled water at 37 °C. After 20 h, the PNA immobilization reaction (amidation) was stopped: the electrode was washed in distilled water (5 min) in order to remove non-covalently bound PNA, then in PBS (2 h at 37 °C). Phosphates in PBS are able to react with NHS-activated ester. Unreacted ester groups are removed after these operations. The surface concentration of probe was estimated measuring the surface concentration of a fluorescent target strand, around 10–20 pmol cm^{-2}.

Table 1
PNA probes and DNA targets

Name	Function	Sequence	Melting temperature[a]
pPNA	Probe	NH2 -TCTTCCTCTCAGCCT-H (5′)	
tDNA-10	Target	5′ GAGAGTCGGA 3′	36.9 °C/50.6 °C
tDNA-15	Target	5′ AGAAGGAGAGTCGGA 3′	53.7 °C/68.5 °C
mDNA-15	Mismatch	5′ AGAAGGAGCGTCGGA 3′	43.8 °C/59.2 °C
rDNA-15	Random	5′ GATCCATGCATTCCG 3′	–

[a] T_m were computed from [44]. The first temperature corresponds to DNA/DNA hybrids, calculated from [44a]. The second temperature corresponds to PNA/DNA hybrids, calculated from [44b].

2.2. Electrochemical methods

For electrochemical experiments, a conventional one-compartment, three-electrode cell was employed. An *EG&G* 263*A* potentiostat was used with the *Echem* software (Ecochemie). The working electrodes were glassy carbon disks (*Tokaï carbon*, *Japan*) of 0.07 cm^2 area. The auxiliary electrode was a platinum grid and the reference electrode a commercial Saturated Calomel Electrode (SCE, MetrOhm).

The electrochemical synthesis of poly(JUG-*co*-JUGA) films was carried out by electrooxidation of a mixture of 5×10^{-2} M JUG + 5×10^{-3} M JUGA + 2×10^{-3} M 1-naphthol + 0.1 M $LiClO_4$ in acetonitrile, on GC electrodes, under dried argon atmosphere, by potential scans from 0.4 to 1 V vs. SCE during 50 cycles at 50 mV s^{-1}. The resulting conducting film presents a thickness of ca. 150 nm. The quinone group embedded in the polymer structure is electroactive in neutral aqueous medium in the potential range [0 V; 1 V] vs. SCE, for a surface concentration of electroactive quinones of around 2×10^{-9} mol cm^{-2}. The chemical structure of this polymer has been described in details elsewhere, and is simply reminded on Scheme 2 [18,19].

Hybridization was detected by recording the modification of the redox process of the quinone group, using square wave voltammetry (SWV). The following parameters were used: pulse height 50 mV, pulse width 50 ms, scan increment 2 mV, frequency 12.5 Hz, potential domain (−0.9; 0 V vs. SCE). The medium was PBS, bubbled with argon for 40 min before and during SWV measurements. The SWV scans were repeated until complete stabilization of the signal (i.e., no difference observed between two successive responses). All electrochemical experiments were conducted at 25 °C.

2.3. Hybridization

For hybridization experiments, 1 mL of PBS (pH 7.4) containing 100 nM of target DNA was used. The electrode (0.07 cm^2) bearing the PNA probe strand was dipped in this target solution then heated at a temperature above the melting temperature of the

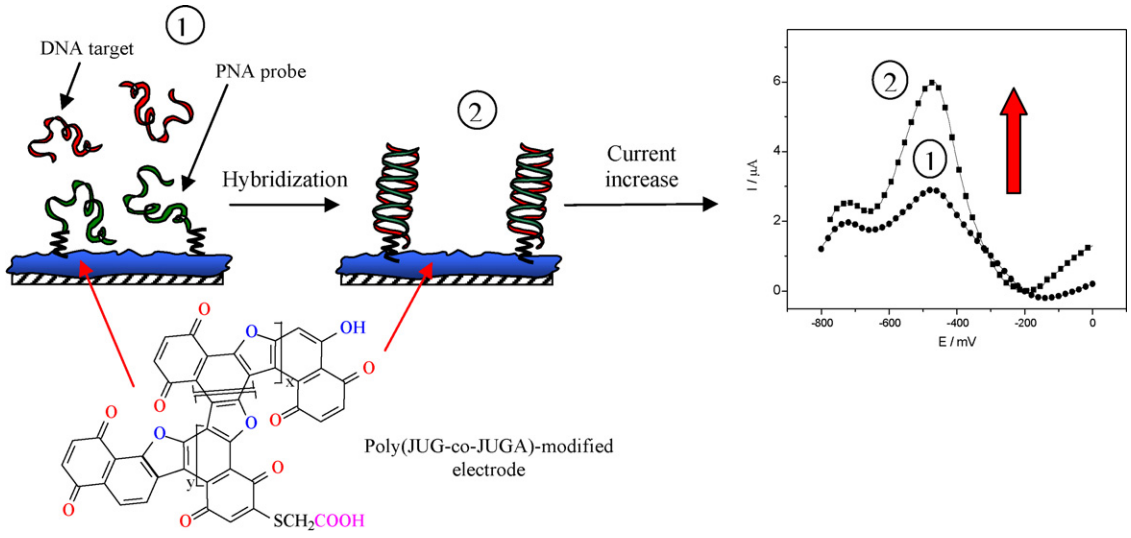

Scheme 2. Polymer structure, hybridization reaction and transduction process.

mismatch duplex (60 °C, see Table 1) during 2 h without stirring, and slowly cooled down to room temperature (at a rate of 0.5 °C per min. down to 25 °C during 1 h). This step is very important. Indeed, it removes mismatch duplexes and non-complementary sequences which could be adsorbed. After that, the electrode was washed again in PBS for 1 h at 25 °C. In our hybridization conditions, for a surface concentration of probe of 10 pmol cm^{-2}, around 6 pmol cm^{-2} of target strands are hybridized.

3. Results and discussion

Table 1 presents the PNA probe and DNA target sequences used in this study. We used as the probe strand a complementary sequence of the anti-gag gene of the HIV virus. Four target sequences were used. A 10 bases tDNA-10, shorter than the probe; a 15 bases tDNA-15 that is the full-complementary sequence of the pPNA probe; a random sequence rDNA-15 which is non specific; and a mismatch sequence mDNA-15 which presents one mismatching base.

Hybridization was detected by recording the modification of the redox process of the quinone group, using square wave voltammetry (SWV) between −0.9 V and 0 V vs. SCE in phosphate buffer saline (PBS) at 25 °C.

In one hand, the quinone group presents a reversible electroactivity in this potential domain, which is particularly sensitive to its chemical environment, for example protons or cations concentrations. In the other hand, ODN strands are polyanionic molecules and carry a high charge density. It is therefore justified to consider that the high charge density carried on ODN can influence its environment, i.e., in our case, the polymer–solution interface and the quinone group. Actually, in previous works in the literature dealing with DNA–DNA hybridization on conducting polymers, explanations of the transduction process were based on ion-exchange hindering and charge screening [10–14,23,43]. However, our idea is that hybridization may be detected more efficiently if only the target strand is charged, and not the probe strand. Indeed, the probe strand may generate a charge screening between the target strand and the electrode. This is why the idea described in this manuscript is to use a PNA (neutral) probe, in order to have only the target strand bearing charges. In other words, binding of the target DNA onto the neutral PNA changes the surfaces charge from neutral to negative to a greater extent than with probe DNA. The polymer structure, hybridization reaction and transduction process are illustrated on Scheme 2.

Initially, hybridization of a 10 bases complementary sequence was performed, using the tDNA-10 target on a pPNA-15 probe. Measurements were made in two steps, before and after tDNA hybridization, with a target concentration of 100 nM. In order to make the result more precise, we present the differential SWV current (Δi) (Fig. 1, curve 1, dotted line). Δi is obtained by subtracting the SWV current before hybridization from the SWV current measured after hybridization. As shown, the current increase is clear. However, the maximum of Δi remains low (about 3 µA at −500 mV/SCE).

Hybridization of the 15 bases complementary sequence (i.e., same length than pPNA) was performed using the tDNA-15 target strand. The results are shown in Fig. 1, curve 2 (plain line). As shown, the current is higher for the tDNA-15 than for the tDNA-10. This effect of the length on hybridization is common and has been previously shown for DNA–DNA hybridization [18,45].

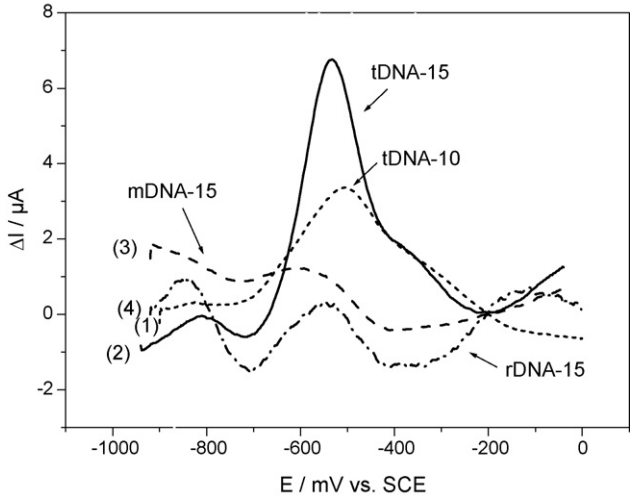

Fig. 1. Differential SWV responses obtained after (1) hybridization of tDNA-10 onto pPNA; (2) hybridization of tDNA-15 onto pPNA; (3) addition of the mismatch sequence mDNA-15; (4) addition of the random sequence rDNA-15. Δi corresponds to the difference $i_h - i_g$; i_h is the SWV current after hybridization and i_g before. Conditions detailed in the Section 2.

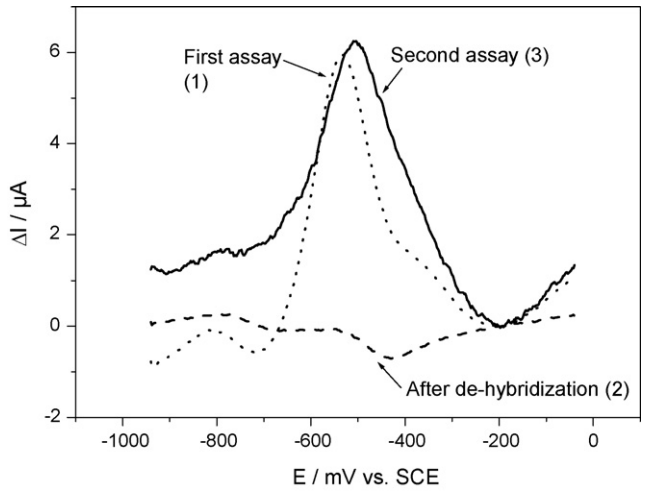

Fig. 2. Differential SWV responses obtained after (1) hybridization of tDNA-15 onto pPNA; (2) dehybridization by a stringent washing procedure; (3) second hybridization of tDNA-15. Same conditions as Fig. 1.

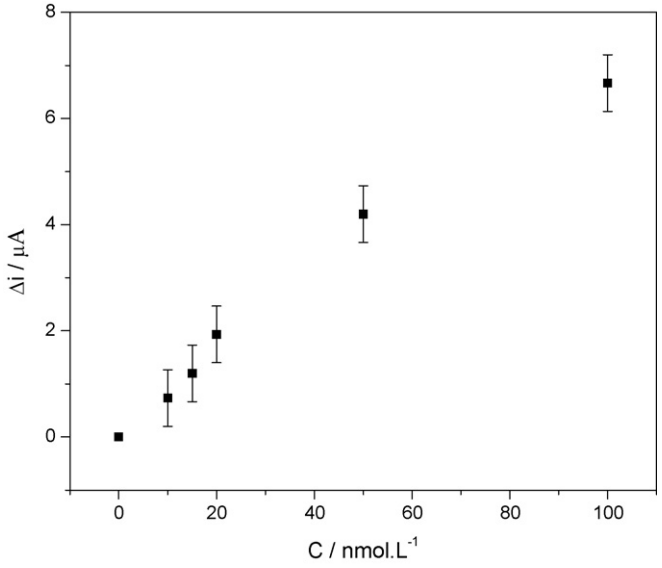

Fig. 3. Differential SWV currents, measured at −500 mV/SCE, after addition of tDNA-15, for increasing concentrations from 10 nM up to 100 nM. Same conditions as Fig. 1.

These results constitute a convincing proof-of-concept for this PNA-based DNA sensor. However, the true challenge, for a DNA sensor, is to achieve a good selectivity for DNA sequence recognition. To demonstrate this, we used a random and a single mismatch target sequences. The first is a random sequence (rDNA-15) which does not present any specificity to the PNA probe. The second is much closer to the genuine target sequence, bearing only one mismatch base (mDNA-15). This is a key-experiment to demonstrate selectivity.

The results obtained for these two targets are shown in Fig. 1 (curve 3, dotted line and curve 4, dash-dotted lines). As shown, incubation with rDNA-15 and mDNA-15 (followed by a washing step at 60 °C) leads to current changes which are not significant, whereas hybridization with the full-complementary sequence tDNA-15 gives a clear current increase.

It is also possible to denature the pPNA–tDNA hybrid, in order to regenerate the electrode surface after a first assay. To illustrate this, after a first hybridization assay, the PNA–DNA hybrid was denaturated in stringent conditions by washing in pure deionised water at 37 °C under stirring during 24 h. The electrode was then re-equilibrated in PBS during 2 h at the same temperature. The results are shown in Fig. 2. It appears that, after the washing step, the differential SWV current recovers a value close to the one obtained before hybridization. This means that the de-hybridization does occur. Moreover, a second hybridization on the same film leads to a current increase which is similar to the one obtained for the first assay. However, further de-hybridizations (>3) lead to a progressive decrease of the current.

Finally, we measured the SWV current response as a function of the concentration of target strand, for concentrations between 10 nM and 100 nM (i.e., 10 pmol and 100 pmol in 1 mL), as shown in Fig. 3. The detection limit appears to be around 10 nM. This is a good value in comparison to most of the results published in the literature concerning DNA sensor using a direct (and reagentless) electrochemical process. All targets present in the hybridization solution do not hybridize. The lowest detectable signal is obtained for a target concentration around 10 nM, i.e., 10 pmol in 1 mL sample. We hope to decrease these values (and therefore increase sensitivity) by using lower volumes and smaller electrodes. This work is in progress, with ultra-microelectrodes and microfluidic cells.

4. Conclusion

A PNA-probe modified electrode based on a conducting polymer was found to transduce the hybridization event to an electrochemical signal with current increase,"signal-on". There is no need for a time-consuming labeling process and external indicators. The electrochemical response is obtained directly by square wave voltammetry. The sensor can discriminate a single mismatch and can be regenerated after a simple dehybridization step in pure water to be re-used. Its detection limit is around 10 nM, but does not constitute a theoretical limit and probably can be improved.

The simplicity of the strategy may open the doors for application in genetic diagnosis and work is under study in this direction.

Acknowledgments

S. Reisberg thanks the French Ministry of Research for a Ph.D. grant, and University Paris-Diderot-Paris 7 for a Post-Doctoral position.

References

[1] E. Bakker, Y. Qin, Anal. Chem. 75 (2006) 3965.
[2] A.B. Steel, T.M. Herne, M.J. Tarlov, Anal. Chem. 70 (1998) 4670.
[3] I.V. Yang, H.H. Thorp, Anal. Chem. 73 (2001) 5316.
[4] J. Wang, D. Xu, A. Kawde, R. Polsky, Anal. Chem. 73 (2001) 5576; J. Wang, The Analyst 130 (2005) 421.
[5] A.M. Oliveira-Brett, M. Vivan, I.R. Fernandes, J.A.P. Piedade, Talanta 56 (2002) 959.
[6] A. Liu, J.I. Anzai, Anal. Chem. 76 (2004) 2975.
[7] E. Dominguez, O. Rincon, A. Narvaez, Anal. Chem. 76 (2004) 3132.
[8] E. Katz, I. Willner, J. Wang, Electroanalysis 16 (2004) 19.
[9] M.V. Del Pozo, C. Alonso, F. Pariente, E. Lorrenzo, Biosens. Bioelectron. 20 (2005) 1549.
[10] H. Korri-Youssoufi, F. Garnier, P. Srivastava, P. Godillot, A. Yassar, J. Am. Chem. Soc. 119 (1997) 7388.
[11] A. Emge, P. Bauerle, Synth. Met. 102 (1999) 1370.
[12] N. Lassalle, E. Vieil, J.P. Correia, L.M. Abrantes, Synth. Met. 119 (2001) 407.
[13] L.A. Thompson, J. Kowalik, M. Josowicz, J. Janata, J. Am. Chem. Soc. 125 (2003) 324.
[14] J. Cha, J.I. Han, Y. Choi, D.S. Yoon, K.W. Oh, G. Lim, Biosens. Bioelectron. 18 (2003) 1241.
[15] G. Marrazza, I. Chianella, M. Mascini, Biosens. Bioelectron. 14 (1999) 43.
[16] B. Wang, L. Bouffier, M. Demeunynck, P. Mailley, A. Roget, T. Livache, P. Dumy, Bioelectrochemistry 63 (2004) 233.

[17] D. Ozkan, A. Erdem, P. Kara, K. Kerman, B. Meric, J. Hassmann, M. Ozsoz, Anal. Chem. 74 (2002) 5931.
[18] S. Reisberg, B. Piro, V. Noël, M.C. Pham, Anal. Chem. 77 (2005) 3351.
[19] S. Reisberg, B. Piro, V. Noel, M.C. Pham, Bioelectrochemistry 69 (2006) 172.
[20] E. Palecek, Anal. Biochem. 170 (1988) 421;
E. Palecek, Talanta 56 (2002) 809.
[21] K.M. Millan, S.R. Mikkelsen, Anal. Chem. 65 (1993) 2317.
[22] E. Souteyrand, J.P. Cloarec, J.R. Martin, C. Wilson, I. Lawrence, S. Mikkelsen, M.F. Lawrence, J. Phys. Chem. B 101 (1997) 2980.
[23] J. Wang, M. Jiang, A. Fortes, B. Mukherjee, Anal. Chim. Acta 402 (1999) 7.
[24] H. Peng, C. Soeller, N. Vigar, P.A. Kilmartin, M.B. Cannell, G.A. Bowmaker, R.P. Cooney, J. Travas-Sejdic, Biosens. Bioelectron. 20 (2005) 1821.
[25] E. Katz, I. Willner, Electroanalysis 15 (2003) 913.
[26] C. Li, Y. Long, J.S. Lee, H. Kraatz, Chem. Commun. (2004) 574.
[27] L. Alfonta, A.K. Singh, I. Willner, Anal. Chem. 73 (2001) 91.
[28] J. Liu, S. Tian, P.E. Nielsen, W. Knoll, Chem. Commun. (2005) 2969.
[29] P.E. Nielsen, M. Egholm, R.H. Berg, O. Buchardt, Science 254 (1991) 1497.
[30] M. Egholm, O. Buchardt, L. Christensen, C. Behrens, S.M. Freier, D.A. Driver, R.H. Berg, S.K. Kim, B. Norden, P.E. Nielsen, Nature 365 (1993) 566.
[31] E. Uhlmann, A. Peyman, G. Breipohl, D.W. Will, Angew. Chem. Int. Ed. Engl. 37 (1998) 2796.
[32] P.E. Nielsen, M. Egholm, Peptide Nucleic Acids: Protocols and Applications, Horizon Scientific Press, Norfolk, UK, 1999.
[33] S. Sen, L. Nilsson, J. Am. Chem. Soc. 123 (2001) 7414.
[34] R. Soliva, E. Sherer, F.J. Luque, C.A. Laughton, M. Orozco, J. Am. Chem. Soc. 122 (2000) 5997.
[35] E. Ortiz, G. Estrada, P.M. Lizardi, Mol. Cell. Probes 12 (1998) 219.
[36] B. Armitage, D. Ly, T. Koch, H. Frydenlund, H. Orum, G.B. Schster, Biochemistry 37 (1998) 9417.
[37] H. Juhn, V.V. Demidov, J.M. Coull, M.J. Fiandaca, B.D. Gildea, M.D. Frank-Kamenetskii, Antisense Nucleic Acid Drug Dev. 11 (2001) 265.
[38] J. Wang, E. Palecek, P.E. Nielsen, G. Rivas, X.H. Cai, H. Shiraishi, N. Dontha, D.B. Luo, P.A.M. Farias, J. Am. Chem. Soc. 118 (1996) 7667.
[39] D. Ozkan, A. Erdem, P. Kara, K. Kerman, J.J. Gooding, P.E. Nielsen, M. Ozsoz, Electrochem. Commun. 4 (2002) 796.
[40] H.X. Ju, H.T. Zhao, Front. Biosci. 10 (2005) 37.
[41] H. Aoki, P. Buhlmann, Y. Umezawa, Electroanalysis 12 (2000) 1272.
[42] H. Aoki, H. Tao, Analyst 132 (2007) 784.
[43] V.V. Demidov, V.N. Potaman, M.D. Frank-Kamenetskii, M. Egholm, O. Buchard, S.H. Sönnichsen, P.E. Nielsen, Biochem. Pharmacol. 48 (1994) 1310.
[44] (a) N. Le Novere, Bioinformatics 17 (2001) 1226;
(b) U. Giesen, W. Kleider, C. Berding, A. Geiger, H. Ørum, P.E. Nielsen, Nucleic Acids Res. 26 (1998) 5004.
[45] B. Piro, S. Reisberg, V. Noel, M.C. Pham, Biosens. Bioelectron. 22 (2007) 3126.

Talanta 76 (2008) 211–225

Contents lists available at ScienceDirect

Talanta

journal homepage: www.elsevier.com/locate/talanta

Multiresidue method for fast determination of pesticides in fruit juices by ultra performance liquid chromatography coupled to tandem mass spectrometry

R. Romero-González, A. Garrido Frenich*, J.L. Martínez Vidal

Department of Analytical Chemistry, Almeria University, E-04071 Almeria, Spain

ARTICLE INFO

Article history:
Received 19 November 2007
Received in revised form 15 February 2008
Accepted 20 February 2008
Available online 6 March 2008

Keywords:
Pesticides
Fruit juices
QuEChERS
UPLC–MS/MS
Routine analysis

ABSTRACT

A new analytical method for the simultaneous determination of 90 pesticides in fruit juices by ultra performance liquid chromatography coupled to tandem mass spectrometry (UPLC–MS/MS) has been developed and validated. Extraction was performed with acetonitrile, applying QuEChERS methodology, and the extracts were analyzed without any further clean-up step, providing better results than solid phase extraction (SPE) procedure. Before chromatographic step, extracts were diluted with water (1:1) in order to obtain good peak shapes. Several chromatographic conditions were evaluated in order to achieve a fast separation in Multiple Reaction Monitoring (MRM) mode, obtaining a run time of only 11 min. Matrix effect was studied for different types of fruit juices (peach, orange, pineapple, apple and multifruit), indicating that multifruit juice can be selected as representative matrix for routine analysis of these food commodities. Pesticides were quantified using matrix-matched calibration with recoveries between 70.4 and 108.5% and relative standard deviation lower than 20%. Limits of quantification were lower than 5 $\mu g\,L^{-1}$ in all the cases. The developed procedure was applied to commercial fruit juices, detecting carbendazim, cyprodinil and thiabendazol in a few samples.

1. Introduction

The use of chemical pesticides in fruit crops is necessary to control pest that could decrease field production, as well as to improve the fruit quality reaches the consumer. Also, pesticides can be applied in fruits for post-harvest protection so pesticide residues may be transferred from fruit into juice, being a significant route to human exposure. Hence, nowadays there is an increasing demand for developing sensitive and selective methods for the determination of multi-class pesticides in fruit juices at trace levels. In addition, for the analysis of pesticides in juices, sample treatment is required in order to isolate the compounds from the complex matrices, followed in certain cases by clean-up steps to eliminate interferences, and improve sensitivity. Several enrichment methods have been developed to accomplish this often time-consuming task using liquid–liquid extraction with organic solvents [1–4], such as acetone, ethyl acetate, cyclohexane, acetonitrile and dichloromethane, or solid phase extraction (SPE) [5,6]. In the last years trends in sample treatment are towards the miniaturization and simplification of the methodologies to overcome the disadvantages caused by using high amounts of toxic solvents. With this aim, several procedures based on solid phase microextraction (SPME) [7–10], matrix-solid phase dispersion (SPMD) [11–13], single-drop microextraction (SDME) [14,15], supported-liquid membrane (SLM) [16], stir bar sorptive extraction (SBSE) and membrane-assisted solvent extraction (MASE) [17] and direct injection of the sample previous dilution with pure water [18] have been used. Recently a quick, easy, cheap, effective, rugged and safe (QuEChERS) extraction procedure has been developed for the extraction of pesticides from fruit and vegetables [19–21]. The original method is based on an acetonitrile extraction/partitioning followed by a clean-up with dispersive-SPE. This is a fast and inexpensive method, which provides good recoveries for a large number of pesticides with different physico-chemical properties with a smaller amount of organic solvent consumption, and high sample throughput. Due to these advantages the QuEChERS method has had worldwide acceptance, becoming an official method of the AOAC for pesticide residue analysis in fruits and vegetables [19], and also drafted as European Norm [22]. Despite the QuEChERS has been applied in many different solid food samples, such as fruits and vegetables [19–21] or baby food [23,24], the method has received a limited attention in liquid samples as olive oil [25] and honey [26]. To our knowledge, there is no report on extraction of pesticides from fruit juices using this method as the sample preparation.

On the other hand, liquid chromatography coupled to mass spectrometry in tandem mode (LC–MS/MS) using triple quadrupole

* Corresponding author. Tel.: +34 950015985; fax: +34 950015483.
E-mail address: agarrido@ual.es (A.G. Frenich).

0039-9140/$ – see front matter © 2008 Elsevier B.V. All rights reserved.
doi:10.1016/j.talanta.2008.02.041

(QqQ) analyzers [6,27] is a very appropriate technique for the determination of pesticides in juices, because it provides sufficient sensitivity, as well as capability of unambiguous evidence for pesticide identification and quantification at trace levels from a single injection, minimizing extensively clean-up steps, and analysis time.

Relatively recent advances in chromatographic instrumentation have enabled the development of alternative methods, such as ultraperformance liquid chromatography (UPLC)–MS/MS [28–30]. UPLC uses a new generation of columns with 1.7 μm diameter particles (a new bridged ethylsiloxane/silica hybrid particles) which can operate at higher back pressures. These advances have important benefits to the chromatographic process, such as an increase in speed of analysis, in resolution, in sensitivity and in peak capacity. UPLC is already a proven technique with a wide range of applications in analysis of multiple pesticides in foods [29,31–33] and water [34,35]. UPLC characteristics in conjunction with MS/MS advantages allow significant decreases in run times, as well as in sample treatment. Bearing in mind this fact, a modification of the buffered QuEChERS method, which entails the elimination of the clean-up step, is proposed in this study.

The aim of this work was to develop and validate a fast analytical method for determination of 90 multi-class pesticides in 11 min in different types of fruit juices using buffered QuEChERS extraction and UPLC–MS/MS, which is not yet documented in literature. The combination of UPLC–QqQ–MS/MS and QuEChERS extraction allows the preparation of a batch of 10 juices samples in about half an hour, and the later chromatographic analysis in less than 2 h. In consequence, this method is suitable to its application in routine analysis where a high sample throughput is required.

2. Experimental

2.1. Reagents and chemicals

Pesticide reference standards (purity higher than 99%) were purchased from Dr. Ehrenstofer (Augsburg, Germany) and Riedel-de-Haën (Seelze-Hannover, Germany). Stock standard solutions of individual compounds (with concentrations ranged from 200 and 300 mg L^{-1}), were prepared by exact weighing of the powder and dissolution in 50 mL of methanol, acetonitrile or acetone and stored at −18 °C in the dark. A multicompound working standard solution (2 mg L^{-1} concentration of each compound) was prepared by appropriate dilutions of the stock solutions with methanol and stored under refrigeration at 4 °C. Anhydrous magnesium sulphate, acetic acid (content > 97%), formic acid (content > 98%) and sodium acetate were obtained from Panreac (Barcelona, Spain). Oasis HLB (200 mg, 6 cm^3; Waters, Milford, MA, USA), C18 C18 Sep-Pak (200 mg, 6 cm^3 Waters) and Strata-X (200 mg, 6 cm^3, Phenomenex, Torrance, CA, USA) cartridges were used for SPE experiments. Methanol, acetone and acetonitrile (pesticide residue grade solvent) were purchased from Panreac. Highly purified water (Milli-Q, Millipore, Bedford, USA) was used throughout for the preparation of buffers, mobile phase and other reagents.

2.2. Instruments and apparatus

Chromatographic analyses were performed in an ACQUITY UPLC™ system (Waters, Midlford MS, USA), using an Acquity UPLC BEH C_{18} column (100 mm × 2.1 mm) from Waters, with 1.7 μm particle size.

Mass spectrometric detection was carried out using an ACQUITY TQD tandem quadrupole mass spectrometer (Waters, Manchester, UK). The instrument was operated using an electrospray ionization source (ESI) in positive mode. ESI parameters were: capillary voltage 3.0 kV, extractor voltage 3 V, source temperature 150 °C, desolvation temperature 350 °C, cone gas flow 80 L h^{-1} and desolvation gas flow 600 L h^{-1} (both gases were nitrogen). Collision-induced dissociation was performed using argon as the collision gas at a pressure of 4×10^{-3} mbar in the collision cell. The multiple reaction monitoring (MRM) transitions as well as the cone and collision energy voltages applied are summarized in Table 1 . Data acquisition was performed using MassLynx 4.0 software with QuanLynx program (Waters).

Centrifugations were performed in a high-volume centrifuge equipped with a bucket rotor (4 mL × 250 mL) from Orto Alresa, Mod. Consul (Madrid, Spain). A Vortex mixer Heidolph, model Reax 2000 and an analytical AB204-S balance (Mettler Toledo, Greinfesee, Switzerland) were also used.

2.3. Extraction procedure

Pesticides were extracted from fruit juices using an extraction procedure based on buffered QuEChERS methodology [20]. Briefly, the procedure was as follows: 10 mL of sample were pippetted to a polypropylene centrifuge tube (40 mL) and 10 mL of 1% of acetic acid in acetonitrile solution was added, and the mixture vortex for 1 min. Afterwards, 4 g of anhydrous magnesium sulfate and 1 g of sodium acetate were added and the tubes were shaken immediately for 1 min. After centrifugation at 4300 × g for 5 min, 1 mL of the supernatant was taken and diluted with 1 mL of water prior UPLC–MS/MS analysis.

During the optimization procedure, a SPE procedure was also evaluated. 2 mL of fruit juice fortified at 50 μg L^{-1} were diluted with 2 mL of Milli Q water and then extracted using cartridges previously conditioned with 4 mL of dichloromethane, 4 mL MeOH and 5 mL water. The flow rate of the samples was 8 mL min^{-1}. The cartridges were then dried for 30 min under vacuum and the analytes were eluted with 5 mL MeOH and 5 mL dichloromethane. The organic solvent was evaporated to dryness and the residue was dissolved in 1 mL of the initial chromatographic mobile phase.

2.4. Chromatographic analysis

Chromatographic analyses were carried out using gradient elution with eluent A being methanol and eluent B consisting of an aqueous solution of formic acid (0.01%). The analysis started with 10% of eluent A, which was increased linearly up to 50% in 2.5 min, and then to 90% in 4.5 min. This composition was held for further 1.5 min before being returned to 10% of eluent A in 1.0 min, followed by a re-equilibration time of 1.5 min, to give a total run time of 11 min. The flow rate was 0.35 mL min^{-1} and the column temperature was maintained at 35 °C. Volumes of 5 μL of extracted samples were injected.

2.5. Validation study

Linearity was evaluated using matrix-matched calibration by analyzing spiked blank samples of juice at five concentration levels between 5 and 100 μg L^{-1}. Repeatability was studied at three concentration levels (10, 50 and 100 μg L^{-1}) using five replicates and interday precision was evaluated at 25 μg L^{-1}, analyzing daily spiked samples for a period of 7 days. Recoveries were determined for five replicates at 10, 50 and 100 μg L^{-1} concentrations. Finally, limits of detection and quantification (LOD and LOQ, respectively) were estimated according to IUPAC recommendations and Sanco guidelines [36,37]. LOD calculations were based on the theory of hypothesis testing and the probabilities of false positives ($\alpha = 0.05$) and false negatives ($\beta = 0.05$), whereas LOQ was established as the lowest concentration tested which gave acceptable recoveries (between 70 and 110%) and precision (R.S.D. lower than 20%).

Table 1
Retention time windows (RTW) and MS/MS parameters of the selected pesticides

Pesticide	Channel	RTW (min)	MRM transition (m/z)[a]	Cone voltage (V)	Collision energy (eV)
Propamocarb	1	1.68–1.72	189 > 102 189 > 74	20 20	17 23
Pymetrozine	1	1.69–1.75	218 > 105 218 > 79	28 28	18 35
Oxamyl	2	2.03–2.09	220 > 72 220 > 90	8 8	14 6
Nitenpyram	2	2.08–2.12	271 > 225 271 > 99	20 20	10 17
Picloram	3	2.22–2.31	241 > 223 241 > 195	26 26	14 22
Methomyl	3	2.27–2.34	163 > 88 163 > 106	15 15	8 8
Carbendazim	3	2.36–2.43	192 > 160 192 > 132	20 20	17 30
Thiamethoxam	3	2.38–2.45	292 > 132 292 > 181	25 25	25 25
Monocrotophos	3	2.47–2.54	224 > 193 224 > 127	15 15	8 14
2,6-dichlorobenzamide	3	2.50–2.57	190 > 173 190 > 145	30 30	16 26
Atrazine desiso-propyl	4	2.68–2.76	174 > 96 174 > 104	20 20	20 20
Thiabendazole	4	2.72–2.79	202 > 175 202 > 131	30 30	26 30
Imidacloprid	4	2.79–2.85	256 > 209 256 > 175	30 30	17 17
Vamidothion	5	3.01–3.05	288 > 146 288 > 118	15 15	13 20
Metamitron	5	3.02–3.09	203 > 175 203 > 104	18 18	15 25
Acetamiprid	5	3.06–3.13	223 > 126 223 > 56	30 30	20 20
Quinmerac	5	3.11–3.16	222 > 204 222 > 141	25 25	15 30
Chloridazon	5	3.13–3.19	222 > 92 222 > 104	30 30	30 30
Thiacloprid	6	3.33–3.39	253 > 126 253 > 186	35 35	22 14
Desethyl atrazine	6	3.35–3.41	188 > 146 188 > 104	20 20	20 30
Metoxuron	7	3.61–3.69	229 > 72 229 > 156	30 30	23 17
Aldicarb	7	3.62–3.69	208 > 191 208 > 89	15 15	8 25
Cinosulfuron	8	3.79–3.86	414 > 183 414 > 157	25 25	15 15
Triasulfuron	9	3.93–4.00	402 > 167 402 > 141	30 30	16 22
Tifensulfuron methyl	9	3.94–4.01	388 > 167 388 > 141	20 20	20 20
Nicosulfuron	9	4.00–4.10	411 > 182 411 > 106	35 35	18 30
Thiophanate methyl	9	4.06–4.15	343 > 151 343 > 311	25 25	20 10
Simazine	10	4.12–4.17	202 > 132 202 > 96	35 35	18 25
Metribuzine	10	4.12–4.20	215 > 187 215 > 131	20 20	20 20

Table 1 (*Continued*)

Pesticide	Channel	RTW (min)	MRM transition (m/z)[a]	Cone voltage (V)	Collision energy (eV)
Carbofuran	10	4.15–4.21	222 > 165 222 > 123	20 20	12 20
Bendiocarb	10	4.15–4.23	224 > 167 224 > 109	20 20	15 10
Ofurace	10	4.17–4.25	282 > 160 282 > 254	20 20	25 15
Chlorsulfuron	11	4.34–4.42	358 > 141 358 > 167	30 30	20 20
Desethyl ter-buthy-lazine	11	4.37–4.42	202 > 146 202 > 79	20 20	16 25
Carbaryl	11	4.37–4.45	202 > 145 202 > 127	20 20	10 30
Imazalil	11	4.38–4.49	297 > 159 297 > 201	40 40	20 20
Monolinuron	12	4.48–4.57	215 > 126 215 > 148	28 28	18 15
Terbumeton	12	4.63–4.72	226 > 170 226 > 114	15 15	15 25
Chlorotoluron	12	4.68–4.77	213 > 72 213 > 46	25 25	15 15
Metobromuron	12	4.74–4.83	259 > 170 259 > 148	28 28	20 20
Atrazine	13	4.81–4.86	216 > 174 216 > 96	30 30	18 25
Metazachlor	13	4.82–4.87	278 > 134 278 > 210	15 15	20 10
Lenacil	13	4.87–4.95	235 > 153 235 > 136	20 20	15 30
Fensulfothion	13	4.89–4.97	309 > 281 309 > 157	30 30	15 26
Isoxaflutole	13	4.92–5.03	360 > 251 360 > 141	30 30	15 15
Isoproturon	13	4.93–5.04	207 > 72 207 > 165	30 30	17 15
Fenpropimorph	14	4.97–5.12	304 > 147 304 > 98	10 10	30 35
Diuron	14	5.04–5.11	233 > 72 233 > 160	30 30	25 18
Azaconazole	14	5.05–5.14	300 > 159 300 > 231	20 20	23 16
Desmediphan	14	5.06–5.17	301 > 182 301 > 136	20 20	8 20
Ethoxyquine	14	5.07–5.19	218 > 174 218 > 160	20 20	30 30
Iodosulfuron methyl	15	5.11–5.19	530 > 163 530 > 390	25 25	16 16
Spiroxamine	15	5.14–5.23	298 > 144 298 > 100	25 25	20 33
Phenmedipham	15	5.17–5.26	301 > 168 301 > 136	30 30	10 20
Bensulfuron methyl	15	5.19–5.27	411 > 149 411 > 182	40 40	18 18
Diethofencarb	16	5.36–5.42	268 > 226 268 > 152	20 20	10 20
Sebuthylazine	16	5.39–5.45	230 > 174 230 > 96	25 25	18 25
Propazine	16	5.42–5.52	230 > 188 230 > 147	25 25	16 20

Table 1 (*Continued*)

Pesticide	Channel	RTW (min)	MRM transition (m/z)[a]	Cone voltage (V)	Collision energy (eV)
Linuron	16	5.47–5.55	249 > 160 249 > 182	30 30	18 18
Methiocarb	17	5.55–5.63	226 > 169 226 > 121	22 22	10 18
Terbuthylazine	17	5.56–5.63	230 > 174 230 > 96	28 28	15 25
Prometryn	17	5.64–5.70	242 > 158 242 > 200	20 20	17 25
Paclobutrazol	17	5.67–5.73	294 > 70 294 > 125	25 25	25 25
Flutalonil	17	5.68–5.75	324 > 242 324 > 262	27 27	25 20
Promecarb	17	5.68–5.75	208 > 151 208 > 109	23 23	9 15
Propyzamide	17	5.76–5.82	256 > 190 256 > 173	25 25	16 23
Triazophos	18	5.90–5.99	314 > 162 314 > 119	35 35	18 34
Tepraloxydim	18	5.95–6.00	342 > 250 342 > 166	20 20	12 20
Iprovalicarb	18	5.97–6.04	321 > 119 321 > 203	20 20	15 8
Triadimenol	18	5.97–6.06	296 > 70 296 > 99	25 25	12 12
Fenhexamide	18	6.02–6.10	302 > 97 302 > 55	25 25	25 30
Epoxiconazole	19	6.10–6.18	330 > 121 330 > 141	25 25	20 20
Tebutam	19	6.16–6.21	234 > 91 234 > 192	27 27	18 18
Metolachlor	19	6.18–6.26	284 > 252 284 > 176	20 20	15 23
Fenbuconazole	19	6.24–6.33	337 > 70 337 > 125	30 30	25 20
Spinosad	19	6.25–6.34	733 > 142 544 > 142	30 30	30 25
Cyprodinil	19	6.27–6.37	226 > 108 226 > 93	20 20	20 20
Diflubemzuron	19	6.30–6.39	311 > 158 311 > 141	25 25	12 22
Thiazopyr	20	6.44–6.50	397 > 377 397 > 335	35 35	28 22
Furmecyclox	20	6.50–6.59	252 > 170 252 > 110	20 20	13 20
Bitertanol	21	6.77–6.84	338 > 269 338 > 99	25 25	10 15
Pencycuron	21	6.86–7.01	329 > 125 329 > 218	40 40	19 14
Trifloxystrobin	22	7.00–7.07	409 > 186 409 > 206	30 30	18 14
Triflumizole	22	7.09–7.20	346 > 73 346 > 278	23 23	17 11
Cycloxydim	22	7.10–7.17	326 > 280 326 > 180	22 22	13 20
Clethodim	22	7.11–7.20	360 > 164 360 > 268	20 20	20 12
Fluazifop buthyl	23	7.24–7.32	384 > 282 384 > 91	35 35	20 30

Table 1 (*Continued*)

Pesticide	Channel	RTW (min)	MRM transition (*m*/*z*)[a]	Cone voltage (V)	Collision energy (eV)
Sethoxydim	23	7.33–7.40	328 > 178 328 > 282	23 23	18 11
Hexythiazox	24	7.59–7.69	353 > 228 353 > 168	25 25	15 20
Fenazaquin	25	8.12–8.21	307 > 161 307 > 147	30 30	16 16

[a] The first transition of each pesticide was used for quantification and the second one for confirmation purposes.

2.6. Fruit juice samples

Several commercial brands of apple, peach, pineapple, orange and multifruit juices were purchased from supermarkets in Almeria (Spain). Juice samples were analyzed following the procedure described below and those samples showing the absence of selected analytes were used as blank juice samples in the preparation of standards and in the recovery study.

3. Results and discussion

3.1. UPLC–MS/MS analysis

First, MS detector conditions were optimized injecting standards of 15 mg L^{-1} of each pesticide using electrospray ionization in positive mode. Full scan mass spectra were recorded in order to select the most abundant *m*/*z* value, optimizing the cone voltage. $[M–H]^+$ ions were found to be the most abundant and were selected as precursor ions for the target pesticides. Then, collision energies were evaluated in order to find the most abundant product ions, selecting the most sensitive transition for quantification purposes and a second one for confirmation. Table 1 indicates MS/MS transitions for quantification and confirmation, as well as the optimized parameters for all the studied pesticides. The optimum values for other parameters in MS/MS determination are indicated in Section 2.

To optimize the chromatographic separation, preliminary experiments were performed checking different mobile phases consisting of methanol, acetonitrile and water with formic or acetic acid at different concentrations. When acetonitrile was used as organic solvent in the mobile phase, bad peak shape was observed for some pesticides such as 2,6-dichlorbenzamide, metamitron and quinmerac. Besides, desmedipham and phenmediphan are not resolved, and bearing in mind that they are isobaric compounds with similar transition (301 > 182), acetonitrile was not selected as organic solvent in the mobile phase. Furthermore, the

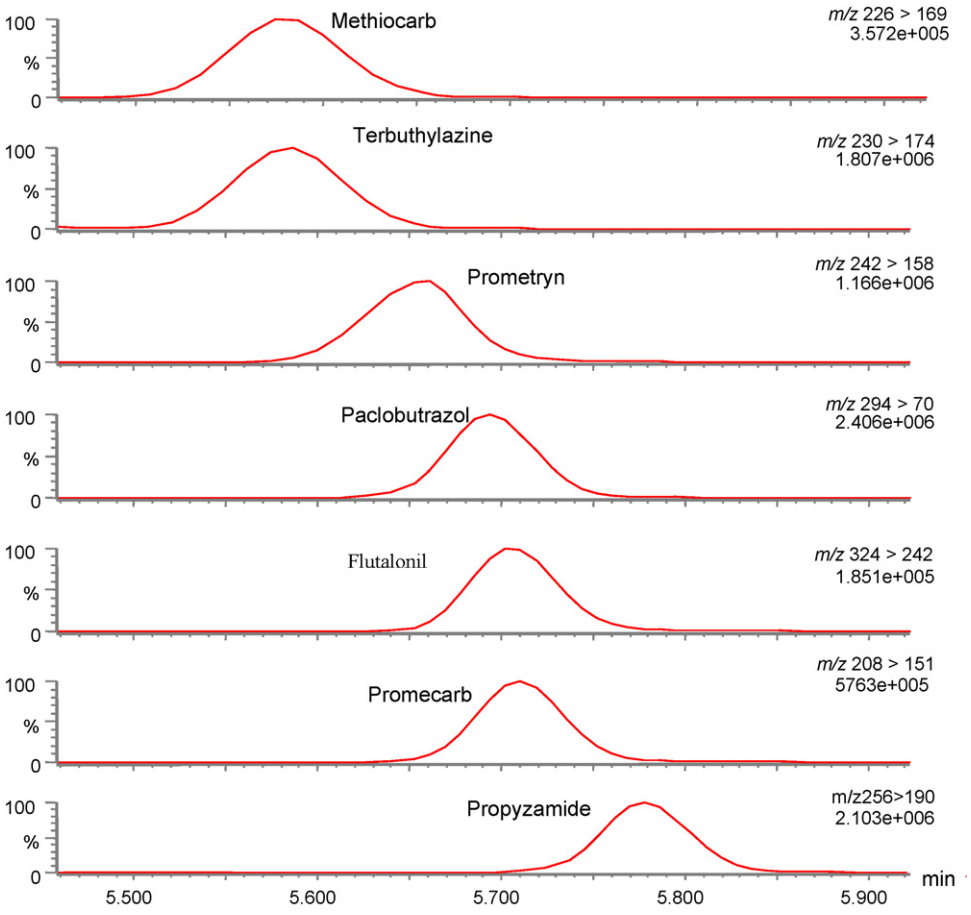

Fig. 1. UPLC–MS/MS chromatogram from a standard mixture of pesticides at 50 μg L^{-1}, monitoring the pesticides selected in acquisition function number 17. Chromatographic and MS/MS conditions are described in the text.

MS signal for most of the pesticides such as propamocarb, monocrotophos, thiabendazol, carbofuran, carbaryl, iodosulphuron methyl and methiocarb, decreased considerably when acetonitrile was used instead of methanol, whereas it was slightly better for a few pesticides such as propazine, lenacil, nicosulfuron and iprovalicarb. On the other hand, the addition of formic acid provided better results than acetic acid and was used to improve the ionization efficiency. The optimal separation of 90 compounds was achieved using a gradient elution with methanol and an aqueous solution of formic acid at 0.01% (v/v), obtaining a gradient elution of 11 min to separate the selected compounds. Other parameters such as flow rate, injection volume and column temperature were optimized, selecting 0.35 mL min^{-1} as optimum flow rate, 35 °C as column temperate and 5 μL as injection volume. When these conditions were used, retention times were constant with a relative standard deviation (R.S.D.) lower than 0.6%, ranging from 1.70 min (propamocarb) to 8.16 min (fenazaquin).

In order to determine the selected pesticides by MRM detection, all compounds were sorted by their retention times and divided into 25 acquisition groups each acquiring 1–7 compounds (2–14 transitions). Good peak shape were obtained when 0.015 s was used as dwell time, except for fenazaquin (last time window), which was monitored using a dwell time of 0.1 s.

Finally, Fig. 1 shows the chromatogram of some coeluting compounds in the same function. It can be observed that complete resolution is not achieved but MS/MS allows the suitable determination of the compounds.

3.2. Optimization of the extraction procedure

Sample preparation is often the most critical part of a multiresidue method due to the diversity of substances that have to be simultaneously extracted. Two procedures were tested: SPE and buffered QuEChERS [20]. SPE procedure was evaluated using three different cartridges: C18, Oasis and Strata-X, showing in Table 2 the obtained results. It can be observed that Oasis and Strata-X provided better results than C18, obtaining for most of the selected pesticides recoveries higher than 50%, whereas recoveries were lower than 50% if C18 cartridges were used. It can be noted that some pesticides such as oxamyl, picloram, methomyl and 2,6-dichlorbenzamide had recoveries lower than 50% when SPE procedure was applied. On the other hand, recoveries higher than 125% were observed for other pesticides such as iodosulfuron methyl, phenmedipham, diuron, desmediphan, methiocarb, triazophos, bitertanol and fenazaquin, indicating that matrix effect is significant when SPE procedure was applied. Furthermore, fruit juices should be diluted with water in order to avoid clogging effects on the cartridges.

In order to overcome these drawbacks, buffered QuEChERS procedure was evaluated. Conventional QuEChERS implies a clean-up step with PSA (primary secondary amine). In this work, this step was avoided, obtaining clean extracts and consistent chromatographic responses. However, the direct injection of 5 μL of acetonitrile sample extracts produced a poor peak shape for pesticides with retention times lower than 3 min, such as propamocarb, pymetrozine, oxamyl, methomyl, carbendazim, and imidacloprid. To select the optimal solvent medium, ratios of acetonitrile/water were regarded as the medium candidates. Besides, nitrogen gas was used to evaporate the acetonitrile residue in extracted samples and then adding 1 mL of methanol/aqueous solution of formic acid 0.01% (50/50, v/v). Better results were obtained when acetonitrile extract was diluted with water (1:1) obtaining good peak shapes and recoveries. Furthermore, evaporation of acetonitrile residue also provided good results, but considering that the direct dilution

Table 2
Comparison of recovery values (%) obtained for the different extraction process evaluated of a blank fruit juice sample fortified with a standard solution of selected pesticides at 50 μg L^{-1}

Pesticide	QuEChERS	SPE procedure		
		Strata	Oasis	C18
Propamocarb	68.0	74.3	115.6	54.0
Pymetrozine	70.2	56.0	92.0	37.6
Oxamyl	72.8	59.1	118.3	86.0
Nitenpyram	82.0	80.0	133.2	57.2
Picloram	90.0	49.7	76.4	*<5.0*
Methomyl	70.4	47.8	51.6	15.4
Carbendazim	72.0	73.9	108.2	101.2
Thiamethoxam	85.2	99.0	92.2	87.6
Monocrotophos	73.2	62.2	105.4	24.4
2,6-dichlorobenzamide	83.3	57.4	82.8	27.2
Atrazine desisopropyl	77.6	40.8	78.4	*<5.0*
Thiabendazole	72.0	51.7	73.0	30.0
Imidacloprid	70.4	60.7	98.2	48.8
Vamidothion	70.0	76.8	67.0	35.2
Metamitron	80.4	71.4	72.6	71.2
Acetamiprid	77.2	61.5	89.2	20.8
Quinmerac	67.3	63.5	95.4	6.6
Chloridazon	78.8	63.3	91.6	8.4
Thiacloprid	76.8	62.6	76.0	35.6
Desethyl atrazine	71.2	53.0	80.0	8.0
Metoxuron	70.4	81.8	78.0	27.6
Aldicarb	71.2	85.3	78.0	24.8
Cinosulfuron	80.0	159.1	164.2	7.6
Triasulfuron	80.8	140.6	190.0	48.8
Tifensulfuron methyl	72.8	114.7	129.2	24.4
Nicosulfuron	86.0	102.6	97.8	31.8
Thiophanate methyl	81.2	66.2	100.4	*<5.0*
Simazine	78.8	87.8	78.6	16.6
Metribuzine	70.0	60.6	73.2	7.4
Carbofuran	73.2	73.3	73.4	41.2
Bendiocarb	74.4	73.8	71.2	18.0
Ofurace	86.0	90.7	97.0	51.6
Chlorsulfuron	70.2	155.5	156.0	25.2
Desethyl terbuthylazine	78.0	77.7	76.6	16.6
Carbaryl	72.4	73.9	100.8	34.8
Imazalil	76.0	94.6	90.2	50.5
Monolinuron	72.4	85.8	99.6	23.6
Terbumeton	76.0	79.8	79.4	5.0
Chlorotoluron	72.6	82.9	88.0	11.6
Metobromuron	82.0	90.2	90.9	8.8
Atrazine	82.4	86.9	90.8	17.4
Metazachlor	76.8	107.1	99.0	17.4
Lenacil	79.1	50.9	58.4	9.6
Fensulfothion	95.2	78.3	109.1	33.6
Isoxaflutole	78.0	101.2	118.6	*<5.0*
Isoproturon	76.0	86.6	101.4	37.2
Fenpropimorph	82.4	106.1	123.4	27.4
Diuron	93.6	80.4	90.2	32.0
Azaconazole	76.4	111.1	102.4	36.8
Desmediphan	71.4	170.9	193.6	60.0
Ethoxyquine	84.0	55.8	51.6	66.8
Iodosulfuron methyl	99.6	190.2	157.5	*<5.0*
Spiroxamine	74.8	93.6	97.6	26.4
Phenmedipham	101.2	178.3	190.4	*<5.0*
Bensulfuron methyl	84.4	143.6	155.7	8.4
Diethofencarb	83.2	127.1	118.0	14.6
Sebuthylazine	74.8	80.7	95.4	17.6
Propazine	83.6	98.3	103.6	*<5.0*
Linuron	82.8	143.7	150.3	*<5.0*
Methiocarb	78.0	151.5	150.6	44.4
Terbuthylazine	76.4	107.8	104.0	11.4
Prometryn	74.8	82.7	101.7	*<5.0*
Paclobutrazol	78.8	85.7	101.2	36.8
Flutalonil	82.8	143.7	140.6	26.8
Promecarb	81.6	98.6	105.4	32.4
Propyzamide	80.2	77.9	101.5	*<5.0*
Triazophos	70.4	157.7	148.8	31.6
Tepraloxydim	82.4	162.1	129.7	22.8
Iprovalicarb	80.4	81.1	107.8	26.8
Triadimenol	72.4	127.7	146.8	26.0
Fenhexamide	76.4	102.9	99.5	57.6

Table 2 (*Continued*)

Pesticide	QuEChERS	SPE procedure		
		Strata	Oasis	C18
Epoxiconazole	85.6	175.3	187.3	30.4
Tebutam	71.2	69.4	79.2	*<5.0*
Metolachlor	82.8	88.3	109.8	5.8
Fenbuconazole	75.3	201.2	207.5	51.6
Spinosad	80.4	192.3	189.4	38.0
Cyprodinil	102.0	100.9	99.6	70.0
Diflubemzuron	99.2	123.0	140.3	33.2
Thiazopyr	78.4	165.4	163.2	19.6
Furmecyclox	76.6	83.4	108.3	22.8
Bitertanol	73.6	156.3	164.9	36.8
Pencycuron	76.0	194.3	198.3	25.6
Trifloxystrobin	70.0	201.3	210.4	16.8
Triflumizole	77.2	164.2	180.0	34.8
Cycloxydim	98.7	93.5	102.2	*<5.0*
Clethodim	94.0	149.3	142.2	*<5.0*
Fluazifop buthyl	80.4	193.4	189.4	6.6
Sethoxydim	82.0	178.9	182.4	9.4
Hexythiazox	89.7	89.2	90.4	25.7
Fenazaquin	78.7	124.5	130.5	29.6

was faster and the limits of quantification lower than 10 $\mu g\,L^{-1}$ were obtained despite the dilution, this procedure was selected. It should be emphasized the sample dilution presents some advantages such as lower amount of matrix loaded in the column, reducing matrix effects of fruit juices, and the compensation of possible variability between samples from different origin or variety [38].

Table 2 shows mean recovery values of blank fruit juices samples fortified at 50 $\mu g\,L^{-1}$, when this procedure was compared to conventional SPE, observing that for most of the selected pesticides better results were obtained when buffered QuEChERS was applied. However, SPE provides better or similar results than QuEChERS for some pesticides such as propamocarb, carbendazim, thiamethoxam, vamidothion, metoxuron, aldicarb, simazine, ofurace, carbaryl, imazalil, monolinuron, terbumeton, metobromuron, atrazine, metazachlor, isoproturon, spiroxamine, prometryn, paclobutrazol, promecarb, propyzamide, iprovalicarb, tebutam and furmecyclox, if Strata-X or Oasis were used as. This procedure yields high recovery rates and clean extracts, allowing the preconcentration of the analytes. However, this approach is laborious and time consuming and it is not suitable for all the pesticides selected in this study, whereas QuEChERS provides a simple, fast and robust sample preparation method based on solvent extraction that did not require any clean-up step, yielding suitable recoveries for all selected compounds, so it was choose for further studies. However, it can be indicated that the main disadvantage of QuEChERS versus SPE is that the 1 g sample/mL final extract concentration is lower than the concentrated extracts obtained when SPE is applied, which could increase the limit of quantification of the final method. Fig. 2 shows a representative chromatogram of blank peach juice fortified at 10 $\mu g\,L^{-1}$ of pesticides, observing clean extracts and high S/N ratios.

Finally it must be emphasized that taking into account the chromatographic analysis time (11 min) and the extraction time (approximately 10 min), the determination of 90 pesticides in one sample can be carried out in less than 22 min, considering the whole process (extraction, chromatographic separation and MS/MS detection).

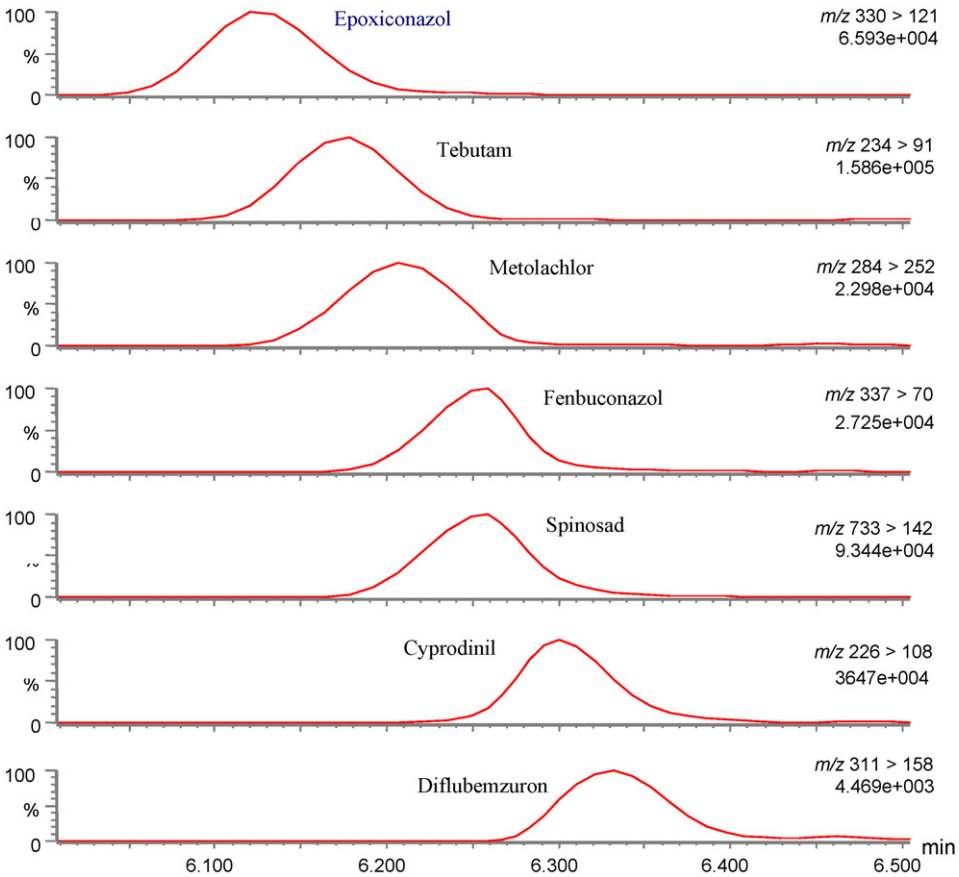

Fig. 2. UPLC–MS/MS chromatograms of seven pesticides spiked at the concentration 10 $\mu g\,L^{-1}$ in blank peach juice. Chromatographic and MS/MS conditions are described in the text.

Table 3
Evaluation of matrix effects, using fruit juice matrix-matched calibration from different fruit juices and solvent-based standards

Pesticide	Solvent	Multifruit[a]	Peach	Pineapple	Orange	Apple	*P* (%)[b]
Propamocarb	694.7	588.0	598.1	469.0	541.3	614.6	*8.9*
Pymetrozine	458.3	347.7	343.2	441.4	288.6	344.7	*5.1*
Oxamyl	10.4	10.7	11.6	13.2	14.6	14.8	*11.1*
Nitenpyram	64.7	52.2	58.5	51.7	59.3	63.9	*10.3*
Picloram	13.7	14.1	13.8	17.0	13.8	16.1	*64.9*
Methomyl	131.3	111.4	116.0	104.5	126.4	134.2	*6.2*
Carbendazim	952.6	771.5	841.1	854.0	790.4	900.5	*16.8*
Thiamethoxam	18.4	21.9	21.5	21.4	19.8	20.0	*72.5*
Monocrotophos	188.7	179.5	186.7	184.8	189.6	191.1	*89.9*
2,6-dichlorobenzamide	50.1	53.1	48.2	52.5	51.7	58.2	*6.3*
Atrazine desisopropyl	68.0	55.9	60.1	66.0	50.0	59.8	*6.0*
Thiabendazole	403.4	381.7	408.1	432.4	404.4	443.9	*5.9*
Imidacloprid	36.9	36.5	37.9	31.0	36.3	35.0	*12.7*
Vamidothion	425.7	431.0	410.9	411.0	408.2	443.9	*13.0*
Metamitron	72.0	56.7	56.1	62.0	65.6	68.6	*9.4*
Acetamiprid	222.6	198.6	190.3	205.6	197.8	212.2	*60.2*
Quinmerac	335.4	264.9	280.6	302.6	295.7	301.1	*43.1*
Chloridazon	30.9	32.1	29.2	29.7	26.1	29.0	*22.0*
Thiacloprid	346.8	292.6	302.6	335.0	285.3	317.3	*8.0*
Desethyl atrazine	387.7	276.0	298.1	315.6	253.5	304.9	*17.5*
Metoxuron	294.3	326.8	311.0	309.2	283.6	316.6	*10.8*
Aldicarb	31.5	56.3	53.0	47.3	48.3	46.0	*26.7*
Cinosulfuron	90.2	96.3	91.6	86.5	81.7	84.4	*7.1*
Triasulfuron	9.2	15.0	13.1	14.7	15.3	14.5	*66.2*
Tifensulfuron methyl	41.5	44.4	39.1	44.1	38.4	41.1	*30.1*
Nicosulfuron	4.8	5.7	5.3	6.5	6.2	6.3	*72.1*
Thiophanate methyl	125.2	121.4	126.6	119.4	99.3	108.9	*5.6*
Simazine	791.2	659.6	723.7	751.3	691.3	760.8	*24.4*
Metribuzine	66.2	58.3	62.2	60.8	55.7	68.7	*33.5*
Carbofuran	277.9	310.7	297.5	299.5	287.2	306.5	*57.8*
Bendiocarb	174.2	186.7	189.3	161.1	149.9	173.4	*6.2*
Ofurace	54.6	46.9	51.6	48.0	49.3	53.6	*52.4*
Chlorsulfuron	9.1	12.3	14.1	13.1	13.4	13.3	*81.5*
Desethyl terbuthylazine	852.5	921.5	943.4	977.5	961.6	1037.2	*35.4*
Carbaryl	172.3	210.9	204.1	210.4	184.9	194.8	*45.5*
Imazalil	198.2	210.2	198.3	226.1	218.6	222.2	*6.2*
Monolinuron	122.6	155.7	157.1	161.2	150.9	157.3	*84.8*
Terbumeton	1145.8	955.4	950.8	937.8	905.9	1032.2	*16.2*
Chlorotoluron	370.2	309.8	361.5	335.9	305.0	330.1	*5.6*
Metobromuron	50.6	52.3	54.1	49.8	49.6	54.7	*46.2*
Atrazine	854.9	703.6	742.6	768.3	695.5	821.2	*12.6*
Metazachlor	359.6	393.0	389.7	338.5	344.1	373.7	*10.4*
Lenacil	129.2	179.9	172.2	156.7	155.7	157.6	*13.2*
Fensulfothion	51.0	70.0	72.1	76.7	64.5	78.4	*48.9*
Isoxaflutole	11.2	12.6	9.3	10.0	10.5	9.8	*40.7*
Isoproturon	98.3	695.6	758.4	604.4	729.4	752.7	*47.4*
Fenpropimorph	362.1	461.9	453.2	448.6	439.2	466.1	*51.2*
Diuron	154.9	149.7	172.5	139.8	158.4	192.3	*20.6*
Azaconazole	193.1	289.7	273.9	296.3	297.0	309.9	*46.2*
Desmediphan	15.0	12.2	13.6	13.8	12.5	13.8	*64.8*
Ethoxyquine	41.9	27.1	23.6	28.3	27.4	27.1	*85.0*
Iodosulfuron methyl	21.5	49.6	50.2	49.5	43.0	50.3	*86.0*
Spiroxamine	2804.4	2707.9	2731.1	2669.7	2674.9	2942.8	*23.7*
Phenmedipham	22.5	23.6	23.9	21.1	21.2	20.7	*52.6*
Bensulfuron methyl	22.9	24.3	24.4	21.6	24.0	23.5	*76.3*
Diethofencarb	95.1	162.7	164.7	155.2	148.3	159.6	*26.2*
Sebuthylazine	82.3	398.1	405.7	389.9	412.3	429.3	*31.5*
Propazine	241.2	384.3	402.7	409.1	394.7	422.7	*29.2*
Linuron	51.9	55.1	53.8	45.3	48.8	48.0	*34.0*
Methiocarb	231.3	255.9	256.9	235.1	244.5	236.4	*49.1*
Terbuthylazine	1297.4	1232.9	1301.4	1249.7	1185.9	1365.3	*18.1*
Prometryn	615.1	628.2	621.0	646.6	594.0	553.4	*23.1*
Paclobutrazol	1443.1	1365.3	1386.4	1276.5	1219.5	1384.5	*26.8*
Flutalonil	98.0	103.8	106.2	108.8	93.5	102.8	*24.7*
Promecarb	299.9	322.4	336.8	303.9	279.9	286.3	*12.6*
Propyzamide	56.9	65.4	60.9	58.6	57.5	60.3	*9.1*
Triazophos	610.0	583.7	569.2	551.5	532.6	525.8	*21.2*
Tepraloxydim	11.3	9.8	9.7	10.0	10.4	10.6	*85.1*
Iprovalicarb	290.1	345.6	350.0	332.1	336.2	337.2	*61.6*
Triadimenol	168.8	224.2	216.7	229.0	229.9	206.9	*57.9*
Fenhexamide	69.1	69.0	73.6	67.7	65.5	66.4	*8.7*
Epoxiconazole	437.0	446.0	452.1	417.2	434.7	495.6	*8.0*
Tebutam	951.0	1065.9	996.8	905.4	947.5	919.9	*9.2*

Table 3 (*Continued*)

Pesticide	Solvent	Multifruit[a]	Peach	Pineapple	Orange	Apple	*P* (%)[b]
Metolachlor	185.2	194.6	209.6	196.9	179.8	195.7	*36.9*
Fenbuconazole	165.6	164.4	171.3	164.3	156.7	182.7	*17.2*
Spinosad	566.6	652.4	632.0	638.2	674.9	708.2	*50.2*
Cyprodinil	254.7	247.1	220.2	217.3	220.9	227.3	*19.2*
Diflubemzuron	36.3	32.3	29.4	28.2	28.8	30.7	*26.7*
Thiazopyr	80.2	79.6	81.5	81.8	77.4	84.2	*66.4*
Furmecyclox	205.0	262.1	258.0	246.2	256.2	250.8	*83.3*
Bitertanol	51.6	55.1	54.8	52.5	55.3	58.8	*53.2*
Pencycuron	247.0	222.8	236.1	204.1	208.8	200.8	*62.9*
Trifloxystrobin	145.0	158.6	156.2	143.5	130.3	138.0	*14.4*
Triflumizole	1097.6	1093.9	1117.9	1029.5	1058.3	1136.7	*49.7*
Cycloxydim	16.4	16.0	15.7	14.0	15.7	15.4	*63.4*
Clethodim	15.8	15.8	15.7	13.4	13.6	14.1	*77.3*
Fluazifop buthyl	92.4	101.9	92.9	98.3	88.2	93.2	*66.7*
Sethoxydim	33.7	26.9	26.9	26.9	25.5	26.5	*74.5*
Hexythiazox	15.8	13.8	13.1	13.6	13.1	13.8	*96.9*
Fenazaquin	1068.3	1211.5	1052.9	1150.2	1255.0	1373.1	*10.9*

[a] Peach and apple.

[b] *P*-value obtained (in %) using the procedure indicated in Ref. [39], when the selected matrices (multifruit, peach, pineapple, orange and apple) were evaluated.

Table 4
Evaluation of recovery (%) in different fruit juice samples, using a common matrix-matched calibration curve

Pesticide	Recovery (%)[a]							
	Peach		Pineapple		Orange		Apple	
	25 μg L^{-1}	75 μg L^{-1}	25 μg L^{-1}	75 μg L^{-1}	25 μg L^{-1}	75 μg L^{-1}	25 μg L^{-1}	75 μg L^{-1}
Propamocarb	91.3 (11.8)	76.1 (18.3)	78.8 (12.3)	76.4 (16.0)	78.8 (17.8)	92.2 (14.1)	109.7 (9.5)	105.7 (6.1)
Pymetrozine	101.5 (3.6)	103.0 (19.8)	104.4 (9.8)	106.9 (18.7)	106.0 (19.2)	105.9 (14.7)	108.4 (5.2)	109.8 (7.8)
Oxamyl	70.8 (20.7)	88.4 (14.6)	106.0 (11.8)	109.9 (19.7)	101.8 (12.2)	109.8 (12.9)	107.3 (12.7)	109.9 (7.1)
Nitenpyram	101.1 (9.4)	97.8 (15.3)	111.2 (17.1)	110.6 (0.5)	104.4 (22.4)	99.3 (21.9)	118.8 (2.9)	119.7 (9.9)
Picloram	105.4 (15.3)	96.8 (6.7)	104.5 (19.8)	109.8 (22.0)	96.2 (10.1)	95.0 (15.2)	102.5 (15.5)	97.2 (9.2)
Methomyl	90.2 (15.0)	95.2 (9.8)	80.7 (13.1)	104.1 (19.9)	106.7 (13.5)	104.7 (11.6)	104.5 (2.9)	107.0 (12.7)
Carbendazim	102.3 (5.7)	109.6 (18.1)	94.0 (19.4)	102.6 (7.9)	88.4 (21.9)	99.0 (12.4)	109.5 (9.4)	108.3 (2.3)
Thiamethoxam	75.3 (22.9)	73.7 (12.9)	78.2 (11.1)	77.4 (10.5)	75.5 (30.8)	93.3 (13.5)	75.5 (9.7)	71.3 (16.8)
Monocrotophos	94.0 (12.9)	96.5 (6.8)	87.5 (19.5)	95.9 (8.1)	97.8 (10.2)	102.6 (11.5)	104.1 (10.0)	101.7 (11.0)
2,6-dichlorobenzamide	96.0 (6.1)	98.0 (7.5)	100.9 (7.5)	96.6 (5.0)	94.7 (10.4)	96.6 (11.0)	94.5 (10.1)	105.0 (6.9)
Atrazine desisopropyl	93.7 (13.4)	95.8 (4.2)	108.7 (12.1)	105.4 (5.0)	88.4 (10.4)	101.6 (14.4)	103.0 (3.3)	105.4 (3.1)
Thiabendazole	99.9 (5.8)	104.8 (5.1)	109.2 (3.5)	102.5 (5.9)	105.4 (15.3)	102.0 (19.7)	103.2 (4.2)	101.0 (2.7)
Imidacloprid	86.2 (16.9)	91.7 (10.8)	81.5 (5.9)	85.8 (6.1)	95.9 (7.0)	94.9 (5.6)	101.3 (6.9)	94.4 (8.5)
Vamidothion	92.7 (5.4)	92.0 (3.4)	89.3 (7.2)	93.8 (5.9)	84.9 (12.3)	93.9 (7.7)	108.4 (4.0)	104.4 (2.9)
Metamitron	98.1 (1.0)	103.8 (6.4)	102.3 (2.5)	103.0 (7.7)	100.6 (13.2)	109.0 (11.2)	102.5 (4.5)	108.4 (1.3)
Acetamiprid	90.5 (10.2)	93.1 (7.7)	93.3 (8.8)	93.7 (6.3)	83.6 (17.4)	93.4 (14.5)	106.3 (2.3)	102.1 (5.8)
Quinmerac	97.7 (11.3)	104.6 (6.4)	105.1 (13.5)	102.2 (6.7)	100.8 (13.8)	107.7 (12.0)	106.5 (0.4)	101.7 (11.5)
Chloridazon	93.8 (11.5)	87.1 (9.0)	89.3 (3.9)	94.1 (4.5)	80.5 (5.3)	82.3 (13.0)	105.2 (15.7)	104.2 (10.8)
Thiacloprid	96.2 (6.8)	99.3 (6.2)	102.9 (12.6)	108.2 (5.0)	92.3 (11.3)	101.2 (8.8)	101.7 (4.0)	108.7 (5.4)
Desethyl atrazine	99.7 (9.4)	104.6 (6.0)	104.6 (8.4)	105.7 (4.8)	82.8 (17.6)	94.4 (14.7)	107.8 (1.8)	105.1 (7.6)
Metoxuron	88.5 (8.4)	89.9 (4.4)	84.7 (10.5)	88.9 (4.1)	80.7 (9.3)	87.5 (7.8)	99.4 (1.0)	95.7 (6.7)
Aldicarb	86.4 (10.7)	85.9 (3.0)	79.1 (9.9)	73.6 (7.7)	74.3 (5.0)	75.9 (4.8)	78.2 (13.5)	70.9 (3.0)
Cinosulfuron	91.5 (8.5)	91.2 (4.9)	89.1 (1.5)	88.8 (5.2)	90.3 (4.1)	87.0 (4.0)	104.3 (16.9)	99.4 (7.5)
Triasulfuron	71.0 (16.0)	86.1 (17.3)	94.0 (16.2)	89.5 (5.2)	88.2 (10.7)	84.8 (12.7)	74.4 (18.3)	74.7 (20.0)
Tifensulfuron methyl	74.3 (19.3)	89.7 (16.9)	86.8 (18.7)	90.9 (5.0)	91.0 (1.5)	89.5 (15.2)	108.5 (24.9)	96.8 (1.8)
Nicosulfuron	101.3 (11.3)	100.5 (16.7)	105.7 (12.6)	106.9 (15.4)	100.8 (11.1)	104.4 (11.9)	104.2 (17.2)	106.4 (18.6)
Thiophanate methyl	99.4 (5.6)	96.3 (8.4)	87.0 (14.1)	89.1 (2.9)	71.7 (9.6)	71.5 (8.5)	107.9 (16.8)	98.7 (2.6)
Simazine	92.3 (17.1)	99.1 (5.8)	94.4 (15.6)	98.7 (4.3)	100.0 (1.5)	101.2 (7.4)	106.8 (1.9)	106.1 (5.6)
Metribuzine	100.3 (4.8)	106.0 (4.9)	91.1 (22.0)	98.2 (8.4)	90.3 (8.2)	90.3 (10.7)	101.5 (1.9)	107.6 (16.8)
Carbofuran	95.8 (4.1)	100.8 (6.0)	92.7 (4.4)	95.8 (6.2)	93.8 (2.5)	91.1 (7.7)	106.2 (12.1)	101.6 (1.4)
Bendiocarb	91.9 (9.7)	91.0 (3.5)	82.4 (7.8)	90.7 (8.6)	81.2 (5.2)	82.6 (7.8)	99.0 (1.2)	96.1 (10.1)
Ofurace	96.2 (15.6)	107.1 (18.7)	95.0 (11.9)	105.1 (8.6)	102.7 (4.7)	106.0 (4.9)	108.7 (6.8)	101.6 (1.4)
Chlorsulfuron	78.1 (14.6)	92.0 (21.4)	95.7 (21.9)	99.2 (9.3)	88.4 (20.7)	89.9 (7.3)	88.7 (6.2)	87.8 (14.7)
Desethyl terbuthylazine	93.8 (10.9)	99.2 (5.8)	97.2 (9.3)	103.0 (7.2)	102.6 (0.8)	104.3 (7.2)	107.2 (2.1)	104.3 (7.3)
Carbaryl	80.2 (23.0)	89.2 (7.5)	76.4 (32.6)	83.7 (8.3)	79.9 (7.4)	80.7 (3.8)	90.5 (3.2)	83.5 (14.8)
Imazalil	101.8 (0.7)	107.7 (4.8)	103.4 (10.7)	105.3 (4.5)	105.2 (14.1)	102.9 (15.5)	109.1 (17.4)	102.2 (6.7)
Monolinuron	87.5 (16.5)	92.8 (6.1)	89.8 (16.4)	93.4 (5.3)	97.8 (2.3)	97.5 (7.3)	107.1 (4.5)	102.4 (4.0)
Terbumeton	97.2 (2.1)	98.9 (3.6)	91.2 (7.1)	98.4 (6.4)	97.2 (1.6)	99.0 (8.2)	107.3 (6.0)	103.3 (1.7)
Chlorotoluron	102.2 (14.8)	109.8 (5.7)	93.0 (18.7)	99.3 (5.5)	98.8 (0.5)	96.6 (5.6)	103.9 (1.2)	99.1 (12.6)
Metobromuron	87.0 (20.0)	91.8 (4.9)	92.9 (2.4)	91.1 (4.7)	85.8 (4.3)	82.2 (6.0)	95.3 (3.3)	94.1 (12.0)
Atrazine	94.4 (14.2)	96.5 (4.2)	90.3 (18.7)	99.2 (9.1)	94.1 (2.2)	96.5 (8.9)	105.2 (1.9)	102.4 (8.8)
Metazachlor	87.7 (11.6)	88.2 (4.7)	81.9 (1.7)	85.3 (3.5)	84.6 (0.4)	82.9 (7.5)	97.5 (2.7)	93.4 (7.4)
Lenacil	87.3 (14.2)	88.7 (6.8)	87.5 (9.8)	88.8 (1.7)	73.9 (17.2)	93.3 (12.4)	95.0 (11.3)	90.8 (10.0)
Fensulfothion	103.7 (17.4)	108.6 (19.7)	104.9 (16.3)	107.4 (8.1)	106.8 (8.6)	100.1 (9.8)	107.6 (16.8)	91.0 (17.9)
Isoxaflutole	81.7 (18.9)	92.9 (13.5)	78.2 (19.4)	75.4 (4.5)	71.5 (15.9)	72.9 (14.5)	79.1 (16.9)	82.3 (1.7)
Isoproturon	94.4 (19.7)	105.8 (9.3)	76.6 (21.5)	87.3 (14.0)	87.1 (8.1)	90.6 (6.2)	106.3 (2.1)	99.4 (13.3)
Fenpropimorph	86.6 (10.6)	90.9 (7.5)	83.8 (9.7)	88.9 (7.0)	89.8 (11.1)	88.2 (10.3)	101.0 (1.6)	98.2 (5.1)

Table 4 (*Continued*)

Pesticide	Recovery (%)[a]							
	Peach		Pineapple		Orange		Apple	
	25 μg L^{-1}	75 μg L^{-1}	25 μg L^{-1}	75 μg L^{-1}	25 μg L^{-1}	75 μg L^{-1}	25 μg L^{-1}	75 μg L^{-1}
Diuron	81.1 (19.2)	102.2 (13.8)	75.5 (21.4)	91.5 (14.6)	90.1 (6.8)	88.3 (4.5)	107.8 (4.9)	103.1 (13.8)
Azaconazole	92.6 (3.3)	91.4 (11.7)	92.2 (8.6)	102.2 (9.3)	98.9 (5.9)	105.2 (3.2)	107.1 (1.8)	101.0 (6.8)
Desmediphan	105.8 (20.7)	109.7 (16.9)	102.4 (15.7)	108.7 (5.9)	90.8 (17.4)	108.0 (10.9)	108.4 (14.7)	105.8 (17.4)
Ethoxyquine	107.6 (17.9)	102.7 (17.3)	105.6 (19.2)	80.3 (17.6)	108.0 (19.5)	91.0 (13.4)	102.5 (17.5)	105.0 (20.2)
Iodosulfuron methyl	106.9 (2.1)	101.9 (16.5)	108.6 (15.9)	102.8 (9.7)	106.6 (4.9)	107.4 (4.0)	108.8 (5.3)	107.5 (24.4)
Spiroxamine	96.4 (6.7)	96.9 (4.4)	87.9 (12.9)	95.6 (7.2)	99.2 (5.9)	96.2 (6.0)	101.9 (5.2)	106.8 (5.8)
Phenmedipham	83.0 (21.6)	83.2 (11.2)	72.7 (7.3)	81.7 (11.8)	76.9 (3.4)	73.6 (12.3)	84.5 (3.9)	78.5 (11.6)
Bensulfuron methyl	78.8 (19.0)	95.1 (14.3)	81.8 (11.5)	88.8 (16.7)	94.4 (15.0)	83.0 (13.5)	107.7 (23.8)	100.3 (8.5)
Diethofencarb	93.3 (10.5	98.6 (6.2)	83.9 (13.6)	90.2 (6.1)	94.6 (5.6)	91.0 (6.7)	100.3 (2.9)	93.2 (10.1)
Sebuthylazine	100.0 (6.0)	103.4 (3.9)	97.3 (3.1)	98.8 (1.7)	107.1 (3.0)	106.3 (5.4)	108.9 (2.4)	105.2 (4.6)
Propazine	106.5 (11.9)	102.2 (7.5)	101.3 (21.3)	107.2 (4.9)	109.1 (2.7)	107.7 (3.7)	108.7 (3.1)	104.6 (8.0)
Linuron	103.7 (10.4)	88.6 (20.6)	85.9 (6.2)	86.0 (3.5)	101.7 (12.3)	93.1 (10.4)	103.3 (15.7)	104.4 (3.9)
Methiocarb	95.3 (6.6)	97.4 (6.4)	79.3 (15.6)	88.7 (9.4)	92.3 (3.2)	89.8 (2.3)	101.0 (8.8)	95.3 (1.7)
Terbuthylazine	99.2 (7.2)	101.1 (4.2)	93.8 (10.0)	95.9 (4.0)	99.3 (0.8)	99.8 (1.3)	105.6 (3.1)	102.4 (4.7)
Prometryn	76.3 (3.6)	77.0 (11.2)	72.2 (6.4)	76.2 (11.8)	70.1 (1.5)	71.2 (6.4)	78.2 (3.5)	76.0 (2.6)
Paclobutrazol	94.2 (7.7)	95.2 (5.2)	79.3 (16.4)	86.2 (7.0)	74.5 (0.7)	85.8 (4.2)	107.9 (3.3)	103.3 (6.0)
Flutalonil	89.2 (18.6)	104.8 (10.9)	90.7 (16.2)	99.5 (8.4)	75.2 (5.4)	81.8 (4.3)	102.1 (11.5)	106.2 (2.6)
Promecarb	97.2 (9.1)	95.7 (3.5)	86.3 (10.4)	93.3 (6.6)	74.6 (3.7)	79.6 (3.2)	97.8 (3.3)	93.0 (8.6)
Propyzamide	89.4 (3.1)	87.8 (7.2)	83.2 (5.7)	87.7 (7.9)	85.9 (8.3)	87.4 (4.5)	109.7 (16.4)	101.6 (5.1)
Triazophos	87.8 (7.0)	92.0 (6.8)	72.9 (15.6)	81.4 (9.2)	76.7 (2.3)	78.2 (3.4)	95.2 (10.3)	91.8 (2.1)
Tepraloxydim	81.5 (14.7)	100.7 (13.5)	77.1 (22.0)	93.9 (19.0)	100.2 (8.6)	108.8 (9.3)	107.9 (6.8)	107.6 (8.6)
Iprovalicarb	97.1 (3.3)	97.7 (4.2)	91.5 (9.2)	93.6 (2.7)	92.9 (1.1)	94.6 (2.3)	108.9 (10.8)	104.1 (2.6)
Triadimenol	90.3 (8.0)	94.8 (4.1)	85.5 (16.3)	94.8 (8.5)	91.5 (6.1)	89.2 (6.3)	99.8 (5.9)	97.7 (4.3)
Fenhexamide	100.6 (9.9)	93.3 (9.6)	80.3 (9.2)	89.0 (9.8)	104.5 (15.9)	98.3 (12.3)	108.9 (13.9)	105.9 (17.3)
Epoxiconazole	88.5 (15.3)	93.5 (4.6)	80.8 (13.0)	91.5 (10.6)	90.7 (5.0)	94.7 (5.3)	102.0 (7.9)	97.5 (17.2)
Tebutam	78.8 (6.2)	72.0 (8.2)	77.8 (1.4)	70.8 (2.7)	71.2 (1.3)	70.5 (5.4)	84.4 (8.1)	79.6 (1.3)
Metolachlor	98.3 (13.5)	103.3 (7.3)	95.2 (9.3)	98.5 (7.3)	93.4 (0.7)	93.3 (0.5)	108.9 (15.0)	108.4 (2.3)
Fenbuconazole	98.7 (5.2)	102.0 (2.3)	92.8 (6.8)	98.3 (6.7)	105.6 (10.2)	99.9 (6.8)	103.1 (9.6)	109.6 (1.7)
Spinosad	97.8 (4.3)	102.8 (3.7)	90.8 (16.0)	101.9 (9.4)	106.9 (3.7)	107.1 (3.2)	104.0 (2.0)	109.9 (9.4)
Cyprodinil	102.5 (20.0)	89.5 (10.6)	89.3 (6.0)	86.6 (3.9)	95.8 (2.1)	95.4 (0.9)	110.3 (6.3)	102.1 (8.2)
Diflubemzuron	91.6 (8.3)	85.1 (12.3)	82.9 (5.7)	87.2 (4.9)	95.2 (7.9)	91.6 (4.9)	103.8 (18.1)	105.8 (14.7)
Thiazopyr	78.1 (16.8)	91.4 (13.2)	85.9 (21.3)	89.5 (3.6)	92.5 (9.3)	90.4 (10.1)	99.7 (4.4)	97.9 (11.4)
Furmecyclox	90.5 (10.1)	91.4 (1.9)	82.5 (14.4)	87.3 (4.8)	96.6 (6.1)	89.9 (4.3)	102.3 (8.2)	95.4 (6.8)
Bitertanol	97.4 (2.2)	96.4 (4.6)	87.2 (8.5)	91.3 (4.1)	82.1 (17.9)	91.2 (14.9)	104.2 (3.5)	103.5 (7.1)
Pencycuron	82.9 (10.3)	80.5 (6.8)	76.8 (18.0)	70.9 (5.1)	78.6 (4.1)	70.6 (2.1)	81.0 (3.7)	73.3 (14.3)
Trifloxystrobin	98.1 (2.4)	96.0 (5.3)	73.8 (16.6)	81.5 (9.0)	79.0 (0.6)	80.2 (2.1)	93.2 (2.9)	89.8 (10.0)
Triflumizole	92.1 (10.7)	95.6 (4.3)	80.8 (18.2)	90.1 (8.9)	93.0 (1.9)	91.8 (2.5)	108.6 (5.4)	104.3 (5.4)
Cycloxydim	72.2 (16.9)	89.0 (17.0)	80.6 (13.6)	90.4 (9.6)	103.6 (7.0)	88.9 (4.5)	107.7 (19.6)	100.8 (7.7)
Clethodim	106.1 (15.6)	89.0 (15.5)	75.5 (19.0)	80.6 (10.8)	106.4 (12.7)	98.5 (10.2)	102.9 (21.4)	99.6 (8.5)
Fluazifop buthyl	89.4 (5.5)	93.8 (3.6)	76.2 (17.0)	79.9 (6.8)	91.6 (4.4)	80.9 (4.3)	104.0 (9.5)	99.3 (6.0)
Sethoxydim	92.5 (4.3)	96.9 (4.0)	88.7 (6.7)	87.2 (3.6)	97.1 (4.6)	90.5 (2.3)	98.4 (2.1)	96.2 (4.7)
Hexythiazox	90.0 (10.0)	89.3 (7.1)	72.9 (19.8)	81.2 (8.8)	90.8 (4.4)	79.3 (2.5)	96.5 (10.6)	92.2 (4.9)
Fenazaquin	91.9 (4.4)	91.3 (2.4)	95.4 (0.6)	103.7 (11.1)	104.4 (5.2)	97.8 (3.2)	105.0 (14.5)	104.6 (8.3)

[a] R.S.D. values are given in brackets ($n = 4$).

3.3. Evaluation of matrix effects

It is well known that matrix components can inhibit or enhance the analyte signal. Matrix effects depend on some factors such as the nature of the pesticide, the type of matrix and the pesticide to matrix ratio. The best way to compensate for matrix effects is the use of isotope internal standards, however, for the most pesticides these compounds are not available, so other approaches such as matrix-matched calibration can be used. In this work, five fruit juices (peach, pineapple, orange, apple and mutifruit) were selected for evaluation of matrix effects, analyzing standards of different concentrations in pure solvents and in the five matrices indicated, and comparing the slopes of the calibration curves. Table 3 shows the obtained results. It can be noted that a matrix effect was observed for most of the pesticides tested, such as lenacil, triadimenol, iodosulfuron methyl (matrix enhancement), and ethoxyquine (matrix inhibition). Besides differences in matrix effects between different types of juice are usually much smaller than the difference between any fruit juice and solvent solutions. No significant difference between the different matrices is observed. Analysis of covariance was carried out in order to compare the slopes obtained for the different pesticides in the five matrices evaluated [39]. It can be observed (see Table 3) that for all the cases, the slopes are not statistically different (P was higher than 5% for all the pesticides) indicating that the selected matrices do not have any significant influence on the extraction procedure. This suggests that the use of matrix-matched calibration provides reliable quantitation capabilities for fruit juice pesticide analysis. The insignificant matrix effect may be due to the relatively diluted samples, considering that 0.5 of commodity/mL was used. For routine analysis, one of this matrix was selected as a representative matrix for the determination of pesticide residues in fruit juices, as only one matrix-matched calibration standard is necessary when analyzing several commodities within the same analytical batch. In this work, multifruit juice (peach and apple) was selected as representative matrix because it contains two fruits which can be frequently used in the preparation of juices. In order to check it, blank fruit samples from different fruits (orange, apple, pineapple and peach) were spiked at two fortification levels, 25 and 75 μg L^{-1} (four replicates) and the samples were quantified using a matrix-matched calibration prepared in a blank multifruit (peach and apple) juice. The results are indicated in Table 4. It can be observed that recoveries ranged from 70 to 110% for the target pesticides in the four types of juices evaluated, indicating that

Table 5
Validation results of the developed method

Pesticide	R^2	Recovery (%)[a]			Intermediate precision[b]	LOD ($\mu g\,L^{-1}$)	LOQ ($\mu g\,L^{-1}$)
		10 $\mu g\,L^{-1}$	50 $\mu g\,L^{-1}$	100 $\mu g\,L^{-1}$			
Propamocarb	0.9903	70.8 (17.2)	71.3 (19.4)	70.1 (10.2)	2.2	1.7	4.2
Pymetrozine	0.9929	79.6 (16.5)	83.3 (13.0)	90.7 (4.9)	5.0	2.2	4.9
Oxamyl	0.9810	89.1 (19.3)	88.3 (21.1)	72.3 (8.7)	19.5	2.8	5.0
Nitenpyram	0.9968	88.9 (24.1)	88.0 (22.7)	79.3 (2.6)	4.5	2.7	4.8
Picloram	0.9951	108.5 (18.8)	75.4 (16.4)	70.2 (14.9)	16.0	2.4	4.6
Methomyl	0.9950	80.9 (7.3)	85.8 (17.6)	72.5 (1.6)	7.9	2.1	4.1
Carbendazim	0.9944	85.1 (10.3)	86.6 (14.5)	77.7 (7.3)	1.5	1.6	4.1
Thiamethoxam	0.9868	93.5 (12.4)	82.8 (20.9)	79.7 (14.1)	10.5	1.6	3.9
Monocrotophos	0.9966	81.7 (19.9)	86.3 (19.9)	74.0 (4.7)	9.3	3.0	4.3
2,6-dichlorobenzamide	0.9981	72.8 (13.8)	88.2 (13.4)	77.2 (8.1)	9.6	1.6	4.0
Atrazine desisopropyl	0.9975	78.3 (19.1)	92.3 (14.5)	73.2 (4.7)	9.7	1.0	2.4
Thiabendazole	0.9981	78.3 (11.0)	87.2 (15.1)	76.8 (5.0)	4.0	1.8	4.6
Imidacloprid	0.9954	91.7 (11.3)	86.3 (18.0)	79.3 (7.1)	2.4	1.9	4.9
Vamidothion	0.9984	83.6 (5.1)	85.7 (17.6)	77.4 (4.5)	1.5	1.5	3.7
Metamitron	0.9951	84.0 (9.3)	85.7 (17.1)	75.6 (8.6)	13.5	2.6	4.7
Acetamiprid	0.9952	79.2 (12.8)	84.6 (13.5)	77.4 (4.4)	5.8	2.0	4.3
Quinmerac	0.9934	75.0 (18.0)	78.9 (13.4)	74.7 (9.4)	4.4	1.3	3.3
Chloridazon	0.9982	93.6 (21.9)	88.9 (19.9)	73.5 (7.9)	11.3	1.5	3.7
Thiacloprid	0.9959	78.2 (11.0)	84.5 (12.9)	77.5 (6.2)	4.4	1.0	2.6
Desethyl atrazine	0.9968	80.7 (11.4)	85.7 (16.0)	75.2 (5.1)	0.6	1.8	4.5
Metoxuron	0.9972	80.5 (8.3)	85.1 (13.9)	78.1 (6.9)	0.9	1.7	4.4
Aldicarb	0.9944	80.4 (10.6)	85.1 (15.1)	75.9 (5.6)	6.7	1.4	3.5
Cinosulfuron	0.9990	83.5 (14.7)	83.9 (14.0)	74.3 (4.1)	5.6	1.4	3.5
Triasulfuron	0.9991	79.5 (19.8)	86.9 (17.3)	77.5 (12.2)	8.2	1.1	2.8
Tifensulfuron methyl	0.9880	77.0 (18.0)	78.1 (19.6)	70.7 (8.2)	11.2	1.9	4.5
Nicosulfuron	0.9878	95.3 (15.4)	70.9 (19.1)	72.1 (14.2)	20.5	2.9	5.0
Thiophanate methyl	0.9951	92.5 (19.8)	86.3 (15.4)	76.8 (4.7)	8.8	2.8	4.8
Simazine	0.9962	81.9 (15.1)	87.7 (13.2)	81.8 (7.3)	9.3	1.1	2.8
Metribuzine	0.9882	76.6 (18.6)	85.0 (15.1)	89.6 (2.4)	6.7	2.9	5.0
Carbofuran	0.9962	76.2 (4.9)	87.8 (15.6)	76.7 (1.8)	4.7	2.7	4.6
Bendiocarb	0.9957	82.0 (18.7)	86.9 (14.4)	76.2 (8.1)	2.6	2.7	4.9
Ofurace	0.9833	79.7 (13.1)	84.2 (14.7)	83.3 (6.2)	9.7	2.7	4.8
Chlorsulfuron	0.9912	95.2 (19.3)	82.0 (17.6)	70.7 (11.8)	7.6	2.6	4.3
Desethyl terbuthylazine	0.9956	78.6 (10.2)	91.0 (15.1)	81.6 (2.1)	3.9	2.4	4.3
Carbaryl	0.9893	84.2 (19.6)	92.3 (16.5)	74.2 (17.6)	8.8	3.1	5.0
Imazalil	0.9965	87.2 (12.0)	85.6 (15.4)	73.0 (3.8)	1.4	2.6	4.1
Monolinuron	0.9954	77.4 (10.3)	84.6 (15.1)	78.8 (2.5)	5.1	1.8	4.7
Terbumeton	0.9976	82.3 (11.5)	88.8 (13.9)	78.7 (4.2)	2.0	1.4	3.5
Chlorotoluron	0.9959	77.3 (8.6)	84.0 (16.1)	76.7 (10.0)	3.8	2.1	4.5
Metobromuron	0.9941	80.0 (14.0)	77.5 (18.0)	80.2 (15.0)	7.8	0.9	2.2
Atrazine	0.9939	88.5 (5.1)	89.1 (12.3)	81.3 (13.8)	4.9	1.9	4.9
Metazachlor	0.9973	85.8 (9.5)	86.8 (13.1)	80.7 (1.7)	3.9	2.9	4.7
Lenacil	0.9964	74.9 (9.3)	91.6 (18.5)	81.3 (4.4)	6.0	0.7	1.7
Fensulfothion	0.9806	85.0 (15.7)	82.5 (7.7)	74.7 (8.1)	9.7	3.0	4.9
Isoxaflutole	0.9925	109.3 (13.9)	72.5 (11.3)	82.6 (18.4)	14.6	2.9	4.8
Isoproturon	0.9895	86.1 (17.7)	79.1 (16.2)	71.9 (2.6)	4.1	3.1	5.0
Fenpropimorph	0.9966	86.6 (10.8)	80.7 (18.1)	74.3 (6.7)	10.6	2.5	4.6
Diuron	0.9842	89.0 (18.9)	90.8 (12.6)	78.9 (7.7)	19.4	1.5	3.7
Azaconazole	0.9975	86.0 (5.1)	85.4 (17.3)	88.1 (10.9)	14.6	1.6	4.0
Desmediphan	0.9886	79.0 (12.4)	91.4 (13.4)	71.8 (11.2)	16.6	2.4	4.8
Ethoxyquine	0.9941	102.9 (10.5)	80.7 (8.4)	83.1 (17.7)	16.3	2.6	4.7
Iodosulfuron methyl	0.9873	88.3 (18.4)	90.4 (18.8)	77.1 (8.6)	16.3	2.9	5.0
Spiroxamine	0.9963	87.8 (11.4)	87.7 (13.9)	78.7 (4.8)	6.4	2.5	4.7
Phenmedipham	0.9980	100.0 (18.6)	86.9 (9.6)	73.1 (17.3)	13.5	2.3	4.6
Bensulfuron methyl	0.9946	94.3 (16.3)	93.2 (16.0)	73.1 (7.6)	11.3	3.0	4.9
Diethofencarb	0.9967	90.0 (18.4)	83.1 (11.8)	71.1 (9.8)	6.4	2.2	4.7
Sebuthylazine	0.9978	86.1 (10.0)	83.4 (13.0)	80.9 (11.0)	1.3	1.7	4.3
Propazine	0.9942	85.6 (15.1)	83.7 (16.9)	72.1 (10.5)	2.9	2.3	4.9
Linuron	0.9919	78.2 (21.9)	90.2 (11.3)	71.4 (16.8)	8.4	1.5	3.7
Methiocarb	0.9946	81.6 (13.8)	84.8 (13.6)	72.1 (10.8)	4.0	2.3	4.1
Terbuthylazine	0.9971	84.1 (9.3)	86.7 (11.8)	81.6 (6.7)	2.7	1.7	4.3
Prometryn	0.9990	76.9 (14.7)	82.9 (10.4)	86.2 (9.1)	3.3	1.5	3.7
Paclobutrazol	0.9957	83.8 (10.5)	89.2 (14.0)	81.9 (4.8)	4.0	1.9	4.9
Flutalonil	0.9947	85.3 (10.4)	87.9 (15.6)	72.8 (12.1)	7.6	3.0	4.5
Promecarb	0.9956	78.4 (10.0)	85.4 (14.8)	74.3 (11.5)	9.5	1.6	4.0
Propyzamide	0.9989	70.5 (18.8)	90.9 (13.1)	83.2 (11.4)	19.6	1.4	4.8
Triazophos	0.9951	78.6 (10.7)	81.7 (17.8)	78.4 (2.7)	2.1	1.5	3.9
Tepraloxydim	0.9853	109.5 (16.6)	103.7 (15.6)	70.8 (13.9)	18.5	2.0	4.6
Iprovalicarb	0.9980	87.2 (18.7)	87.0 (16.8)	76.1 (5.6)	4.7	1.6	4.1
Triadimenol	0.9941	81.2 (9.1)	86.3 (17.8)	77.7 (1.0)	2.1	1.9	4.9
Fenhexamide	0.9961	90.6 (18.7)	84.5 (14.8)	71.0 (12.0)	8.4	2.6	4.5

Table 5 (*Continued*)

Pesticide	R^2	Recovery (%)[a]			Intermediate precision[b]	LOD ($\mu g\,L^{-1}$)	LOQ ($\mu g\,L^{-1}$)
		10 $\mu g\,L^{-1}$	50 $\mu g\,L^{-1}$	100 $\mu g\,L^{-1}$			
Epoxiconazole	0.9956	91.2 (16.5)	92.7 (14.6)	75.5 (3.6)	7.2	2.1	4.3
Tebutam	0.9979	76.7 (12.6)	78.4 (10.0)	76.1 (5.2)	1.9	1.2	3.0
Metolachlor	0.9955	81.5 (17.4)	88.1 (15.6)	74.5 (6.7)	3.8	2.4	4.3
Fenbuconazole	0.9966	85.0 (8.9)	86.1 (15.5)	75.6 (5.7)	2.6	2.4	4.4
Spinosad	0.9949	77.4 (16.9)	89.7 (14.3)	83.0 (5.7)	3.1	2.1	4.5
Cyprodinil	0.9998	79.0 (18.2)	84.2 (10.1)	79.9 (4.4)	8.0	1.9	4.8
Diflubemzuron	0.9953	102.8 (15.8)	88.0 (10.6)	72.3 (4.1)	12.6	2.5	4.6
Thiazopyr	0.9964	80.1 (16.1)	84.3 (13.9)	76.9 (6.8)	6.4	2.9	4.9
Furmecyclox	0.9929	84.6 (8.5)	85.5 (13.0)	77.1 (6.3)	2.0	2.0	4.3
Bitertanol	0.9982	76.6 (15.7)	83.9 (16.3)	75.7 (7.2)	6.7	1.0	2.6
Pencycuron	0.9954	80.3 (16.9)	72.1 (12.2)	75.5 (6.0)	2.6	1.1	2.7
Trifloxystrobin	0.9970	75.9 (13.8)	77.9 (19.1)	73.0 (12.4)	0.7	1.3	3.4
Triflumizole	0.9944	80.1 (11.6)	84.1 (12.5)	75.1 (7.9)	2.7	1.5	3.8
Cycloxydim	0.9889	88.3 (20.1)	85.6 (7.4)	72.9 (3.9)	14.5	1.2	2.9
Clethodim	0.9821	72.2 (16.0)	82.2 (4.8)	72.5 (8.8)	5.4	2.9	4.1
Fluazifop buthyl	0.9870	74.9 (15.8)	76.1 (10.2)	70.8 (9.1)	5.2	3.0	5.0
Sethoxydim	0.9992	75.4 (14.6)	85.3 (8.5)	79.8 (10.5)	12.6	1.5	3.9
Hexythiazox	0.9803	74.5 (16.4)	70.8 (10.2)	70.4 (14.5)	19.2	2.6	4.8
Fenazaquin	0.9940	77.3 (14.3)	76.8 (18.9)	79.8 (6.0)	4.7	1.7	4.3

[a] R.S.D. values of repeatability are given in brackets ($n = 5$).
[b] R.S.D. values obtained at 25 $\mu g\,L^{-1}$ ($n = 7$).

multifruit juice matrix can be used as representative matrix in routine analysis.

3.4. Validation study

Performance characteristics of the optimized method were established by a validation procedure with spiked blank multifruit juice (as representative matrix), studying linearity, selectivity, accuracy (expressed as recovery), repeatability, interday precision, LODs and LOQs.

First, the identification of the selected compounds was based on the retention time windows (RTWs), defined as the mean retention time ± three standard deviations of the retention time of ten blank samples spiked at 50 $\mu g\,L^{-1}$ for each compound (Table 1). Then, confirmation was performed by acquisition of two MS/MS transitions and comparing the intensity ratios of both of them (quantitation and confirmation). Confirmation was considered reliable if the ratio was within the criteria laid down in the European Commission Decision 2002/657/EC [40]. Besides it also establishes the concept of identification points (IPs). For low resolution mass spectrometry such as QqQ–MS, this document sets a minimum of 3 IPs for the confirmation of pesticides, which was fulfilled in this work monitoring two product ions.

Selectivity was evaluated extracting and analyzing blank fruit juices. The absence of any signal at the same elution time as the target pesticides indicated that no matrix or chemical compounds are extracted and give a false positive signal.

Calibration was performed by the use of matrix-matched calibration standards prepared as described in Section 2. Peak area was used as response and good linearity was obtained for all pesticides at concentrations within the tested interval (from 5 to 100 $\mu g\,L^{-1}$), with determination coefficient higher than 0.98 (Table 5).

Accuracy was evaluated through recovery studies, spiking blank samples at three fortification levels: 10, 50 and 100 $\mu g\,L^{-1}$, processing five samples in each experiment. Recoveries ranged from 70.8 to 108.5 at 10 $\mu g\,L^{-1}$, from 70.8 to 103.7 at 50 $\mu g\,L^{-1}$ and from 70.4 to 90.7 at 100 $\mu g\,L^{-1}$ (Table 5). These results indicate that good recoveries from juice samples were obtained throughout the proposed method.

Precision was studied by performing repeatability and interday precision studies, expressed as R.S.D. It can be observed (Table 5) that repeatability was lower than 20% for the three level assayed. Interday precision was evaluated by running one batch of blank samples spiked at 25 $\mu g\,L^{-1}$ on 7 days. R.S.D.s lower than 20% were obtained for all the compounds analyzed except for nicosulfuron. For this compound a value slightly higher than 20% was obtained (20.5%). In short, interday precision of the method was below 10% for 68 of the 90 analyzed compounds, and they were in the range 10–20% for the other compounds, indicating the good precision of the developed method.

Finally LODs and LOQs were evaluated, showing in Table 5 the obtained values. Good results were obtained, with LOD and LOQ values lower than 0.7 and 5.0 $\mu g\,L^{-1}$, respectively. It should be stressed that the MRLs fixed by the European legislation are referred to fruits and not to derivate products such as juices; however it is worth noting that LOQ levels are equal or below the MRLs even considering the dilution factor.

3.5. Sample analysis

The validated analytical methodology was applied to analyze 30 samples of fruit juices (orange, apple, pineapple, peach and multifruit) obtained from local supermarkets. Internal quality control was applied in every batch of samples in order to check if the system is under control. This quality control implies a matrix-matched calibration, a reagent blank, a matrix blank and a spiked blank sample at 10 $\mu g\,L^{-1}$ in order to evaluate stability of the proposed method with time.

Table 6 summarizes the pesticide levels found in the fruit juices analyzed. The pesticides found in the commercial juices were only carbendazime, thiabendazol and cyprodinil, although traces of thiamethoxam were found in a pineapple juice. It must be indicated that benzimidazole fungicides, such as carbendazim and thiabendazole are widely used for the pre- or post-harvest treatment for

Table 6
Detected pesticides in analyzed samples

Type of juice	Concentration range ($\mu g\,L^{-1}$) of pesticide		
	Carbendazim	Thiabendazol	Cyprodinil
Peach juice	6.0–26.5		Traces-5.1
Pineapple juice			
Orange juice		9.2–24.9	Traces
Apple juice			Traces
Multifruit juice	33.6		

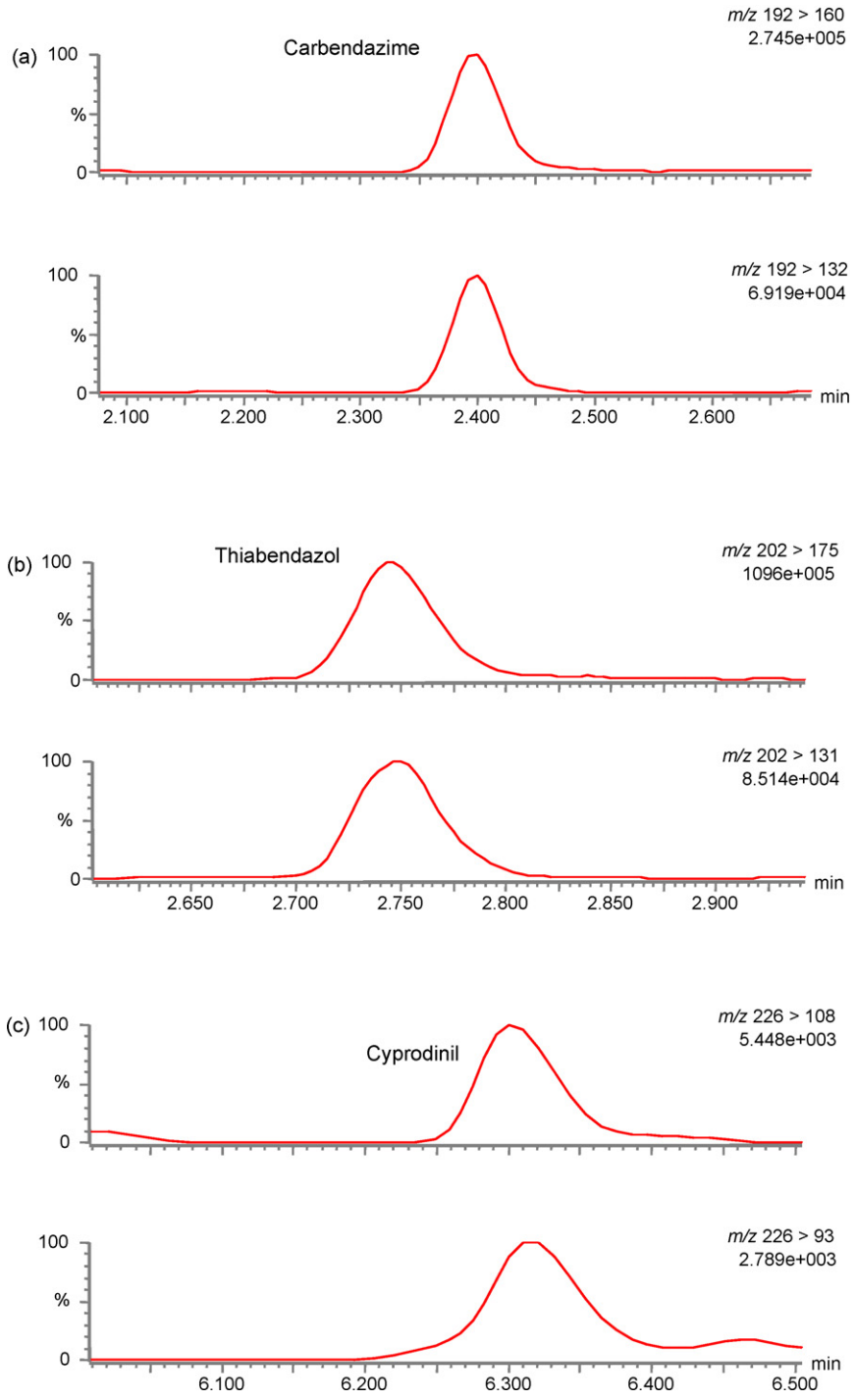

Fig. 3. UPLC–MS/MS chromatograms for: (a) multifruit juice containing carbendazim at 33.6 μg L^{-1}; (b) orange fruit containing thiabendazol (9.6 μg L^{-1}) and (c) peach juice containing cyprodinil at 5.1 μg L^{-1}. Quantification and confirmation transitions were shown for the 3 positive samples.

the control of a wide range of fruit and vegetable pathogens, so they can persist over the season and appear in processed products for human consumption such as fruit juices. In this sense, carbendazime was detected in 4 samples, 3 peach and 1 multifruit juices which also contains peach. On the other hand, thiabendazole, which is usually used as a fungicide on citrus fruit to protect it from decay, was found in two orange juices. Finally, cyprodinil was detected at low concentrations in peach, orange and apple juices.

It can be emphasized that pesticides were detected in 26% of the samples analyzed, although were lower than the MRL established by the EU for the raw fruits of the pesticides analyzed. As an example, Fig. 3 shows a positive result of carbendazim in a multifruit juice sample, thiabendazol in an orange juice, and cyprodinil in a peach juice sample.

4. Conclusions

A new multiresidue method was developed and validated for rapid and simultaneous determination of more than 90 pesticides in fruit juices by UPLC–MS/MS, using QuEChERS methodology as

the proposed extraction method. The developed method combines the selectivity, high resolution capacity and fast analysis of UPLC–MS/MS with the advantages of QuEChERS (easy to use, fast and cheap), providing a simple, rapid and reliable analysis of pesticides in fruit juices, which requires a low volume consumption of organic solvents. Basically, analysis time (less than 22 min), including sample preparation and determination is shorter compared to traditional methods, so high sample throughput can, therefore, be achieved, which is useful in monitoring food programs, in which a large number of samples is normally analyzed.

Acknowledgments

The authors gratefully acknowledge Spanish Ministry of Education and Science (MEC-FEDER) (Project Ref. AGL2006-12127-C02-01) for financial support. RRG is also grateful for personal funding through the Juan de la Cierva program (Spanish Ministry of Education and Science).

References

[1] A. Sannino, Rapid Commun. Mass Spectrom. 21 (2007) 2079.
[2] J.H. Wang, Y.B. Zhang, X.L. Whang, J. Sep. Sci. 29 (2006) 2330.
[3] N. Kolbe, J.T. Andersson, J. Agric. Food Chem. 54 (2006) 5736.
[4] E. Orejuela, M. Silva, J. Chromatogr. A 1007 (2003) 197.
[5] S. Topuz, G. Özhan, B. Alpertunga, Food Control 16 (2005) 87.
[6] Y. Picó, C. Kozmutza, Anal. Bioanal. Chem. 389 (2007) 1805.
[7] S. Cortés-Aguado, N. Sánchez-Morito, F.J. Arrebola, A. Garrido Frenich, J.L. Martínez Vidal, Food Control 107 (2008) 1314.
[8] G. Sagratini, J. Mañes, D. Giardiná, P. Damiani, Y. Picó, J. Chromatogr. A 1147 (2007) 135.
[9] C.G. Zambonin, M. Quinto, N. De Vietro, F. Palmisano, Food Chem. 86 (2004) 269.
[10] D.A. Lambropoulou, T.A. Albanis, J. Agric. Food Chem. 50 (2002) 3359.
[11] X.G. Chu, X.Z. Hu, H.Y. Yao, J. Chromatogr. A 1063 (2005) 201.
[12] B. Albero, C. Sánchez-Brunete, A. Donoso, J.L. Tadeo, J. Chromatogr. A 1043 (2004) 127.
[13] B. Albero, C. Sánchez-Brunete, J.L. Tadeo, J. Agric. Food Chem. 51 (2003) 6915.
[14] E. Zhao, L. Han, S. Jiang, Q. Wang, Z. Zhou, J. Chromatogr. A 1114 (2006) 269.
[15] Q. Xiao, B. Hu, C. Yu, L. Xia, Z. Jiang, Talanta 69 (2006) 848.
[16] M.V. Khrolenko, P.P. Wieczorek, J. Chromatogr. A 1093 (2005) 111.
[17] V. Gomes Zuin, M. Schellin, L. Montero, J.H. Yariwake, F. Augusto, P. Popp, J. Chromatogr. A 1114 (2006) 180.
[18] T. Goto, Y. Ito, H. Oka, I. Saito, H. Matsumoto, H. Sugiyama, C. Ohkubo, H. Nakazawa, H. Nagase, Anal. Chim. Acta 531 (2005) 79.
[19] S.J. Lehotay, J. AOAC Int. 90 (2007) 485.
[20] S.J. Lehotay, K. Mastovska, A.R. Lightfield, J. AOAC Int. 88 (2005) 615.
[21] M. Anasstassiades, S.J. Lehotay, J. AOAC Int. 86 (2003) 412.
[22] CENT/TC 275, N236, Draft, Food of plant origin, Determination of pesticide residues using GC–MS and LC–MS/(MS) following acetonitrile extraction/partitioning and clean-up by dispersive SPE, QuEChERS method, European Committee for Standardisation (2006).
[23] A. Hercegová, M. Dömötörová, E. Matisová, J. Chromatogr. A 1153 (2007) 54.
[24] A. Hercegová, M. Dömötörová, D. Kruzlicová, E. Matisová, J. Sep. Sci. 29 (2006) 1102.
[25] S.C. Cunha, S.J. Lehotay, K. Mastovaska, J.O. Fernándes, M.B.P.P. Oliveira, J. Sep. Sci. 30 (2007) 620.
[26] A.A. Barakat, H.M.A. Badawy, E. Salama, E. Attallah, G. Maatook, J. Food, Agr. Environ. 5 (2007) 97.
[27] F. Hernández, T. Portolés, E. Pitarch, F.J. López, J. Beltrán, C. Vázquez, Anal. Chem. 77 (2005) 7662.
[28] K. Yu, D. Little, R. Plumb, B. Smith, Rapid Commun. Mass Spectrom. 20 (2006) 544.
[29] T. Kovalczuk, M. Jech, J. Poustka, J. Hajslová, Anal. Chim. Acta 57 (2006) 8.
[30] K.A. Johnson, R. Plumb, J. Pharm. Biomed. Anal. 39 (2005) 805.
[31] A. Garrido Frenich, J.L. Martínez Vidal, E. Pastor Montoro, R. Romero González, Anal. Bioanal. Chem. 390 (2008) 947.
[32] C.C. Leandro, P. Hancock, R.J. Fussell, B.J. Keely, J. Chromatogr. A 1144 (2007) 161.
[33] C.C. Leandro, P. Hancock, R.J. Fussell, B.J. Keely, J. Chromatogr. A 1103 (2006) 94.
[34] E. Pastor Montoro, R. Romero González, A. Garrido Frenich, M.E. Hernández Torres, J.L. Martínez Vidal, Rapid Commun. Mass Spectrom. 21 (2007) 3585.
[35] M. Mezcua, A. Agüera, J.L. Lliberia, M.A. Cortés, B. Bagó, A.R. Fernández-Alba, J. Chromatogr. A 1109 (2006) 222.
[36] L.A. Currie, Anal. Chim. Acta 391 (1999) 127.
[37] Quality control procedures for pesticide residue analysis, European Commission, Directorate General Health and Consumer Protection, Document No SANCO/10232/2006, March 2006.
[38] S. Grimalt, J.V. Sancho, O.J. Pozo, J.M. García-Baudin, M.L. Fernández-Cruz, F. Hernández, J. Agric. Food Chem. 54 (2006) 1188.
[39] A. Garcia-Campaña, L. Cuadros-Rodriguez, J. Aybar-Muñoz, F. Ales-Barrero, J. AOAC Int. 80 (1997) 657.
[40] Commission Decision 2002/657/EC of 12 August 2002 implementing Council Directive 96/23/EC concerning the performance of analytical methods and the interpretation of results, Official Journal of the European Union, L 221, 17 August 2002.

Talanta 76 (2008) 166–171

Contents lists available at ScienceDirect

Talanta

journal homepage: www.elsevier.com/locate/talanta

Flow injection spectrofluorimetric determination of carvedilol mediated by micelles

Raúl A. Silva[a], Chien Chun Wang[d], Liliana P. Fernández[b,d], Adriana N. Masi[c,d,*]

[a] Área de Farmacotecnia, Facultad de Química, Bioquímica y Farmacia, Universidad Nacional de San Luis, 5700 San Luis, Argentina
[b] Área de Química Analítica, Facultad de Química, Bioquímica y Farmacia, Universidad Nacional de San Luis, 5700 San Luis, Argentina
[c] Área de Bromatología-Ensayo y Valoración de Medicamentos, Facultad de Química, Bioquímica y Farmacia, Universidad Nacional de San Luis, 5700 San Luis, Argentina
[d] CONICET, Chacabuco y Pedernera, 5700 San Luis, Argentina

ARTICLE INFO

Article history:
Received 28 December 2007
Received in revised form 15 February 2008
Accepted 18 February 2008
Available online 29 February 2008

Keywords:
Carvedilol determination
Flow injection spectrofluorimetry
Micellar enhancement
Pharmaceuticals

ABSTRACT

A novel flow injection (FI)-spectrofluorimetric methodology for the determination of carvedilol in micro-heterogeneous medium has been developed. In the sodium dodecyl sulfate (SDS) surfactant medium, an additional fluorescence enhancement was produced by the electrolyte NaCl. A total enhancement of 3.1-fold in the native fluorescent response was achieved respect to aqueous medium. Using an excitation and emission wavelength of 286 and 341 nm, respectively, a good linear relationship was obtained in the range of 9×10^{-8} to 1×10^{-6} mol L^{-1} with a detection limit of 3.63×10^{-9} mol L^{-1} ($S/N = 3$). This method was applied to determine carvedilol in commercial pharmaceutical formulations. Good concordance was found between the nominal (6.25, 12.5 and 25.0 mg) and experimental values. The new methodology developed showed high selectivity respect to the common excipients used in pharmaceuticals. The sampling rate was 30 samples h^{-1}. From the fluorescent properties, binding constant for carvedilol–SDS determined was 3.2×10^{2} L mol^{-1}.

1. Introduction

Carvedilol (1-(9H-carbazol-4-yloxy)-3-[2-(2-methoxyphenoxy)ethylamino]propan-2-ol, Fig. 1) is a nonselective β-adrenergic blocking agent with α_1-blocking activity, indicated for the treatment of hypertension and mild or moderate heart failure of ischemic or cardiomyopathic origin. Relative to other beta blockers, carvedilol has minimal inverse agonist activity; the use of carvedilol has been shown to provide additional morbidity and mortality benefits in congestive heart failure [1].

Since its use for pharmaceutical purposes is relatively recent, literature reveals that methods available for carvedilol determination are scarce. Different analytical techniques have been employed for the determination of carvedilol in biological fluids [2,3], specially those applied to the analysis of plasma [4–8] and urine [9] should be highlighted. Some chemists have developed methods for determining carvedilol by HPLC with high sensitivity, but the procedures for sample preparing were tedious and time consuming [2–8,10–12], with poor reproducibility and recovery. Also spectrophotometric methods have been reported [13,14], but in these cases sensitivities obtained were low. A differential pulse voltammetric procedure using a glassy carbon electrode was developed for the analysis of tablets [15]. However, this method presented various limitations, including time-consuming sample clean-up and laborious extraction steps, low sensitivity and long run times, being then less suitable for routine analysis.

Some luminescent methods have been proposed for the determination of carvedilol in pharmaceutical drugs and biological samples [16–18], using chemioluminometry and sinchronofluorescence. Table 1 resumes the main characteristics of the reported methodologies for carvedilol determination.

For routine laboratory quality control of final products, for research tasks and/or for rapid screening of biological samples, development of fast, simple, reliable, rugged and automatized analytical procedures are required. High quality chemical data collected at run-time are essential for the control of modern chemical manufacturing facilities.

It is widely known the ability of organized media to provide an appropriate microenvironment able to modify the catalytic and luminescence properties of reactants and products [19]; the effect of organized media over the carvedilol has not yet been broadly studied.

This paper reports a rapid spectrofluorimetric method for determining the content of carvedilol in pharmaceuticals. Effects of pH,

* Corresponding author at: Área de Bromatología-Ensayo y Valoración de Medicamentos, Facultad de Química, Bioquímica y Farmacia, Universidad Nacional de San Luis, 5700 San Luis, Argentina. Tel.: +54 2652425385; fax: +54 2652430224.
E-mail address: amasi@unsl.edu.ar (A.N. Masi).

0039-9140/$ – see front matter © 2008 Elsevier B.V. All rights reserved.
doi:10.1016/j.talanta.2008.02.029

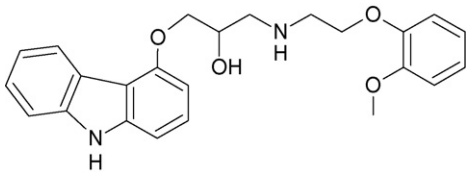

Fig. 1. Chemical structure of carvedilol.

presence of different surfactant agents and ionic strength on the relative fluorescent intensity and fluorescent spectrum of carvedilol were examined. The method has a wide linear range and low detection limit. It was successfully applied for determining carvedilol in tablets without interferences from pharmaceuticals excipients. In addition, sample preparation is easy, fast and without prior separation steps.

2. Experimental

2.1. Instruments

A Shimadzu RF-5301PC spectrofluorimeter (Shimadzu Corporation, Analytical Instrument Division, Kyoto Japan), equipped with a Xenon discharge lamp and 1 cm quartz cells was used for the fluorescence measurements. For flow measurements a LC flow cell unit (12 μL cell) was used.

A pH meter (Orion Expandable Ion Analyzer, Orion Research, Cambridge, MA, USA), model EA 940 with combined glass electrode was used for monitoring pH adjustment.

2.2. Reagents

Carvedilol was kindly provided by Gador S.A. (Buenos Aires, Argentina). Chemicals of analytical grade were used: sodium dodecyl sulfate (SDS), Triton® X-100 and hexadecyl trimethylammonium bromide (HTAB) were purchased from Tokyo Kasei Industries. Chuo-Ku, Tokyo, Japan. High-purity water was obtained from a Millipore (Milford, MA, USA) Milli-Q Plus System.

The pH values in optimization stage were adjusted by the addition of solutions of NaOH 0.01 mol L^{-1}, NaOH (c), HCl 0.01 mol L^{-1} or HCl (c) until the target pH value was reached.

2.2.1. Solutions

Carvedilol standard solution containing 1 mg mL^{-1} was prepared dissolving the reagent in ethanol. During the experiments, this solution was found to be stable for several weeks when was kept in dark at 5 °C. Standard working solution of 1 μg mL^{-1} was prepared daily by dilution of stock standard solution with ultra pure water and stored in a dark bottle at 5 °C. In these conditions, carvedilol was stable for almost 4 weeks.

A 0.1 mol L^{-1} SDS, was prepared with an adequate weight of SDS and dissolving in ultra pure water. A 2 mol L^{-1} NaCl solution was prepared dissolving an adequate weight of the salt in ultra pure water. A 0.1 mol L^{-1} HCl solution was prepared mixing an adequate volume of concentrated acid with ultra pure water.

2.2.2. Sample solutions

Ten tablets containing 6.25 mg carvedilol each were weighed and finely powdered. A portion of the powder, equivalent to 6.25 mg of carvedilol, was weighed and treated with 10 mL of ethanol, shaken for 15 min, centrifuged during 10 min. The supernatant was separated and the residue was treated with another portion of 10 mL ethanol. The two portions were then joined and filtrated through Millipore membranes of 0.45 μm pore size. Two hundred milliliters of the filtered solution were transferred to a 100 mL volumetric flask and taken to volume with ultra pure water. The same procedure was applied with tablets containing 12.5 and 25 mg carvedilol. The final concentrations were 0.625, 1.25 and 2.5 μg mL^{-1}, respectively.

2.3. FIA configuration

In Fig. 2, a schematic representation of the FIA system used for the on line spectrofluorimetric determination of carvedilol is shown. The manifold used was built using a four-channel Gilson Minipuls-3 peristaltic pumps fitted with rate selectors; a Rheodyne Model 5041 injection valve, acting as selecting valve, and PVC tubing of 0.8 mm i.d.

Under the conditions described in Table 1, a stream of SDS/NaCl (position 3 in Fig. 2), was mixed in reaction coil (R) with a stream of water (position 4) as reagent blank for producing the baseline. After changing the valve position a stream of carvedilol/HCl (position 1) was mixed in reaction coil (R) with a stream of SDS/NaCl and impelled then through the spectrofluorimeter for measurement.

2.4. General procedure

A stream of sample or standards solutions containing carvedilol at pH 2 was combined with the carrier stream. The carrier stream consisted of a solution prepared with SDS (0.04 mol L^{-1}) and sodium chloride (0.4 mol L^{-1}) to obtain the optimal conditions for carvedilol fluorescent emission. The drug contained in the sample/standards and the carrier stream interacted in reactor (R) and flowed to the fluorescence detector. The valve was switched in such manner that allowed, in one position, to pass the carrier stream and ultra pure water, and in the second position allowed to pass the sample/standards and carrier solution. In this way the fiagram had always the same background produced by the same concentration of carrier solution.

2.5. Method validation procedure

In order to demonstrate the validity of this method 10 tablets containing 6.25 mg carvedilol each, were weighed and finely powder. The powder was divided into 10 equal portions. The proposed method was applied to six portions and the average quantity of carvedilol obtained was taken as a base value. Then, increasing quantities of carvedilol were added to the other five aliquots of sample and carvedilol was determined applying the same method.

3. Results and discussion

3.1. Spectral characteristics of carvedilol

3.1.1. Fluorescence characteristics of carvedilol in aqueous media

Fig. 3 shows the excitation and emission spectra obtained for a 1 μg mL^{-1} aqueous solution of carvedilol at pH 2. As can be seen, the drug showed a maximum emission at 341 nm when was excited at 286 nm. These wavelengths were selected for the following assays to measure the fluorescence intensity.

Carvedilol showed a strong native fluorescence signal at acid or extremely alkaline pHs, but showed a decrease in fluorescent emission at intermediate pHs. Fig. 4 resumes the effect of pH value in the fluorescence signal. Analysis of spectrofluorimetric data for carvedilol in water shows that the intensity increase at pH 2–3 decrease between 4 and 8, and increase again at pH 10–11. The working pH selected was 2 due to the higher intensity obtained and the additional advantage of preparing systems without adding buffer solutions. Thus, an HCl 0.01 mol L^{-1} medium was chosen for future studies.

Table 1
Comparative table for carvedilol determination

Instrumental methodology	Experimental detail	LOD	LOQ	LOL	Samples	Ref.
HPLC-fluorimetry	SPE. Column: Spherisorb C_6. Mobile phase: 65% ACN, 35% potassium acetate buffer (0.25 M, pH 4)	WD	0.40 ng mL^{-1}	242 ng mL^{-1}	Human plasma	[2]
HPLC-fluorimetry	Ether extraction	WD	WD	WD	Serum	[3]
HPLC-fluorimetry	Monolithic column. Isocratic mobile phase: 0.01 M disodium hydrogen phosphate buffer–ACN (40:60, v/v) pH 3.5	WD	1 ng mL^{-1}	80 ng mL^{-1}	Human plasma	[4]
HILIC–MS/MS	Extraction methyl *tert*-butyl ether, basic pH. Mobile phase: ACN–ammonium form-ate (50 mM, pH 4.5) (90:10, v/v)	WD	0.1 ng mL^{-1}	200 ng mL^{-1}	Human plasma	[5]
HPLC	Brownlee C8 column, isocratic elution, on-line deproteination	WD	0.8 ng mL^{-1}	WD	Human plasma	[6]
HPLC-fluorimetry	Protein precipitation with methanol. Column: Develosil 3 μm ODS 100 × 4.6 mm i.d. Mobile phase: ACN–30 mM potassium dihydrogen-phosphate buffer, pH 2	1.3 ng mL^{-1}	WD	WD	Human plasma	[7]
HPLC-ECD	Mobile phase: 53% (v/v) methanol, 47% (v/v) phosphate buffer (pH 3.8)	WD	0.10 ng mL^{-1}	WD	Human plasma	[8]
LC-MS	ESI. Liquid–liquid extraction with ethyl acetate	–	WD	WD	Human urine	[9]
HPLC-fluorimetry	SPE: reversed-phase octadecyl silica column	3.6 ng mL^{-1}	WD	1000 ng mL^{-1}.	Rat plasma	[10]
HPLC	Extracted with acetone. Internal Standard: naftopidil. pH 3.5. Samples clean-up: SPE columns	WD	0.01 ng mg^{-1}	0.35 ng mg^{-1} (wet weight)	Human Cardiac Tissue	[11]
HPLC–MS/MS	Internal standard (IS): metoprolol. LLE: die-thylether	WD	0.1 ng mL^{-1}	200 ng mL^{-1}	Human plasma	[12]
Spectrophotometry	Apparent molar absorptivity 15.4×10^3 L mol^{-1} cm^{-1}. λ = 285 nm. Solvent: methanol	WD	4 μg mL^{-1}	36 μg mL^{-1}	Bulk and formulations	[13]
Spectrophotometry	λ = 244 nm. Solvent: ethanol	WD	2 μg mL^{-1}	7 μg mL^{-1}	Tablets and compounded capsules	[14]
Nonaqueous volumetry	Medium: 0.01 M perchloric acid. Indicator: 1% violet crystal					
Differential pulse voltammetry	pH: 2.0–11.0 (glassy carbon electrode)	0.10 μg mL^{-1}	0.25 μg mL^{-1}	10.00 μg mL^{-1}	Tablets dosage form	[15]
Fluorimetry	λ_{em} = 356 nm, λ_{ex} = 254 nm	0.19 ng mL^{-1}	0.50 ng mL^{-1}	270 ng mL^{-1}	Tablets	[16]
Synchronous fluorimetry	λ_{em} = 356 nm, λ_{ex} = 254 nm, Δλ = 80 nm. Sensing reagent: isopropanol	1 ng mL^{-1}	0.005 μg mL^{-1}	0.1 μg mL^{-1}	Medicine dosage	[17]
Chemiluminometry	Reaction: oxidation of luminol by hypochlorite. Multi-pumping flow system multiple solenoid actuated μ-pumps	8.7×10^{-9} mol L^{-1}	1.2×10^{-7} mol L^{-1}	3.0×10^{-6} mol L^{-1}	Pharmaceuticals	[18]
FI-fluorimetry	λ_{em} = 341 nm, λ_{ex} = 286 nm. pH 2.0. Ionic strength: 0.1 mol L^{-1} SDS: 1.10^{-2} mol L^{-1}. Flow rate: 35 rpm. $K_B = 3.2 \times 10^2$ L mol^{-1}. Sampling rate: 30 samples h^{-1}	3.63×10^{-9} mol L^{-1}	9×10^{-8} mol L^{-1}	1×10^{-6} mol L^{-1}	Pharmaceuticals	This method

HILIC–MS/MS: hydrophilic interaction liquid chromatography with tandem mass spectrometry. WD: without datum. ACN: acetonitrile. ESI: electrospray ionization. SPE: solid phase extraction. LLE: liquid–liquid extraction.

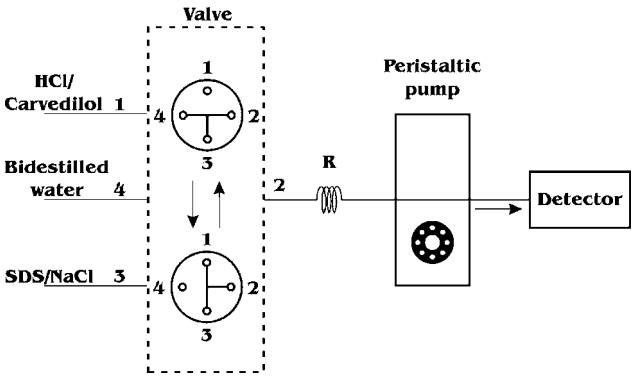

Fig. 2. FIA configuration.

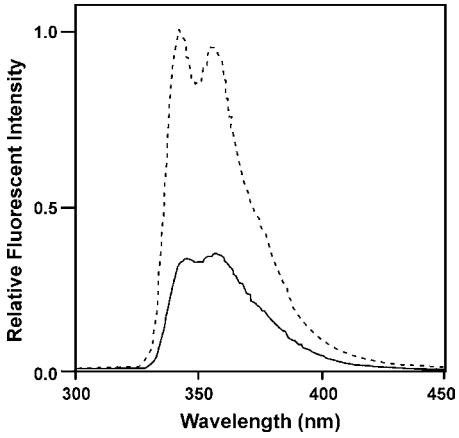

Fig. 3. Emission spectrum of carvedilol at pH 2 (λ_{exc} = 286 nm). (—) Carvedilol 0.1 μg mL^{-1}; (- - -) carvedilol 0.1 μg mL^{-1}, NaCl 0.1 mol L^{-1} and SDS 0.01 mol L^{-1}.

3.1.2. Fluorescence characteristics of carvedilol in micellar media

3.1.2.1. Nature and concentration of surfactant agent. In order to perform the luminescent emission, the fluorescence properties of carvedilol in various surfactant media were studied: anionic surfactant (SDS, 0–9 × 10^{-3} mol L^{-1}), cationic surfactant (CTAB, 0–5 × 10^{-2} mol L^{-1}) and non-ionic surfactant (TX-100, 0–1 × 10^{-3} mol L^{-1}). Experimental data showed that the enhancement factor for carvedilol–SDS system (2.5-fold respect to carvedilol fluorescence in water medium) was higher than carvedilol–CTAB; for TX-100, an important spectrum interference was observed; thus, the anionic surfactant SDS was chosen for further work.

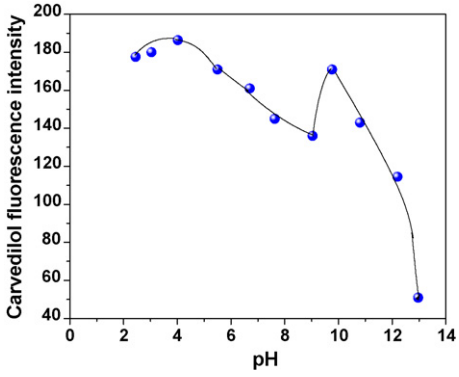

Fig. 4. Effect of pH on cavedilol fluorescence intensity.

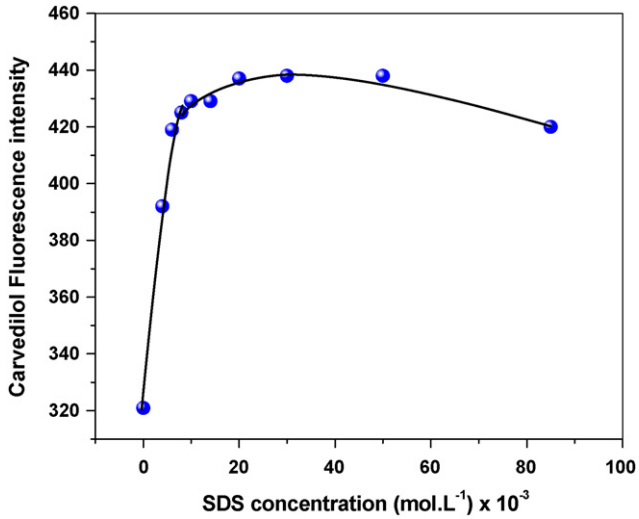

Fig. 5. Effect of surfactant concentration on carvedilol fluorescence intensity.

The fluorescence spectrum of carvedilol in ultra pure water and aqueous SDS revealed that the fluorescence intensity increased, above the cmc, with SDS concentration, and that this increase was more evident at 10 mmol L^{-1} (Fig. 5). The fluorescence increase in micellar media was attributed to a stabilization/protection of the excited state singlet, that hinders decay by quenching and other non-radiative deactivation processes [20,21].

3.1.2.2. Binding constant for the SDS–carvedilol system. The binding constant value (K_B) was obtained from fluorescence data of carvedilol as a function of SDS surfactant concentration using Eq. (1) [22,23]:

$$\frac{I_\alpha - I_0}{I_S - I_0} = 1 + \frac{1}{K_B[M]} \quad (1)$$

where I_α is the emission intensity at infinite micellar concentration; I_0 the emission intensity without micelles; I_S the emission intensity at intermedia micellar concentration; K_B the binding constant; [M] the micellar concentration in mol L^{-1}.

The concentration of the micelles [M] can be determined using the relation below [24]:

$$[M] = \frac{[\text{surfactant}] - \text{CMC}}{N_{av}} \quad (2)$$

where [surfactant] = total surfactant concentration; N_{av} = aggregation number. N_{av} is ca. 62 [25].

According to this model, the solubilization process is considered as an addition reaction of solute molecules (S) in the micellar aggregations (M), giving MS_i adducts (a micelle containing i molecules of solute). From the slope of the plot of $(I_\alpha - I_0)/(I_S - I_0)$ versus inverse micellar concentration, the binding constant K_B was determined, giving a value of 3.2 × 10^2 L mol^{-1}.

3.1.3. Effects of electrolytes on the fluorescence intensity of carvedilol

In aqueous surfactant media, the role of NaCl is to push the organic compounds inside the micelle. In this work it was found that in the presence of 0.1 mol L^{-1} NaCl, the fluorescence signal of carvedilol in surfactant media increased almost 3.1-fold respect to the same in absence of salt. The effect produced by the addition of inert salts to the system is shown in Fig. 6. The working concentration chosen was 0.1 mol L^{-1}.

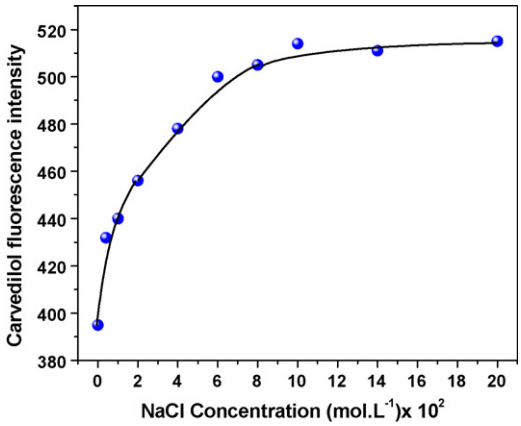

Fig. 6. Effect of ionic strength on carvedilol fluorescence intensity. SDS concentration 0.01 mol L^{-1}.

3.2. Effect of flow rate

The effect of flow rate of FIA system on fluorescent signal was studied. Although the fluorescent signal was highest for 45 rpm, from 40 rpm a great turbulence was observed due to the introduction of bubbles into the flow system, the flow selected was 35 rpm. Under these optimal conditions the sampling rate was 30 samples h^{-1}.

3.3. Validation method

3.3.1. Linearity and sensitivity

Calibration curve was constructed covering a concentration range from 9×10^{-8} to 2×10^{-6} mol L^{-1}. Fig. 7 shows the fiagram obtained with different standards of carvedilol. The triplicate signals demonstrated good reproducibility. Equation for calibration graph was obtained by least-square linear regression analysis of the areas of analyte standard fluorescent signals versus analyte concentrations: $F = 2030x + 100.7C$. Where F is the relative fluorescence intensity and C the concentration of carvedilol. The method was linear up to 1×10^{-6} mol L^{-1} of carvedilol. Correlation coefficient was 0.9998. The LOD was defined as the compound concentration that produced a signal-to-noise ratio greater than three, while the limit of quantitation of the assay was evaluated as the concentration equal to 10 times the value of the signal to-noise ratio. LOD and LOQ values for this method based upon these criteria are shown in Table 1.

3.3.2. Precision and accuracy

The precision of the method based on repeatability was performed, by replicating injections ($n = 6$) of four standard solutions prepared by the standard addition method covering different concentration levels. Accuracy was determined and expressed by percentual relative error which was always under 1.5%.

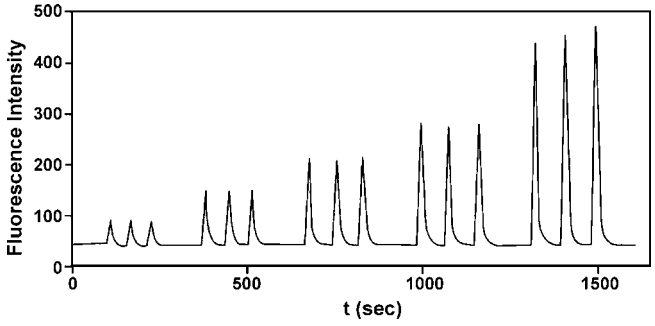

Fig. 7. Carvedilol fiagram for calibration curve.

Table 2
Validation of the method for the determination of carvedilol in commercial pharmaceutical formulae

Sample ($n = 6$)	Base value (mg)	Added (mg)	Found (mg)	E%
A	6.29	1	7.40	1.50
B	6.29	2	8.22	0.84
C	6.29	3	9.18	1.10
D	6.29	4	10.31	0.19

Table 3
Analysis of carvedilol tablets

Sample[a]	Nominal quantity (mg)	Carvedilol found (mg)	E%
1	6.25	6.29	0.64
2	12.50	12.40	0.80
3	25.00	25.30	1.20

[a] Rotiaz from Richmond Lab. ($n = 6$).

The optimum working conditions for the on line fluorimetric determination of carvedilol are resumed in Table 1. The validation method results are shown in Table 2.

3.3.3. Analysis of pharmaceuticals

The developed method was applied to the determination of carvedilol in commercial pharmaceutical samples containing 6.25, 12.5 and 25 mg of carvedilol, respectively. The results are shown in Table 3.

4. Conclusions

The FIA spectrofluorimetric method proposed for the determination of carvedilol in pharmaceuticals samples has the advantages of simplicity, speed, accuracy and the use of inexpensive equipment and reagents. The fluorescent detection gives a special selectivity without interference from the common excipients found in commercial pharmaceutical forms. The use of SDS micellar system provides a simple means to enhance the fluorescence of carvedilol. This phenomenon can be explained by the protection of lowest excited state of fluorophore in micellar microenvironment from non-radiative processes that normally readily occur in bulk aqueous solutions. The association constant for carvedilol–SDS system was determined using the adduct model. The addition of SDS/NaCl gives a 3.1-fold increase in sensitivity and improves the limit of detection without further sample manipulation. Additionally, it can be remarked the wide range linearity obtained in the calibration curve, with high sensitivity and high sampling rate results adequate for the quality control and routine analysis of tablets.

Acknowledgments

The authors wish to thank CONICET (Consejo Nacional de Investigaciones Científicas y Tecnológicas), FONCYT (Fondo Nacional de Ciencia y Tecnología), National University of San Luis (Project 22/Q528) for the financial support.

References

[1] M. Packer, M.B. Fowler, E.B. Roecker, Circulation 106 (2002) 2194.
[2] F. Behn, S. Läer, T.S. Mir, H. Scholz, Chromatographia 53 (2001) 641.
[3] F. Varin, L.X. Cubeddu, J.R. Powell, J. Pharm. Sci. 75 (1986) 1195.
[4] A. Zarghi, S.M. Foroutan, A. Shafaati, A. Khoddam, J. Pharm. Biomed. Anal. 44 (2007) 250.
[5] D.W. Jeong, Y.H. Kim, H.Y. Ji, Y.S. Youn, K.C. Lee, H.S. Lee, J. Pharm. Biomed. Anal. 44 (2007) 547.

[6] G. Lamprecht, K. Stoschitzky, Chromatographia 59 (2004) 551.
[7] P. Ptacek, J. Macek, L. Klima, J. Chromatogr. B 789 (2003) 405.
[8] M. Machida, M. Watanabe, S. Takechi, S. Kakinoki, A. Nomura, J. Chromatogr. B. 798 (2003) 187.
[9] K. Deventer, P. Van Eenoo, F.T. Delbeke, Rapid Comm. Mass Spectrom. 19 (2005) 90.
[10] N. Hokama, N. Hobara, H. Kameya, S. Ohshiro, M. Sakanashi, J. Chromatogr. B: Biomed. Sci. Appl. 732 (1999) 233.
[11] F. Behn, S. Läer, H. Scholz, J. Chromatogr. Sci. 30 (2001) 121.
[12] N.C do C. Borges, G. Duarte Mendes, D. de Oliveira Silva, V. Marcondes Rezende, R. Barrientos-Astigarraga, G. De Nucci, J. Chromatogr. B 822 (2005) 253.
[13] P.S. Jain, G.S. Talele, S.G. Talele, S.J. Surana, Indian J. Pharm. Sci. 67 (2005) 358.
[14] C. Viana Silva Ieggli, S. Gonçalves Cardoso, L. Potrich Belle, J. AOAC Int. 88 (2005) 1299.
[15] A. Radi, T. Elmogy, Il Farmaco 60 (2005) 43.
[16] L.X. Xu, N. Hui, L.Y. Ma, H.Y. Wang, Spectrochim. Acta A: Mol. Biomol. Spectrosc. 61 (2005) 855.
[17] Y. Xiao, H.Y. Wang, J. Han, Spectrochim. Acta A: Mol. Biomol. Spectrosc. 61 (2005) 567.
[18] C.K. Pires, K.L. Marques, J.L.M. Santos, R.A.S. Lapa, J.L.F.C. Lima, E.A.G. Zagatto, Talanta 68 (2005) 239.
[19] W.L. Hinze, K.L. In:, Mittal (Eds.), Use of Surfactant and Micellar Systems in Analytical Chemistry in Solution Chemistry Surfactants, vol. 1, Plenum Press, New York, 1979, p. 79.
[20] C.D. Tran, T.A. Van Fleet, Anal. Chem. 60 (1988) 2478.
[21] H. Singh, W.L. Hinze, Anal. Lett. 15 (1982) 221.
[22] S. De, A. Girigoswami, S. Mandal, Spectrochim. Acta Part A 58 (2002) 2547.
[23] M. Almgren, F. Greiser, J.K. Thomas, J. Am. Chem. Soc. 101 (1979) 279.
[24] F.H. Quina, V.G. Toscano, J. Phys. Chem. 81 (1977) 1750.
[25] W. Hinze, In: W.L. Hinze, D.W. Armstrong (Eds.), Ordered Media in Chemical Separations, ACS Symposium Series 342, American Chemical Society, Washington, DC, 1987, p. 4.

Talanta 76 (2008) 189–199

Contents lists available at ScienceDirect

Talanta

journal homepage: www.elsevier.com/locate/talanta

Analysis of phenolic compounds by high performance liquid chromatography and ultra performance liquid chromatography

Zdeněk Spáčil, Lucie Nováková, Petr Solich*

Department of Analytical Chemistry, Faculty of Pharmacy, Charles University in Prague, Heyrovského 1203, 500 05 Hradec Králové, Czech Republic

ARTICLE INFO

Article history:
Received 26 October 2007
Received in revised form 15 February 2008
Accepted 20 February 2008
Available online 4 March 2008

Keywords:
UPLC
HPLC
Phenolic compounds
Gradient analysis

ABSTRACT

Two novel chromatographic methods both based on utilization of sub-2-micron particle columns were developed for the analysis of phenolic compounds in this work. An HPLC system was equipped with C_{18} silica-based analytical column (50 mm × 4.6 mm, 1.8 μm) and a UPLC system with ethylene-bridged hybrid C_{18} analytical column (100 mm × 2.1 mm, 1.7 μm).

In total 34 phenolic substances were divided into groups of phenolic acids, flavonoids, catechins and coumarins and were analysed in sequence using different gradient methods. System suitability test data, including repeatability of retention time and peak area, mean values of asymmetry factor, resolution, peak capacity and the height equivalent of a theoretical plate were determined for each gradient method by 10 replicate injections. The developed methods were applied in the analysis of real samples (grape wines, teas).

1. Introduction

In recent years considerable attention has been paid to natural substances with antioxidant activity, due to increasing incidence of serious pathologies such as cancer, cardiovascular diseases or inflammation. These disorders are caused, amongst other things, by the harmful effects of free radicals [1]. Free radicals can participate in the development of atherosclerosis and thus increase the risk of blood clot formation [2]. They can also accelerate the process of body tissue aging and they quite possibly have some relationship to the occurrence of diabetes, rheumatoid arthritis, Alzheimerĭs disease and Parkinsonĭs disease. Antioxidants are both natural and synthetic compounds able to scavenge free radicals and to inhibit oxidation processes. Antioxidants are a very large and diverse group of substances. These include: vitamins (A, B_6, C, E), zinc, selenium and phenolic compounds (namely phenolic acids and flavonoids) [3].

The phenolic acids are hydroxylated derivatives of either benzoic or cinnamic acid, their structures are depicted in Fig. 1. They are substances widely distributed in the plant kingdom and occur in a free state as well as combined into esters or glycosides. Especially the derivates of cinnamic acid are very common, for instance caffeic acid with its esters, ferulic acid or sinapic acid are the most frequent. Ferulic acid is often associated with food fibre (ester bond to hemicelullose). Chlorogenic acid (ester of caffeic acid) is broadly present in many kinds of fruit, vegetables and coffee.

Flavonoid compounds (also known as flavonoids) are an extensive group of plant phenols. They possess a basic structural element, the flavan (2-phenylchromane) skeleton and fall into different classes, e.g. flavonols (kaempferol, quercetin), flavan-3-ols (catechin), flavones (luteolin) or flavanones (naringenin). Natural flavonoids occur most frequently in the form of *O*-glycosides, which means, that they contain a non-sugar group in their molecule (aglycone) and a sugar group (monosacharides or oligosacharides). Structures of flavonoids used for the purpose of this work are given in Fig. 1. Catechins, sometimes classified as condensed tannins, are abundant in the tea leaves. They are indicating strong antioxidant activity. Some studies have proven, that the antioxidant activity of (−)-epigallocatechin gallate exceeds the effect of vitamin C at least 100 times [4]. Coumarins are 2H-1-benzopyran-2-ones substituted by hydroxyl groups often either methylated or engaged in a glycosidic linkage [5].

The recent methods dealing with the analysis of phenolics are summarized in review articles [6–8]. It can be seen that the high performance liquid chromatography (HPLC) occupies a leading position in the analysis of phenolics. In general, HPLC separations are based on C_{18} reverse-phased columns and a binary solvent gradient. The mobile phase usually consists of an aqueous solution of acid and an organic solvent (acetonitrile or methanol). Traditional HPLC is most frequently coupled with simple ultraviolet (UV) [9] or photodiode array (DAD) [10] detection, but HPLC applying a

* Corresponding author. Tel.: +420 495067294; fax: +420 495067164.
E-mail address: solich@faf.cuni.cz (P. Solich).

0039-9140/$ – see front matter © 2008 Elsevier B.V. All rights reserved.
doi:10.1016/j.talanta.2008.02.021

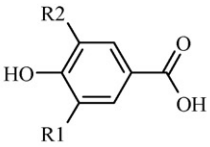

Benzoic type	R^1	R^2
Gallic acid	-OH	-OH
Protocatechuic acid	-OH	-H
Vanillic acid	$-OCH_3$	-H
Syringic acid	$-OCH_3$	$-OCH_3$

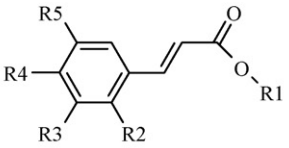

Cinnamic type	R^1	R^2	R^3	R^4	R^5
Chlorogenic acid	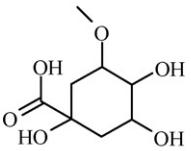	-H	-OH	-OH	-H
Caffeic acid	-H	-H	-OH	-OH	-H
p-Coumaric acid	-H	-H	-H	-OH	-H
Ferulic acid	-H	-H	$-OCH_3$	-OH	-H
Sinapic acid	-H	-H	$-OCH_3$	-OH	$-OCH_3$
o-Coumaric acid	-H	-OH	-H	-H	-H
Cinnamic acid	-H	-H	-H	-H	-H

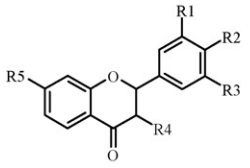

Flavonoid	Bond type	R^1	R^2	R^3	R^4	R^5
Rutin	C_3=C_4	-H	-OH	-OH	-rhamnoglucoside	-OH
Naringin	C_3–C_4	-H	-OH	-H	-H	-rhamnoglucoside
Quercitrin	C_3=C_4	-H	-OH	-OH	-rhamnoside	-OH
Quercetin	C_3=C_4	-OH	-OH	-H	-OH	-OH
Hesperetin	C_3–C_4	-OH	$-OCH_3$	-H	-H	-OH
Kaempferol	C_3=C_4	-H	-OH	-H	-OH	-OH
Rhamnetin	C_3=C_4	-OH	-OH	-H	-OH	$-OCH_3$
Galangin	C_3=C_4	-H	-H	-H	-OH	-OH

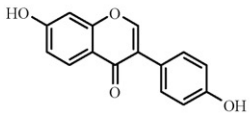

Daidzein

Fig. 1. Structural types of analysed phenolic acids and flavonoids.

mass spectrometric (MS) detector has proven to be the method of choice, particularly in the identification of phenolics [11–14]. The electrochemical detection [15] provides in some cases additional selectivity, compared to the classical UV and DAD techniques. Apart from the HPLC methods, several electromigration methods such as capillary electrophoresis (CE) and micellar electrokinetic capillary chromatography (MEKC) have been also used [16–18]. These methods show higher efficiency, selectivity and speed compared to HPLC, but difficulties in sensitivity and reproducibility have been observed. Another possibility for the separation of phenolics is provided by gas chromatography (GC). The GC analysis can be performed with or without derivatization applying mainly MS detection. GC analysis without derivatization is suitable only for the identification of aglycones, but excellent selectivity and sensitivity was achieved using silylating agents.

There is a need for a method allowing simultaneous detection of a wide range of phenolics in a single analysis, in order to decrease the time necessary for the analysis of complex samples and reduce the analysis costs. This method should be able to characterize the occurrence of flavonoids and phenolic acids in various materials with sufficient selectivity and sensitivity during a short analysis time based on efficient separation. However recent methods often show weak points in one or more of these requirements. According to the table presented in a review article by Molnár-Perl et al. [7] the number of analytes detected simultaneously by most HPLC methods is usually around 10. Such number of phenolic compounds is usually satisfactorily separated in 45 or 50 min. The brief summary of more recent published separation methods in the field of simultaneous analysis of phenolics is presented in Table 1. On average, a similar figure was observed for the number of analytes (12), but the time of analysis was shorter (35 min).

In order to further increase the speed of analysis for phenolic compounds, a liquid chromatography system utilizing a sub-2-micron analytical column was used in this work. A conventional HPLC system and a ultra performance liquid chromatography (UPLC) system, equipped with columns containing similar stationary phases, were compared.

The conventional HPLC system was equipped with a Zorbax Stable Bond (SB) C_{18} analytical column packed with 1.8 μm silica-based particles containing diisobutyl groups in order to provide steric protection for the siloxane bonds. Acid labile end-capping reagents were not utilized. These adjustments improved column lifetime, as well as increased temperature and chemical stability in the pH 1–6 range. The use of this column in a conventional HPLC system was compared with a UPLC column containing hybrid sorbents based on BEH technology.

The main advantage of UPLC, in terms of separation efficiency, arises from the use of 1.7 μm, particles. This is in accordance with the Van Deemter theory [20]. As an LC technique, UPLC is still relatively new and has the potential for more pioneering research. It has enhanced sensitivity and separation power which results in decreased analysis time and solvent consumption. Using sub-2-micron particles provide maximum efficiency, leading to column back-pressures of more than 60 MPa, which are not achievable by conventional liquid chromatographic systems or columns [21]. UPLC systems allow work at extreme pressures, up to 100 MPa [22], due to the hardware adjustments.

The aim of this study was to compare HPLC and UPLC for the analysis of phenolic compounds. Both conventional HPLC, equipped with a sub-2-micron particle column, and a UPLC–UV method for determination of phenolic compounds was not published yet.

2. Experimental

2.1. Chemicals and reagents

The working standards of caffeic acid, cinnamic acid, ferulic acid, gallic acid, chlorogenic acid, *o*-coumaric acid, *p*-coumaric acid, protocatechuic acid, sinapic acid, syringic acid, vanillic acid, (+)-catechin (C), (−)-catechin gallate (Cg), (−)-epicatechin (EC), (−)-epicatechin gallate (ECg), (−)-epigallocatechin (EGC), (−)-epigallocatechin gallate (EGCg), (−)-gallocatechin (GC),

Table 1
Recent methods for the simultaneous analysis of phenolic compounds

Method	Analytes	Run time (min)	Time per analyte (min)	Reference
HPLC–UV	Rutin; quercetrin; fisetin; myricetin; morin; luteolin; quercetin; apigenin; kaempferol; isorhamnetin; rhannetin; galangin	60	5	[9]
HPLC–DAD	Gallic acid; 3,5-dihydroxybenzoic acid; (−)-epigallocatechin; (−)-epigallocatechin gallate; (−)-epicatechin; (−)-epicatechin gallate; caffeine; (−)-catechin gallate; *p*-anisic acid; myricetin; 3,4,5-trimethoxycinnamic acid	25	2	[10]
HPLC–MS	6-*O*-Feruloylsucrose; 6-*O*-sinapoylsucrose; ferulic acid; sinapinic acid; *p*-coumaric acid; chlorogenic acid; caffeic acid; protocatechuic acid; hydroxybenzoic acid; vanillic acid; syringic acid	40	4	[11]
HPLC–MS/MS	Naringenin; genistein; kaempferol; apigenin; pinocembrin; galangin; acacetin; chrysin	35	4	[12]
HPLC–MS/MS	Gallic acid; protocatechuic acid; catechin; isorhoifolin; epicatechin; procyanidin; rutin; hesperidin; hyperoside; isoquercitrin; quercetin-*O*-pentose; naringenin-7-*O*-glucoside; rhamnetin-*O*-rutinoside; quercetin; luteolin; naringenin	20	1	[13]
HPLC–DAD–MS–FD–ED	Gallic acid; 5-HMF; protocatechuic acid; epigallocatechin; furfural; caftaric acid; *p*-hydroxybenzoic acid; *cis*-coutaric acid; catechin; caffeic acid; fertaric acid; epicatechin; vanillin; ferulic acid; *trans*-piceid; quercetin-3-glucuronide; quercetin-3-glucoside; *cis*-piceid; kaempferol-3-glucoside; quercetin-3-rutinoside; *trans*-resveratrol; *cis*-resveratrol; quercetin	80	3	[14]
HPLC–ECD	Gallic acid; protocatechuic acid; 4-hydroxybenzoic acid; 4-hydroxyphenylacetic acid; catechin; vanillic acid; chlorogenic acid; caffeic acid; syringic acid; *p*-coumaric acid; ferulic acid; sinapic acid; isoferulic acid; *o*-coumaric acid	50	4	[15]
CE–DAD	Protocatechuic acid; salicylic acid; *p*-hydroxybenzoic acid; vanillic acid; syringic acid; *p*-coumaric acid; ferulic acid; sinapic acid	4	1	[16]
CE–ECD	*Tert*butylhydroquinone; propyl gallate	7	4	[17]
MEKC–UV	Chlorogenic acid; syringic acid; ferulic acid; *p*-coumaric acid; vanillic acid; *p*-hydroxybenzoic acid; caffeic acid; cichoric acid; caftaric acid; 3,4-dihydroxybenzoic acid	35	4	[18]

(−)-gallocatechin gallate (GCg), daidzein, galangin, hesperetin, kaempferol, naringin, quercetin, quercitrin, rhamnetin, rutin, 4-hydroxycoumarin, 6-methylcoumarin, daphnoretin, aesculin, scopoletin, umbelliferone and caffeine used for the purposes of this study were purchased from Sigma–Aldrich (Prague, Czech Republic).

Mobile phase additive formic acid 98% p.a., LC–MS grade methanol (UPLC analysis) and HPLC grade methanol for the HLPC analyses were supplied by Sigma–Aldrich (Prague, Czech Republic).

HPLC grade water was prepared by Milli-Q reverse osmosis Millipore (Bedford, MA, USA) and additionally filtered through a 0.22 μm membrane (UPLC), 0.45 μm for HPLC, respectively immediately before use.

The red wine, Blue Frankish 2005 vintage, was a product of Moravian Winery (Bzenec, Czech Republic) and the white wine, Kerner 2004 vintage, was manufactured in the winery Mikrosvín (Mikulov, Czech Republic). The green tea, Formosa Gunpowder and black tea, Nepal SFTGFOP-Maloom, were obtained from (OXALIS, Slusovice, Czech Republic).

2.2. Liquid chromatography instruments

A UPLC system Acquity (Waters, Prague, Czech Republic) consisting of a binary solvent manager and a sample manager was coupled to a tunable UV detector. All UPLC analyses were performed on a bridged ethylene hybrid (BEH) C_{18} analytical column (100 mm × 2.1 mm, 1.7 μm, Waters, Prague, Czech Republic). The analytical column was kept at 50 or 25 °C by column oven. The auto sampler stored run solutions at 4 °C. A partial loop injection mode with a needle overfill was set up, enabling 1.5 μL injection volumes when 5 μL injection loop was used. Mobile phase generated from 0.1% formic acid in water and methanol was mixed directly in the instrument. The flow rate was 0.45 mL min^{-1}. The UV detection wavelength was set at 280 nm, with a data acquisition rate of 40 Hz. Empower 2 software was used for chromatographic data gathering and integration of chromatograms.

An LC system consisting of a Waters 1525 binary HLPC pump, a Waters 717plus auto sampler and a Waters 2487 Dual λ Absorbance detector (Waters, Prague, Czech Republic) was utilized for HPLC analyses. The analytical column Zorbax SB C18 (50 mm × 4.6 mm, 1.8 μm, Agilent Technologies, Prague, Czech Republic) used was kept at 25 °C. The injection volume was 5 μL. The mobile phase contained 0.1% formic acid in water and methanol in a ratio dependant on the gradient profile, at a flow rate of 1.0 mL min^{-1}. The UV detector wavelength was set at 280 nm. Data acquisition was carried out by Breeze software.

2.3. Preparation of standard solutions

The stock solutions of standards were prepared with analytical accuracy dissolving 1 mg of standard substance in 1 mL of methanol. The working solutions for the standards used for the sensitivity comparisons, were prepared by diluting the stock solutions by a factor of 10, using methanol. These run solutions were also used for the HPLC system suitability test (SST) data measurement. UPLC SST run solutions were prepared by further dilution of the same stock solutions. The SST data run solution for phenolic acids was 50 times diluted, for catechins 80 times diluted, for coumarins and flavonoids 30 times diluted.

2.4. SST data measurement

Ten replicate standard solutions were injected into either the UPLC or HPLC systems. More diluted run solutions for UPLC than for HPLC were used in order to work in the linear detector range, according to the Lambert–Beer law. All HPLC analyses were performed at 25 °C. The UPLC analyses were performed at 50 or 25 °C. The R.S.D. data of retention times, peak areas and mean values of asymmetry and resolution were calculated for all components. The

rules for the measurements and the limits for the acceptance are given by appropriate guidelines [23] and pharmacopoeias [24,25]. The peak capacity values and the height equivalents of the theoretical plate were also calculated for each peak. Although the peak capacity is a more suitable tool to determine the quality of a gradient separation [26], height equivalents of the theoretical plate were presented as well in order to illustrate the correlation between both parameters.

2.5. Pretreatment of the samples

The wine samples were prepared without any extraction. They were filtrated through a 0.22 μm membrane and directly used for the injections. The tea infusions were prepared by pouring 100 mL of hot water (90 °C) over 1 g of dry tea mixture and 5 min of maceration with mild stirring. The then cooled down tea infusion was filtrated through a 0.22 μm membrane and was diluted, using methanol: water 50:50 (v/v) solution, by a factor of 2.

3. Results and discussion

Four groups of important phenolic compounds were chosen for the purpose of the study. The results presented in this work were obtained by comparing the methods of UPLC with HPLC using similar conditions and analytical columns with analogous particle size. The length of the analytical column for HPLC was 50 mm and for UPLC it was 100 mm. The reason behind this bipolar approach was the very high back-pressure in the HPLC system, generated by the column with the sub-2-microne particles, when keeping 100 mm column length. The UPLC system copes with this feature of sub-2-micron particle sorbents, but such a back-pressure is unacceptable for conventional HPLC system. Typical values of the back-pressures reached during the HPLC analyses, using 50 mm Zorbax analytical column, were around 30 MPa. Another reason for the usage of a short column was also the achievement of faster analysis.

The comparative data for the sensitivities of both systems were derived from the relationship between injection volumes and peak areas of the same concentrated solution.

In spite of the predominantly aqueous mobile phase, methanol was used as the solvent for the stock solutions. This was due to the poor solubility of some phenolic substances in water. The different solvent strength of methanol caused broadening and distortion of early eluting peaks. This phenomenon was observed despite using very small injection volumes.

3.1. Column temperature

The higher temperature (50 °C) was used during UPLC separations with the view of shortening the retention time and lowering backpressure and organic solvent consumption [27]. This high temperature was selected for the analyses because, in the case of phenolic acids, catechins and coumarins, it resulted in a high resolution of the chromatographic peaks. The negative effects on resolution were observed when the higher temperature was applied in the analysis of flavonoids. Due to these results, it was decided to keep lower temperature (25 °C). Higher column temperatures were applied to the HPLC analyses as well, but the impaired resolution for ionic compounds was evident. Therefore, the 25 °C column temperature was used.

3.2. Equilibration times

Both chromatographic methods were suitable for the analysis of phenolic compounds, but the UPLC method brought some advantages. It was not only faster, more sensitive and more efficient, but also a more reliable and ecologic method. The speed of the analysis was improved in two steps. Obviously the run time of analysis yielded first reduction, but secondly the equilibration time for bringing the column to the initial conditions after gradient analysis was much shorter. Between 10 and 15 min is recommended for returning a HPLC column to its equilibrated state, but according to our experiences, only 1.5–3 min were required for UPLC to regain its equilibrium. An equilibration time of 15 min was used for HPLC analyses. However, satisfactory results in the UPLC analyses were obtained using an equilibration time of 90 s for catechins and phenolic acids, and 3 min for flavonoids and coumarins. This disproportion was demanded by several factors. Firstly, methanol was used to flush out the system after these two gradient analyses, in order to prevent the retention of some residues on the column. Secondly, an increase of 50–60% of methanol was used in these gradient runs. Finally, the analysis of flavonoids was performed at a lower temperature.

3.3. Phenolic acids

UPLC analyses were performed 4.6 times faster than those by HPLC. Solvent consumption was decreased by a factor of 10. Injecting just 1.5 μL to the UPLC system decreased the peak area by half when compared to 5 μL injections into the HPLC, using the same concentrated solution. That means that about 1.7 times higher sensitivity was achieved with UPLC.

SST data comparing both methods are presented in Table 2. Retention time, peak area repeatability and symmetry factor values were significantly better for UPLC. The HPLC method indicated problems with the resolution of chlorogenic, vanillic and caffeic acid. Chromatographic peaks of these acids were partially overlapped. This same poor resolution of chlorogenic, vanillic and caffeic acid was not seen using the UPLC method. The separation

Table 2
SST data for phenolic acids

	SST parameters											
	Retention time (%R.S.D.)		Peak area (%R.S.D.)		Asymmetry factor		Resolution		Peak capacity		HETP (μm)	
	HPLC	UPLC	HPLC	UPLC	HPLC	UPLC	HPLC	UPLC	HPLC	UPLC	HPLC	UPLC
Gallic acid	0.40	0.08	0.53	0.18	1.37	1.14	–	–	34.13	82.47	72.78	7.31
Protocatechuic acid	0.45	0.06	0.61	0.19	1.23	1.05	4.61	7.97	34.06	83.26	29.62	4.69
Chlorogenic acid	0.69	0.07	0.88	0.20	0.67	1.00	13.01	5.42	34.13	67.84	9.08	4.81
Vanillic acid	0.47	0.08	0.44	0.15	–	1.02	0.89	8.08	44.60	62.17	14.40	4.18
Caffeic acid	0.56	0.07	0.44	0.13	–	1.03	1.37	2.47	27.67	61.05	10.71	3.91
Syringic acid	0.44	0.08	0.22	0.16	0.88	0.91	4.39	3.02	31.02	51.84	5.01	3.98
p-Coumaric acid	0.39	0.07	0.49	0.26	0.87	1.02	6.74	9.78	30.96	44.78	2.61	3.98
Ferulic acid	0.27	0.07	1.02	0.26	0.86	0.99	5.17	7.58	37.95	39.36	1.34	3.74
Sinapic acid	0.23	0.09	0.46	0.28	0.83	1.01	2.97	1.56	28.44	41.15	0.92	3.33
o-Coumaric acid	0.20	0.05	0.60	0.31	0.85	1.03	6.06	12.30	39.37	113.33	1.08	0.27
Cinnamic acid	0.11	0.05	0.21	0.75	0.88	1.02	11.62	7.66	42.78	97.55	0.69	0.34

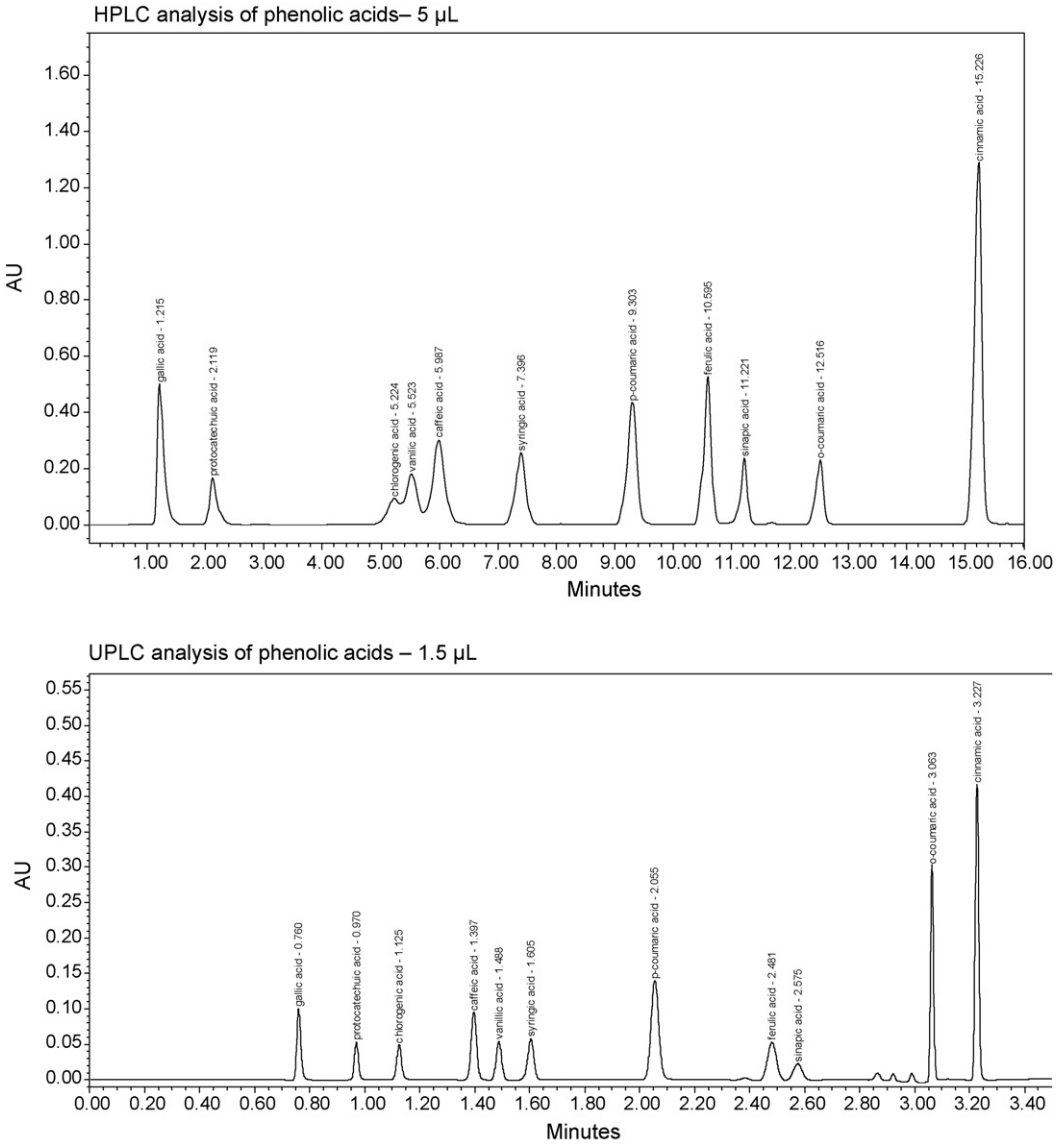

Fig. 2. Analysis of phenolic acids: HPLC, 0.1% formic acid–methanol, from 85:15 to 50:50 (v/v), 1.0 mL min^{-1}; UPLC, 0.1% formic acid–methanol, from 88.5:11.5 to 30:70 (v/v), 0.45 mL min^{-1}.

efficiency determined by peak capacity was higher for UPLC method.

There was found a difference in selectivity, since chromatographic peaks in HPLC conditions were currently eluting in the sequence of vanillic acid followed by caffeic acid. These peaks of vanillic and caffeic were switched over in the UPLC chromatogram (Fig. 2).

3.4. Catechins

The UPLC analysis time of the catechins was seven times shorter in comparison to the HPLC method. Solvent consumption for each individual analysis was reduced almost 16 times in this way, as can be seen in Fig. 3. Sensitivity of detection was 1.5 higher for UPLC. Peak retention time and the area repeatability parameters for UPLC

Table 3
SST data for catechins

	SST parameters											
	Retention time (%R.S.D.)		Peak area (%R.S.D.)		Asymmetry factor		Resolution		Peak capacity		HETP (µm)	
	HPLC	UPLC	HPLC	UPLC	HPLC	UPLC	HPLC	UPLC	HPLC	UPLC	HPLC	UPLC
GC	0.57	0.02	0.71	0.51	1.18	1.21	–	–	21.00	38.04	18.68	4.16
EGC	0.05	0.06	0.69	0.58	1.12	1.08	15.31	4.45	41.00	30.70	0.56	4.12
C		0.07		0.54		1.06		2.12		33.97		3.94
EGCg	0.03	0.09	0.76	0.42	1.19	1.09	9.05	2.45	31.00	26.66	0.40	4.19
EC	0.04	0.08	0.74	0.55	1.15	1.05	2.95	2.62	45.94	27.75	0.35	4.26
GCg	0.03	0.07	0.68	0.41	1.19	1.05	2.37	2.00	45.94	30.83	0.33	3.78
ECg	0.05	0.07	0.86	0.64	1.25	1.03	4.75	7.35	31.00	20.06	0.31	4.40
Cg	0.05	0.08	0.70	0.63	1.17	1.04	2.96	2.45	36.93	18.50	0.27	4.59

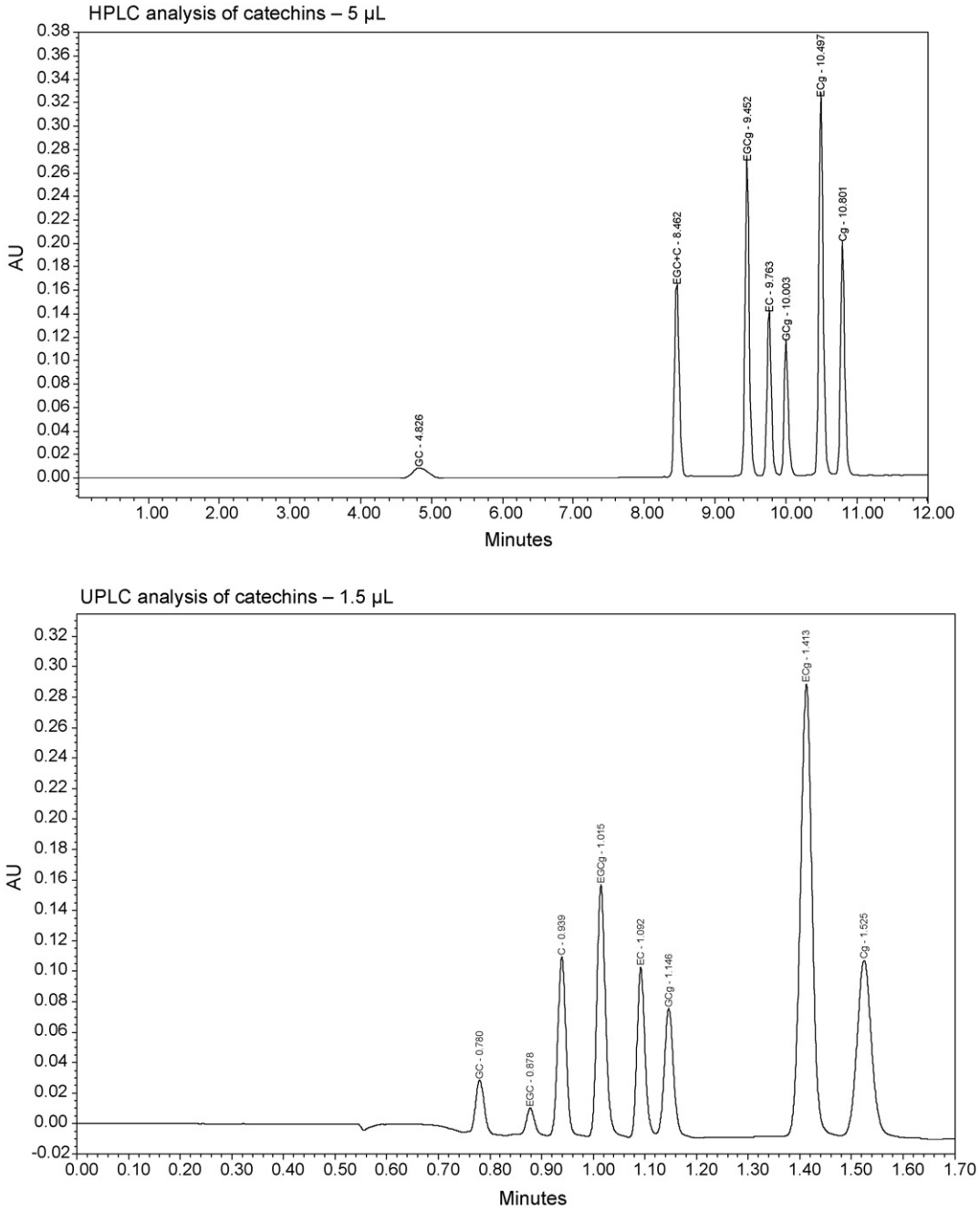

Fig. 3. Analysis of catechins: HPLC, 0.1% formic acid–methanol, from 95:05 to 40:60 (v/v), 1.0 mL min^{-1}; UPLC, 0.1% formic acid–methanol, from 88.5:11.5 to 60:40 (v/v), 0.45 mL min^{-1}.

analysis (Table 3) resembled the data gained for the HPLC method. Peak asymmetry values revealed less peak "tailing" in favour of the UPLC technique. The UPLC method has shown slightly lower peak capacity, probably due to the extremely fast analysis. On the other hand all peaks were separated by this method with satisfactory resolution, even the peaks of (−) -epigallocatechin and (+) -catechin. No separation was achieved using HPLC, even though several mobile phase modifications and different gradient methods were tested.

3.5. Coumarins

Using UPLC approach, the analysis time was three times shorter and the solvent consumption was decreased by a factor of 6.7 in comparison with HPLC. The sensitivity of the UPLC system was about twice as high. The use of 1.5 µL injection volumes caused a 1.7 multiple decrease in the peak area.

The comparison of the SST values is in Table 4. The UPLC analyses indicated excellent repeatability for retention time, but slightly worse repeatability for peak area. Other SST parameters such as asymmetry factor, resolution and peak capacity, were slightly superior for the UPLC analyses.

Despite of using the similar type of stationary phase, another change in selectivity was observed. The peak of daphnoretin, eluting at the end of chromatogram in HPLC analysis, moved ahead of 6-methyl-coumarin peak performing the UPLC method (Fig. 4).

Table 4
SST data for coumarins

	SST parameters											
	Retention time (%R.S.D.)		Peak area (%R.S.D.)		Asymmetry factor		Resolution		Peak capacity		HETP (μm)	
	HPLC	UPLC	HPLC	UPLC	HPLC	UPLC	HPLC	UPLC	HPLC	UPLC	HPLC	UPLC
Aesculin	0.36	0.06	0.46	0.76	1.54	0.92	–	–	21.00	43.90	71.12	22.91
Umbelliferone	0.19	0.03	0.59	0.80	0.88	1.01	12.03	23.52	21.00	30.24	14.03	4.48
Scopoletin	0.18	0.04	0.59	0.70	–	0.96	1.31	2.30	18.14	34.33	15.67	2.89
4-Hydroxycoumarin	0.15	0.08	0.50	0.81	0.88	1.06	13.22	13.58	20.48	81.81	1.40	0.36
Daphnoretin	0.06	0.15	0.49	0.97	0.90	1.07	6.11	3.17	21.55	78.36	0.93	0.36
6-Methylcoumarin	0.11	0.10	0.41	0.71	0.99	1.06	4.99	2.59	31.00	69.42	0.45	0.42

3.6. Flavonoids

Analysis duration was 2.5 times shorter due to UPLC and solvent consumption was decreased by 5.5 times. The comparison of chromatograms can be seen in Fig. 5. The UPLC system also showed very good sensitivity (1.7 times higher), allowing injection of only 1.5 μL volume for reliable analysis results.

There are comparable values of retention time repeatability, peak area repeatability, asymmetry factor and resolution as well. The separation of rutin and naringin bears difficulties for both chromatographic methods. It was not possible to obtain satisfac-

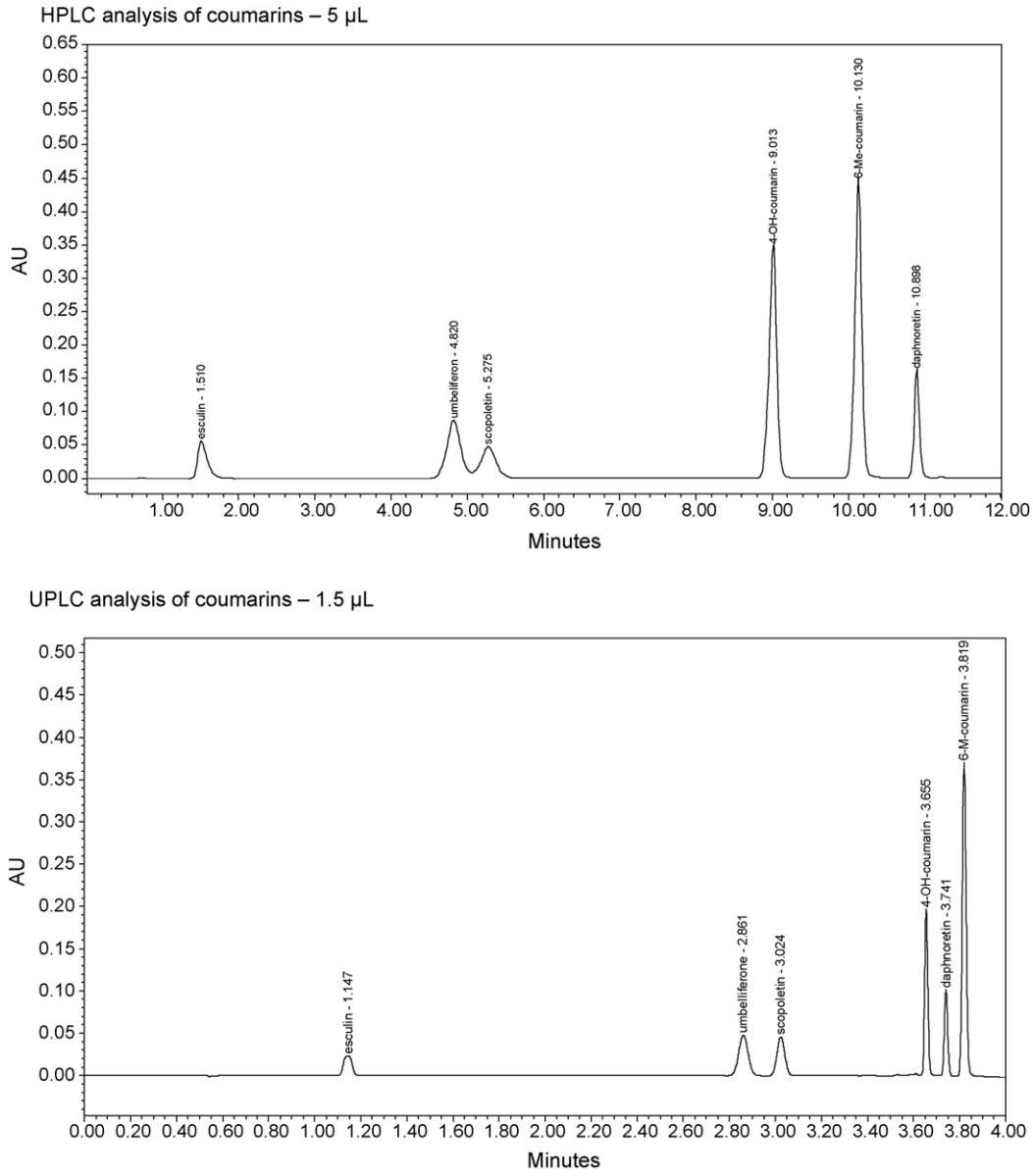

Fig. 4. Analysis of coumarins: HPLC, 0.1% formic acid–methanol, from 75:25 to 50:50 (v/v), 1.0 mL min^{-1}; UPLC, 0.1% formic acid–methanol, from 88.5:11.5 to 40:60 (v/v), 0.45 mL min^{-1}.

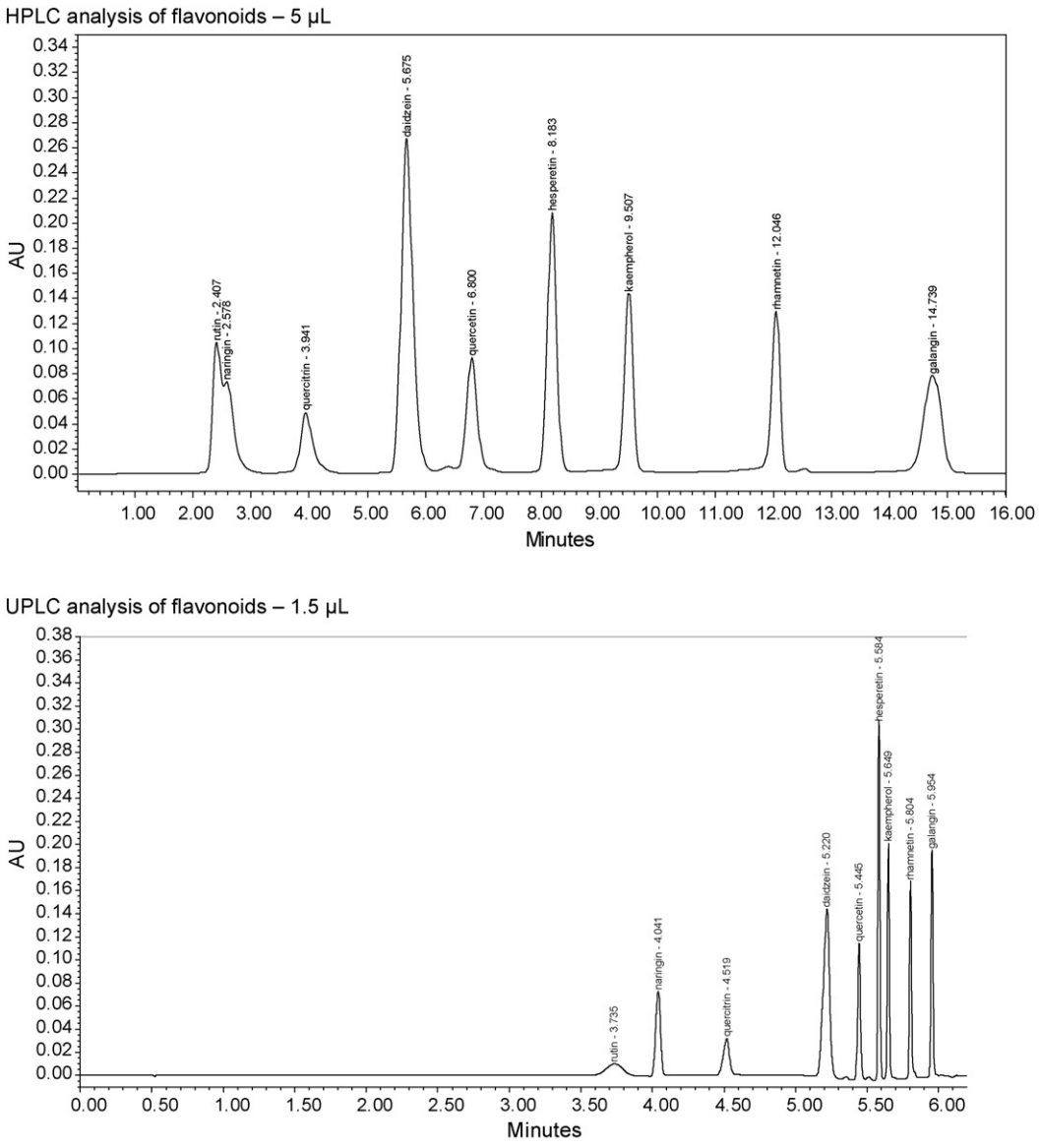

Fig. 5. Analysis of flavonoids: HPLC, 0.1% formic acid–methanol, from 60:40 to 40:60 (v/v), 1.0 mL min^{-1}; UPLC, 0.1% formic acid–methanol, from 69:31 to 10:90 (v/v), 0.45 mL min^{-1}.

tory resolution for these peaks using the HPLC method at all. In the UPLC method it was needed to use lower column temperature (25 °C) in order to reach acceptable chromatographic peak resolution. The UPLC system had significantly higher peak capacity number than the HPLC system. The first two peaks were excluded from this comparison, because of partial overlap in the HPLC analysis. The results of SST measurements could be seen in Table 5.

Table 5
SST data for flavonoids

	SST parameters											
	Retention time (%R.S.D.)		Peak area (%R.S.D.)		Asymmetry factor		Resolution		Peak capacity		HETP (µm)	
	HPLC	UPLC	HPLC	UPLC	HPLC	UPLC	HPLC	UPLC	HPLC	UPLC	HPLC	UPLC
Rutin	0.53	0.60	6.83	0.76	0.83	0.97	–	–	46.71	19.91	29.76	21.66
Naringin	0.66	0.21	8.36	0.84	–	0.97	–	2.06	29.22	58.71	–	2.80
Quercitrin	0.66	0.19	0.90	0.90	1.20	0.93	–	5.63	23.32	49.92	26.90	1.93
Daidzein	0.40	0.15	1.01	0.82	1.06	0.89	4.73	8.72	20.21	48.79	13.44	1.50
Quercetin	0.38	0.07	1.03	1.09	0.97	0.94	3.21	3.99	24.39	108.51	7.36	0.23
Hesperetin	0.26	0.02	1.02	0.83	0.93	0.95	4.29	4.73	30.09	155.30	4.33	0.13
Kaempferol	0.24	0.04	0.88	0.85	0.90	0.98	4.49	2.64	31.95	152.16	2.82	0.13
Rhamnetin	0.18	0.02	0.84	0.82	0.85	0.99	8.71	5.90	30.09	156.69	1.87	0.13
Galangin	0.22	0.02	1.04	0.90	0.99	0.99	5.74	5.82	20.21	152.31	5.46	0.12

Table 6
The analysis of grape wine and tea

	Blue Frankish (red wine) HPLC/UPLC	Kerner (white wine) HPLC/UPLC		Gunpowder (green tea) HPLC/UPLC	Nepal (black tea) HPLC/UPLC
Gallic acid	+/+	−/?	GC	?/+	−/?
Protocatechuic acid	+/+	+/+	EGC	?/+	?/+
Chlorogenic acid	−/−	−/−	C	?/?	?/?
Vanillic acid	+/+	?/?	EGCg	+/+	?/+
Caffeic acid	?/+	+/+	EC	+/+	?/?
Syringic acid	+/+	−/?	GCg	+/+	+/?
p-Coumaric acid	+/+	+/+	ECg	+/+	+/+
Ferulic acid	?/+	?/?	Cg	?/?	?/−
Sinapic acid	−/?	−/?			
o-Coumaric acid	?/?	−/−			
Cinnamic acid	−/−	−/−			

(+) detected; (−) not detected; (?) confirmation needed.

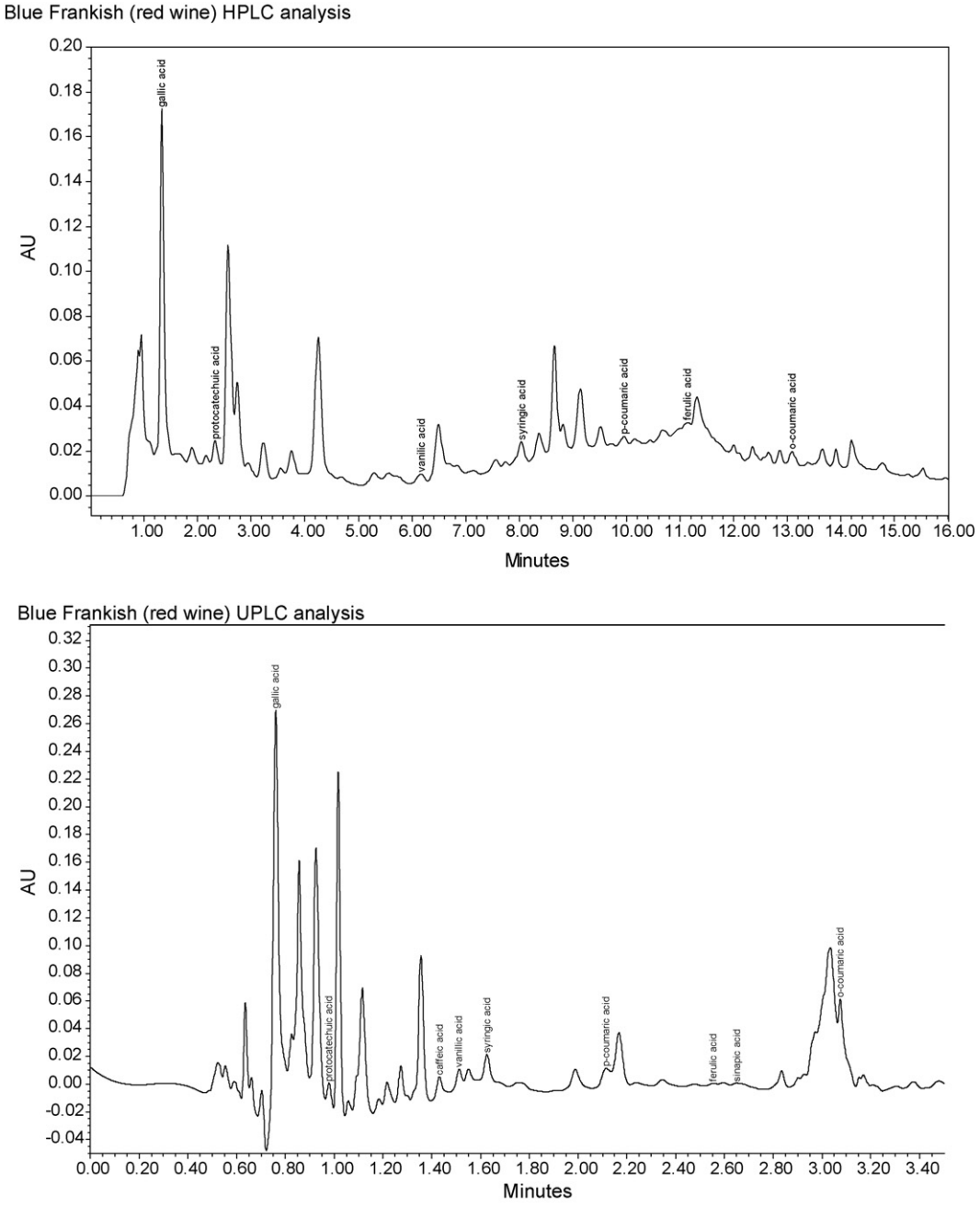

Fig. 6. Comparison of HPLC and UPLC method in the analysis of real samples.

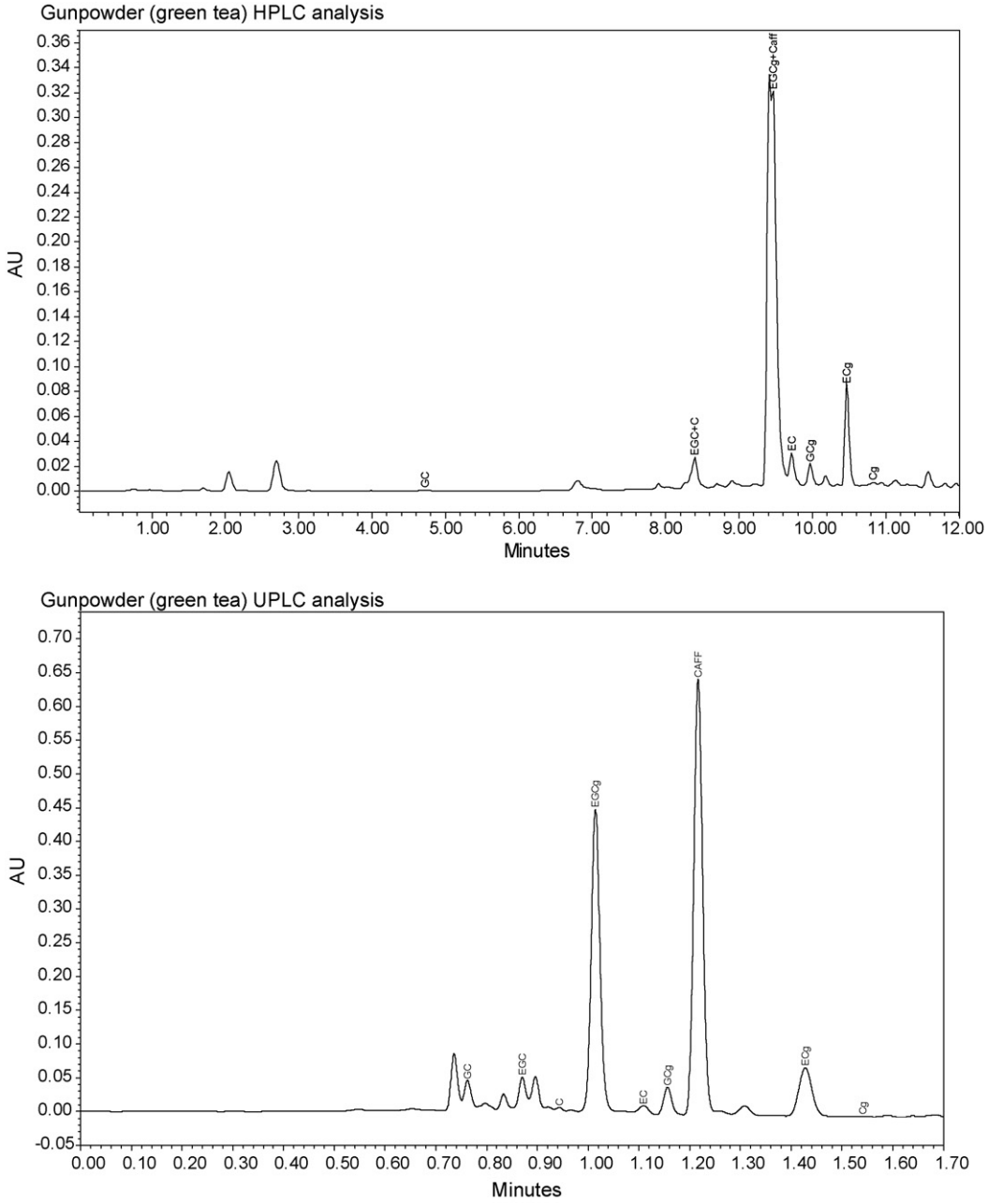

Fig. 6. (*Continued*).

Table 7
Comparison of analysis duration and solvent consumption

		Flow rate (mL min^{-1})	Analysis duration (min)	Solvent consumption (mL)	Time per analyte (min)
Phenolic acids	HPLC	1.00	16.0	16.0	1.5
	UPLC	0.45	3.5	1.6	0.3
Catechins	HPLC	1.00	12.0	12.0	1.5
	UPLC	0.45	1.7	0.8	0.2
Coumarins	HPLC	1.00	12.0	12.0	2.0
	UPLC	0.45	4.0	1.8	0.7
Flavonoids	HPLC	1.00	16.0	16.0	1.8
	UPLC	0.45	6.5	2.9	0.7

3.7. Analysis of phenolic acids in grape wines and catechins in teas

The real samples of grape wines and teas were selected in order to demonstrate the applicability of the methods for the analysis of real matrix samples. The results of the analyses are summarized in Table 6. Seven phenolic acids in red wine and three in white wine were reliably identified using the UPLC method. It is possible that other phenolic acids were observed. Nevertheless the confirmation using more selective detection is needed to be sure. The HPLC method enables to detect five phenolic acids, the presence of other two needs to be confirmed (Fig. 6).

In the matrix of the green tea infusion six catechins and caffeine were reliably identified. The remaining two catechins probably occur in minor concentrations. The black tea was a less abundant source of catechins, but in spite of this four catechins were identified. The presence of another three of them is suspected. On the other hand, the results obtained by the HPLC method are less informative due to the low sensitivity and in particular low separation efficiency. Only the peaks of GCg and ECg have good response and are sufficiently separated. The co elution of EGC and C was observed already on standard solution. Newly ascertained was the partial co elution of EGCg/caffeine and insufficient resolution of EC. The responses of GC and Cg were negligible (Fig. 6).

4. Conclusions

It is of course not possible to provide the strict comparison of HPLC and UPLC system, because there is more than one different parameter. The basic limitations are represented by the impossibility of the connection of both the columns to the same chromatographic system. The sorbent particle size and chemistry is different as well. On the other hand, the mobile phase constituents were the same and the gradient programs were constructed with respect to analysis speed and good resolution in both cases. The system suitability parameters gained for each method were compared. Generally, both analytical methods showed good results, but the UPLC system appeared to be superior.

The UPLC gradient method development brought a substantial saving in time (a factor of 2–8), which was needed for method optimization (Table 7) The average analysis time of one analyte using UPLC was only 30 s, whereas in the developed HPLC method it was approximately 90 s. Accompanying the minimal solvent consumption (5–18 times lower) UPLC was more ecological and had lower analyses costs. The peak capacity measured as the gradient run time, divided by the peak width showed higher values for three UPLC gradient analyses. Only the peak capacity in the case of catechins was somewhat higher for HPLC, but it was outweighed by better utility of the UPLC method in the analysis of real samples. It is necessary to underline the excellent retention time and peak area repeatability of the UPLC method, most importantly in terms of use in routine pharmaceutical analyses. The UPLC method met all criteria required for pharmaceutical analyses. The great precision indicated for UPLC was achieved despite the use of negligible injection volumes in partial loop injection mode. Considering the shorter column washout time, UPLC methods can be rated as "green" methods. The UPLC method was more sensitive, the area of the detected peak increased by a factor 1.5–2, when using the same concentrated solution.

UPLC is becoming a more widely spread analytical method, nowadays found in many laboratories around the world. The practical value of both UPLC and HPLC, was confirmed by analysing real samples. The narrow peaks gained using the UPLC approach enable the detection of analytes at very low concentrations and with high resolution, making it appear preferable to HPLC.

Acknowledgement

The authors gratefully acknowledge the financial support of the Czech Ministry of Education, project MSM 0021620822.

References

[1] N. Getoff, Radiat. Phys. Chem. 76 (2007) 1577.
[2] H. Xi, M. Akishita, K. Nagai, W. Yu, H. Hasegawa, M. Eto, K. Kozaki, K. Toba, Atherosclerosis 191 (2007) 281.
[3] A. Chiou, V.T. Karathanos, A. Mylona, F.N. Salta, F. Preventi, N.K. Andrikopoulos, Food Chem. 102 (2007) 516.
[4] C. Hu, D.D. Kitts, Mol. Cell Biochem. 218 (2001) 147.
[5] J. Brunton, Pharmacognosy, Phytochemistry, Medicinal Plants, 2nd edn., Lavoisier, 1999, pp. 240–369.
[6] M. Naczk, F. Shahidi, J. Chromatogr. A 1054 (2004) 95.
[7] I. Molnár-Perl, Z. Füzfai, J. Chromatogr. A 1073 (2005) 201.
[8] E. Rijke, P. Out, W.M.A. Niessen, F. Ariese, C. Gooijer, U.A.T. Brinkman, J. Chromatogr. A 1112 (2006) 31.
[9] F. Fang, J.-M. Li, Q.-H. Pan, W.-D. Huang, Food Chem. 101 (2007) 428.
[10] Y. Zuo, H. Chen, Y. Deng, Talanta 57 (2002) 307.
[11] S. Tian, K. Nakamura, T. Cui, H. Kayahara, J. Chromatogr. A 1063 (2005) 121.
[12] N. Volpi, G. Bergonzini, J. Pharm. Biomed. Anal. 42 (2006) 354.
[13] Z. Charrouf, M. Hilali, O. Jauregui, M. Soufiaoui, D. Guillaume, Food Chem. 100 (2007) 1398.
[14] M.N. Bravo, S. Silva, A.V. Coelho, L. Vilas Boas, M.R. Bronze, Anal. Chim. Acta 563 (2006) 84.
[15] M. Nardini, A. Ghiselli, Food Chem. 84 (2004) 137.
[16] J. Hernández-Borges, G. González-Hernández, T. Borges-Miquel, M.A. Rodríguez-Delgado, Food Chem. 91 (2005) 105.
[17] B.-B. Sha, X.-B. Yin, X.-H. Zhang, X.-W. He, W.-L. Yang, J. Chromatogr. A 1167 (2007) 109.
[18] R. Pomponio, R. Gotti, M. Hudaib, V. Cavrini, J. Chromatogr. A 945 (2002) 239.
[20] D. Guillarme, D.T.-T. Nguye, S. Rudaz, J.-L. Veuthey, J. Chromatogr. A 1149 (2007) 20.
[21] D.T.-T. Nguye, D. Guillarme, S. Rudaz, J.-L. Veuthey, J. Chromatogr. A 1128 (2006) 105.
[22] S.A.C. Wren, J. Pharm. Biomed. Anal. 38 (2005) 337.
[23] International Conference on Harmonization (ICH), Q2(R1), Text on Validation of Analytical Procedures, US FDA Federal Register, 2003.
[24] European Pharmacopoeia, 6th edn, Council of Europe, Strasbourg, 2007.
[25] United States Pharmacopoeia 30, United States Pharmacopoeial Convention, Rockville, MD 20852, United States, 2006.
[26] U.D. Neue, J. Chromatogr. A 1079 (2005) 153.
[27] S.A.C. Wren, P. Tchelitcheff, J. Chromatogr. A 1119 (2006) 140.

Talanta 76 (2008) 66–71

Contents lists available at ScienceDirect

Talanta

journal homepage: www.elsevier.com/locate/talanta

Interpretative optimization and artificial neural network modeling of the gas chromatographic separation of polycyclic aromatic hydrocarbons

Snežana Sremac[a], Aleksandar Popović[b], Žaklina Todorović[a], Đuro Čokeša[a], Antonije Onjia[a,*]

[a] The Vinča Institute of Nuclear Sciences, P.O. Box 522, 11001 Belgrade, Serbia
[b] Faculty of Chemistry, Studentski trg 12-16, 11000 Belgrade, Serbia

ARTICLE INFO

Article history:
Received 25 August 2007
Received in revised form 25 January 2008
Accepted 8 February 2008
Available online 17 February 2008

Keywords:
PAHs
Factorial design
ANN
GC
Resolution product

ABSTRACT

An interpretative strategy (factorial design experimentation + total resolution analysis + chromatogram simulation) was employed to optimize the separation of 16 polycyclic aromatic hydrocarbons (PAHs) (naphthalene, acenaphthylene, acenaphthene, fluorene, phenanthrene, anthracene, fluoranthene, pyrene, chrysene, benzo(*a*)anthracene, benzo(*k*)fluoranthene, benzo(*b*)fluoranthene, benzo(*a*)pyrene, indeno(1,2,3-*c*,*d*)pyrene, dibenzo(*a*,*h*)anthracene, benzo(*g*,*h*,*i*)perylene) in temperature-programmed gas chromatography (GC). Also, the retention behavior of PAHs in the same GC system was studied by a feed-forward artificial neural network (ANN). GC separation was investigated as a function of one (linear temperature ramp) or two (linear temperature ramp + the final hold temperature) variables. The applied interpretative approach resulted in rather good agreement between the measured and the predicted retention times for PAHs in both one and two variable modeling. The ANN model, strongly affected by the number of input experiments, was shown to be less effective for one variable used, but quite successful when two input variables were used. All PAHs, including difficult to separate peak pairs (benzo(*k*)fluoranthene/benzo(*b*)fluoranthene and indeno(1,2,3-*c*,*d*)pyrene/dibenzo(*a*,*h*)anthracene), were separated in a standard (5% phenyl–95% dimethylpolysiloxane) capillary column at an optimum temperature ramp of 8.0 °C/min and final hold temperature in the range of 260–320 °C.

1. Introduction

A large number of compounds of the polycyclic aromatic hydrocarbon group (PAHs) are being released into the environment from the combustion of organic compounds. Since some of the PAHs are known to be carcinogenic and mutagenic [1], increasing importance is being attached to their presence in the environment. Sixteen PAHs compounds classified by the U.S.EPA as priority pollutants require monitoring in the environment. Nevertheless, the measurement of the content of these micropollutants in environmental materials is mandated by most regulatory agencies worldwide [1].

PAHs analysis can be well accomplished using gas chromatography (GC) [2,3], gas chromatography/mass spectrometry (GC–MS) [4], high-performance liquid chromatography (HPLC) [5], or HPLC–MS [6]. There has been a lot of controversy over which of the chromatographic techniques, GC or HPLC, is more favorable. In general, there are some clear advantages of HPLC over GC and vice versa. Reversed phase and particularly liquid crystal HPLC columns [7] are capable of separating a number of PAHs that are difficult to separate by capillary GC. Also, the sample preparation procedure is less tedious.

However, many PAHs are thermally stable and exhibit low polarity, and as such suitable for GC analysis. The advantages of GC separation of PAHs over the HPLC one are better peak resolution and, when coupled with MS, more reliable confirmation. Unlike separation of PAHs by isothermal GC that is somewhat obsolete nowadays, the temperature-programmed GC has the ability to separate both weakly and strongly retained PAHs in the same run.

Though chemical properties of many PAHs, such as water-solubility and reactivity [1] are different, some of them are very similar, which may cause overlapping of their chromatographic peaks. In general, whichever chromatographic technique we use the chromatographic separation has to be optimized.

Computer-assisted approach to the optimization of chromatographic separations has been extensively used recently. Thus, a number of articles on HPLC of PAHs dealt with factorial design [8–10] and simplex [8,11–13] methodology, while chemometric GC separations of PAHs were manly focused on Quantitative Structure–Retention Relationships (QSRRs) studies using multiple

* Corresponding author. Tel.: +381 11 2455 654; fax: +381 11 3422 900.
E-mail address: onjia@vin.bg.ac.yu (A. Onjia).

0039-9140/$ – see front matter © 2008 Elsevier B.V. All rights reserved.
doi:10.1016/j.talanta.2008.02.004

linear regression (MLR) [14–18] or artificial neural networks (ANNs) [19,20].

In the present work, the factorial design in conjunction with objective function (total resolution) analysis and computer simulation of chromatograms, so called the interpretative approach, was applied to study the retention behavior of 16 high priority PAH pollutants and to optimize their temperature-programmed GC separation. In addition, the retention modeling of PAHs by ANN was evaluated.

2. Experimental

All measurements were made using a Varian model 3400cx gas chromatograph coupled with Saturn 3 ion trap mass spectrometer and 8200cx autosampler. The initial column temperature of 50 °C was selected, while the linear temperature ramp and the final hold temperature was varied in the range 5–25 °C/min. and 260–320 °C, respectively. The injector and the transfer line were maintained at 260 and 220 °C, respectively. Helium was used as the carrier gas with a column head pressure of 12 psi. The mass spectrometer operated in EI ionization mode and all spectra were acquired using m/z 150–300 mass range and automatic gain control (AGC). The advantage of mass spectra in chromatographic retention studies is that they provide a reliable peak identification that is very critical when dealing with overlapped peaks and peak reversal phenomenon.

A certified mixture of 16 priority PAH pollutants (20 μg/ml each) from Ultra Scientific Inc. (North Kingstown, RI, USA) was diluted 10-fold with *n*-hexane to prepare a working mixture containing 2.0 ppm of each PAH. An aliquot of 1.0 μl was injected into a Varian FactorFour™ VF-5ms (5% phenyl–95% dimethylpolysiloxane) capillary column (30 m, 0.25 mm, 0.25 μm).

The retention time for each PAH was measured in duplicate using temperature programs with different linear ramp/hold temperature combinations. This data set was used to calibrate/train the retention or the ANN model, while unseen data for the temperature program for which the interpretative calculation gives good total resolution was used to test these models.

All calculations in interpretative strategy were made using a MathCAD 2001 software package (Mathsoft Inc., USA) with laboratory-written program. This program can simulate retention times of chromatographic runs by entering the retention times from three (for one variable) or nine (for two variables) actual injections. It enables a better visualization of the separation. Besides simulation, the program also calculates automatically the resolutions of all consecutive peaks, as well as the total resolution. It can also handle the peak reversal phenomenon during the calculation. Separately, the ANN systems were simulated using a QwikNet ANN simulator (Craig Jensen, Redmond, USA).

3. Results and discussion

3.1. Interpretative optimization

To study the GC separation of a mixture of PAHs, retention behavior of each PAH in the mixture has to be investigated. First step in interpretative optimization is the choice of a proper retention model. The model should provide adequate precision in estimation of the variable effect with a minimum of experiments. In general, there should be more experiments than variables. In temperature programmed GC, the most significant variable that influences the retention behavior is the temperature ramp [21]. By analogy with common retention models in gradient HPLC separation, the logarithm of the temperature ramp may be related to the logarithm of the retention factor. However, low volatile analytes often elute from the column after the column temperature increase finished. This elution requires the final hold temperature to be included in the retention model. Assuming higher order terms in the Taylor series approximation of the response function to be of lesser importance in the experimental domain [22], a quadratic function can be used in the retention model. For two variables, the form of this model can be written as

$$\log k = A + B \times (\log S_T) + C \times (\log T_F) + D \times (\log S_T)^2 + E \times (\log T_F)^2 + F \times (\log S_T) \times (\log T_F) \quad (1)$$

where k is the capacity factor, S_T is the temperature ramp (°C/min), T_F is the final hold temperature (°C), while A–E and F are the estimated model parameters for PAHs. If we assume that T_F is of minor influence on PAHs retentions, than the parameters C, E and F in Eq. (1) approach 0. The effect of T_F can surely be neglected for several early eluting PAHs, but it needs to be evaluated for strongly retained ones. The model parameters and the sum of squares of deviation (SSE) for each PAH (see Table 1) were estimated from the experimentally obtained retention times for: (a) nine S_T/T_F combinations in the two factor three level experimental domain (S_T = 5.0, 15.0, and 25.0 °C/min and T_F = 260, 290 and 320 °C) and (b) three temperature ramps (S_T = 5.0, 15.0, and 25.0 °C/min and T_F = 290 °C). In both cases, a non-linear regression fitting was employed for the parameter estimation.

It is obvious that the SSE values are much lower for one-variable model for which the fitting is more simple. In order to check the

Table 1
Estimated parameters in model equation and SSE for: (a) two-variable model; (b) one-variable model

Br.	PAHs	*A*		*B*		*C*	*D*		*E*	*F*	SSE × 10^4	
		(a)	(b)	(a)	(b)	(a)	(a)	(b)	(a)	(a)	(a)	(b)
1.	Naphthalene	1.121	0.990	−0.732	−0.573	−0.045	−0.109	0.081	−0.011	−0.008	86.1	0.09
2.	Acenaphthylene	1.169	1.235	−0.751	−0.693	−0.065	0.054	0.053	−0.014	−0.004	104	0.05
3.	Acenaphthene	1.177	1.323	−0.770	−0.880	−0.051	0.118	0.025	−0.009	−0.008	78.2	0.97
4.	Fluorene	1.251	1.451	−0.789	−0.946	−0.058	−0.127	0.039	−0.015	−0.011	136	0.66
5.	Phenanthrene	1.289	1.587	−0.808	−1.091	−0.061	0.116	0.011	−0.021	−0.007	79.2	0.96
6.	Anthracene	1.319	1.592	−0.827	−1.094	−0.063	0.118	0.005	−0.02	−0.009	37.1	0.52
7.	Fluoranthene	1.359	1.658	−0.846	−1.145	−0.027	0.138	0.020	−0.022	−0.010	27.3	6.38
8.	Pyrene	1.398	1.729	−0.865	−1.157	−0.047	0.145	0.036	−0.025	−0.013	24.5	0.31
9.	Chrysene	1.448	1.817	−0.884	−1.359	−0.087	0.249	0.051	−0.027	−0.016	21.8	0.07
10.	Benzo(*a*)anthracene	1.478	1.850	−0.903	−1.363	−0.092	0.252	0.067	−0.029	−0.011	22.3	0.79
11.	Benzo(*k*)fluoranthene	1.528	1.984	−0.922	−1.380	−0.108	0.337	0.082	−0.031	−0.012	35.2	2.32
12.	Benzo(*b*)fluoranthene	1.558	2.095	−0.941	−1.387	−0.177	0.339	0.085	−0.033	−0.021	30.8	1.37
13.	Benzo(*a*)pyrene	1.597	2.103	−0.961	−1.396	−0.379	0.355	0.113	−0.035	−0.026	29.7	0.96
14.	Indeno(1,2,3-*c*,*d*)pyrene	1.647	2.293	−0.979	−1.404	−0.441	0.377	0.129	−0.037	−0.033	18.4	1.09
15.	Dibenzo(*a*,*h*)anthracene	1.677	2.302	−0.998	−1.408	−0.471	0.375	0.144	−0.039	−0.046	91.5	2.11
16.	Benzo(*g*,*h*,*i*)perylene	1.717	2.360	−1.017	−1.425	−0.609	0.345	0.159	−0.041	−0.051	18.9	1.87

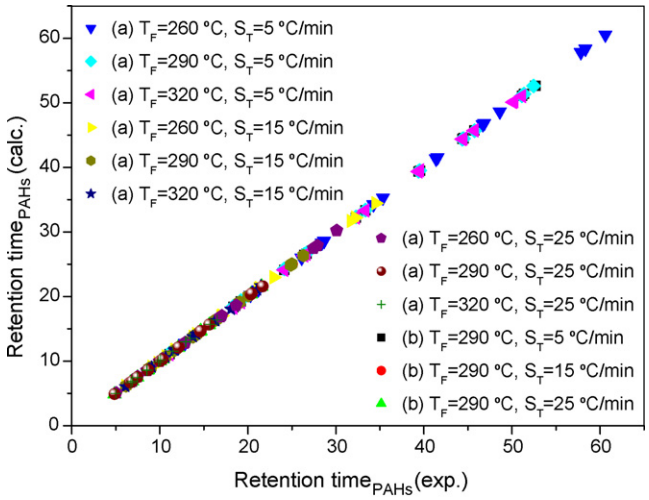

Fig. 1. Predicted (calc.) by the retention model and measured (exp.) GC retention times (min) of PAHs for: (a) two-variable model; (b) one-variable model.

retention model, estimated and experimentally obtained retention times using these temperature programs were compared (see Fig. 1). One can see a rather good agreement between these retention data.

The major step in chromatographic separation study is the selection of an appropriate response function, and it depends on the overall goal of the separation. In practical applications, a compromise has to be made between the quality of separation and the analysis time. Here, the normalized resolution product criterion [23,24] was chosen to quantify numerically the chromatograms. This is a global separation criterion with which all peaks of interest are considered. Namely, it quantifies the global resolution taking into account not only the resolution of peak pairs but also the total analysis time, i.e. spacing of peaks.

The normalized resolution product (r) is calculated from the expression:

$$r = \prod_{i=1}^{n-1} \left\{ \frac{R_{Si,i+1}}{\left[(n-1)^{-1} \sum_{i=1}^{n-1} R_{Si,i+1} \right]} \right\} \quad (2)$$

where n is the number of peaks and $R_{Si,i+1}$ is the resolution between the peaks i and $i+1$. This criterion gives a zero value to a chromatogram that has at least one peak fully overlapped, and one for the chromatogram with evenly spaced peaks. Using this expression, the resolution product as a function of temperature program for all PAHs was calculated and presented in Fig. 2.

Both the resolution surface (Fig. 2a) and line (Fig. 2b) show a strong influence of S_T on the resolution product. In both cases, linear S_T of 8.0 °C/min was selected as the optimum one with maximum value of the resolution product. At this S_T, for which the retention times are not excessively long, the separation of PAHs is acceptable.

The final hold temperature, T_F, however, has a much smaller effect on the resolution. Any T_F in the studied range may be selected for this separation. In order to test the prediction power of the interpretative model, we selected T_F of 290 and 275 °C, for one- and two-variable model, respectively. By keeping relatively high T_F, the elution of other strongly retained analytes commonly present in real samples is made possible.

It should be pointed out that the resolution surface and the curve in Fig. 2 might be different for different chromatographic systems. How these shapes will look depends on the analytes chromatographed as well as on the chromatographic column used. It means that the optimum S_T and T_F may change if we add or omit

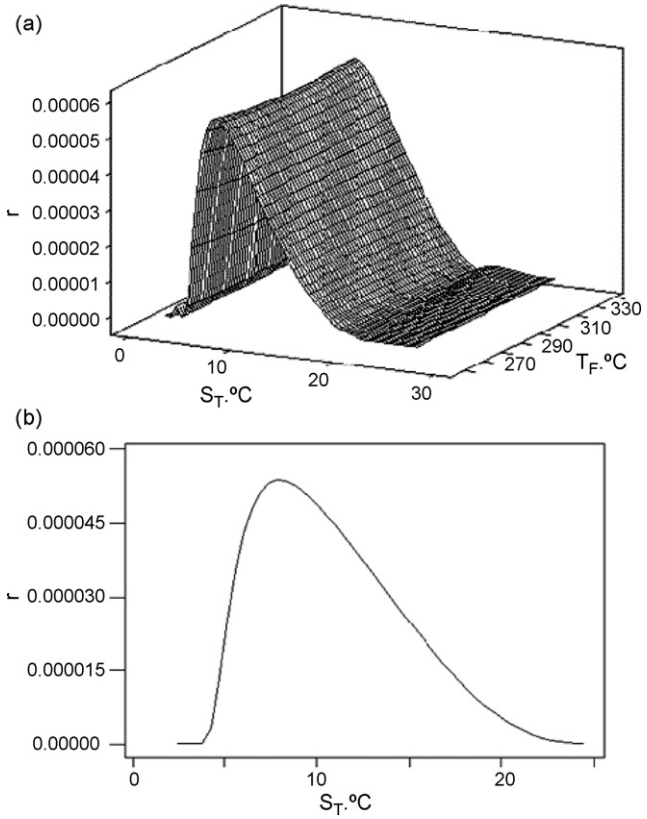

Fig. 2. Resolution product for 16 PAHs as a function of: (a) linear temperature ramp and final hold temperature; (b) linear temperature ramp.

some PAHs or change the column. For this study we chose a general-purpose column, which is not the best one for the GC separation of PAHs. The main goal was to develop the interpretative approach for difficult, i.e. non-ideal, chromatographic conditions.

The next step in the interpretative approach is the simulation of chromatograms. This approach enables the calculation of a chromatogram for any point on the surface (Fig. 2a) and the curve (Fig. 2b). Among several mathematical functions for the representation of chromatographic peaks [25], the Exponentially Modified Gaussian (EMG) equation was chosen in this study to simulate peaks of both fronted and tailed shapes.

Fig. 3 illustrates experimentally obtained and calculated chromatograms for GC run at selected S_T of 8.0 °C/min and T_F of 275 and 290 °C. It can be seen that the predicted retention times are satisfactorily close to the measured ones. The dotted line represents a chromatogram estimated from two-variable model with a fixed T_F of 275 °C. Since no significant deviation in estimated peak positions for most PAHs whether we use T_F = 275 °C or T_F = 290 °C has been observed, the role of T_F in this modeling may be neglected.

A characteristic baseline increase with temperature can be noticed on the chromatogram (II) (Fig. 3). In order to take into account this common phenomenon in temperature programmed GC, further modification of equation for the chromatogram simulation is needed.

3.2. Artificial neural networks

Out of several systematic approaches to GC retention modeling, only artificial neural networks (ANNs) offer the possibility to model the retention with no prior knowledge of the separation mechanism. The theory behind ANNs and their use in chromatography has been described elsewhere [19,20,26–30]. Here, ANN was employed

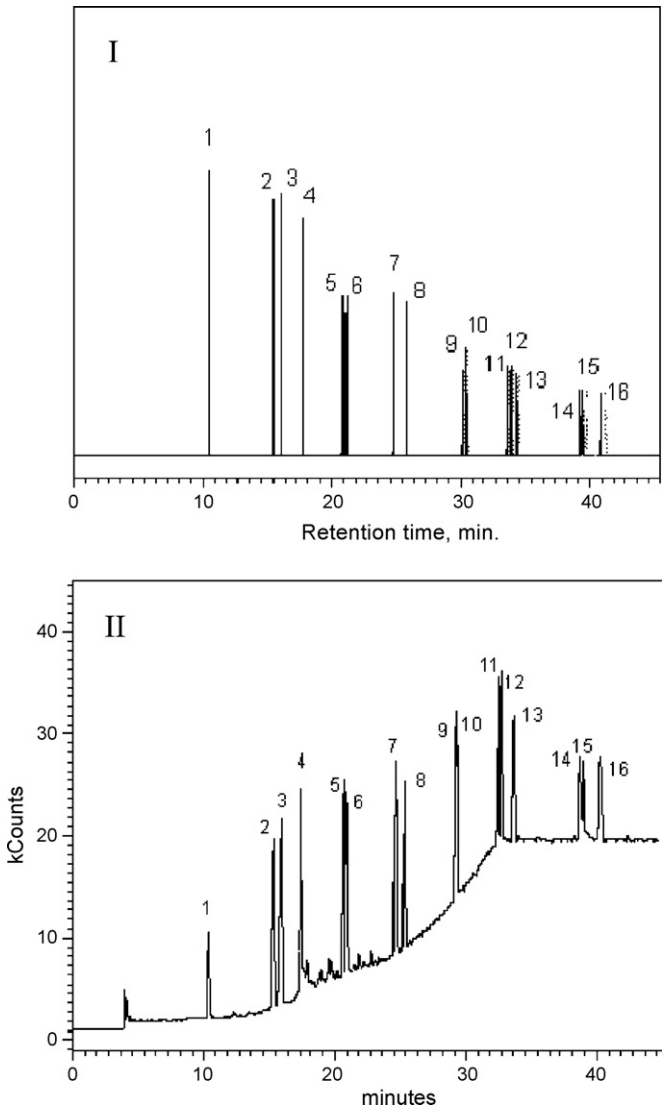

Fig. 3. Chromatograms of 16 PAHs for linear temperature ramp of 8.0 °C/min and (I) calculated for one variable (T_F = 290 °C, solid line) and two variables (T_F = 275 °C, dotted line); (II) measured (T_F = 275 °C). PAHs identities as in Table 1.

to study the effect of changing of GC temperature program, i.e. S_T and T_F, on retention times of 16 PAHs.

The topological structure of the ANN employed in this study consists of three layers: an input layer with one or two nodes (S_T or $S_T + T_F$), output layer with 16 nodes (PAH retention times), and a hidden layer with the number of nodes to be optimized. To find the best ANN parameters, a trial and error approach has been used. The employed root mean square (RMS) error function was computed with the following formula:

$$\text{RMS error} = \frac{\left[\sum_{i=1}^{n}(d_i - o_i)/n\right]^{1/2}}{x} \quad (3)$$

where d_i is the desired output, o_i is the actual output, n is the number of retention time data, and x is the average value of desired outputs in the testing set. Details on applied ANN algorithm and training method were given elsewhere [19,20,27].

Fig. 4a shows a curve of the RMS error of the training set versus the number of hidden layer nodes. The optimum number of hidden

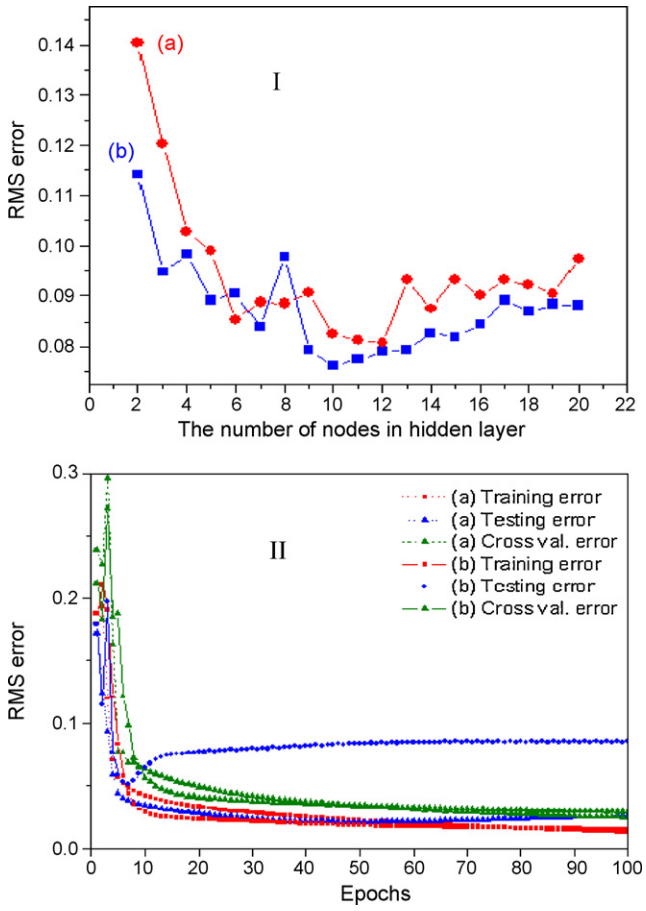

Fig. 4. RMS error vs. (I) hidden node number; (II) training epochs for: (a) two-variable ANN model and (b) one-variable ANN model.

layer nodes was found to be 10 for ANN with one input node and 12 for ANN with two input nodes. To illustrate the learning process, the curves of RMS error values of training, cross-validation, and testing set versus learning epochs for the optimum number of hidden layer nodes are shown in Fig. 4b. For one-variable model, the minimum average RMS error value for the testing set is 0.05 and was reached after seven epochs, while ANN converges slower (60 epochs) and RMS error value of 0.02 for two-variable model was obtained.

It was reported [27,26] that the size of the experimental data set used for the ANN training had a significant influence on the ANN accuracy. The more input data points, the more prediction power an ANN model can get. However, a reduction in the number of experiments is crucial for the development of the ANN model in a time-saving way. For that reason it is important to determine the optimal number of input chromatographic runs to be used for the training set. Fig. 5 shows the influence of the number of levels in the experimental design on the RMS error. It can be seen that that a more evenly (and in more detail) covered experimental domain is needed to get a well-trained ANN. For further ANN evaluation, five points in one-variable and 25 points in two-variable modeling were used. It means that the ANNs were trained using five-level experimental designs.

3.3. Comparison of ANN and interpretative strategy

The retention and the trained ANN models were used to predict the retention data for 16 PAHs at optimum S_T of 8.0 °C/min and T_F of 290 and 275 °C for one- and two-variable modeling, respectively. These optima were previously estimated by interpretative

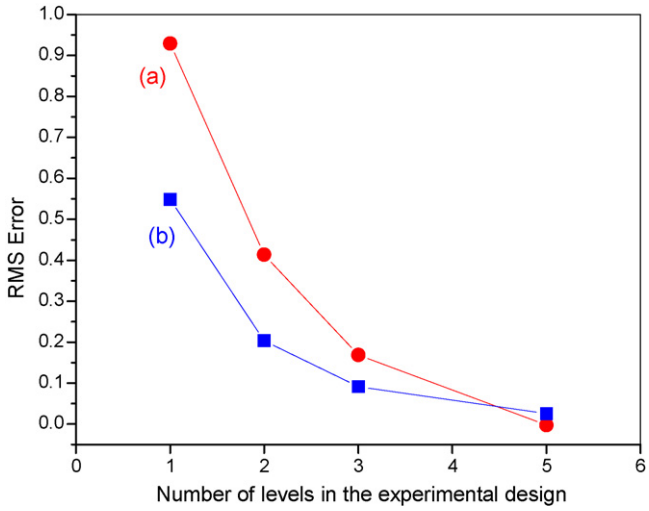

Fig. 5. Average RMS error vs. number of levels in the experimental design for: (a) two variables ANN model; (b) one-variable ANN model.

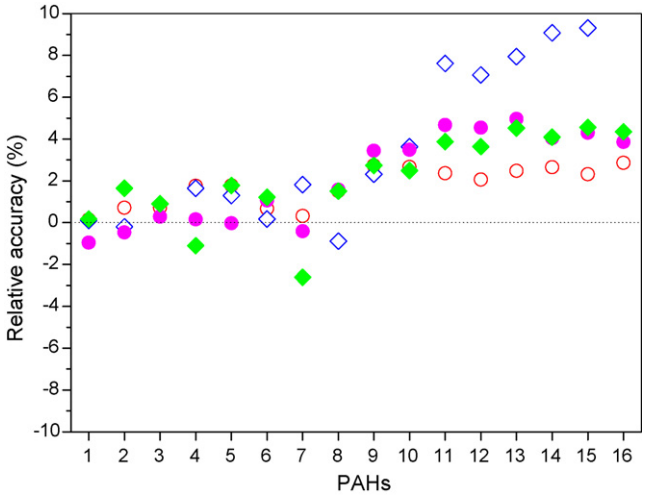

Fig. 6. Relative accuracy as a degree of agreement between the measured and the predicted retention times (S_T = 8.0 °C/min) for 16 PAHs for: (●) two variables interpretative model (T_F = 275 °C); (○) one-variable interpretative model (T_F = 290 °C); (◆) two variables ANN model (T_F = 275 °C); (◇) one variable ANN model (T_F = 290 °C). PAHs identities as in Tables 1 and 2.

approach. It should be stressed that the measured retention data for these optimal temperature programs were included neither in the ANN training data set nor in the retention model calibration data set. Having in mind that the ANN prediction power is strongly affected by the number of input experiments, we applied five-level experimental design for ANN training. The predicted retention data and the experimentally obtained ones were compared (see Table 2).

A quantitative comparison between the observed and the predicted retentions for the linear S_T of 8.0 °C/min and T_F of 290 and 275 °C is also illustrated in Fig. 6. For two-input variable models, the average absolute magnitude of the difference between the measured and the calculated values for most PAHs is generally within 5%. This percentage approaches the magnitude of the experimental precision. The interpretative approach gives even better results (3%) with one input variable, while the prediction power of ANN with one input node is somewhat lower for the late-eluting PAHs.

The greater difference between predicted and experimentally obtained retention times for strongly retained PAHs in one-variable ANN model can be ascribed to their elution during the isothermal hold at the end of the temperature program. This phenomenon diminishes the role of GC temperature ramp and causes wrong input to both the retention and ANN model. In general, the retention model seems to be more robust and as such can more easily cope with this problem. This problem is fixed by including a second variable, i.e. the final-hold temperature, in the ANN model.

4. Conclusion

A good agreement between the obtained and the calculated values of retention times for 16 PAHs indicates that the optimization of their GC separation can be performed in a fast and accurate way by using both the interpretative and the ANN modeling. The interpretative approach can be readily applied to predict the retention behavior of PAHs in temperature-programmed GC as a function of linear temperature ramp only, while ANN needs an additional input variable, i.e. final hold temperature. The advantages of the ANN model over numerical ones are very fast optimization, no need for a mathematical form of the relationship between input and output data, and the analyst can be unfamiliar with the analyte GC retention. These advantages are particularly

Table 2
Predicted and measured GC retention times (min) of PAHs at optimum temperature ramp (8.0 °C/min) for: (a) two-variable models (T_F = 275 °C); (b) one-variable models (T_F = 290 °C)

Br.	PAHs	(a)			(b)		
		Exp. values	Interp. model	ANN model	Exp. values	Interp. model	ANN model
1.	Naphthalene	10.426	10.327	10.444	10.425	10.441	10.437
2.	Acenaphthylene	15.393	15.322	15.647	15.391	15.502	15.360
3.	Acenaphthene	15.960	16.007	16.106	15.959	16.075	16.101
4.	Fluorene	17.469	17.498	17.277	17.469	17.776	17.757
5.	Phenanthrene	20.602	20.597	20.969	20.603	20.972	20.870
6.	Anthracene	20.976	21.201	21.233	20.977	21.118	21.012
7.	Fluoranthene	24.676	24.576	24.032	24.676	24.758	25.125
8.	Pyrene	25.429	25.831	25.812	25.428	25.814	25.203
9.	Chrysene	29.204	30.210	30.003	29.202	30.001	29.880
10.	Benzo(*a*)anthracene	29.393	30.420	30.126	29.390	30.174	30.457
11.	Benzo(*k*)fluoranthene	32.582	34.104	33.846	32.532	33.302	35.012
12.	Benzo(*b*)fluoranthene	32.805	34.298	33.998	32.782	33.461	35.097
13.	Benzo(*a*)pyrene	33.993	35.683	35.528	33.843	34.683	36.533
14.	Indeno(1,2,3-*c*,*d*)pyrene	39.801	41.415	41.432	38.789	39.822	42.311
15.	Dibenzo(*a*,*h*)anthracene	39.976	41.694	41.800	39.040	39.944	42.675
16.	Benzo(*g*,*h*,*i*)perylene	41.349	42.945	43.147	40.293	41.450	44.575

significant in GC analysis of a large number of analytes. However, ANN needs more experimental input points than the interpretative method and is more difficult to interface online to the total resolution analysis. The latter is particularly straightforward in GC optimization.

Acknowledgment

The authors gratefully acknowledge financial support of the Ministry of Science of the Republic of Serbia (Project No. ON142039).

References

[1] R.G. Harvey, Polycyclic Aromatic Hydrocarbons: Chemistry and Carcinogenicity, Cambridge University Press, Cambridge, 1991.
[2] J.C. Fetzer, Polycyclic Aromatic Hydrocarbons Chemistry and Analysis, vol. 158, in: J.D. Winefordner, Series Editor, Chemical Analysis: A Series of Monographs on Analytical Chemistry and its Applications, Wiley Interscience, 2000, pp. 163–204.
[3] C.D. Simpson, W.R. Cullen, K.B. Quinlan, K.J. Reimer, Chemosphere 31 (1995) 4143.
[4] M. Àngels Olivella, Talanta 69 (2006) 267.
[5] J.L. Capelo, M.M. Galesio, G.M. Felisberto, C. Vaz, J. Costa Pessoa, Talanta 66 (2005) 1272.
[6] O. Delhomme, M. Millet, P. Herckes, Talanta 74 (2008) 703.
[7] K. Jinno, Y. Saito, R.M. née Chopra, J.J. Pesek, J.C. Fetzer, W.B. Biggs, J. Chromatogr. 557 (1991) 459.
[8] A.M. Siouffi, R. Phan-Tan-Luu, J. Chromatogr. A 892 (2000) 75.
[9] A.M. Dorthe, J.L. Ramberti, A. Thienpont, Analusis 28 (2000) 587.
[10] W.G. Lan, K.K. Chee, M.K. Wong, H.K. Lee, Y.M. Sin, Analyst 120 (1995) 281.
[11] P. Araujo, Trends Anal. Chem. 19 (2000) 524.
[12] R.W. Fedeniuk, S. Ramamurthi, A.R. McCurdy, J. Chromatogr. B 677 (1996) 291.
[13] N. Kuppithayanant, M. Rayanakorn, S. Wongpornchai, T. Prapamontol, R.L. Deming, Talanta 61 (2003) 879.
[14] S. Liu, C. Yin, S. Cai, Z. Li, Chem. Intell. Lab. Syst. 61 (2002) 3.
[15] E.R. Collantes, W. Tong, W.J. Welsh, W.L. Zielinski, Anal. Chem. 68 (1996) 2038.
[16] J. Kang, C. Cao, Z. Li, J. Chromatogr. A 799 (1998) 361.
[17] J.R. Wilmhust, J. Chromatogr. 17 (1965) 50.
[18] R. Kaliszan, H. Lamparczyk, J. Chromatogr. Sci. 16 (1978) 246.
[19] S. Sremac, B. Škrbić, A. Onjia, J. Serb. Chem. Soc. 70 (2005) 1301.
[20] B. Škrbić, A. Onjia, J. Chromatogr. A 1108 (2006) 279.
[21] T.C. Gerbino, G. Castello, U. Pettinati, J. Chromatogr. 634 (1993) 338.
[22] S.L. Morgan, S.N. Deming, J. Chromatogr. 112 (1983) 267.
[23] P. Haddad, A. Drouen, H. Billiet, L. De Galan, J. Chromatogr. 282 (1983) 71.
[24] A. Onjia, T. Vasiljević, Đ. Čokeša, M. Laušević, J. Serb. Chem. Soc. 67 (2002) 745.
[25] V.B. Di Marco, G.G. Bombi, J. Chromatogr. A 931 (2001) 1.
[26] S. Dragović, A. Onjia, S. Stanković, I. Aničin, G. Bačić, Nucl. Inst. Method Phys. Res. A 540 (2005) 455.
[27] T. Vasiljević, A. Onjia, Dj. Čokeša, M. Laušević, Talanta 64 (2004) 785.
[28] S. Agatonović-Kuštrin, M. Zečević, Lj. Živanović, I. Tucker, Anal. Chim. Acta 364 (1998) 265.
[29] R. Zhang, A. Yan, M. Liu, H. Liu, Z. Hu, Chem. Intell. Lab. Syst. 45 (1999) 113.
[30] M.H. Fatemi, J. Chromatogr. A 955 (2002) 273.

Talanta 76 (2008) 116–121

Contents lists available at ScienceDirect

Talanta

journal homepage: www.elsevier.com/locate/talanta

Electrochemical study of the interaction between dsDNA and copper(I) using carbon paste and hanging mercury drop electrode

Z. Stanić[b], S. Girousi[a,*]

[a] Laboratory of Analytical Chemistry, Department of Chemistry, Aristotle University, Thessaloniki 54124, Greece
[b] Department of Chemistry, Faculty of Sciences, University of Kragujevac, R.Domanović 12, P.O. Box 60, 34000 Kragujevac, Serbia

ARTICLE INFO

Article history:
Received 14 November 2007
Received in revised form 6 February 2008
Accepted 14 February 2008
Available online 26 February 2008

Keywords:
Copper(I)
DNA interaction
Carbon paste electrode
Hanging mercury drop electrode

ABSTRACT

The interaction of copper(I) with double-stranded (ds) calf thymus DNA was studied in solution and at the electrode surface by means of transfer voltammetry using a carbon paste electrode (CPE) as working electrode in 0.2 M acetate buffer solution (pH 5.0). As a result of the interaction of Cu(I) between the base pairs of the dsDNA, the characteristic peaks of dsDNA, due to the oxidation of guanine and adenine, increased and after a certain concentration of Cu(I) a new peak at +1.37 V appeared, probably due to the formation of a purine–Cu(I) complex (dsDNA–Cu(I) complex).

Accordingly, the interaction of copper(I) with calf thymus dsDNA was studied in solution as well as at the electrode surface using hanging mercury drop electrode (HMDE) by means of alternating current voltammetry (AC voltammetry) in 0.3 M NaCl and 50 mM sodium phosphate buffer (pH 8.5) as supporting electrolyte. Its interaction with DNA is shown to be time dependent. Significant changes in the characteristic peaks of dsDNA were observed after addition of higher concentration of Cu(I) to a solution containing dsDNA, as a result of the interaction between Cu(I) and dsDNA.

All the experimental results indicate that Cu(I) can bind to DNA by electrostatic binding and form an association complex.

1. Introduction

More than 20 years ago it was shown that the nucleic acid bases and some other purine and pyrimidine derivatives can be determined at nanomolar concentrations by cathodic stripping voltammetry (CSV) [1,2]. Then, Glodowski et al. [3] found that sparingly soluble compounds of copper(I) with adenine (A) and adenosine can be accumulated at the electrode surface either by reduction of copper(II) ions or by oxidation of the copper liquid amalgam electrode. The copper(I)/adenine deposit can be stripped either anodically or cathodically with detection limits 20 and 5 nM, respectively. Shiraishi and Takahashi [4] accumulated copper(I) compounds of adenine and guanine at carbon electrodes to determine the bases by anodic stripping voltammetry. Electrochemical methods were applied in studies of interactions of nucleic acid monomeric constituents with copper [1–4]. Farias et al. [5] used the hanging mercury drop electrode (HMDE) to determine low concentrations of adenine in the presence of copper.

The reactivity and damage to deoxyribonucleic acid (DNA) are of importance from both chemical and medical points of view. Oxidative DNA damage by active oxygen species plays a critical role in several biological processes including mutagenesis, carcinogenesis and ageing [6–8]. When some kinds of metal complexes interacted with DNA, they could induce the breakage of DNA strands. Metal chelates with heterocyclic ligands such as 1,10-phenanthroline (phen) and 2,2′-bipyridyl (bpy) were studied as DNA probes [9–12]. A number of copper complexes that can be used for inducing the lesion of double-stranded DNA has been developed [13–17] since the chemical nuclease activity of copper–phenanthroline complex was discovered in the 1980's [18–20]. In the investigation of DNA damage or cleavage, a great deal of works was performed by metal ion or its complexes-mediate strand cleavage [21–23]. Some strong reductive agents such as ascorbate, GSH, NADH or phenolic compounds [24,25] as the inducing agents of producing a radical were required to be added into system of DNA cleavage reaction. Ueda et al. [26] investigated that $Cu(phen)_2^{2+}$ could cleave DNA in the presence of ascorbate or hydroquinone and $Cu(en)_2^{2+}$ complexes also could cleave DNA in the presence of ascorbate, but $Cu(en)_2^{2+}$ could not cleave DNA in the presence of hydroquinone. It was suggested the reductive capability of the reductants had critical influence on DNA cleavage. Rodriguez et al. [27] studied nicking

* Corresponding author. Tel.: +30 2310 997722; fax: +30 2310 997719.
E-mail address: girousi@chem.auth.gr (S. Girousi).

0039-9140/$ – see front matter © 2008 Elsevier B.V. All rights reserved.
doi:10.1016/j.talanta.2008.02.017

of supercoiled (sc) DNA by oxygen reduction at electrode in the presence of transition metals, observing potential-modulated DNA cleavage during electrolysis of aerobic DNA solution (detected by gel electrophoresis). Fojta et al. [28] showed that redox processes involved in DNA damage could be controlled by the potential of scDNA-modified HMDE. Using this approach, the scDNA-modified electrode is capable not only to detect chemical or biochemical DNA/cleavage agents, but also to modulate the DNA cleavage by generating the DNA damage species electrochemically. This method has been paid much attention because its system of DNA cleavage reaction is simple, and the cleavage efficiency is very high.

In this study, we used the DNA-modified carbon paste electrode (CPE) in combination with cyclic voltammetry (CV) and especially differential pulse voltammetry (DPV) to obtain information about the interaction of Cu(I) with double-stranded DNA. This cleavage and, also, the changes in the experimental parameters (the concentration of Cu(I), the incubation time of Cu(I)) were studied by using DPV. Using this method, it needs no extra agents to produce electron transfer, which makes the system simple and some chemical interference factors are excluded. Furthermore, the present work reports the voltammetric behavior of dsDNA in the presence of Cu(I) using hanging mercury drop electrode and alternating current voltammetry.

2. Experimental

2.1. Reagents

Double-stranded (ds) calf thymus DNA (D-1501, highly polymerized) was purchased from Sigma. Copper standard solution was prepared by dissolving CuCl in hydrochloric acid, purchased from Merck. The working solutions of copper(I) were prepared by dilution of the standard solution with doubly distilled water.

The supporting electrolyte used to perform the differential pulse voltammetric experiments was acetate buffer solution 0.2 M (pH 5.0), while the one used to perform the alternating current voltammetric experiments was 0.3 M NaCl, 50 mM sodium phosphate buffer (pH 8.5).

For the study of the electrochemical behaviour of dsDNA on the CPE surface, the stock solutions (0.14 g L^{-1}) was prepared in 10 mM Tris–HCl and 1 mM EDTA at pH 8.0, while for the electrochemical behavior on the HMDE the stock solution of dsDNA (0.08 g L^{-1}) was prepared in 10 mM Tris–HCl at pH 7.5 [29].

Ultra pure argon was used to bubble the solutions of dissolved oxygen for 1 min before each experiment.

2.2. Apparatus

Differential pulse and alternating current voltammetric measurements were performed with a PalmSens potensiostat purchased from IVIUM Technologies (The Netherlands, www.ivium.nl) and PalmSensPC software. The working electrode for the differential pulse voltammetric measurements was a carbon paste electrode of 6 mm diameter, the reference electrode was a saturated Ag/AgCl and the counter electrode was a platinum wire electrode, while the working electrode for the alternating current voltammetric measurements was a hanging mercury drop electrode.

2.3. Preparation of working electrodes

2.3.1. Carbon paste electrode

The carbon paste was prepared in the usual way by hand-mixing graphite powder and nujol oil. The ratio of graphite powder to nujol oil was 75:25. The resulting paste was packed tightly into a PTFE sleeve. Electrical contact was established with stainless steel screw. The surface was polished to a smooth finish before use. The electrode was pre-treated by applying a potential at +1.7 V for 1 min without stirring prior to the accumulation step. The electrochemical pre-treatment produces a more hydrophilic surface state and a concomitant removal of organic layers [30].

2.3.2. Hanging mercury drop electrode

(a) dsDNA was adsorbed at the electrode surface from 10 μL of 0.08 g L^{-1} dsDNA solution containing 10 mM Tris–HCl, pH 7.5 for 120 s.
(b) dsDNA (0.08 g L^{-1}) was incubated with varying concentrations of Cu(I) for 25 min prior to immobilization at the electrode surface. The electrode was immersed into 10 μL of the previously mentioned solution for 120 s.

3. Procedures

3.1. Interaction of surface-confined dsDNA with Cu(I) on the CPE surface

The procedure consists of DNA immobilization, interaction of Cu(I) with immobilized DNA and measurement of the peak current, by transfer voltammetry, using differential pulse as the stripping mode. Prior to each medium exchange, the electrode was rinsed carefully with water for 5 s. After the pretreatment of the CPE, as previously described, the nucleic acid was subsequently immobilized onto the activated electrode surface by adsorptive accumulation for 5 min at +0.5 V. The dsDNA-coated electrode was transferred to the stirred sample solution (analyte and 0.2 M acetate buffer solution, pH 5.0) for 6 min. The modified electrode was then removed from the solution and washed twice with doubly distilled water and with the background electrolyte solution. The washed electrode was then placed into a voltammetric cell. The measurement was carried out in the background electrolyte, blank acetate buffer solution, with an initial potential of +0.1 V. The conditions were E_{step} = 0.005 V, E_{pulse} = 0.025 V and scan rate = 0.050 V s^{-1}.

3.2. Treatment of dsDNA with Cu(I) in solution and immobilization on the CPE surface

The analysis of solution-phase DNA with Cu(I) consisted of mixing the two components, followed by accumulation and measurement of the peak current, by transfer voltammetry, using differential pulse as the stripping mode. The electrode was rinsed for 5 s prior to each medium exchange. Stock DNA (0.14 g L^{-1}) and Cu(I) solutions were added to 0.2 M acetate buffer to produce the required concentrations and the mixture was left to stand for 10 min. A freshly polished and pretreated carbon paste surface was immersed into the solution. The accumulation of the mixture was performed by applying a potential of +0.5 V for 5 min. The modified electrode was then removed from the solution and washed twice with doubly distilled water and with the background electrolyte solution. The metal tightly bound to DNA remains at the electrode, while the rest of Cu(I) is washed away. The washed electrode was then placed into a voltammetric cell. The measurement was carried out in the blank acetate buffer solution, with an initial potential of +0.1 V. The conditions were E_{step} = 0.005 V, E_{pulse} = 0.025 V and scan rate = 0.050 V s^{-1}.

3.3. Interaction of surface-confined dsDNA with Cu(I) on the HMDE surface

The mercury electrode saturated by the adsorbed DNA (dsDNA was adsorbed at the electrode surface from 10 μL of 0.08 g L^{-1}

dsDNA solution in 10 mM Tris–HCl, pH 7.5 for 120 s). The dsDNA-coated electrode was transferred to the stirred sample solution (analyte and 0.05 M phosphate buffer solution, pH 8.5). The modified electrode was then removed from the solution and washed twice with doubly-distilled water and with the background electrolyte solution. Argon was passed through both media during the wash procedures. The washed electrode was then placed into a voltammetric cell. Argon was bubbled through the solution for 60 s. The measurement was carried out in the blank, previously deoxygenated, supporting electrolyte with an initial potential of −0.1 V, a scan rate of 0.020 V s^{-1}, a frequency of 230 Hz, and peak amplitude of 10 mV.

3.4. Treatment of DNA with Cu(I) in solution and immobilization on the HMDE surface

dsDNA (0.08 g/L) was incubated with Cu(I) at different concentrations for 25 min prior to adsorption at the electrode surface. Ten microliters of the solution was adsorbed at the surface of the mercury electrode for 120 s and the purine base residue–Cu(I) complex (dsDNA–Cu(I) complex) was accumulated at the electrode surface [31]. The modified electrode was washed twice by doubly distilled water and once more by the solution containing the supporting electrolyte. This electrode was then immersed into the blank supporting electrolyte which was previously deareated with argon. The measurement was carried out with an initial potential of −0.1 V, a scan rate of 0.020 V s^{-1}, a frequency of 230 Hz, and peak amplitude of 10 mV.

4. Results and discussion

4.1. Study of the interaction between DNA and Cu(I) using a carbon paste electrode

For our studies we used 0.2 M sodium acetate buffer (pH 5.0) as a background electrolyte. Native double-stranded DNA, dsDNA, yielded two positive peaks, one peak at +0.98 V and another one at +1.25 V. The first peak corresponds to the oxidation of the guanine (G) residues and the second one corresponds to the oxidation of adenine (A) residues [32]. The nature of these peaks at the above conditions were studied elsewhere [33].

A cyclic voltammogram in a 1.0×10^{-4} M Cu(I) solution was recorded at a carbon paste working electrode in 0.2 M sodium acetate buffer pH 5.0, at scan rate of 100 mV s^{-1} is displayed in Fig. 1.

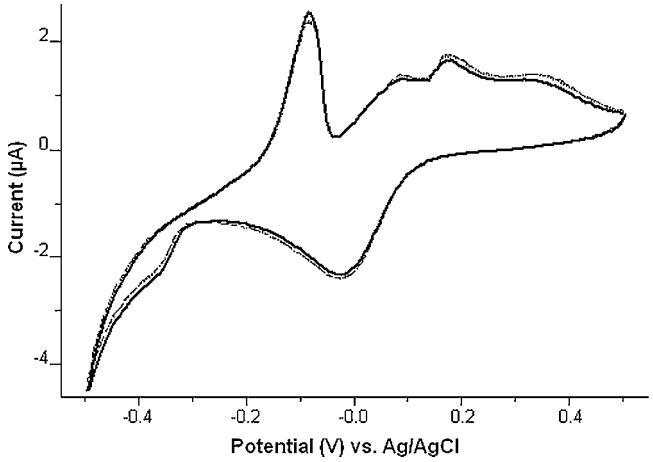

Fig. 1. Cyclic voltammogram of Cu(I) ($c = 1.0 \times 10^{-4}$ M) using CPE, scan rate = 100 mV s^{-1}, E_{step} = 0.005 V, and 0.2 M sodium acetate buffer + 20 mM NaCl pH 5.0 as electrolyte.

Table 1
The effect of interaction time between the immobilized dsDNA (0.14 g L^{-1}) and a constant concentration of Cu(I) (1.89×10^{-6} M) into the solution at pH 5.0

Interaction time (s)	*I* (nA) dsDNA peak at +0.98 V	*I* (nA) dsDNA peak at +1.25 V	*I* (nA) a new peak at +1.37 V
0	193	201	–
120	325	269	–
240	441	352	43
300	499	382	68
360	547	398	135
480	504	328	81
600	488	262	52

As it can be seen, a well-defined oxidation peak at about −0.08 V appeared and the cathodic peak can be observed at −0.02 V.

4.1.1. Interaction of surface-confined dsDNA with a solution of Cu(I)

The DNA-modified electrode was prepared by immersing the CPE in a solution of dsDNA at a concentration of 0.14 g L^{-1} in 0.2 M sodium acetate buffer, pH 5.0, as previously described. The electrode was washed and subsequently immersed into Cu(I) solutions of concentrations ranging from 9.95×10^{-10} to 1.10×10^{-5} M (in 0.2 M sodium acetate buffer, pH 5.0).

Differential pulse voltammograms were recorded after the transfer of the electrode into a blank background electrolyte. The selection of the interaction time was made according to the potential changes of the characteristic oxidation peaks of DNA and the appearance of a new peak probably due to the formation of a complex between Cu(I) and DNA. Table 1 indicates the changes of the peak current of the guanine and adenine residues, while the concentration of Cu(I) was constant at 1.89×10^{-6} M. The optimal interaction time was selected to be 6 min.

Fig. 2 shows the dependence of the peak current of the three peaks in relation to increasing concentrations of Cu(I). The interaction at pH 5.0 is very strong, the characteristic peaks of dsDNA are gradually increased and a new peak appears at +1.37 V (Fig. 3), when the concentration of Cu(I) became 1.1×10^{-7} M.

4.1.2. Interaction between dsDNA and Cu(I) in solution

The incubation time of the two components is a very important factor affecting the DPV response. Figs. 4 and 5 show the effect of the incubation time of Cu(I) at a constant concentration of 2.51×10^{-6} M and dsDNA (0.14 g L^{-1}) in solution, namely that the current response increased at the beginning, and later slowly decreased with increasing incubation time. The time selected was

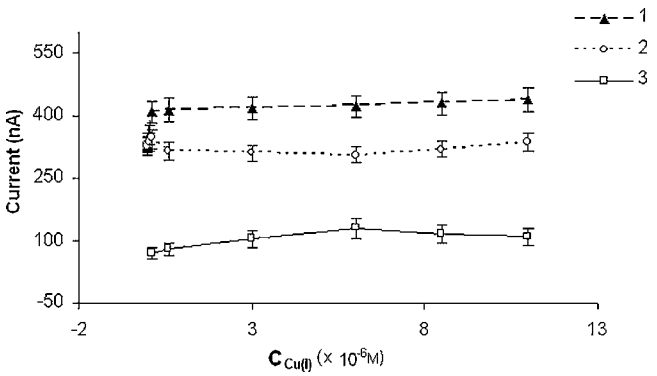

Fig. 2. Dependence of peak oxidation current for (1) guanine and (2) adenine residues in dsDNA immobilized on the electrode surface on increasing concentrations of Cu(I). (3) Dependence of peak current of dsDNA–Cu(I) complex on concentration of Cu(I) in the solution. Error bars show standard deviations for three trials. Other conditions as described in the experimental part.

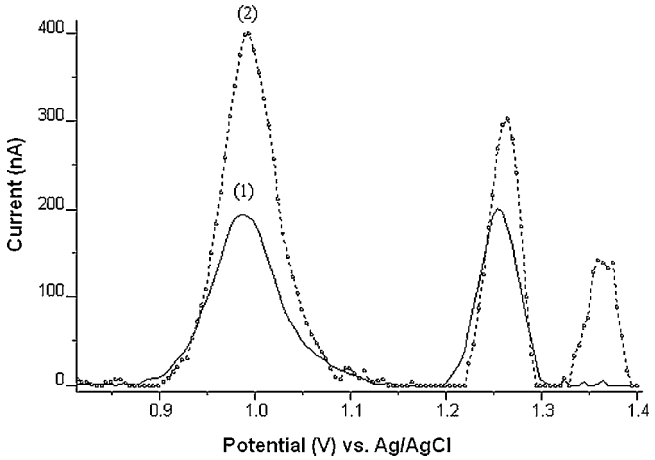

Fig. 3. Differential pulse voltammogram of: (1) dsDNA (0.14 g L^{-1}) immobilized on the CPE surface at pH 5.0 and (2) surface confined dsDNA (0.14 g L^{-1}) and Cu(I) (1.10×10^{-6} M) in solution where a new peak at +1.37 V appears, probably due to the formation of a complex.

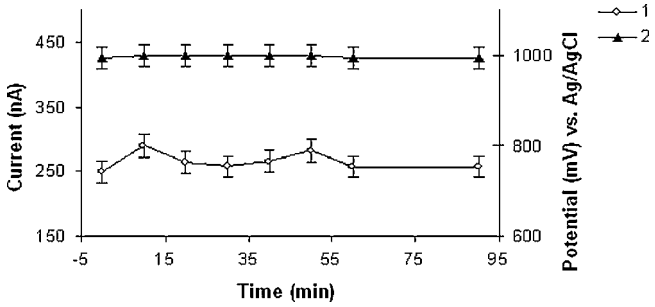

Fig. 4. (1) Dependence of peak oxidation current for guanine residues in dsDNA in solution with a constant concentration of Cu(I) (2.51×10^{-6} M) on the incubation time in the relation to the potential (left scale). (2) Dependence of the oxidation potential on the incubation time under the above conditions (right scale).

10 min, since no dramatic change in the peak current occurs after this point.

A solution of 0.14 g L^{-1} double-stranded DNA solution was left to react for 10 min with different concentrations of Cu(I) ranging from 5.0×10^{-7} to 1.1×10^{-5} M. The peak current due to the oxidation of guanine and adenine residues gradually increased with increasing concentrations of Cu(I). In Fig. 6 are presented the differentiations at the peak current of both peaks of dsDNA in relation to increasing concentrations of Cu(I) after incubation in solution.

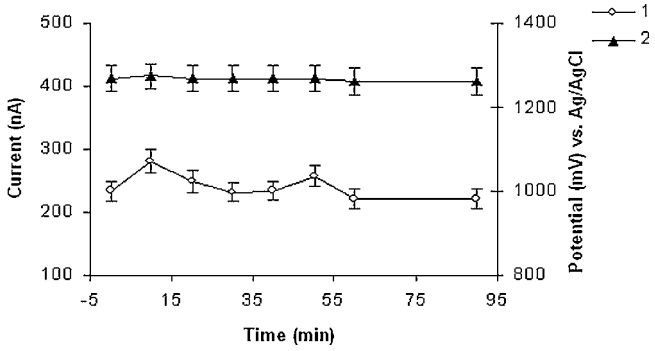

Fig. 5. (1) Dependence of peak oxidation current for adenine residues in dsDNA in solution with a constant concentration of Cu(I) (2.51×10^{-6} M) on the incubation time in the relation to the potential (left scale). (2) Dependence of the oxidation potential on the incubation time under the above conditions (right scale).

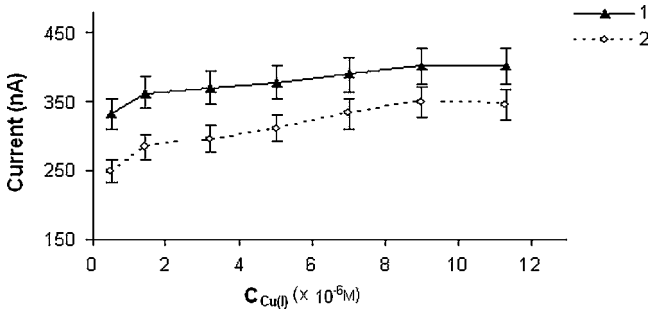

Fig. 6. (1) Dependence of peak oxidation current for guanine residues in dsDNA upon increasing concentrations of Cu(I) after incubation of stock dsDNA with the drug in 0.2 M acetate buffer, pH 5, for 10 min. The CPE was immersed in the mixture solution, the accumulation was performed by applying a potential at +1.7 V for 1 min followed by application of a potential at +0.5 V for 5 min. (2) Dependence of peak of oxidation of adenine residues in dsDNA after incubation with increasing concentrations of Cu(I) as described above. Experimental conditions are as above.

The result of the interaction of Cu(I) with the immobilized dsDNA was different from the behavior of dsDNA and Cu(I) incubated in solution, in terms of the characteristic peaks of dsDNA. In both of these cases, the characteristic peaks of guanine and adenine residues in dsDNA increased, but the increase was much more in the second case. The increase of the characteristic oxidation peaks of dsDNA with increasing concentrations of Cu(I) in the bulk solution could be attributed to a bending of the DNA molecule and its ability to adhere to the rough CPE surface [34]. In contrast to the second case, in the first one, a more positive peak at +1.37 V appeared due to the formation of a complex between Cu(I) and dsDNA.

4.2. Study of the interaction between DNA and Cu(I) using a hanging mercury drop electrode

A hanging mercury drop electrode (HMDE) and particularly the DNA-modified HMDE are useful tools in the study of the interfacial properties of DNA, including changes in DNA conformation at the electrode surface. On the other hand, mercury electrode can be also used in the study of changes in DNA conformation in solution. If HMDE is used, the surface changes in the DNA structure can be viewed by choosing proper conditions, including concentration of dsDNA, pH, scan rate.

In our investigation, the mercury electrode was immersed into 10 μL drop of DNA solution for an accumulation time of t_A = 120 s. The DNA concentration was adjusted to secure full coverage of the electrode surface under the given conditions. The concentration of dsDNA was 0.08 g L^{-1}. All the solutions were prepared in 10 mM Tris–HCl at pH 7.5. The electrode was washed and transferred into the electrolytic cell containing a blank background electrolyte and the alternating current voltammetric measurement was performed. dsDNA yielded peak I at −1.17 V and a higher peak II at −1.42 V in very good agreement with the results obtained from the other researchers [35,36].

4.2.1. Interaction of surface-confined dsDNA with a solution of Cu(I)

After dsDNA immobilization as previously described, Cu(I) was added to the solution and, after transfer into the electrolytic cell containing blank supporting electrolyte, alternating current voltammetry was performed.

The selection of the interaction time was made according to the current changes to the characteristic peaks of DNA. Fig. 7 shows the effect of incubation time between immobilized dsDNA and Cu(I). It is shown that the current response decreased with increasing incubation time, and the time selected was 5 min.

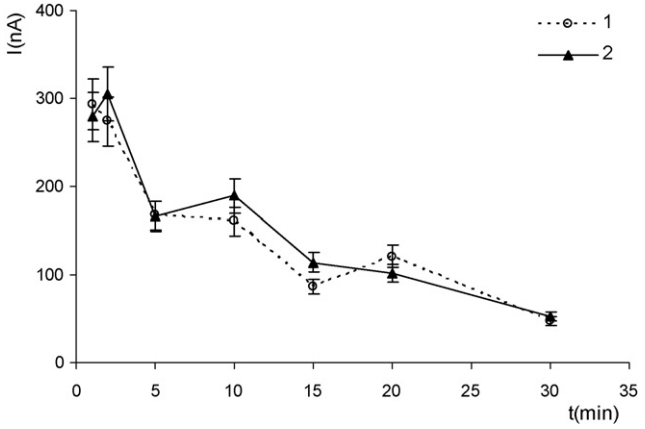

Fig. 7. (1) The effect of incubation time on the peak at −1.42 V between the immobilized dsDNA and the constant concentration of Cu(I) (2.51×10^{-6} M). (2) The effect of incubation time on the peak at −1.17 V between the immobilized dsDNA and the constant concentration of Cu(I) (2.51×10^{-6} M).

By increasing the concentration of Cu(I) in the solution, peak at −1.17 V becomes wider, while peak at −1.42 V decreases (Fig. 8). The presence of Cu(I) causes local distortions of DNA double-helix and/or overall unwinding of dsDNA molecules thus leading to the decrease of peak at −1.17 V. In addition, the adsorption of the underwound DNA segments prevent surface DNA denaturation and formation of DNA regions with freely accessible bases resulting in decreased intensity of peak at −1.42 V [37].

4.2.2. Interaction between dsDNA and Cu(I) in solution

Different concentrations of Cu(I) between 2.2×10^{-7} and 2.2×10^{-5} M were studied in relation with the double-stranded form of DNA.

The mercury electrode was immersed into a 10 μL drop of a DNA solution for an accumulation time of 120 s. The electrode was washed and transferred into the electrolytic cell containing blank background electrolyte to perform the alternating current voltammograms. Then, dsDNA and Cu(I) were incubated for a certain time interval. Ten microliters of this solution were immobilized at the HMDE surface and alternating current voltammetry was performed in blank supporting electrolyte. Fig. 9 shows the effect of the incubation time of Cu(I) and DNA in solution. It is shown that the current response is decreased as the incubation time is increased. The incubation time selected was 25 min, since no dramatic change at the peak current occurs after this point.

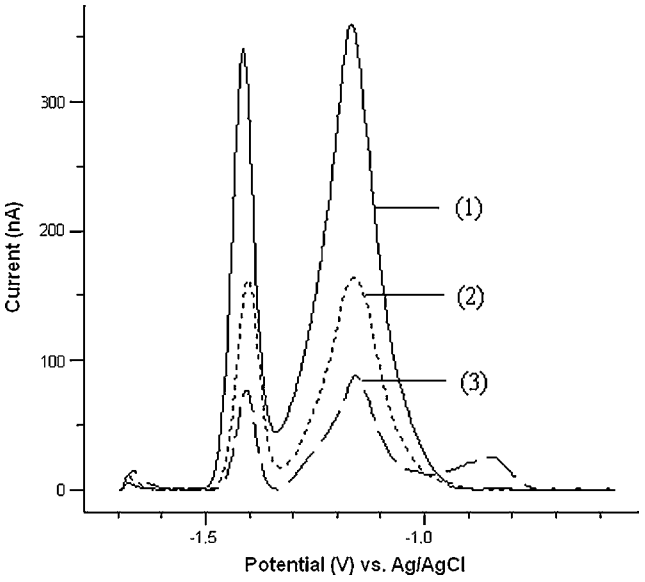

Fig. 8. (1) Alternating current voltammogram of dsDNA (80 mg L^{-1}) immobilized on the HMDE surface; (2) as in (1) and 2.51×10^{-6} M Cu(I) in solution; (3) as in (1) and 1.13×10^{-5} M Cu(I) in solution. Experimental conditions as described in the text.

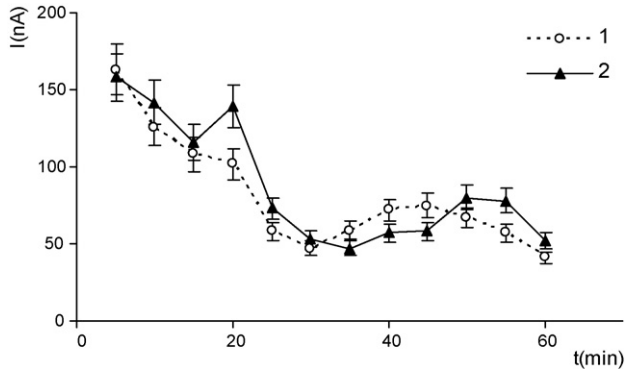

Fig. 9. (1) The effect of incubation time on peak (−1.42 V) between dsDNA (0.08 g L^{-1}) and Cu(I) (2.2×10^{-6} M). (2) The effect of incubation time on peak (−1.17 V) between dsDNA (0.08 g L^{-1}) and Cu(I) (2.2×10^{-6} M).

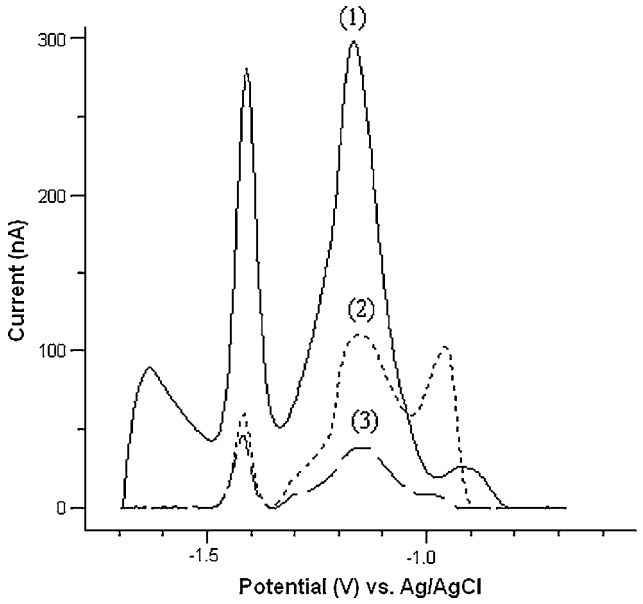

Fig. 10. (1) Alternating current voltammogram of dsDNA (0.08 g L^{-1}) immobilized on the HMDE surface; (2) alternating current voltammogram of the mixture dsDNA (0.08 g L^{-1}) + 2.2×10^{-6} M Cu(I) incubated in solution prior to immobilization on the HMDE surface; (3) alternating current voltammogram of the mixture dsDNA (0.08 g L^{-1}) + 2.2×10^{-5} M Cu(I) incubated in solution prior to immobilization on the HMDE surface. Experimental conditions as described in the text.

The interaction of dsDNA and Cu(I) resulted in a clear evidence of the differentiation in DNA configuration. The characteristic peaks of dsDNA greatly decreased. Peak II which appears due to the desorption of the DNA segments firmly adsorbed via bases, is a very important indicator of DNA cleavage at the electrode surface [35]. Fig. 10 presents the differentiations in dsDNA form after incubation with increasing concentrations of Cu(I).

The result of the interaction of Cu(I) with the immobilized dsDNA was different compared to the behaviour of dsDNA with Cu(I), incubated in solution. These behaviors can be differentiated according to the second characteristic peak of dsDNA, which was drastically decreased during interaction of Cu(I) and dsDNA in solution.

5. Conclusion

In this paper we have shown that interaction of Cu(I) with DNA being in solution or being immobilized on the CPE surface can be monitored by adsorptive transfer stripping voltammetry with differential pulse mode. Furthermore, the interaction at the HMDE surface with alternating current voltammetry can play a complementary role in order to study the results of the interaction. The interaction dsDNA with Cu(I) is shown to be time dependent and the optimal reaction time was investigated.

In the case of the interaction of Cu(I) with dsDNA immobilized at the CPE, characteristic peaks of dsDNA increased, but the increase was lower than in the case of interaction of Cu(I) with dsDNA is solution. We have to take into account that DNA is electrostatically adsorbed at the CPE surface through the negatively charged sugar-phosphate backbone by forming a flat layer at the electrode surface and that the side of the duplex that is in intimate contact with the electrode surface is not easily accessible. In addition, by immersing the dsDNA-modified carbon paste electrode in Cu(I) solution, we observed a peak at 1.37 V which started to appear by increasing concentrations of Cu(I). This observation can lead us to the conclusion that dsDNA is capable of interacting with Cu(I) diffusing to the surface from the bulk solution.

In the case of the incubation of dsDNA and the Cu(I) and subsequent immobilization at the CPE surface, both of the characteristic peaks of dsDNA increase and then level off probably due to easier accessibility of guanine and adenine residues at the CPE surface. It is obvious that we cannot speak about an intercalative complex formed as a result of the interaction between dsDNA and Cu(I), but other modes of DNA binding should be taken into account, such as electrostatic binding. Based on this kind of interaction, DNA could be efficiently cleaved by an electrochemically induced method. The different results of the interaction at the CPE surface or in the solution will be further investigated.

It is shown that the HMDE surface (in combination with alternating current voltammetry) responses of dsDNA form and presents high sensitivity to damage to the DNA double helix. As a result of the interaction between Cu(I) and dsDNA, we observed that the characteristic peaks of dsDNA increased. As an overall conclusion from the interaction between Cu(I) and dsDNA using HMDE arises that the differences at peaks I (−1.17 V) and II (−1.42 V) after interaction of surface-confined dsDNA with Cu(I) are much lower than that observed after interaction of solution phase dsDNA with Cu(I), probably due to the steric positioning of DNA at the electrode surface which prohibited a favorable interaction between them [38].

In this article, we applied a dsDNA-modified electrode which can be used in the detection of Cu(I). The changes of the characteristic peaks of guanine and adenine, can be used in the determination a very low concentrations of this element. Finally, it is shown that adsorptive transfer stripping voltammetry combined with differential pulse or alternating current as stripping modes, can be used in order to study the effects of chemical substance into the DNA structure.

Acknowledgement

Z. Stanić wish to thank the Ministry of Science of the Republic of Serbia, for financial support.

References

[1] E. Palecek, Anal. Biochem. 108 (1980) 129.
[2] E. Palecek, J. Osteryoung, R.A. Osteryoung, Anal. Chem. 54 (1982) 1389.
[3] S. Glodowski, R. Bilewicz, Z. Kublik, Anal. Chim. Acta 201 (1987) 11.
[4] H. Shiraishi, R. Takahashi, Bioelectrochem. Bioenerg. 31 (1993) 203.
[5] P.A.M. Farias, A. de, L.R. Wagener, A.A. Castro, Talanta 55 (2001) 281.
[6] R.A. Floyd, Carcinogenesis 11 (1990) 1447.
[7] M. Dizdaroglu, Mutat. Res. 275 (1992) 331.
[8] J. Tchou, A.P. Grollman, Mutat. Res. 299 (1993) 277.
[9] M.T. Carter, M. Rodriguez, A.J. Bard, J. Am. Chem. Soc. 111 (1989) 8901.
[10] D.W. Pang, M. Zhang, Z.L. Wang, Y.P. Qi, J.K. Cheng, Z.Y. Liu, J. Electroanal. Chem. 403 (1996) 183.
[11] S. Mahadevan, M. Palaniandavar, Inorg. Chem. 37 (1998) 693.
[12] D.W. Pang, H.D. Abruna, Anal. Chem. 70 (1998) 3162.
[13] E. Lamour, S. Routier, J.L. Bermier, J.P. Catteau, C. Bailly, H. Vezin, J. Am. Chem. Soc. 121 (1999) 1862.
[14] C.J. Burrows, J.G. Muller, Chem. Rev. 98 (1998) 1109.
[15] F.P. Bossu, K.L. Chellappa, D.W. Margerum, J. Am. Chem. Soc. 99 (1977) 2195.
[16] J. Labuda, M. Buckova, M. Vanickova, J. Mattusch, R. Wennrich, Electroanalysis 11 (1999) 101.
[17] K.H. Reddy, P.S. Reddy, P.R. Babu, J. Inorg. Biochem. 77 (1999) 169.
[18] D.S. Sigman, D.R. Graham, V.D. Aaurora, A.M. Stern, J. Biol. Chem. 254 (1979) 12269.
[19] K.M. Downey, B.G. Que, A.G. So, Biochem. Biophys. Res. Commun. 93 (1980) 264.
[20] L.E. Marshall, D.R. Graham, K.A. Reich, D.S. Sigman, Biochemistry 20 (1981) 244.
[21] D.S. Sigman, Acc. Chem. Res. 19 (1986) 180.
[22] M. Murata, M. Kobayashi, S. Kawanishi, Biochemistry 38 (1999) 7624.
[23] S. Oikawa, S. Kawanishi, Biochim. Biophys. Acta 1399 (1998) 19.
[24] W. Lytollis, R.T. Scannell, H. An, V.S. Murty, K.S. Reddy, J.R. Barr, S.M. Hecht, J. Am. Chem. Soc. 117 (1995) 12683.
[25] U.S. Singh, R.T. Scannell, H. An, B.J. Carter, S.M. Hecht, J. Am. Chem. Soc. 117 (1995) 12691.
[26] J.I. Ueda, M. Takai, Y. Shimazu, T. Ozawa, Arch. Biochem. Biophys. 357 (1998) 231.
[27] M. Rodriguez, T. Kodadek, M. Torres, A.J. Bard, Bioconjug. Chem. 1 (1990) 123.
[28] M. Fojta, T. Kubicarova, E. Palecek, Biosens. Bioelectron. 15 (2000) 107.
[29] P. Palaska, E. Aritzoglou, S. Girousi, Talanta 72 (2007) 1199.
[30] M.E. Rice, Z. Galus, R.N. Adams, J. Electroanal. Chem. 143 (1983) 89.
[31] S. Hasoň, F. Jelen, L. Fojt, V. Vetterl, J. Electroanal. Chem. 577 (2005) 263.
[32] V. Brabec, Bioelectrochem. Bioenerg. 7 (1980) 69.
[33] E. Palecek, F. Jelen, C. Teijeiro, V. Fucik, T.M. Jovin, Anal. Chim Acta. 273 (1993) 175.
[34] C. Teijeiro, P. Perez, D. Marin, E. Palecek, Bioelectrochem. Bioenerg. 38 (1995) 77.
[35] E. Palecek, Electroanalysis 8 (1996) 7.
[36] F. Jelen, V. Vetterl, P. Belusa, S. Hason, Electroanalysis 12 (2000) 987.
[37] M. Fojta, L. Havran, J. Fulneckova, T. Kubicarova, Electroanalysis 12 (2000) 926.
[38] M. Ozsoz, A. Erdem, P. Kara, K. Kerman, D. Ozkan, Electroanalysis 15 (2003) 613.

Available online at www.sciencedirect.com
ScienceDirect
Talanta 76 (2008) 9–14
Talanta
www.elsevier.com/locate/talanta

2,1,3-Benzoxadiazole-based selective chromogenic chemosensor for rapid naked-eye detection of Hg^{2+} and Cu^{2+}

Jin Tan, Xiu-Ping Yan *

Research Center for Analytical Sciences, College of Chemistry, Nankai University, 94 Weijin Road, Tianjin 300071, China

Received 14 November 2007; received in revised form 24 January 2008; accepted 25 January 2008
Available online 6 February 2008

Abstract

We report a simple twisted intramolecular charge transfer (TICT) chromogenic chemosensor for rapid and selective detection of Hg^{2+} and Cu^{2+}. The sensor was composed of an electron-acceptor 4-fluoro moiety and an electron-donor 7-mercapto-2,1,3-benzoxadiazole species where the S together with the 1-N provided the soft binding unit. Upon Hg^{2+} and Cu^{2+} complexation, remarkable but different absorbance spectra shifts were obtained in CH_3CN–H_2O mixed buffer solution at pH 7.6, which can be easily used for naked-eye detection. The sensor formed a stable 2:1 complex with Cu^{2+}, and both 2:1 and 3:1 complexes with Hg^{2+}. While alkali-, alkaline earth- and other heavy and transition metal ions such as Na^+, Mg^{2+}, Mn^{2+}, Co^{2+}, Ni^{2+}, Ag^+, Zn^{2+}, Pb^{2+} and Cd^{2+} did not cause any significant spectral changes of the sensor. This finding is not only a supplement to the detecting methods for Hg^{2+} and Cu^{2+}, but also adds new merits to the chemistry of 4,7-substituted 2,1,3-benzoxadiazoles.

Keywords: Chromogenic chemosensor; 2,1,3-Benzoxadiazole; Naked eye; Hg^{2+}; Cu^{2+}

1. Introduction

The design of sensors for highly noxious heavy and transition metal (HTM) ions such as Hg^{2+} and Cu^{2+} is of topical interest owing to their fundamental role in biological, environmental and chemical processes [1–6]. Over the years, a great effort has gone into the development of sensing devices for Hg^{2+} and Cu^{2+}, involving chromogenic [7–9] and fluorescent [10–12] chemosensors, electrochemical devices [13,14] and sensors based on mass changes [15]. Among these methods, colorimetric sensors are especially promising due to their simple naked-eye applications requiring less labor and expensive equipment than closely related methods such as fluorescent sensors. To date, a number of colorimetric sensors have been developed for Hg^{2+} and Cu^{2+} [16–23].

However, most of these systems display shortcomings for practical use, such as interference from other metal ions, delayed response to target ions and especially complicated and expensive synthesis. Therefore the convenient synthesis of selective chromogenic chemosensor for rapid detection of Hg^{2+} and Cu^{2+} is of great importance in practical use. 4,7-Substituted 2,1,3-benzoxadiazole derivatives were a group of widely used fluorophores [24–29]. The fluorescence characteristics of 4,7-substituted 2,1,3-benzoxadiazole derivatives greatly depend on the substituent groups at the 4- and 7-positions of the benzoxadiazole skeleton. By introducing different substituent groups at the 4- and 7-positions, various 2,1,3-benzoxadiazole derivatives were obtained [28]. However, most of these derivatives were used as fluorophores and only few works focused on their chromogenic properties toward metal ions [30].

Herein, we report a simple chromogenic chemosensor for Hg^{2+} and Cu^{2+} based on such 4,7-substituted 2,1,3-benzoxadiazole derivatives. We introduced mercapto moiety into the benzoxadiazole skeleton and two novel compounds 4-fluoro-7-mercapto-2,1,3-benzoxadiazole (**1**) and 4-(4-fluoro-2,1,3-benzoxadiazol-7-ylthio)-7-mercapto-2,1,3-benzoxadiazole (**2**) (Fig. 1) were easily obtained. Upon Hg^{2+} and Cu^{2+} complexation, remarkable but different absorbance spectra shifts of **2** in CH_3CN–H_2O mixed buffer solution at pH 7.6 were obtained with obvious color changes which makes **2** a selective naked-eye chemosensor for rapid and selective detection of Hg^{2+} and Cu^{2+}.

* Corresponding author. Fax: +86 22 23506075.
E-mail address: xpyan@nankai.edu.cn (X.-P. Yan).

0039-9140/$ – see front matter © 2008 Elsevier B.V. All rights reserved.
doi:10.1016/j.talanta.2008.01.056

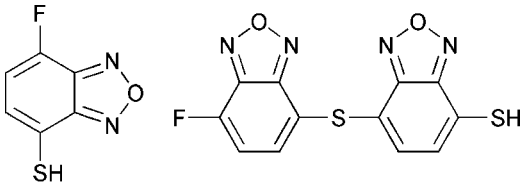

1 2

Fig. 1. Molecular structures of **1** and **2**.

2. Experimental

2.1. Chemicals

All reagents used were of at least analytical grade. Doubly deionized water (DDW, 18.2 MΩ cm^{-1}) obtained from a WaterPro water system (Labconco Corporation, Kansas City, USA) was used throughout the experiments. 4-Chlorosulfonyl-7-fluoro-2,1,3-benzoxadiazole (CBD-F) was synthesized according to Toyo'oka and Imai [31]. Aqueous metal ion solutions of Cu^{2+}, Hg^{2+}, Na^{+}, Mg^{2+}, Mn^{2+}, Co^{2+}, Ni^{2+}, Ag^{+}, Zn^{2+}, Pb^{2+} and Cd^{2+} were prepared from $Cu(NO_3)_2{\cdot}3H_2O$, $HgCl_2$, NaCl, $MgSO_4$, $MnCl_2{\cdot}4H_2O$, $CoCl_2{\cdot}6H_2O$, $NiCl_2{\cdot}6H_2O$, $AgNO_3$, $ZnSO_4{\cdot}7H_2O$, $Pb(NO_3)_2$ and $CdCl_2{\cdot}2.5H_2O$, respectively.

2.2. Instrumentation

^{1}H NMR and ^{13}C NMR spectra were recorded on a Varian MERCURY VX300 spectrometer. High resolution mass spectra (HRMS) were determined on an Ionspec 7.0T FT-ICR mass spectrometer. Absorption spectra were measured with a Shimadzu UV-3600 UV–vis spectrophotometer.

2.3. Synthesis and characterization of Compounds *1* and *2*

4-Fluoro-7-mercapto-2,1,3-benzoxadiazole (**1**): CBD-F (160 mg) was dissolved in CH_2Cl_2 (4.0 mL). After the addition of acetic acid (6.0 mL), concentrated HCl (2.0 mL) and $SnCl_2{\cdot}2H_2O$ (1.0 g), the mixture was stirred at room temperature (RT) for 30 min. The solution was poured into ice water (100 g) and extracted with CH_2Cl_2. The organic layer was then washed with DDW and dried over anhydrous Na_2SO_4. The organic solvent was removed by evaporation to give **1** as orange oil (110 mg, 95%). ^{1}H NMR (300 MHz, $CDCl_3$) δ = 7.19 (dd, ^3J(H,H) = 7.8 Hz, ^4J(F,H) = 3.9 Hz, 1H, ArH), 6.98 (dd, ^3J(H,H) = 7.8 Hz, ^3J(F,H) = 9.3 Hz, 1H, ArH), 4.22 ppm (s, 1H, SH). ^{13}C NMR (75 MHz, $CDCl_3$) δ = 150.1, 146.6, 143.0, 128.4, 117.8, 114.2 ppm. HRMS (ESI) Calcd for $C_6H_3FN_2OS$ $(M-H)^-$, 168.9877; Found, 168.9879.

4-(4-Fluoro-2,1,3-benzoxadiazol-7-ylthio)-7-mercapto-2,1,3-benzoxadiazole (**2**): **1** (100 mg) was dissolved in CH_3OH (10.0 mL). After the addition of triethyl amine (0.5 mL), the mixture was stirred at RT for 2 h and then evaporated in vacuum. The residue was chromatographed on silica gel using CH_2Cl_2–CH_3OH (4:1). The organic solvents were removed by evaporation to give **2** as red powder (80 mg, 85%). ^{1}H NMR (300 MHz, [D$_6$]DMSO) δ = 7.32 (dd, ^3J(H,H) = 7.8 Hz, ^4J(F,H) = 2.2 Hz, 1H, ArH), 7.23 (dd, ^3J(H,H) = 7.8 Hz, ^3J(F,H) = 10.6 Hz, 1H, ArH), 7.03 (d, J = 7.2 Hz, 1H, ArH), 6.74 (d, J = 7.2 Hz, 1H, ArH), 3.38 ppm (br, 1H, SH). ^{13}C NMR (75 MHz, [D$_6$]DMSO) δ = 152.0, 151.4, 150.8, 149.2, 144.0, 139.2, 136.1, 133.7, 132.9, 123.2, 120.1, 115.9 ppm. HRMS (ESI) Calcd for $C_{12}H_5FN_4O_2S_2$ $(M-H)^-$, 318.9765; Found, 318.9763.

2.4. UV–vis absorption titration studies

The pH effect on the UV–vis absorption of **2** was measured in CH_3CN–H_2O (4:1 v/v) using a constant host concentration (2.0×10^{-5} M) with aliquots of diluted HCl added to yield final pH range from 7.6 to 2.8. The binding ability of receptor **2** for Cu^{2+} and Hg^{2+} was investigated by UV–vis spectroscopy in CH_3CN–H_2O (4:1 v/v) at pH 7.6 using a constant host concentration (5.0×10^{-5} M) and increasing concentrations of cations. All the UV–vis absorption tests were carried on just after the addition of cations.

3. Results and discussion

3.1. Design of chemosensors

In order to bind Hg^{2+} and Cu^{2+}, soft mercapto moiety was easily introduced into benzoxadiazole skeleton by reduction of commercial available CBD-F. **1** was composed of an electron-acceptor 4-fluoro moiety and an electron-donor 7-mercapto-2,1,3-benzoxadiazole species where the S together with the 1-N provided the soft binding unit for Hg^{2+} and Cu^{2+}. The electronic properties of such an intramolecular charge transfer (ICT) [5,6] complex should be strongly affected when Hg^{2+} or Cu^{2+} was present. Unfortunately, **1** was unstable and would gradually change to disulfide at RT. While under basic condition, **1** reacted with itself and formed a structurally similar compound **2**. **2** also had a soft S and N binding unit but with two benzoxadiazole skeletons connected by a sulfur bridge. Both **1** and **2** were easily synthesized at RT with high yield. **2** in solid state was stable for more than 3 months in the dark at RT as judged by UV–vis absorption spectroscopy. The effect of light on the stability of **2** in solid state was not remarkable but was fatal to **2** in solution state. When stored under light, the UV–vis absorbance of **2** in solution state maintained stable within 1 day and then decreased gradually. In this work, the solution of **2** was prepared just before use and all the UV–vis absorption tests were carried on just after the addition of cations within 1 day, so the effect of light on the process can be negligible.

3.2. UV–vis absorption spectra of *1* and *2*

1 and **2** show good solubility in CH_3CN and optimization of assay conditions required 80% CH_3CN and 20% H_2O. The UV–vis absorption spectra of **1** and **2** were then measured in CH_3CN–H_2O (4:1 v/v) as shown in Fig. 2. **1** shows a maximal absorption band at 475 nm ($\varepsilon = 2.8 \times 10^3$ cm^{-1} M^{-1})

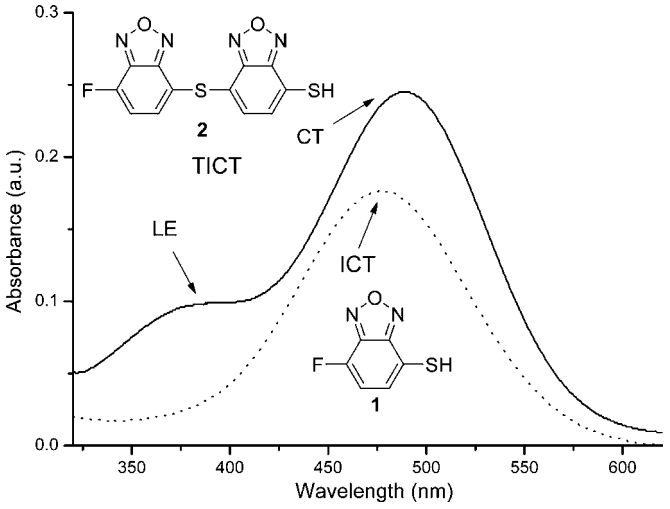

Fig. 2. UV–vis absorption spectra of **1** (6.0×10^{-5} M) (dotted line) and **2** (5.0×10^{-5} M) (solid line) in CH_3CN–H_2O (4:1 v/v). ICT: intramolecular charge transfer; TICT: twisted intramolecular charge transfer; LE: locally excited and CT: charge transfer.

assigned to ICT. While **2**, with the two rotational benzoxadiazole skeletons, shows a twisted intramolecular charge transfer (TICT) [5,6,32,33] characteristic dual absorption spectrum: a short wavelength absorption at 394 nm attributed to the transition to the locally excited (LE) state along with a long wavelength absorption at 489 nm ($\varepsilon = 5.1 \times 10^3$ cm^{-1} M^{-1}) attributed to the transition to the charge transfer (CT) state. Further investigations on the spectral properties of **2** were performed in the following sections.

3.3. Effect of pH

Considering the benzoxadiazole nitrogens with lone pair electrons, the photophysical property of **2** was influenced by its protonation states. Fig. 3 shows the changes in the UV–vis spectra of **2** at various pH with titration of diluted HCl solution. When pH gradually decreased from 7.6 to 2.8, the CT band centered at 489 nm decreased and the LE band centered at 394 nm developed. Correspondingly, the solution color changed from salmon pink to yellow. A clear isosbestic point at 430 nm indicates the formation of a new species corresponding to the protonation of the benzoxadiazole nitrogens. As the lone pair electrons of nitrogen were engaged with H^+, the charge transfer possibilities died out, resulting in the disappearance of the CT band [32,33]. Additionally, these changes were fully reversible as the addition of diluted NaOH solution reversed these effects. Plotting the absorbance change at 489 nm as a function of pH

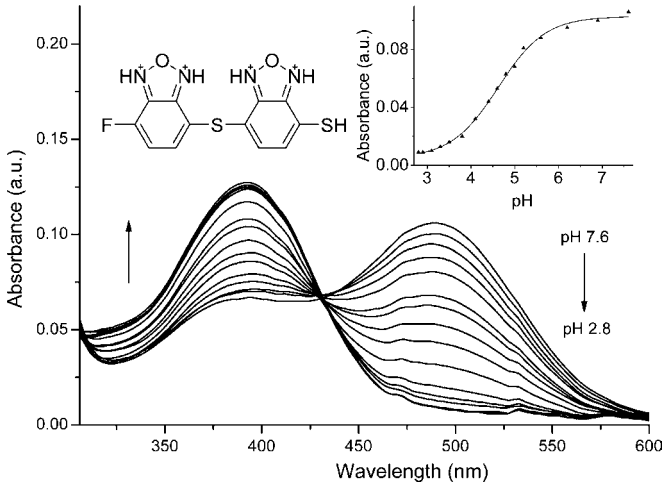

Fig. 3. The effect of pH on the UV–vis absorption of **2** (2.0×10^{-5} M) in CH_3CN–H_2O (4:1 v/v). Aliquots of diluted HCl were added to yield final pH of 7.6, 6.9, 6.2, 5.6, 5.2, 5.0, 4.8, 4.6, 4.4, 4.1, 3.8, 3.5, 3.3, 3.1, 2.9 and 2.8. Inset: structure of the protonated **2** and changes in the UV–vis spectra of **2** at 489 nm as a function of pH.

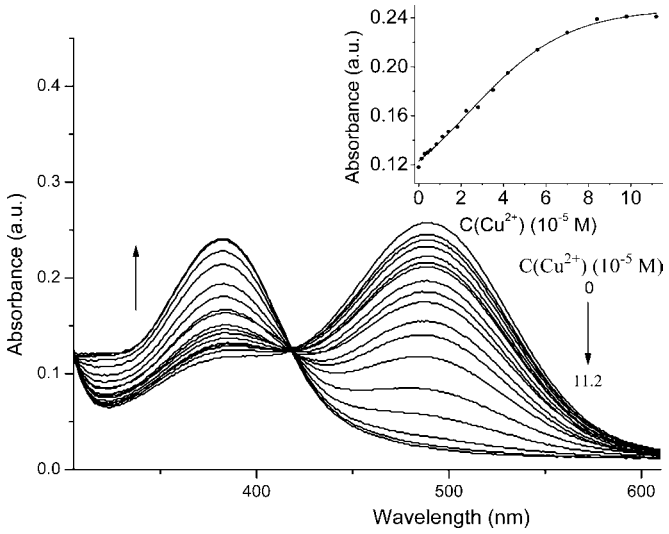

Fig. 4. UV–vis absorption spectra of **2** (5.0×10^{-5} M) in CH_3CN–H_2O (4:1 v/v) at pH 7.6 (20 mM Tris–HCl) upon Cu^{2+} titration. Aliquots of 5.0×10^{-3} M $Cu(NO_3)_2$ were added to yield final Cu^{2+} concentrations of 0, 0.14, 0.28, 0.42, 0.56, 0.84, 1.12, 1.40, 1.82, 2.24, 2.80, 3.50, 4.20, 5.60, 7.00, 8.40, 9.80 and 11.20×10^{-5} M. Inset: changes in the UV–vis spectra of **2** at 383 nm as a function of Cu^{2+} added.

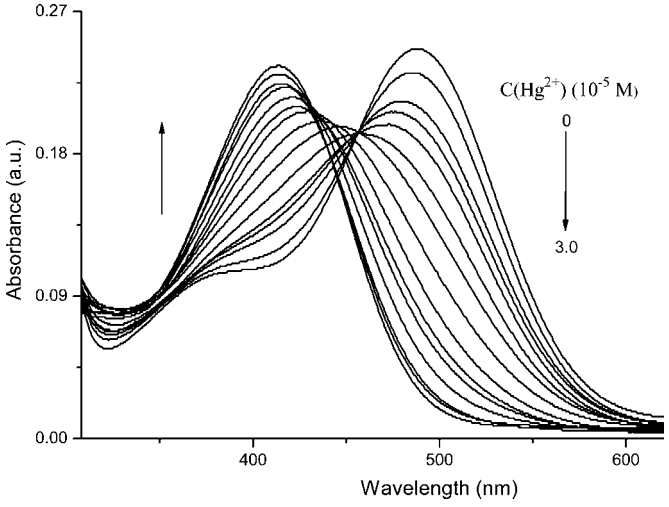

Fig. 5. UV–vis absorption spectra of **2** (5.0×10^{-5} M) in CH_3CN–H_2O (4:1 v/v) at pH 7.6 (20 mM Tris–HCl) upon Hg^{2+} titration. Aliquots of 5.0×10^{-3} M $HgCl_2$ were added to yield final Hg^{2+} concentrations of 0, 0.10, 0.20, 0.25, 0.30, 0.40, 0.50, 0.63, 0.75, 0.88, 1.00, 1.25, 1.50, 1.75, 2.00, 2.25, 2.50, 2.75 and 3.00×10^{-5} M.

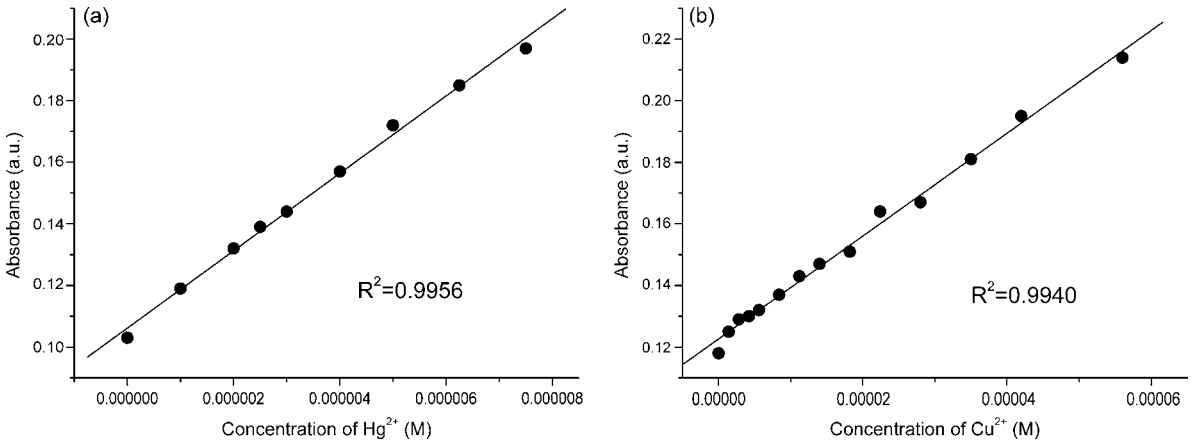

Fig. 6. The linear relationships between the absorbance at 413 nm and concentration of Hg^{2+} (a) and the absorbance at 383 nm and concentration of Cu^{2+} (b).

gave a sigmoidal curve. As can be seen from the inset of Fig. 3, only minor changes occurred above ca. pH 6.0. Finally, treating the protonated **2** as a monobasic acid, a pK_a value of 4.7 ± 0.1 was derived from this curve. These results demonstrate that **2** could be used in the environment where pH ranged from 6.0 to 7.6, which covered the physiological range of pH. We next investigated the complexation abilities of **2** with Cu^{2+} and Hg^{2+} in CH_3CN–H_2O (4:1 v/v) at pH 7.6 (20 mM Tris–HCl).

3.4. UV–vis titration of 2 with Cu^{2+} and Hg^{2+}

Fig. 4 shows UV–vis absorption spectra of **2** with various concentrations of Cu^{2+}. Upon titration of Cu^{2+}, the CT band centered at 489 nm decreased and a new band centered at ca. 383 nm arose. Correspondingly, the solution color changed from salmon pink to pale green, nearly colorless. A well-defined isosbestic point at 420 nm indicates the formation of a new compound. Plotting the absorbance change at 383 nm as a function of concentrations of Cu^{2+} added gave a sigmoidal curve as shown in the inset of Fig. 4. The 2:1 binding stoichiometry of **2**-Cu^{2+} was supported by the nice nonlinear fitting [34] of the titration curve. A log K value of 8.8 ± 0.1 in CH_3CN–H_2O (4:1 v/v) at pH 7.6 (20 mM Tris–HCl) was derived from this curve. The binding of the soft Cu^{2+} with the soft S and N unit diminished the degree of charge transfer, resulting in the blue shift of the absorption band of **2**. The 2:1 binding stoichiometry of **2**-Cu^{2+} was also supported by the ESI-MS spectrum of the Cu^{2+} titration solution of **2** (See Fig. S1 in Supporting Information). The peak at m/z 672.9 was assigned to the $[(\mathbf{2})_2\text{-}2H + Cl]^-$ species. The peak at m/z 701.0 was assigned to the $[Cu(\mathbf{2})_2\text{-}2H]$ species and it was in well accordance with the pattern simulated by Xcalibur™.

The experimental phenomenon was different from that of Cu^{2+} when Hg^{2+} was added to the solution of **2**. As shown in Fig. 5, an isosbestic point was obtained at 457 nm in the range less than 5×10^{-6} M of Hg^{2+}, indicating a new compound formed and coexisted with free **2**. Further addition of $HgCl_2$ gave multiple spectral intersections instead of a precise isosbestic point, suggesting the formation of new species [34]. During the titration, the absorbance at 489 nm gradually decreased and that at 413 nm arose. As a result, the solution color changed from salmon pink to yellow.

Similar excursion in spectra when large amount of $HgCl_2$ was added was obtained using **1** instead of **2**. Similar excursion in spectra of both **1** and **2** when large amount of $HgCl_2$

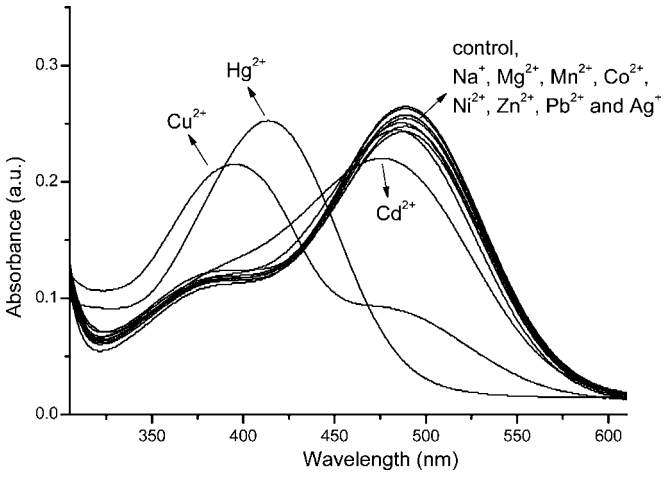

Fig. 7. UV–vis absorption spectra of **2** (5.0×10^{-5} M) in CH_3CN–H_2O (4:1 v/v) at pH 7.6 (20 mM Tris–HCl) with different metal ions (2.5×10^{-5} M).

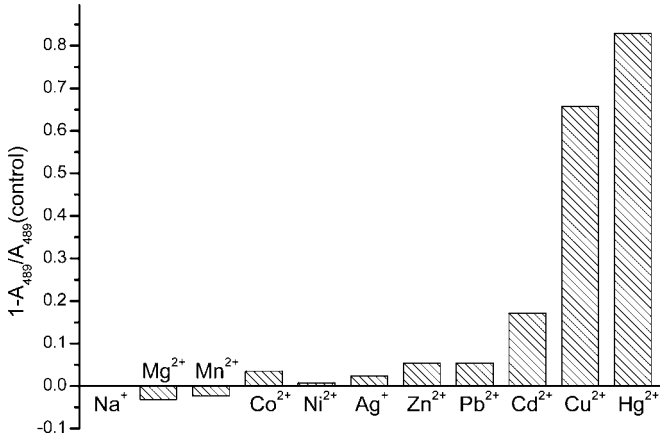

Fig. 8. Absorbance changes at 489 nm of **2** (5.0×10^{-5} M) in CH_3CN–H_2O (4:1 v/v) at pH 7.6 (20 mM Tris–HCl) with different cations (2.5×10^{-5} M).

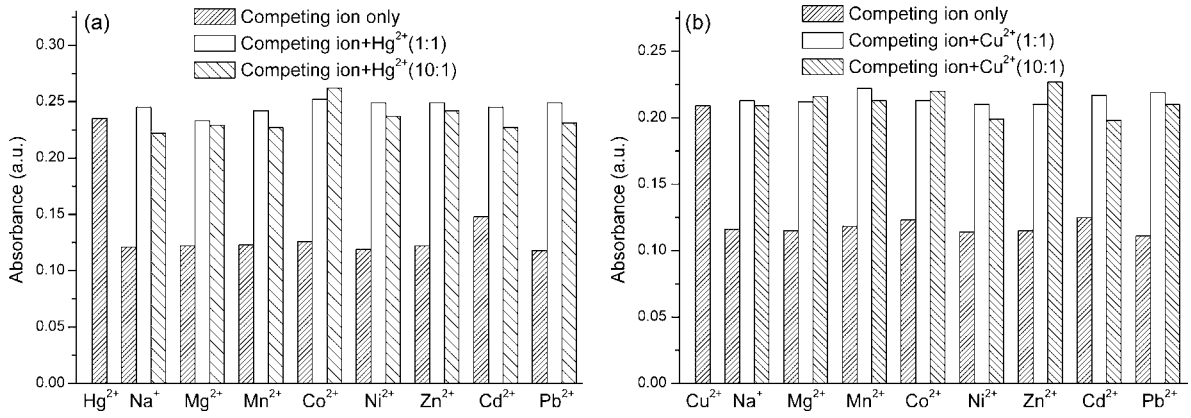

Fig. 9. The absorbance change profiles of **2** (5.0×10^{-5} M) with Hg^{2+} (2.5×10^{-5} M) at 413 nm (a) and Cu^{2+} (2.5×10^{-5} M) at 383 nm (b) in the presence of selected metal ions at two ratios of 1:1 and 10:1 (competing ion/Hg^{2+} or Cu^{2+}) in CH_3CN–H_2O (4:1 v/v) at pH 7.6 (20 mM Tris–HCl).

was added indicates that it depended on the inherent chemistry between the soft Hg^{2+} and the soft S and N binding unit. We assigned this excursion to the multi-stoichiometries of **2**-Hg^{2+}, which was confirmed by the ESI-MS spectrum of the Hg^{2+} titration solution of **2** (see Fig. S2 in Supporting Information). The peak at *m/z* 672.9 was assigned to the $[(\mathbf{2})_2\text{-}2H + Cl]^-$ species. The peaks at *m/z* 874.8 and 1158.6 were assigned to the $[Hg(\mathbf{2})_2\text{-}2H + Cl]^-$ and $[Hg(\mathbf{2})_3\text{-}3H]$ species, respectively. The ESI-MS results reveal the 2:1 and 3:1 binding stoichiometries of **2**-Hg^{2+}, accounting for the excursion in Hg^{2+} titration spectra. Similar phenomenon of such multiple spectral intersections was found in Lazarides and co-workers' recent work [35], which was attributed to the 1:1 and 1:2 binding stoichiometries of host–guest.

3.5. Quantitative study

The quantitative responses of **2** toward Hg^{2+} and Cu^{2+} were studied and the linear calibration plots are shown in Fig. 6. The dynamic ranges for the determination of Hg^{2+} and Cu^{2+} were determined to be linear up to 7.5×10^{-6} M and 5.6×10^{-5} M with correlation coefficient (R^2) of 0.9956 and 0.9940, respectively. The limit of detection (LOD) is evaluated using $3\sigma/s$, where σ is the standard deviation of the blank signals and s is the slope of the linear calibration plot. The LODs for determination of Hg^{2+} and Cu^{2+} were thus calculated to be 3.4×10^{-7} M and 2.9×10^{-6} M, respectively.

3.6. Interference from other metal ions

The influences of other metal ions such as Na^+, Mg^{2+}, Mn^{2+}, Co^{2+}, Ni^{2+}, Ag^+, Zn^{2+}, Pb^{2+} and Cd^{2+} on the absorption spectrum of **2** were investigated. As shown in Fig. 7, the presence of these alkali-, alkaline earth- and HTM ions did not cause any significant spectral changes of **2** in CH_3CN–H_2O (4:1 v/v) at pH 7.6 (20 mM Tris–HCl). Plotting the absorbance changes at 489 nm in the UV–vis spectra of **2** with different cations gives Fig. 8. Compared to the response of **2** with Hg^{2+} and Cu^{2+}, no obvious change at 489 nm was observed upon addition of Na^+, Mg^{2+}, Mn^{2+}, Co^{2+}, Ni^{2+}, Ag^+, Zn^{2+} and Pb^{2+}, indicating that **2** shows high selectivity for Hg^{2+} and Cu^{2+} upon these metal ions. Only Cd^{2+} caused relatively smaller blue shifts of the spectrum. UV–vis titration of **2** with Cd^{2+} was then investigated. As shown in Fig. S3 (See Supporting Information), a ca. 45 nm blue shift was observed without obvious color change (shift of wavelength < 60 nm). An isosbestic point at 461 nm indicates the formation of a new compound. As shown in the inset, the nice linear fitting of the Benesi–Hildebrand plot [34] indicates the 1:1 binding stoichiometry of **2**-Cd^{2+} and a $\log K$ value of 4.4 ± 0.1 in CH_3CN–H_2O (4:1 v/v) at pH 7.6 (20 mM Tris–HCl) which is much smaller than that of **2**-Cu^{2+} was derived. Furthermore, by plotting the relative absorbance changes at 489 nm as a function of pM, where pM = −log[M] where M is the cations used, the sensitivity and the selectivity of these ion recognitions can be evaluated. From Fig. S4 (See Supporting Information), it is apparent that Cd^{2+} modulates the absorption spectra, but this change occurs at much higher concentrations than that of Cu^{2+} and Hg^{2+}. In fact, the presence of Hg^{2+} and Cu^{2+} can be easily distinguished by the naked eye (See Fig. S5, Supporting Information). The affinity for Cu^{2+} and Hg^{2+} of **2** is not strange considering its soft S and N binding unit and is similar to that encountered with several S and/or N containing ligands that exhibit selectivity for metal ions in the "copper triangle" of the periodic table [16,36].

To explore further the utility of **2** as an ion-selective chromogenic chemosensor for Hg^{2+} and Cu^{2+}, the competition experiments were conducted in coexistence of other metal ions including Na^+, Mg^{2+}, Mn^{2+}, Co^{2+}, Ni^{2+}, Zn^{2+}, Pb^{2+} and Cd^{2+} at two ratios of 1:1 and 10:1 (competing ion/Hg^{2+} or Cu^{2+}) and the results are illustrated in Fig. 9. Notes that the interference of Ag^+ was not investigated because it would be precipitated in coexistence of $HgCl_2$. Clearly, the presence of alkali-, alkaline earth- and transition metals such as Na^+, Mg^{2+}, Mn^{2+}, Co^{2+}, Ni^{2+}, Zn^{2+}, Pb^{2+} and Cd^{2+} do not cause any significant absorbance variation of **2** and Hg^{2+} or Cu^{2+}. The presence of a 10 mole ratio of these competing ions does not change the absorbance more than 12%. The competing experiments reveal that the absorbance for Hg^{2+} or Cu^{2+} is unaffected in a background of 10 equivalents mole ratio of these competing ions. The above results imply that the selectivity of **2** toward Hg^{2+} and Cu^{2+} was remarkable

and made **2** a selective chromogenic chemosensor for Hg^{2+} and Cu^{2+}.

4. Conclusions

In conclusion, a novel selective colorimetric chemosensor **2** based on TICT was developed for Hg^{2+} and Cu^{2+} incorporating 2,1,3-benzoxadiazole skeletons. Upon Hg^{2+} and Cu^{2+} complexation, remarkable but different absorbance spectra shifts were obtained with obvious color changes, which can be easily used for naked-eye detection. **2** formed a single stable 2:1 complex with Cu^{2+}, and both 2:1 and 3:1 complexes with Hg^{2+}. This finding is not only a supplement to the detecting methods for Hg^{2+} and Cu^{2+}, but also adds new merits to the chemistry of 4,7-substituted 2,1,3-benzoxadiazoles.

Acknowledgement

This work was supported by the National Natural Science Foundation of China (No. 20775037) and the National Basic Research Program of China (2006CB705703).

Appendix A. Supplementary data

Supplementary data associated with this article can be found, in the online version, at doi:10.1016/j.talanta.2008.01.056.

References

[1] P.B. Tchounwou, W.K. Ayensu, N. Ninashvili, D. Sutton, Environ. Toxicol. 18 (2003) 149.
[2] H.H. Harris, I.J. Pickering, G.N. George, Science 301 (2003) 1203.
[3] Z.L. Harris, J.D. Gitlin, Am. J. Clin. Nutr. 63 (1996) 836S.
[4] R. Uauy, M. Olivares, M. Gonzalez, Am. J. Clin. Nutr. 67 (1998) 952S.
[5] A.P. de Silva, H.Q.N. Gunaratne, T. Gunnlaugsson, A.J.M. Huxley, C.P. McCoy, J.T. Rademacher, T.E. Rice, Chem. Rev. 97 (1997) 1515.
[6] B. Valeur, I. Leray, Coord. Chem. Rev. 205 (2000) 3.
[7] F. Sancenón, R. Martínez-Máñez, J. Soto, Chem. Commun. (2001) 2262.
[8] T. Gunnlaugsson, J.P. Leonard, N.S. Murray, Org. Lett. 6 (2004) 1557.
[9] N. Kaur, S. Kumar, Tetrahedron Lett. 47 (2006) 4109.
[10] S.H. Kim, J.S. Kim, S.M. Park, S.-K. Chang, Org. Lett. 8 (2006) 371.
[11] N.J. Youn, S.-K. Chang, Tetrahedron Lett. 46 (2005) 125.
[12] S. Yoon, A.E. Albers, A.P. Wong, C.J. Chang, J. Am. Chem. Soc. 127 (2005) 16030.
[13] L.P. Singh, J.M. Bhatnagar, Talanta 64 (2004) 313.
[14] Z. Liu, S. Huan, J. Jiang, G. Shen, R. Yu, Talanta 68 (2006) 1120.
[15] L. Manganiello, A. Ríos, M. Valcárcel, Anal. Chem. 74 (2002) 921.
[16] R. Martínez, A. Espinosa, A. Tárraga, P. Molina, Org. Lett. 7 (2005) 5869.
[17] Z. Xu, X. Qian, J. Cui, Org. Lett. 7 (2005) 3029.
[18] J.V. Ros-Lis, M.D. Marcos, R. Martínez-Máñez, K. Rurack, J. Soto, Angew. Chem. Int. Ed. 44 (2005) 4405.
[19] Y.-K. Yang, K.-J. Yook, J. Tae, J. Am. Chem. Soc. 127 (2005) 16760.
[20] S. Tatay, P. Gaviña, E. Coronado, E. Palomares, Org. Lett. 8 (2006) 3857.
[21] Y.-F. Cheng, D.-T. Zhao, M. Zhang, Z.-Q. Liu, Y.-F. Zhou, T.-M. Shu, F.-Y. Li, T. Yi, C.-H. Huang, Tetrahedron Lett. 47 (2006) 6413.
[22] R.R. Avirah, K. Jyothish, D. Ramaiah, Org. Lett. 9 (2007) 121.
[23] R. Martínez, F. Zapata, A. Caballero, A. Espinosa, A. Tárraga, P. Molina, Org. Lett. 8 (2006) 3235.
[24] H. Sakamoto, J. Ishikawa, S. Nakao, H. Wada, Chem. Commun. (2000) 2395.
[25] S. Uchiyama, T. Santa, K. Imai, Anal. Chem. 73 (2001) 2165.
[26] A.L. Graham, C.A. Carlson, P.L. Edmiston, Anal. Chem. 74 (2002) 458.
[27] N. Lavignac, C.J. Allender, K.R. Brain, Tetrahedron Lett. 45 (2004) 3625.
[28] S. Uchiyama, T. Santa, N. Okiyama, T. Fukushima, K. Imai, Biomed. Chromatogr. 15 (2001) 295.
[29] N.T. Greene, K.D. Shimizu, J. Am. Chem. Soc. 127 (2005) 5695.
[30] M. Boiocchi, L. Fabbrizzi, M. Licchelli, D. Sacchi, M. Vázquez, C. Zampa, Chem. Commun. (2003) 1812.
[31] T. Toyo'oka, K. Imai, Anal. Chem. 56 (1984) 2461.
[32] P.R. Bangal, S. Panja, S. Chakravorti, J. Photochem. Photobiol. A 139 (2001) 5.
[33] A. Chakraborty, S. Kar, N. Guchhait, Chem. Phys. 324 (2006) 733.
[34] K.A. Conners, Binding Constants, Wiley, New York, 1987, pp. 141–168.
[35] T. Lazarides, T.L. Easun, C. Veyne-Marti, W.Z. Alsindi, M.W. George, N. Deppermann, C.A. Hunter, H. Adams, M.D. Ward, J. Am. Chem. Soc. 129 (2007) 4014.
[36] T.H. Cooper, M.J. Mayer, K.-H. Leung, L.A. Ochrymowycz, D.B. Rorabacher, Inorg. Chem. 31 (1992) 3796.

Talanta 76 (2008) 80–84

Contents lists available at ScienceDirect

Talanta

journal homepage: www.elsevier.com/locate/talanta

Selection and fingerprints of the control substances for plant drug *Eucommia ulmodies Oliver* by HPLC and LC–MS

Ling Tong[a], Yuzhi Wang[a,*], Jinfang Xiong[a], Yue Cui[a], YigangZhou[b], Lunchao Yi[c]

[a] *State Key Laboratory of Chemo/Biological Sensing & Chemometrics, College of Chemistry and Chemical Engineering, Hunan University, Changsha 410082, PR China*
[b] *Department of Microbiology, College of Basic Medicine, Central South University, Changsha 410083, PR China*
[c] *Department of Chemistry, Central South University, Changsha 410083, PR China*

ARTICLE INFO

Article history:
Received 12 December 2007
Received in revised form 1 February 2008
Accepted 8 February 2008
Available online 10 March 2008

Keywords:
E. ulmodies
Chlorogenic acid
Control substance of plant drug
Fingerprint
Extraction

ABSTRACT

Eucommia ulmodies Oliver (*E. ulmodies*) has been used as herbal medicine for thousands years in China. The selection of the control substances and their fingerprints of this plant medicine were investigated by using high performance liquid chromatography (HPLC) and liquid chromatography–mass spectrometry (LC–MS). The gradient elution mode was applied in chromatographic separation, and the data was analyzed by "Computer Aided Similarity Evaluation" software to compare the similarity of the *E. ulmodies* from different habitats. Low similarity was found in the samples from nonadjacent provinces, while high similarity was obtained in those from the adjacent provinces. The LC–MS fingerprints of *E. ulmodies* showed the main active constituents and could be used for its original identification and quality evaluation.

1. Introduction

Eucommia ulmodies Oliver, with a Chinese name Duzhong, is a precious plant medicine used for nourishing the liver and kidney, strengthening the bone and muscle, preventing abortion, and so on for thousands years [1]. As one of very important active compounds in *E. ulmodies*, chlorogenic acid (a kind of phenylpropanoids) is cultivated by aerobic respiration of the plant, showing anti-bacterial, phlogosis, mutagenic, oxidant and other biological activities [2,3]. It is well known that the therapeutic effect of herbal medicine is based on the synergic effect of its various constituents, which is different from western medicines. Recently, the chromatographic fingerprint technique [4–7], which was a more significant formulation for controlling the quality of herbal medicines or their products in comparison to conventional methods, has attracted more and more attention because this technique emphasizes the systemic characterization of samples' compositions and focuses on identifying and assessing the stability of the plants. Due to the variation of the collecting seasons, sites, processing methods, there are some differences in the content and the variety of active components in the same plant. Therefore, it is necessary to establish fingerprints of *E. ulmodies* for its quality control. The control substances of a plant can be selected by using high performance liquid chromatography (HPLC) and liquid chromatography–mass spectrometry (LC–MS). The similarity, often represented by the correlation coefficient, of fingerprints between the reference material and a sample was usually measured for the evaluation of quality that is considered as great, eligible or unqualified for the fingerprint with a corresponding correlation coefficient above 0.9, between 0.8 and 0.9, or below 0.8, respectively. In conventional methods [8–14], the sample preparation of herbal medicines was accomplished by heating, boiling, refluxing or ultrasonic extraction [15–17]. Although the microwave-assisted extraction [18–23] has been extensively used for herbal medicine analysis, its application in the study on the fingerprint of *E. ulmodies* has been rarely reported. In this article, different sample preparation procedures were compared, including microwave-assisted and ultrasonic extraction, condensing reflux and marinated extraction at room temperature, microwave-assisted extraction and microwave-assisted extraction was utilized with HPLC and LC–MS for control substance selection and fingerprint establishment of *E. ulmodies*.

2. Experimental

2.1. Apparatus

An Agilent HP1100 series HPLC system consisting of a vacuum degasser, thermo-stated column compartment and DAD (Agilent, Palo Alto, CA, USA) was used to obtain chromatograms, and LC–MS

* Corresponding author. Tel.: +86 731 8822286; fax: +86 731 8713642.
E-mail address: wyzss@tom.com (Y. Wang).

0039-9140/$ – see front matter © 2008 Elsevier B.V. All rights reserved.
doi:10.1016/j.talanta.2008.02.012

system was Advantage LCQ model from Thermo Finnigen. Pressure Self-Control Microwave Decomposition System (Shanghai, China) and an ultrasonic cleaner were used for extraction.

2.2. Reagents and materials

Standard chlorogenic acid (>97%) was purchased from Alfa Aeser. Roasted leaves, dried and unroasted barks of *E. ulmodies* came from Traditional Chinese Medicine Co. Ltd. (Hunan, PRC). Duzhong Pingya Tablets was purchased from Guizhou province. Ethanol of A.P. grade was used for extraction and triple-distilled water was used for preparation of sample solutions. HPLC grade methanol, glacial acetic acid and redistilled water were filtrated through a 0.45 μm membrane before used.

2.3. Extraction methods

Before extraction, the dried leaves of *E. ulmodies* were cut into pieces (5 mm × 5 mm), and bark (roasted and unroasted) of *E. ulmodies* was ground into powder with particle diameter of 0.2–0.9 mm).

2.3.1. Microwave-assisted extraction

A 0.5 g aliquot of sample was placed into the pressure self-control microwave decomposition system, and then extraction solvent consisting of ethanol and water (60:40, v/v) (solvent to sample ratio 50/1, v/w) was added. The irradiation time was kept for 2 min, then the extraction solution was cooled down to ambient temperature. After that, the resulted solution was centrifuged and filtrated through 0.45 μm membrane before the analysis by HPLC.

2.3.2. Ultrasonic extraction

A 0.5 g aliquot of sample was mixed with the ethanol–water (60:40, v/v) solvent (solvent/sample ratio, 50/1, v/w), and then placed into the ultrasonic bath, followed by sonication for 80 min and filtration through 0.45 μm membrane. The prepared filtrate was directly used for HPLC analysis.

2.3.3. Marinated extraction

A 0.5 g aliquot of sample was mixed with the ethanol–water (60:40, v/v) solvent (solvent/sample ratio, 50/1, v/w), and then placed into the sealed vessel, followed by the extraction for 30 h and filtration through 0.45 μm membrane. The prepared filtrate was directly injected into HPLC for analysis.

2.3.4. Condensing reflux

A 0.5 g aliquot of sample was mixed with the ethanol–water (60:40, v/v) solvent (solvent/sample ratio, 50/1, v/w), and then placed into the sealed vessel, followed by the extraction for 6 h and filtration through 0.45 μm membrane. The prepared filtrate was directly used for HPLC analysis.

2.3.5. Preparation of standard solution

Certain amount of chlorogenic acid was weighted exactly, and dissolved in ethanol–water (60:40, v/v) solution in a 100 ml volumetric flack. Then, it was diluted to different concentrations for construction of calibration curves.

2.3.6. HPLC conditions

A reversed-phase C_{18} column (150 mm × 4.6 nm, i.d. 5 μm) from Agilent was used with the mobile phase consisted of methanol (A) and 0.5% acetic acid in water (B). Gradient elution was programmed from 30% (A) at 0–16 min, then from 30% (A) to 60% (A) during 17–25 min, finally from 60% (A) to 30% (A) during 25–26 min. The column temperature was set at 30 °C and chromatograms were monitored by DAD at 332 nm. The sample volume injected was 10 μl. External standard method was used for determination of chlorogenic acid and other active components in *E. ulmodies*.

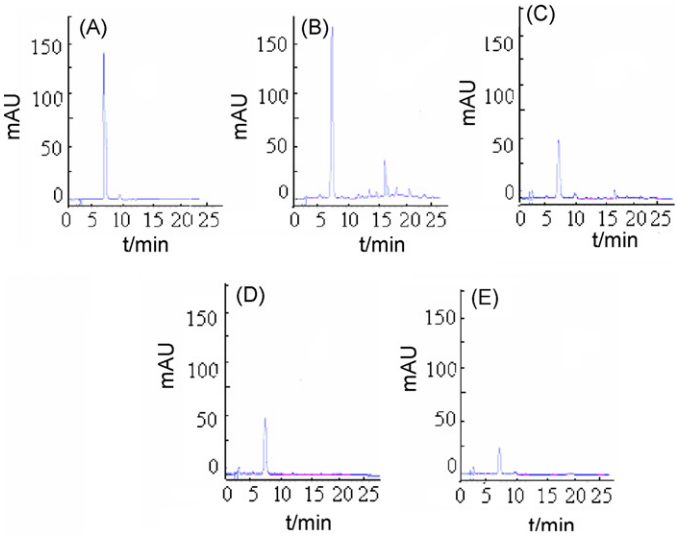

Fig. 1. The HPLC fingerprints of *E. ulmodies* extracted by different methods. (A) Standard chlorogenic acid; (B) microwave extraction; (C) ultrasonic extraction; (D) condensing reflux; (E) marinated extraction.

2.3.7. LC–MS conditions

The chromatographic conditions were as following: ODS-3 column (150 mm × 2.1 mm, i.d. 5 μm), sample injection volume of 20 μL, column temperature of 30 °C, the mobile phase consisting of methanol and 0.5% acetic acid in water (30:70, v/v) at a flow rate of 1.0 ml/min. APCI source was employed in LC–MS analysis, with vaporizer temp of 450 °C, discharge current of 50 μA, capillary temp of 200 °C, capillary voltage of 10 V and Tabe lens offset of 50 V.

3. Results and discussion

3.1. Selection of extraction method

The extraction efficiency of different methods was investigated in this work, including microwave-assisted extraction for 2 min (B), ultrasonic extraction for 80 min (C), condensing reflux for 6 h and marinated extraction for 30 h. The results are illustrated in Fig. 1. It is found that microwave-assisted extraction is most suitable for complete extraction of main components, especially chlorogenic acid. The extraction efficiency of different solvents containing ethanol from 20% to 80% was also investigated, showing that the most components in the herb can be quantitatively extracted by using 60% ethanol solution.

3.2. Preliminary test of microwave-assisted extraction conditions

In microwave-assisted extraction of chlorogenic acid and others from *E. ulmodies*, there were many factors affecting the extraction efficiency, among which the irradiation time, pressure, solid–liquid ratio and solvent are the main factors. In order to reduce the times of experiment, a L_9 (3^4) orthogonal design graph was used. As a result, the following conditions were selected: 2 min of irradiation time, 50 ml solvent per gram of sample, 60% ethanol solution, 3 atm. The results were shown in Tables 1 and 2.

Table 1
Factors and levels

No.	*A*, ethanol concentration (ml:ml)	*B*, ratio of material to solvent (g/ml)	*C*, time (min)	*D*, pressure (atm)
1	4:6	1:50	1	1
2	5:5	1:25	2	2
3	6:4	1:15	3	3

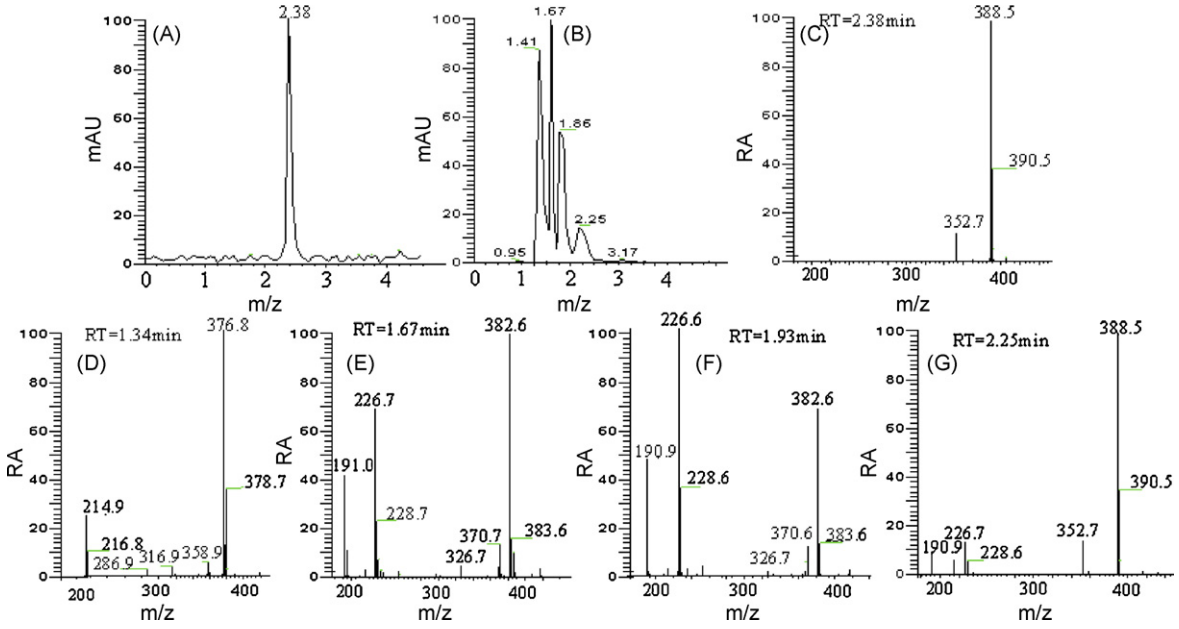

Fig. 2. The LC–MS spectrums of chlorogenic acid and the leave of *E. ulmodies*. (A) The HPLC chromatogram of chlorogenic acid (t_R = 2.38 min); (B) the HPLC chromatogram of the leaves of *E. ulmodies*; (C) the MS spectrum of chlorogenic acid (t_R = 2.38 min); (D) the MS spectrum of the leave of *E. ulmodies* (t_R = 1.34 min); (E) the MS spectrum of the leave of *E. ulmodies* (t_R = 1.67 min); (F) the MS spectrum of the leave of *E. ulmodies* (t_R = 1.93 min); (G) the MS spectrum of the leave of *E. ulmodies* (t_R = 2.25 min).

3.3. Fingerprints of E. ulmodies

3.3.1. LC–MS analysis

The standard chlorogenic acid and the leaves of *E. ulmodies* were extracted by microwave apparatus and analyzed by LC–MS. As shown in Fig. 2, most of the constituents exhibited quasi-molecular ions $[M+Cl]^-$ and $[M+CH_3COO]^-$ in MS spectra. The structures of these compounds [24] were shown in Table 3. Therefore, these compounds can be used as references for quality control.

3.3.2. The establishment of the reference fingerprint

For the establishment of the reference fingerprint [25,26], 10 groups of super roasted bark of *E. ulmodies* were analyzed by HPLC. Then the results were treated by the"computer aided similarity evaluation" software. The reference fingerprints of super samples are shown in Fig. 3.

Table 2
Arrangement and results of L9 (3^4) orthogonal test

No.	*A*	*B*	*C*	*D*	Extraction ratio (mg/g)
1	1	1	1	1	17.41
2	1	2	2	2	18.69
3	1	3	3	3	13.95
4	2	1	2	3	22.35
5	2	2	3	1	13.73
6	2	3	1	2	15.09
7	3	1	3	2	22.80
8	3	2	1	3	19.80
9	3	3	2	1	14.10
Kj1	50.05	62.56	52.30	45.24	
Kj2	51.17	52.22	55.14	56.58	
Kj3	56.70	43.14	50.48	56.10	
R	6.65	19.42	4.66	11.34	

3.3.3. The fingerprints of roasted bark of E. ulmodies collected in different locations

To investigate the effects of various conditions on the roasted bark of *E. ulmodies*, 13 samples were extracted by microwave-assisted extraction and then analyzed by HPLC system (as shown in Fig. 4). According to the similarity values of all herbal chromatograms as shown in Table 4, all samples were divided into three groups, group A, B and C. The similarity values of the three groups are above 0.9, between 0.8 and 0.9 and below 0.8 in turn, which were consistent with their habitats. While the habitats of the herbal were nearer, the similarity values were larger. Consequently, a conclusion can be obtained that the compositions of the Chinese herbal were similar when the corresponding locations were close to each other. This can be used to collect high quality Chinese herbal.

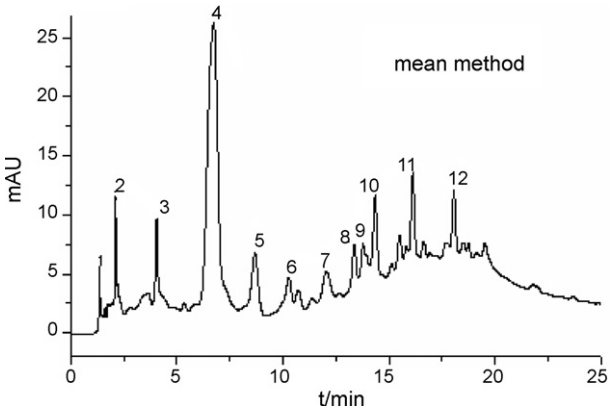

Fig. 3. The reference fingerprint of samples (super roasted bark of *E. ulmodies*).

Table 3
MS spectra for the identification of fingerprint peak

No.	t_R (min)	MI	MS/MS	MW	Name	Structure
C	2.38	388.5	352.7	354	Chlorogenic acid	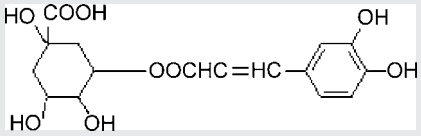
D	1.34	376.8	358.9 316.9 286.9 214.9	374	Geniposidic acid	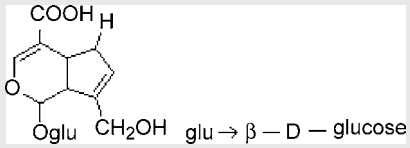
E	1.67	382.6	370.7 326.7 226.7 191.0	384	Neochlorogenic ethyl ester	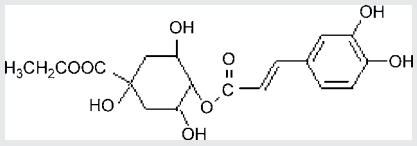
F	1.93	382.6	370.6 326.7 226.6 190.9	384	Isochlorogenic ethyl ester	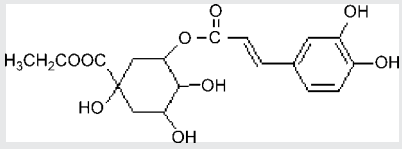
G	2.25	388.5	352.7 226.7 190.9	354	Chlorogenic acid	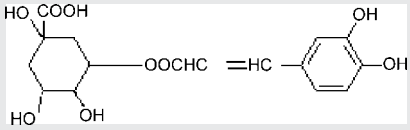

3.3.4. *The fingerprints of different kinds of E. ulmodies*

The leaves, unroasted bark, roasted bark of *E. ulmodies* and Duzhong Pingya Tablets were extracted by microwave apparatus, and analyzed by HPLC system. The results were shown in Fig. 5. Although they all contained chlorogenic acid, there were obvious differences in the variety and the content, which resulted in differences in utilizations.

3.4. *Methodology study*

3.4.1. *Precision test of the apparatus*

Apparatus precision was evaluated by the analysis of five successive injections of the same sample solution. The correlation coefficients between the reference HPLC fingerprint and the sample HPLC fingerprint were: 0.9960, 0.994, 0.9961, 0.9995 and 0.9983, respectively. These data showed that the precision of the apparatus was satisfactory.

3.4.2. *Stability test of the solution*

Stability was evaluated by the analysis of five injections of the same sample solution every 4 h. The correlation coefficients were 0.9989, 0.9996, 0.9983, 0.9992 and 0.9995, respectively. The data indicated that the stability of the solution was very nice.

3.4.3. *Repeatability of analytical method*

Repeatability was evaluated by the analysis of five injections of five samples solutions prepared by the same method. The correlation coefficients were 0.9986, 0.9993, 0.9997, 0.9995 and 0.9988, respectively, showing that the repeatability of the analytical method is very suitable.

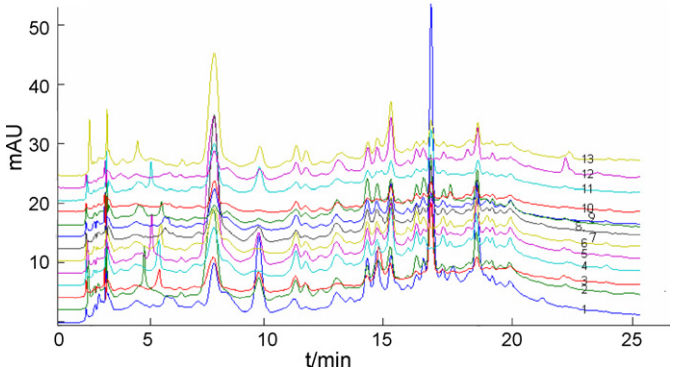

Fig. 4. HPLC fingerprints of the roasted bark of *E. ulmodies* from different habitats.

Table 4
The similarity of the bark of *E. ulmodies* from different habitats

Number	Habitat	Similarity	Common peak ratio
1	Mianyang	0.8033	0.9890
2	Zhangjiajie	0.9538	0.9770
3	Zigong	0.8965	0.9685
4	Fenghuang	0.9172	0.9759
5	Meishan	0.8843	0.9769
6	Jishou	0.9192	0.9735
7	Changde	0.9350	0.9743
8	Yiyang	0.9387	0.9721
9	Xinyang	0.7976	0.9971
10	Hengyang	0.9229	0.9991
11	Xiangtan	0.9627	0.9819
12	Yibin	0.8711	0.9775
13	Guangyuan	0.8730	0.9714

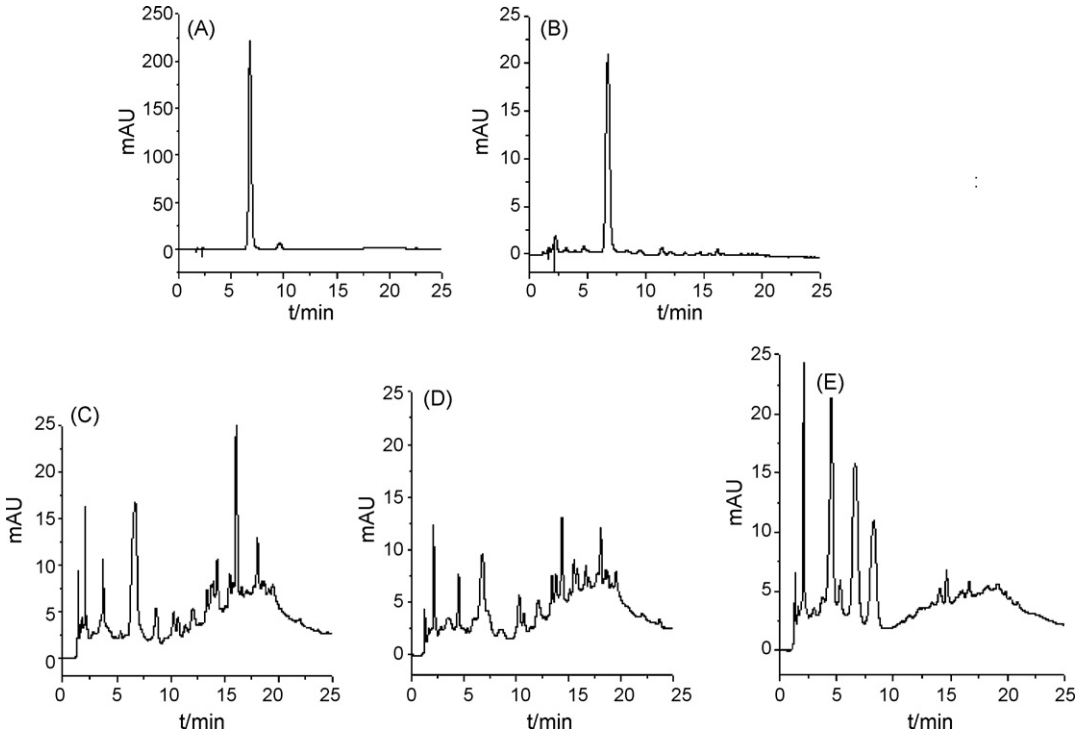

Fig. 5. The HPLC fingerprints of different kinds of *E. ulmodies*. (A) The standard of chlorogenic acid; (B) the leaves of *E. ulmodies*; (C) unroasted bark of *E. ulmodies*; (D) roasted bark of *E. ulmodies*; (E) Duzhong Pingya Tablets.

3.5. Discussion

Herbal medicine usually consists of hundreds of phytochemicals with a dependence on climate, regions of cultivation, season of harvest and so on. Moreover, the concentration of different ingredients is varied dramatically. With extensive application of *E. ulmodies*, it is urgent to develop a novel standard for the quality control. Comparing with the quantification of a few markers or pharmacologically active constituents, the chromatographic fingerprint has more predominance in reporting the authenticity of herbal. So we used HPLC with DAD to develop a simple, rapid and valid chromatographic fingerprint method for qualitative analysis of *E. ulmodies*. Combining the MS result, the substance composition and substance structure can be further identified. So HPLC and LC–MS fingerprints can be used for original identification and quality evaluation.

4. Conclusion

In summary, the microwave-assisted extraction were very suitable for the simple preparation of *E. ulmodies* by compared different preparation procedures including microwave-assisted and ultrasonic extraction, condensing reflux and marinated extraction at room temperature. It has the characters of speediness, high efficiency and no-pollution. The present studies in this paper also demonstrated that the HPLC and LC–MS can be used to select control substances and to construct fingerprints of *E. ulmodies*. The method is very simple with high precision, stability and repeatability. The resulting HPLC and LC–MS fingerprints can be used for original identification and quality evaluation of related herbal medicines, and will become a key technique for Chinese herbal quality control and a powerful support for the progress of Chinese herbal medical prescription

Acknowledgements

The authors are indebted to the financial supports from the Hunan Provincial Natural Science Foundation (No. 07JJ3018) and the State Key Laboratories Open Foundation of China (2007).

References

[1] D. Takeshi, N. Sansci, N. Yoshihisa, Acta Pharmacol. Sin. 22 (2001) 1057.
[2] T. Nakamura, Y. Nakazawa, S. Onizuka, Mutat. Res. 338 (1997) 7.
[3] Y.F. Sasaki, A. Chiba, M. Murakam, Mutat. Res. 371 (1996) 203.
[4] M. Ohmishi, H. Morishita, H. Iwahashi, Phytochemistry 36 (1994) 576.
[5] M.H. Wu, C.Y. Huang, L.H. Zhao, L.H. Mei, Chin. J. Nat. Med. 69 (2005) 106.
[6] J.N. Cai, G.J. Xu, R.L. Jin, L.S. Xu, J. Chin. Pharm. Univ. 6 (1991) 345.
[7] K.J. James, A.G. Bishop, R. Craisci, L. Palleschi, J. Chromatogr. A 844 (1999) 53.
[8] S. Conannon, V.N. Ramachandran, W.F. Smyth, Rapid Commun. Mass Spectrom. 14 (2000) 1157.
[9] H. Sakuma, S. Matsushima, S. Munakata, S. Sugawara, Agric. Biol. Chem. 46 (1982) 1311.
[10] G. Paganga, N. Miller, C.A. Rice-Evans, Free Radic. Res. 30 (1999) 153.
[11] X. Yan, M. Suzuki, M. Ohnishi-Kameyama, Y. Sada, T. Nakanishi, T. Nagata, J. Agric. Food Chem. 47 (1999) 4711.
[12] J. Yu, T. Vasanthan, F. Temelli, J. Agric. Food Chem. 49 (2001) 4352.
[13] T. Deyama, T. Ikawa, S. Kigagawa, Chem. Pham. Bull. 35 (1987) 1785.
[14] T.J. Mason, E.D. Cordemans, Trans. Inst. Chem. Eng. 74 (1996) 511.
[15] B. Sun, M.J. Peng, X.Y. Yang, Chem. Ind. Forest Prod. 19 (1999) 67.
[16] M. Romdhane, C. Gourdon, Chem. Eng. J. 87 (2002) 11.
[17] M. Palma, C.G. Barroso, Anal. Chim. Acta 458 (2002) 119.
[18] A.V. Filgueiras, J.L. Capelo, I. Lavilla, C. Bindicho, Talanta 53 (2000) 433.
[19] Z.K. Guo, Q.H. Jin, G.Q. Fan, Y.P. Duan, C. Qin, M.J. Wen, Anal. Chim. Acta 436 (2001) 41.
[20] E.D. Conte, C.Y. Shen, P.W. Perschbacher, D.W. Miller, J. Agric. Food Chem. 44 (1996) 829.
[21] B. Kaufmann, P. Christen, J.L. Venuthey, Phytochem. Anal. 12 (2001) 327.
[22] N. Hong, V.A. Yaylayan, G.S. Raghavan, J.R. Park, J.M. Blanger, Nat. Prod. Lett. 15 (2001) 197.
[23] W.H. Ho, S.J. Hsieh, Anal. Chim. Acta 428 (2001) 111.
[24] H.Y. Zhang, Y.L. Wang, P. Hu, K.S. Yan, G.A. Luo, Y.M. Wang, Chin. Tradit. Patent Med. 28 (2006) 469.
[25] S. Wang, H.Q. Ma, Y.J. Sun, C.D. Qiao, S.J. Shao, S.X. Jiang, Talanta 72 (2007) 434.
[26] H.Z. Lian, Y. Wei, Talanta 71 (2007) 264.

Talanta 76 (2008) 226–229

Contents lists available at ScienceDirect

Talanta

journal homepage: www.elsevier.com/locate/talanta

Short communication

External polyacrylate-coating as alternative material for preparation of photopolymerized sol–gel monolithic column

Fernando Antonio Simas Vaz[a], Patrícia Mendonça de Castro[a], Celso Molina[b], Sidney José Lima Ribeiro[b], Ferminio César Polachini[b], Younes Messaddeq[b], Adriana Palombo Nunes[c], Marcone Augusto Leal de Oliveira[a,*]

[a] *Departamento de Química, Universidade Federal de Juiz de Fora, UFJF, 36036-330 Juiz de Fora, MG, Brazil*
[b] *Instituto de Química, Universidade Estadual Paulista Júlio de Mesquita Filho, UNESP, 14801-970 Araraquara, SP, Brazil*
[c] *Central Analítica, Instituto de Química, Universidade de São Paulo, 05508-900 São Paulo, SP, Brazil*

ARTICLE INFO

Article history:
Received 5 October 2007
Received in revised form 8 February 2008
Accepted 14 February 2008
Available online 7 March 2008

Keywords:
Electrochromatography
Monolithic stationary phase
Photopolymerization
Sol–gel
Polyacrylate-coating

ABSTRACT

Photopolymerized sol–gel monolithic columns for use in capillary electrochromatography were prepared in 125 μm i.d. polyacrylate-coated fused-silica capillaries. The polyacrylate-coating, unlike the polyimide one, is transparent to the radiation used (≈370 nm), and thus, no coating removal is necessary. This is a very important particularity since intrinsic capillary column characteristics, such as flexibility and mechanical resistance, are unchanged. A mixture containing metacryloxypropyltrimethoxysilane (MPTMS) as the polymeric precursor, hydrochloric acid as the catalyst, toluene as the porogen and bis(2,4,6-trimethylbenzoyl)-phenylphosphine oxide (Irgacure 819) as the photoinitiator was irradiated at 370 nm for 20 min inside the capillaries to prepare the columns through sol–gel approach. The versatility and viability of the use of polyacrilate as a new capillary external coating were shown through preparation of two columns under different conditions, which were tested in electrochromatography for separation of standard mixture containing thiourea (marker compound), propylbenzene, phenanthrene and pyrene.

1. Introduction

The investigation of new analytical techniques intended to perform faster and more efficient analysis of different kinds of compounds in complex matrixes have become remarkably attractive for separation area in the last decade. The applications involving the use of monolithic stationary phases for capillary electrochromatography (CEC) in order to carry out analysis of simple molecules, peptides, proteins, polycyclic aromatic hydrocarbons, enantiomers and other important compounds have presented significant growth [1–5].

In general, the polymerization of monolithic stationary phases in fused-silica capillary is thermally initiated [6], but it can also be activated by means of light radiation incidence [7]. The choice will depend on the availability of reagents and physical–chemical features of the capillary coating.

As regards the photopolymerized monolithic column preparation, Svec reported the use of photopolymerization in ultraviolet (UV) transparent tubing such as Teflon-coated fused-silica capillaries, which are fragile and hard to handle when compared with polyimide-coated capillaries [8,9]. On the other hand, the polyimide fused-silica tubing absorbs UV light and some range of the visible one. Thus, the photopolymerization is only possible after removing a stripe of the coating [10,11].

The preparation of photopolymerized monolithic stationary phases (PMSP) using fused-silica capillary with an alternative coating, like polyacrylate, which is transparent over 370 nm and presents features and performances similar to the polyimide one [12,13] offers other advantages such as the control of the segment length filled inside the capillary, the evaluation of the macroscopic homogeneity of the dry monoliths and, mainly, the unchanged flexibility and mechanical resistance of the capillary since the removal of a stripe of the polymer coating before photopolymerization is unnecessary.

Within this context, this work describes an alternative procedure for *in situ* one-step preparation of a PMSP with a porous

* Corresponding author. Tel.: +55 32 21023310; fax: +55 32 21023314.
E-mail address: marcone.oliveira@ufjf.edu.br (M.A.L. de Oliveira).

0039-9140/$ – see front matter © 2008 Elsevier B.V. All rights reserved.
doi:10.1016/j.talanta.2008.02.007

structure and the ability to separate neutral species in a liquid stream by application of an electric field through the polyacrylate-coated capillary. As a demonstration, a standard mixture containing neutral compounds in a solution of methanol has been pressure-injected into the column and separated.

2. Experimental

2.1. Materials, reagents and chemicals

Fused-silica polyacrylate-coated capillaries (125 μm i.d. × 375 μm o.d.) were purchased from Micro Tube (Araraquara, Brazil). Metacryloxypropyltrimethoxysilane (MPTMS) was purchased from Acros Organics (New Jersey, USA) and bis(2,4,6-trimethylbenzoyl)-phenylphosphine oxide (Irgacure 819) was donated by Ciba Specialty Chemicals (São Paulo, Brazil). Toluene (Beckman, Fullerton, USA), acetonitrile (ACN) (J.T. Baker, Phillipsburg, USA), ethanol, methanol and ammonium hydroxide (Quimex, Tubarão, Brazil), hydrochloride acid and acetic acid (Vetec, Rio de Janeiro, Brazil) were purchased with analytical grade. Pyrene (Buchs, Switzerland), phenanthrene (Tokyo, Japan) and propylbenzene (Sacramento, USA) standards were purchased from Fluka.

2.2. Instrumentation

An agilent HP3d capillary electrophoresis instrument (Palo Alto, USA) equipped with a diode array detector, a temperature control device in cartridge and acquisition and treatment data software (HP ChemStation, rev A.06.01) was used to carry out all CEC experiments. A homemade UV–vis cross-linker equipped with six 15 W black light tubes of predominantly 370 nm wavelength was used to irradiate the reaction solutions. The emission measurements from this chamber set-up were carried out in a UV–vis spectrophotometer system (model USB 2000, Ocean Optics, USA) equipped with optic fiber and CCD detector. The absorption spectra measurements were carried out in a UV–vis spectrophotometer system (model UV-1601PC, Shimadzu, Kyoto, Japan) equipped with double-beam in time by using quartz regular cells of optical way equal to 1.0 cm. Scanning electron microscopy (SEM) analyses were performed on a Field Emission Scanning Electron Microscope JSM 7401F (*Jeol*) (Tokyo, Japan). In the present work, a low voltage (1 kV) was used to scan the monoliths in order to avoid burning them, as the segment was not sputtered with gold.

2.3. Preparation of the PMSP

In order to show the viability and versatility of the use of polyacrylate-coated capillary in the monolith preparation, two different conditions have been performed. A monomer solution A containing 1000 μL of MTPMS and 300 μL of HCl (0.12 mol L^{-1}) and a monomer solution B containing 750 μL of MTPMS and 150 μL of HCl (0.12 mol L^{-1}) were prepared separately. These two

Table 1
Monomer and porogene solutions used for PMSP preparation

	Monomer solution		Porogene solution	
	MPTMS (μL)	HCl (μL)	Toluene (%)[a]	Irgacure 819 (%)[b]
Column A[c]	1000	300	87	0.44
Column B[d]	750	150	82	0.98

[a] Percentage (v/v) of porogenic solution to the monomer solution.
[b] Percentage (m/v) of Irgacure 819 relative to the toluene amount.
[c] Filling with disposable syringe.
[d] Filling with CE equipment. Conditions: 40 mbar × 10 s from the outlet.

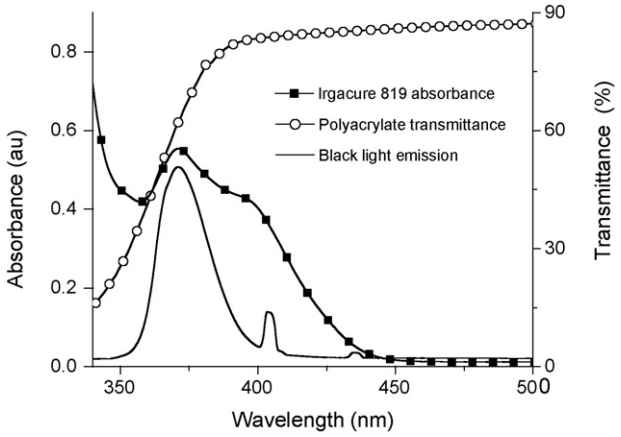

Fig. 1. Absorbance of Irgacure 819 (0.03% m/v, dissolved in toluene) transmittance of a polyacrylate film (0.3 mm of thickness) and emission (scale not shown) of a black light.

solutions were stirred at room temperature, in dark, for approximately 20 min to afford monophasic solutions. The sol is formed in these solutions through a series of hydrolysis and condensation, as described by Dulay et al. [10]. Two other solutions were prepared

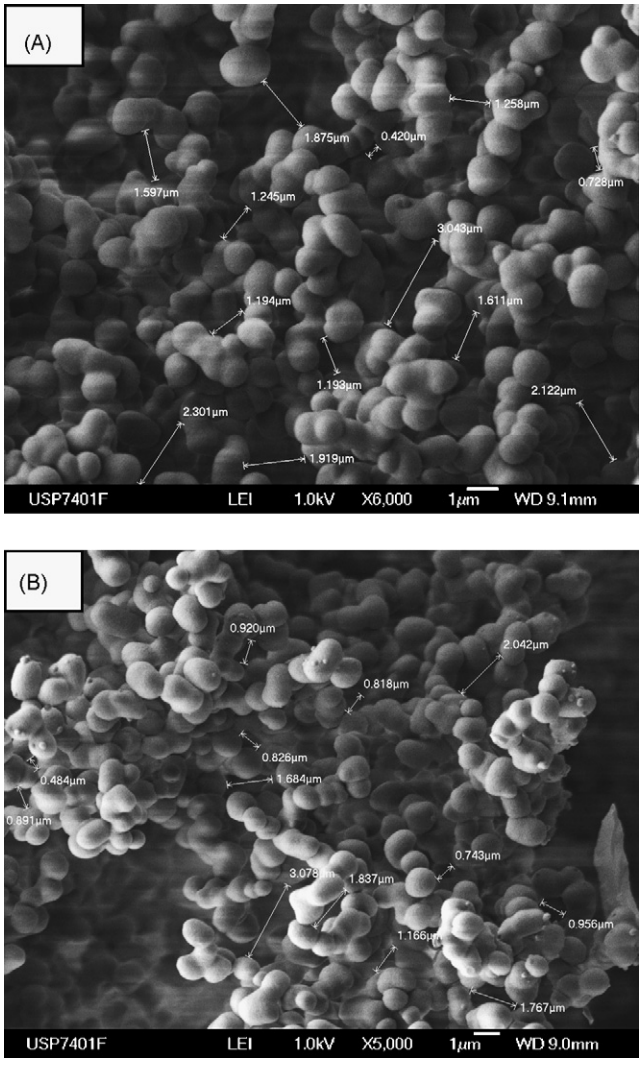

Fig. 2. Scanning electron micrographs of the cross-section of columns A and B.

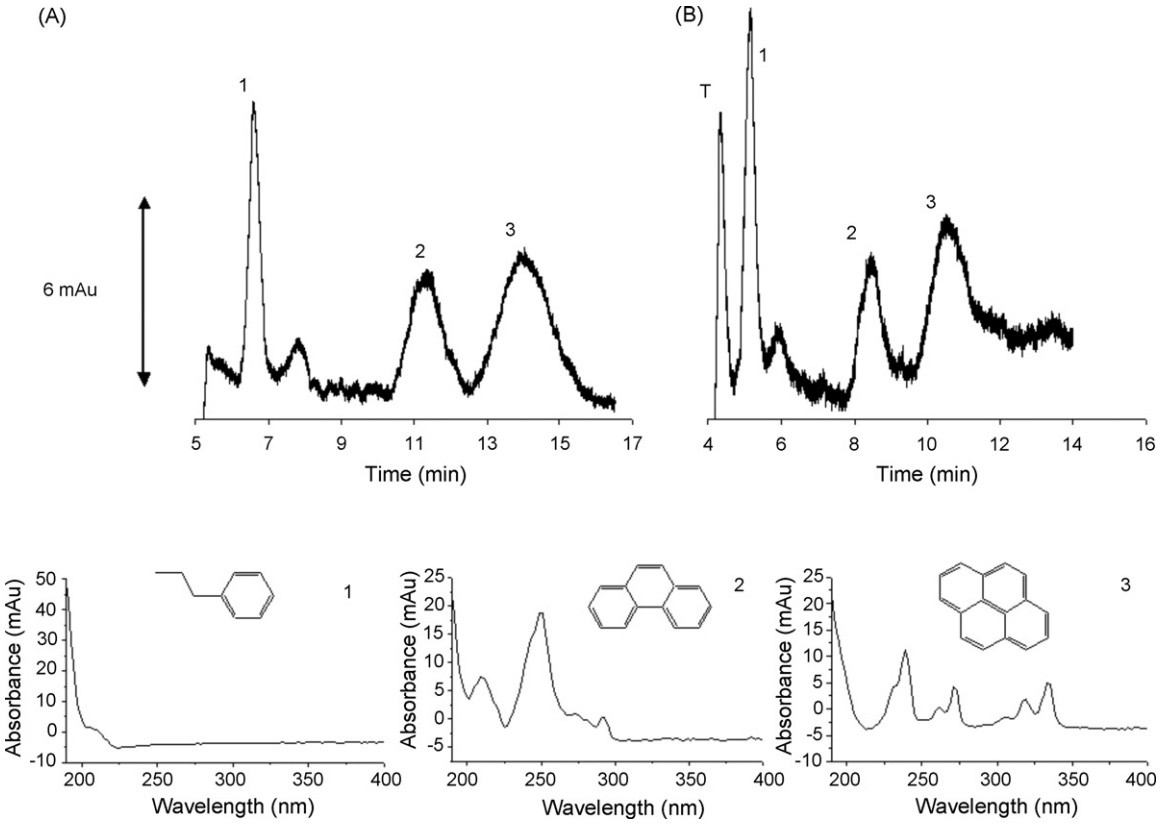

Fig. 3. Electrochromatograms of (1) propylbenzene, (2) phenantrene, (3) pyrene and (T) thiourea (marker compound) obtained from monolithic columns A and B, 36 cm (27.5 cm effective length), 125 μm i.d and 10 cm of PMSP. Mobile phase, 50 mmol L^{-1} NH_4Ac buffer/H_2O/ACN (1:2:2); voltages: +20 kV and +25 kV for columns A and B, respectively; temperature: 20 °C; injection: 40 mbar for 10 s; detection: 200 nm.

diluting 0.44% and 0.98% (m/v) of Irgacure 819 (photoinitiator) in toluene (porogene). The porogenic solutions were stirred for about 10 min, then added to the corresponding amount of monomer solutions A and B as showed in Table 1. The mixture were stirred for 30 min at room temperature, in dark, to afford a yellow solution. Then, the inner wall of two capillaries was pretreated by pressure flush with 1.0 mol L^{-1} NaOH solutions (20 min), deionized water (5 min) and air (5 min). The 36 cm pretreated capillaries were filled with sol up to 10 cm using a disposable syringe (column A) or CE equipment (column B). The column B was filled from the outlet to inlet by applying 40 mbar pressure for 10 s, corresponding to 10 cm of filling.

The filled capillaries were irradiated in the homemade UV–vis chamber for 20 min to form the PMSP. After that, column A was placed in an oven with temperature set at 60 °C for 12 h while column B was not. After this period of time, each capillary containing the PMSP was normally installed in the cartridge and conditioned by pressure rinsing (900 mbar) in the CE instrument with methanol (20 min) and the separation electrolyte (10 min). The electrokinetic conditioning (+20 kV column A or +25 kV column B) with electrolyte solution was done until a stable baseline was achieved. In between runs, the capillary containing the PMSP was replenished with electrolyte solution (5 min, pressure flush).

2.4. Standard solutions

Stock solutions containing 4.2 mg of thiourea, 30.1 mg (35 μL) of propylbenzene, 8.9 mg of phenanthrene and 11.6 mg of pyrene were separately dissolved in 5 mL of methanol and stored in the freezer. The standard mixture containing 1.0 mmol L^{-1} of each standard was dissolved in the electrolyte solution before injection.

2.5. Electrolyte system preparation

The buffer solutions were prepared with purified water (Milli-Q system, Millipore, Bedford, USA). A 50 mmol L^{-1} ammonium acetate buffer was prepared through the addition of 143 μL of acetic acid (99.7%) with 664 μL of ammonium hydroxide (29%). The optimized electrolyte solution was obtained through the mixture of the buffer, water and ACN (1:2:2) v/v/v. This mixture was sonicated for 10 min.

3. Results and discussion

3.1. Considerations on photopolymerization

The term photopolymerization used in this work is actually a combination of a photolysis process (called photoinitiation) and the propagation of a radical polymerization. The first one, which uses the photochemical reactor light, occurs due to the photoinitiator absorption of the UV radiation leading to homolyse to form radicals, which are added to C=C groups present in the molecules of the polymeric precursors. Each reactive intermediary generates polymerization until there are no more radicals or precursor's double bonds [11,14].

A simultaneous evaluation among the spectra plotted in Fig. 1 shows that 370 nm is an optimal wavelength for photoinitiation, because Irgacure 819 and the lamp present maximum absorption and emission at this wavelength, where the polyacrylate exhibits transmittance over 50%.

It is important to note that the polyacrylate film used to measure the transmittance is 0.3 mm thick and the capillary coating

is only about 0.015 mm, which means that the measured transmittance obtained is underestimated. Additionally, it is important to stress that, as the polyacrylate-coated capillary transmits in a large wavelength interval (over 350 nm), it is possible to select other photoinitiators and lamps if their spectra are compatible. In the present case, Irgacure 819 has been chosen because it presented satisfactory results for polymerization in comparison with other tested photoinitiators such as Irgacure 184 and canforquinone.

3.2. Characterization

The prepared PMSP were characterized by means of SEM. Fig. 2 shows images obtained from the cross-sections of columns A and B. The comparative evaluation between the two columns shows that both PMSP segments present network with 1 μm linked spherical structures.

3.3. PMSP qualitative evaluation

Fig. 3 shows the separation profile obtained for standard mixture containing propylbenzene, phenanthrene and pyrene with spectral confirmation for columns A and B. In column B thiourea was used as a marker compound. The electropherograms profile exhibited typical behaviour of a reversed-phase, with less hydrophobic molecules eluting first. For columns A and B, RSD values in migration time of 1.28, 0.38 and 0.21 for propylbenzene, phenanthrene and pyrene, and 0.47, 0.10, 1.08, 0.02 for thiourea, propylbenzene, phenantrene, pyrene, respectively, were obtained for two consecutive injections. An observed problem was the peak tailing due to convective diffusion, since the capillary internal diameter is large (125 μm) and more favorable for zone spreading [15]. However, these results can be considered satisfactory since it is possible to demonstrate that the PMSP have been formed despite different ways of preparation and filling.

4. Conclusions

This work described a PMSP preparation by using of polyacrylate as external coating capillary. In fact, the use of polyacrylate-coating, unlike polyimide and Teflon ones, keeps important features of the capillary unchanged, such as flexibility and mechanical resistance, when photopolymerization via *sol–gel* approach is considered. Once the preliminary results presented in this work were satisfactory, new trials for the preparation of PMSP using polyacrylate-coated capillary with internal diameters of 100 μm and 75 μm, respectively, will be carried out in order to improve the electrochromatographic parameters such as efficiency and resolution.

Acknowledgments

The authors wish to acknowledge the Coordenação de Aperfeiçoamento de Pessoal de Nível Superior (CAPES), Conselho Nacional de Desenvolvimento Científico e Tecnológico (CNPq: 400618/2004-4, 154931/2006-3 and 476386/2007-1) and Fundação de Amparo à Pesquisa do Estado de Minas Gerais of Brazil (FAPEMIG: EDT-161/05 and CEX-APQ 1906-5.02-07) for fellowships and financial support.

References

[1] E.F. Hilder, F. Svec, J.M.J. Fréchet, J. Chromatogr. A 1044 (2004) 3.
[2] W. Li, D.P. Fries, A. Malik, J. Chromatogr. A 1044 (2004) 23.
[3] F. Svec, E.C. Peters, D. Sykora, J.M.J. Frechet, J. Chromatogr. A 887 (2000) 3.
[4] Á. Végvári, J. Chromatogr. A 1079 (2005) 50.
[5] M. Lämmerhofer, F. Svec, J.M.J. Fréchet, W. Lindner, Trends Anal. Chem. 19 (11) (2000) 676.
[6] I. Gusev, X. Huang, C. Horváth, J. Chromatogr. A 855 (1999) 273.
[7] M. Kato, K. Sakai-K., T. Toyo'oka, M.T. Dulay, J.P. Quirino, B.D. Bennett, R.N. Zare, J. Chromatogr. A 961 (1) (2002) 45.
[8] Q. Tang, M.L. Lee, Trends Anal. Chem. 19 (11) (2000) 648.
[9] J. Zheng, S.A.A. Rizvi, S.A. Shamsi, J. Hou, J. Liq. Chromatogr. Relat. Technol. 30 (1) (2007) 43.
[10] M.T. Dulay, J.P. Quirino, B.D. Bennett, M. Kato, R.N. Zare, Anal. Chem. 73 (2001) 3921.
[11] W.J. Gong, Y.-J. Zhang, Y.-P. Zhang, S.-H. Choi, Chin. Chem. Lett. 17 (6) (2006) 813.
[12] M.R. Balesteros, A.F. Faria, M.A.L. Oliveira, J. Braz. Chem. Soc. 18 (3) (2007) 554.
[13] L.C.G. Filho, G.A. Micke, J. Chromatogr. A 1154 (2007) 477.
[14] S. Jockusch, N.J. Turro, J. Am. Chem. Soc. 120 (1998) 11773.
[15] D.R. Baker, Capillary Electrophoresis, John Wiley & Sons, Inc., New York, 1995, p. 5.

Talanta 76 (2008) 96–101

Contents lists available at ScienceDirect

Talanta

journal homepage: www.elsevier.com/locate/talanta

Application of a metal ion-imprinted polymer based on salen–Cu complex to flow injection preconcentration and FAAS determination of copper

Stanisław Walas*, Anna Tobiasz, Marta Gawin, Bartosz Trzewik, Marcin Strojny, Halina Mrowiec

Jagiellonian University, Faculty of Chemistry, ul. Ingardena 3, 30-060 Kraków, Poland

ARTICLE INFO

Article history:
Received 3 October 2007
Received in revised form 7 February 2008
Accepted 14 February 2008
Available online 10 March 2008

Keywords:
On-line preconcentration
Salen-based ion-imprinted polymer
Copper
Flow injection-flame atomic absorption spectrometry

ABSTRACT

A new Cu(II)-imprinted polymer (Cu-IIP) for preconcentration of copper by liquid–solid extraction via flow injection technique has been proposed. Cu-IIP was obtained by copolymerization of salen–Cu(II) complex with styrene and divinylbenzene using suspension polymerization technique. Granules fraction of 60–80 μm in diameter was used as a microcolumn packing. Cu(II) sorption was proved to be the most effective from solutions of pH 7, whereas similar elution effectiveness was observed when applying as eluents hydrochloric or nitric acid in the concentration range of 0.5–10% (v/v). The system exhibited good long-term stability and acid resistance. Batch sorbent capacity was found to be 0.11 mmol g^{-1} of a dry polymer. Enrichment factor (EF) for 30 s loading time was 16. Preconcentration of Cu(II) and potentially interfering metal ions is strongly pH dependent. Examination of Cu(II) sorption in the presence of Pb(II), Cd(II), Zn(II) and Ag(I) showed significant influence of cadmium and zinc ions only and that was for the interferent concentrations above 0.5 mg L^{-1} (Cu-IIP mass of ca. 35 mg). The interference effect was reduced with the sorbent mass increase. Fe(III) and Mn(II) ions, present in treated tap water in relatively high concentrations, did not interfere. Effective pH adjusting of the loaded solution in on-line mode, when applying diluted Clark–Lubs buffering solution, allowed accurate copper determination in tap water (compared to graphite furnace atomic absorption spectrometry, GFAAS) using standard addition or combination calibration method.

1. Introduction

Sensitivity of many popular analytical techniques, e.g. flame atomic absorption spectrometry (FAAS), is generally insufficient for trace analysis [1], therefore analyte preconcentration is required. Flow methods are universal tools for sample pretreatment, including preconcentration of analyte preceding its subsequent determination [2,3]. They improve selectivity of the analytical method and provide flexibility of enrichment factors appropriate for given analytical needs.

Although FAAS is generally a specific determination method, introducing a preconcentration step may lead to interferences in this stage due to sorbents insufficient selectivity. For that reason new packing materials are still being proposed and examined. Recent achievements in this field have been summarized in a review by de Pereira and Arruda [4]. Ion-imprinted polymers (IIPs), based on the idea of molecular imprinting technique, have attracted much attention as selective sorbents for preconcentration of metal ions [5–8]. In ion imprinting it is a metal ion which serves as a template. The choice of a complexing ligand is of great importance here, as it directly influences selectivity of the sorbent. Also the coordination geometry and the coordination number of a metal ion together with the charge and the size of the ion play an important role in obtaining selective IIPs [9]. Ion-imprinted polymers have already found various applications, e.g. in separation, preconcentration and purification processes with regard to metal ions including transition elements [10], actinides [11], lanthanides [12] and noble metals in diverse matrices [13].

Shiff bases may be perspective complexing ligands for ion imprinting purposes due to their complexing abilities towards heavy metals. They have been applied both as reagents in simple spectrophotometric determinations [14] and as modifying agents for various sorbents [15–17]. Among Shiff bases especially salens have been used for forming organometallic complexes but to the authors' knowledge they have not served as complexing ligands for IIPs yet.

Here we present a salen-based copper-imprinted polymer for on-line flow injection microcolumn preconcentration of Cu(II). The system was coupled with flame atomic absorption spectrometer in order to improve the sensitivity of copper determination.

* Corresponding author. Fax: +48 12 634 05 15.
E-mail address: walas@chemia.uj.edu.pl (S. Walas).

0039-9140/$ – see front matter © 2008 Elsevier B.V. All rights reserved.
doi:10.1016/j.talanta.2008.02.008

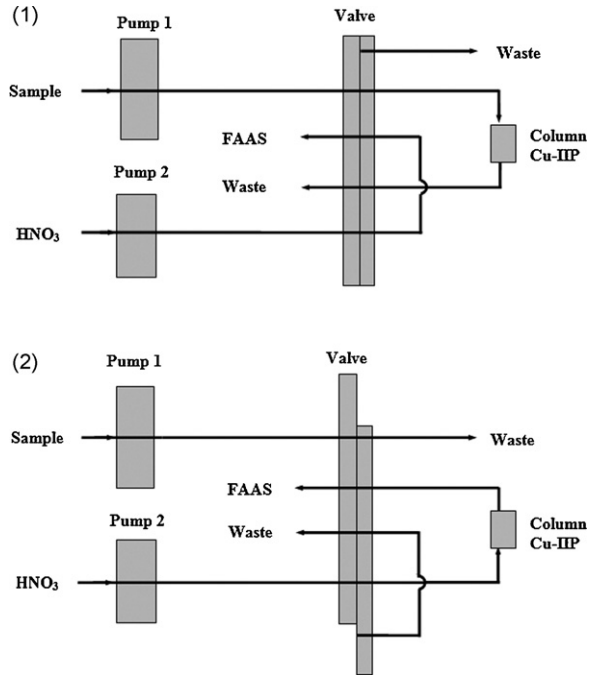

Fig. 1. A scheme of the flow injection preconcentration system FIAS 400: valve positions for sorption (1) and elution (2) step.

2. Experimental

2.1. Apparatus

PerkinElmer FIAS 400 flow injection system coupled with AAnalyst 300 flame atomic absorption spectrometer was applied. Air/acetylene flame was used and copper was determined at the wavelength of 324.8 nm. Deuterium background correction was applied in all measurements. Fig. 1 illustrates the on-line flow injection preconcentration system coupled with FAAS with the use of a capillary of 16 cm in length. FIAS 400 preconcentration system comprises two peristaltic pumps, a two-positional valve and a preconcentration column. Two TYGON R3607 red-red pump tubes (I.D. 1.14 mm) were applied for both pumps in most of the experiments. Only for on-line pH adjusting one yellow-blue tube (I.D. 1.52) and one red-red tube were used for pump 1.

Elmetron (Zabrze, Poland) CPI-551 pH-meter was used for pH measurements.

For GFAAS analyses SpectrAA Zeeman 220 (Varian) was applied.

NMR, IR spectra and elemental analysis were performed with the use of Bruker Avance II 300 MHz spectrometer, Bruker Equinox 55 spectrometer and EuroEA 3000 Elemental Analyzer, respectively.

Scanning electron microscope (SEM), ZEISS Leo 435 VP was applied to take microphoto of obtained microbeads.

2.2. Reagents and solutions

For organic synthesis of salen–Cu complex: 97% allyl bromide, Aldrich (Milwaukee, USA), ethylenediamine pure for analysis, Aldrich (Milwaukee, USA), salicylaldehyde pure, Aldrich (Milwaukee, USA), copper acetate pure for analysis, Merck (Darmstadt, Germany) were used. During polymerization process pure styren and 55% divinylbenzene, Aldrich (Milwaukee, USA) were applied. All solvents were of pure for analysis grade.

Standard stock solutions ($1\,g\,L^{-1}$) of copper, lead, cadmium, cobalt, nickel, chromium, manganese, iron, mercury, magnesium, silver and zinc were prepared from Merck (Darmstadt, Germany) Titrisol solutions. Standard solutions were prepared by dilution of the stock solutions with deionized water. Eluent solutions (0.5; 1.0; 5.0 and 10.0% (v/v)) were prepared by dilution of concentrated nitric and hydrochloric acid, pure for analysis, Merck (Darmstadt, Germany). Deionized water after reversed osmosis was used throughout the work, also for preparation of blanks.

Britton–Robinson and Clark–Lubs buffer solutions were prepared according to Ref. [18]. In the former case, the buffers were prepared by mixing acidic solution (a mixture of 0.04 mol phosphoric acid, 0.04 mol boric acid and 0.04 mol acetic acid per litre) with 0.2 mol L^{-1} sodium hydroxide solution in appropriate ratios. In the latter case, 0.1 mol L^{-1} KH_2PO_4 solution and 0.1 mol L^{-1} NaOH were the buffer components.

2.3. Preparation of salen–Cu complex

The chelating ligand—salen was obtained in a three-step organic synthesis. Salicylaldehyde (0.33 mol) was dissolved in acetone (0.5 mL), then allyl bromide (0.35 mol) and potassium carbonate (55.7 g) were added to the solution. The mixture was heated under reflux for 3 h, then the solvent was removed using rotary evaporator and finally the residue was distilled under reduced pressure. The intermediate product (refractive index (RI) 1.557) was subsequently subjected to Claisen rearrangement by heating. Thus, obtained product (0.06 mol) (RI = 1.564) and ethylendiamine (0.03 mol) were dissolved in ethanol (110 mL) and heated under reflux for 2 min. Yellow crystals of salen were obtained and filtered. ^{1}H NMR ($CDCl_3$): δ = 13.52 (s, 1H, OH), 8.36 (s, 1H, CH═N), 7.19 (dd, J = 7.5, 1.8 Hz, 1H, H-3), 7.12 (dd, J = 7.5, 1.8 Hz, 1H, H-5), 6.82 (t, J = 7.5 Hz, 1H, H-4), 6.03 (ddt, J = 23.2, 10.5, 6.6 Hz, 1H, —CH═), 5.10 (ddd, J = 8.6, 3.6, 1.5 Hz, 1H, CH_2═), 5.06 (t, J = 1.5 Hz, 1H, CH_2═), 3.93 (s, 2H, N—CH_2), 3.74 (s, 3H, OCH_3), 3.44 (d, J = 6.6 Hz, 2H, CH_2). ^{13}C NMR ($CDCl_3$): δ = 166.7 (C═N), 158.9 (C-1), 136.6, 132.6, 129.7, 127.8, 118.3, 118.1, 115.6, 59.6 (CH_2—N), 33.6 (CH_2═). FT-IR (KBr, cm^{-1}): 3500 (ν (OH); broad), 1631 (ν (C═N)), 1448 (ν (C═C)), 912 (γ (═C—H); vinyl), 744 (γ (C—H); aromatic). Calculated for $C_{22}H_{24}N_2O_2$ (%): C, 75.84; H, 6.95; N, 8.04. Analytically found: C, 75.70; H, 6.98; N, 8.14.

Complexation reaction was performed as follow: salen (2 mmol) was dissolved in ethanol (15 mL) and added to solution of copper acetate (2.4 mmol) in water (5 mL) upon stirring. Dark violet crystals of salen–Cu complex were obtained and filtered. FT-IR (KBr, cm^{-1}): 1624 (ν (C═N)), 1546 (ν (C═C); vinyl), 916 (γ (C—H); aromatic), 462 (ν (N—Cu)). Calculated for $C_{22}H_{22}N_2O_2Cu$ (%): C, 64.14; H, 5.38; N, 6.82. Analytically found: C, 64.65; H, 5.52; N, 6.89.

2.4. Preparation of copper(II)-imprinted polymer microbeads

IIP microbeads were prepared by suspension polymerization technique. The procedure was as follow: (i) dispersion medium was prepared by dissolving sodium chloride (0.3 g) and gelatine (2.1 g) in water (100 mL); (ii) salen–Cu complex (0.11 g) was dissolved in chloroform (11 mL) and subsequently mixed with styrene (7.5 mL) and divinylbenzene (1.5 mL); then benzoylperoxide (BPO) (0.5 g) was added as an initiator; (iii) both solutions were transferred to thermostatted reactor and mechanically stirred. The reactor temperature was kept constant at 90 °C for 4 h. The scheme of the Cu-IIP preparation process is presented in Fig. 2.

Thus, obtained spherically shaped microbeads were separated from the polymerization medium, thoroughly washed with water and dried in a vacuum oven for 24 h. Control (non-imprinted) polymer was prepared in a similar way but salen ligand (0.10 g) was used instead of salen–Cu complex. Both imprinted and non-imprinted polymers were subsequently sieved and the fraction of

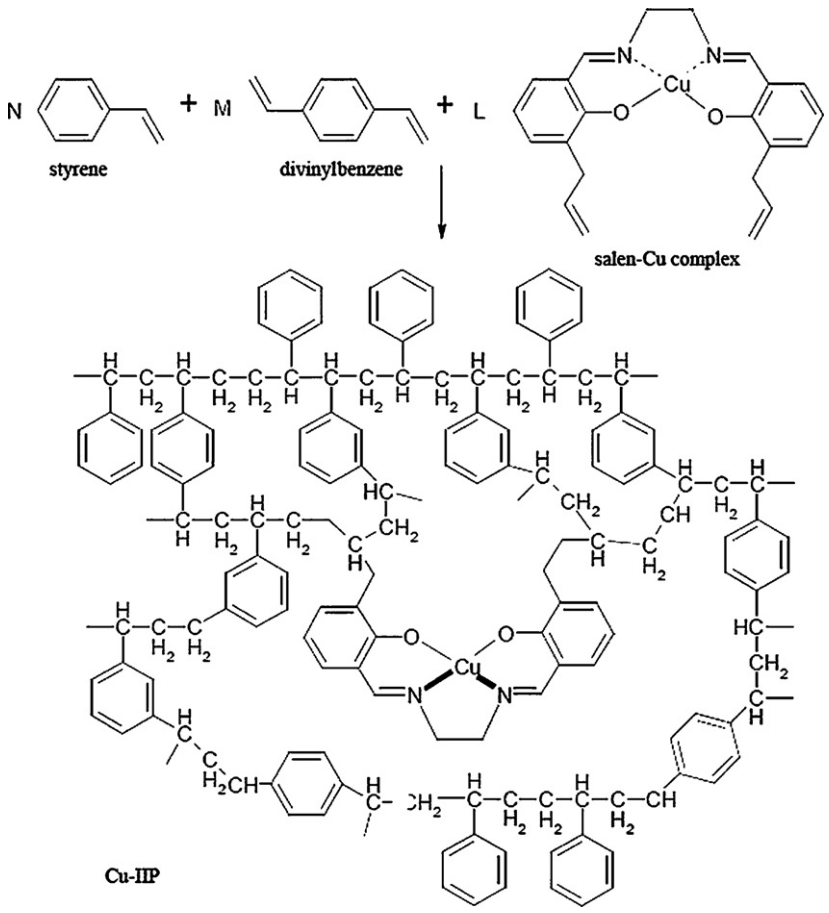

Fig. 2. Scheme of the proposed Cu(II)-imprinted polymer preparation.

diameter range of 60–80 μm (Fig. 3) was used as a microcolumn filling.

2.5. Extraction procedure

Cylindrical column (0.5 cm in length and 3 mm in diameter) packed with ca. 35 mg of the prepared polymer was used for most of the experiments—such a small portion of the sorbent was applied intentionally to show the polymer properties in detail. A column of 3.0 cm in length (3 mm in diameter; 150 mg sorbent) was applied for special purposes. In order to prevent leakage of the sorbent SPE polyethylene frits were used. FI-FAAS set was controlled by a computer program including: pre-filling, filling, loading and elution step (Table 1).

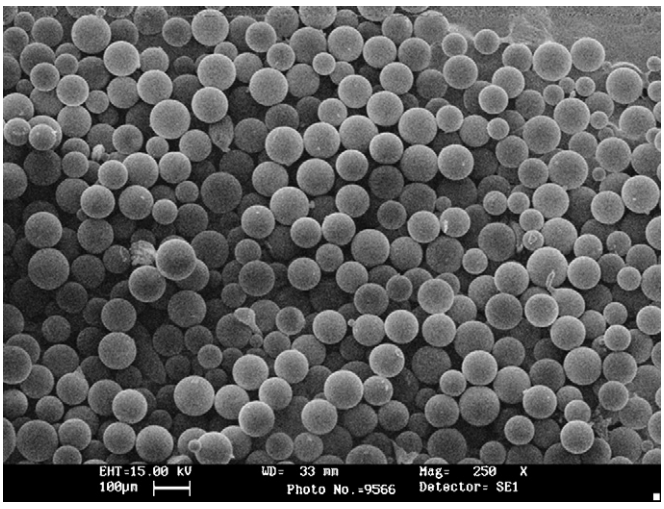

Fig. 3. Scanning electron microscope photo of the Cu(II)-imprinted polymer microbeads.

Each preconcentration cycle was proceeded by a short loading and elution step performed to fill the tubes. Loading time was 30 s for most of the experiments. Elution, including 10 s reading time, lasted for another 30 s. During the sample loading step, 10 s before the valve was moved to the elution position, the signal readings were stabilized with the eluent solution and finally set zero. To assure effective and stable nebulization, the flow rate in the elution step was set at 8 mL min^{-1}. Absorbance peak was registered and its height was the analytical signal. For every standard and sample solution four series of measurements were carried out in a random order. Each measurement was followed by a blank check.

Table 1
FI program for preconcentration of copper; +: on; −off.

Step	Time (s)	Pump 1	Pump 2	Loading	Elution	Reading
Pre-fill	1	+	+	+	–	–
1	10	+	–	+	–	–
2	20	–	+	–	+	–
3	20	+	–	+	–	–
4	10	+	+	+	–	–
5	30	–	+	–	+	+
6	1	–	–	–	+	–

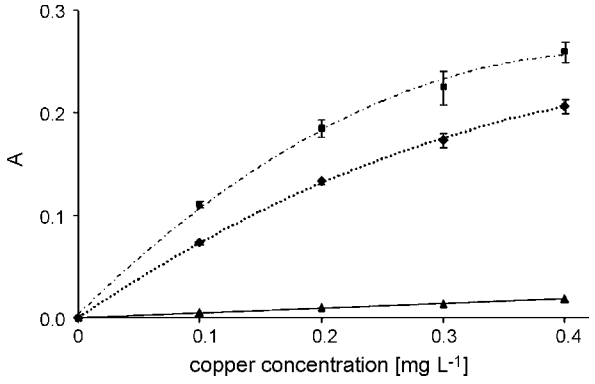

Fig. 4. Signal dependence on copper concentration with and without preconcentration step; — FAAS; ··· FI-FAAS; sorption time 30 s; -·-·-· 60 s; sorbent mass 35 mg; pH 7.

3. Results and discussion

3.1. Copper extraction from Cu-imprinted polymer

Copper ions acting as a template in the imprinting process were removed from the polymer to free the active sites in the polymeric net. Extraction was carried out directly in the flow system and various eluents including EDTA, nitric or hydrochloric acid solutions of different concentrations were used. 5% HNO_3 (v/v) appeared to be the most effective of the above-mentioned solutions, hence it was used as eluent for template extraction. Elution efficiency of copper sorbed on the polymer in the preconcentration process was also evaluated and 1% HNO_3 was chosen for this purpose.

3.2. Optimum pH range for preconcentration of copper

Complex formation between salen immobilized in the polymeric net and copper ions present in a sample was expected to be pH dependent. For this reason pH influence of the loading solution on the preconcentration of copper was tested. Copper standard solutions (0.3 mg Cu L^{-1}) within a wide range of pH (2.87–11.98) were prepared and analyzed according to the above-mentioned procedure. For buffering purposes Britton–Robinson (phosphate–borate) buffers were used. In low pH range copper preconcentration was hindered due to strong protonation of the active sites in the sorbent. The medium pH increase facilitated complex formation and the maximum was reached at pH 7. For higher pH values the signal decrease was observed. Therefore, for further preconcentration experiments pH of copper solutions was set at 7.

3.3. Enrichment factor

Enrichment factor was calculated as a ratio of the calibration curve slope obtained when applying the preconcentration step (FI-FAAS) and the slope obtained without it (FAAS). For standards buffered to pH 7 and 30-s loading time EF accounted for 16. Although the enrichment factor was higher when 60-s loading time was applied (EF 23), to assure satisfactory sample throughput for further studies 30-s loading time was accepted. The mentioned calibration functions are presented in Fig. 4.

3.4. Sorption capacity

To estimate sorption capacity of the tested polymer experiments were performed both in a flow injection and a batch mode. In the former case the dependence of the analytical signal on a wide concentration range of the loaded solution (0.1–10 mg Cu L^{-1}) was determined as follow. 35 mg of the sorbent was packed into a microcolumn and used for copper preconcentration. Loading time was set at 30 s. The absorbance was rising with growing concentration of copper, although the increase was non-linear. No plateau was reached in the tested range of concentration. To find the percentage of copper ions retained on the sorbent standard solutions of 0.1–0.4 mg Cu L^{-1} were loaded onto the sorbent and the effluent was collected for subsequent copper determination by graphite furnace atomic absorption spectrometry (GFAAS). The obtained results indicated that only about 70% of copper ions was retained on the sorbent. This result is an effect of a compromise between the sample loading rate (higher than the optimal one) and determination sensitivity resulting from total quantity of coper ions loaded on the sorbent in 30-s sorption time.

Batch sorption capacity was examined as follow: 35 mg of the polymer was added to 20 mL of a standard solution (3, 5, 10, 20, 50 mg L^{-1}) and the mixture was magnetically stirred for 60 min. After that time an aliquot was analyzed with the use of FAAS. Mass of the retained copper was calculated as a difference of initial Cu(II) mass in the solution and the one left after reaching the equilibrium. Batch sorption capacity was found to be 0.11 mmol g^{-1} (7.22 mg g^{-1}).

3.5. Sorbent stability

Sorbent stability in the working conditions was evaluated for one hundred repetitive preconcentration cycles (0.3 mg Cu L^{-1}, pH 7) and 30-s loading time. The obtained absorbance values did not form any trend which proved good sorbent stability in the working conditions.

3.6. Interference studies

Selectivity of the polymer was investigated in a three-stage procedure. In the preliminary stage a possibility of different metal ions sorption was evaluated for two concentration levels of a particular ion (0.2 and 1.0 mg L^{-1}) both with and without preconcentration step. As different elements determination sensitivity vary when applying AAS as a detector, enrichment factors (EFs) for potential interfering ions were calculated and compared instead of comparing absorbance values obtained in a single measurement. Among Cu(II), Cd(II), Co(II), Cr(III), Mn(II), Hg(II), Ag(I), Mg(II), Zn(II), Fe(III), Ni(II), Pb(II) significant enrichment was found for Cu(II), Pb(II), Cd(II), Ag(I) and Zn(II).

In the second stage influence of the loading solution pH on preconcentration of a given ion was evaluated. The results presented in Fig. 5 indicate that in the pH range optimal for copper sorption the

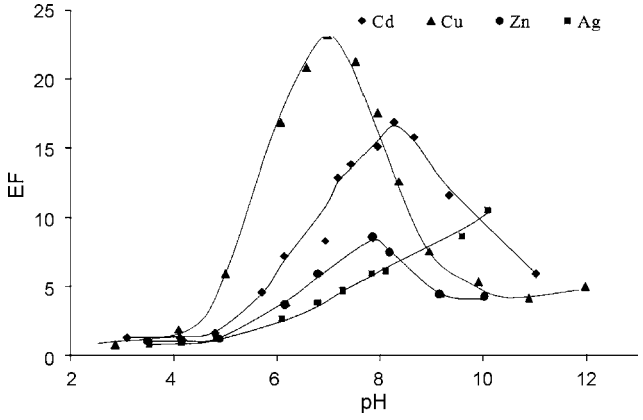

Fig. 5. Influence of pH on preconcentration of Cu(II), Cd(II), Zn(II), Ag(I); Cu-IIP mass: 35 mg, concentration of the standard solutions: 0.3 mg L^{-1}.

Table 2
Influence of Zn(II), Cd(II), Ag(I) and Pb(II) on copper(II) preconcentration

Concentration of interferent ($mg\,L^{-1}$)	Recovery (%)			
	$0.2\,mg\,L^{-1}$ [a]		$0.4\,mg\,L^{-1}$ [a]	
	Control polymer	Cu-IIP	Control polymer	Cu-IIP
Zn((II)				
0.1	**95.6 ± 0.3**[b]	**94.7 ± 0.3**	88.5 ± 0.6	**100.3 ± 0.9**
0.2	94.0 ± 0.2	**104,8 ± 0.2**	86.3 ± 0.7	**96.5 ± 0.5**
0.5	87.4 ± 0 **1**	**99.5 ± 0.1**	85.4 ± 0.3	94.2 ± 0.2
1.0	76.2 ± 0.3	**91.3** ± 0.4	84.4 ± 0.1	**77.1** ± 0 **1**
Cd(II)				
0.1	**98.7 ± 0.5**	**100.0 ± 0.9**	**100.8 ± 0.4**	**96.9 ± 0.1**
0.2	**100.5 ± 0.5**	**94.9 ± 0.3**	**90 5** ± 02	**95.2 ± 0.8**
0.5	90.4 ± **0.1**	**94.9 ± 0.3**	87.9 ± **0.1**	**96.3 ± 0.2**
1.0	**86.1** ± 0.5	74.2 ± 0.3	88.9 ± 0.4	93.4 ± **0.1**
Ag(I)				
0.1	**100.3 ± 0.1**	**95.3 ± 0.3**	**103.8 ± 0.1**	**101.9 ± 0.2**
0.2	**100.6 ± 0.2**	**101.9 ± 0.5**	**99.1 ± 0.2**	**95.7 ± 0.4**
0.5	91.3 ± 0.2	**103.1 ± 0.3**	**994 ± 0.3**	**97.0 ± 0.3**
1.0	87.7 ± 0.3	**102.7 ± 0.2**	**99.8 ± 0.6**	**100.5 ± 0.7**
2.0	84.7 ± 0 5	**100.4 ± 0.2**	**92.1** ± 0.2	**96.8 ± 0.2**
5.0	85.9 ± 0.3	**96.5 ± 0.7**	79.8 ± 0.2	**96.5 ± 0.2**
Pb(II)				
0.1	**97.5 ± 0.0**	**99.5 ± 0.2**	**97.8 ± 0.8**	**101.5 ± 0.6**
0.2	89.9 ± 0.2	**99.6 ± 0.4**	**99.8 ± 0.3**	**104.0 ± 0.4**
0.5	91 0 ± 0.1	86.0 ± 0.2	**91.8** ± 0.6	89.8 ± 0.5
10	87 7 ± 0.2	76 3 ± 0 2	85.7 ± 0.5	87.5 ± 0.3

[a] Concentration of Cu(II).
[b] Recovery values higher than 95 % were bolded.

potential interfering ions are also complexed but to a lesser extent. In spite of lower interferent co-extraction in acidic medium it was decided to adjust the samples pH to 7 in subsequent experiments due to significant loss of sensitivity for copper in other pH regions.

In the third stage individual influence of each interfering metal ion on copper preconcentration at pH 7 was examined. Solutions containing copper at two concentration levels (0.2 or $0.4\,mg\,L^{-1}$) and an interferent at concentration ranging from 0 to $5.0\,mg\,L^{-1}$ were analyzed both for Cu-imprinted and non-imprinted polymer. For Cu-imprinted polymer presence of Cd(II), Zn(II) at concentrations higher than $0.5\,mg\,L^{-1}$ resulted in copper signal decrease. Pb(II) at concentration lower than $0.2\,mg\,L^{-1}$ did not influence copper sorption. Silver ions did not affect copper preconcentration. For non-imprinted polymer interference effect (recovery <95%) occurred for lower interferent concentration than for Cu-imprinted polymer as presented in Table 2.

3.7. Preconcentration of copper present in water samples

The imprinted polymer was applied to determination of copper in tap water samples from water installation containing copper elements. Two procedures of adjusting a sample pH: (a) manual and (b) on-line were applied and copper concentration was determined with the use of the following calibration methods: the set of standards method (SSM), the standard addition method (SAM) or the combination calibration method (CCM). The applied combination calibration method integrates the virtues of the set of standards method and the standard addition method. In this approach concentration of a given analyte in one sample is determined as in SAM (i.e. in interpolative way), while for the rest of the samples the analyte concentration is found as in SSM (i.e. in interpolative way). Regression equations for SSM and SAM with manual pH adjusting (pH 7, sorbent mass 150 mg) were: $A = 0.516\ c_{Cu}$ and $A = 0.578\ c_{Cu} + 0.043$, respectively.

GFAAS analyses were performed in order to compare the results obtained for copper when applying the proposed method. Relative error (RE) was calculated according to Eq. (1):

$$RE = \frac{c_{Cu}(FI - FAAS) - c_{Cu}(ETAAS)}{c_{Cu}(ETAAS)} \times 100\% \quad (1)$$

Relative error of 12.8% and 5.7% was found for SSM and SAM, while relative standard deviation (R.S.D.) accounted for 2.4% and 3.4%, respectively. The limit of detection (LOD) for the set of standard calibration method was calculated as a standard deviation (3σ) from 10 readings of the blank divided by the slope of the calibration line and was found to be $9.0\,\mu g\,L^{-1}$.

In the on-line procedure of pH adjustment the flow rate for a standard or a sample was kept as in the manual one ($8\,mL\,min^{-1}$) while a buffering solution was transported with an additional tube ($4\,mL\,min^{-1}$) and mixed with a standard/sample before reaching the column. In order to find the optimal working conditions parameters like: the sort of a buffering solution and its concentration, loading time, length and shape of a mixing coil were optimized. At first application of sodium hydroxide of different concentrations was tested for adjusting the standards pH and the highest signal for copper was achieved when $4 \times 10^{-5}\,mol\,L^{-1}$ NaOH was applied. However, for real samples pH adjustment with sodium hydroxide could be inadequate, hence several other buffering solutions were examined and Clark–Lubs buffer (pH 7) diluted 8 times was chosen as optimal.

Influence of the loading time on the sorption process was evaluated taking into account EF values. Calibration equation in the concentration range 0–$0.2\,mg\,Cu\,L^{-1}$ was found both for FAAS and FI-FAAS technique (preconcentration time: 30, 60, 120 s; sorbent mass 150 mg; on-line pH adjustment, pH 7) and thus obtained slopes were used for calculating the EF values. The dependence was found linear up to 60-s and changed to non-linear when longer loading time was applied. The EF values for 30-, 60- and 120-s sorption time were: 14, 26 and 43, respectively.

Table 3
Copper concentration in tap water samples obtained for CCM

Sample	FI-FAAS ($\mu g\,L^{-1}$)	ETAAS ($\mu g\,L^{-1}$)	RE (%)	R.S.D. (%)
Extrapolative method				
1	19	21	9.4	5.9
Interpolative method				
2	27	24	13.2	12.4
3	23	21	9.6	8.3
4	156	146	7.0	1.6

Calibration equation $y = 0.5701x + 0.0106$; correlation coefficient: $R = 0.9975$; standard addition range 0–0.2 $mg\,L^{-1}$.

On-line buffering system was applied to determination of copper in tap water samples by CCM. For the first sample copper concentration was obtained via extrapolation according to SAM, whereas for the rest of the samples it was calculated in interpolative way using the calibration line established for the first sample. Copper concentration found and relative error calculated for exemplary samples are presented in Table 3.

To evaluate trueness of the proposed method synthetic water of composition adequate to SPS-SW2 (Reference Material for Measurement of Elements in Surface Waters, Spectrapure Standards AS, Oslo Norway) with copper concentration 100 $\mu g\,L^{-1}$ was prepared and analyzed. Comparison of copper concentration found (98 ± 1) and theoretical one proved good trueness of the method.

4. Conclusions

The salen based Cu-IIP prepared by suspension polymerization technique fulfils the most important requirements needed for FIA preconcentration: spherical shape resulting in low flow back pressure, good ion-exchange effectiveness, acid resistance and long-term stability—no significant loss of activity was observed.

The proposed sorbent does not require the analyte to be converted into a complex prior to retention and the only parameter strongly influencing sorption and selectivity is pH of the loading solution, thus sample pretreatment is very easy and incorporates only pH adjusting which can be done on-line with the same setup.

The enrichment factor obtained for 30 s loading time is typical for the applied preconcentration procedure (when the analyte peak obtained in the elution process appears in about 2 s) and is of the same order or even better than EFs reported for other sorbents [19–21], when recalculating data to comparable preconcentration conditions. Longer loading time resulted in EF increase, albeit no linear correlation was observed in the tested conditions (sorbent mass and flow rate).

LOD value obtained for the new salen based copper-imprinted polymer, loading solution volume 4 mL and sample sorption time 30 s is comparable with those found for other sorbents. For some comparison LOD values: 0.2 $\mu g\,L^{-1}$ [19], 8.4 $\mu g\,L^{-1}$ [20], 0.4 $\mu g\,L^{-1}$ [22], were obtained for loading solution volumes: 11.3, 13 and 14.4 mL, and sample sorption: 90, 120 and 120 s, respectively.

The proposed IIP although appeared not specific for copper showed good selectivity. The only significant influence on Cu(II) preconcentration was observed for cadmium and zinc ions at concentrations above 0.5 $mg\,L^{-1}$, however the aforesaid metal ions are not to be found in tap water on this level. Moreover, thanks to the sorbent selectivity copper is separated from iron or manganese ions which are present in water due to its treatment. When compared to non-imprinted polymer, the presented IIP exhibits much higher selectivity towards all tested ions.

The proposed method may find application in copper determination in water samples, as was exemplified in analysis of tap water. The method shows good accuracy especially when the standard addition method or combination calibration method are used for potential matrix effects elimination.

References

[1] J.A. Broekaert, Analytical Atomic Spectrometry with Flames and Plasmas, Wiley–VCH, Weinheim, 2002.
[2] Z. Fang, Flow Injection Atomic Absorption Spectrometry, John Wiley & Sons, Chichester, 1995.
[3] Z. Fang, Flow Injection Separation and Preconcentration, Wiley–VCH, Weinheim, 1993.
[4] M.G. de Pereira, M.A.Z. Arruda, Microchim. Acta 141 (2003) 115.
[5] T. Prasada Rao, R. Kala, S. Daniel, Anal. Chim. Acta 578 (2006) 105.
[6] T. Prasada Rao, S. Daniel, J.M. Gladis, TrAC 23 (2004) 28.
[7] R.A. Bartsch, M. Maeda (Eds.), Molecular and Ionic Recognition with Imprinted Polymers, American Chemical Society, Washington, DC, 1998.
[8] B. Sellergren (Ed.), Molecularly Imprinted Polymers: Man-made Mimics of Antibodies and Their Applications in Analytical Chemistry, Elsevier, Amsterdam, 2001.
[9] G. Wulff, Angew. Chem. Int. Ed. Engl. 34 (1995) 1812.
[10] H. Yavuz, R. Say, A. Denizli, Mater. Sci. Eng. C 25 (2005) 521.
[11] P. Metilda, J.M. Gladis, T. Prasada Rao, Anal. Chim. Acta 512 (2004) 63.
[12] O. Vigneau, C. Pinel, M. Lemaire, Anal. Chim. Acta 435 (2001) 75.
[13] S. Daniel, P.E.J. Babu, T. Prasada Rao, Talanta 65 (2005) 441.
[14] G. Tanaru, V. Dorneanu, M. Stan, J. Pharm. Biomed. Anal. 27 (2002) 827.
[15] P. Hashemi, H. Hassanvand, H. Nagimi, A.R. Ghiasvand, Microchim. Acta 150 (2005) 147.
[16] M. Shamsipur, A.R. Ghiasvand, H. Sharghi, H. Naeimi, Anal. Chim. Acta 408 (2000) 271.
[17] F. Shemirani, A.A. Mirroshandel, M.S. Niassari, R.R. Kozani, J. Anal. Chem. 59 (2004) 228.
[18] L. Meites (Ed.), Handbook of Analytical Chemistry, McGraw-Hill Book Company, New York, Toronto, London, 1963.
[19] E.L. da Silva, A.O. Martins, A. Valentini, V.T. de Fávere, E. Carasek, Talanta 64 (2004) 181.
[20] S.V.M. de Moraes, J.L. Brasil, C.D. Milcharek, L.C. Martins, M.T. Laranjo, M.R. Gallas, E.V. Benvenutti, E.C. Lima, Spectrochim. Acta A 62 (2005) 398.
[21] S. Wang, R. Zhang, Microchim. Acta 73 (2006) 154.
[22] E.L. da Silva, E.M. Ganzarolli, E. Carasek, Talanta 62 (2004) 727.

Talanta 76 (2008) 85–90

Contents lists available at ScienceDirect

Talanta

journal homepage: www.elsevier.com/locate/talanta

Capillary electrophoresis with gold nanoparticles enhanced electrochemiluminescence for the detection of roxithromycin

Jingwu Wang [a,*], Zhiming Yang [a], Xiaoxia Wang [b], Nianjun Yang [c,*]

[a] Department of Chemistry, Nanchang University, Nanchang 330031, China
[b] Graduate School of Engineering, University of Fukui, Fukui 910-8507, Japan
[c] Diamond Research Center, National Institute of Advanced Industrial Science and Technology (AIST), Umezono 1-1-1, Tsukuba 305-8568, Japan

ARTICLE INFO

Article history:
Received 21 January 2008
Received in revised form 11 February 2008
Accepted 13 February 2008
Available online 19 February 2008

Keywords:
Enhanced electrochemiluminescence
$Ru(bpy)_3^{2+}$
Gold nanoparticles
Roxithromycin
Capillary electrophoresis

ABSTRACT

Tris(2,2′-bipyridyl) ruthenium(II) ($Ru(bpy)_3^{2+}$)–roxithromycin based electrochemiluminescence (ECL) was enhanced greatly by gold nanoparticles 10 nm in diameter. Capillary electrophoresis (CE) was coupled with the resultant ECL system as a detector for roxithromycin. This ECL emission is explained by the *coreactant* mechanism where roxithromycin behaves as a *coreactant* to generate strong reducing species and gold nanoparticles act as "floating nanoelectrodes". The reaction of $Ru(bpy)_3^{3+}$ with the generated strong reducing species on the Pt working electrode as well as on "floating nanoelectrodes" releases $Ru(bpy)_3^{2+*}$, resulting in enhancement of ECL emission. The selectivity of this detection system towards roxithromycin was examined by CE. Under the optimized conditions, the intensity of ECL emission varies linearly with the concentration of roxithromycin from 24 nM to 0.24 mM. The detection limit is 8.4 nM, while without adding gold nanoparticles it is only 84 nM. The detection of roxithromycin in pharmaceutical and urine samples was also performed by the proposed CE–ECL method.

1. Introduction

Electrochemiluminescence or electrogenerated chemiluminescence (ECL), which is defined as that electrochemically generated reactants undergo a high-energy electron transfer reaction to generate an excited state, was investigated in detail by Hercules and Lytle [1] for the first time. Tokel and Bard [2] pioneered the study on the reaction mechanisms of ECL systems by use of tris(2,2′-bipyridyl) ruthenium(II) ($Ru(bpy)_3^{2+}$) as an ECL reagent. It has been well-known that $Ru(bpy)_3^{2+}$ based ECL emission originates from its excited state $Ru(bpy)_3^{2+*}$, which is possible to be generated in the ways called *annihilation* and *coreactant* mechanism [2–5]. In the *annihilation* reaction mechanism, the excited species $Ru(bpy)_3^{2+*}$ are produced by the reaction of $Ru(bpy)_3^{+}$ with $Ru(bpy)_3^{3+}$, which are produced by applying a suitable voltage on the working electrode in a $Ru(bpy)_3^{2+}$ solution. The excited species $Ru(bpy)_3^{2+*}$ produce an orange emission centered around 610 nm. $Ru(bpy)_3^{2+*}$ can also be produced by oxidizing $Ru(bpy)_3^{2+}$ in the presence of a strong reducing reagent. This is termed as an *oxidative-reduction* mode. Another method to form $Ru(bpy)_3^{2+*}$ is to reduce $Ru(bpy)_3^{2+}$ in the presence of a strong oxidizing reagent. This is named as the *reductive-oxidation* mode. In the cases of *oxidative-reduction* and *reductive-oxidation* mode, a new reactant so-called *coreactant* has to be added into the solution, and thus the reaction mechanism for ECL emission is called *coreactant* mechanism. When the *coreactants* are oxidized or reduced, the strong reducing or oxidizing species are generated. Besides the investigation of ECL emission of $Ru(bpy)_3^{2+}$ in the bulk solution, immobilization of $Ru(bpy)_3^{2+}$ on the electrode surface [6–12] to generate excited species has been also investigated intensively. Recently artificially adding nanometer sized materials (e.g. nanoparticles, carbon nanotubes) into $Ru(bpy)_3^{2+}$ based ECL systems as catalysts [13–16] has been paid much attention. However, few reports [15] focused on the reaction mechanisms of the resultant ECL emissions in the presence of nano-structured materials.

Since the intensity of $Ru(bpy)_3^{2+}$ based ECL emission shows linearity with the concentration of *coreactants* in a wide concentration range and also because $Ru(bpy)_3^{2+}$ based ECL emission is of high-stability and -capability of being generated at room temperature, even in the buffer solutions, $Ru(bpy)_3^{2+}$ based ECL systems have been adopted widely by analytical chemists for the detection of various analytes [2–5,17–20] (e.g. amines, amines surfactants, amino acids, glucose, ethanol, oxalate, naphthlene, erythomycin, codeine, pyruvate, polymerase chain reaction products, and DNA). Unfortunately, they [3] lack selectivity and depend greatly on the environmental conditions (e.g. viscosity, temperature, surfactant, ion strength, and pH values of buffer solutions).

* Corresponding authors. Tel.: +81 29 861 5080; fax: +81 29 861 2771.
E-mail addresses: wangjingwu@ncu.edu.cn (J. Wang), nianjun-yang@aist.go.jp (N. Yang).

0039-9140/$ – see front matter © 2008 Elsevier B.V. All rights reserved.
doi:10.1016/j.talanta.2008.02.006

Nevertheless, the marriage of above ECL detection systems with capillary electrophoresis (CE) [2–5], flow injection analysis (FIA), and high-performance liquid chromatography (HPLC) [17–20] has dissolved the above problems successfully. In this contribution, we report about the enhanced $Ru(bpy)_3^{2+}$ ECL emission in the presence of roxithromycin by gold nanoparticles and the combination of enhanced ECL with CE for the detection of roxithromycin.

Roxithromycin ($C_{41}H_{76}N_2O_{15}$) is a semi-synthetic acid-stable 14-membered macrolide with an esterified oxime side-chain, and has been frequently adopted as a safe and effective treatment for several different infections, including some sexually transmitted diseases, upper and lower respiratory tract infections and asthma, gum infections like gingivitis, and bacterial infections associated with stomach and intestinal ulcers. Although, it has been detected by various routes, for examples, by the microbiological assay [21], by HPLC with various detectors like UV–vis [22], mass spectroscopy [23,24], electrochemical detectors [25,26], and by the coupled FIA with chemiluminescence [27], no reports have been found on CE–ECL detection of roxithromycin in literatures up-till-now. In this paper, we investigated the ECL emission of $Ru(bpy)_3^{2+}$–roxithromycin *coreactant* system before and after adding gold nanoparticles. CE was coupled with the resultant ECL system to improve the selectivity towards roxithromycin during measurements. Under the optimized conditions, the determination of roxithromycin in tablets and urine samples by the proposed CE–ECL method was performed.

2. Experimental

2.1. Chemicals and apparatus

Tris(2,2′-bipyridyl) ruthenium(II) chloride hexahydrate was purchased from Aldrich Chemical (Milwaukee, WI, USA) and roxithromycin was from Vitalpharms Company Ltd. (Zhuhai, China). Other chemicals are commercially available and of analytical grade. The stock solution of 1.0 mg mL^{-1} roxithromycin in pH 8.0 phosphate buffer solution (PBS) was stored in the refrigerator at 4 °C. The roxithromycin solutions were prepared by diluting the stock solution with PBS just before measurements. The water used for the preparation of solutions was purified in a Mili-Q System (Milipore, Bedford, MA, USA). Prior to CE analysis, the required sample solutions and PBS buffer were filtered through 0.22 μm membrane filters (Shanghai Xinya Purification Material Factory, Shanghai, China).

Gold nanoparticles were prepared through the well-known wet-synthetic route [28]. The as-prepared gold nanoparticles were inspected by transmission electron microscopy (TEM) and UV–vis spectroscopy. The gold nanoparticles were suspended in water and were stored in a dark glass bottle in a refrigerator. Please note here that the glassware used for the synthesis of gold nanoparticles is always better to be cleaned carefully.

The CE–ECL detection system (Xi'an Remax Electronics Co. Ltd., Xi'an, China) consists of a high-voltage power supply for electrophoretic separation and electrokinetic injection, a potential control system, a chemiluminescence detector, and a data processor. The electrophoresis is driven by the high-potential apparatus and the high voltage is applied at the end of the injection. This high-potential apparatus provides a separation voltage across the capillary to drive sample, but also introduces the samples by electromigration injection at a definite time. The construction of ECL cell has been presented previously [29]. The ECL cell is mainly composed of a three-electrode system with a 300-μm diameter Pt disc electrode as the working electrode, a Pt wire electrode as the auxiliary electrode, and an Ag/AgCl electrode as the reference electrode. A piece of fused-silica capillary (25 μm i.d., 375 μm o.d.) with a length of 45 cm (Yongnian Ruipu chromatogram equipment Co. Ltd., Hebei, China) was used as the separation capillary and placed between the injection reservoir and the reaction reservoir. The detection cell has a volume of about 300 μL and is fixed in a dark detection chamber. The capillary and the Pt working electrode were screwed in an opposite direction inside the ECL cell [29]. The reference electrode and counter electrode were inserted into the cell from punched holes of the upper side of the cell. To avoid blocking photo detection by the photomultiplier tube (PMT), the reference electrode and counter electrode were inserted into the solution just above the working electrode. An optical glass was adopted as ECL detection window and put directly at the top of a PMT. The glass slide and PMT were fixed in the chamber in order to keep the same distance between the working electrode and PMT photo detector. The outlet of the capillary was grounded by a stainless tube which was fixed on the capillary by epoxy. A Model CHI600 voltammetric analyzer (CH Instruments, Austin, TX, USA) was used to supply the potential for the redox reaction of $Ru(bpy)_3^{2+}$ on the Pt working electrode. The detection cell was placed directly above PMT. The output of ECL intensity was amplified and recorded with MPI-B software by a computer.

Transmission electron microscopy (Hitachi H-600, Japan) was utilized to investigate the size and size distribution of gold nanoparticles. The UV–vis spectra of gold nanoparticles were recorded at room temperature on a UV-570 spectrometer (JASCO, Tokyo, Japan).

2.2. Procedure

Prior to electrochemical measurements, the Pt disc-working electrode was polished with 0.3 and 0.05 μm Al_2O_3 slurry, cleaned with water in an ultrasonic cleaner, and then carefully put on an opposite position to the capillary outlet end. In order to make CE effluent contact the electrode surface directly, the distance between Pt working electrode and the outlet of the capillary was controlled strictly in the range of 70 ± 5 μm [30,31] with the aid of an optical microscope. Elimination of the oxide layer on the Pt electrode was always performed via scanning the potential of the Pt disc electrode from −0.5 to 0.0 V for ten cycles. 250 μL of $Ru(bpy)_3^{2+}$ solution was added into the reservoir before analysis, and replaced every 2 h to eliminate depletion effect or potential interference from reaction during the analysis.

The capillary is always flushed with 0.1 M sodium hydroxide for overnight followed by rinsing with distilled water for 30 min at the first use. Before each run, the capillary was flushed with distilled water and the corresponding running buffer until the baseline of ECL is flat. A series of extraction procedures was done before electrophoresis to eliminate the influence of ionic strength in sample and obtain clear electrophoretic profile.

The measurement of ECL intensity of $Ru(bpy)_3^{2+}$–roxithromycin *coreactant* system in the presence of gold nanoparticles was performed [15] in the following procedure: 300 μL of 5 mM $Ru(bpy)_3^{2+}$ was first injected into the ECL cell containing roxithromycin. The ECL emission was inspected. 30 μL mixed solution was then extracted from the ECL cell and 30 μL gold nanoparticles suspension was injected into the ECL cell and mixed immediately with a syringe. The ECL spectra were then recorded. The experimental conditions were also changed during these measurements and the corresponded ECL spectra were recorded.

For the detection of roxithromycin in tablets and urine samples, the sample solutions have to be filtered through a membrane (0.22 μm) and then injected by electrokinetic injection for 10 s at 10 kV (about 4.5 nL). The electropherograms of analytes were recorded at 15 kV.

2.3. Sample treatment

Roxithromycin capsule and human urine were collected for the detection of roxithromycin by the proposed CE–ECL route. More than ten capsules of roxithromycin were weighed and grounded to a fine powder by use of a pestle and mortar. The powder was dissolved in water, and the resulting solution was diluted to 100 mL in a calibrated flask. Suitable aliquots from this solution were taken for the determination of roxithromycin.

The urine samples were collected from the volunteers in our laboratory who were orally administrated to one capsule containing 150 mg roxithromycin with empty stomach. Then urine samples were periodically collected up to 6 h. Firstly, 500 μL ethyl ether and 50 μL 0.1 M sodium hydroxide were added into a 1.0 mL aliquot of urine sample in a 2.0 mL Eppendorf tube. The sample was then mixed using a medium motion on a shaker for 2 min and centrifuged at 2000 rpm for 5 min. The top separated organic layer was transferred into a new Eppendorf tube and evaporated at 40 °C until dry under a gentle steam of nitrogen. The dry residue was dissolved in 500 μL water and the resultant solution was used as urine sample.

3. Results and discussion

3.1. ECL of $Ru(bpy)_3^{2+}$ in presence of roxithromycin

Fig. 1 shows cyclic voltammograms of (curve a) 5.0 mM $Ru(bpy)_3^{2+}$ and (curve b) the mixture of 0.1 mg mL^{-1} roxithromycin with 5.0 mM $Ru(bpy)_3^{2+}$ in pH 8.0 PBS buffer on the Pt electrode within the potential range from 0 to 1.40 V at a scan rate of 0.1 V s^{-1}. Curve (c) in Fig. 1 shows cyclic voltammogram of a Pt electrode in pH 8.0 PBS buffer without $Ru(bpy)_3^{2+}$ as a control experiment which shows only capacitive current and the huge anodic current at potential higher than 1.2 V due to electrochemical oxidation of Pt electrode surface and/or water. While in curve (a), a couple of waves were noticed and the anodic peak current was equal to the cathodic one. Their peak separation was about 59 mV and did not alter with scan rates or during the continuous cycling. However, adding of 0.1 mg mL^{-1} roxithromycin solution resulted in increasing anodic and cathodic peak current (curve b). The magnitude of anodic peak current is larger than the cathodic one. Please note here that $Ru(bpy)_3^{2+}$ and roxithromycin were always driven out of the cell by CE and also the concentration of $Ru(bpy)_3^{2+}$ is relatively high (5.0 mM). Therefore, the generated $Ru(bpy)_3^{3+}$ was only partially reduced by strong reducing species, which originate from the coreactant of roxithromycin during oxidation process, to generate $Ru(bpy)_3^{2+*}$ [2–5]. While other part of $Ru(bpy)_3^{3+}$ ions will reduce on the Pt electrode directly, resulting a cathodic current, as shown in curve (b). Subsequently, the intensity of the resultant ECL is possible to be utilized as a quantitative parameter for the detection of coreactant, roxithromycin.

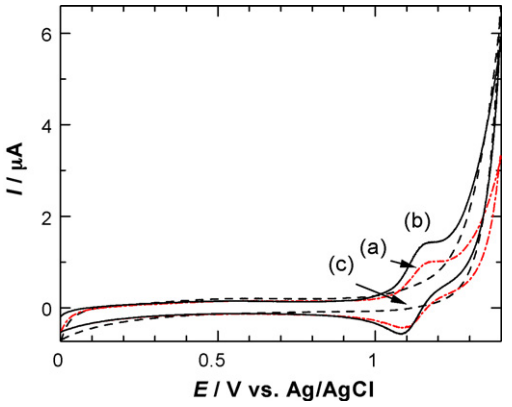

Fig. 1. Cyclic voltammograms of 5.0 mM $Ru(bpy)_3^{2+}$ (a) and the mixture of 5.0 mM $Ru(bpy)_3^{2+}$ with 0.1 mg mL^{-1} roxithromycin (b) in pH 8.0 PBS buffer on a Pt working electrode at a scan rate of 0.1 V s^{-1}. Curve (c) is cyclic voltammogram of Pt electrode in pH 8.0 PBS buffer at a scan rate of 0.1 V s^{-1}.

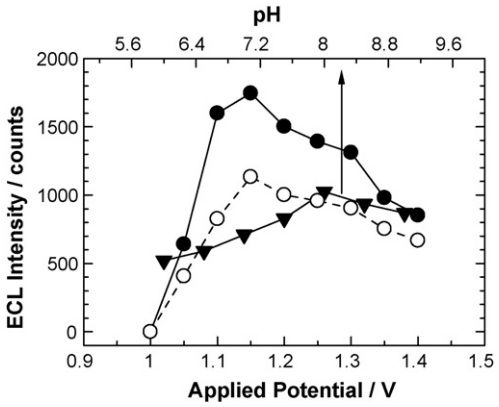

Fig. 2. The intensity of $Ru(bpy)_3^{2+}$ based ECL emission as a function of the applied potential on Pt working electrode in the presence (full circles) and absence (open circles) of 10 μg mL^{-1} roxithromycin and as a function of pH value of PBS buffer (full triangles). The concentration of $Ru(bpy)_3^{2+}$ and separation buffer were 5 and 10 mM, respectively. The electrokinetic injection time and voltage were 10 s and 10 kV, respectively. For circles dots, pH 8.0 PBS buffer was used. For triangles, the applied potential of 1.15 V was applied.

Since the ECL emission of $Ru(bpy)_3^{2+}$ itself has been well-known [2–16], only ECL emission of $Ru(bpy)_3^{2+}$–roxithromycin *coreactant* system was investigated. Fig. 2 shows the ECL intensity of this *coreactant* system as a function of the potential applied on Pt working electrode (full circles) and of pH value of PBS buffer (full triangles). The ECL intensity of $Ru(bpy)_3^{2+}$ system as a function of applied potential without adding roxithromycin was also shown (open circles) as a reference. Although the background of ECL emission was very strong (because high concentration of $Ru(bpy)_3^{2+}$ solution was used), it is still very clear to tell the difference of ECL intensity after adding roxithromycin. The potential applied on Pt working electrode and pH value of PBS buffer affected greatly the ECL intensity of $Ru(bpy)_3^{2+}$–roxithromycin coreactant system. No light emission was observed when the potential applied was lower than 1.00 V. An increase in the potential applied from 1.00 V led to an increase in the ECL intensity and then to the maximum value around 1.15 V. The maximum intensity of ECL light emission at 1.15 V is in accordance with the highest anodic peak current in Fig. 1. The ECL intensity of $Ru(bpy)_3^{2+}$–roxithromycin coreactant system was almost 1.5 times stronger than $Ru(bpy)_3^{2+}$ only based system, indicating that roxithromycin might act as a *coreactant*. Potential higher than 1.15 V resulted in weakening the ECL light intensity. This is probably caused by the oxidation of Pt electrode surface and/or water, which prevents the generation of excited species, $Ru(bpy)_3^{2+*}$. These results agree well with the previous reports in literature [2–16]. The potential of 1.15 V was then applied in the following experiments for the detection of roxithromycin.

The effect of pH value on the ECL intensity (full triangles) was investigated in the pH range of 6.0–9.0. The ECL intensity increased with pH value from 6.0 to 8.0 and then decreased when the pH value of buffer was larger than 8.0. The reason for the decrease of the ECL intensity might be the involvement of the competition of the reduction of $Ru(bpy)_3^{3+}$ with the reduction of OH^- ions at higher pH values [18]. The pH value of buffer was then

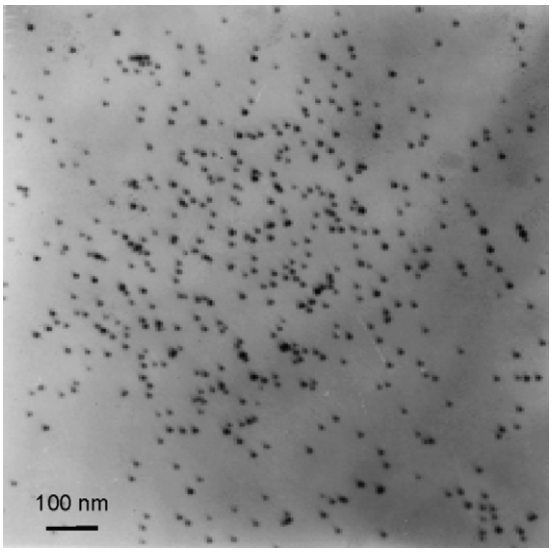

Fig. 3. TEM images of as-prepared citric-acid-stabilized gold nanoparticles.

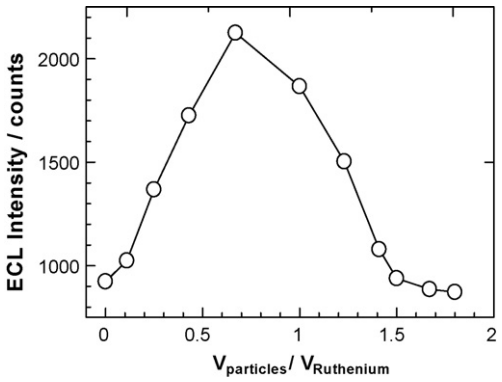

Fig. 4. Variation of the intensity of 5.0 mM $Ru(bpy)_3^{2+}$ based ECL emission in the presence of 10 μg mL^{-1} roxithromycin with the volume ratio of the suspension of gold nanoparticles to $Ru(bpy)_3^{2+}$ solution. The potential applied at the Pt working electrode was 1.15 V. The separation buffer was 10 mM pH 8.0 PBS buffer. The electrokinetic injection time and voltage were 10 s and 10 kV, respectively.

fixed at 8.0 in the following experiments for the detection of roxithromycin.

The variation of the ECL intensity of $Ru(bpy)_3^{2+}$–roxithromycin coreactant system with other experimental conditions has also been examined, including the concentration of $Ru(bpy)_3^{2+}$ in the range of 0–10 mM, the concentration of PBS buffer. The intensity of ECL emission increased with an increase in $Ru(bpy)_3^{2+}$ concentration because the number of electrogenerated excite species $Ru(bpy)_3^{2+*}$ increases with an increase in the concentration of $Ru(bpy)_3^{2+}$ [32]. Unfortunately, the background current increased remarkably when its concentration was too high. 5 mM $Ru(bpy)_3^{2+}$ was thus chosen for the detection of roxithromycin.

The concentration of buffer solution also affected the ECL intensity. When the concentration of PBS buffer was smaller than 50 mM, the ECL intensity was relatively weak, while the concentration was larger than 50 mM, the background was unexpectedly enlarged. The strong and stable ECL emission was noticed when the concentration of PBS buffer was 50 mM. Then 5 mM $Ru(bpy)_3^{2+}$ in 50 mM PBS buffer was selected in the following experiments to obtain a stable ECL signal with higher intensity.

3.2. Gold nanoparticles enhanced ECL of $Ru(bpy)_3^{2+}$ in presence of roxithromycin

Morphology and optical properties of the as-prepared citric-acid-stabilized gold nanoparticles by wet-synthetic route [28] were examined with UV–vis spectroscopy and TEM. The maximum absorption wave of the suspension of these nanoparticles in UV–vis spectra was at 524 nm and its intensity varied linearly with their mass concentration, indicating optical behavior of gold spherical nanoparticles [28]. Fig. 3 shows TEM image of gold nanoparticles, which shows they are mostly spherical and uniform in size. Their average diameter was measured about 10 nm from 250 randomly sampled particles with a standard deviation of 0.69 nm.

The intensity of $Ru(bpy)_3^{2+}$–roxithromycin *coreactant* system was enhanced greatly after adding gold nanoparticles. In order to give quantitative analysis of ECL enhancement by gold nanoparticles, we recorded ECL intensity as a function of the amount (volume) of gold nanoparticles added. Fig. 4 shows the variation of ECL intensity as a function of the ratio of the volume of gold nanoparticles suspension to the volume of $Ru(bpy)_3^{2+}$-roxithromycin solution. The ECL intensity was only 900 counts before adding gold nanoparticles. After adding gold nanoparticles, the ECL intensity was enhanced greatly. When the volume ratio was 0.7, the maximum ECL intensity was noticed to be 2100 counts, which is 2 times stronger than that without adding gold nanoparticles. Higher volume ratio than 0.7 resulted in a decrease in the ECL intensity. It has also confirmed that gold nanoparticles did not change their optical properties before and after the ECL measurements. These experimental facts agree with the results reported in literature [15].

The enhancement of $Ru(bpy)_3^{2+}$ based ECL emission by gold nanoparticles has been reported in literature [15] where the enhancement of ECL intensity was attributed to the electrostatic interaction of negative-charged stabilizers on the surface of gold nanoparticles with positive-charged $Ru(bpy)_3^{2+}$, which decreases the energy gap of the ligand π–π^* bond since the energy gap of the ligand π–π^* bond actually determines the rate and efficiency of the charge transfer transitions between a d-orbital on the ruthenium and a π^* anti-bonding orbital on the ligand [33]. This interaction makes transition of the excited species $Ru(bpy)_3^{2+*}$ into ground state easier and more efficient, resulting in an enhancement of ECL emission. Moreover, the larger surface area of gold nanoparticles [28] and the catalytic ability of gold nanoparticles [28,34,35] will also improve the number of transmission state, which are other important parameters for the intensity of ECL emission.

We would like to propose here a new concept named “floating nanoelectrodes” [36,37] to explain the enhancement of ECL emission of $Ru(bpy)_3^{2+}$ by gold nanoparticles. Actually, light emission from ECL is believed to originate from the solution in vicinity of the electrode surface where the reacting species (alternatively generated at the electrode surface via a series of potential steps into the oxidation and reduction diffusion plateau) are recombined by electron transfer to give rise to a luminescent excited state. It is generally found that the ECL spectrum correlates very well with the solution luminescence spectrum for the species involved. Therefore, in the solutions containing gold nanoparticles and $Ru(bpy)_3^{2+}$, the ECL emission not only produces in vicinity of the Pt working electrode surface but also on the surface of gold nanoparticles in the same way described on Pt working electrode because gold nanoparticles can behavior as “floating nanoelectrodes” [36,37]. The floating of nanoelectrodes is of electric floating since the potential required to oxidize $Ru(bpy)_3^{2+}$ to $Ru(bpy)_3^{3+}$ on the surface of the Pt working electrode is very high and this high potential can provide an electric filed for gold nanoparticles move between Pt working electrode and counter electrode. Please note here that floating nanoelec-

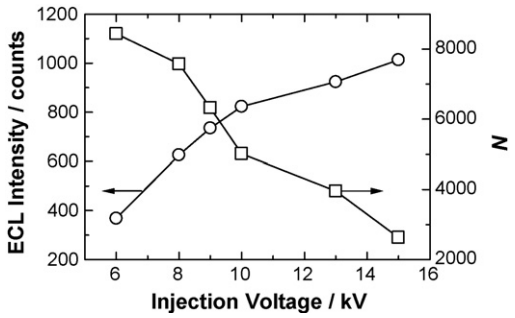

Fig. 5. Dependence of injection voltage on the ECL intensity (circles) and on the calculated number of theoretical plates, *N* (squares). The concentration of roxithromycin was 10 μg mL^{-1} and the concentration of $Ru(bpy)_3^{2+}$ was 5.0 mM. 10 mM pH 8.0 PBS buffer was used as separation buffer. The potential applied at the Pt working electrode was 1.15 V. The electrokinetic injection time was 10 s. The volume ratio of the suspension of gold nanoparticles to $Ru(bpy)_3^{2+}$ solution was 0.7.

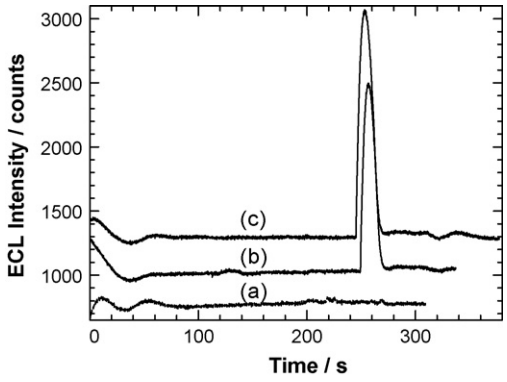

Fig. 6. Electropherograms of urine sample (a), urine sample after 2 h administration (b), the mixture of urine sample after 2 h administration with standard roxithromycin solution (c). 10 mM pH 8.0 PBS buffer was used as separation buffer. The electrokinetic injection voltage and time was 10 kV and 10 s, respectively. The separation voltage was 15 kV. The potential applied at the Pt working electrode was 1.15 V. The volume ratio of the suspension of gold nanoparticles to $Ru(bpy)_3^{2+}$ solution was 0.7.

trodes indicate that the nanoparticles are not connected directly to the working electrodes, apart from via their surroundings such as a conductive solution in the vessel. Further experiments related with the effect of size and the effect of the type of nanoparticles on the enhancement of $Ru(bpy)_3^{2+}$ based ECL emission, especially the enhancement of ECL emission of $Ru(bpy)_3^{2+}$ by gold nanoparticles in the presence of other analytes, are currently undergoing in our laboratory to confirm the explanations we proposed here.

3.3. Optimization of the CE–ECL system for roxithromycin detection

In the CE–ECL system, CE conditions not only decide the separation efficiency but also influence ECL intensity. In order to obtain high ECL signal and good separation efficiency for roxithromycin detection, the injection voltage and injection time of sample solutions, the separation voltage, and the concentration of separation buffer, and the pH value of the separation buffer were examined.

Fig. 5 shows dependence of the intensity of ECL emission on the injection voltage of the samples from 6 to 15 kV (circles). Higher injection voltage resulted in stronger ECL emission, because the ECL intensity depends on the concentration of analytes (roxithromycin and $Ru(bpy)_3^{2+}$) in the diffusion layer at the working electrode. At higher injection voltage, more roxithromycin and $Ru(bpy)_3^{2+}$ can diffuse to the diffusion layer and react on the working electrode and generate excited species, $Ru(bpy)_3^{2+*}$. On the other side, the sample zone might expand in the capillary during its running. Moreover, too much roxithromycin and $Ru(bpy)_3^{2+}$ will not react on the electrode immediately and diffuse back into the solution. Overloading effect often takes place. This negative effect can be seen clearly when the theoretical plates of the capillary, *N*, is calculated by the equation of $N = 5.54\ (t_m/W_{1/2})^2$, where t_m is the migration time and $W_{1/2}$ is the width at half height of the electrophoretic peak. As expected, *N* decreased with an increase in injection voltage (squares). Similarly, longer injection time enhanced ECL intensity, but decreased theoretical plates (not shown). Taking two opposite effects into account, injection voltage of 10 kV and injection time of 10 s were chosen in the next experiments to obtain higher ECL intensity and a larger *N* for the detection of roxithromycin.

The separation voltage affected greatly ECL intensity and migration time of analytes like roxithromycin. When the separation voltage varied from 8 to 18 kV, the ECL intensity kept increasing and reached the maximum value at 14 kV, and then slowly decreased. However, the migration time kept decreasing from 800 to 180 s. The separation voltage higher than 14 kV resulted in much higher noise of the baseline, which is attributed to the increase of Joule heating in capillary. Furthermore, the strong flow of effluent from the capillary might reduce the concentration of $Ru(bpy)_3^{3+}$ near the Pt working electrode surface, resulting in reducing the efficiency of light emitting [38]. In order to obtain a short migration time and high ECL intensity for the detection of roxithromycin, the 14 kV was selected as the optimum separation voltage.

It has been known that the pH value of separation buffer influences not only the net charge of the analytes (e.g. roxithromycin), but also affects the electroosmotic flow (EOF) inside the capillary which actually determines migration times of analytes. On the other side, different pH values of separation buffer with detection buffer will result in a pH gradient along the capillary. Therefore, pH 8.0 PBS buffer, the same one as detection buffer, was used for the detection of roxithromycin.

The effect of the concentration of separation buffer (pH 8.0 PBS) in the range from 5 to 50 mM on the separation efficiency was investigated. Light variation in the ECL intensity was noticed when the concentration of PBS buffer was changed. The highest ECL signal was obtained when the concentration was 10 mM. As for the migration time of roxithromycin, it increased with an increase in the concentration of buffer while the baseline became unstable. This is due to the increase of Joule heating caused by the increased ionic strength. Meanwhile, EOF decreased with an increase in the concentration of buffer and the migration time also became longer. Thus, we chose 10 mM pH 8.0 PBS buffer as separation solution for the detection of roxithromycin.

Under the optimized conditions, the separation of roxithromycin from other materials existing in tablets and urine samples were conducted. Fig. 6 shows electropherograms of urine sample without roxithromycin (curve a), urine samples after administration for 2 h (curve b), and the mixture of urine samples after administration for 2 h with standard roxithromycin solution. Neither shift on migration time nor occurrence of additional peaks was noticed, indicating no interference from the co-existed species

Table 1
Determination results of roxithromycin in capsules

Number	Labeled (mg capsule^{-1})	Found[a] (mg capsule^{-1})	Recovery (%)	R.S.D. (%)
20060201	150	149.2	98.7	3.94
20061008	150	152.7	102.4	4.05
20070219	150	154.6	101.9	4.31

[a] Average value of five measurements.

Table 2
Determination results of roxithromycin excretive in human urine after administration

Time (h)	Found ($\mu g\,mL^{-}$)[1]	Added ($\mu g\,mL^{-1}$)	Total ($\mu g\,mL^{-}$)[1]	Recovery (%)	R.S.D. (%)	Roxithromin in urine ($\mu g\,mL^{-1}$)
0.5	0.03	1.00	1.02	99.0	3.15	0.03
1.0	0.27	1.00	1.14	87.0	4.62	0.20
2.0	6.34	1.00	7.39	105	3.24	6.34
3.0	1.24	1.00	2.21	97.0	3.35	1.24
4.0	0.82	1.00	1.90	108	3.98	0.82
6.0	0.45	1.00	1.34	89.0	4.43	0.45

(matrix materials) in urine sample. This fact confirms good separation of CE towards roxithromycin under these experimental conditions.

3.4. CE–ECL for detection of roxithromycin

Under the optimized conditions before adding gold nanoparticles (the potential applied on Pt working electrode, 1.15 V; concentration of $Ru(bpy)_3^{2+}$, 5.0 mM in 50 mM pH 8.00 PBS buffer; electrokinetic injection voltage, 10 kV; electrokinetic injection time, 10 s; separation buffer, 10 mM pH 8.00 PBS buffer, separation voltage, 14 kV), the intensity of ECL emission, I, varied linearly with the concentration of roxithromycin, c with an equation of $I = 54.6 + 190.6c$ ($r = 0.998$) in the lower roxithromycin concentration range from 0.24 to 9.6 μM and of $I = 1658.0 + 12.1c$ ($r = 0.997$) in the concentration range from 9.6 μM to 0.24 mM. The detection limit was 84 nM (S/N = 3).

However, after adding gold nanoparticle into ECL cell (the volume ratio of the suspension of gold nanoparticles to that of $Ru(bpy)_3^{2+}$ was 0.7), I still enhanced linearly with c. The linear regression equations were $I = 60.4 + 281.9c$ ($r = 0.991$) in the lower roxithromycin concentration range from 24 nM to 4.8 μM and $I = 1272.1 + 12.9c$ ($r = 0.987$) in the concentration range from 4.8 μM to 0.24 mM. The detection limit was 8.4 nM (S/N = 3), which is 10-times lower than the detection limit without adding gold nanoparticles as catalyst. The reproducibility was tested by consecutive injection of 1.0 $\mu g\,mL^{-1}$ roxithromycin standard solution ($n = 7$) and the relative standard derivation (R.S.D.) values of ECL intensity and migration time were 3.85 and 1.12%, respectively.

Tables 1 and 2 show the results for roxithromycin tablets and urine sample by use of the proposed method, respectively. The maximum content of roxithromycin was found to be reached about 2.0 h after the administration and the excreted roxithromycin through urine was 6.34 $\mu g\,mL^{-1}$ in 2 h. The values of relative standard derivation for these detections were less than 4.62% and the recovery was in the range of 87.0–108%. These results indicate the proposed CE–ECL method for the detection of roxithromycin in tablets and urine samples is practical and successful.

4. Conclusion

Enhancement of electrochemiluminescent intensity of tris(2,2′-bipyridyl) ruthenium(II)-roxithromycin coreaction system by gold nanoparticles is probably due to the ECL emission on Pt working electrode as well as on gold nanoparticles which act as “floating nanoelectrodes”. The size of gold nanoparticles and the type of nanoparticles might affect the intensity of the ECL emission greatly and this topic will be reported in near future. In term of analytical applications, the most interesting point is that this ECL system coupled with CE not only showed high selectivity towards roxithromycin but also decrease the detection limit of roxithromycin from 84 to 8.4 nM after adding gold nanoparticles into the ECL system. The proposed CE–ECL method has the potential to be adopted as official route in clinic and pharmaceutical analysis in near future.

References

[1] D.M. Hercules, F.E. Lytle, J. Am. Chem. Soc. 88 (1966) 4745.
[2] N.E. Tokel, A.J. Bard, J. Am. Chem. Soc. 94 (1972) 2862.
[3] X.-B. Yin, S. Dong, E. Wang, Trends Anal. Chem. 23 (2004) 432.
[4] X.-B. Yin, E. Wang, Anal. Chim. Acta 533 (2005) 113.
[5] S. Kulmala, J. Suomi, Anal. Chim. Acta 500 (2003) 21.
[6] I. Rubinstein, A.J. Bard, J. Am. Chem. Soc. 102 (1980) 6642.
[7] C.H. Lyons, E.D. Abbas, J.-K. Lee, M.F. Rubner, J. Am. Chem. Soc. 120 (1998) 12100.
[8] C.J. Miller, P. McCord, A.J. Bard, Langmuir 7 (1991) 2781.
[9] Y. Sato, K. Uosaki, J. Electroanal. Chem. 384 (1995) 57.
[10] W.-Y. Lee, T.A. Nieman, Anal. Chem. 67 (1995) 1789.
[11] H.Y. Wang, G.B. Xu, S. Dong, Electroanalysis 14 (2002) 853.
[12] A.N. Khramov, M.M. Collinson, Anal. Chem. 72 (2000) 2943.
[13] Z. Guo, S. Dong, Anal. Chem. 76 (2004) 2683.
[14] Z. Guo, Y. Shen, M. Wang, F. Zhao, S. Dong, Anal. Chem. 76 (2004) 184.
[15] Y. Liu, W. Pan, Q. Liu, S. Yao, Electrophoresis 26 (2005) 4468.
[16] J.-Z. Guo, H. Cui, S.-L. Xu, Y.-P. Dong, J. Phys. Chem. C 111 (2007) 606.
[17] R.D. Gerardi, N.W. Barnett, S.W. Lewis, Anal. Chim. Acta 378 (1999) 1.
[18] W.Y. Lee, Mikrochim. Acta 127 (1997) 19.
[19] K.A. Fahnrich, M. Pravda, G.G. Guilbault, Talanta 54 (2001) 531.
[20] A.V. Kukoba, A.I. Bykh, I.B. Svir, Fresenius' J. Anal. Chem. 368 (2000) 439.
[21] A.L. Barry, R.R. Packer, Eur. J. Clin. Microbiol. 5 (1986) 536.
[22] V. DeOliveira, A.M. Bergold, E.E.S. Schapoval, Anal. Lett. 29 (1996) 2377.
[23] M.P. Schlusener, K. Bester, M. Spiteller, Anal. Bioanal. Chem. 375 (2003) 942.
[24] J.H. Lim, B.S. Jang, R.K. Lee, S.C. Park, H.I. Yun, J. Chromatogr. B 746 (2000) 219.
[25] M.J. Gonzalez de la Huebra, G. Bordin, A.R. Rodríguez, Anal. Bioanal. Chem. 375 (2003) 1031.
[26] M.J. Gonzalez de la Huebra, G. Bordin, A.R. Rodríguez, Electroanalysis 15 (2003) 473.
[27] Z.H. Song, Y.H. Liu, X.F. Xie, Curr. Drug. Metab. 7 (2006) 389.
[28] M.-C. Daniel, D. Astruc, Chem. Rev. 104 (2004) 293.
[29] X.H. Sun, J.F. Liu, W.D. Cao, X.R. Yang, E. Wang, Y.S. Fung, Anal. Chim. Acta 470 (2002) 137.
[30] J.F. Liu, J.L. Yan, X.R. Yang, E. Wang, Anal. Chem. 75 (2003) 3637.
[31] W.D. Cao, J.F. Liu, X.R. Yang, E. Wang, Electrophoresis 23 (2002) 3683.
[32] W.Y. Lee, T.A. Nieman, Anal. Chem. 67 (1995) 1789.
[33] S. Workman, M.M. Richter, Anal. Chem. 72 (2000) 5556.
[34] M.M. Maye, Y.B. Lou, C.-J. Zhong, Langmuir 16 (2000) 7520.
[35] Y. Xiao, H.X. Ju, H.Y. Chen, Anal. Biochem. 278 (2000) 22.
[36] A.-K. Timo, H. Keijo, J. Pentti, K. Jouko, K. Sakari, K. Rainer, L. Kari, N. Mauri, P. Jyrki, S. Timo, V. Raili, Method for luminescence measurements. U.S. Patent (2000), p. 11 CODEN: USXXAM US 6136268 A 20001024 CAN 133:305085 AN 2000:752078 CAPLUS.
[37] M. Andreas, A. Arun. Electrochemiluminescence cell with floating reaction electrodes. PCT Int. Appl. (2000), p. 47. CODEN: PIXXD2 WO 2000003233 A1 20000120 CAN 132:90343 AN 2000:54048 CAPLUS.
[38] P.R. Haddad, Anal. Lett. 32 (1999) 2909.

Talanta 76 (2008) 122–127

Contents lists available at ScienceDirect

Talanta

journal homepage: www.elsevier.com/locate/talanta

Investigation of voltammetric enzyme-linked immunoassay based on a new system of HAP-H_2O_2-HRP

Shusheng Zhang*, Jin Zou, Fengli Yu

Key Laboratory of Eco-chemical Engineering, Ministry of Education; College of Chemistry and Molecular Engineering, Qingdao University of Science and Technology, Qingdao 266042, China

ARTICLE INFO

Article history:
Received 23 November 2007
Received in revised form 10 February 2008
Accepted 14 February 2008
Available online 4 March 2008

Keywords:
Electrochemical immunoassay
Horseradish peroxidase
3-Hydroxyl-2-aminopyridine
α-Fetoprotein

ABSTRACT

By introducing heterocyclic compound to immunoassay system as an electrochemical substrate for the fist time, a new voltammetric enzyme-linked immunoassay system of 3-hydroxyl-2-aminopyridine (HAP)-H_2O_2-horseradish peroxidase (HRP) has been developed. HAP was oxidized with H_2O_2 catalyzed by HRP, and the resulting electroactive product produced a sensitive voltammetric peak at potential of −0.36 V (vs. SCE) in Britton–Robinson (BR) buffer solution. The process of the enzyme-catalyzed reaction and the electro-reduction of the product have been investigated in detail. The linear range for detection of free HRP was from 4.0×10^{-13} to 1.0×10^{-9} g/mL with a detection limit of 1.2×10^{-13} g/mL. The new system has been successfully applied for the assay of α-fetoprotein (αFP) in human serum ranging from 0.1 to 200 ng/mL with a detection limit of 0.1 ng/mL, which was 10 times lower than that of traditional spectrophotometric enzyme-linked immunosorbent assay (ELISA) method. HAP-H_2O_2-HRP voltammetric enzyme-linked immunoassay showed a promising alternative approach in the detection of αFP in clinical diagnosis.

1. Introduction

Electrochemical immunoassay with high sensitivity and selectivity has incorporated enzyme label, immunotechnique and electrochemical detection methods, which has been applied for plant virus identification and clinical malady diagnoses [1–7]. A number of recent studies have utilized enzymes to the detection of some antigens and drugs, most of which are involved in amperometric enzyme-linked immunoassay [8–12].

Voltammetric enzyme-linked immunoassay has coupled voltammetric detection with enzyme immunoassay. The excellent advantages of almost unrivaled sensitivity, wide dynamic range, low detection limit and good reproducibility make it competitive with other analytical techniques. In addition, the miniaturization and low cost of the instrumentation have contributed to the practical application of voltammetric enzyme-linked immunoassay [13,14]. HRP is widely used as labeled enzyme in immunoassay due to its high stability and low cost. Free HRP or labeled HRP catalyzes the oxidation reaction of substrate with H_2O_2, the electroactive product of which can be reduced in negative electrode and produces a sensitive voltammetric peak. By using this voltammetric peak, free HRP and labeled HRP can be measured. Additionally, different antibodies and antigens can also be identified through HRP-linked immunoassay. A variety of substrates in HRP-linked immunoassay have been employed, such as 3,3′-5,5′-tetramethylbenzidine [15], *o*-, *m*- *and p*-aminophenol [16], *o*-, *m*- and *p*-phenylenediamine [17], 3,4-diaminobenzoic [18] and, etc. Some voltammetric enzyme-linked immunoassay systems based on substrate-H_2O_2-HRP have been applied for the determining of some antigens and antibodies with satisfactory results [19]. Sensitivity and stability vary with substrate in electrochemical immunoassay. Therefore, seeking for appropriate electrochemical substrate may be key to acquire higher sensitivity and higher stability.

Up to now, there has been no report related to the study on heterocycle substrate in electrochemical immunoassay according to our best knowledge. In this paper, *N*-heterocyclic compound has been firstly introduced to immunoassay system and a new voltammetric enzyme-linked immunoassay system of HAP-H_2O_2-HRP has been developed. The study has showed that HAP-H_2O_2-HRP system owned higher sensitivity for the detection of free HRP and labeled HRP than the traditional spectrophotometric enzyme-linked immunosorbent assay (ELISA) method. The linear range for detection of free HRP was from 4.0×10^{-13} to 1.0×10^{-9} g/mL with a detection limit of 1.2×10^{-13} g/mL.

α-Fetoprotein (αFP) is an important ingredient of human serum. The sensitive detection of αFP is a key means of liver cancer diagnoses and prevention. Agar double diffusion, immunoelectrophoresis, reverse indirect hemagglutination and ELISA are now employed for the detection of αFP, but the sensitivities of these

* Corresponding author. Tel.: +86 532 84022750; fax: +86 532 84022750.
E-mail address: shushzhang@126.com (S. Zhang).

0039-9140/$ – see front matter © 2008 Elsevier B.V. All rights reserved.
doi:10.1016/j.talanta.2008.02.024

techniques are poor [20,21]. Radioimmunoassay (RIA) used in most modern hospitals has advantages of automatization and excellent sensitivity. Whereas, the technique needs expensive instrumentation, and radiate isotope as a label is harmful to human health. Heineman has utilized labeled alkaline phosphatase and flow injection electrochemical immunoassay to the detection of αFP [22]. The sensitivity was improved, but the complicated equipment and manipulation made the use of the technique limited. Voltammetric enzyme-linked immunoassay based on *o-*, *m- and p*-aminophenol-H_2O_2-HRP have been applied for the detection of αFP by Zhang et al. [16], which have improved the sensitivity and the practicality. The detection limits for αFP are 1.25, 0.5 and 0.2 ng/mL, respectively.

The proposed new voltammetric enzyme-linked immunoassay system HAP-H_2O_2-HRP has been successfully applied for the assay of αFP ranging from 0.1 to 200 ng/mL with a detection limit of 0.1 ng/mL, which is ten times lower than that of traditional spectrophotometric enzyme-linked immunosorbent assay. The sensitivity of the method is comparable with *p*-aminophenol-H_2O_2-HRP voltammetric enzyme-linked immunoassay system. The method appears to be practical, conventional and reliable, showing a potential for determination of αFP in clinical diagnosis.

2. Experimental

2.1. Apparatus

The electrochemical measurement was carried out with a MP-2 voltammetric analyzer (Shandong No. 7 Electric Communication Factory, China) with three-electrode system composed of a dropping mercury electrode or a hanging mercury drop electrode as working electrode, a platinum wire electrode as auxiliary electrode and a saturated calomel electrode (SCE) as reference electrode. G-03 hanging mercury drop electrode was form Shandong No. 7 Electric Communication Factory. Model PHS-25 pH meter was purchased from Shanghai Leici Apparatus Factory. Model OG3022A enzemy labeled meter was produced by Nanhua Electric Group Medical Appliance Company. Incubation for the immune reaction was carried out in a Model HH.W21.Cr420 incubator (Guangdong Shantou Instrument Factory, China).

2.2. Reagents

3-Hydroxyl-2-aminopyridine (HAP, MERCK): 98%, 8.0×10^{-3} mol/L HAP solution was prepared by dissolving 0.0881 g HAP in water and diluted to 100 mL. HRP solution: Shanghai Xueman Biochemical Technique Company, 250 units per mg enzyme (RZ > 3.0), 1.0×10^{-3} g/mL stock solution of HRP was prepared by dissolving 0.0100 g HRP in 100 mL water, which was stored in a refrigerator at 4 °C. H_2O_2 solution: 5.0×10^{-4} mol/L, prepared before use. BR solution: 0.2 mol/L, pH 6.0 and 0.2 mol/L, pH 7.0. The substrate solution in the electrochemical enzyme immunoassay system was prepared as follows: 3.0 mL of 8.0×10^{-3} mol/L HAP solution, 1.5 mL of 5.0×10^{-4} mol/L H_2O_2 solution and 1.0 mL of 0.2 mol/L pH 6.0 BR buffer solution were added to a colorimetric tube of 10 mL in sequence, then diluted to the desired scale and shaken to uniformity. The αFP EIA Kit was purchased from Zhengzhou Bosai Biotechnique Academe. The kit included 48-well immunoplates precoated by anti-αFP serum; HRP-conjugated anti-αFP (anti-αFP-HRP); 0–200 ng/mL of αFP quality control sera; rinsing solution (PBS-Tween 20 buffer solution). All other reagents were of analytical grade and doubly deionized water was used throughout.

2.3. Electrochemical measurement of free and labeled HRP

The 3.0 mL of 8.0×10^{-3} mol/L HAP solution, 1.5 mL of 5.0×10^{-4} mol/L H_2O_2 solution, 1.0 mL of 0.2 mol/L pH 6.0 BR buffer solution and 1.0 mL of 1.0×10^{-8} g/mL HRP solution were added to a 10 mL colorimetric tube in sequence. The mixture was diluted to the scale and shaken to uniformity. Then, let the solution react for 30 min at 37 °C. 5.0 mL of above reaction solution was transferred into another 10 mL colorimetric tube and 1.0 mL of 0.2 mol/L pH 7.0 BR buffer solution was subsequently added. The mixture was diluted to the scale and shaken to uniformity. Then, the solution was transferred to an electrochemical cell of 10 mL. The second-order derivative linear-sweep voltammogram was recorded with the MP-2 voltammetric analyzer. The instrumental conditions were as follows: initial potential, −0.00 V; final potential, −0.80 V; mercury drop standing time, 7 s; potential scanning rate, 400 mV/s.

2.4. Determination of αFP

The wells of the polystyrene immunoplates precoated by anti-αFP serum were written numbers and rinsed with PBS-Tween 20 buffer solution three times for 3 min each. After removing the rinsing solution, 100 μL of different concentrations of the αFP quality control sera or the serum samples were added to each well and incubated at 37 °C for 30 min. The wells were then rinsed as above. Following this step, 100 μL of anti-αFP-HRP was added to each well and incubated at 37 °C for 30 min. The wells were then rinsed as above and once more with double deionized water. Following this step, 400 μL of HAP substrate solutions were added to each well, and the enzymatic reaction was allowed to proceed for 40 min at 37 °C. The reaction solution was transferred into a cell of 1 mL. 80 μL of 0.2 mol/L BR buffer (pH 7.0) and 200 μL doubly deionized water were added into the cell. The second-order derivative linear-sweep voltammogram was recorded as above.

For comparison, spectrophotometric detection of ELISA was also preformed in parallel using OG3022A enzemy labeled meter.

3. Results and discussion

3.1. Second-order derivative linear-sweep voltammograms

Fig. 1 showed the results of the second-order derivative linear-sweep voltammograms of the HAP-H_2O_2-HRP voltammetric

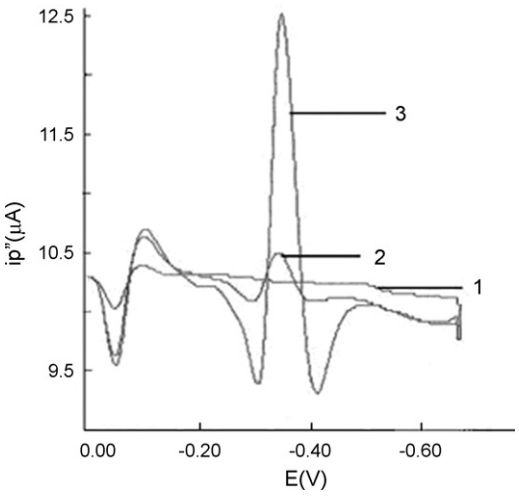

Fig. 1. Second-order derivative linear-sweep voltammograms: (1) 0.02 mol/L pH 6.0 BR buffer; (2) reaction in the absence of HRP (0.02 mol/L pH 6.0 BR buffer +2.4×10^{-3} mol/L HAP +7.5×10^{-5} mol/L H_2O_2); (3) reaction in the presence of HRP (2 + 1.0×10^{-7} mol/L HRP).

enzyme-linked immunoassay system. Curve 1 was the voltammogram of BR buffer solution, in which no voltammetric peak was observed. Curve 2 was that of BR + HAP + H_2O_2, in which a small voltammetric peak at −0.36 V was found. The small peak was due to the product of slow oxidation of HAP by H_2O_2. Curve 3 was that of the enzyme-catalyzed reaction solution, in which a large and well-defined voltammetric peak at −0.36 V appeared. The results showed that the addition of HRP quickened greatly the oxidation of HAP with H_2O_2. When the HRP content was controlled as low as 1.2×10^{-13} g/mL, a distinctive increase of this voltammetric peak could still be observed.

3.2. Conditions for enzyme-catalyzed reaction

HRP efficiently catalyzed the oxidation reaction of HAP by H_2O_2, and the electroactive product produced a sensitive voltammetric peak at potential of −0.36 V (vs. SCE) in BR solution. Referring to the oxidation reaction of *o*-aminophenol (OAP) by H_2O_2 in voltammetric enzyme-linked immunoassay system [16], the process of the enzyme-catalyzed oxidation reaction of HAP could be expressed as follow:

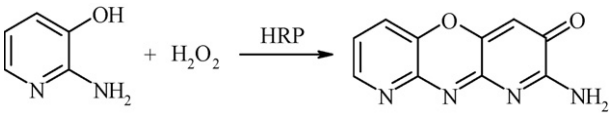

(1)

The activity of HRP was greatly influenced by the reaction conditions. The effect of the pH of the BR buffer solution on enzyme-catalyzed reaction was studied by varying pH between 2.0 and 10.0. When pH was in the range of 5.5–6.5, a most sensitive and stable voltammetric peak could be observed. Therefore, pH 6.0 of BR buffer solution was chosen for enzyme-catalyzed reaction.

Additionally, the concentration of each component in substrate solution including BR buffer solution, HAP and H_2O_2 was also investigated. The optimized conditions were that the 10 mL reaction solution consisted of 1.0 mL of 0.2 mol/L pH 6.0 BR buffer solution, 3.0 mL of 8.0×10^{-3} mol/L HAP solution and 1.5 mL of 5.0×10^{-4} mol/L H_2O_2 solution. Under such enzyme-catalyzed reaction conditions, the equilibrium was achieved in 40 min at 37 °C, and the highest electrochemical peak kept stable within 1 h. 40 min was selected as the time for the enzyme-catalyzed reaction at 37 °C.

3.3. Optimization of voltammetric detection conditions

The fine second-order derivative linear-sweep voltammetric peak of the product of the enzyme-catalyzed reaction could be obtained in certain buffer solutions, such as BR or HAc-NaAc. BR buffer solution affording better electrochemical peak was selected as the supporting electrolyte for the polarographic measurement. The effect of pH of BR buffer as supporting electrolyte on the voltammetric peak was investigated. Results showed that the peak height was the highest and stable in BR buffer solution at pH 7.0. In addition, the optimized amount of BR buffer solution as supporting electrolyte was 1.0 mL for 10 mL of the overall electrolyte solution.

3.4. The electrode procedure of the enzymatic product

For the HRP-catalyzed oxidation reaction of HAP by H_2O_2, the reduction peak height of the product increased with rising static period using the hanging mercury drop electrode. When the static period was more than 140 s, the reduction peak height did not increase any longer. For pH 6.0 BR buffer solution, the linear-sweep voltammetric peak increased by increasing the rate of scanning. The plot of peak current against the square root of the rate of scanning was not linear, but an upward curve in the range of 200–900 mV/s. The peak potential values shifted to more negative values with increasing rate of scanning. The electrocapillary curve of HAP-H_2O_2-HRP was compared to those of HAP-H_2O_2 and BR buffer solution, respectively. Between 0.00 and −1.80 V, the surface tension of the former solution was much smaller. All the above results indicated that the product of the enzymatic reaction was adsorbed on the mercury electrode.

Under the optimum conditions, multiple-sweep voltammograms were recorded. There were good cathodic and anodic peaks and these two peaks were similar in height. Moreover, the heights of both peaks increased with the increase of scanning cycle. After scanning seven times, the heights of two peaks kept stable, indicating that the adsorption of product on the mercury electrode reached saturation.

After enzyme-catalyzed reaction in pH 6.0 BR buffer solution, the cyclic voltammetric experiment in different pH BR buffer solution were performed. The results were shown in Fig. 2.

When pH < 4.0, there was no cyclic voltammetric wave. Between pH 4.0 and 10.0, both anodic peak and cathodic peak appeared with the equal height, which indicated that the voltammogram of the product was a reversible adsorption process. When pH ≥ 12.0, anodic peak decreased, indicating an irreversible redox process. The reaction electron number was two from the relation between the width of the peak at half height and the reaction electron number based on the theory developed by Nicholson [23]. As we could see, the heights of two peak increased with the increase of pH from 4.0 to 7.0. Whereas, the heights of two peaks decreased when pH > 7.0.

From above experimental results, the enzymatic product appeared a two-electron adsorptive reversible redox process in pH 4.0–10.0 BR buffer solution. The process was expressed as follow:

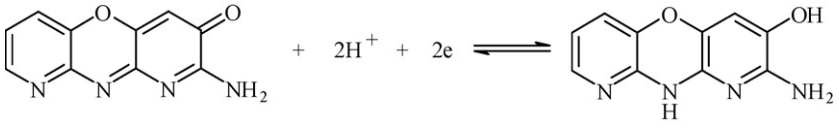

(2)

3.5. Determination of free HRP

According to the experimental method, different quantities of HRP were used to catalyze the oxidation reaction of HAP with H_2O_2 and the second-order derivative linear-sweep voltammograms were recorded. The peak height exhibited a good linear relation with free HRP concentration from 4.0×10^{-13} to 1.0×10^{-9} g/mL. The relative standard deviation was 4.1% for 11 parallel determinations with 1.0×10^{-11} g/mL HRP. The detection limit of free HRP was 1.2×10^{-13} g/mL.

3.6. Determination of labeled HRP

Similar with free HRP, labeled HRP could also be determined. Five HRP conjugated antibodies such as α-fetoprotein (anti-αFP-HRP, 1), carcinoma embryo antigen (anti-CEA-HRP, 2), human chorionic gonadotropin (anti-HCG-HRP, 3), prostate specific antigen (anti-PSA-HRP, 4) and thyroxine (anti-T_4-HRP, 5) were detected under the optimum experimental condi-

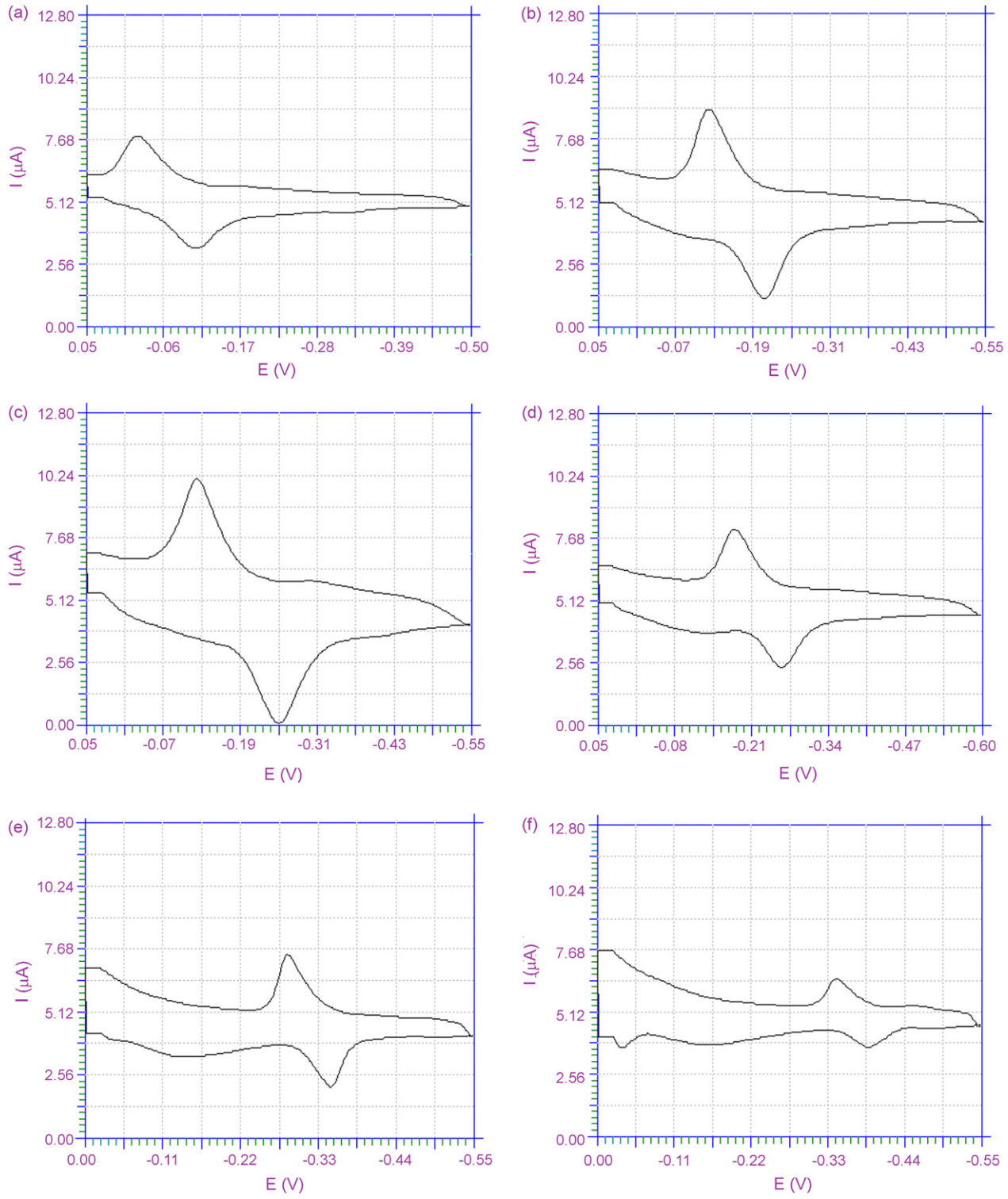

Fig. 2. The cyclic voltammograms in different pH BR buffer solutions. (a) pH 4 (b) pH 6 (c) pH 7 (d) pH 8 (e) pH 10 (f) pH 12.

tions. In comparison with the OPD spectrophotometric ELISA, the new method showed higher sensitivity for detection of labeled HRP. The dilution curves of two methods were exhibited in Fig. 3. The highest dilution ratios detected by our electrochemical method were $1{:}4.1 \times 10^6$, $1{:}1 \times 10^4$, $1{:}5.6 \times 10^4$, $1{:}8.4 \times 10^5$ and $1{:}6 \times 10^3$, respectively. The highest dilution ratio detected by the spectrophotometric ELISA method was $1{:}3.9 \times 10^5$, $1{:}5.0 \times 10^3$, $1{:}8.0 \times 10^3$, $1{:}6.0 \times 10^4$ and $1{:}1 \times 10^3$, respectively. The detection limits of electrochemical method based on HAP-H_2O_2-HRP system were lowered by 10, 5, 7, 15 and 6 times than those of the OPD spectrophotometric ELISA method.

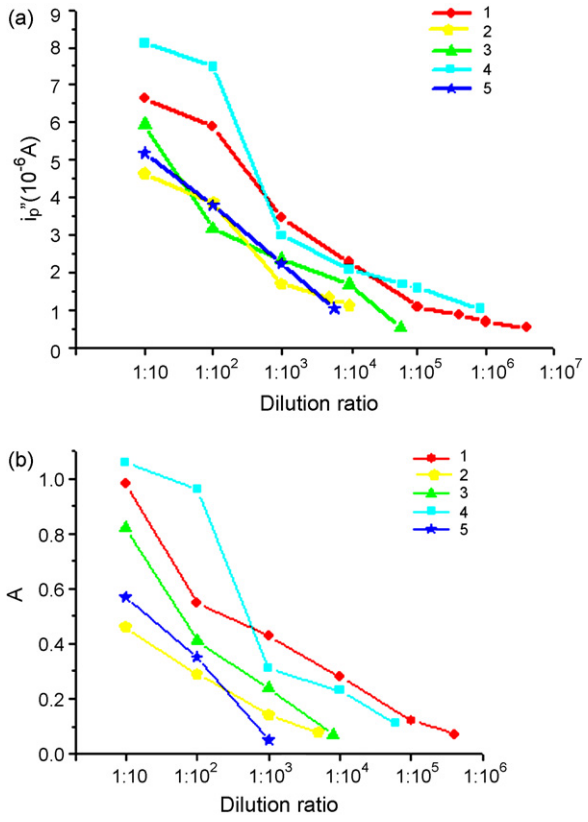

Fig. 3. The determination result of labeled HRP dilution ratio with electrochemical method (a) and spectrophotometric ELISA method (b). 1. anti-αFP-HRP; 2. anti-CEA-HRP; 3. anti-HCG-HRP; 4. anti-PSA-HRP; 5. anti-T_4-HRP.

3.7. Determination of αFP

The determination of αFP was carried out with double-antibody-sandwich immunoassay method. Under the optimum conditions, the linear range of the αFP quality control serum was 0.1–200 ng/mL and the detection limit was 0.1 ng/mL. The equation of linear regression was $y_1 = 0.6084 + 0.4284x_1$ (y represented $\Delta i_p''$, i_p'' was the peak current, μA; x was the concentration of αFP, 0.1–20 ng/mL, $n = 8$, $\gamma = 0.9955$) and $y_2 = 7.169 + 0.06927x_2$(y represented $\Delta i_p''$, i_p'' was the peak current, μA; x was the concentration of αFP, 20–200 ng/mL, $n = 5$, $\gamma = 0.9970$). The repeatability of the assay was studied by running 11 replicate assays on 5 ng/mL of αFP in serum, and the relative standard deviation was 3.8%. Under the same conditions, the linear range of the αFP quality control serum was 1.0–200 ng/mL and the detection limit was 1.0 ng/mL with OPD spectrophotometric ELISA method. The equation of linear regression was $A = 0.23318 + 0.006C$ (A was the absorbance, C was the concentration of αFP, $n = 7$, $\gamma = 0.9968$). Therefore, the detection limit of our electrochemical enzyme-linked immunoassay method was 10 times lower than that of the OPD spectrophotometric ELISA method.

3.8. Determination of αFP in human serum samples

Under the optimum conditions, the αFP content in human serum samples was assayed. The compared results with OPD spectrophotometric ELISA method were listed in Table 1. The results of two methods showed good agreement. The results of the HAP-H_2O_2-HRP voltammetric enzyme-linked immunoassay system was linearly proportional to those of OPD spectrophotometric ELISA method, and the equation of linear regression was $y = 1.0607x + 0.9250$ (x was the result of electrochemical method; y was the result of spectrophotometric method; $n = 12$, $\gamma = 0.9988$). Satisfactory results were obtained. The proposed new assay system showed a potential for detecting αFP in clinical examination.

Table 1
Comparison of results of the electrochemical method with the spectrophotometric ELISA method for the detection of αFP in human serum

Sample	Electrochemical method (ng/mL)	Spectrophotometric method (ng/mL)
1	7.21	6.86
2	0.57	–
3	15.27	13.14
4	4.50	4.32
5	10.58	12.54
6	33.65	35.97
7	0.52	–
8	21.03	19.33
9	0.41	–
10	19.56	20.68

4. Conclusions

It has been demonstrated here, for the first time, that *N*-heterocyclic compound is used as a substrate in electrochemical enzyme-linked immunoassay. A new voltammetric enzyme-linked immunoassay system based on HAP-H_2O_2-HRP has been developed and exhibited potential performance for detection of free HRP, labeled HRP and αFP in human serum. The new immunoassay has provided a convenient, low cost, and versatile method for specific and highly sensitive detection of virus and tumor, and exploited a new field of *N*-heterocyclic substrates for seeking more superior electrochemical enzyme-linked immunoassay system. In addition, the structures of many biologically active molecules in organism body contain pyridine ring or other *N*-heterocyclic compounds. The redox study of *N*-heterocyclic compounds is highly significative to better understand the process and mechanism of biological activity in life science.

Acknowledgement

This work was supported by the National Natural Science Foundation of China (No.20775038), the Natural Science Foundation of Shandong Province (No. Z2006B01), and the National High-tech R&D Program (863 Program, No. 2007AA09Z113).

References

[1] P. Sarker, P.S. Pal, D. Ghosh, S.J. Steford, I.E. Tothill, Int. J. Pharm. 238 (2002) 1.
[2] M. Antonini, P. Ghisellini, C. Paternolli, C. Nicolini, Talanta 62 (2004) 945.
[3] J.H. Thomas, S.K. Kim, P.J. Hesketh, H.B. Halsall, W.R. Heineman, Anal. Chem. 76 (2004) 2700.
[4] W. Vastarella, R. Nicastri, Talanta 66 (2005) 627.
[5] S.H. Alarcon, G. Palleschi, D. Compagnone, M. Pascale, A. Visconti, I. Barna-Vetro, Talanta 69 (2006) 1031.
[6] R. Jain, N. Jadon, K. Radhapyari, Talanta 70 (2006) 383.
[7] A. Salimi, H. Mamkhezri, R. Hallaj, Talanta 70 (2006) 823.
[8] Y. Zhang, A. Heller, Anal. Chem. 77 (2005) 7758.
[9] E.M. Abad-Villar, M.T. Fernaindez-Abedul, A. Costa-Garcia, Anal. Chim. Acta 453 (2002) 63.
[10] M.S. Wilson, W. Nie, Anal. Chem. 78 (2006) 2507.
[11] H.S. Jung, J.M. Kim, J.W. Park, H.Y. Lee, T. Kawai, Langmuir 21 (2005) 6025.
[12] D.-G. Maria, M.B. Gonzalez-Garci, A. Costa-Garcia, Electroanalysis 17 (2005) 1901.

[13] K. Jiao, W. Sun, S.S. Zhang, Fresen J. Anal. Chem. 367 (2000) 667.
[14] W. Sun, K. Jiao, S.S. Zhang, Anal. Lett. 33 (2000) 2653.
[15] Y.N. He, H.Y. Chen, J.J. Zheng, G.Y. Zhang, Z.L. Chen, Talanta 44 (1997) 823.
[16] S.S. Zhang, K. Jiao, H.Y. Chen, Anal. Lett. 32 (1999) 1761.
[17] K. Jiao, W. Sun, S.S. Zhang, G. Sun, Anal. Chim. Acta 413 (2000) 71.
[18] S.S. Zhang, P. Du, F. Li, Talanta 72 (2007) 1487.
[19] S.S. Zhang, K. Jiao, H.Y. Chen, Electroanalysis 11 (1999) 511.
[20] T.P. Whitehead, G.H.G. Thorpe, T.J.N. Carter, C. Groucutt, L.J. Kricka, Nature 305 (1983) 158.
[21] M. Maeda, A. Tsuji, Anal. Chim. Acta 167 (1985) 241.
[22] Y. Xu, H.B. Halsall, W.R. Heineman, Clin. Chem. 36 (1990) 1941.
[23] R.S. Nicholson, Anal. Chem. 37 (1965) 1351.

Talanta 76 (2008) 44–48

Contents lists available at ScienceDirect

Talanta

journal homepage: www.elsevier.com/locate/talanta

Quality control of piperaquine in pharmaceutical formulations by capillary zone electrophoresis

Qin Zhang, Yuan Fang Li, Cheng Zhi Huang*

College of Pharmaceutical Sciences, CQKL-LRTA, Southwest University, Chongqing 400715, China

ARTICLE INFO

Article history:
Received 24 October 2007
Received in revised form 30 January 2008
Accepted 31 January 2008
Available online 10 March 2008

Keywords:
Piperaquine
Quality control
Capillary zone electrophoresis
Pharmaceutical formulations

ABSTRACT

Quality control (QC) is of great importance since the pharmaceutical quality not only directly affects the curative effect of the drugs, but also relates to human health and safety closely. Capillary electrophoresis (CE) has recently become a good alternative for pharmaceutical analysis and a complementary technique to high-performance liquid chromatography since it possesses many unique advantages. In this contribution, we propose a simple and reliable capillary zone electrophoretic method for the detection of piperaquine (PQ) in pharmaceutical formulations in terms of quality control, which might be of use to those working on similar compounds. The influence of buffer type, buffer pH, buffer concentration, buffer additive, applied voltage, capillary temperature and injection amount was systemically investigated and the proposed method was then successfully applied to the quality control of piperaquine in its pharmaceutical formulations. With quinine (QN) as an internal standard to improve precision, this method was suitably validated with respect to the linearity, limit of detection and quantification, accuracy, precision, specificity and stability.

1. Introduction

Capillary electrophoresis (CE) has become one of the most advanced separation techniques for pharmaceutical analysis in recent years, although quality control analysis of pharmaceuticals currently is performed predominantly with high-performance liquid chromatography (HPLC). It has proved that CE is a useful and reliable alternative and a complementary technique to HPLC in many areas, including main component assay, impurity determination, enantiomeric separations, identity confirmation and stoichiometry determination. In many instances, CE can have distinct advantages over HPLC in terms of rapid method development, reduced operating costs and increased simplicity. In addition, a single set of CE operation conditions may be appropriate for a wide range of pharmaceuticals leading to very significant efficiency gains [1]. A number of studies have shown that modern CE system can be very reproducible; the biggest variable is probably migration time that changes due to EOF variations. On the other hand, a major drawback of CE is the perceived lack of precision, which has been widely adopted in the area of main component assay. The major source of imprecision when using commercial instrumentation is injection volume variability. To cope with this problem, in present work, an internal standard (IS) was employed as a means of increasing precision according to Refs. [2–3].

Malaria is an established public health problem in several third world countries. There are 300–500 million clinical cases each year, and between one and three million deaths, mostly children (and pregnant women) are attributable to this disease [4]. To improve therapeutic efficacy and delay the development of resistance to monotherapies, artemisinin-based combination therapies (ACTs) has been recommended by World Health Organization (WHO), and generally considered as the best current treatment for uncomplicated falciparum malaria [5–7]. As a suitable ACTs partner, piperaquine (PQ, Fig. 1), a bisquinoline antimalarial drug, in combination with dihydroartemisinin (DHA) has shown to be safe over the last couple of years, highly efficacious and tolerable in controlled clinical trials [8–13], and has been adopted as first-line treatment of uncomplicated malaria in Viet Nam [14]. Moreover, in 2004, Chongqing Holley Holding, Sigma-Tau, Oxford University and the Medicines for Malaria Venture (MMV) have initiated a joint project for the international development of the promising fixed-dose drug combination, PQ–DHA (Artekin®) [4].

To date there are only few publications concerning the detection of PQ in pharmaceutical preparations [15] and biological samples [16–21], and all of them are HPLC methods, which involve in the use of Cyano column, solid-phase extraction (SPE) column and a relatively large amount of organic solvent. The aim of the work described herein is to develop a simple and readily applicable capillary zone electrophoresis (CZE) method for the quality

* Corresponding author. Tel.: +86 23 68254659; fax: +86 23 68866796.
E-mail address: chengzhi@swu.edu.cn (C.Z. Huang).

0039-9140/$ – see front matter © 2008 Elsevier B.V. All rights reserved.
doi:10.1016/j.talanta.2008.01.066

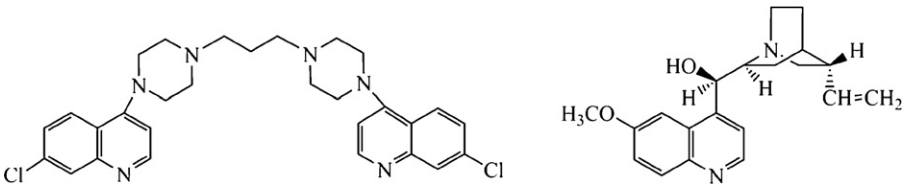

Fig. 1. Molecular structure of piperaquine (PQ, left) and quinine (Q, right).

control of PQ in pharmaceutical formulations. Quinine (QN, Fig. 1), an antimalarial compound, was chosen to be IS in this contribution since its migration time is close to PQ and it has smooth peak shape in optimized conditions. Validation of the proposed method was performed according to the International Conference on Harmonization (ICH) Guidelines [22]. The developed and validated method was successfully applied to the quality control of PQ in Artekin® tablets.

2. Experimental

2.1. Apparatus

All CE experiments were performed on a Beckman P/ACE MDQ capillary electrophoresis system (Beckman, Fullercon, CA, USA) equipped with a photodiode array detection system. The electrophoregrams were recorded and integrated with 32-karat software version 7.0 (Beckman). Electrophoretic separations were carried out with an uncoated fused-silica capillary (i.d. 75 μm, Yongnian Optic Fiber Factory, Heibei, China) of total length 50 cm and effective length 40 cm. Samples were injected with pressure at 0.5 psi for 5 s and separated at +20 kV. The CZE was run under the temperature of 25 °C with the detection wavelength at 240 nm for the photodiode array detection system.

Prior to the first use, new capillary should be conditioned following the flushing with 0.1 mol l^{-1} NaOH for 30 min, water and the running buffer for 10 min, respectively, and be kept with buffer overnight. At the beginning of each working day, the capillary was rinsed sequentially with 0.1 mol l^{-1} NaOH for 5 min, water for 3 min, the running buffer for 10 min, and finally pre-equilibrated with the running buffer under the separation voltage for 10 min. Between runs, the capillary was rinsed with 0.1 mol l^{-1} NaOH, water and the running buffer, respectively, for 2 min each. Buffers and samples were filtered through a 0.45 μm membrane filter and degassed ultrasonically before use.

2.2. Chemicals and reagents

Piperaquine (PQ) phosphate reference standard was purchased from the National Institute for the Control of Pharmaceutical and Biological Products (Beijing, China). Quinine sulfate (QN) salt was obtained from Sinopharm Chemical Reagent Co. Ltd. (Shanghai, China). Artekin® tablets (320 mg piperaquine phosphate per tablet) were kindly provided by Chongqing Institute for Drug Control (Chongqing, China), which were manufactured by Holley Pharmaceuticals Co. Ltd. (Chongqing, China). Other reagents used were analytical grade purchased from local chemical company. Water used throughout was doubly distilled (18.2 Ω). The separation buffer, consisted of 65 mmol l^{-1} phosphoric acid, was adjusted to pH 3.00 with triethanolamine (TEA).

2.3. Standard and sample solutions

The stock solutions of PQ (200 μg ml^{-1}) and QN (200 μg ml^{-1}) were prepared in 10 mmol l^{-1} HCl and kept in the dark at 4 °C. Standard solutions of PQ were prepared daily by appropriate dilution of the stock solution with 10 mmol l^{-1} HCl. Into various aliquots of standard solutions was added QN solution and then diluted to 1 ml with 10 mmol l^{-1} HCl to give a final analytical concentration of 5, 10, 20, 30, 40, 60, 80 and 100 μg ml^{-1}, respectively.

Ten tablets of Artekin® were accurately weighed and finely powdered. A portion of the powder, which was equivalent to about 40 mg piperaquine phosphate according to the label content of the tablet supplier, was transferred to a 50-ml volumetric flask. With the addition of 35 ml of 10 mmol l^{-1} HCl, the mixture was sonicated for 15 min, and diluted with 10 mmol l^{-1} HCl to volume, mixed and filtered, and 50 μl of the filtrate was transferred to a vial. Following the addition of 100 μl QN (200 μg ml^{-1}), the mixture was diluted with 10 mmol l^{-1} HCl to 1 ml, and then transferred for CZE analysis.

3. Results and discussion

3.1. Restraint of PQ adsorption

PQ is highly lipophilic with four pK_a values of 6.9, 6.2, 5.7, and 5.4 [23], and it should be at least partially positively charged at all pH values lower than 6.9. Preliminary investigations showed that the adsorption of PQ on the fused silica capillary wall was serious in acidic condition owing to electrostatic interaction, hydrophobic interaction and some other various two-phase distribution mechanisms. Therefore, it was very important to restrain or completely eliminate the interaction between PQ and capillary wall. Strategies for reducing solute adsorption include use of buffer additives of extremes pH, high salt concentration and internally coated capillaries [24–26].

In order to achieve the good peak shape of PQ, highest sensitivity and short analysis time in this contribution, running buffers, such as disodium hydrogen phosphate–citric acid, H_3PO_4–NaOH and H_3PO_4–TEA at pH 3.0 had been tested. By evaluating the factors of migration time, peak area, height, theoretical plates, resolution, symmetry of PQ and QN, we found that H_3PO_4–TEA buffer could provide the best results, which was in accordance with earlier reports that TEA could be used as the coupled ion of buffer to reduce peak tailing [27–28].

Operation at extremes of pH beneficially alters the charged nature of both the solutes and capillary wall and can reduce electrostatic interactions. Fig. 2 shows the effects of pH upon the migration time or theoretical plates of PQ in the H_3PO_4–TEA buffer with pH ranging from 2.0 to 3.5. It could be seen that the migration time and the theoretical plates of PQ got dramatically increased with pH increasing from 2.0 to 3.0, and the maximum values occurred at pH 3.0. If pH was further higher than 3.0, the migration time and the theoretical plates of PQ would decrease sharply, and the peak height got declined with serious tailing. These results were mainly attributed to the increased ionization of the silanol groups on the capillary wall at higher pH values, leading to a strong absorption of PQ on the capillary wall.

It was found that buffer concentration affects the migration time and separation efficiency. Upon increasing the buffer concentration ranging from 20 to 80 mmol l^{-1}, the migration time and the

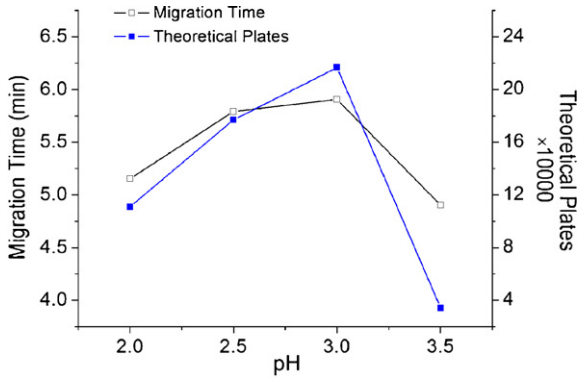

Fig. 2. Effect of pH on migration time and theoretical plates of PQ. Running buffer, 65 mmol l^{-1} H_3PO_4–TEA; capillary, 50 cm × 75 μm i.d., effective length 40 cm; applied voltage, +20 kV; UV detection, 240 nm; column temperature, 25 °C. PQ, 40 μg ml^{-1} and Q, 20 μg ml^{-1}, pressure injection at 0.5 psi for 5 s.

theoretical plates of PQ got increased significantly until 65 mmol l^{-1}, and then the increase got lessened (Fig. 3). In addition, the separations of QN and two impurities were improved from part to complete separation whereas the resolution of PQ and QN decreased gradually with increase in the buffer concentration. An increased peak height ratio of PQ and QN was also observed, which indicated higher sensitivity.

Injection solvents also influence the peak shape of PQ. Our experiments showed that the peak shape of PQ and QN were deformed either with the flat top or with peaking tailing if the stock solutions were diluted with buffer or water for injection analysis. To overcome this problem, various additives to the running buffer were considered in the present investigations. The organic modifier such as acetonitrile (5 and 10%, v/v) and surfactants including Triton X-100 (0.001 and 0.01%, v/v) and cetyltrimethylammonium bromide (CTAB, 0.5 mM) had been added to the buffer. Regrettably, the results demonstrated that the peak tailing of PQ was not improved. It was found that the best way is to dilute the stock solution with 10 mmol l^{-1} HCl as it could alleviate the adsorption of PQ on the capillary wall, giving a good peak shape.

3.2. Optimization of the CZE conditions

The effect of applied voltage was tested in the range 14–26 kV. In the buffer of 65 mmol l^{-1} H_3PO_4–TEA at pH 3.0, increasing applied voltage gave both shorter migration times and sharper peaks. On the other hand, high voltages exhibited high currents with the

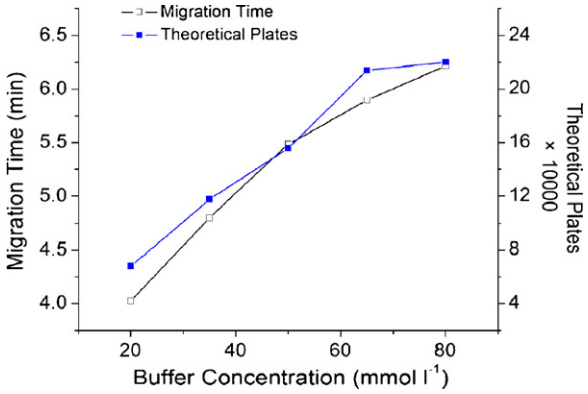

Fig. 3. Effect of buffer concentration on migration time and theoretical plates of PQ. Running buffer, H_3PO_4–TEA (pH 3.0). Other conditions were as described in the caption to Fig. 2.

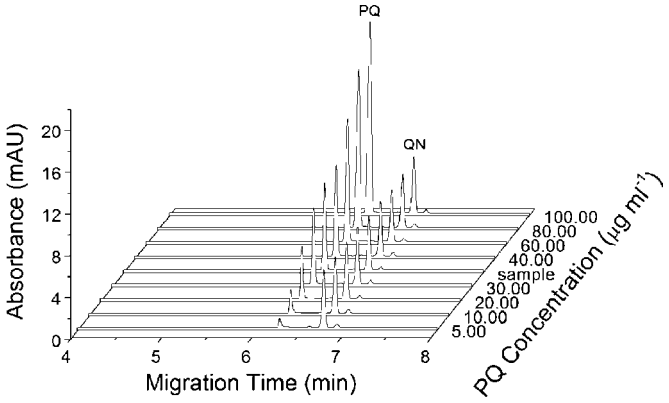

Fig. 4. Capillary electrophoretic determination of PQ in pharmaceutical tablets. Electrophoretic conditions: running buffer, 65 mmol l^{-1} H_3PO_4–TEA (pH 3.0). Other conditions were as described in the caption to Fig. 2. Concentration of standard, PQ: 5.00, 10.00, 20.00, 30.00, 40.00, 60.00, 80.00 and 100.00 μg ml^{-1}, QN: 20 μg ml^{-1}. Linear regression, $y = 0.0426x - 0.0594$ (where y is the peak area ratio of PQ to QN, and x is the concentration of PQ). The correlation coefficient was 0.9996. From the standard curve and linear regression, the quantity of PQ in Artekin® tablets was 320.65 mg, R.S.D. was 0.73% ($n = 6$).

results of increasing Joule heat and decreasing separation efficiency. Based on the experiments, 20 kV was chosen as the optimum voltage to accomplish a good compromise.

Changes in capillary temperature can cause variations in EOF, migration time, injection volume, separation efficiency and repeatability. The effect of temperature on analysis was investigated at 20, 25 and 30 °C. An increase of the capillary temperature resulted in a decrease of migration times for PQ and QN due to smaller electrolyte viscosity. It was noted that the temperature giving the best compromise between resolution and run time, with a good level of baseline noise, was 25 °C.

In order to improve the sensitivity, sample solutions were injected with pressure at 0.5 psi while the injection time was varied from 3 to 10 s. The peak area increased with increasing injection time. It was noticed that the peak shapes of PQ and QN were deformed after 5 s.

Under these optimized conditions, the migration times of PQ and QN were 6.24 ± 0.01 and 6.73 ± 0.01 min, respectively. The total time for the analysis was less than 8 min (Fig. 4).

3.3. Validation of the method

In order to demonstrate whether the present method is suitable for the quality control of PQ in pharmaceutical formulations, we made validation of the method with respect to linearity, limit of detection (LOD) and limit of quantification (LOQ), accuracy, precision, specificity and stability.

3.3.1. Linearity range

Under the optimum conditions for quality control, linearity was investigated in the concentration range of 5.00–100.00 μg ml^{-1} for PQ, and 20.00 μg ml^{-1} of QN was added as IS in all cases. Calibration curve was constructed with a series of PQ concentrations. Each point of the calibration graph corresponded to the mean value obtained from 6 independent measurements. The linearity curve was defined by the equation of $y = 0.0426x - 0.0594$, where y is the peak area ratio of PQ to QN, and x is the concentration of PQ expressed in μg ml^{-1}. The correlation coefficient was 0.9996. The ratio of peak area (PQ/QN) was chosen for plotting calibration curve because of only providing slight higher R.S.D. (0.61%) than the ratio of peak normalization (as the ratio PQ peak area/migration

Table 1
Repeatability of migration time, peak area, peak normalization, ratio of peak area and ratio of peak normalization values (PQ: 40.00 μg ml^{-1} and QN: 20.00 μg ml^{-1}) (n = 6)

	PQ			QN			Ratio of peak area	Ratio of PN
	Migration time (min)	Peak area	PN	Migration time (min)	Peak area	PN		
$\overline{X}$ ± S.E.	6.24 ± 0.01	25142 ± 364	4031 ± 53	6.73 ± 0.01	15314 ± 195	2274 ± 27	1.64 ± 0.004	1.77 ± 0.004
S.D.	0.02	891	131	0.05	478	65	0.01	0.01
R.S.D.%	0.32	3.54	3.25	0.74	3.16	2.86	0.61	0.56

$\overline{X}$ ± S.E.: mean ± standard error; S.D.: standard deviation; R.S.D.%: relative standard deviation; PN (peak normalization): peak area/migration time.

Table 2
Precision and accuracy data for the proposed method (n = 3)

Added (μg ml^{-1})	Intra-day			Inter-day		
	Found[a] (μg ml^{-1})	Precision (R.S.D.%)	Accuracy[b] (bias%)	Found[a] (μg ml^{-1})	Precision (R.S.D.%)	Accuracy[b] (bias%)
10.00	10.08 ± 0.04	1.19	0.80	9.76 ± 0.09	2.66	−2.40
40.00	39.70 ± 0.07	0.50	−0.75	40.08 ± 0.22	1.65	0.20
90.00	90.39 ± 0.25	0.82	0.43	90.51 ± 0.60	1.99	0.57

[a] Found: mean ± standard error; R.S.D.%: relative standard deviation.
[b] Accuracy: bias% = [(founded − added)/added] × 100.

time-QN peak area/migration time) (0.56%) for simpler calculation. All raw data were calculated using calibration curve.

3.3.2. Sensitivity

A signal-to-noise ratio (S/N) of approximately 3:1 is generally considered to be acceptable for estimating the LOD. The measured LOD value of PQ was 2.00 μg ml^{-1}, and the relative standard deviation (R.S.D.) is 2.10% (n = 6). The LOQ is the lowest concentration of PQ that can be quantified with acceptable precision and accuracy, which was defined as S/N = 10. The measured LOQ value was 3.00 μg ml^{-1} (R.S.D. = 2.04% and bias = 0.33%, n = 6) for the proposed method.

3.3.3. Precision

The precision was investigated with respect to repeatability and intermediate precision. In order to measure repeatability of the system, six consecutive injections were made with a standard solution containing 40.00 μg ml^{-1} of PQ and 20.00 μg ml^{-1} of QN, and the results were evaluated by considering migration time, peak area, and peak normalization (peak area/migration time), ratio of peak normalization and ratio of peak area values of PQ to QN. The precision values with their R.S.D. are shown in Table 1. The amount of PQ was found to be 39.93 ± 0.10 with R.S.D. of 0.58% for CZE method. Percentage recovery of PQ was calculated as 99.82 ± 0.24% with R.S.D. of 0.59%. These values indicated that the proposed method have high repeatability and precision for the PQ analysis.

To evaluate intermediate precision in terms of intra- and inter-day precisions, three different concentrations of PQ in the linear range (10.00, 40.00 and 90.00 μg ml^{-1}) were analyzed in three independent series in the same day (intra-day precision) and three consecutive days (inter-day precision), and within each series every sample was injected three times. The precision of the analysis was determined by calculating R.S.D.%, which should not exceed 5%. The R.S.D. values of intra-day and inter-day studies varied from 0.50 to 2.66% showed that the intermediate precision of the method was satisfactory (Table 2).

3.3.4. Accuracy and recovery

The accuracy is determined by calculating the percentage relative error (bias%), which is acceptable between −5 and +5%. Table 2 shows the results obtained for intra- and inter-day accuracy. Recovery studies for the accuracy of the method were performed by injecting the sample solutions spiked with known amounts of PQ in the range 75–125% of the target concentration (30.00, 40.00 and 50.00 μg ml^{-1}). Samples were treated as described in the procedure for sample preparation. The acceptable recovery was set as between 95 and 105%. The results were shown in Table 3. The mean recovery of PQ was between 99.20 and 100.15%, and R.S.D. was between 0.21 and 0.64%.

3.3.5. Specificity

The specificity was evaluated by peak purity check using the pharmaceutical tablet solution containing PQ and QN optimizing separation and detection. Spectral scans for the individual peak of PQ and QN were made between 200 and 400 nm. Spectra at predetermined intervals across per-peak were normalized and then compared to the spectrum collected at the peak apex. Peak was considered pure when there was a coincidence between the spectra (similarity index was greater than 0.99). These data showed that there was no significant interference of related compounds and excipients in the analysis of PQ in pharmaceutical formulations by the proposed method. The method can be considered selective.

3.3.6. Stability

Stability of the standard solution of PQ in 10 mmol l^{-1} HCl, stored in the dark and at 4 °C, was evaluated at various time points over 2 months. The absorption spectrum of this solution was checked and PQ solution was found unchanged within this period. Stability of the sample solution of PQ stored in the dark at room temperature was also assessed at various time points over 12 h. The R.S.D. value of the peak area radios of PQ to QN was 0.91%, which indicated that the sample solution was stable within this period.

Table 3
The results of recovery in spiked tablets of PQ for the proposed method (n = 3)

Added (μg ml^{-1})	Found[a] (μg ml^{-1})	Mean recovery (%)	R.S.D.%
30.00	29.76 ± 0.11	99.20	0.64
40.00	39.92 ± 0.10	99.81	0.45
50.00	50.08 ± 0.06	100.15	0.21

[a] Found: mean ± standard error; R.S.D.%: relative standard deviation.

3.4. Analysis of Artekin® tablets

The optimized proposed CZE method was applied to the determination of PQ in Artekin® tablets. The amounts of PQ in tablets were calculated using calibration curve method. The results obtained (99.39–101.33%, 0.73%R.S.D., $n = 6$) were in good agreement with the label claim for tablet content.

4. Conclusion

A simple and reliable CZE method of PQ in pharmaceutical formulations has been developed and validated in terms of quality control. Although method sensitivity is not outstanding (LOQ = 3 $\mu g\,ml^{-1}$) due to the intrinsic limitations of the system (short optical path, injection by pressure), the method is quite rapid and feasible. With respect to the reported HPLC methods, this method only consumes lower amounts of polluting and toxic organic solvents. Furthermore, the method is characterized by good linearity, accuracy and precision (correlation coefficient 0.9996, mean recovery 99.20–100.15%, R.S.D. < 2.7%). Thus, this method is suitable for routine quality control of PQ in pharmaceutical formulations.

Acknowledgements

We thank the supports of the National Natural Science Foundation of China (NSFC, NO. 20425517), and Chongqing Institute for Drug Control.

References

[1] K.D. Altria, LCGC 18 (2000) 33.
[2] B.X. Mayer, J. Chromatogr. A 907 (2001) 21.
[3] E.A. Pereira, G.A. Micke, F.M. Tavares, J. Chromatogr. A 1091 (2005) 169.
[4] J.G. Breman, Am. J. Trop. Med. Hyg. 64 (2001) 1.
[5] The use of antimalarial drug. Report of a WHO Informal Consultation. World Health Organization, 2000. (WHO/CDS/RBM/2001.33).
[6] Antimalarial drug combination therapy. Report of a WHO technical consultation. World Health Organization, 2001. (WHO/CDS/RBM/2001.35).
[7] Guidelines for the treatment of malaria. World Health Organization, 2006. (WHO/HAM/MAL/2006.1108).
[8] H.Y. Myint, E.A. Ashley, N.P. Day, F. Nosten, N.J. White, Trans. R. Soc. Trop. Med. Hyg. 101 (2007) 858.
[9] M.R. Kamya, A. Yeka, H. Bukirwa, M. Lugemwa, J.B. Rwakimari, S.G. Staedke, A.O. Talisuna, B. Greenhouse, F. Nosten, P.J. Rosenthal, F. Wabwire-Mangen, G. Dorsey, PLoS Clin. Trials. 2 (2007) e20.
[10] Q.L. Fivelman, I.S. Adagu, D.C. Warhurst, Antimicrob. Agents Chemother. 51 (2007) 2265.
[11] A.R. Hasugian, H.L. Purba, E. Kenangalem, R.M. Wuwung, E.P. Ebsworth, R. Maristela, P.M. Penttinen, F. Laihad, N.M. Anstey, E. Tjitra, R.N. Price, Clin. Infect. Dis. 44 (2007) 1067.
[12] A. Ratcliff, H. Siswantoro, E. Kenangalem, R. Maristela, R.M. Wuwung, F. Laihad, E.P. Ebsworth, N.M. Anstey, E. Tjitra, R.N. Price, Lancet 369 (2007) 757.
[13] B. Janssens, M. van Herp, L. Goubert, S. Chan, S. Uong, S. Nong, D. Socheat, A. Brockman, E.A. Ashley, W. Van Damme, Trop. Med. Int. Health. 12 (2007) 251.
[14] World Health Organization, Facts on ACTs (Artemisinin-Based Combination Therapies), January 2006 Update, 2006.
[15] M.Q. Li, Q. Fan, X.S. Zhang, West China J. Pharm. Sci. 19 (2004) 221.
[16] N. Lindegardh, N.J. White, N.P.J. Day, J. Pharm. Biomed. Anal. 39 (2005) 601.
[17] T.Y. Hung, T.M. Davis, K.F. Ilett, J. Chromatogr. B 791 (2003) 93.
[18] N. Lindegardh, M. Ashton, Y. Bergqvist, J. Chromatogr. Sci. 41 (2003) 44.
[19] N. Lindegardh, M. Ashton, Y. Bergqvist, Ther. Drug Monit. 25 (2003) 544.
[20] M. Malm, N. Lindegardh, Y. Bergqvist, J. Chromatogr. B 809 (2004) 43.
[21] J. Tarning, T. Singtoroj, A. Annerberg, M. Ashton, Y. Bergqvist, N.J. White, N.P.J. Day, N. Lindegardh, J. Pharm. Biomed. Anal. 41 (2006) 213.
[22] ICH Harmonised Tripartite Guideline, International Conference on Harmonisation of Technical Requirements for Registration of Pharmaceuticals for Human Use, "Validation of Analytical Procedure: Methodology", 1996.
[23] D.C. Warhurst, J.C. Craig, I.S. Adagu, R.K. Guy, P.B. Madrid, Q.L. Fivelman, Biochem. Pharmacol. 73 (2007) 1910.
[24] J.M. Armenta, B. Gu, C.D. Thulin, M.L. Lee, J. Chromatogr. A 1148 (2007) 115.
[25] X.F. Guo, J. Lv, W.D. Zhang, Q.J. Wang, P.G. He, Y.Z. Fang, Talanta 69 (2006) 121.
[26] H. Wätzig, M. Degenhardt, A. Kunkel, Electrophoresis 19 (1998) 2695.
[27] S.A. Berkowitza, H.J. Zhong, M. Berardinoa, Z. Sosica, J. Siemiatkoskia, I.S. Krullb, R. Mhatrea, J. Chromatogr. A 1079 (2005) 254.
[28] J.W. Kang, A. Van Schepdael, J.A. Orwa, E. Roets, J. Hoogmartens, J. Chromatogr. A 879 (2000) 211.

Talanta 76 (2008) 230–232

Contents lists available at ScienceDirect

Talanta

journal homepage: www.elsevier.com/locate/talanta

Short communication

Tryptophan-contained peptide-functional nanomaterials as general spectrofluorometric reagents for enzyme

Shu Jun Zhen [a], Yuan Fang Li [a,*], Cheng Zhi Huang [b,*], Yun Fei Long [c]

[a] College of Chemistry and Chemical Engineering, CQKL-LRTA, Southwest University, Chongqing 400715, China
[b] College of Pharmaceutical Sciences, CQKL-LRTA, Southwest University, Beibei, Chongqing 400715, China
[c] Institute of Chemistry and Chemical Engineering, Hunan University of Science and Technology, Hunan 411201, China

ARTICLE INFO

Article history:
Received 28 November 2007
Received in revised form 15 February 2008
Accepted 18 February 2008
Available online 29 February 2008

Keywords:
Peptide
Au-nanoparticles
Thrombin
Fluorescence
Tryptophan

ABSTRACT

By designing and coupling a functional peptide, Gly-Leu-Ala-Cys-Ser-Gly-Phe-Pro-Arg-Gly-Arg-Trp, which could be cleaved by thrombin at the site of Arg-Gly (R-G), to the surface of gold nanoparticles (Au-NPs), we propose a simple spectrofluorometry for thrombin (TRB) in this contribution. Experiments showed that the peptide coupled to the surface of Au-NPs in a Tris–HCl buffer at 37 °C could be cleaved, leaving the fluorescent fragment of Gly-Arg-Trp in the Au-NPs suspension. By centrifuging the suspension and measuring the fluorescence signals resulting from the Trp residue of Gly-Arg-Trp fragment in the supernatant, we found that the fluorescence intensity is proportional to thrombin concentrations in the range of 1–100 nM with the limit of the detection of 0.1 nM. Since there are a lot of enzymes that can hydrolyze peptide with special sequence, and novel nanomaterials that can bind with the tryptophan-contained peptide and understand centrifugation, this spectrofluorometric method is general and it is possible to develop a variety of detection method for target enzymes.

1. Introduction

Enzymes can catalyze biological processes specifically, promoting the rate of reactions of their substrates by orders of magnitude relative to the corresponding rates in solutions [1]. As one of the most important enzyme in biological processes, thrombin is a trypsin-like serine protease, which can selectively cleave Arg-Gly bonds and convert fibrinogen to fibrin and active factor XIII as the last step of coagulation [2,3]. It can promote the platelet aggregation, and active protease-activated receptors (PARs) that play a particularly important role in the pathogenesis of clinical disorders [4]. Thrombin can also mediate the formation of acute thrombus under arterial flow conditions [5] and promote tumor cells to acquire malignancy [6]. Therefore detection of thrombin plays an important role in clinical diagnosis and pathological research.

Several approaches have been developed successfully to detect thrombin including fluorescence assay [7,8], colorimetry [9], capillary electrophoresis [10–12], matrix-assisted laser-desorption ionization time-of flight mass spectrum (MALDI-ToF-MS) [13], electrochemical methods [14–19], nanogap impedance [20], electrogenerated chemiluminescence [21], and so on. Most of these methods, however, are based on the aptamer [22], DNA or RNA oligonucleotides, as the specific detection probe, which should have to be labeled with functional groups like fluorophore [7]. To our knowledge, there are few reports dealing with the peptide-functionalized nanoparticles to detect thrombin or to monitor its proteolytic activity, in which FRET is the most used [23] and the peptides still need labeling with functional groups, too. In addition, the times needed in these methods are always long and some even more than 20 h [15,18].

Herein we report a simple spectrofluorometric method of thrombin with peptide-functionalized Au-nanoparticles (peptide-Au-NPs) based on the fluorescence signals resulting from the tryptophan contained in the cleavage fragment from the peptide by thrombin. In contrast to previous methods, present method is simple and it is not necessary to label the peptide with signal reporter or other functional groups such as fluorophore, NH_2, SH, and so on. Since there are a lot of enzymes that can hydrolyze peptide with special sequence, our method is general and could be applied to the development of detecting a variety of target enzymes.

2. Experimental

2.1. Materials

The peptide we designed has the sequence of Gly-Leu-Ala-Cys-Ser-Gly-Phe-Pro-Arg-Gly-Arg-Trp (GLACSGFPRGRW, SciLight

* Corresponding authors. Tel.: +86 23 68254659; fax: +86 23 68866796.
E-mail addresses: liyf@swu.edu.cn (Y.F. Li), chengzhi@swu.edu.cn (C.Z. Huang).

0039-9140/$ – see front matter © 2008 Elsevier B.V. All rights reserved.
doi:10.1016/j.talanta.2008.02.030

Biotechnology, LLC). Thrombin was purchased from Haematologic Technologies Inc. (USA). BSA, HSA, cellulas, and lysozyme were purchased from Beijing BioDev-Tech Scientific & Technical Co. Ltd. Tris–HCl buffer solution (pH 7.4, 0.05 M) was used to control the acidity, and Mili-Q purified water was used throughout.

2.2. Apparatus

The fluorescence measurements were made with an F-2500 fluorescence spectrophotometer (Hitachi, Tokyo, Japan). A U-3010 spectrophotometer (Hitachi, Tokyo, Japan) was used for the measurement of the plasmon absorption spectrum of the Au-NPs. A vortex mixer QL-901 (Haimen, China) was used to blend the solution. A high-speed TGL-16M centrifuge (Hunan, China) was used for the centrifugation of the solution.

2.3. Synthesis of Au-NPs

Au-NPs were prepared based on the reduction of $HAuCl_4$ according to the literature procedure [24]. Briefly, 485 μL aqueous solution consisting of 0.02 M $HAuCl_4$ was brought to 40 mL vigorous boiling water with stirring in a conical flask, and 1 mL trisodium citrate (1%) was added rapidly to the solution. The solution was boiled for another 8 min. During that time the color of the mixture changed from pale yellow to deep red. The solution was then cooled to room temperature with continuous stirring, and Au-NPs with the plasmon absorption at 518.0 nm were prepared.

2.4. General procedure

1.0 μM peptide solution was incubated with 0.17 mM as-prepared Au-NPs in Tris–HCl buffer (pH 7.4, 6 mM) for 30 min at 37 °C to allow the complete binding, then thrombin with different concentrations was added into the solution and incubated for another 20 min at the same temperature. After centrifugation for 20 min at 16,000 rpm (17,800 × *g*), the supernatant was transferred for fluorescence measurements with the F-2500 fluorescence spectrophotometer by fitting the excitation wavelength at 280.0 nm.

3. Results and discussion

3.1. General strategy for enzyme assay

Peptide used in this method should be designed to have the amino acid sequence cleavable by the proteolytic enzyme thrombin, and the end of the peptide should have tryptophan residue (W) that can emit strong fluorescence. Fig. 1 depicts the strategy of thrombin assay. The designed peptide was first covalently coupled to the surfaces of Au-NPs based on the formation of gold-thiol bonds through HS– of cysteine, and then the Arg-Gly bonds was hydrolytically cleaved by thrombin, leaving the fragment containing tryptophan in the supernatant after centrifugation. Then the supernatant could emit strong fluorescence owing to the tryptophan. Thus we can use the enhanced fluorescence signals to detect thrombin.

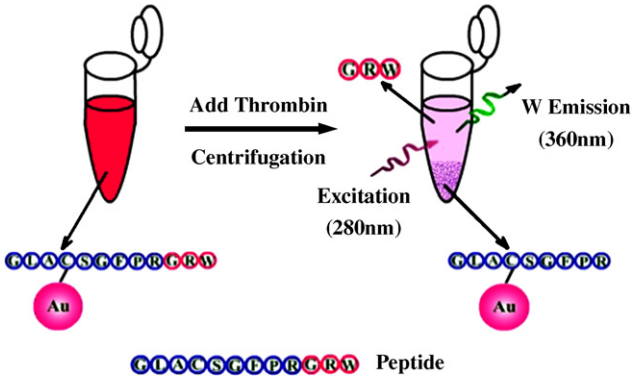

Fig. 1. Design strategy of thrombin assay. The designed peptide covalently bonded on the Au-NPs can be cleaved by thrombin on the specific site. As a result, the fragment "GRW" leaves from the surface of Au-NPs and stays in the supernatant after centrifugation, which emits fluorescence due to the strong fluorescence of tryptophan (W).

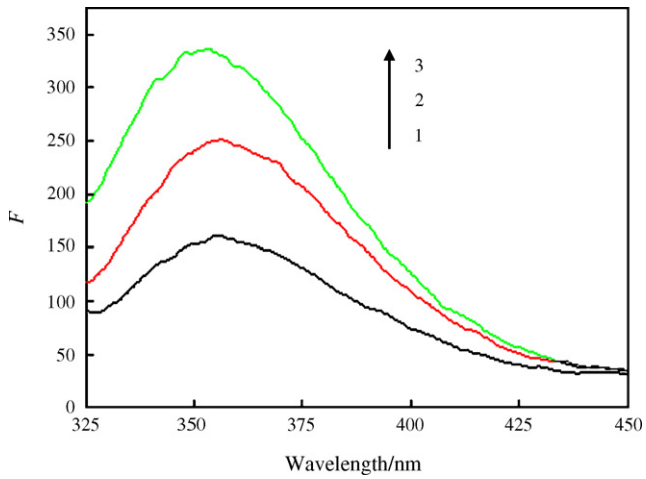

Fig. 2. The fluorescence emissions of the supernatant before and after the reaction of peptide-Au-NPs with thrombin: 1, peptide-Au-NPs; 2, peptide-Au-NPs + 40 nM thrombin; 3, peptide-Au-NPs + 60 nM thrombin. Concentrations: peptide, 1 μM; Au-NPs, 0.17 mM. All data were recorded in 6 mM Tris–HCl buffer, pH 7.4; λ_{ex}, 280.0 nm.

3.2. Spectral feature

Fig. 2 shows the fluorescence emissions of the supernatant after centrifuging peptide-Au-NPs suspension both in the presence and absence of thrombin. The fluorescence signal of the supernatant after centrifuging peptide-Au-NPs suspension is weak in the absence of the thrombin. After the addition of thrombin to the

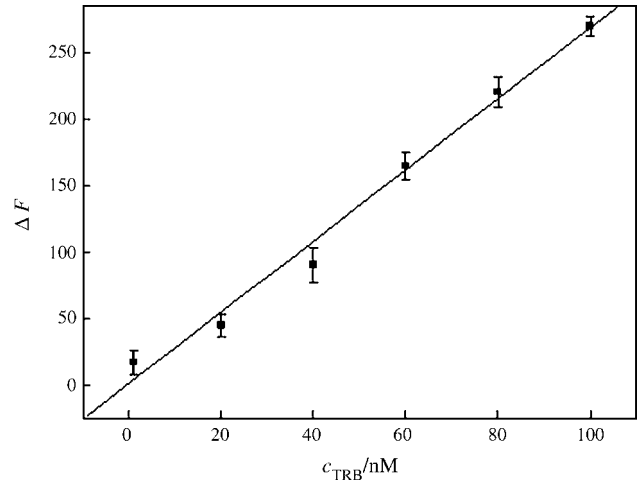

Fig. 3. The calibration curve, which could be expressed as $\Delta F = -0.56 + 2.69c_{TRB}$ with correlation coefficient of 0.9938. ΔF, the enhanced fluorescence intensity after adding thrombin to the peptide-Au-NPs solution. All data were collected at 360.0 nm from three measurements and error bars indicate the standard deviation. Concentrations: peptide, 1 μM; Au-NPs, 0.17 mM. All data were recorded in 6 mM Tris–HCl buffer, pH 7.4.

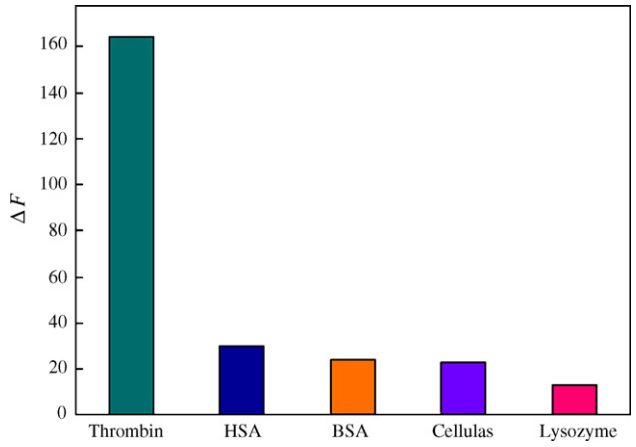

Fig. 4. The selectivity of the detection of thrombin. Concentrations: peptide, 1 μM; thrombin, 60 nM; HSA, 60 nM; BSA, 60 nM; cellulas, 60 nM; lysozyme, 60 nM; Au-NPs, 0.17 mM, pH 7.4. All data were collected at 360.0 nm.

Table 1
Analytical results for synthetic sample

$c_{thrombin}$ (nM)	60.0
Main additives[a]	HSA, BSA, lysozyme, cellulas
Found (nM) (n = 5)	61.18
Recovery range (%) (n = 5)	94.4–107.2
R.S.D.[b] (%)	4.67

[a] Concentrations of additives: BSA, 5.0 nM; HSA, 5.0 nM; lysozyme, 10.0 nM; cellulas, 10.0 nM.
[b] Relative standard deviation for five measurements.

solution, however, the enzyme selectively cleaves the Arg-Gly (R-G) bond, and the fragment with the sequence "GRW" at the end of the peptide leaves from the surface of Au-NPs and stays in the supernatant that separated from the centrifugation with the Au-nanoparticles. Then the supernatant can emit fluorescence strongly because of the fluorescent tryptophan residue.

3.3. Detection of thrombin

According to the method above, calibration curve of thrombin are constructed (shown in Fig. 3). All the data were obtained at 360.0 nm. There is linear relationship between the enhanced fluorescence intensities and the concentrations of thrombin in the range of 1–100 nM with the correlation coefficient, 0.9938. The calibration equation is $\Delta F = -0.56 + 2.69c_{TRB}$, and the limit of the determination is 0.1 nM.

To evaluate the selectivity of this method, four nonspecific proteins including HSA, BSA, cellulas, and lysozyme were tested, as shown in Fig. 4. The enhanced fluorescence intensities of the four proteins are much lower than that of thrombin, indicating that the four proteins cannot selectively cleave the peptide. The relatively low enhanced fluorescence intensities probably because that the four proteins can be absorbed to the surface of Au-NPs nonspecifically and make some peptides that can also emit fluorescence leave from the surface of Au-NPs to the aqueous solution.

To testify the practical feasibility of our method, synthetic sample was analyzed and the determination results were listed in Table 1. All of the results indicate that this method is possible for the real application of blood sample.

4. Conclusions

In summary, we propose a simple method to detect thrombin sensitively and selectively. Thrombin can selectively cleave the peptide with special sequence, which was coupled to the surface of Au-nanoparticles, and lead to the enhanced fluorescence intensity emitted by tryptophan of the fragment that cleaved from the peptide. This method is simple, and without labeling the peptide with fluorophore to report the signal or other functional groups, such as NH_2, SH, and so on. The time needed in our method, about 1 h, is very short. Since there are a lot of enzymes that can hydrolyze peptide with special sequence, it will be possible to develop the designation of this method to detect a variety of target enzymes.

In addition, it should be noted that we employed gold nanoparticles mainly considering that the easy covalently coupling reaction between peptide and Au-NPs based on the formation of gold-thiol bonds through HS– of cysteine. In fact, other solid materials such as magnetic nanoparitlces also could be employed since the gold nanoparticles only take the role of seperation of the fluorescence fragment of the hydrolytic cleavage product by thrombin.

Acknowledgement

This research was supported by the National Natural Science Foundation of China (NSFC, no. 20425517).

References

[1] A. Warshel, Proc. Natl. Acad. Sci. U.S.A. 75 (1978) 5250.
[2] L.A. Linkins, J.I. Weitz, Annu. Rev. Med. 56 (2005) 63.
[3] J.M. Fernindez-Romero, M.D. Luque de Castro, Talanta 43 (1996) 1531.
[4] S.F. Steinberg, Mol. Pharmacol. 67 (2005) 2.
[5] A.B. Kelly, U.M. Marzec, W. Krupski, A. Bass, Y. Cadroy, S.R. Hanson, L.A. Harker, Blood 77 (1991) 1006.
[6] H. Inuyama, T. Saito, J. Takagi, Y. Saito, J. Cell. Physiol. 173 (1997) 406.
[7] E. Heyduk, T. Heyduk, Anal. Chem. 77 (2005) 1147.
[8] I.L. Medintz, A.R. Clapp, F.M. Brunel, T. Tiefenbrunn, H.T. Uyeda, E.L. Chang, J.R. Deschamps, P.E. Dawson, H. Mattoussi, Nat. Mater. 5 (2006) 581.
[9] H.A. Ho, M. Leclerc, J. Am. Chem. Soc. 126 (2004) 1384.
[10] M. Berezovski, R. Nutiu, Y. Li, S.N. Krylov, Anal. Chem. 75 (2003) 1382.
[11] C.C. Huang, Z. Cao, H.T. Chang, W. Tan, Anal. Chem. 76 (2004) 6973.
[12] I. German, D.D. Buchanan, R.T. Kennedy, Anal. Chem. 70 (1998) 4540.
[13] L.W. Dick Jr., L.B. McGown, Anal. Chem. 76 (2004) 3037.
[14] S. Centi, S. Tombelli, M. Minunni, M. Mascini, Anal. Chem. 79 (2007) 1466.
[15] R. Polsky, R. Gill, L. Kaganovsky, I. Willner, Anal. Chem. 78 (2006) 2268.
[16] F.L. Floch, H.A. Ho, M. Leclerc, Anal. Chem. 78 (2006) 4727.
[17] A.E. Radi, J.L.A. Sanchez, E. Baldrich, C.K. O'Sullivan, J. Am. Chem. Soc. 128 (2006) 117.
[18] Y. Xiao, B.D. Piorek, K.W. Plaxco, A.J. Heeger, J. Am. Chem. Soc. 127 (2005) 17990.
[19] D.A. Di Giusto, W.A. Wlassoff, J.J. Gooding1, B.A. Messerle, G.C. King, Nucl. Acids. Res. 33 (2005) e64.
[20] U. Schlecht, A. Malavé, T. Gronewold, M. Tewes, M. Löhndorf, Anal. Chim. Acta 573 (2006) 65.
[21] X. Wang, J. Zhou, W. Yun, S. Xiao, Z. Chang, P. He, Y. Fang, Anal. Chim. Acta 598 (2007) 242.
[22] J.L.A. Sanchez, E. Baldrich, A.E.-G. Radi, S. Dondapati, P.L. Sanchez, I. Katakis, Electroanalysis 18 (2006) 1957.
[23] L. Shi, V.D. Paoli, N. Rosenzweig, Z. Rosenzweig, J. Am. Chem. Soc. 128 (2006) 10378.
[24] P.C. Lee, D. Meisel, J. Phys. Chem. 86 (1982) 3391.

Available online at www.sciencedirect.com
ScienceDirect
Talanta 76 (2008) 15–20
Talanta
www.elsevier.com/locate/talanta

An online field-amplification sample stacking method for the determination of diuretics in urine by capillary electrophoresis-amperometric detection

Xinyu Zheng [a,b], Minghua Lu [a], Lan Zhang [a,*], Yuwu Chi [a], Lihui Zheng [a], Guonan Chen [a,*]

[a] *Key Laboratory of Analysis and Detection Technology for Food Safety, Ministry of Education, Fuzhou University, Fuzhou, Fujian 350002, China*
[b] *School of Life Sciences, Fujian Agriculture and Forestry University, Fuzhou, Fujian 350002, China*

Received 3 November 2007; received in revised form 26 January 2008; accepted 28 January 2008
Available online 15 February 2008

Abstract

A simple and sensitive online field-amplification sample stacking (FASS) pre-enrichment method following by capillary electrophoresis with amperometric detection has been developed for the determination of diuretics, such as indapamide (IDP), hydrochlorothiazide (HCT) and bumetanide (BMTN) in urine. Under the optimum conditions, it was found that the low concentration buffer solution could be used as the diluents for simultaneous field-amplification injection of three diuretics after electrokinetically injecting a short water plug (15 kV, 3 s). Three analytes could be well separated within 10 min in an uncoated fused-silica capillary with H_3BO_3–$Na_2B_4O_7$ (BB) buffer solution (pH 8.98). The detection limits (S/N = 3) were 9.0 ng/mL for IDP, 20 ng/mL for HCT and 1.5 ng/mL for BMTN, respectively. The detection limits of three diuretics were much lower by FASS than that by conventional sample injection, of which the detection limits were 340, 890 and 330 ng/mL for IDP, HCT and BMTN, respectively. Especially, for bumetanide the detection limit was 220-time lower by FASS. The linear ranges of three diuretics were all over three orders of magnitude. The proposed method has been successfully applied to analyze the diuretics in human urine samples without off-column sample pre-concentration.

Keywords: Capillary electrophoresis; Amperometric detection; Field-amplification sample stacking; Diuretic

1. Introduction

Diuretics have been widely used to treat the congestive heart failure and hypertension. Indapamide (IDP), hydrochlorothiazide (HCT) and bumetanide (BMTN) are three kinds of diuretics. IDP and HCT belong to medium effective diuretics. IDP is an extensively metabolized drug, and only 7% of the total dose administered was recovered in urine unchangeably. But 75–95% of HCT administered was recovered in urine unchangeably. BMTN is a highly effective diuretic, and 35–44% of BMTN excreted unchangeably in urine [1]. These three diuretics are used to treat edema in clinic. IDP is usually administered individually, while BMTN and HCT are used to treat the serious edema together.

Diuretics are considered as banned drugs to lose the athletes' avoirdupois before the competitions related weight categories, such as wrestling, boxing, judo, and weight lifting. On the other hand, diuretics were used illegally in sport competition to reduce the concentration of the other banned substances in urine. Moreover, diuretics may also destroy the thermoregulatory balance of human body, which would cause the exhaustion, irregular heartbeat and ultimate stoppage of the heart [2]. Diuretics have been forbidden by the Medical Commission of the International Olympic Committee (IOCMC) [3]. Thus, it is very important to develop a sensitive and time-saving method for the determination of diuretics in urine.

* Corresponding authors. Fax: +86 591 3713866.
E-mail addresses: zlan@fzu.edu.cn (L. Zhang), gnchen@fzu.edu.cn (G. Chen).

0039-9140/$ – see front matter © 2008 Elsevier B.V. All rights reserved.
doi:10.1016/j.talanta.2008.01.064

The techniques for determination of individual diuretic include HPLC [4], spectrophotometry [5], chemiluminescence [6] and GC–MS [7]. GC–MS is commonly used to analyze the diuretics in complex mixtures [8], but derivatization must be carried out before analysis due to the low volatility and thermal stability of diuretics. Another method for the simultaneous determination of multiple mixture diuretics is liquid chromatography [9]. However, it requires large sample consumption and complicated sample preparation, and sometimes it lacks of adequate sensitivity. Nowadays, high-performance capillary electrophoresis (HPCE), which offers the advantages of excellent high resolution, rapid analysis and especially minimal sample volume requirement, has become a useful analytical technique for drug analysis [10,11]. Some sensitive detectors, such as laser-induced fluorescence and amperometric detectors (AD) provide ultimate sensitivity while maintaining the extreme separation efficiency of CE. Gonzalez et al. [12] proposed the method for the determination of four diuretics by capillary zone electrophoresis (CZE) coupled with fluorescence detection. Our group has also developed the methods for determination of multiple diuretics in urine by CZE-AD and CE-MS in the previous works [13,14]. However, CE method suffers from low concentration sensitivity because of some factors, such as a short optical path length and a small injection volume. These above methods are still not sensitive enough to determine these diuretics in body fluids without extensive sample pre-concentration. Although CZE-AD could obtain good sensitivity and selectivity for the analysis of some diuretics, it could not satisfy the extreme low detection limit of bumetanide in urine after the oral administration (usually lower than 10 ng/mL) [15]. So some on-column sample stacking approaches were used to enhance the sensitivity of CE method for determination of diuretics in urine. On-column isotachophoresis [16,17], pH-mediated sample stacking [17] and field-amplification sample stacking (FASS) [18–20] have been applied to pre-concentrate the polar analytes which can be loaded into the capillary and improve the analytical sensitivity. FASS, developed by Mikker et al. [21], is a convenient and practical on-column pre-concentration technique based on the difference of conductivity between the sample solution and background electrolyte. And its performance has been successfully confirmed and improved [17,22,23].

In this paper, a simple, sensitive and pre-treatment-free new method based on CZE-FASS-AD was developed for the simultaneous determination of IDP, HCT and BMTN. The limits of detection (S/N = 3) were in the ng/mL concentration range, and the linear range was about three orders of magnitude. Finally, the proposed method has been successfully applied to analyze the corresponding diuretics in human urine.

2. Experimental

2.1. Apparatus

In this study, a home-made CE-AD system has been established for analysis. A ±30 kV high-voltage dc power supply (Shanghai Institute of Nuclear Research, Shanghai, China) provided the separation voltage between the two ends of capillary. An uncoated fused-silica capillary was used in the study (63 cm length × 25 μm i.d. × 360 μm o.d., Yongnian Optical Fiber Factory, Hebei, China). A three-electrode electrochemical cell including a 300 μm diameter carbon disc working electrode, a platinum auxiliary electrode and an Ag/AgCl (saturated KCl) electrode as reference electrode, was connected to a BAS LC-4C amperometric detector (Bioanalytical Systems Inc., West Lafayette, IN, USA). The data were recorded by the TL9902 analytical system of chromatogram (Beijing Teleh Electronic Tech. Co., Ltd.).

2.2. Chemicals

IDP, HCT and BMTN were obtained from the Chinese Institute of Biological Products Control (Beijing, China). Indapamide tablets were obtained from Tianjin Lisheng Pharmaceutical Co., Ltd. Hydrochlorothiazide tablets were purchased from Beijing Double-Crane Pharmaceutical Co., Ltd. Bumetanide tablets were provided by Fuzhou Neptunus Fuyao Pharmaceuticals Co., Ltd. All chemicals were of analytical reagent grade.

2.3. Preparation of standard solution and buffer solutions

All solutions were prepared with fresh deionized water and passed through a 0.22 μm membrane filter before use. Stock solution of IDP (1.00 mg/mL), HCT (1.12 mg/mL) and BMTN (1.00 mg/mL) were prepared by the use of 3/7 (v/v) methanol–buffer solution, respectively. Buffer solution was prepared by mixing 50.0 mmol/L $Na_2B_4O_7$ and 200 mmol/L H_3BO_3 solutions to form a H_3BO_3–$Na_2B_4O_7$ buffer solution (200 mmol/L). The running buffer used for electrophoresis in this experiment was 25.0 mmol/L BB (pH 8.98) buffer solution.

2.4. Preparation of human urine sample

Healthy male volunteers were divided to two groups. One group of volunteers took a single does of hydrochlorothiazide tablets (25 mg). The other volunteers took a single does of hydrochlorothiazide (25 mg) and two doses of bumetanide (2 mg). All administrations were according to the principle of Public Health Bureau of China. The urine samples were collected at regular intervals of time and then stored in the refrigerator at 4 °C. Before analysis, the sample was thawed at room temperature and centrifuged for 15 min at 4000 rpm in order to remove precipitated proteins and other particulate matters.

2.5. Separation preconditions

The new capillary was flushed by 0.100 mol/L sodium hydroxide solution for 4 h before use, and then rinsed with 0.100 mol/L HCl and deionized water, respectively for 10 min. Between each run, the capillary was rinsed with 0.0500 mol/L sodium hydroxide solution, water and running buffer for 2 min, respectively.

For FASS, the standard solution was diluted to desired concentration by 15.0 mmol/L BB buffer solution (pH 8.98). Prior

to sample injection a short plug of water was injected into the capillary with 15 kV for 3 s, and then the diuretics were injected with 15 kV for 15 s. Then, 25.0 mmol/L BB (pH 8.98) running buffer was used during CE separation.

3. Results and discussion

3.1. Detection of three diuretics using conventional CE-AD

3.1.1. Optimization of separation conditions

Two kinds of buffers, namely sodium phosphate and H_3BO_3–$Na_2B_4O_7$ (BB) buffer solutions were tried to be used for separation of diuretics. The results showed that under the same condition a good sensitivity and resolution were achieved by using of BB buffer. Moreover, the pH value was the important parameter to affect the separation efficiency and the current response because of its effect on the electroosmotic flow. Thus, it is very important to optimize the pH value of the buffer. Fig. 1 showed the electropherograms of three analytes with the pH range from 8.08 to 9.21 (25 mmol/L BB buffer solution). When pH value was between 8.98 and 9.21, a good separation of three compounds was obtained. Meanwhile, the peak current achieved maximum at the point of pH 8.98. Therefore, pH 8.98 was selected for subsequent experiments.

The concentration of buffer would influence the viscosity coefficient of the running solution and further affect the resolution and migration time of the analytes [17]. It was also an influential factor on the stacking efficiency. Higher running buffer concentration would increase the conductivity of the background buffer. It would lead to enlarge the difference of conductivity between the background running buffer and sample matrix zone. And then the higher stacking efficiency may be obtained. However, it should be noted that higher buffer concentrations would result in longer separation times and reduced resolution. Thus, the effect of concentration of the running solution on the separation was studied by use of 15.0, 20.0, 25.0, 30.0 and 35.0 mmol/L BB (pH 8.98) buffer solution, respectively. 25.0 mmol/L of BB (pH 8.98) buffer solution was employed to achieve a good compromise between resolution and analysis time.

Also, the dependence of the migration velocities of the solute on the applied electrical field strength was examined for various voltages in the BB running buffer solution of 25.0 mmol/L, pH 8.98. The migration time of analytes was significantly shortened and their corresponding current peaks were sharpened when separation voltage was increased. However, if the separation voltage was too high, more Joule heat was produced. It would make the peak shape broadening. As a comprehensive thought, a separation voltage of 15 kV was selected as the optimum separation voltage in this experiment. The amount sampling was also tested in this experiment. It was found that good analytical sensitivity could be obtained when injection time was 10 s at 15 kV.

Fig. 3(A) shows the electropherogram under the optimum conditions for the three diuretics. It is clear that by using the normal injection condition of CZE-AD the three diuretics can be fully separated within 10 min.

3.1.2. Linearity and detection limit

Under the optimum conditions, a series of different concentrations of the standard mixture solutions of IDP, HCT and BMTN ($n = 5$) were analyzed to determine the linear response range. The regression equations, coefficient correlation and detection limits are listed in Table 1. The detection limits for IDP, HCT and BMTN by normal injection were 340, 890 and 330 ng/mL (S/N = 3), respectively. Obviously, the detection limits of BMTN by normal injection mode of CE-AD could not fit the request of direct determination in urine (lower than 10 ng/mL).

3.2. Field-amplified sample stacking

Compared with CE-UV, CE-AD has the conspicuous superiority in the aspects of sensitivity and selectivity, but sometimes it still cannot meet the actual requirements for the determination of diuretics in biological samples. In order to improve the sensitivity, several approaches have been described to pre-concentrate samples in the CE capillary prior to separation [17,21–23]. As one of the conventional on-column pre-concentration approaches, the practical and useful FASS is very suitable for the AD detection. For FASS, the sample solvent, the length of water plug, injection voltage and injection time of the sample solution are all the key factors needing optimization.

3.2.1. Effect of the background solution in the sample zone

In order to decrease the conductivity, the analytical sample is normally prepared in a lower conductivity solution than that of running buffer solution. Adding organic solvents to the sample solution is the most useful method to decrease the conductivity. In this experiment, several kinds of organic solvent were tested to add to the sample solution. However, the result suggested that addition of organic solvents to the sample solution did not result in the sensitivity increasing. Then sample ions were tried to prepare in a more diluted buffer whose concentration was lower than that of running buffer solution in order to enhance the electric field strength of sample zone. A series of BB buffer solutions with different concentrations (5, 10, 15, 20, 25 and 30 mmol/L) were used as the diluted sample solutions. The results indicated that the highest peak currents of these three analytes were obtained when 15 mmol/L BB buffer solution was used as the sample solution.

3.2.2. Effect of water plug length

It was noticed that introducing a short plug of water before electrokinetic injection could provide a high electric field strength from the beginning of the injection. The basic functions of short water plug were as following: (1) making the boundary between the sample solution and the background electrolyte much clearer for the higher analytical sensitivity; (2) reducing the electricity discrimination; (3) concentrating positive and negative ions simultaneously; and (4) achieving good reproducibility [20].

The experiments showed that better peak current response and shape could be gained when water plug was used. Prior to the sample injection, a water plug was injected into the capil-

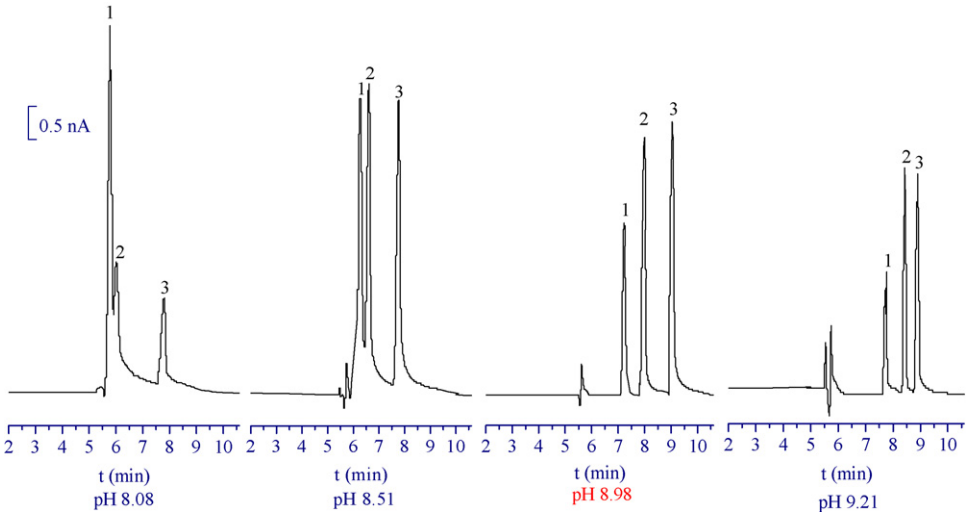

Fig. 1. Effect of the pH on the separation of three diuretics. 1: IDP (80.0 μg/mL); 2: HCT (65.0 μg/mL); 3: BMTN (55.0 μg/mL). Capillary: 63 cm × 25 μm; separation voltage: 20 kV; buffer solution: 25 mmol/L BB; temperature: 20 ± 0.5 °C. The working electrode: carbon disk electrode; the auxiliary electrode: platinum wire; injection: 15 kV × 10 s; the reference electrode: Ag/AgCl; working potential: 800 mV.

lary immediately to enhance stacking and sample loading. Since the length of the water plug in the capillary would significantly influence the sensitivity, the injection time of the water plug in the range of 1–10 s at 15 kV was examined. The results showed that 3 s of injection time (about 0.34 cm water plug length equivalently) provided the highest peak current.

3.2.3. *Effect of the injection voltage and injection time*

For FASS, the injection conditions were the most important factor to affect the behavior of stacking [24]. Effect of the injection voltage on the peak currents was shown in Fig. 2. The peak currents increased with the injection voltage from 9 to 15 kV. When the injection voltage was 15 kV, the peak current enhancement attained the maximum for all the three analytes. The effect of sample injection time was also investigated, and the results showed that the peak currents of the three analytes increased with the injection volumes in the range of 10–20 s. A series of different injection time for the standard mixture solutions of IDP, HCT and BMTN ($n = 5$) were performed to investigate the linearity of injection volume against peak height of three analytes. The regression equations and coefficient correlation (R) were

$$\text{IDP}: y = 2.87x - 0.0275 \quad (R = 0.9993)$$

$$\text{HCT}: y = 2.86x + 0.0205 \quad (R = 0.9996)$$

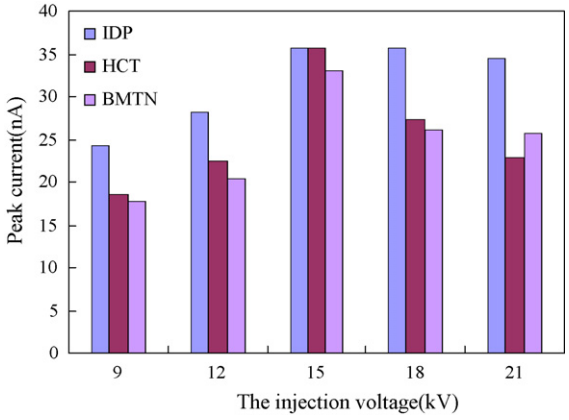

Fig. 2. Effect of the injection voltage on the peak current of three diuretics. IDP (64.0 μg/mL); HCT (65.0 μg/mL); BMTN (40.0 μg/mL). Water injection: 15 kV × 3 s; diluent solvent: 15 mmol/L BB (pH 8.98); other conditions are the same as Fig. 1.

$$\text{BMTN}: y = 2.63x + 0.0574 \quad (R = 0.9994)$$

where the y and x are the peak current (nA) and the injection volume of analytes (nL), respectively.

However, when injection time was longer than 15 s (about 12.5 nL), the resolution reduced because of the peak-broadening. "The possible reasons for this phenomenon might be explained

Table 1
The comparison of the linear ranges and detection limits by CE-FASS-AD and conventional injection CE-AD[a]

Compound	Linear ranges (μg/mL)		Detection limits (ng/mL)[b]	
	Conventional injection	FASS	Conventional injection	FASS
IDP	1.0–250	0.03–25.0	340	9.0
HCT	3.3–220	0.06–110	890	20
BMTN	1.0–50.0	0.005–12.9	330	1.5

[a] All conditions are the same as Fig. 3.
[b] The detection limits are estimated on the basis of a signal-to-noise ratio of 3 (S/N = 3).

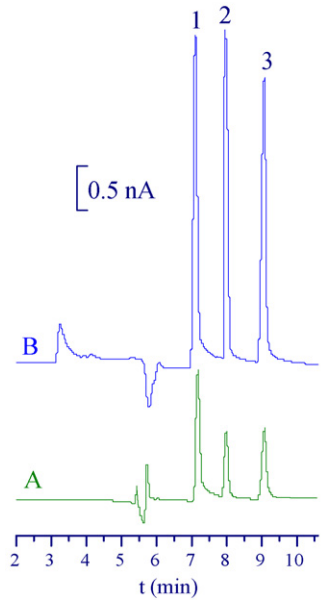

Fig. 3. The comparison electropherograms between post-concentration (A) and pre-concentration (B). 1. IDP; 2. HCT; 3. BMTN. Capillary: 63 cm × 25 μm; separation voltage: 15 kV; buffer solution: 25 mmol/L BB (pH 8.98); temperature: 20 ± 0.5 °C. The working electrode: carbon disk electrode; the auxiliary electrode: platinum wire; the reference electrode: Ag/AgCl; working potential: 800 mV. (A) Concentration: IDP (40.0 μg/mL), HCT (22.5 μg/mL), BMTN (20.0 μg/mL); injection: 15 kV × 10 s; (B) concentration: IDP (6.5 μg/mL), HCT (7.5 μg/mL), BMTN (4.0 μg/mL); water injection: 3 s; diluent solvent: 15 mmol/L BB (pH 8.98); electrokinetic injection: 15 kV for 15 s.

as follows: (1) the increasing of electric field distribution for sample solution zone would reduce electric field strength for BGE. It leads the electrophoretic speed of sample ion to very small and sample ion mainly relied the EOFs to migrate from anode to cathode. This was the main reason to result in the resolution descended when injection time was too long [25,26]; (2) too large injection amount might cause the increasing of laminar flow and then peak-broadening; (3) the high electric field of sample solution zone could produce the partially Joule heat, which would generate the bubble and broaden the peaks. Therefore, the resolution was decreased when the injection time was too long in stacking. ” Thus, the best injection time for FASS mode were 15 s.

Electrophorograms obtained under the above optimum conditions for pre-concentration and post-concentration were illustrated in Fig. 3(A and B). Concentration of IDP, HCT and BMTN were 40.0, 22.5 and 20.0 μg/mL, respectively by use of conventional injection, while they were 6.5, 7.5 and 4.0 μg/mL, respectively by using FASS. It can be seen from Fig. 3 that the peak currents of three diuretics were drastically increased after pre-concentration.

3.2.4. Detection limit, linear response range and repeatability

Under the optimum conditions for FASS, a series of different concentrations of the standard mixture solutions of IDP, HCT and BMTN were analyzed to determine the linear response range. The regression equations and coefficient correlation (R) were

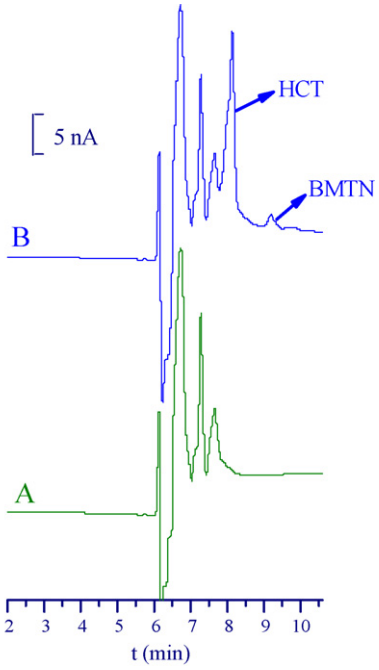

Fig. 4. Electropherograms of blank urine (A) and real urine sample (B). Other conditions are the same as Fig. 3(B).

$$\text{IDP}: y = 0.557x + 0.0535 \quad (R = 0.9997)$$

$$\text{HCT}: y = 0.531x - 0.0104 \quad (R = 0.9993)$$

$$\text{BMTN}: y = 0.812x + 0.0761 \quad (R = 0.9999)$$

where the y and x are the peak current (nA) and the concentration of analytes (μg/mL), respectively. The linear response ranges by FASS mode were 0.03–25.0 μg/mL for IDP, 0.06–110 μg/mL for HCT and 0.005–12.9 μg/mL for BMTN with the detection limits of 9.0, 20 and 1.5 ng/mL, respectively. In addition, some experiments of the repeatability of the CE-FASS-AD method were carried out. The repeatability of the peak current and migration time for the three analytes was tested by duplicated injections of a standard mixture solution ($n = 5$). The R.S.D.s of peak current for IDP, HCT and BMTN were 2.5, 1.9 and 2.0%,

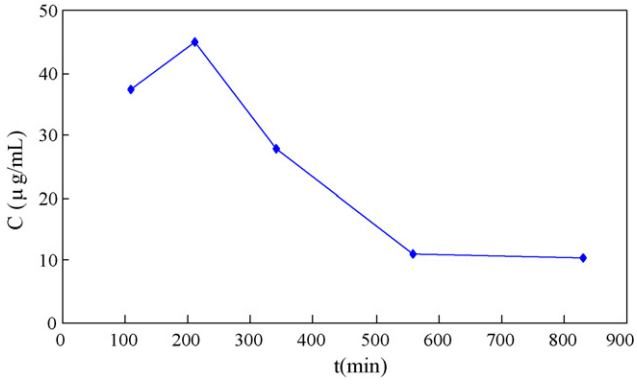

Fig. 5. Study of the urinary excretion of HCT. Other conditions are the same as Fig. 3(B).

Table 2
Recoveries of IDP, HCT and BMTN in the urine samples ($n = 5$)[a]

Compound	Added (μg)	Found (μg)	Recovery (%)	R.S.D. (%)
IDP	0.50	0.51	102	1.6
	2.50	2.38	95.2	2.2
HCT	0.72	0.67	93.1	3.3
	6.22	6.75	108	3.0
BMTN	0.40	0.38	95.0	4.0
	1.82	1.76	96.8	4.2

[a] All conditions are the same as Fig. 3(B).

and the R.S.D.s of migration time for IDP, HCT and BMTN were 0.4, 1.0 and 0.5%, respectively. Comparison of the detection limits of the three analytes by FASS mode with those of conventional injection mode was shown in Table 1. According to the data in Table 1, the detection limits of the three analytes by FASS mode were 37.8, 44.5 and 220 times lower than those by the conventional injection for IDP, HCT and BMTN, respectively. And meantime the linear response ranges by FASS mode achieved three orders of magnitude. Therefore, the results showed that the proposal CE-FASS-AD system provided a convenient tool for the determination for the trace diuretics in biological sample.

3.3. Analytical applications

As HCT can work as synergetic function coupling with BMTN, they can be used together in clinic. In this study one group of healthy volunteers were given with oral doses of HCT (12.5 mg) and BMTN (2.0 mg) simultaneously. The preparation of human urine sample was according to Section 2.4. The urine sample was diluted 50-fold with buffer solution (15 mmol/L, pH 8.98, BB) without any pre-treatment. Due to average 200 mmol/L salts existed in real urine, the sample contained about 4 mmol/L salts after 50-fold dilution. In order to offset salt effect and ensure the efficiency of FASS, 4 mmol/L NaCl was added to the sample solution. The urine sample was injected into the capillary by FASS mode directly without any pre-treatment. Fig. 4 illustrated the electropherograms of the blank urine sample and the real urine sample of volunteers taking corresponding diuretic doses after 200 min. In order to identify the peaks of HCT and BMTN, the standard solutions were added to the urine sample and then it was found that the peak currents were obviously increased accordingly. The results suggested that both HCT and BMTN could be successfully detected in real urine samples without the interference of high salt, proteins and endogenetic compounds.

Another group of healthy volunteers were given the single oral dose of HCT (25 mg). The preparation of human urine sample was also according to Section 2.4. Five urine samples were collected within a half-life (when 110, 210, 340, 560 and 830 min after drug ingestion). Fig. 5 showed the changing trends of the concentration of HCT during urinary excretion. The total unchangeable percentages of HCT in five urine samples were 91.78%, which were calculated according to the regression equations. This result agrees well with the literature, which was 75–95% of HCT excreted unchangeably in urine [1].

In order to study the recovery of this method, three diuretic standard solutions were added into the diluted blank urine. Table 2 showed the recoveries of three analytes in this method. The average recoveries were in the range of 93.1–108%, and the R.S.D.s were less than 4.2% ($n = 5$).

4. Conclusions

A sensitive and time-saving CE-FASS-AD method for determination of three diuretics (IDP, HCT and BMTN) has been developed in this paper. By using FASS technique the detection sensitivity has been greatly improved (220-time higher than that of the normal injection), and the linear response range was over about three orders of magnitude. Direct injection and online CE-FASS-AD method have been applied to analyze diuretics in real human urine samples successfully. The developed CE-FASS-AD method would promise to application in the field of pharmaceutical and routine doping analysis.

Acknowledgements

The authors are grateful for the National Nature Sciences Funding of China (20675016, 20735002, 20775014), the Key Program of Science and Technology Department of Fujian Province (2007I0020), the Key Special Purpose Funding of Physical Education Bureau of Fujian Province, China (HX2005-74).

References

[1] P.W. Feit, K. Roholt, H. Sorensen, J. Pharm. Sci. 62 (1973) 375.
[2] United States Olympic Committee on Substance Abuse, Questions and Answers, USOC, Colorado Springs, 2006.
[3] International Olympic Committee, Medical Commission, International Olympic Charter Against Doping in sport, IOC, Lausanne, 1990.
[4] H.J. Guchelaar, L. Chandi, O. Schouten, et al., Anal. Chem. 363 (1999) 700.
[5] M.L. Luis, J.M.G. Fraga, F. Jimenez, et al., Talanta 53 (2001) 761.
[6] J. Ouyang, W.R.G. Baeyens, J. Delanghe, et al., Talanta 46 (1998) 961.
[7] R. Ventura, J. Segura, J. Chromatogr. B 687 (1996) 127.
[8] V. Morra, P. Davit, P. Capra, et al., J. Chromatogr. A 1135 (2006) 219.
[9] L. Politi, L. Morini, A. Polettini, Clin. Chim. Acta 386 (2007) 46.
[10] N. Helai, N.T. Tran, L. Monser, et al., Talanta 74 (2008) 694.
[11] L. Zhang, G.N. Chen, Q. Hu, Y.Z. Fang, Anal. Chim. Acta 431 (2001) 287.
[12] E. Gonzalez, A. Becerra, J.J. Laserna, J. Chromatogr. B 687 (1996)145.
[13] L. Zhang, P. Tong, Y. He, et al., Chin. J. Chromatogr. 23 (2005) 22.
[14] M.H. Lu, P. Tong, L. Zhang, et al., Electrophoresis 28 (2007) 1461.
[15] C.Y. Gradeen, D.M. Billay, S.C. Chan, J. Anal. Toxicol. 14 (1990) 123.
[16] A. Jastrzebska, Talanta 69 (2006) 1018.
[17] Y. Chen, Capillary Electrophoresis Technology and Application, Chemical Industry Press, Beijing, 2006, pp. 43–46.
[18] Z. Zhu, L. Zhang, A. Marimuthu, Z. Yang, Electrophoresis 23 (2002) 2280.
[19] Y.F. Shi, Y. Huang, J.P. Duan, et al., J. Chromatogr. A 1125 (2006) 124.
[20] S.M. Wu, Y.H. Ho, H.L. Wu, et al., Electrophoresis 22 (2001) 2717.
[21] F.E.P. Mikker, F.M. Everaets, T.P. Verheggen, J. Chromatogr. 169 (1979) 1.
[22] Z.K. Shihabi, J. Chromatogr. A 853 (1999) 3.
[23] Y.Z. Yang, R.I. Boysen, M.T.W. Hearn, Anal. Chem. 78 (2006) 4752.
[24] R.L. Chien, D.S. Burgi, J. Chromatogr. 559 (1991) 141.
[25] D.M. Osbourn, D.J. Weiss, C.E. Lunte, Electrophoresis 21 (2000) 2768.
[26] M.C. Breadmore, P.R. Haddad, Electrophoresis 22 (2001) 2464.